

Large-scale Roll-to-Roll Fabrication of Organic Solar Cells for Energy Production

Hösel, Markus; Krebs, Frederik C

Publication date:
2013

Document Version
Publisher's PDF, also known as Version of record

[Link back to DTU Orbit](#)

Citation (APA):
Hösel, M., & Krebs, F. C. (2013). Large-scale Roll-to-Roll Fabrication of Organic Solar Cells for Energy Production. Department of Energy Conversion and Storage, Technical University of Denmark.

DTU Library

Technical Information Center of Denmark

General rights

Copyright and moral rights for the publications made accessible in the public portal are retained by the authors and/or other copyright owners and it is a condition of accessing publications that users recognise and abide by the legal requirements associated with these rights.

- Users may download and print one copy of any publication from the public portal for the purpose of private study or research.
- You may not further distribute the material or use it for any profit-making activity or commercial gain
- You may freely distribute the URL identifying the publication in the public portal

If you believe that this document breaches copyright please contact us providing details, and we will remove access to the work immediately and investigate your claim.

Large-scale Roll-to-Roll Fabrication of Organic Solar Cells for Energy Production

Markus Hösel

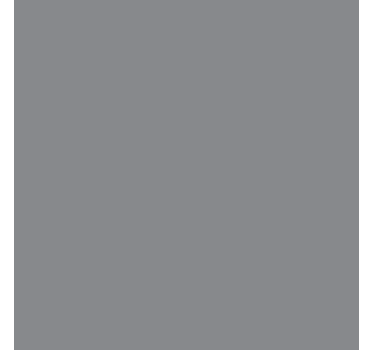
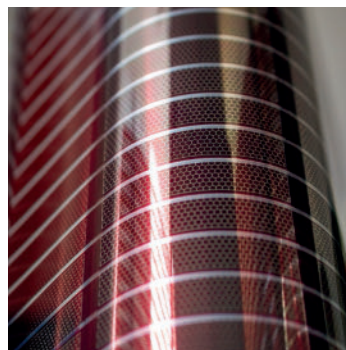
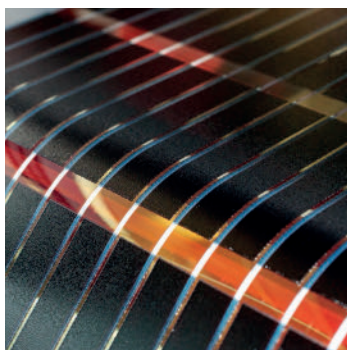
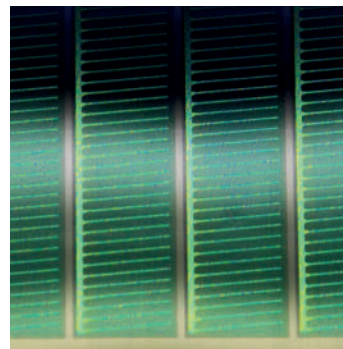
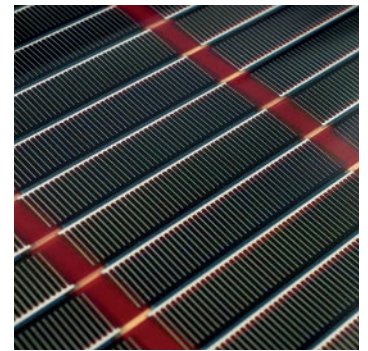
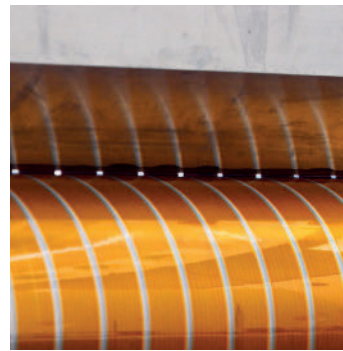
Department of Energy Conversion and Storage

Ph.D. Thesis, December 2013

Thermoelectrical Generators / Superconducting Components
High Temperature Polymer Electrolyte Membrane Fuel Cells

Energy Conversion

Colloidal Chemistry / Electrochemistry
Polymer Solar Cells
Solid State Physics
Electron Microscopy
Ceramic Membranes
Solid Oxide Fuel Cells
Shaping Processes / Electron Microscopy / Solid State Physics / Computational Materials Design / Modelling / Heterostructures
Solid Oxide Electrolysis Cells
Computational Materials Design
X-Ray and Neutron Scattering
High Temperature Polymer Electrolyte Membrane Electrolysis Cells
Fuel Cells and Hydrogen Test Center
Shaping Processes / Defect Chemistry
Electrochemical Flue Gas Purification
Batteries / Hydrogen Storage
Synthesis / Colloidal Chemistry / Heterostructures / X-Ray and Neutron Scattering
Magnetic Refrigeration
Energy Storage
Sintering
Synthetic Fuels
Magnetism
Synthesis
Modelling



Large-scale Roll-to-Roll Fabrication of Organic Solar Cells for Energy Production

PhD Thesis

Markus Hösel



Roskilde, December 2013

PhD thesis title:

Large-scale Roll-to-Roll Fabrication of Organic Solar Cells for Energy Production

Author:

Markus Hösel

Supervisor:

Prof. Frederik C. Krebs

Technical University of Denmark, Denmark
Department of Energy Conversion and Storage
Solar Energy

Assessment committee:

Prof. Panagiotis Lianos, University of Patras, Greece
Prof. Bo Wegge Laursen, University of Copenhagen, Denmark
Dr. Jens Wenzel Andreasen, Technical University of Denmark, Denmark

Date of defense:

5 February 2014

Funding:

Project "Largecells", EU-Indian framework (EU FP7/2007-2013, grant no. 261936)

Address:

Technical University of Denmark
Department of Energy Conversion and Storage
Frederiksborgvej 399
DK-4000 Roskilde, Denmark
Phone +45 4677 5800
info@ecs.dtu.dk
www.ecs.dtu.dk

ISBN: 978-87-92986-15-3

Abstract

The global energy consumption is increasing steadily while natural energy sources are running out sooner or later. Solar electricity is one of many renewable energy sources that contributes to the world's demand. Organic solar cells (OPV) are an attractive 3rd generation solar technology that can be produced cheaply and very fast from solution with printing processes. The current research all around the world is still focused on lab-scale sized devices $\ll 1 \text{ cm}^2$, ITO-glass substrates, and spin coating as the main fabrication method. These OPV devices are far from any practical application although record efficiencies beyond 10 % could be achieved.

This dissertation describes process workflows and roll-to-roll (R2R) fabrication methods for upscaling the OPV technology to solar module sizes that enable real power production even at efficiencies $< 2 \%$. The fundamental cell technology was based on flexible plastic substrates and ITO-free transparent conductive electrodes made from special designed flexo printed silver grids, rotary screen printed PEDOT:PSS, and slot-die coated ZnO (= Flextrode). The organic solar cell was fabricated by slot-die coating a light absorbing photoactive layer (e. g. P3HT:PCBM) on top of the Flextrode substrate and completed by rotary screen printed PEDOT:PSS and silver electrodes. All layers were R2R printed and coated from solution under full ambient vacuum-free conditions with fabrication speeds reaching 25 m min^{-1} for some of the layers.

Fabrication of modules with high power output requires intelligent connection of single cells that should involve as less as possible manual processes such as wiring or soldering. The problem was solved by serially connecting thousands of single cells entirely during the R2R processing by printing thin-film silver conductors. High voltage networks require only thin conductors to efficiently transport the relatively low current of the organic solar cells. The serial connection was possible through a special designed pattern layout that combined 1-dimensional coating and 2-dimensional printing processes. The so-called Infinity concept allowed the fabrication of virtually infinitely large module sizes without manual wiring. High voltage modules with 21000 cells, open circuit voltage $> 10 \text{ kV}$ and power output $> 220 \text{ W}_{\text{peak}}$ could be successfully manufactured while having only two terminal contacts.

Real energy production from these modules was studied by setting up a whole solar park based on OPV modules. Infinity modules with a length of 100 m (width 0.3 m) were rolled out and taped onto a wooden structure. The maximum power output of six parallel-connected modules with a total active area of 88.2 m^2 was beyond 1.3 kW while having energy payback times $\ll 1$ year. Alternative installation concepts such as a balloon or special designed solar tubes on land or water were proved to be functional as well. Solar tubes with Infinity modules of around 200 W generated 18 kWh in 5 weeks. The energy was fed back into the Danish power grid.

The dissertation contains a brief introduction of organic solar cell technology and reviews important R2R compatible manufacturing methods including photonic sintering. The fabrication, design, and challenges of Flextrode and Infinity modules are described in detail. The potential future energy production is presented through large-scale OPV installation scenarios and performance analyses. Fatal failures such as fully burned cells are described while easy repair mechanisms are shown that avoid costly replacements of full modules. A conclusion and outlook finalizes the dissertation.

Resumé

Energiforbruget i verden er støt stigende, mens jordens naturlige energi ressourcer er begrænsede og før eller siden vel være opbrugte. Konvertering af solenergi til elektricitet er en af mange bæredygtige energikilder, som bidrager til at dække verdens energi behov. Organiske sol celler (OPV) er en attraktiv tredje generations solcelle teknologi, som kan produceres billigt og meget hurtigt fra aktivt blæk opløsninger ved brug af printe og coate teknikker. Meget af den nuværende forskning er stadig fokuseret på laboratorie-skala solceller med størrelser $\ll 1 \text{ cm}^2$, ITO-glas substrater og spin coating som den primære fabrikations metode. Disse OPV devices er langt fra praktisk anvendelse, på trods af at en rekord effektivitet på over 10 % har kunnet opnås.

Denne afhandling beskriver proces flowet og rulle-til-rulle (R2R) fabrikationsmetoder for opskalering af OPV teknologien til solcellemodul størrelser, der muliggør egentlig energi produktion selv med effektiviteter $< 2\%$. Den fundamentale celle teknologi er baseret på fleksible substrater og ITO-fri transparente ledende elektroder, fremstillet med specialdesignede flexografisk printede sølv gitre, rotationstrykt PEDOT:PSS og slot-die coatet zinkoxid (= Flextrode). De organiske solceller blev fabrikeret ved slot-die coating af et lys-absorberende fotoaktivt lag (f. eks. P3HT:PCBM) oven på det Flextrode substrat og færdiggjort ved rotationstryk af PEDOT:PSS og sølv elektroder. Alle lag blev R2R printet eller coatet fra blæk under normal luft og vakuum-fri betingelser, med fabrikationshastigheder op til 25 m min^{-1} ved nogle af lagene.

Fabrikation af moduler med høj effekt kræver intelligent sammenkobling af enkeltceller, med minimal manuel indsats, såsom kabling og lodning. Problemet blev løst ved at serieforbinde tusindvis af enkeltceller udelukkende ved brug af R2R processering og printing af tyndfilms sølvledere. Højspændingsnetværk kræver kun tynde ledere for effektivt at transportere den relativt lave strøm fra de organiske solceller. Serieforbindelsen blev gjort mulig gennem et specielt designet maskelayout, som kombinerer 1-dimensionel coating og 2-dimensionel print processer. Dette såkaldte Infinity koncept tillader fabrikation af næsten uendeligt store modulstørrelser uden behov for manuel elektrisk forbindelse. Højspændingsmoduler med 21000 celler, en åben-kreds spænding på $> 10 \text{ kV}$ og en effekt på $> 220 \text{ W}$, blev fremstillet med kun to tilslutningsterminaler.

Energi produktionen fra disse moduler blev studeret ved opsætning af en solcellepark baseret på OPV moduler. Infinity moduler med en længde på 100 m blev rullet u dog tapet fast på et træ-skellet. Den maksimale effekt fra seks parallel-forbundne moduler med et total aktivt areal på 88.2 m^2 var over 1.3 kW og med energitilbagebetalingstider på $\ll 1$ år. Alternative installationskoncepter, såsom en ballon eller specialdesignede solrør på land eller vand blev testet som funktionelle. Solrør med Infinity moduler på cirka 200 W ydede 18 kWh i løbet af en 5 ugers periode. Energien blev ført tilbage ind i det danske el-net.

Afhandlingen indeholder en kort introduktion af organisk solcelle teknologi og gennemgår deslige vigtige R2R kompatible fremstillingsmetoder så som fotonisk sintering. Fabrikationen, designet, og udfordringerne i forbindelse med udviklingen af Flextrode substratet og Infinity moduler er beskrevet i detaljer. Den potentielle fremtidige energi-produktion præsenteres gennem stor-skala OPV installationsscenarier og ydelses analyser. Fatale udfald, såsom fuldstændig brændte celler beskrives, mens lette reparationsmekanismer vises, således at dyre udskiftninger af fulde moduler undgås. En konklusion og fremtidige perspektiver afslutter afhandlingen.

Preface

This PhD thesis presents the main results of my work carried out at the Solar Energy section of the Department of Energy Conversion and Storage of the Technical University of Denmark. The three years of research between 2011 and 2013 under the supervision of Prof. Frederik C. Krebs has been financed by the Project "Largecells" under the EU-Indian framework of the European Commission (EU FP7/2007-2013, grant no. 261936). I was heavily involved in the EU project and it allowed me to contribute with project reports and the active participation at project meetings in India and Israel. Parts of the study were carried out during a 5 month long external research stay at the Jawaharlal Nehru Centre for Advanced Scientific Research (JNCASR) in Bangalore, India.

My engineering background and specialization in large-scale processing and printing allowed me to contribute in a plenty of different projects as can be seen by the number of publications listed in Section 1.4. This thesis contains only the main publications that describe the upscaling efforts and fabrication background of organic solar cell devices for energy production. The main goal was to create a compact and consistent storyline with as much information as necessary instead of a collection of different projects.

All of the above has been made possible through my supervisor Frederik C. Krebs. His contagious passion, energy, and activity in the laboratory and in front of the printing machines is amazing and allowed me to discuss and ask questions straight away. Thank you! I would also like to thank the other large-scale processing and Infinity team members Mikkel Jørgensen and Roar R. Søndergaard for their time to discuss project related problems. The time with all of you during the print-runs and outside in the solar park was great and we often had a lot to laugh!

Special thanks go to my office mate Dechan Angmo. We not only shared and solved scientific problems together but also laughed a lot and amused our office neighbors from time to time. I like to thank Nieves Espinosa for all the crazy experiments and collaboration within the Infinity project, and the very nice relationship during work and leisure time. Furthermore, I like to thank Henrik, Thomas T., Morten, "Bondo", Suren, Thue, Thomas R., Birgitta, Arvid, Jon, Martin, Jacob, and all the newcomers for the good discussions, collaborations, and fun at work and outside. Last but no least I like to thank the whole Solar Energy group for the last three years. It was a pleasure to work with you! Finally, I like to thank my family and friends back in Germany and all my friends here in Denmark for their support.

Contents

1. Introduction	1
1.1. Background	1
1.2. OPV working principle	3
1.3. Device geometries and materials	5
1.4. List of publications and contributions	7
2. Large-scale manufacturing methods for organic solar cells	13
2.1. Coating technologies	13
2.1.1. Slot-die coating	14
2.1.2. Blade coating	16
2.1.3. Spray coating	17
2.2. Printing technologies	18
2.2.1. Screen printing	18
2.2.2. Flexography	19
2.2.3. Gravure printing	21
2.2.4. Inkjet printing	22
2.3. Further fabrication methods	25
2.4. Manufacturing strategies	26
2.5. Reports on printed and coated devices	28
3. Photonic sintering methods	35
3.1. Technology and working principle	35
3.2. Photonic sintering of flexo printed silver electrodes	37
3.2.1. Experimental	37
3.2.2. Results and discussion	38
3.3. Conclusion	43
4. Large-scale R2R fabrication of OPV devices	45
4.1. ITO-free transparent electrode for OPVs	45
4.1.1. Flextrode	46
4.1.2. Flextrode improvements	48
4.2. Infinity module fabrication	50
4.3. Back electrode printing	57
4.3.1. Experimental	57
4.3.2. Results and discussion	58
4.3.3. Conclusion	62

4.4. Encapsulation	62
4.4.1. Experimental	63
4.4.2. Results and discussion	65
4.4.3. Conclusion	69
5. Large-scale OPV installation scenarios and operation	71
5.1. Installation scenarios	72
5.1.1. Solar park	72
5.1.2. Alternative concepts	74
5.2. Performance	76
5.2.1. Solar park	76
5.2.2. Alternative concepts	79
5.3. Failure modes and repair procedures	81
5.3.1. Mechanical failures	82
5.3.2. Electrical failures, hot-spots, burns	83
5.3.3. Repair procedures	85
6. Conclusion & outlook	87
Bibliography	89
A. Appendix	121

List of Abbreviations

Ag	Silver
AgNP	Silver nanoparticle
AgNW	Silver nanowire
ALD	Atomic layer deposition
AZO	Aluminium doped zinc oxide
BTU	British thermal unit, 1 BTU = 1055 J
C	Carbon
CD	Cross direction
CdS	Cadmium sulfide
CIGS	Copper indium-gallium diselenide
CIJ	Continuous inkjet
CMYK	Cyan, Magenta, Yellow, Key (Black)
Cs ₂ CO ₃	Caesium carbonate
CTE	Coefficient of thermal expansion
Cu(In,Ga)	Copper (Indium, Gallium)
CuNW	Copper nanowire
DOD	Drop on demand
dpi	Dots per inch
DSSC	Dye sensitized solar cell
EGBE	Ethylene glycol butyl ether
EHD	Electrohydrodynamic
EPBT	Energy payback time
EQE	External quantum efficiency
FBSP	Flatbed screen printing
FDTS	1H, 1H, 2H, 2H perfluorodecyltrichlorosilane
FESEM	Field emission scanning electron microscopy
FITS	Field- or flow-induced tip streaming
IJ	Inkjet
IPL	Intense pulsed light (sintering)
IR	Infrared
ITO	Indium tin oxide
LCA	Life cycle assessment
LCOE	Levelized cost of electricity
LDPE	Low density polyethylene
MDMO-PPV	...	Poly [2-methoxy,5-(3',7'-dimethyl-octyloxy)]-p-phenylene vinylene
MEH-PPV	Poly(2-methoxy-5-(2'-ethyl-hexyloxy)-1,4-phenylene vinylene)
MEMS	Microelectromechanical system

MoO _x	Molybdenum oxide
NP	Nanoparticle
OLED	Organic light emitting diode
OPV	Organic photovoltaics
OTFT	Organic thin film transistor
OTR	Oxygen transmission rate
P3HT	Poly(3-hexylthiophene)
P3MHOCT	Poly-(3-(2-methylhexan-2-yl)-oxy-carbonyldithiophene)
P3OT	Poly(3-octylthiophene-2,5-diyl)
PCBM	[6,6]-phenyl-C ₆₁ -butyric acid methyl ester
PCBTDP	Poly-[N-9-heptadecan-2,7-carbazole-alt-3,6-bis(thiophen-5-yl)-2,5-diethylhexyl-2,5-dihydropyrrolo-[3,4-pyrrole-1,4-dione]
PCDTBT	[N-9-heptadecan-2,7-carbazole-alt-5,5-(4,7-di-2-thienyl-2,1,3-benzothiadiazole)]
PCE	Power conversion efficiency
PECVD	Plasma-enhanced physical vapor deposition
PEDOT:PSS ...	Poly(3,4-ethylenedioxythiophene):poly(styrenesulfonate)
PET	Polyethylene terephthalate
PFDTBT	Poly[9,9-dioctylfluorenyl-2,7-diyl-co-(10,12-bis(thiophen-2-yl)-3,6-dioxooctyl-11-thia-9,13-diaza-cyclopenta[b]triphenylene]
PMMA	Poly(methyl methacrylate)
PSA	Pressure sensitive adhesives
PTE	polyoxyethylene tridecyl ether
PV	Photovoltaics
PVK	Poly(N-vinyl carbazole)
QD	Quantum dot
R2R	Roll-to-roll
RSP	Rotary screen printing
S(TPA-DPP) ...	Triphenylamine-diketopyrrolopyrrole
Si-PCPDTBT ..	Poly[(4,4'-bis(2-ethylhexyl)dithieno[3,2-b:2',3-d] silole)-2,6-diyl-alt-(4,7-bis(2-thienyl)-2,1,3-benzothiadiazole)-5,5'-diyl]
T ₈₀	Time to reach 80 % of an initial value
Ti	Titanium
TiO _x	Titanium oxide
TQ-1	Poly-[thiophene-2,5-diyl-alt-(2,3-bis(3-octyloxyphenyl)quinoxaline-5,8-diyl]
V ₂ O ₅	Vanadium(V) oxide
WD	Web direction
WVTR	Water vapor transmission rate
XRD	X-ray diffraction
ZnO	Zinc oxide

List of Figures

1.1.	Primary energy consumption and electric power generating capacity	1
1.2.	Band diagram and BHJ structure of an OPV device	4
1.3.	Characteristic J–V curve of an organic solar cell	4
1.4.	Principal device geometries of organic solar cells	6
1.5.	Modified inverted ITO-free layer stack (IOne)	6
1.6.	Chemical structure of common materials used in OPV devices	7
2.1.	R2R coating and printing setup	14
2.2.	Simplified schematics of non-contact coating technologies	15
2.3.	Simplified schematics of screen printing technologies	18
2.4.	Simplified schematics of flexo and gravure printing	20
2.5.	Simplified schematics of inkjet printing	23
2.6.	Process workflow principles	27
3.1.	Illustration of the nanoparticle sintering process	36
3.2.	R2R photonic sintering setup	37
3.3.	Flexo printing of silver nanoparticle ink	38
3.4.	Sheet resistances after static flash light exposure.	39
3.5.	Barrier substrate with flexo printed AgNP, static and R2R exposure	40
3.6.	Sheet resistance behavior of AgNP ink during R2R processing	41
3.7.	FESEM images of flexo printed nanoparticle ink	42
3.8.	Microscopic photographs of cracked AgNP layers after flashing	43
4.1.	Photographs of the Flextrode with hexagonal grid pattern	47
4.2.	Flextrode transmittance and device performance	47
4.3.	Photographs and transmittance of Flextrode with slanted grids	49
4.4.	Overlay simulation of front and back electrode	50
4.5.	R2R printing and coating processes used for Infinity modules	52
4.6.	Printing forms and slot-die coating stripe layout for Infinity module	54
4.7.	Overlay simulation of Infinity module concept	55
4.8.	Quality control data of a 700 m long Infinity print-run	56
4.9.	Photographs of silver back electrode print results	59
4.10.	J–V curves of single cells and modules with different back electrodes	61
4.11.	Simplified schematics of three different R2R encapsulation strategies	64
4.12.	Photographs of three different R2R encapsulation processes	65
4.13.	Edge bleaching behavior of single-side encapsulated modules	67
4.14.	Lifetime study of single and double-side encapsulated modules	68

5.1. Panorama photograph of the solar park	72
5.2. Detailed view on solar installation wagon and mounted modules	73
5.3. Photographs of alternative solar cell installation concepts.	75
5.4. Transmittance and effect of LDPE foil on the solar cell performance	76
5.5. Photographs of the airborne solar cell installation concept.	77
5.6. Solar cell behavior of the first installed Infinity modules	77
5.7. Lifetime of the first installed Infinity modules	78
5.8. Solar cell characteristics over 3000 h under outdoor conditions	79
5.9. Characteristics of six parallel connected solar cell modules	80
5.10. Solar cell characteristics of alternative deployment strategies.	80
5.11. Irradiance and energy production for onshore solar tubes.	81
5.12. Large-scale defects in form of scratching and delamination	82
5.13. IR imaging photographs of OPV modules under operational conditions.	83
5.14. Various burns on the OPV module	84
5.15. I–V curves and photographs of a forced burning test	85
5.16. Simple repair procedures of an Infinity module.	86
5.17. Power and I–V curves of a repaired module	86
6.1. Upscaling achievements using the Infinity module layout	88

List of Tables

2.1. Reports in literature on slot-die coating for OPV	28
2.2. Reports in literature on doctor blading for OPV	29
2.3. Reports in literature on spray coating for OPV	30
2.4. Reports in literature on screen printing for OPV	31
2.5. Reports in literature on flexo printing for OPV	32
2.6. Reports in literature on gravure printing for OPV	33
2.7. Reports in literature on inkjet printing for OPV	34
3.1. Measured width w of the sintered area of AgNP ink	41
4.1. Back electrode process parameters and silver layer characteristics	60
4.2. Solar cell and module parameters for each printing method	62
5.1. Solar cell parameters of a forced burning test	86

1. Introduction

1.1. Background

Despite financial and economical crises the global energy demand is steadily increasing. The total worldwide primary energy consumption is estimated with 18.3 TW for the year 2013 and projected to be >27 TW in 2040 based on assumptions from the U.S. Energy Information Administration that were reported in the International Energy Outlook 2013.^a Although TW (terawatt) is a unit of power it will be adopted here as unit for energy use.[1] Renewable energy sources including solar power contribute with around 2.1 TW (11.4%) to the primary energy consumption in 2013 as can be seen in Figure 1.1a. Primary energy is transformed to energy carriers such as electricity through conversion processes. The global installed electric power capacity is estimated with 5413 GW in 2013 (8254 GW in 2040) while 29% (1596 GW) is covered by renewable energy sources. Solar power contributes with just 94 GW (1.7%) in 2013 to the globally installed energy mix and is projected to be 266 GW in 2040. A breakdown of the world total installed electric power generating capacity is illustrated in Figure 1.1b.

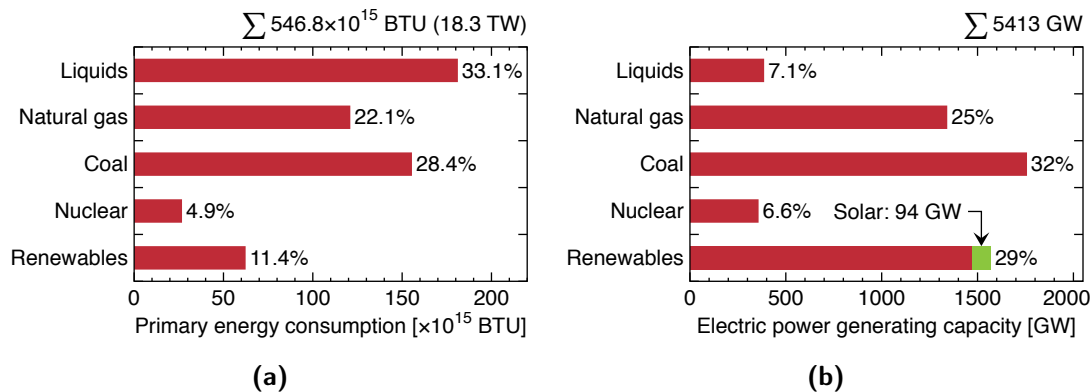


Figure 1.1.: Breakdown of global primary energy consumption (a) and installed electric power generating capacity (b) for the year 2013.

The small role of renewable energy sources in the energy mix is still related to their apparently higher cost, which is therefore often subsidized by local governments to force energy transitions. The advantage of renewables energy sources, in particular solar energy, is the possibility to fully substitute the global primary energy demand.[2] Technically feasible solar photovoltaic energy supply is >65 TW based on a usage of just

^a[http://www.eia.gov/forecasts/ieo/pdf/0484\(2013\).pdf](http://www.eia.gov/forecasts/ieo/pdf/0484(2013).pdf) (28.12.2013)

2% land area and a power conversion efficiency (PCE) of 12%.^[1] The solar irradiation on a cloudless day is 1000 W m^{-2} according to the ASTM G173-03 standard reference for the AM1.5G spectrum. While solar energy alone can theoretically supply more energy than necessary, a mix with other (renewable) energy sources is the favorable approach due to its intermittent nature and lack of adequate energy storage.

Solar photovoltaic (PV) cells are the only devices that allow the direct conversion of sunlight into electricity without CO_2 emission. Finding ways to cheaply utilize the vast amount of abundant solar energy could potentially close the projected primary energy gap of roughly 1 GW day^{-1} until 2050, which corresponds to an average nuclear power plant per day.^[3] Although conventional PV saw rapid growth in the recent years with the consequence of dropping module prices $<1 \text{ US\$ W}^{-1}$,^[4] the current annual 1st and 2nd generation solar PV module production capacity was just around 40 GW in 2013 and will most likely reach around 50 GW in 2014.^b

Today's solar cell technologies can be categorized into three generations, whereby 1st generation cells are based on thick mono- or polycrystalline silicon wafers ($>100 \mu\text{m}$) with efficiencies reaching 25% for lab-scale devices.^[4] Commercial modules typically have efficiencies $<20\%$. Manufacturing requires energy intensive processes with high temperatures while cutting wafers from ingots results in large material loss. The 2nd generation solar cell technologies address the amount of material used in the fabrication and focus on thin-film deposition methods (PVD, CVD, plasma-based, etc.) of a variety of materials such as amorphous silicon, CIGS, CdTe/CdS on substrates like glass or metal foil.^[5] Lab-scale efficiencies are around 20% while module-based efficiencies are in the range of 16% or less.^[6] A bottleneck of all these types of solar cells is their high levelized cost of electricity (LCOE) with around 0.14 € kWh^{-1} for PV installations in southern Germany. This is roughly twice as much as electricity costs from conventional power plants and grid parity is expected to be as early as 2022 in Germany.^[7] The energy payback time (EPBT) of conventional PV is typically >1 year.^[3]

Further concepts for cost reduction or methods to increase the efficiency beyond 30% by stacking multiple devices are summarized in 3rd generation solar cell technologies. The category of potential candidates for cheap solar cells are based on organic materials and include dye sensitized solar cells (DSSC),^[8] small-molecule solar cells,^[9] and polymer solar cells.^[10–12] Record efficiencies $>10\%$ were achieved for lab-scale sized organic PV devices.^[6] Especially polymer solar cells are of particular interest because they offer the potential of very low cost through solution-based fabrication methods such as printing or coating at temperatures $<140 \text{ °C}$ and very low EPBTs $\ll 1$ year.^[3, 13] The history of organic solar cells goes back to 1986 with first reports on small molecule cells,^[14] and developed through the early '90s with the introduction of polymer- C_{60} heterojunction PV.^[15, 16] Since more than 25 years of development an enormous amount of different device architectures and materials were developed and are covered in numerous reviews and books.^[10, 12, 17–24]

^bhttp://www.pv-tech.org/news/npd_solarbuzz_solar_module_production_to_hit_50gw_in_2014
(28.12.2013)

This thesis will purely focus on technological upscaling methods of organic solar cells (OPV) with polymer:fullerene light absorbing active layers to device sizes with high power outputs never shown before for single modules. The basic working principle of OPVs and typical materials will be introduced briefly in the following sections. The advanced chemistry and physics of OPV devices will not be detailed further since the scope of this thesis will be the applied large-scale fabrication technologies from the engineer's point of view.

1.2. OPV working principle

Solution-processed OPV devices can have a broad range of polymer:acceptor material systems and device structures where the acceptor part can be fullerenes, polymers, semiconductor nanoparticles, or metal oxides. The latter are often named hybrid solar cells. Here, the scope is on the widely studied polymer:fullerene material system based on the bulk heterojunction (BHJ) concept. In short, the soluble donor and acceptor material is mixed in an organic solvent such as chlorobenzene and deposited on a conductive substrate. After evaporation of the solvent and post-treatment steps, an interpenetrated network of electron donor and acceptor is formed by microphase separation. The large interface area between donor and acceptor improves the charge separation after the exciton generation due to illumination while the interconnected domains with continuous paths to the electrodes allow efficient charge transport to anode and cathode.

The working principle of a bulk heterojunction OPV device can be described in four basis steps,^[10, 25] whereby the supporting band diagram and BHJ structure is illustrated in Figure 1.2:

1. **Exciton generation:** A photon is mainly absorbed in the donor material upon illumination of the active layer and promotes the electron to the lowest unoccupied molecular orbital (LUMO). The same time, a positive charge carrier (hole) remains in the highest occupied molecular orbital (HOMO). The charge carriers are attracted to each other and bound by Coulomb forces forming an electron-hole pair, the exciton.
2. **Exciton diffusion:** Excitons diffuse inside the donor phase to the interface of the donor and acceptor material. Charge carrier recombination or exciton decay may appear if they are generated too far from the interface. The intermixed BHJ concept decreases the diffusion length compared to a stacked bilayer structure and reduces the decay rate of the exciton. The dimensions of the two phases should be in the range or smaller than the diffusion length of 4–20 nm.^[26–28]
3. **Exciton dissociation:** The exciton dissociates into a free electron and hole at the interface of donor and acceptor material.
4. **Charge carrier transport:** Free charge carriers are separated by an internal electric field due to the different work functions of the electrodes. The charges are transported through the donor and acceptor material and collected at the cathode (electrons) and anode (holes). The photocurrent is generated by short circuiting or applying a load to an external circuit.

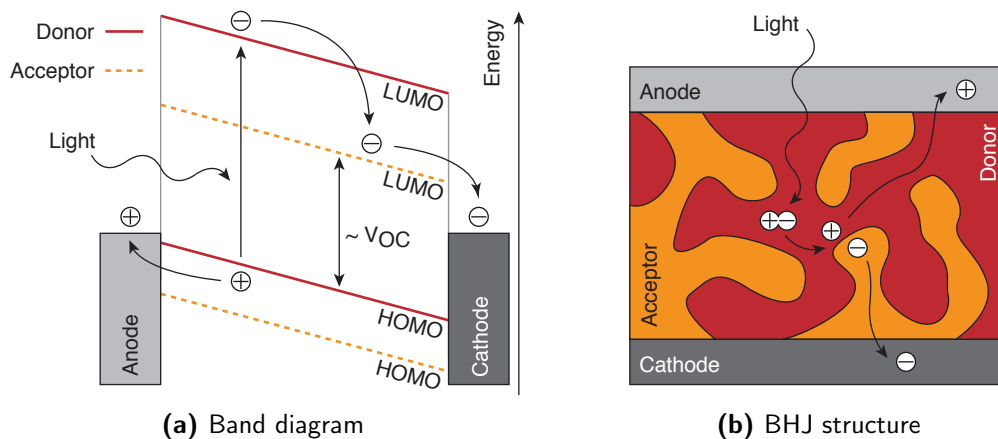


Figure 1.2.: (a) Schematic band diagram of the photocurrent generation in a BHJ solar cell. (b) Intermixed BHJ structure with charge carrier transportation paths.

The optimization of each step enables an efficient power generation while the difference between HOMO and LUMO (optical band gap) is a very crucial parameter. Organic materials with a large absorption range (low band gap) can be synthesized and directly influence the exciton generation.[29] Low band gap materials can harvest photons at longer wavelength and improve the efficiency due to higher currents and better overlap with the solar spectrum. Energy level tuning of donor and acceptor can also increase the open circuit voltage (V_{OC}) that ultimately lead to high efficiencies beyond 10%.[30–32] The microphase separation can be largely affected by processing parameters.[33, 34]

In the dark, the solar cell acts like a simple diode but upon lighting the electrical models can be quite complex including single, two-diode, and three-diode models.[21, 35] The basic current density–voltage characteristics (J – V curve) are shown in Figure 1.3 and include the key parameters open circuit voltage V_{OC} measured in V, short-circuit current density J_{SC} measured in mA cm^{-2} , the fill factor FF specified in %, and the current density J_{MPP} and voltage V_{MPP} for the maximum power point MPP.

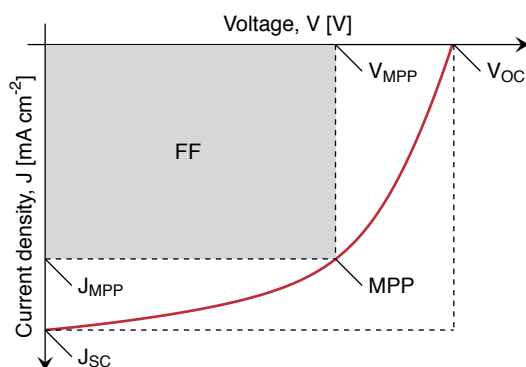


Figure 1.3.: Characteristic J – V curve of an organic solar cell.

The power conversion efficiency (PCE, η) describes the ratio between the maximum electrical power ($= I_{\text{MPP}} \cdot V_{\text{MPP}}$) of a cell and the power of the incident light P_{in} on a given active area A :

$$\eta = \frac{I_{\text{MPP}} \cdot V_{\text{MPP}}}{P_{\text{in}} \cdot A} = FF \cdot \frac{I_{\text{SC}} \cdot V_{\text{OC}}}{P_{\text{in}} \cdot A} = FF \cdot \frac{J_{\text{SC}} \cdot V_{\text{OC}}}{P_{\text{in}}} \quad (1.1)$$

where the fill factor FF is defined as a ratio between practical produced power and the theoretically possible:

$$FF = \frac{I_{\text{MPP}} \cdot V_{\text{MPP}}}{I_{\text{SC}} \cdot V_{\text{OC}}} = \frac{J_{\text{MPP}} \cdot V_{\text{MPP}}}{J_{\text{SC}} \cdot V_{\text{OC}}} \quad (1.2)$$

The fill factor for state of the art OPV devices is in the range of 60–70% and should be as high a possible. It is influenced by the series resistance R_s that includes all resistances at the interfaces in the layers, the conductivity of the semiconductors and the electrodes. It should be low for a good performing device. The shunt resistance R_{sh} needs to be high and includes all the current leakage through shunts as a result of defects in the layers. Open circuit voltage is directly related to the difference of the energy levels of donor and acceptor material. Empirical studies found an additional loss factor, whereby the origin is still under discussion.[30, 36]

$$V_{\text{OC}} = \frac{1}{q} (|E_{\text{HOMO,D}}| - |E_{\text{LUMO,A}}|) - 0.3 \text{ V} \quad (1.3)$$

where q is the elementary charge, $E_{\text{HOMO,D}}$ is the HOMO level energy of the donor and $E_{\text{LUMO,A}}$ is the LUMO level energy of the acceptor.

1.3. Device geometries and materials

The standard layer stack of an OPV device comprises two electrodes with a sandwiched photoactive layer in between. At least one of the electrodes must be transparent and is typically made of indium tin oxide (ITO) sputtered or evaporated on a transparent substrate such as glass or polyethylene terephthalate (PET). Nowadays, intermixed layers of donor and acceptor (bulk heterojunction, BHJ) are widely used, whereby other concepts such as bilayer or highly ordered structures are existing.[37] The BHJ concept largely improves the charge separation and transport by its nanoscale morphology in the range of the exciton diffusion length. Buffer layer between the active layer and the electrodes serve as charge selective transport layer, either transporting just holes (HTL) or just electrons (ETL).

Two reference device geometries, namely normal and inverted geometry, are actually used to fabricate OPV devices and illustrated in Figure 1.4. Traditional normal devices are favorable and most often used for lab-scale devices to study new materials and device physics. One drawback is the use of vacuum steps to evaporate the low work function aluminum electrode on top of the active layer.

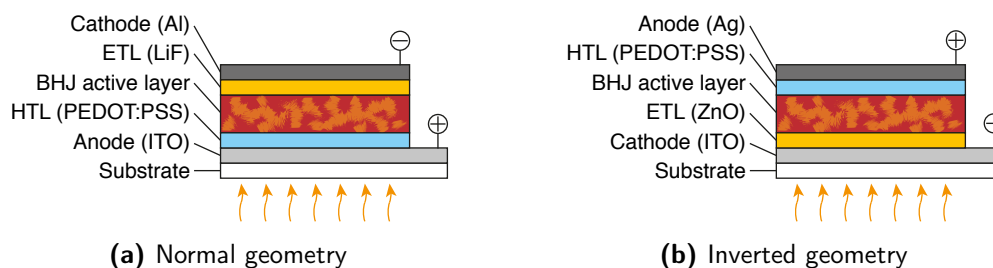


Figure 1.4.: Principal device geometries of organic solar cells.

To allow full solution processing of the anode the layer stack has to be flipped. This inverted structure avoids vacuum steps for all layers except the transparent conductive electrode ITO, and has been proved a better choice for large-scale processing.[13, 38] Furthermore, this design integrates a higher work function back electrode such as silver, which significantly improves the device lifetime.[39]

The fabrication of ITO electrodes involves vacuum steps and subtractive patterning processes, which ultimately leads to a high embodied energy.[40] Full solution-based devices need to replace ITO and therefore a modified inverted design is introduced that will be the fundamental design for all upscaling approaches discussed in this PhD thesis. The IOne stack introduced through Krebs *et al.* as shown in Figure 1.5 replaces ITO with silver grids, highly conductive polymer PEDOT:PSS, and zinc oxide ZnO as ETL.[41–43] This transparent conductive electrode, named Flextrode, is fully printable using low-temperature processes and will be detailed in Section 4.1.

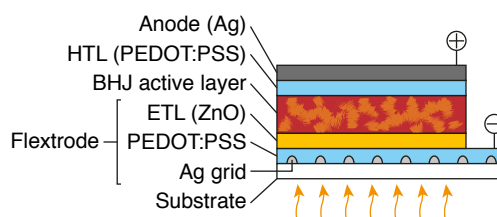


Figure 1.5.: Modified inverted layer stack (IOne) that replaces ITO with silver grids and PEDOT:PSS.

Organic solar cells are normally not purely organic and involve metals, metal oxides, conductive and semi-conductive conjugates polymers, and molecules. Intermediate or buffer layers between electrode and active layer act as charge selective conductor and may also smooth the surface.[44, 45] In normal geometries, poly(3,4-ethylenedioxythiophene)-poly(styrenesulfonate) (PEDOT:PSS) is the most used hole transport layer and dissolved or dispersed in aqueous solution. Calcium or lithium fluoride (LiF) acts as ETL for efficient current extraction through the aluminum electrode.

Inverted devices typically have metal oxides such as titanium oxide (TiO_x) or zinc oxide (ZnO) as ETL. They can be coated from solution-based precursors or nanoparticles. Hole conducting PEDOT:PSS is typically used in inverted OPVs, but metal oxides such as

MoO_3 and V_2O_5 have been reported as well.[46, 47] Special modified highly conductive PEDOT:PSS solutions can also act as replacement for ITO. Silver is either used as printable back electrode or as current collection grid in hybrid front electrodes such as realized for the Flextrode in the IOne layer stack.

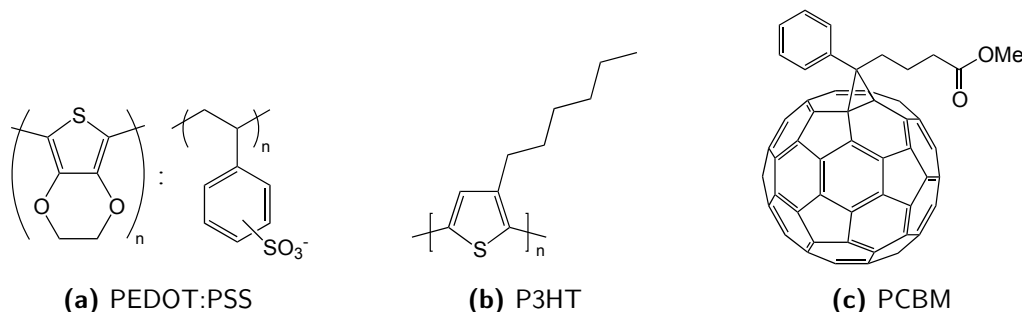


Figure 1.6.: Chemical structure of common materials used in OPV devices.

The main part of the OPV device is the light absorbing active layer containing donor and acceptor materials. Probably the best studied material combination is Poly(3-hexylthiophene) (P3HT) as donor and the fullerene derivate [6,6]-phenyl-C61 -butyric acid methyl ester (PCBM) as acceptor, whereby efficiencies up to around 5% were achieved.[48, 49] The chemical structures are illustrated in Figure 1.6b and 1.6c. These materials are fairly easy to produce and commercial available in large scale, which is crucial for upscaling approaches as discussed later. They can be dissolved in a variety of solvents such as chlorobenzene, dichlorobenzene, or chloroform. Since the absorption spectrum of P3HT is not matched to the solar spectrum and absorbs only wavelength below 650 nm there has been a tremendous research in new polymers. Low band gap materials can harvest more light in the higher wavelength and enable higher efficiencies while further details can be found elsewhere.[29]

1.4. List of publications and contributions

During the 3 years of PhD study a long list of publications has been produced, whereby this PhD thesis focuses mainly on large-scale processing and deployment of organic solar cells for energy production. My personal background as an engineer in microtechnology/mechatronics with specialization in printing technology allowed me to concentrate on the fabrication, characterization, and deployment of multiple functional devices beyond organic solar cells. I basically designed and simulated all printing forms to enable correct multilayer printing with several different fabrication methods. The main focus was then on R2R fabrication of functional groups or full devices as member of the R2R processing team. Furthermore, a variety of small-scale and large-scale organic solar cell devices have been completed and characterized indoors and outdoors. A big contribution was in the final encapsulation and customization of test samples. The photonic sintering equipment was experimentally studied and operated to support further research such as

improving electrodes for electrochromic devices or annealing of thermo-cleavable active layer polymers. My role was very application-oriented and allowed me to support and contribute in multiple projects as described below. Furthermore, a lot of the publications include my artwork, photographs, and illustrations. Only the most relevant publications that are fundamental for this thesis are attached in the appendix.

The five first-authored publications are mainly focussed on the applied R2R fabrication processes of Flextrode substrates, back electrodes, and encapsulation procedures for OPVs. Photonic sintering as a post-treatment process for printed silver nanoparticle electrodes has been studied as well. All devices were carefully characterized and analyzed. The publication on failure modes and repair procedures of OPVs shows problems and challenges with the first large-scale produced high power OPV modules for energy production:

- **M. Hösel**, R. R. Søndergaard, M. Jørgensen and F. C. Krebs, Fast inline roll-to-roll printing and coating of electrodes for indium-tin-oxide free polymer solar cells using automatic registration, *Energy Technology*, 2013, **1**, 102–107.
- **M. Hösel**, R. R. Søndergaard, D. Angmo and F. C. Krebs, Comparison of fast roll-to-roll flexographic, inkjet, flatbed and rotary screen printing of metal back electrodes for polymer solar cells, *Adv. Eng. Mater.*, 2013, **15**, 995–1001.
- **M. Hösel**, R. R. Søndergaard, M. Jørgensen and F. C. Krebs, Comparison of UV-curing, hotmelt and pressure sensitive adhesive as roll-to-roll encapsulation methods for polymer solar cells, *Adv. Eng. Mater.*, 2013, **15**, 1068–1075.
- **M. Hösel** and F. C. Krebs, Large-scale roll-to-roll photonic sintering of flexo printed silver nanoparticle electrodes, *J. Mater. Chem.*, 2012, **22**, 15683–15688.
- **M. Hösel**, R. R. Søndergaard, M. Jørgensen and F. C. Krebs, Failure modes and fast repair procedures in high voltage organic solar cell installations, *Adv. Energy Mater.*, 2014, in press.

Functionality and upscaling potential of OPVs based on the Infinity concept has been shown in three publications. Main contribution was in pattern design, R2R fabrication, testing, data analysis, realization of alternative deployment concepts, and partial manuscript preparation:

- P. Sommer-Larsen, M. Jørgensen, R. R. Søndergaard, **M. Hösel** and F. C. Krebs, It is all in the pattern - high efficiency power extraction from polymer solar cells through high voltage serial connection, *Energy Technology*, 2013, **1**, 15–19.
- F. C. Krebs, N. Espinosa, **M. Hösel**, R. R. Søndergaard and M. Jørgensen, 25th Anniversary Article: Rise to Power - OPV-Based Solar Parks, *Adv. Mater.*, 2014, **26**, 29-39.
- N. Espinosa, **M. Hösel**, M. Jørgensen and F. C. Krebs, Large scale deployment of polymer solar cells on land, on sea and in the air, *Energy Environ. Sci.*, 2014, **7**, 855-866.

Devices with semi-transparent silver front electrodes were introduced in two publications. The silver electrode was studied in detail with respect to ink mixtures, electrical and

optical properties. Devices were fully R2R processed for the first time directly on barrier foil and characterized afterwards. Furthermore, it was used as a calculation basis for a potential OPV design with very low energy payback times:

- D. Angmo, **M. Hösel** and F. C. Krebs, All solution processing of ITO-free organic solar cell modules directly on barrier foil, *Sol. Energy Mater. Sol. Cells*, 2012, **107**, 329–336.
- N. Espinosa, **M. Hösel**, D. Angmo and F. C. Krebs, Solar cells with one-day energy payback for the factories of the future, *Energy Environ. Sci.*, 2012, **5**, 5117–5132.

Pattern design, R2R fabrication, characterization, and preparation of freely available demonstrators based on the ITO-free IOne layer stack:

- F. C. Krebs, **M. Hösel**, M. Corazza, B. Roth, M. V. Madsen, S. A. Gevorgyan, R. R. Søndergaard, D. Karg and M. Jørgensen, Freely available OPV - The fast way to progress, *Energy Technology*, 2013, **1**, 378–381.

Contribution in the manuscript preparation (experimental part) with focus on the evaluation of the optical R2R inline inspection:

- N. Espinosa, F. O. Lenzmann, S. Ryley, D. Angmo, **M. Hösel**, R. R. Søndergaard, D. Huss, S. Dafinger, S. Gritsch, J. M. Kroon, M. Jørgensen and F. C. Krebs, OPV for mobile applications: an evaluation of roll-to-roll processed indium and silver free polymer solar cells through analysis of life cycle, cost and layer quality using inline optical and functional inspection tools, *J. Mater. Chem. A*, 2013, **1**, 7037–7049.

Development and setup of an outdoor test stand in Bangalore/India. Lifetime study of IOne modules, data handling, and analysis on-site in India:

- D. Angmo, S. A. Gevorgyan, T. T. Larsen-Olsen, R. R. Søndergaard, **M. Hösel**, M. Jørgensen, R. Gupta, G. U. Kulkarni and F. C. Krebs, Scalability and stability of very thin, roll-to-roll processed, large area, indium-tin-oxide free polymer solar cell modules, *Org. Electron.*, 2013, **14**, 984–994.

Pattern design and electrode characterization (inkjet and flexo printed):

- J.-S. Yu, I. Kim, J.-S. Kim, J. Jo, T. T. Larsen-Olsen, R. R. Søndergaard, **M. Hösel**, D. Angmo, M. Jørgensen and F. C. Krebs, Silver front electrode grids for ITO-free all printed polymer solar cells with embedded and raised topographies, prepared by thermal imprint, flexographic and inkjet roll-to-roll processes, *Nanoscale*, 2012, **4**, 6032–6040.

Contribution to two review publications and one book chapter with focus on R2R methods for organic solar cells and organic functional devices (literature study, manuscript preparation):

- R. Søndergaard, **M. Hösel**, D. Angmo, T. T. Larsen-Olsen and F. C. Krebs, Roll-to-roll fabrication of polymer solar cells, *Mater. Today*, 2012, **15**, 36–49.
- R. R. Søndergaard, **M. Hösel** and F. C. Krebs, Roll-to-Roll fabrication of large area functional organic materials, *J. Polym. Sci. B Polym. Phys.*, 2013, **51**, 16–34.

- **M. Hösel**, D. Angmo and F. C. Krebs, Organic Solar Cells (OSCs), in *Handbook of organic materials for optical and (opto)electronic devices*, Woodhead Publishing Ltd, Sawsten, 2013, pp. 473–507.

Printing form design, R2R fabrication, and characterization of thermoelectric devices. An Infinity pattern was modified to allow flexo printed silver front and back electrodes:

- R. R. Søndergaard, **M. Hösel**, N. Espinosa, M. Jørgensen and F. C. Krebs, Practical evaluation of organic polymer thermoelectrics by large-area R2R processing on flexible substrates, *Energy Science & Engineering*, 2013, **1**, 81–88.

Printing form design and flexo printing of silver grids. Photonic sintering of printed silver grids to remove organic residues for improved device performance:

- J. Jensen, **M. Hösel**, I. Kim, J.-S. Yu, J. Jo and F. C. Krebs, Fast switching ITO free electrochromic devices, *Adv. Funct. Mater.*, 2014. in press
- R. R. Søndergaard, **M. Hösel**, M. Jørgensen and F. C. Krebs, Fast printing of thin, large area, ITO free electrochromics on flexible barrier foil, *J. Polym. Sci. B Polym. Phys.*, 2013, **51**, 132–136.

Operation of photonic sintering setup and pre-studies on the effect of active layers. Contribution to manuscript (experimental part):

- M. Helgesen, J. E. Carlé, B. Andreasen, **M. Hösel**, K. Norrman, R. Søndergaard and F. C. Krebs, Rapid flash annealing of thermally reactive copolymers in a roll-to-roll process for polymer solar cells, *Polym. Chem.*, 2012, **3**, 2649–2655.

Flectrode preparation and electrode design for roll coater:

- T. R. Andersen, H. F. Dam, B. Andreasen, **M. Hösel**, M. V. Madsen, S. A. Gevorgyan, R. R. Søndergaard, M. Jørgensen and F. C. Krebs, A rational method for developing and testing stable flexible indium- and vacuum-free multilayer tandem polymer solar cells comprising up to twelve roll processed layers, *Sol. Energy Mater. Sol. Cells*, 2014, **120**, 735–743.

Sample fabrication, customization, and preparation of small OPV samples for a round robin study in China. Sample characterization and handling of different types of OPVs for the ISOS-3 publication series.

- T. T. Larsen-Olsen, S. A. Gevorgyan, R. R. Søndergaard, **M. Hösel**, Z. Gu, H. Chen, Y. Liu, P. Cheng, Y. Jing, H. Li, J. Wang, J. Hou, Y. Li, X. Zhan, J. Wu, J. Liu, Z. Xie, X. Du, L. Ding, C. Xie, R. Zeng, Y. Chen, W. Li, T. Xiao, N. Zhao, F. Chen, L. Chen, J. Peng, W. Ma, B. Xiao, H. Wu, X. Wan, Y. Chen, R. Chang, C. Li, Z. Bo, B. Ji, W. Tian, S. Chen, L. Hu, S. Dai and F. C. Krebs, A round robin study of polymer solar cells and small modules across China, *Sol. Energy Mater. Sol. Cells*, 2013, **117**, 382–389.
- D. M. Tanenbaum, M. Hermenau, E. Voroshazi, M. T. Lloyd, Y. Galagan, B. Zimmermann, **M. Hösel**, H. F. Dam, M. Jørgensen, S. A. Gevorgyan, S. Kudret, W. Maes, L. Lutsen, D. Vanderzande, U. Würfel, R. Andriessen, R. Rösch, H. Hoppe, G. Teran-Escobar, M. Lira-Cantu, A. Rivaton, G. Y. Uzunoglu, D. Germack, B. Andreasen, M. V. Madsen, K. Norrman and F. C. Krebs, The ISOS-3 inter-laboratory collaboration focused on the stability of a variety of organic photovoltaic devices, *RSC Adv.*, 2012, **2**, 882–893.

- R. Rösch, D. M. Tanenbaum, M. Jørgensen, M. Seeland, M. Bärenklau, M. Hermenau, E. Voroshazi, M. T. Lloyd, Y. Galagan, B. Zimmermann, U. Würfel, **M. Hösel**, H. F. Dam, S. A. Gevorgyan, S. Kudret, W. Maes, L. Lutsen, D. Vanderzande, R. Andriessen, G. Teran-Escobar, M. Lira-Cantu, A. Rivaton, G. Y. Uzunoglu, D. Germack, B. Andreasen, M. V. Madsen, K. Norrman, H. Hoppe and F. C. Krebs, Investigation of the degradation mechanisms of a variety of organic photovoltaic devices by combination of imaging techniques — the ISOS-3 inter-laboratory collaboration, *Energy Environ. Sci.*, 2012, **5**, 6521–6540.
- G. Teran-Escobar, D. M. Tanenbaum, E. Voroshazi, M. Hermenau, K. Norrman, M. T. Lloyd, Y. Galagan, B. Zimmermann, **M. Hösel**, H. F. Dam, M. Jørgensen, S. A. Gevorgyan, S. Kudret, W. Maes, L. Lutsen, D. Vanderzande, U. Würfel, R. Andriessen, R. Rösch, H. Hoppe, A. Rivaton, G. Y. Uzunoglu, D. Germack, B. Andreasen, M. V. Madsen, E. Bundgaard, F. C. Krebs and M. Lira-Cantu, On the stability of a variety of organic photovoltaic devices by IPCE and in situ IPCE analyses – the ISOS-3 inter-laboratory collaboration, *Phys. Chem. Chem. Phys.*, 2012, **14**, 11824–11845.
- B. Andreasen, D. M. Tanenbaum, M. Hermenau, E. Voroshazi, M. T. Lloyd, Y. Galagan, B. Zimmermann, S. Kudret, W. Maes, L. Lutsen, D. Vanderzande, U. Würfel, R. Andriessen, R. Rösch, H. Hoppe, G. Teran-Escobar, M. Lira-Cantu, A. Rivaton, G. Y. Uzunoglu, D. S. Germack, **M. Hösel**, H. F. Dam, M. Jørgensen, S. A. Gevorgyan, M. V. Madsen, E. Bundgaard, F. C. Krebs and K. Norrman, TOF-SIMS investigation of degradation pathways occurring in a variety of organic photovoltaic devices – the ISOS-3 inter-laboratory collaboration, *Phys. Chem. Chem. Phys.*, 2012, **14**, 11780–11799.

2. Large-scale manufacturing methods for organic solar cells

In this chapter, a variety of different coating and printing technologies are described with respect to working principle and applicability for the large-scale manufacturing of organic solar cells. Most of the methods are used in the traditional coating and printing industry for a long time and were adapted in recent years for the fabrication of functional devices such as OPV or other printed electronics applications.[13, 50, 51] Here, only the most prominent and promising methods for OPV are described. Not every method is suitable for the different layers in a solar cell so a combination of the best processes has to be found for an efficient fabrication of the layer stack. Spin coating will not be described as it is a well known standard method for the majority of lab-scale based studies and the results cannot be directly transferred to large-scale processes.

Each technology could be analyzed very theoretically but for large-scale application the hands-on experience combined with the basic understanding of the technical principles is very important. There is an uncountable variety of processes available that go beyond the scope of this chapter. A deeper insight into technical details of all methods can be found elsewhere.[52–60] Here, the focus is on full-solution processes without the use of vacuum. This chapter also serves as a comprehensive review of the methods with extensive tabular listings of scientific reports that employ at least one method for the fabrication of the OPV layer stack. The tables with references can be found at the end of this chapter in Section 2.5. Some reports are not related to OPV but have importance for the potential usage in one of the functional layers of the device. A small outlook of rather exotic deposition methods and potential R2R manufacturing strategies for the efficient fabrication of OPV devices are presented as well.

A photograph of the most often used R2R machinery throughout the experimental work of this PhD study is shown in Figure 2.1. It does not contain all of the methods described later in this section but allows flexo printing, slot-die coating, and rotary screen printing with speeds of up to 25 m min^{-1} on a web width of 305 mm. The machine is operated under full ambient conditions without any clean-room infrastructure or special lighting.

2.1. Coating technologies

Coating technologies are in general used for large-scale deposition of homogeneous large area functional films on a carrier substrate. Patterning is, with some exceptions, not possible or limited to coarse stripes. The methods are contact-based or contact-free and enable film thickness variations from nanometers to millimeters.

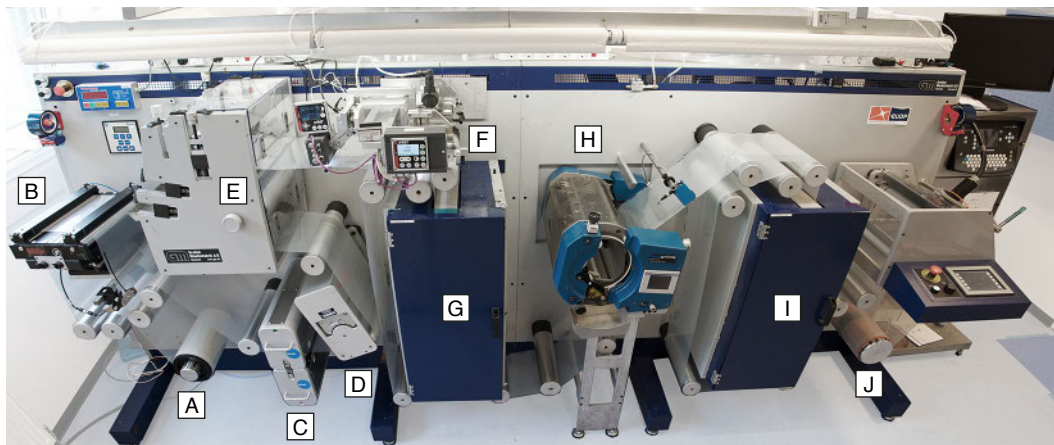


Figure 2.1.: Photograph of a R2R coating and printing setup employed for the large-scale fabrication of OPV cells and modules. The main components in direction of web movement: (A) unwinder, (B) edge guide, (C) web cleaner, (D) corona treatment, (E) flexo printing, (F) slot-die coating, (G) dryer, (H) rotary screen printing, (I) dryer, (J) rewinder. Adapted from Ref. [61] with permission from Woodhead Publishing Limited.

2.1.1. Slot-die coating

Slot-die coating is a non-contact large-area processing method for the deposition of homogeneous wet films with high cross-directional uniformity. It can handle a broad range of viscosities between less than 1 mPa·s and several thousand Pa·s while the coating speed has a similar wide spectrum between less than 1 m min⁻¹ and more than 600 m min⁻¹. The method belongs to the pre-metered coating processes, whereby all of the supplied liquid is deposited on the substrate. The wet film thickness is controlled by the flow rate, coating width, and speed. The resulting dry layer thickness d in cm for a given ink can be expressed with the formula

$$d = \frac{f}{v \cdot w} \cdot \frac{c}{\rho} \quad (2.1)$$

where f is the flow rate in cm³ min⁻¹, v is the coating speed in cm min⁻¹, w the coating width in cm, c is the concentration of the solids in the ink in g cm⁻³, and ρ the density of the material in the final film in g cm⁻³. [13] Depending on the viscosity the ink is pumped into the head with a piston pump, gear pump, or pressure tank. Piston and gear pumps allow the most precise setting of the flow rate.

The slot-die coating head made from stainless steel is illustrated in Figure 2.2a and contains an ink distribution chamber, feed slot, and an up- and downstream lip. The two main designs of the ink distribution chamber are T-shaped constant cross-sectional manifolds and coat-hanger volumetrically diminishing manifolds to enable an adequate flow of the ink to the ends of the head. [52] An internal mask (shim) defines the feed slot width and allows stripe coating. [62, 63] The mask thickness depends on the viscosity of the ink and is typical in the range of 25–50 μm for low-viscous inks

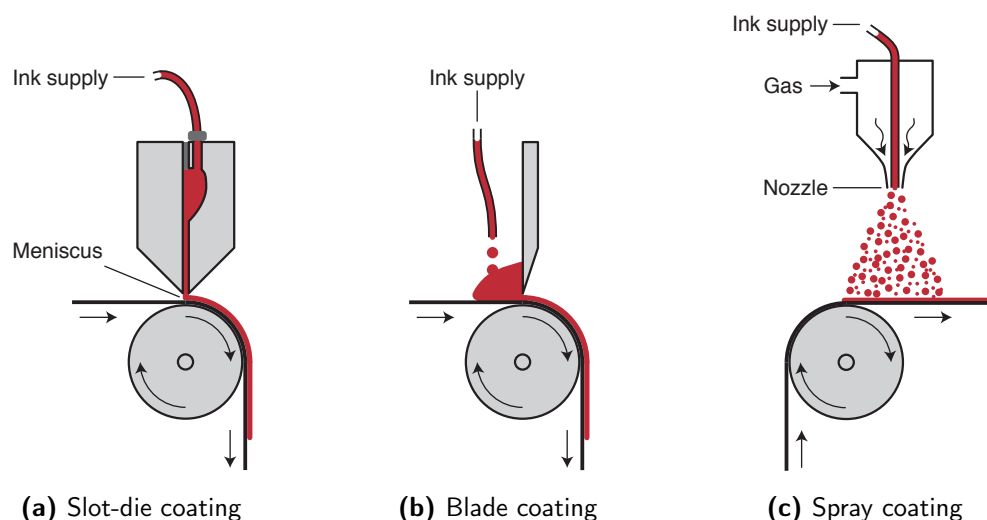


Figure 2.2.: Simplified schematics of non-contact coating technologies for large-area deposition of functional layers used in the manufacturing of organic solar cells. Adapted from [50] © 2012 Wiley Periodicals, Inc.

<20 mPa·s. Furthermore, stripe coating at slow speed is supported by a second internal mask with small protrusions (meniscus guide) at the coating lip that prevent the joining of the menisci between two adjacent stripes.[64] Stripe gaps of down to 1 mm can be achieved, while stripe width can be millimeters to centimeters. The main purpose of slot-die coating are full layers or 1-dimensional stripes but it also allows intermittent batch coating of high viscous slurries as used in the fabrication of battery electrodes.[65] Slot-die coating operates in certain parameter regimes (coating windows) that can be calculated or evaluated experimentally.[54] The slot-die process has been extensively studied in all its varieties beginning from lip forms, manifold design, coating windows, over flow-simulations to meniscus forming, while a selection of literature can be found elsewhere.[54, 62, 66–73]

The stripe coating capability is favorable for the fabrication OPV devices as it allows easy stacking and cross-directional alignment of the layer stack for modules with serially connected cells. The fully closed system between pump and ink exit is ideal for highly volatile solvents. It has been extensively used for the coating of ZnO, active layers, PEDOT:PSS, and silver.[38, 64, 74, 75] More or less all of the currently R2R fabricated OPV devices from Krebs *et al.* contain at least slot-die coated ZnO and active layers in its layer stack. A list of reports with slot-die coated layers for OPV devices is summarized in Table 2.1, whereby the maximum achieved PCE is around 3.2%. Important work on the fluid-dynamic properties of the active layer and PEDOT:PSS with different solvents and additives was carried out by Wengeler *et al.*, while the coating speed limitation was determined by Jakubka *et al.*[76–78] Slot-die coating could also be used for the fabrication of polymer light emitting diodes.[79, 80] The advantage of the pre-metered processing is the control over flow rate and wet layer thickness, which makes it to an ideal

tool for gradient studies of functional layers along the web direction. A huge parameter space of different material ratios or layer thickness in OPV devices can be tested very fast under real production conditions.[81] Ink from two reservoirs was mixed prior entering the head and pumped separately to enable different ratios over time.

2.1.2. Blade coating

Blade coating, also known as knife coating, is a processing method for the fabrication of large area films on rigid or flexible substrates. The well-defined thickness is mainly controlled by the gap size of the blade to the surface. For lab-scale processing the blade is often moved with a defined speed using a motorized stage, but a careful manual operation is possible as well. For large-scale R2R processes the blade is fixed over the moving substrate. The ink is placed in front of the fixed blade whereby the substrate moves relatively to the blade as shown in Figure 2.2b. Adjustable gap widths allow the deposition of wet layer thicknesses from low tens to hundreds of micrometers. The final wet layer thickness is roughly half of the gap width depending on the coating speed and flow behavior.[58] Further coating parameters that influence the film formation are surface energy of the substrate, surface tension of the fluid, coating speed, viscosity, and surface temperatures. The dry layer thickness d can be calculated from the empirical relationship

$$d = \frac{1}{2} \cdot g \cdot \frac{c}{\rho} \quad (2.2)$$

where g is the gap width, c the concentration of the solids in the ink in g cm^{-3} , and ρ the density of the material in the final film in g cm^{-3} . [13]

Patterning during coating is virtually not possible and needs to be kept in mind for a potential upscaling to R2R fabrication of module based OPV devices. The advantage of blade coating is minimal ink waste during coating and almost all ink will be applied. The ink lost can be extensive in initial coating trials while finding proper process parameters. This is a large advantage compared to spin coating where only a fraction of the ink is utilized.

The lab-based coating is rather slow and the ink in front of the blade is exposed to the environment. The processes and ink conditions have to be carefully selected to avoid drying or aggregation before the actual blade coating process. Nevertheless, this method has seen an increasing attraction for the fabrication of small lab-scale devices. The variety of processed materials and layers from active layer to electrodes are listed in Table 2.2. Some reports use doctor blading only for one layer of the device but several devices were successfully fabricated in an all blade coated approach. The resulting efficiencies are comparable with spin coating. The use of blading in a R2R process has not been reported except for a full layer coating of ZnO on patterned ITO .[64] An ohmic ITO-silver contact through ZnO for serially connected cells could be formed but the performance of the modules was poor. Doctor blading is a very simple technology and has therefore also been used for studying drying kinetics and morphologies of the active layer film.[82–86]

2.1.3. Spray coating

Spray coating is widely known as an (industrial) method for car body painting and from graffiti artists using spray cans. The functional fluid or ink is atomized at the nozzle of the spray head, which generates a continuous flow of droplets as shown in Figure 2.2c. Pneumatic-based systems use a stream of pressurized air or gas (e.g. nitrogen or argon) that breaks up the liquid into droplets at the nozzle.[87] The main parameters for the atomization process are surface tension, viscosity, fluid density, gas flow properties, and nozzle design. The quality of the coated layer is defined by the wetting behavior, surface properties, working distance, coating speed, droplet sizes, and the amount of sprayed layers. Besides the fluid-surface interaction the kinetic impact of the droplets influence the spreading of the droplets. Surface temperature plays an important role as well.[88] The simplest form of a pneumatic-based system is an airbrush gun. More advanced spray generation methods that are commonly available are ultrasonication with directed carrier gases,[89] or electro-spraying.[90]

The advantage of spray coating is its high throughput and low material waste for large area depositions without patterning. Spray mist should be avoided through electrostatic control. Patterning through masks naturally involves a lot of ink waste. The combination of multiple spray head enables large area covering and/or multilayer coating. It is fully R2R compatible and the fast drying of the small droplets enable multilayer coatings with single solvent systems.[91] Spray mist can be seen as disadvantage as it tends to contaminate the machinery. Ink waste will be generated for patterned coating through shadow masks that enable only limited structuring. Edge quality and accumulated ink on the mask with the tendency of uncontrolled drops will decrease the usage for a patterned deposition over long runs. Nevertheless, spray coating has seen an increasing impact in the lab-scale fabrication of organic solar cells as can be seen in Table 2.3.

Spray coating allows a broad range of solvent systems and a versatile selection of material systems. Therefore, it shows its applicability in several layers of the OPV device, namely intermediate layers, active layers, and electrodes as summarized in Table 2.3. The material variety includes silver nanowires, nanoparticles, polymers, and nanotubes. The typical research focus is on compatible solvent systems, substrate temperatures, flow rates, and layer thicknesses to achieve the desired film morphology and optimized efficiencies.[92] The utilization of spray coating for all layers of the OPV stack has been shown by some groups.[93–95] An advantage is the possibility to bypass orthogonal solvents for bilayer coatings.[96]

A lot of studies on spray coating have been carried out in detail but the application in large-scale R2R fabrication of OPV has yet to be shown. The majority of the reports in Table 2.3 simply claim R2R possibility. The problem in the realization can be seen in the patterning requirements for full additive manufacturing or the lack of equipment. Using masks or stencils in combination with spray coating in a R2R line is very challenging.

2.2. Printing technologies

Printing is typically a contact-based ink deposition method that allows the transfer of an image or motif from a solid printing form to the substrate. An exception is the fully digital inkjet printing process that is contact-free and employs no physical printing form, it can be changed on demand. Printing methods allow 2-dimensional pattern formation in a wide range of thicknesses, resolutions, and speeds.

2.2.1. Screen printing

Screen printing as illustrated in Figure 2.3a was probably the first and therefore the oldest method for the fabrication of "printed electronics". It was already used during the 1940s for the mass production of electronic circuits, more than half a century before anybody thought about printing OPVs.[60] Nowadays it is common in the graphics art industry, manufacturing of printed circuit boards, and metallization of silicon solar cells.

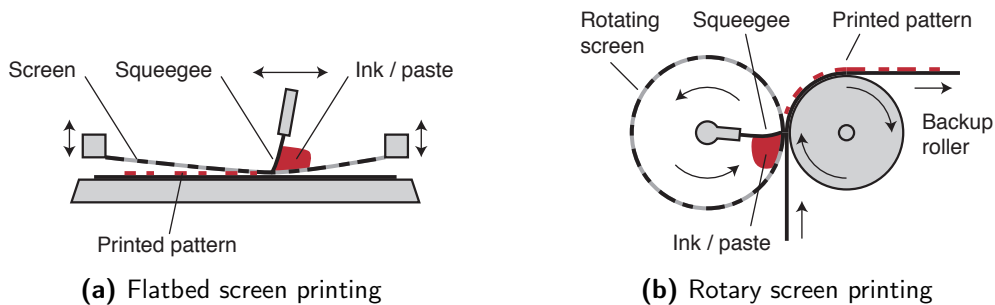


Figure 2.3.: Simplified schematics of screen printing technologies for the structured deposition of functional layers such as PEDOT:PSS and silver. Adapted from [50]
© 2012 Wiley Periodicals, Inc.

The mesh is placed in a certain snap-off distance atop the substrate and a floodbar distributes the ink and fills the mesh. The printing process is initiated by the squeegee that presses against the screen mesh onto the substrate. The moving squeegee forces the ink through the open areas while the rebound of the screen induces shear to the columns of materials. Typically, high-viscous thixotropic ink formulations with shear thinning properties are used for screen printing. This prevents the instantaneous run through the mesh and enables the ink flow once a force is applied. The imprint of the mesh on the deposited ink is minimized throughout the subsequent leveling that depends strongly on the ink characteristics and drying procedures.

Screen printing is a characteristic thick layer deposition method with wet layer thicknesses from less than $10\ \mu\text{m}$ up to more than $500\ \mu\text{m}$. It is given by the screen volume V_{screen} measured in $\text{cm}^3\ \text{m}^{-2}$. The final pickout ratio k_p depends on the process parameters such as squeegee force, printing speed, snap-off distance, snap-off angle, and ink rheology. The dry layer thickness d can be empirically calculated with

$$d = V_{\text{screen}} \cdot k_p \cdot \frac{c}{\rho} \quad (2.3)$$

where c is the concentration of the solids in the ink in g cm^{-3} , and ρ the density of the material in the final film in g cm^{-3} .^[13] Printing resolution of way less than $100\ \mu\text{m}$ are possible when using special screens. Very detailed studies of the fundamentals of screen printing are introduced elsewhere and go beyond this introduction.^[60]

Flatbed screen printing is basically limited to a semi-continuous process workflow due to the up and down movement of the screen, although specialized machine designs allow a full continuous R2R process (i.e. Kammann K61-OS). True continuous prints with the possibility of gapless infinitely long repeating pattern are achieved through rotary screen printing as illustrated in Figure 2.3b. The basic functionality is similar to flatbed screen printing, whereby the squeegee is fixed inside a cylindrical screen that rotates relatively to the squeegee with the same speed as the substrate. The screen is typically an electroformed nickel mesh tube, either seamless or wrapped containing a seam. End rings stabilize the printing form and enable the mounting in the printing unit. A variety of mesh parameters are available to achieve different wet layer thicknesses and print resolutions. The continuous process can easily reach very high speeds of $180\ \text{m min}^{-1}$.

The required ink properties (i.e. viscosity, low volatility) for screen printing are limiting factors in the broad usage in the field of OPV. Although commercial silver and PEDOT:PSS inks are available, ink adjustments are sometimes necessary. Nevertheless, flatbed screen printing has also been used for the deposition of active layers.^[97] The main usage is the printing of PEDOT:PSS and silver electrodes, either full layer or grids. An important study was made to evaluate the influence of different silver paste solvents on the OPV behavior.^[98] The full upscaling potential has been shown in several reports where rotary screen printing was used for the deposition of front and back electrode PEDOT:PSS and silver grids. All processes were printed in register to enable virtually infinitely long modules with thousands of serially connected solar cells.^[43, 99] An overview where screen printing has been employed in the fabrication of OPV is summarized in Table 2.4.

2.2.2. Flexography

Flexography or flexo printing is a commonly used technology in the commercial printing industry, especially for foil substrates. It is a very fast method for a wide range of substrates with web widths beyond $1.5\ \text{m}$. Industrial flexo printing presses can run at hundreds of meters per minute.

The printing method is illustrated in Figure 2.4a and is based on a soft printing plate whereby the raised areas transfer the ink. The material can be rubber or photopolymer of different hardnesses and material qualities depending on the application and ink. The printing plate is taped onto the printing cylinder or manufactured as a gapless sleeve. The plate making process can be carried out through light exposure, developing and washing, or through direct laser engraving.

The second important part of the printing unit is the anilox roller made from ceramics. It contains an engraved surface with small cavities/cells of a certain ink volume (ml m^{-2}) that can be transferred to the substrate depending on the overall pick-out and transfer ratio. The anilox roller is filled with ink through a fountain roller (3-roller-

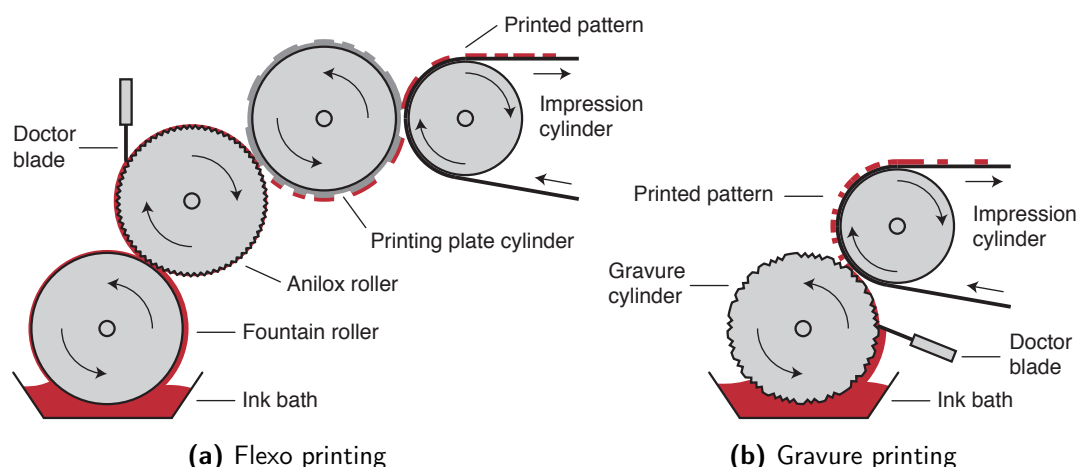


Figure 2.4.: Simplified schematics of traditional high throughput printing methods used in the fabrication of specific layers for organic solar cells. Adapted from [50] © 2012 Wiley Periodicals, Inc.

system) or directly through a closed chambered blade system (2-roller-system). Excess ink is scraped off with a doctor blade. It is then brought into contact with the printing form cylinder that picks out the ink and transfers it to the substrate. Contact pressure between printing form cylinder and impression cylinder is kept low to avoid typical flexo printing phenomena such as halos (squeezed edges). The ink splitting between printing form and substrate surface induces viscous fingering of the printed layers that results in slightly inhomogeneous layers.[100] The ink rheology is similar to gravure printing inks with low to medium viscosities below 500 mPa·s. Further printing parameters that can be adjusted for achieving optimized print results are anilox cell geometries, ink surface tension, nip pressure, and printing speed. Furthermore, the ink rheology and drying time has an effect on the ink leveling after exiting the printing nip.

Conventional 4-color flexo printing is based on half-tone images but in functional printing full layers or fine line patterns are required. Resolutions below 100 μm can be easily achieved. The flexo printing process is not yet broadly employed for OPV like the other printing methods and limited to a narrow range of functional inks such as AgNP or PEDOT:PSS. The interaction of the ink solvents with the soft printing form and the ink transfer characteristics can be seen as a critical factor. An overview of reports on OPV can be found in Table 2.5. The applicability on other printed electronics devices was reported with the fabrication of paper-thin loudspeakers,[101] OTFT electrodes and dielectrics,[102–105] and electroluminescent layers.[106]

In OPV devices flexo printing is mainly used for the fabrication of silver electrodes. An exception is the deposition of a transparent PEDOT:PSS anode on top of the active layer using a highly optimized ink mixture. The paper based solar cell achieved a PCE of 1.31% ($A_{\text{active}} = 9 \text{ mm}^2$). Otherwise, AgNP grid front electrodes for the fabrication of transparent conductive substrates are currently the main application for flexography. The Flextrode substrates with honeycombs or slanted grid fingers and PEDOT:PSS|ZnO have

been heavily used for the fabrication of a variety of devices from small-scale cells to multi square meter large modules.[41, 99, 107] Finger widths below 100 μm and fabrication speeds of 20 m min^{-1} and beyond are possible. Back electrodes based on micro flake based silver paste are flexo printed on a rollcoater and employed in several studies as shown in Table 2.5.

The drawback of flexo printed silver grid lines and layers can be spikes that may appear after leaving the printing nip. Several parameter studies for the flexo-based fabrication of silver grid networks have been carried out and show promising results for the employment of this production method.[108–110] Line widths down to 32 μm could be achieved. The reports show the importance of printing pressure and ink volume on the achievable line width, height and layer morphology. In all cases the printed line is wider than the nominal line width of the printing form.

2.2.3. Gravure printing

Gravure printing is a traditional printing method for high-volume applications such as magazines, catalogs or packaging with printing speeds beyond 15 ms^{-1} . It founds the way into printed electronics due to its potential of high resolution prints, smooth layers, and the variety of processable materials.

The working principle is illustrated in Figure 2.4b. The gravure cylinder is made from steel and a thin copper layer that holds the printing image consisting of engraved cells. A final chromium layer acts as a wear resisting layer. The cells of the printing form can be fabricated through etching, electro-mechanical engraving, or laser engraving. Depending on the application and the desired printing results the cells have different depths, sizes, screen ruling, or shape that define the print volume in ml m^{-2} . The printing cylinder is immersed in an ink bath that fills the cells with ink while rotating. The doctor blade scrapes off excess ink leaving the unpatterned chrome surface blank. A second way of inking the gravure cylinder is through a chambered blade system that keeps the ink in an enclosed system without exposing it to the environment. The ink is transferred to substrate through surface interactions as the web runs through the nip between impression roller and gravure cylinder. The nip force between the hard gravure cylinder (driven) and the soft impression roller (idle) is generally quite high compared to flexo printing. The ink transfer is based on complex interactions between the cell characteristics, printing parameters and ink rheology. Detailed background on the theory can be found elsewhere and goes beyond this introduction.[111–120] The transferred ink of low viscosity with tens of $\text{mPa}\cdot\text{s}$ requires good leveling after deposition to form a homogenous layer due to the structured printing image based on small cells. A variety of direct gravure printing is gravure offset, whereby the image is first transferred to a soft blanket roller and then onto the substrate.

Gravure has the ability to print a variety of functional materials and fine lines with resolutions below 30 μm . It can therefore be used for printing transistor structures[103, 121–126] or functional traces for printed electronics.[127–131] A high resolution grid pattern with line widths down to 20 μm was printed through a gravure offset process and

silver salt ink.[132] Furthermore, surface treatment and drying studies on PEDOT:PSS were carried out using R2R gravure printing.[133]

Gravure printing has the ability for very homogenous and thin layers, and was therefore used in the fabrication of OPVs and similar structured OLEDs as listed in Table 2.6. The typical materials printed in these reports are PEDOT:PSS and P3HT:PCBM and studied on wetting behavior, solvent compositions for best printability, and morphology. Small modules with efficiencies of 1.92 % could be successfully printed on a tabletop gravure proofer but required evaporated electrodes.[134] The preparation of printable solvent systems for PEDOT:PSS and P3HT:PCBM, and the interaction with multiple printing process parameters to achieve smear-free layer is described by *Kopola et al.*[135] The maximum efficiency achieved was 2.8 %, which is by now the highest for gravure printed OPVs. Print process parameters such as ink concentration, speed and drying time on the morphology of the active layer were studied in [136, 137] and led to an efficiency of 1.0 %. Furthermore, detailed ink compositions and additives for an inverted device structure were analyzed and achieved a maximum PCE of 1.2 %.[138, 139] Characteristic for the majority of the gravure experiments is the usage of active layers with high solid loads beyond 10 wt%. Although some R2R processes were carried out most of the studies were performed on flatbed gravure tester. All test cells required evaporated back electrodes except for gravure printed OPV on paper.[140] Gravure printing was often used just for printing full layers or continuous stripes where the cell was later on built up. The 2-dimensional pattern generation that is important for material efficient cell structuring and module fabrication has been shown only by a minority of the reports.[134, 135, 141]

2.2.4. Inkjet printing

Inkjet printing is a well recognized technology from the daily (home-) office use and gained relevance in other areas outside of conventional printing in the late 1990s.[56, 59, 142] It can be divided into the three categories: continuous inkjet (CIJ), drop on demand (DOD), and field- or flow-induced tip streaming (FITS).[56]

Here, the focus is mainly on DOD because of its current relevance and increased application in the field of print functionalities. CIJ has its focus in the graphical industry, industrial labeling, and imprinting of individual information, e.g. during newspaper printing at full speed of several hundred meters per minute. FITS methods such as electrohydrodynamic (EHD) inkjets are special technologies that go beyond this introduction. Even thermal DOD inkjet will be left out because of its limited ink parameter space and irrelevance for printed electronics, although they are relatively cheap. It is mainly used in home inkjet printers.

The majority of today's inkjet printheads employed in functional printing use piezoelectrically actuated transducers to eject droplets on demand out of the nozzle. A simplified schematic is shown in Figure 2.5. An applied voltage waveform (firing pulse) to the piezo induces a mechanical actuation and propagates a pressure pulse through the ink held in the chamber behind the printing nozzle. The droplets get ejected once the pressure exceeds the threshold at the nozzle. Ink is held inside the chamber due

to surface tension and static pressure that stabilizes the meniscus at the nozzle.[59] A similar actuation method is achieved using microelectromechanical systems (MEMS) and electrostatic forces.

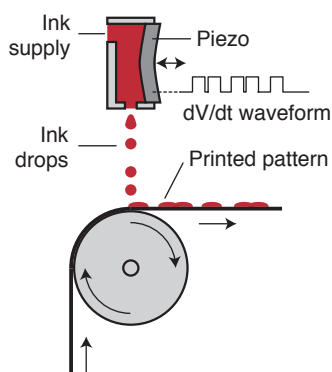


Figure 2.5.: Simplified schematics of drop-on-demand piezoelectric inkjet printing. Adapted from [50] © 2012 Wiley Periodicals, Inc.

State of the art industrial printheads have e.g. a native resolution of 300 dpi but can go beyond 1000 dpi of effective resolution due to variable drop size volumes. Multiple small sub-drops can be ejected and form bigger droplets in air to achieve variable gray levels. Firing frequencies over 40 kHz are commercially available with typical drop volumes between 5–80 picoliter depending on type and manufacturer. Lab-scale based systems such as the often-used Fujifilm Dimatix DMP printer can print with small drops down to 1 pl. This system is perfect for research studies due to its cartridge system (1.5 ml ink volume) and only 16 nozzles. For R2R systems inkjet heads with large print swathe widths are preferred. They often have >1000 nozzles and can print >70 mm wide at speeds beyond 50 m min⁻¹. These setups often rely on high-volume ink circulation systems that prevent frequent ink changes and are preferably used just for production runs. Drop positioning is achieved by a relative movement of the print head to the substrate, depending on which one is fixed. Continuous R2R applications have fixed heads that are carefully aligned over the web width for gap-free printing.

The interplay between ink fluid rheology (viscosity $\ll 50$ mPa·s), inkjet head, surface energies of the substrate, surface tension of the ink, and print parameters such as print speed and drop distance is very critical and has to be adjusted carefully for a satisfying drop generation, layer homogeneity and line definition.[55, 59, 142, 143]. The theoretical background, including the introduction of dimensionless numbers (e.g. Ohnesorge (Oh) number, Z -number) describing the behavior of liquid drops, has been studied in detail but goes beyond this technological introduction.[59, 144, 145] In general, the pattern resolution is limited by the drop spreading on the surface, the drop overlap, and the coalescence with adjacent drops. The drop footprint (diameter) is approximately 3× the drop diameter in flight. Feature sizes down to 30 μm without additional surface modifications can be achieved.[59] Different line formations and the coffee ring effect are characteristics of the droplet interaction with the surface and the environment.[146–150].

Print parameter settings and the choice of solvents mixtures (low and high boiler) have a crucial impact on the layer print results. Just based on this very brief introduction it can be seen that inkjet printing is a very complex technology with a huge parameter space that needs to be taken into account for the fabrication of functional structures. The big advantage is virtually waste-free printing using additive processes and digital printing forms, which are literally free and can be changed on-the-fly.

The variety of printable inks and materials is huge as long as the printhead requirements are maintained (viscosity, particle size, solvent system, etc.). Inkjet can probably be used for the fabrication of more devices than it would be possible with all other printing and coating methods combined.[59, 142, 143, 151, 152]

Inkjet printing for the fabrication of OPV devices has an increasing attention within the last years as summarized in Table 2.7 The aim for printing active layers and PEDOT:PSS electrodes or intermediate layers are homogenous full layers whereas AgNP ink was preferably used for current collecting grid structures. The most efficient cells produced so far are reportedly in the range of 3.7%.[153, 154] It was found that inkjet printing can produce active layer morphologies compared to spin coating without sacrificing the device performance. Inkjetting requires optimized ink that must be technically printable but also suitable for the surface that it is printed on. That's why the majority of the studies report on tailored solvent systems and process conditions. Lange *et al.* used chloro-/trichlorobenzene, anisole/tetralin, p-xylene/tetralin, p-xylene/mesitylene/tetralin or pure tetralin for finding suitable chlorine-free solvents but finally chloro-/trichlorobenzene still gave the best efficiencies with up to 3.5%.[155] Anisole/tetralin resulted in a coarser phase separation due to partial solubility of the polymer PFDTBTP and PCBM in anisole. Additives have a strong influence on the morphology and optoelectronic properties of the active layer and it was found that 1,8 octanedithiol gave the best efficiency with 3.71% (active area 3×3 mm²).[153] Surface morphology and printability of PEDOT:PSS layers for normal-structured OPVs could be improved with additives such as glycerol and ethylene glycol butyl ether (EGBE), which finally lead to efficiencies of 3.16%.[156] Furthermore, inkjet printing was used for material screening regarding blend ratios, concentrations, solvent ratios, layer morphologies, and film thicknesses of two donor polymers with two acceptor fullerenes.[157] The minimal material loss during printing makes it favorable to other dispensing techniques and enables probing of large material libraries.

The strength of inkjet printing is the digital patterning of fine line and grid structures that can be used in OPV devices, especially for front grid electrodes,[42, 158–161] but also for back electrodes.[162, 163] For front electrodes, different current collecting grid shapes were evaluated in detail with respect to printing parameters, line topology, and electrical simulations.[158, 159] Line thicknesses beyond 600 nm have been found to be challenging to overcoat and therefore the right combination of thickness, line width, shadow loss, and conductivity has to be selected. The challenge of inkjet printed back electrodes on R2R fabricated inverted devices is the difference in surface morphologies, thicknesses, step heights, and surface energies.[164] The inkjet print of low-viscous inks on such layer structures has been shown very complex and rather unsuccessful leading to poor layer qualities with low device performances and will be described in detail in Section 4.3.

Although inkjet printing has been used a lot for OPVs the holy grail in real-world upscaling has not yet been shown and virtually no reports on R2R printed OPVs except for conductive grid structures exist.[42] A lot of authors claim full upscalability to R2R level but all keep staying at their lab-scale system. The complexity of large-scale inkjet setups that typically involves recirculation systems, the required ink volumes and the change of drying conditions that has an impact on the layer formation and finally on the device performance tend to be the main bottleneck.

2.3. Further fabrication methods

Despite the more conventional fabrication methods as described before some interesting concepts have been reported that eventually have an impact in the upcoming field of OPV although most of them are rather academic. Detailed descriptions of the methods can be found in the references given below.

Zone-casting (similar to slot-die) was used to produce highly ordered P3HT:PCBM layers, whereby the P3HT nanofibers are aligned due to the shear stress and solute concentration gradient during the processing.[165] The substrate speed is very low with $60 \mu\text{m s}^{-1}$ but the PCE could be raised by 50% compared to spin coated cells.

Horizontal dipping using a small cylindrical bar moving in a certain distance over the substrate was used to produce high quality active layer films.[166–169] This method can be used to fabricate gradient layers for material screening and thickness optimizations. The speed was typically below 1 m min^{-1} in all of the experiments and was so far only used for lab-scale sized applications. Conventional dip coating has also been used to produce pinhole-free and self-assembled active films for fully solution processed OPV devices.[170] The authors achieved more than 4% efficiency and foresee an alternative to R2R fabrication but the speed with 0.18 m min^{-1} is far off from any upscaling goals. Dip-coated AgNW electrode films for small-molecule solar cells have been reported as well.[171] A similar method is called meniscus coating and was used to prepare bilayer solar cell with a maximum PCE of 1.6%.[172] The ink meniscus is built between a flat bar and the substrate. The same technique was used for a pinhole-free coating of fullerene acceptor and cyanine dye donor layers.[173]

Simple painting with an ordinary brush has successfully been used for the fabrication of AgNW networks,[174] carbon nanotubes,[175] and the deposition of PEDOT:PSS and P3HT:PCBM through a mask.[176, 177] The achieved efficiencies were 3.2%, 1.63%, 2.1% and 3.6%, respectively. Wiper coating was used to deposit PEDOT:PSS in a normal structured device with a PCE of 4.46%.[178] Another method employed for the P3HT:PCBM active layer is roller painting. Efficiencies of up to 4.6% could be achieved due to the given shear and normal stresses, and slow drying of the method.[179] These processes induce an improved crystallization of P3HT and PCBM compared to spin coating. Actually, all these painting methods are the first principle demonstration of the often proclaimed dream of direct painting of roofs or walls with solar cells. Nevertheless, and often forgotten by all visionaries and forecasters is that painting of one or two layers is not enough for the fabrication of a working solar cell. The cells in the examples given before required at least on evaporated electrode.

Oxygen plasma patterning of the PEDOT:PSS electrode through a shadow mask has been used to fabricate a cell with an efficiency of 2.2%.^[180] The drawback of this method is the subtractive character with material loss and the long plasma etching time of 3 min for removing unprotected parts of the PEDOT:PSS film. Surface treatment using inkjet printed lines of 1H, 1H, 2H, 2H perfluorodecyltrichlorosilane (FDTS) has been used for the patterning of the active layer. The primary solvent ortho-dichlorobenzene of the active layer is repelled from the FDTS due to the high contact angle and enables a fast and economic patterning without material loss. The drawback of this procedure is the built up of slightly thicker active layers along the FDTS and the low conductivity of FDTS that decreases the fill factor in serially connected cells. Patterning resolution down to 120 μm and efficiencies of close to 2.4% could be achieved for small modules. The process is R2R compatible.^[181]

Finally, laser processing has been used in the fabrication of OPV devices. The method is highly upscalable und R2R compatible but high investment costs have to be taken into account to achieve these requirements.^[182–184] The advantage of laser scribing is the achievement of very high geometrical fill factors of more than 90%.^[185] It is a subtractive process but only a minimum of material is ablated to the pattern the electrodes (P1 and P3 cut) and interfaces and semiconductors layer (P2 cut). The laser parameters (pulse length, wavelength, energy, focus) need to be adjusted for each layer of the layer stack. Several studies have been carried using laser patterning and showed notable results. Small modules of 10 serially connected tandem cells could reach a PCE of 3.3%.^[186] The general goal is to minimize the dead area between the cell by decreasing the scribe width to tens of micrometers.^[185] The structuring of ITO,^[187] PEDOT:PSS,^[183] and active layers ^[184, 188] has been carried with picosecond and femtosecond lasers at different wavelength. Beside the costs, ablation debris and protrusion at the laser cuts has to be taken into account. It requires optimal parameter tuning and debris removal systems (i.e. suction). Laser cutting systems can also be used to cut out fully finished devices from the processed substrate.^[107]

2.4. Manufacturing strategies

Multilayer or multicolor printing is very common in the conventional high-volume commercial printing industry. The sheet-fed and roll-to-roll printing machines are designed to print at least four colors (CMYK) in registry. With front and backside printing, spot colors and special coatings the number of print units in one machine can easily add up to 12 or more. All printing and drying steps are optimized to run at the same speed. This inline concept (Figure 2.6a) is the most practical workflow in an efficient print shop.

Fully printed solar cells with an inverted stack design on ITO substrate need at least four printing and coating steps (i.e. ZnO, active layer, PEDOT:PSS, Ag), not considering the subtractive pre-structuring of the ITO. The ITO-free concept employed for the Flextrode substrate requires 6 or more process steps. The most efficient production workflow would be the inline concept as used in the conventional printing industry. Nevertheless, the field of large-scale solar cell printing is relatively new and mostly research

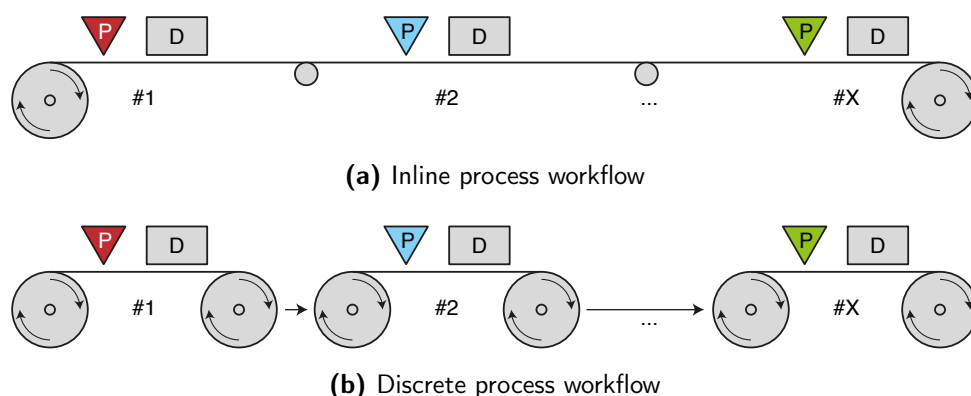


Figure 2.6.: Basic process workflow principles during the multilayer deposition of functional layers. Each layer requires an optimized printing/coating (P) and drying unit (D), whereby the process speed can be maximized individually during a discrete workflow. The inline workflow is limited to the slowest process.

driven. Finding the most adequate process workflow and best material combination with low embodied energies has a high priority until an industrialization is meaningful. Each ink has different solvents, requires various thicknesses, or has variable drying and annealing times. The layers are often processed with different deposition methods that have optimal process windows to achieve the required layer characteristics.

The discrete workflow as illustrated in Figure 2.6b allows the process optimization and monitoring of each layer without interacting with other processes. Optimized single machines and variable machines can be used to maximize the output of one layer under the required conditions. The ultimate inline process workflow requires a machine design that is tailored to a specific layer stack and vice versa. The order of print units, dryer lengths and methods would be fixed, whereby the maximum speed is limited to the slowest deposition step. The risk of failure in the deposition of one layer during an inline process is currently too high and cost intensive, which makes it impractical at the current stage of development. Printing in registry over multiple print units is a further challenge and very critical for the patterned deposition of the functional layers.

An appropriate intermediate solution is a combination of inline and discrete processes. It has been shown during experiments that flexo printing of silver grids and rotary screen printing of PEDOT:PSS can be easily combined in one print run to halve the overall processing time.[41] Each of the layers has similar process windows that allow for a simultaneous print in registry at high speed. Furthermore, the intermediate rewinding of the substrate during a discrete workflow was not necessary. Similar results could be achieved during the inline coating of ZnO and active layer at the same speed. Although the results were promising the best workflow to date is the discrete print of one specific layer under optimized parameters.

2.5. Reports on printed and coated devices

The following tables contain all important reports and studies mainly on printed and coated OPVs, where at least one layer was fabricated through a large-scale compatible solution-based fabrication process. Related devices such as OLEDs are listed as well because of similar layer characteristics and methods.

Table 2.1.: Overview of important studies that employ **slot-die coating** as a manufacturing method for the electrode, active layer, and electron selective layer in OPV devices.

Material	PCE [%]	Notes	Ref.
PEDOT:PSS	–	Electrode for OPV devices	[189]
ZnO, Polymer:Fullerene, PEDOT:PSS	–	Krebs <i>et al.</i> , various studies	[38, 40–42, 64, 98, 190–204]
ZnO, P3HT:PCBM	1.53	88.2 m ² active area	[99]
ZnO, PDTSTTz-4:PCBM	3.2	Module, ITO-free	[205]
ZnO, P3HT:PCBM, PEDOT:PSS, V ₂ O ₅ , MoO _x	1.33	Tandem cell	[206]
P3HT:PCBM, PEDOT:PSS	2.8	Metal wrap through	[207]
ZnO, P3HT:PCBM, PEDOT:PSS	–	Coating + wetting study	[76]
P3HT:PCBM, PEDOT:PSS, AgNP	–	Shear rate study	[78]
PEDOT:PSS, P3HT:PCBM	3.07	Stripe & meniscus study	[208]
H-blocking, Active, E-Blocking	3	Environmental chamber tests	[209]
ZnO, P3HT:PCBM, PEDOT:PSS	1	Coating window study	[77]
ZnO, P3HT:PCBM	–	ITO-free device, Krebs <i>et al.</i>	[210, 211]
Ag, ZnO, P3HT:PCBM, PEDOT:PSS	0.44	Semi-transparent Ag electrode	[75]
PEDOT:PSS, P3HT:PCBM	3.2	Solvent study	[212]
PEDOT:PSS, P3HT:PCBM	–	Coating method study	[58]
ZnO, P3HT:PCBM, V ₂ O ₅ , TQ-1:PCBM, PEDOT:PSS	0.1	Tandem cell	[213]
ZnO, P3HT:PCBM, PEDOT:PSS	0.03	Double slot-die	[214]
PEDOT:PSS, P3HT:PCBM	2.5	ITO-free device	[215]
ZnO, Polymer:PCBM, PEDOT:PSS	0.55	Aqueous processing	[216]
ZnO, P3HT:PCBM, V ₂ O ₅	0.4	PEDOT:PSS-free cells	[47]
P3HT:PCBM, PEDOT:PSS	1	ITO-free device	[217]
PEDOT:PSS, QD:P3HT	0.06	Hybrid solar cells	[218]
ZnO, P3HT:PCBM, PEDOT:PSS	–	Differentially pumped slot-die	[81]
P3HT:PCBM, PEDOT:PSS	0.7	Non-chlorinated solvent	[219]
Ag, ZnO, P3HT:PCBM, PEDOT:PSS	0.3	Backside illumination	[74]
PEDOT:PSS, P3HT:PCBM	1.74	General device preparation	[220]
PEDOT:PSS, P3HT:PCBM	0.061	ITO-free device, monolithic	[221]
PEDOT:PSS, MDMO-PPV:PCBM	–	Large-area cells	[222]
ZnO, PEDOT:PSS, S(TPA-DPP):PCBM	0.21	Small-molecule activer layer	[223]

Table 2.2.: Overview of important studies that employ **doctor blading** as a manufacturing method for the active layer, electron selective layer, or electrode. Some reports utilize doctor blading for more than one layer of the OPV.

Material	PCE [%]	Notes	Ref.
P3HT:PCBM	3.11	Additive studies	[224]
POD2T-DTBT:PCBM	6.74	Thickness, solvent studies	[225]
P3HT:PCBM	3.58	Comparison with inkjet	[226]
P3HT:PCBM	3.85	600 nm layer	[227]
P3HT:PCBM	4.4	Smooth surface, fast drying	[228]
P3HT:PCBM	2.1	Indane solvent, drying study	[229]
P3HT:PCBM	1.8	Morphology studies, X-Ray	[82]
P3HT:PCBM	3.6	XRD study	[230]
P3HT:PCBM	3.49	Fill factor > 70%	[231]
P3HT:PCBM	4.1	Multilayer studies, OLED	[232]
P3HT:PCBM	–	Drying kinetics	[233]
P3HT:PCBM	3.8	High material yield	[234]
P3HT:PCBM	4.05	Comparison with inkjet	[235]
P3HT:Nanoparticles	1.18	Hybrid solar cell	[218]
P3HT:PCBM	4.4	Regioregularity study	[236]
PEDOT:PSS	2.2	Solar cell on fabric substrate	[237]
PEDOT:PSS	3.1	Comparison with spraying	[238]
ZnO	–	R2R, modules	[64]
AgNP	1.4	Thermal imprinted grid	[239]
AgNP	2.5	Back electrode	[240]
AgNW	2.5	Front electrode	[241]
P3HT:Si-PCPDTBT:PCBM, PEDOT:PSS	4.7	Tandem cell	[186]
ZnO, pDPP5T-2:PCBM, PEDOT:PSS	6.09	Multijunction cell	[242]
AgNW, AZO, PEDOT:PSS, P3HT:Si-PCPDTBT:PCBM	3.3	Four layers blade coated	[243]
AZO, P3HT:PCBM, PEDOT:PSS	2.79	Three layers blade coated	[244]
TiO _x , PTE, P3HT:PCBM, PEDOT:PSS	3.45	Four layers blade coated	[245]
AZO, P3HT:PCBM, PEDOT:PSS	2.0	Three layers blade coated	[246]
AZO, P3HT:PCBM, PEDOT:PSS	4.32	Intermediate layer studies	[247]
AZO, P3HT:Si-PCPDTBT:PCBM, PEDOT:PSS	4.0	Three layers blade coated	[248]
PEDOT:PSS, P3HT:PCBM	3.3	Comparison with inkjet	[249]
PEDOT:PSS, P3HT:PCBM	3	Optical simulations	[250]
PEDOT:PSS, P3HT:PCBM	–	Thick active layer, EQE	[251]
TiO _x , P3HT:PCBM, PEDOT:PSS	3.1	Inverted structure	[252]
PEDOT:PSS, P3HT:PCBM	4	Comparison to spin coating	[253]
PEDOT:PSS, MDMO-PPV:PCBM	–	Large cells	[254]
Cs ₂ CO ₃ , P3HT:PCBM, PEDOT:PSS	3.92	Co-solvent study	[255]
PEDOT:PSS, Si-PCPDTBT:PCBM	4.91	Ag front grid electrode	[256]

Table 2.3.: Report and studies on **spray coating** as a manufacturing method for the active layer, electron selective layer, or electrode.

Material	PCE [%]	Notes	Ref.
P3HT:PCBM	2.86	Ag-grid/PEDOT:PSS Electrode	[160]
P3HT:PCBM	3.61	Solvent annealing using spray	[257]
P3HT:PCBM	4.1	Concurrent spraying, ratio study	[258]
PCDTBT:PCBM	4.3	Low band gap polymer	[259]
P3HT:PCBM	1.5	Donor acceptor ratio studies	[260]
PCDTBT:PCBM	5.8	Thickness and solvent study	[261]
P3HT:PCBM	2.83	Additional spraying of solvent	[262]
P3HT:PCBM	–	Succesive spraying of components	[263]
P3HT:PCBM	2.17	Succesive spraying, multilayer	[264]
PCBM	0.55	Nanoimprinting (P3HT) + spray	[265]
PCBM	1.94	Spray on active layer	[266]
P1:PCBM	5.8	Low band gap polymer	[267]
P3HT:PCBM	4.1	Co-solvent mixtures	[268]
P1:PCBM	3.0	Low band gap polymer	[269]
P3HT:PCBM	3.06	Additional spraying of solvent	[270]
P3HT:PCBM	2.8	Multi-source/component spraying	[271]
P3HT:PCBM	3.4	Droplet size studies	[87]
P3HT:PCBM	3.2	Solvent studies	[89]
P3HT:PCBM	2.8	Realization of structural gradients	[91]
PCBTDP:PCBM	3.92	Solvent, additive studies	[272]
P3HT:PCBM	2.99	Electrospray, solvent study	[273]
PEDOT:PSS	2.65	Smoothing layer	[274]
PEDOT:PSS	2.44	Lifetime studies, inverted device	[275]
PEDOT:PSS	3.5	Comparison with other methods	[276]
ZnO	3.17	Comparison with other methods	[277]
PEDOT:PSS	2.0	Shadow masking	[278]
PEDOT:PSS	0.25	AgNW/PEDOT:PSS composite	[279]
PEDOT:PSS	1.25	Back-electrode	[280]
PEDOT:PSS	1.9	Double spray process, seed layer	[281]
PEDOT:PSS	0.5	Wetting improvement studies	[282]
AgNW/PEDOT:PSS	2.16	Spraying of material mixture	[274]
CuNW	3.1	Front electrode, pressing required	[283]
AgNW	2.2	Back electrode	[243]
AgNW	5.27	Front electrode, mask	[284]
AgNW	0.25	AgNW/PEDOT:PSS composite	[279]
AgNW	2.13	Back electrode, semi-transparent	[246]
AgNW	4.02	Back electrode, semi-transparent	[285]
AgNW	2.8	Front electrode	[286]
AgNP	3.0	Back electrode, > 20 layers	[287]
AgNP	2.5	Back electrode, shadow mask	[288]
SWCNT	3.6	Front electrode, mask	[289]
ZnO, P3HT:PCBM, PEDOT:PSS	3.17	All three layers in one cell	[93]
ZnO, P3HT:PCBM, PEDOT:PSS	2.41	All three layers in one cell	[94]
CS ₂ CO ₃ , P3HT:PCBM, PEDOT:PSS	1.8	All three layers in one cell	[95]
TiO ₂ , P3HT:PCBM, 2×PEDOT:PSS	1.53	All four layers in one cell	[290]
PEDOT:PSS, P3HT:PCBM	3.75	All two layers in one cell	[92]
PEDOT:PSS, P3HT:PCBM	2.17	All two layers in one cell, ITO-free	[291]
PEDOT:PSS, P3HT:PCBM	2.95	All two layers in one cell	[292]
PEDOT:PSS, P3HT:PCBM	2.7	All two layers in one cell	[238]

Table 2.4.: Overview of important studies that employ **screen printing** as a manufacturing method mainly for the active layer and electrodes. Screen printing is also used for conventional solar cells.

Material	PCE [%]	Notes	Ref.
P3HT:PCBM	–	Poor performance	[293]
P3HT:PCBM	4.23	Solvent study	[97]
MEH-PPV:PCBM	1.25	Viscosity studies	[294]
MEH-PPV	0.0046	Feasibility study	[295]
MDMO-PPV:PCBM	4.3	Monochromatic 422 nm illumination	[296]
Ag, PEDOT:PSS	2.1	Front + back electrode, rotary, flatbed	[164]
Ag, C, PEDOT:PSS	–	Back electrode, LCA analysis	[297]
Ag	0.1	Back electrode for tandem cells	[213]
Ag, C, PEDOT:PSS	1.9	Back electrode	[210]
Ag	–	Back electrode, LCA analysis	[3]
Ag	0.55	Back electrode, water based active layer	[216]
Ag	–	Back electrode, different silver, LBIC	[98]
Ag	0.36	Back electrode, large monolithic cells	[217]
Ag	1.93	Front electrode	[298]
Ag	0.7	Back electrode, all water-processed cell	[299]
Ag	1.02	Back electrode and conductors	[196]
Ag	0.061	Front electrode, monolithic, metal foil	[221]
Ag	3	Back electrode, environmental tests	[209]
AgNP	2.15	Front electrode, embedded	[300]
PEDOT:PSS	–	Front electrode, comparison with ITO	[301]
Ag, (PEDOT:PSS)	–	Electrodes, F. C. Krebs <i>et al.</i>	[38, 47, 64, 74, 81, 99, 193–195, 197, 201, 211]
ZnO, P3MHOCT:PCBM, PEDOT:PSS, Ag	0.013	All screen printed	[302]
Ti, C	5.38	DSSC cells	[303]
Ag	–	Silicon solar cell, electrodes, review	[4]
Ag	20.3	Silicon solar cell, electrodes	[304]

Table 2.5.: Overview of important studies that employ **flexo printing** as a manufacturing method for the electrodes, and supporting layers of the OPV. Some reports utilize flexo printing for the metallization of Si-based solar cells.

Material	PCE [%]	Notes	Ref.
AgNP	1.82	R2R, grid front electrode, slanted comb	[107]
AgNP	1.62	R2R, grid front electrode, honeycomb	[198]
AgNP	0.55	R2R, front + back electrode	[164]
AgNP	1.6	R2R, general Flextrode report	[41]
AgNP, Ag	1.5	R2R, rollcoated cells	[199]
AgNP	1.53	R2R, slanted grid, for > 200 W modules	[99]
AgNP, Ag	1.33	R2R, rollcoated, tandem cells	[206]
AgNP	1.82	R2R, comparison with inkjet, imprinting	[42]
PEDOT:PSS	1.3	Paper based solar cell	[140]
n-octanol	2.75	R2R, prewetting prior PEDOT:PSS	[193]
Adhesive	–	R2R adhesive deposition for encapsulation	[305]
Ag	18.1	Si solar cell metallization	[306]
Ag		Si solar cell metallization	[307]

Table 2.6.: Overview of important studies that employ **gravure printing** as a manufacturing method for the active layer, electrode, or the intermediate layer. Some reports utilize gravure printing for OLED devices that employ a similar layer stack.

Material	PCE [%]	Notes	Ref.
P3HT:PCBM	2.21	Solvent study	[308]
P3HT:PCBM	1.3	R2R, paper substrate	[140]
PEDOT:PSS	2.0	Bending tests	[309]
ITO	–	Photodiode, printability study	[310]
PEDOT:PSS, P3HT:PCBM	0.3	R2R, morphology study	[136]
PEDOT:PSS, P3HT:PCBM	–	R2R, optical properties study	[311]
PEDOT:PSS, P3HT:PCBM	1.0	R2R, drying, morphology study	[137]
PEDOT:PSS, P3HT:PCBM, ZnO	1.02	Modules, printability study	[312]
TiO _x , P3HT:PCBM, PEDOT:PSS	1.2	Ink property study	[138]
PEDOT:PSS, P3HT:PCBM	1.92	Small modules	[134]
TiO _x , P3HT:PCBM, PEDOT:PSS	0.6	Solvent and wetting study	[139]
PEDOT:PSS, LG1300	–	OLED, printability study	[313]
PEDOT:PSS, P3HT:PCBM	2.8	Printability, wetting study	[135]
PEDOT:PSS, P3HT:PCBM	2.4	R2R, printability study	[314]
PEDOT:PSS, P3HT:PCBM	1.68	Printability, wetting study	[141]
PEDOT:PSS, P3HT:PCBM	0.74	R2R reverse gravure	[315]
MEH-PPV	–	OLED, roughness control	[316]
PVK/Ir(ppy) ₃	–	OLED, annealing study	[317]
ITO, PEDOT:PSS, LEP	–	OLED, printability study	[318]
PEDOT:PSS, SM:UHMW-PS	–	OLED, printability study	[319]
PEDOT:PSS, LEP	–	OLED, printability study	[320]
MEH-PV, Rubrene	–	OLED, bilayer printing	[321]
PEDOT:PSS, SuperYellow	–	OLED, printability study	[322]

Table 2.7.: Overview of important studies that employ **inkjet printing** as a manufacturing method for the active layer, electrode, or the intermediate layer in OPV device.

Material	PCE [%]	Notes	Ref.
PFDTBTP:PCBM	3.7	Comparison with spin coating	[154]
P3HT:PCBM	2.4	Drying and annealing study	[323]
PFDTBTP:PCBM	2.7	Chlorine-free solvents	[155]
P3HT:PCBM	3.07	Process parameter study	[226]
Polymer:fullerene	–	Material screening	[157]
P3HT:PCBM	2.4	Solvent studies	[324]
P3HT:PCBM	1.29	Tetraline solvent	[249]
P3OT:PCBM	0.00078	Printing parameter study	[325]
P3HT:PCBM	3.5	Regioregularity study	[236]
P3HT:PCBM	3.5	Regioregularity and solvent study	[235]
P3HT:PCBM	1.4	Solvent study	[326]
P3HT:PCBM	2.9	Solvent study	[327]
P3HT:PCBM	2.2	Morphology, printability study	[328]
PEDOT:PSS	1.5	Front electrode	[329]
AgNP	0.21	Back electrode	[330]
AgNP	2.86	Front grid electrode	[160]
AgNP	0.83	R2R, Back electrode	[164]
AgNP	–	R2R, front electrode, LCA study	[297]
AgNP	1.96	Back electrode	[162]
AgNP	2.64	Aerosol jet printing	[331]
AgNP	1.7	R2R, front electrode	[211]
AgNP	0.79	R2R, front electrode	[42]
AgNP	1.96	Front electrode	[161]
AgNP	–	Front electrode, silicon solar cell	[332]
AgNP	4.91	Front electrode, sintering study	[256]
AgNP, PEDOT:PSS	1.52	Front electrode, grid spacing	[159]
AgNP, PEDOT:PSS	1.95	Front and back electrode	[163]
AgNP, PEDOT:PSS	1.54	Front electrode, different grids	[158]
AgNP, PEDOT:PSS	1.38	Front electrode, photonic sintering	[333]
ITO	2.13	Front electrode	[334]
IZTO	0.81	Front electrode	[335]
ITO	1.8	Active area study	[336]
PEDOT:PSS	3.16	Additive study	[156]
PEDOT:PSS	3.3	Comparison spin coating and spray	[276]
AgNP, P3HT:PCBM, PEDOT:PSS	–	Photodetector	[337]
ZnO, P3HT:PCBM, P-Layer, Ag	2.1	Small modules	[338]
P3HT:PCBM, PEDOT:PSS	3.71	Solvent studies	[153]

3. Photonic sintering methods

Solution processed layers typically require post-printing processes such as thermal drying for solvent evaporation or UV exposure for cross-linking to form the functional dry film. The maximum temperature has to be compatible with the substrate parameters and the layer stack, and is limited to roughly 140 °C for polyethylene terephthalate (PET), which is a flexible standard substrate for large-scale processed OPVs.

Replacing ITO-based electrodes with metal-based grids in conjunction with conductive polymers can enable full additive processing and eliminates the need of vacuum that raises the embodied energy significantly.[40, 41] Nevertheless, nanoparticle (NP) inks such as silver often require further heat treatments (>200 °C) and/or long sintering steps (>30 min) to achieve conductivity, which eliminate the use of cheap plastic substrates (PET).[339–342] Introduction of optimized ink systems or customized rapid post-printing processes such as photonic sintering can increase the fabrication speed without harming the heat-sensitive substrate.

In this chapter, R2R photonic sintering of flexo printed electrodes based on silver nanoparticle ink is evaluated by comparing two different ink samples in their sintering behavior and surface morphology.[343] The focus is on the R2R behavior, electrical characteristics and the impact on the electrodes layer quality in conjunction with thin barrier foil. Although OPV devices were not directly manufactured throughout the experiments the results were used for benchmarking the sintering equipment to justify the general necessity with respect to the used inks. Nevertheless, the photonic sintering process was used in the manufacturing workflow of small OPV modules,[211] and for the improvement of grid electrodes in fast switching electrochromic devices.[344] It was also used for the rapid annealing of thermocleavable active layer polymers in OPVs, which has not been carried out by anyone else before.[345]

3.1. Technology and working principle

Metallic nanoparticle inks contain NPs with diameters typically below 100 nm. The melting point of the NPs is decreasing, the smaller the particle radius is,[346] which is finally much lower than the melting temperature of the bulk metal.[347, 348] Having such NPs in dispersion would make an ideal ink but to prevent agglomeration and enable printability organic binders are added. Thin layers around the NPs ensure a stable colloidal dispersion.

After depositing the NP ink (e. g. with printing methods) further steps are required to transform it into a conductive layer. First, the solvent is evaporated and the organic coating will be removed to achieve direct contact of the particles.[349] Second, large particles will be formed due to grain growth, sintering, and Ostwald ripening (small grains dissolve and large grains grow further, the average grain size increases). [350]

Sintering is the welding or merging of nanoparticles and formation of percolation paths to create conductivity. The lowered melting point enhances self-diffusion of the metal atoms that supports the initial neck formation between the NPs. After bonding of the NPs the grain size increases and densification takes places.[351] High conductivity is achieved through the formation of long necks and large densification, ideally with the formation of metallic crystalline structures and minimized grain boundaries.[340] A simplified workflow of the sintering process is illustrated in Figure 3.1. Further details on the physical background including modeling can be found elsewhere.[341, 350, 352–354]

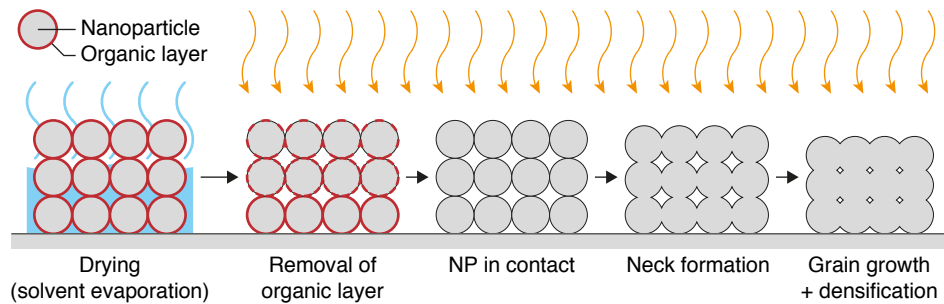


Figure 3.1.: Schematic illustration of the nanoparticle sintering process once the solvent is evaporated during the drying phase.

Beside conventional thermal sintering,[341] many other methods have emerged such electrical sintering,[355] microwave sintering,[356] plasma sintering,[357] infrared sintering,[358] chemical sintering,[359] and laser sintering.[360] Several reviews on the development of the various technologies can be found elsewhere.[339, 340, 351]

Finally, photonic sintering, also often named intense pulsed light (IPL) sintering or flash sintering, has been employed in the recent years and can be seen as the fastest method to sinter nanoparticles. In principle, it is a thermal sintering method whereby the nanoparticles heat up through absorption of a high intensity pulsed light with a broad spectrum. The impact on the sintering can be controlled by the light intensity, flash duration and amount of pulses. The advantage of the short pulses (<2 ms) is heating and fusing of the metal nanoparticles without significantly heating the substrate. Metal nanoparticles are typically of black nature and have a good light absorption, whereby the high surface to mass ratio enables fast heating of the layers. Thin micron-sized layers do not retain the heat very well and cool fast, which minimizes the impact on the substrate.[361] The pulse length is so short that no thermal equilibrium with the substrate will be achieved. Photonic sintering of conductive metal nanoparticles was introduced in 2006, [362] although early reports on rapid thermal processing go back to the 70ies,[363] followed by several studies investigating the physical background by modeling the rapid thermal processes. [361, 364, 365] The simulations show that a 3 μm silver layer can heat up to more than 700 $^{\circ}\text{C}$ in less than 300 μs . [365–367] Peak temperatures beyond 1000 $^{\circ}\text{C}$ can be achieved for thinner layers.[366] The ideal energy was found to be around 1 J cm^{-2} but it is highly dependent on particle type and size, film thickness, substrate, and organic binders.[362]

Photonic sintering of printed nanoparticle layers requires careful experimental studies to achieve the best correlation between conductivity and morphological impact on the printed layer and substrate. A huge amount of reports explore the technology and shows its applicability on a variety of metallic nanoparticles such as gold,[368] copper,[369–375] Cu(In,Ga) alloys,[376] CdS,[372] nickel,[377] and of course silver.[362, 378–389] Intense pulsed light sintering is not necessarily limited to nanoparticles as it was also shown to be suitable for welding of Ag nanowires.[390, 391] It is noteworthy that the studies are mostly carried out on small test patterns without real-world applicability.

3.2. Photonic sintering of flexo printed silver electrodes

3.2.1. Experimental

Photonic sintering can be carried out using an ordinary camera flash,[389] custom built setups,[379, 382] or commercial systems.[386, 390] Basically all reports employed static setups except one, where a proprietary flash system was installed into a R2R setup.[392]

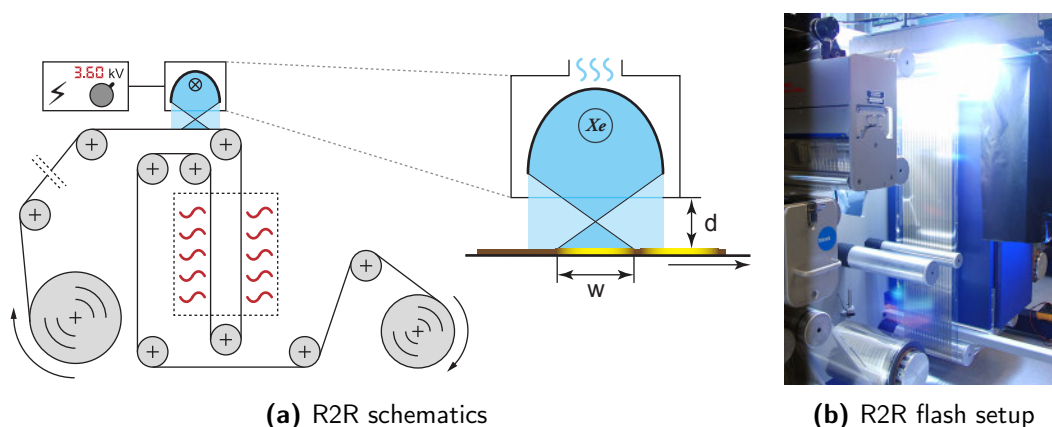


Figure 3.2.: (a) Simplified schematics of the R2R photonic sintering setup with a magnified illustration of the lamp housing including the mirror and xenon flash lamp. (b) Photograph of the R2R setup captured during an active flash with an exposure time of 0.5 ms. Adapted and reproduced from Ref. [343] with permission from The Royal Society of Chemistry.

Here, a commercial xenon flash lamp system (Sinteron 2000, Xenon Corp.) has been permanently installed into a R2R setup as shown in Figure 3.2. The pulse forming controller can deliver electrical pulse energies from 150 to 2000 Joules by changing the voltage settings between 1.6 and 3.8 kV. The pulse duration was set to 0.5 ms with a maximum electrical pulse energy of 830 J, and a fixed flash frequency of 1.8 Hz. These setting parameters can be changed by changing hardware components. The air-cooled 16" linear xenon flash lamp (lamp type C) delivers a broadband spectrum from 190 to 1000 nm. The distance d between the lamp housing and the unsupported substrate was set to 2" (out of focus) to gain a larger exposure area for an increased processing speed although the optical energy density will be decreased. The optical energy density values given later are based on datasets from the system's manual and represent approximate numbers.

The substrate used in this study was a thin PET barrier foil from Amcor with a thickness of 60 μm . Two different silver nanoparticle inks were flexo printed on a R2R system as described in Chapter 2. The commercial water-based flexo silver ink PFI-722 (PChem Associates) was printed at 15 m min^{-1} using an anilox volume of 1.5 ml m^{-2} and an elastomeric printing form (65 Shore). The silver content of the ink was 60 wt% with a particle size of 10–30 nm. Corona treatment was used for improved adhesion and print quality. The second silver ink (AgNP) was a dispersion of Ag nanoparticles (40–70 nm) in a 1:1 mixture of triethyleneglycolmonomethylether and o-xylene with a final concentration of 25 wt% and filtered through a $2.7\text{ }\mu\text{m}$ filter prior to printing.[74] This ink was flexo printed at 10 m min^{-1} using an anilox volume of 11 ml m^{-2} and an elastomeric printing form (40 Shore). Here, the barrier substrate was not corona treated to achieve better print quality. Drying was carried out using hot air ovens ($140\text{ }^\circ\text{C}$, $2\times 2\text{ m}$) and additional IR heating. The printed electrode pattern consisted of 16 stripes (13 mm wide, 2 mm gap) with a gap of 1 mm between the stripes along the print direction. Photographs of the printing processes are shown in Figure 3.3.

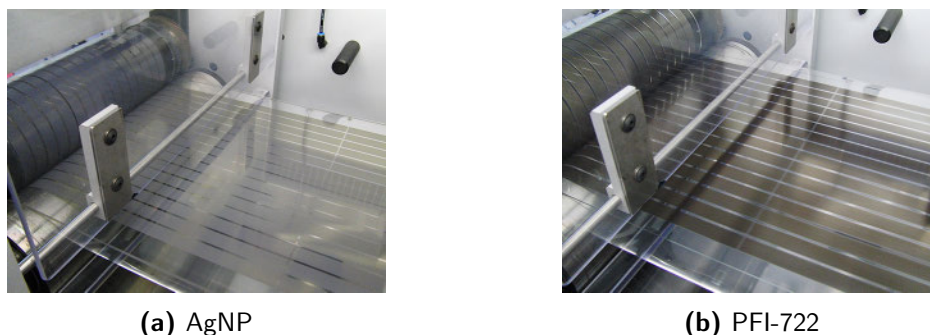


Figure 3.3.: Photographs showing the flexo printing of full layer silver nanoparticle electrodes directly on thin barrier substrate. Reproduced from [343] with permission from The Royal Society of Chemistry.

3.2.2. Results and discussion

Both silver inks showed good printability and edge definition but suffered from viscous fingering effects due to Saffman-Taylor instabilities as known from nip-based methods (see Section 2.2.2).[393] The low-viscous AgNP ink (not optimized for flexography) achieved a dry layer thickness of 150–200 nm, whereas the commercial flexo-optimized PFI-722 ink was measured with an average thickness of less than 250 nm. The electrical characterization of the electrodes was based on sheet resistance due to the slightly uneven layer as the calculation of the resistivity would deliver incorrect results due to the varying cross-sections in the area of interest.

Prior R2R sintering the electrodes were electrically characterized under static conditions for finding suitable parameter settings. The PFI-722 ink already showed highly conductive behavior directly after conventional drying in the printing machine and in principle needed no further treatment. The ink is optimized by manufacturer for fast

and low-temperature drying/sintering with hot air and IR. The sheet resistance was measured to $1.55 \Omega \square^{-1}$. On the other hand, the AgNP ink showed no conductivity after printing and drying at even slower processing speeds. After an additional 4 min long heat treatment at 140°C conductivity was achieved and measured with a sheet resistance of $271 \Omega \square^{-1}$. Interestingly, the same ink was highly conductive with $10 \text{ m} \Omega \square^{-1}$ after only 1 min at 130°C when using slot-die coating as deposition method.[74] One reason for this can be seen in the thinner and less dense layer when printed with flexography. Nevertheless, the effect of the intensive pulsed flashlight was tested on both printed electrodes to study the effect on sheet resistance and layer morphology on further energy input.

The printed electrode patterns were sintered with single flash exposure (0.5 ms), quadruple exposure ($4 \times 0.5 \text{ ms}$) at 1.8 Hz, and later on R2R at different speeds up to 2.5 m min^{-1} . The voltage setting (pulse energy) was varied between minimum (1.6 kV) and maximum (3.8 kV) in steps of 200 V. The in-focus distance of the flash lamp housing to the substrate is 1" due to the reflector design, which results in an optical footprint of $19 \text{ mm} \times 305 \text{ mm}$. Here, twice the distance was used to increase the exposure area for potentially faster R2R processing.

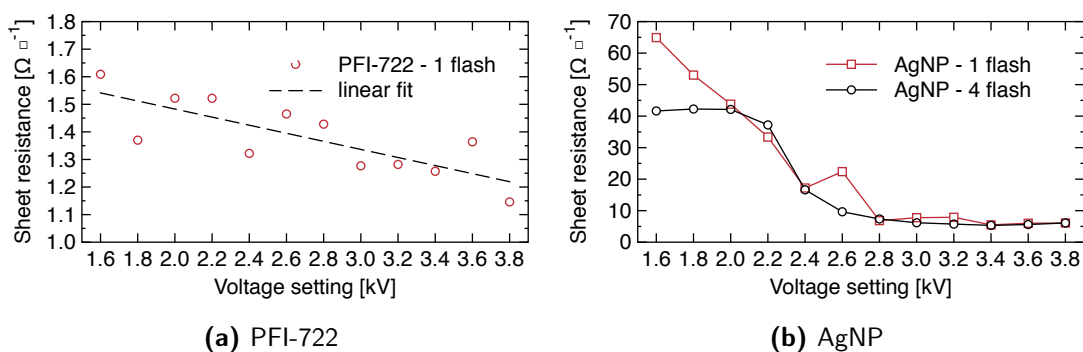


Figure 3.4.: Sheet resistances of the two ink types after static flash light exposure. Adapted from Ref. [343] with permission from The Royal Society of Chemistry.

The effect of different voltage settings on the sheet resistance of the printed inks is shown in Figure 3.4a. The lowest sheet resistance of $1.15 \Omega \square^{-1}$ on PFI-722 could be achieved with a single flash and a voltage setting of 3.8 kV, which corresponded to an optical energy density of around 1.75 J cm^{-2} . The sheet resistance decreases linearly with increasing energy input. The good conductivity without flashing is caused by the already sintered silver nanoparticles after drying due to the optimized ink recipe from manufacturer's side. Further grain growth and densification was most likely the reason for the slightly improved conductivity.

The AgNP ink, which was not conductive after processing, tremendously improved the conductivity through photonic sintering. The impact of single and quadruple exposures is illustrated in Figure 3.4b. For single exposures, the sheet resistance linearly decreased to about $6.8 \Omega \square^{-1}$ at a voltage setting of 2.8 kV, which corresponded to around 0.95 J cm^{-2} . Only minor changes could be measured with increasing energies and implies an almost fully sintered layer. The minimum resistance was found at 3.4 kV with

$5.5 \Omega \square^{-1}$. The impact of multiple flashes could only be measured for low energies up to a voltage setting of 2.0 kV (0.48 J cm^{-2}). Further increase of the energy showed similar behavior as single exposures. The result implied that multiple flashes are not necessarily required and the substrate can eventually run faster during R2R photonic sintering. The AgNP ink showed a color change from black to golden starting from 2.8 kV upwards as shown in Figure 3.5a and the adhesion significantly improved. Because of this, it was possible to visually measure the impact area and the sintered width w . The thin barrier foil substrate showed no deformation after single exposure at maximum energy but small wrinkles appeared for 4 pulses at 1.8 Hz with voltage settings above 2.6 kV. The silver layer absorbed too much energy that heated the substrate beyond the critical temperature and caused permanent deformation.

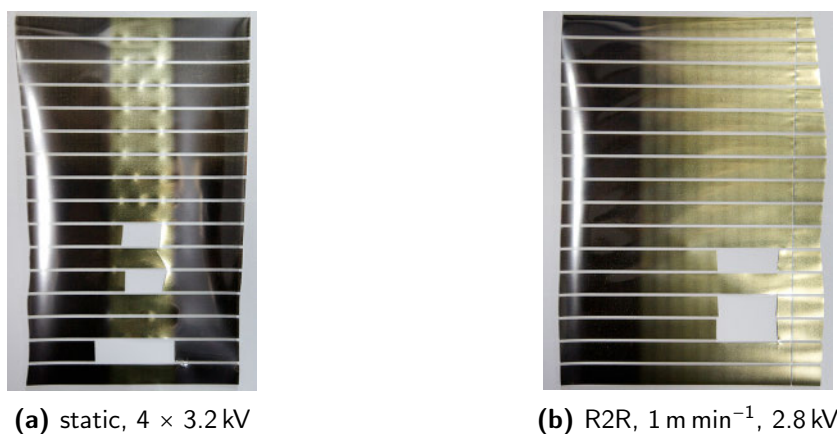


Figure 3.5.: Barrier substrate with flexo printed AgNP ink electrode stripes under different exposures. (a) The sintered width w is clearly visible with its color change from black to golden. (b) The pulsed light exposure under R2R conditions shows the overlapped areas. Photos were taken from the substrate backside. Adapted from Ref. [343] with permission from The Royal Society of Chemistry.

The sintered width w for a flash distance of 2" is larger than the optical footprint based on the manufacturer recommendation with 1". It was more than doubled with a sintered width of up to 42 mm after one flash (see Table 3.1) on AgNP electrodes. Multiple exposures were measured with up to 44 mm. That means it should be possible to increase the R2R processing speed by a factor of two. The theoretical web speed v in m min^{-1} can be calculated with

$$v = \frac{f \cdot (w - w_O) \cdot 60}{1000} \quad (3.1)$$

where f is the flash frequency in Hz, w the sintered width in mm of a single flash, and w_O the desired overlap in mm. An overlap of exposed areas is often required due to unsharp sinter edges caused by decreased optical energy densities at the edge.

Table 3.1.: Measured width w of the sintered area of AgNP ink for different voltage settings (kV) with single and quadruple exposure. The R2R web speed v for two scenarios is calculated based on the w of the single exposure. Adapted from Ref. [343] with permission from The Royal Society of Chemistry.

kV	w [mm] 1 × flash	w [mm] 4 × flash	v [m min ⁻¹] $w_O = 5$ mm	v [m min ⁻¹] $w_O = 0$ mm
2.0	–	37	–	–
2.2	–	38	–	–
2.4	–	38	–	–
2.6	–	39	–	–
2.8	25	40	2.16	2.70
3.0	33	41	3.02	3.56
3.2	34	42	3.13	3.67
3.4	40	42	3.78	4.32
3.6	41	43	3.89	4.43
3.8	42	44	4.00	4.54

R2R flash sintering was only carried on the flexo printed AgNP ink electrodes because the PFI-722 ink was already highly conductive without additional flashing. One experiment was carried out at 1 m min⁻¹ with different voltage settings and another one at fixed 3 kV but with increasing web speeds up to 2.5 m min⁻¹. The measured sheet resistance behavior is shown in Figure 3.6. The sheet resistance at 1 m min⁻¹ was decreased compared to a single flash, as the resulting overlap at low speed led to multiple exposures with increased evaporation of organic residues and further nanoparticle densification. The difference could be observed especially for low voltage settings. As the silver nanoparticles were already sintered and densified above 2.8 kV, multiple exposures had minor impact. A R2R sintered sample from the substrate backside, exposed with 2.8 kV at 1 m min⁻¹ and additional 140 °C thermal treatment is shown in Figure 3.5b. The thermal treatment alone had no further impact on the sheet resistance.

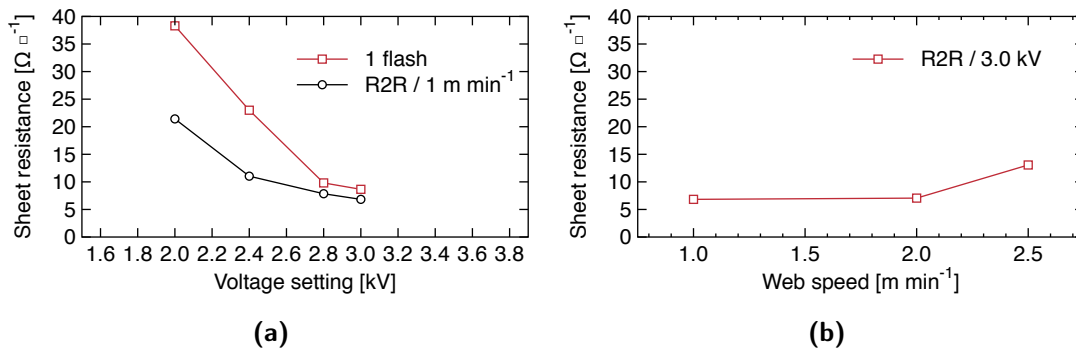


Figure 3.6.: Sheet resistance behavior of AgNP ink during R2R processing. Adapted from Ref. [343] with permission from The Royal Society of Chemistry.

R2R sintering with 3 kV at 2.5 m min^{-1} led to a slightly higher sheet resistance as can be seen in Figure 3.6b. At 1 m min^{-1} the silver was exposed with 6 pulses (23.7 mm overlap), and almost 2 pulses at 2 m min^{-1} (14.5 mm overlap). At 2.5 m min^{-1} the overlap was calculated with only 9.8 mm resulting in alternating single and double exposures that explained the change in conductivity.

The sintering of the silver nanoparticles could be observed using scanning electron microscopy techniques (FEI Nova NanoSEM 600) as shown in Figure 3.7. The PFI-722 ink already had fully sintered particles with long neck and large grain sizes directly after the drying during the printing process. An effect of the photonic sintering post-process is hardly visible. The AgNP ink was not conductive after drying and the unsintered nanoparticles are clearly visible in Figure 3.7c. A percolation network and fused particles are responsible for the evolved conductivity after a single flash as can be seen in Figure 3.7d. With flashlight sintering the heat is generated through the enhanced photothermal effect [389] and once the particles are sintered they lose their nanoparticle behavior and only grain growth and densification occurs.

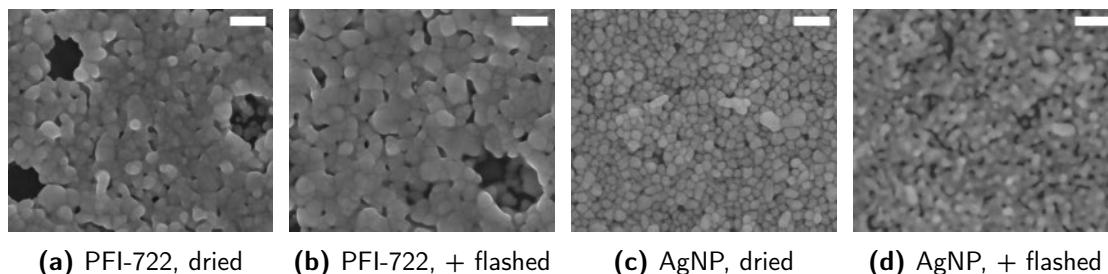


Figure 3.7.: FESEM images of two different flexo printed silver nanoparticle inks before and after photonic sintering. Scale bar is 200 nm. Adapted from Ref. [343] with permission from The Royal Society of Chemistry.

Surface damage and crack formation is an important factor of the sintering process and has to be avoided, especially if subsequent layers are deposited on top. The process upscaling depends on the right level between conductivity and surface morphology. Some crucial damage on the AgNP silver ink layer occurred only at higher energy input with voltage settings above 3.4 kV for single exposure whereas multiple exposures at high voltage settings led to significant surface damage including cracks as can be seen in Figure 3.8. Silver layers printed using the PFI-722 ink showed no cracks. These cracks might not be critical for large areas but fine line structures such as grids can be completely interrupted.

Densification of the sintered nanoparticles is one reason for the crack formation. Furthermore, the cracks are often observed in thicker areas due to inhomogeneous stress distribution and the difference of the coefficient of thermal expansion (CTE) of silver and the barrier foil substrate, which is $19 \mu\text{m m}^{-1} \text{K}^{-1}$ and $59 \mu\text{m m}^{-1} \text{K}^{-1}$, respectively. [341, 394] Homogeneous layers and reduced energy input <3.4 kV can result in crack-free and fully sintered silver electrodes.

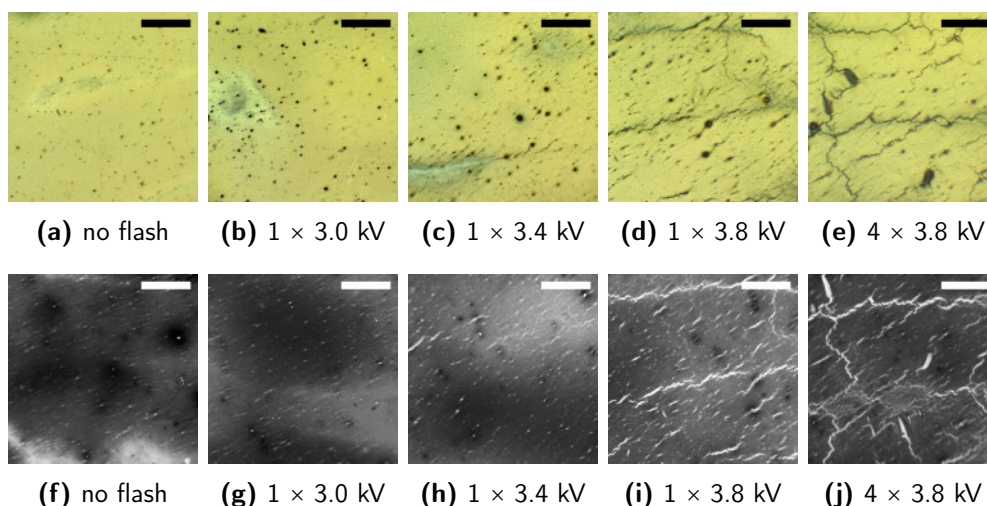


Figure 3.8.: Microscopic photographs of AgNP ink layers with reflected light (a – e) and transmitted light (f – j) show the evolution of cracks with increasing flash light intensities. Scale bar is 100 μm . Adapted from Ref. [343] with permission from The Royal Society of Chemistry.

3.3. Conclusion

The main finding is that properly engineered low-temperature inks do not require additional photonic sintering process steps at all. Anyway, the inks should be dried to avoid wet contact with rollers and to avoid rapid solvent blow-off caused by the fast flash light heating, although shown to be solvable.[383] Hot air and IR as used here or by others is obviously a reliable process in itself and can dry and sinter silver nanoparticle inks in about 2 seconds.[358] The PFI-722 ink was later on the only ink used for high speed processing of front electrode grids during the R2R fabrication of large OPV modules that did not need further photonic flash treatment (Section 4).

Pre-dried nanoparticle inks with higher sintering temperatures can benefit from flashing with respect to both conductivity and adhesion, it might even be necessary. Contrary to existing reports it was shown that a single flash is already enough to achieve high conductivity without damaging the layer morphology and thin barrier foil substrate. Photonic sintering is an ultra-fast technology and has potential for direct inline processing with fast printing technologies when multiple flash systems are synchronized or the flash frequency of a single lamp system is increased. The R2R experiments clearly show the challenges in homogeneous sintering over a large area while the interaction of web speed, exposure area, and overlap plays an important role. The exposure area itself depends on flash distance, optical energy density distribution and the material characteristics (e.g. absorption behavior).

Photonic sintering can be justified for special use-cases such as removing organic residues from the silver electrodes. Basically, it can only be used for the treatment of the first printed layer. Flashing of silver layer electrodes deposited on already printed layers

seems to be very challenging due to the absorption and heat-up of the other layers. This can result in a complete blow-off of the layer stack.

Organic solar cells with flash sintered inkjet printed silver grids have been demonstrated by some groups and showed no big difference in performance to thermal treated grids.[333] The sintering time was drastically reduced from 6 h to 5 s but the sintered grid line had a more pronounced profile due to the coffee stain effect. Small modules with R2R flashed inkjet printed silver grids showed a slightly better performance due to an improved sheet resistance.[211]

4. Large-scale R2R fabrication of OPV devices

This chapter describes the R2R processing and layout strategies for the fabrication of OPV modules with active areas beyond $>14\text{m}^2$ to enable high power output for real energy production. First, the processing and improvement of the Flextrode substrate, an ITO-free alternative, will be described. This transparent conductive electrode can be manufactured directly on barrier foil under full ambient conditions using additive and successive deposition methods. The Flextrode and intelligent subsequent print layouts allow the serial connection of thousands of cells just through printing processes. The conceptual design and fabrication of virtually infinitely large modules with high power output will be described in detail. Finally, four silver back electrode printing methods and three encapsulation procedures are compared with respect to R2R processing and upscaling challenges. This chapter contains information extracted from five first-authored and co-authored publications.[41, 43, 99, 164, 305]

4.1. ITO-free transparent electrode for OPVs

The majority of organic solar cells fabricated in the laboratories around the world are made on glass substrates (99%) with ITO as transparent conductive electrode (95%), which incorporates substantial drawbacks.[395] Low abundance (0.05 ppm of continental earth crust), high demand from the display industry, and localized mining (50% from China) make indium to be a scarce and expensive element.[396] The fabrication of ITO layers is highly inefficient, requires sputtering processes, and employs $>85\%$ of the embodied energy in ITO-PET-based OPV devices.[204, 396] The sheet resistance of typical flexible ITO-based plastic substrates is around $60\ \Omega\ \square^{-1}$ (transmittance $>80\%$), which limits the upscaling of subcells in serially connected modules due to limited current collection.[397] Furthermore, the brittleness of the ceramic-like ITO leads to cracks upon bending, which ultimately destroys the functionality of the OPV device.[398, 399]

Although all record cells are manufactured on ITO substrate, the research on alternative transparent conductive electrodes with comparable and even better properties is increasing constantly. Ideally, the electrode should be highly flexible, solution-processible, have high transmittance and low sheet resistance. Transmittance is not required once the solar cell is illuminated through the backside. Full additive processing and R2R compatibility without the use of vacuum would allow fast and efficient upscaling.

Many different approaches emerged for the replacement of ITO in general and for OPV in particular, and can be categorized into polymers, metal grid and polymers, metal nanowires, ultrathin metals, carbon nanotubes, and graphene.[400, 401] A hybrid

electrode with a combination of metal grids and polymers, typically highly conductive PEDOT:PSS, is most likely the method with the highest impact for large-area organic solar cells as it allows full additive processing with a variety of deposition methods, high mechanical flexibility and comparable or better electrical/optical parameters with respect to ITO. A variety of studies on hybrid electrodes for OPV, typically silver grid and PEDOT:PSS, have been reported that show promising results with transmittance values $>80\%$, sheet resistances $\ll 20 \Omega \square^{-1}$, or efficiencies $>2\%$ for cells with P3HT:PCBM as active layer.[158, 159, 161, 256, 298, 333, 402–405] Embedded grid structures minimize the chance of shorts with the counter electrode that might appear with too thick printed grid lines and not fully covering PEDOT:PSS layers.[298, 300, 406]

Although all of these reports provide highly useful information regarding grid dimensioning, layer stacking, and eventually printing methods, none of the cells were actually produced using R2R processes for all layers. Here, the so-called Flextrode electrode will be described, which is based on a fully R2R produced layer stack of silver grids, PEDOT:PSS, and ZnO as electron transport layer.[41] All processes are additive, solution-based, vacuum-free, and enable the fabrication of inverted OPV devices with thousands of serially connected cells and virtually infinitely large modules sizes – the Infinity concept.

4.1.1. Flextrode

The first unnamed presentation of the Flextrode electrode was in summer 2012 with a comparison of different fabrication methods of the silver grid itself.[42] Inkjet printing, thermal imprinting, and flexo printing (all R2R) of nanoparticle-based silver ink resulted in P3HT:PCBM-based cells with efficiencies of 0.75 %, 1.92 %, and 1.82 %, respectively. Inkjet printing suffered from high sheet resistance while thermal imprinting was very slow with $<0.5 \text{ m min}^{-1}$ and required special equipment, which was made available through a Korean collaboration. Flexo printing produced the thickest grid lines with some spikes but it had the highest fabrication speed of 25 m min^{-1} , moderate printing form costs and was found to be a very reliable method for the fabrication of grid structures and solar cells with considerable high efficiencies $>1.8\%$. Comparable R2R produced ITO-based cells and modules following the ProcessOne method achieved efficiencies of around 2 % depending on the size.[38, 194]

The final introduction and detailed fabrication procedure of the Flextrode electrode was presented early 2013 and will be detailed here.[41] The electrode was based on flexo printed hexagonal grid patterns with rotary screen printed PEDOT:PSS and slot-die coated ZnO. The macroscopic pattern shape was similar to the former ITO stripe pattern and comprised 16 stripes with a width of 13 mm. Photographs of the final electrode on PET are shown in Figure 4.1

The hexagonal (honeycomb) grid had a pitch size of 2 mm and a nominal line width of $100 \mu\text{m}$ on the printing form. The water-based silver nanoparticle ink PFI-722 introduced in Section 3 was R2R flexo printed at a speed of 10 m min^{-1} using an anilox roller with a volume of 1.5 ml m^{-2} and 480 L cm^{-1} . The ink was dried using two 2 m long hot air ovens at 140°C and supportive IR lamps. Additional processes such as photonic sintering or

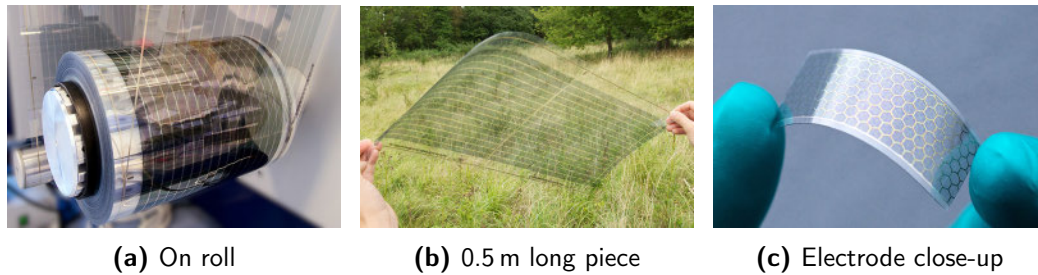


Figure 4.1.: Photographs of the Flextrode transparent conducting electrode substrate with hexagonal grid pattern. (a) Adapted from [41] © 2013 WILEY-VCH Verlag GmbH & Co. KGaA, Weinheim

long thermal treatments were not necessary as shown earlier in Section 3. The width of the grid lines increased during the printing processes to roughly $160\ \mu\text{m}$. The average thickness was in the range of $200\ \text{nm}$ but viscous fingering and ink splitting effects formed areas with peak heights of up to $750\ \text{nm}$. The measured sheet resistance of the silver grid itself was in the range of $7.4\ \Omega\ \square^{-1}$ while having a transmittance of 77 % at $550\ \text{nm}$ simply through shadow losses of the light blocking grids (see Figure 4.2a).

The highly conductive PEDOT:PSS (Clevios PH1000, Heraeus) was rotary screen printed on top of the grid pattern to achieve a homogeneous large-area electrode. It was mixed 10:3 by weight with isopropanol to ensure proper printing results and satisfying wetting. The printing form was an electroformed nickel screen with a 215 mesh and an open area of 25 % for a theoretical wet deposit of $20\ \mu\text{m}$. The printing speed was set to $10\ \text{m}\ \text{min}^{-1}$ and dried with a 2 m long oven at $140\ ^\circ\text{C}$ and IR support. The PEDOT:PSS fully covered the printed grid structure and had a roughness of around $80\ \text{nm}$ measured inside a hexagonal grid. The overall transmittance dropped to 68 % at $550\ \text{nm}$ as shown in Figure 4.2a while the sheet resistance increased slightly to around $10.4\ \Omega\ \square^{-1}$, which is still $6\times$ less than typical flexible ITO-based substrates.

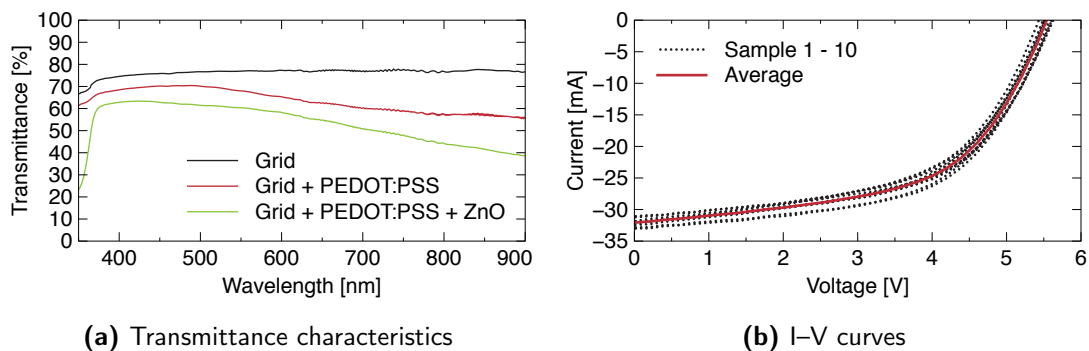


Figure 4.2.: (a) Optical characteristics of the Flextrode substrate with hexagonal grid. (b) Device performance of 10 fully R2R produced OPV modules on Flextrode. Adapted from [41] © 2013 WILEY-VCH Verlag GmbH & Co. KGaA, Weinheim

The finalization of the Flextrode stack was achieved through slot-die coating of ZnO stripes on the Ag-grid|PEDOT:PSS stack. The nanoparticle-based ZnO suspension (55 mg ml^{-1} in acetone) was coated at a speed of $5\text{--}10 \text{ m min}^{-1}$ and dried at $70/140^\circ\text{C}$ in two 2 m long ovens. The dry layer thickness of around 100 nm followed the surface metrology of the pre-printed layer and smoothed them further. The roughness decreased to $<7 \text{ nm}$ because the ZnO nanoparticles filled the PEDOT:PSS that was slightly dissolved from the acetone. The transmittance dropped furthermore to around $>60\%$ at 550 nm .

The common speed of 10 m min^{-1} for each process was chosen to enable inline processing of several printing steps in one print run. It was shown to be functional for simultaneous printing of the silver grid and PEDOT:PSS, and for slot-die coating of ZnO and active layer in one run. The inline processing saved considerable amount of time with less substrate handling compared to individual prints at the same speed but it was not optimized for the optimum speed of each process. Flexo for example should run much faster for better print results. All Flextrode substrates, in particular for the Infinity and freeOPV modules, were later on fabricated in individual print runs at optimized speeds. The advantage of the Flextrode process is the possibility to apply it on different kinds of substrates. The test modules were fabricated on plain PET foil but a direct application on thin barrier was possible as well.

Sample modules of 11 serially connected cells and an active area of 66 cm^2 were manufactured based on the ITO layer stack to verify the performance of the fabricated ITO substitute. The cells comprised of Flextrode|P3HT:PCBM| $2\times$ PEDOT:PSS|Ag-comb, whereby the active layer was slot-die coated at 10 m min^{-1} and the back electrode PEDOT:PSS (Agfa 5010) and silver (Dupont 5025) were rotary screen printed at 2 m min^{-1} and dried sufficiently. All cells had to be electrically switched to transform the layer stack to a functional solar cell device by dedoping the PEDOT:PSS layer at the active-layer|PEDOT:PSS interface.[210] The test modules were edge-sealed with UV-curable adhesive and $72 \mu\text{m}$ thick Amcor barrier foil. The resulting I-V curves of 10 sample devices are shown in Figure 4.2b. All samples performed similar with an average PCE of 1.5% (max. 1.6%), V_{OC} of 5.54 V , I_{SC} of 32.09 mA , and FF of 55.64% (max. 57.34%). The slightly lower performance compared to similar ITO devices is most likely caused by the shadow loss of the grid lines and the lower transmittance in general. The fill factor is highly improved due to the low sheet resistance.

4.1.2. Flextrode improvements

The results from these Flextrode experiments were starting point for further grid improvements. It has been shown through experimental runs that honeycomb electrodes are not necessary while grid lines in the direction of the current flow are suitable enough to achieve a sufficient current extraction over the whole area. This could also be proved by others through simulations and current mapping.[159, 405] The nominal line width could be lowered to $50 \mu\text{m}$ due to an improved flexo process. The grid fingers were tapered from $50 \mu\text{m}$ to $>100 \mu\text{m}$ on the printing form, which resulted in an increasing printed line width starting from $>80 \mu\text{m}$. The lines of one cell were just connected to a busbar and not framed by a printed outline as in the honeycomb grid. The distance between the

lines was set to 1.5 mm. Photographs of the improved Flextrode under different light conditions are shown in Figure 4.3a. Visual quality control during the fabrication of the PEDOT:PSS and ZnO layer was carried out by observing the optical interferences from printed and coated thin films. This "snake skin" effect was suitable to verify dry and evenly distributed layers over the web width based on hands-on experience gained from a vast amount of experiments.

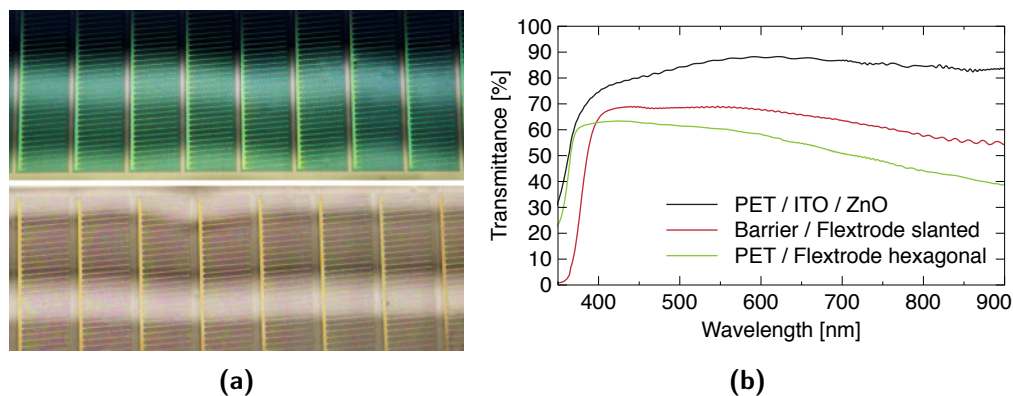


Figure 4.3.: (a) Photographs of improved Flextrode electrode with slanted grids. (b) Transmittance of the improved Flextrode substrate with slanted grids vs. ITO-PET and honeycomb Flextrode. (a, top) Adapted from [99] © 2013 WILEY-VCH Verlag GmbH & Co. KGaA, Weinheim.

The biggest drawback of the honeycomb grid was the amount of overlaps with the printed comb back electrode (see Figure 4.4a) that could lead to shorts in case silver spikes occurred or the intermediate layers were too thin. The best solution for this problem would be parallel front and back comb electrodes that are slightly separated, but since the foil expands in web direction and shrinks across the web due to heating it can happen that some grid fingers from front and back electrode are exactly on top of each other. Secondly, the available registration control was not precise and reliable enough to print exactly in register. This problem could be solved and the amount of overlaps could be minimized by introducing $+5^\circ$ and -5° slanted front and back electrodes that form an overlapping moiré pattern as can be seen in Figure 4.4b–4.4g. In worst case, just two direct point overlaps per front and back electrode finger are possible independently from shrinkage and web directional (WD) or cross directional (CD) registration errors.

The latest version of the Flextrode layer stack was flexo printed using the PFI-722 silver ink and an anilox volume of 3 ml m^{-2} at 20 m min^{-1} to achieve better printing quality. The full layer sheet resistance was $<500 \text{ m } \Omega \square^{-1}$. Highly conductive PEDOT:PSS (PH1000) was rotary screen printed using a 305 mesh (8% open area) with a wet layer deposit of just $6 \mu\text{m}$. This allowed faster processing with up to 20 m min^{-1} while having increased transmittance. ZnO was slot-die coated as usual. The resistance is anisotropic since the dominating conductive silver grid lines are only in the direction of the current flow and tapered. Measurements in the direction of the current flow revealed a sheet resistance of $<20 \text{ } \Omega \square^{-1}$. The transmittance was highly improved although it was di-

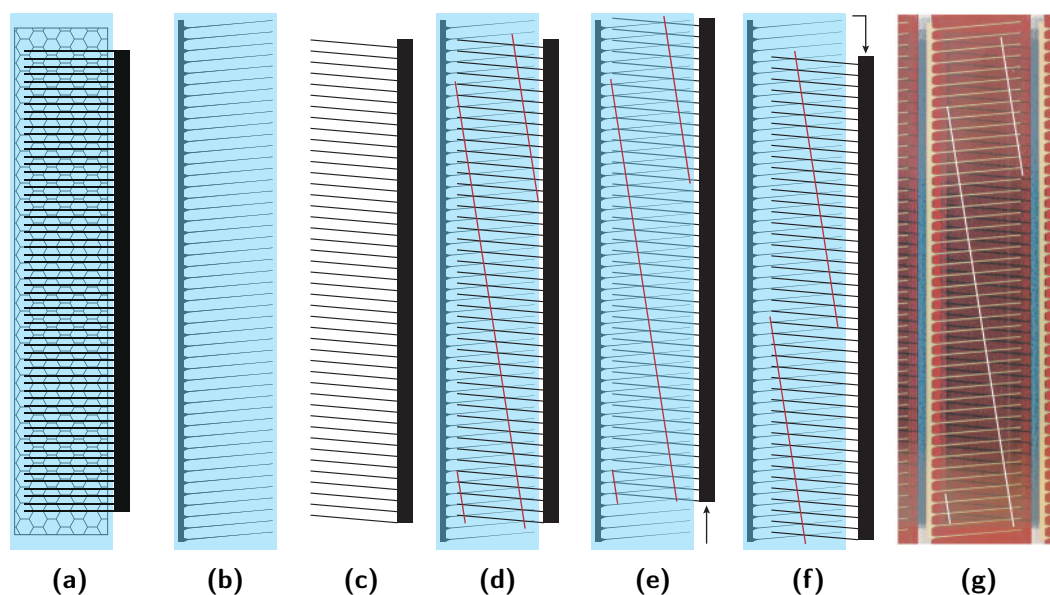


Figure 4.4.: Overlay simulation of front and back electrode under different registration. A moiré pattern is built up for the slanted grid design. The red and white lines show the points where front and back electrode fingers overlap.

- (a) Hexagonal front electrode with PEDOT:PSS + comb back electrode
- (b) Grid front electrode (slanted $+5^\circ$) with PEDOT:PSS.
- (c) Grid back electrode (slanted -5°).
- (d) Print in register.
- (e) Print out of register (WD offset).
- (f) Print out of register (WD + CD offset).
- (g) Photograph of a randomly selected printed solar cell.

Partially reproduced from [99] © 2013 WILEY-VCH Verlag GmbH & Co. KGaA, Weinheim.

rectly printed on Amcor barrier substrate, which has already a lower transmittance than plain PET. A comparison of slanted Flextrode, hexagonal Flextrode and standard ITO substrate with ZnO is shown in Figure 4.3b.

4.2. Infinity module fabrication

All large-scale OPV modules produced so far were limited by the size of the R2R machinery, the motif length of one print, and the serially connected stripe design. The biggest demonstrators were in the range of A4–A3 sheet sizes.[194] Modules of these sizes could charge batteries and drive LED lamps, but real energy production was limited due to limited efficiency.[196] An efficient upscaling procedure was necessary that enabled full R2R production of large OPV modules with high power output for actual energy production. The former OPV company "Konarka Technologies" solved this with a proprietary bus bar embedding method to parallel connect submodules to larger high-current low-voltage

modules with a maximum output of $27 \text{ W}_{\text{peak}}$.^a The bus bar processing and encapsulation of the modules was sheet-to-sheet based, time consuming and labour intensive, while the basic OPV production was R2R-based.[407]

A new and improved concept for the fabrication of OPV modules will be presented here that allowed virtually infinitely large modules manufactured with a full R2R workflow from the first printed layer to the final installation of the modules. Since the efficiency of the available materials is still low the module has to be huge to extract sufficient power. Printed thin films are unable to transport high electrical currents from many parallel connected cells, which limits the maximum size of a module. The upscaling challenge was solved with a fully printed serial connection of all cells employed in one module. The obvious problem of such a configuration is that one poor cell, for example a shadowed cell, can compromise the whole module performance. Conventional silicon-based modules employ bypass diodes to resolve these effects but is found to be challenging for organic solar cells since the manufacturing should be kept simple. Surprisingly, it was found that OPV modules are relatively insensitive to partial shadowing due to their lower fill factor and current density compared to silicon PV.[43]

The IOne layer stack and the availability of the in-house produced Flextrode substrate allowed the design of an intelligent layout for the serial connection of thousands of cells along the web direction just by using R2R printing and coating methods. The design had to be very robust during the fabrication since catastrophic failures such as an open circuit of just one cell would prevent any power extraction. Short circuit cells could be tolerated although it generates a series resistance, which causes poorer performance.

^aKonarka Power Plastic 40 Series https://web.archive.org/web/20120516144714/http://konarka.com/media/pdf/konarka_40series.pdf

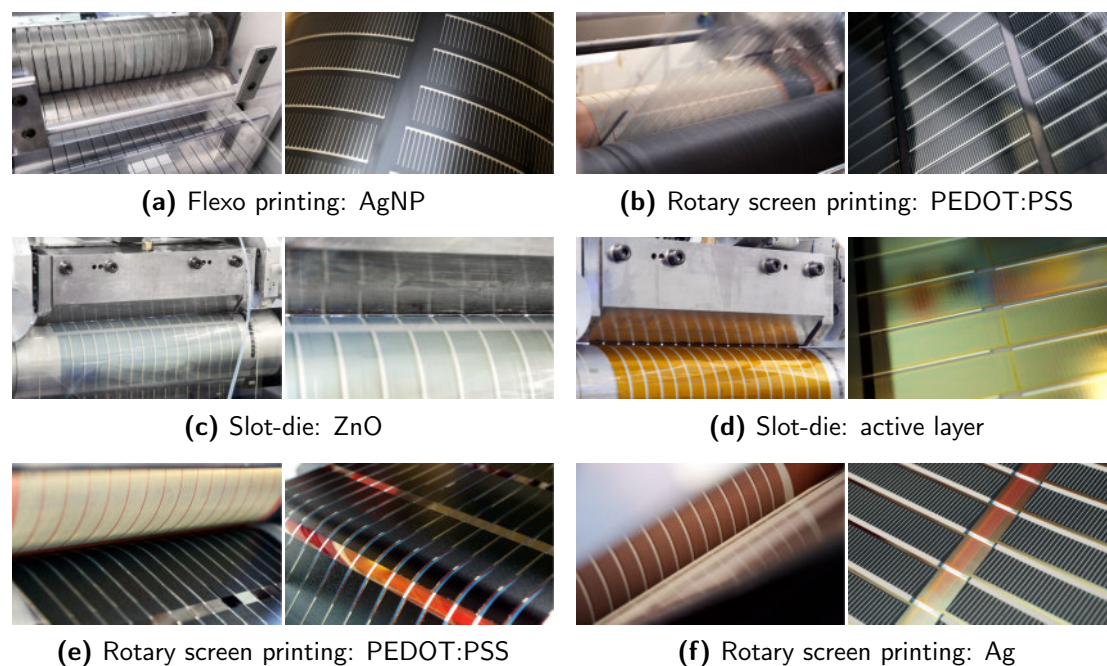


Figure 4.5.: R2R fabrication methods for fabricating Infinity modules. Partially adapted from [99] © 2013 WILEY-VCH Verlag GmbH & Co. KGaA, Weinheim.

Photographs of Infinity fabrication processes are shown in Figure 4.5, while the process workflow is illustrated in Figure 4.6 together with a detailed illustration of the serial interconnection in Figure 4.7. It employed a combination of seven R2R printing and coating steps with a pattern design that accommodated 1-dimensional and 2-dimensional film forming methods. The layout described here was designed for a web width of 305 mm and a print motif length of 12" (304.8 mm). First, the slanted silver front electrode was flexo printed together with register marks and continuous guidelines that allowed automatic register corrections for the subsequent print and coating steps (Figure 4.6a). Each motif comprised 4 rows of 16 cells. Next, the highly conductive PEDOT:PSS front electrode was rotary screen printed exactly on top of the silver grid electrode (Figure 4.6b). ZnO was slot-die coated in form of 16 stripes with a width of 13 mm on top of the cells leaving the alternating bus bar open for each single cell (Figure 4.6c and 4.7c). The first three layers built the Flextrode electrode and were processed according standard procedures described earlier.

Active layer was slot-die coated exactly on top of ZnO using the same 16×13 mm stripe mask. The typical fabrication speed for P3HT:PCBM dissolved in chlorobenzene was around 5 m min⁻¹ although higher speeds could be achieved. The dry layer thickness was in the range of 500 nm to enable reliable switching. The PEDOT:PSS (Agfa 5010) hole transporting full back electrode layer was rotary screen printed with a cross directionally shifted pattern to cover the active layer of each cell while contacting the bus bars of the adjacent cells (Figure 4.6e and 4.7e). Printing was typically carried out using a 75 mesh screen (32% open area) with a wet deposit of 40 μm at a speed of 2 m min⁻¹. Hot air drying at 140 °C was supported by IR lamps. The print parameters were not fixed, thus thinner PEDOT:PSS layers could be printed faster.

The silver back electrodes (Dupont PV410) with slanted grids and 2 mm wide bus bars had the same pattern shift as the underlying PEDOT:PSS layer and connected the bus bar of the flexo printed front electrode (Figure 4.6f and 4.7f). The bus bars were localized exactly inside the 2 mm gap of the active layer stripes and allowed good contact with the spring loaded pins of the automatic R2R switcher.[41] The large contact areas on the outer cells of the serially connected 16-cell submodules were finally connected with silver connector pads in a seventh print run using rotary screen printing (Figure 4.6g). A printing form with a 215 mesh (25 % open area) and a wet deposit of 20 μm was typically used while printing speed of 10 m min^{-1} could be achieved. The printing parameters were subject to change and just a rule of thumb. The two final silver prints could also be combined using a seamless screen with a motif length of 18" comprising six submodules per motif. Individual printing steps were preferred due to higher tolerance in the web directional registration and the possibility for different layer thicknesses of grid and Infinity connector.

The shifted pattern on every submodule generated a flipped polarization that enabled the meandering serial connection along the web direction as shown in Figure 4.6h. The final module had therefore only two terminal connectors independently of the length of the module. The active area of one cell was 7 cm^2 while 100 m of foil comprised circa 21000 cells ($V_{\text{OC}} > 10 \text{ kV}$) and a total active area of 14.7 m^2 . Modules processed according the Infinity concept were generally fabricated in lengths of at least 700 m without any open circuits (technical yield of 100 %). The Flextrode substrate itself was prepared on web lengths $> 1.5 \text{ km}$. These dimensions were necessary for filling one row of the solar park (Section 5.1) with six stripes of 100 m length each. Furthermore, it minimized the relative amount of material waste compared to short runs. The performance of such Infinity modules is described in Section 5.2.

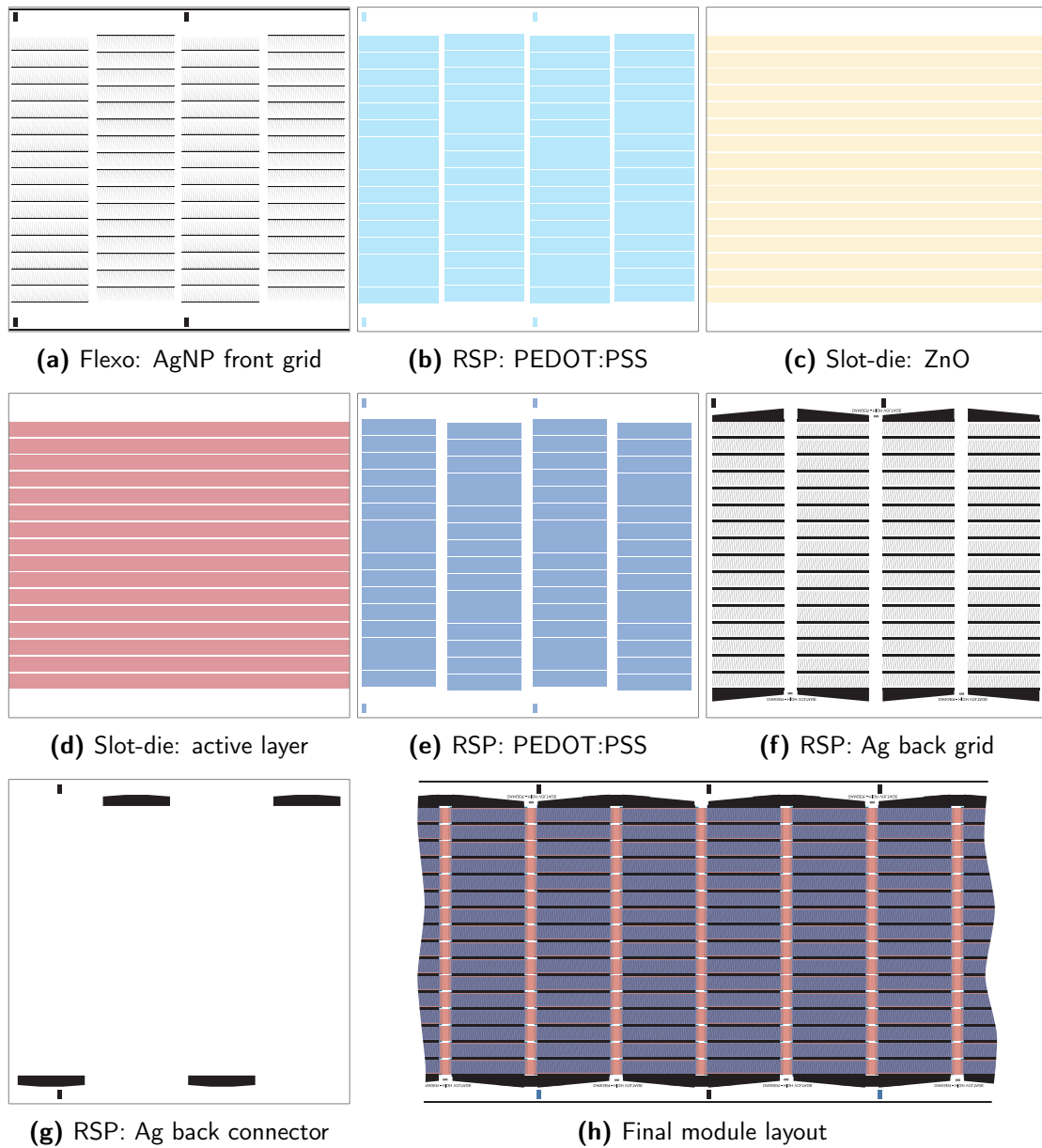


Figure 4.6.: Printing forms and slot-die coating stripe layout for the Infinity modules. The final Ag connector (g) serially connects the submodules to a virtually infinitely large module (h). Print and coating direction is from left to right (a → g).

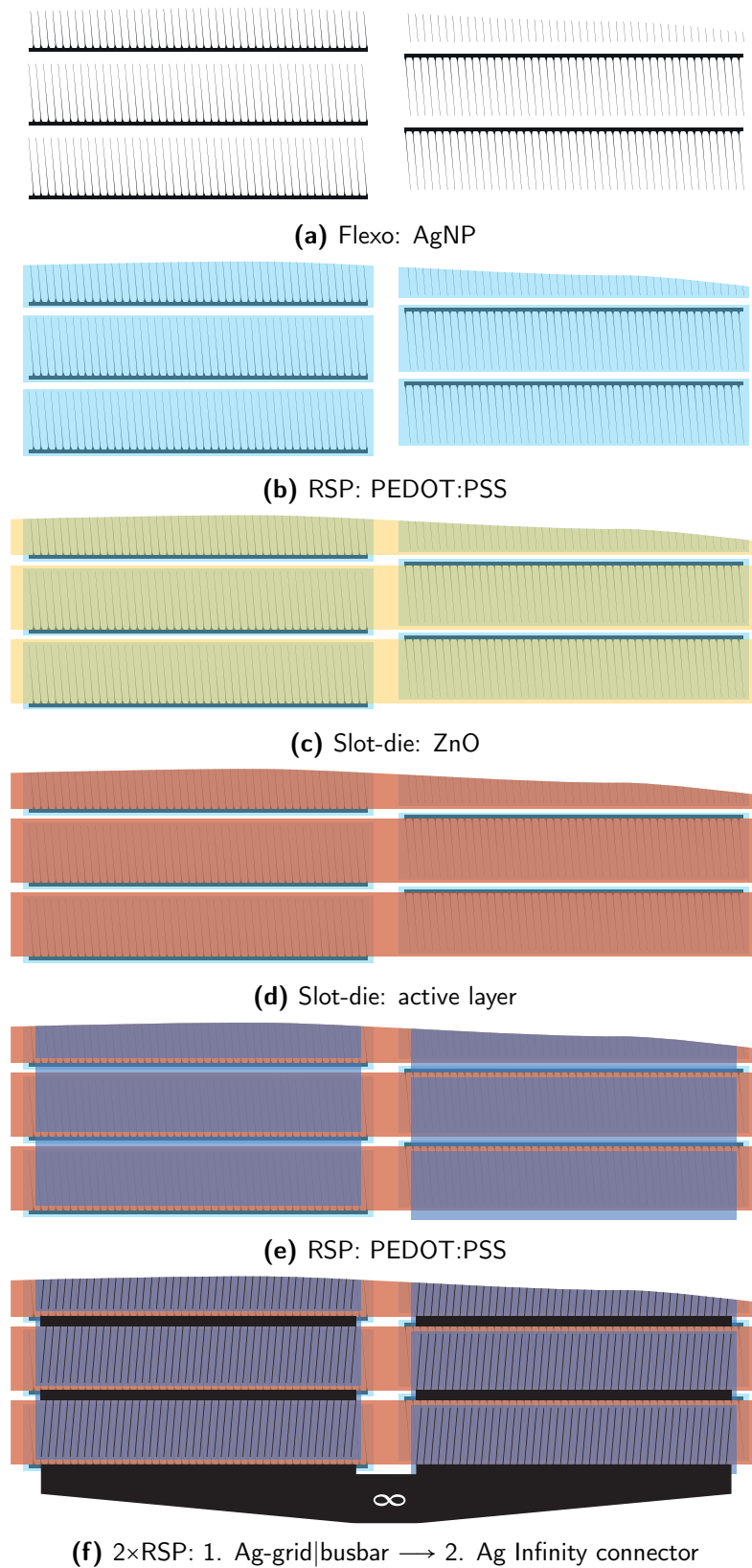


Figure 4.7.: Overlay simulation of Infinity module concept with at least 6 subsequent print and coating steps. It is possible to combine step (f) to one single print using a seamless RSP printing form.

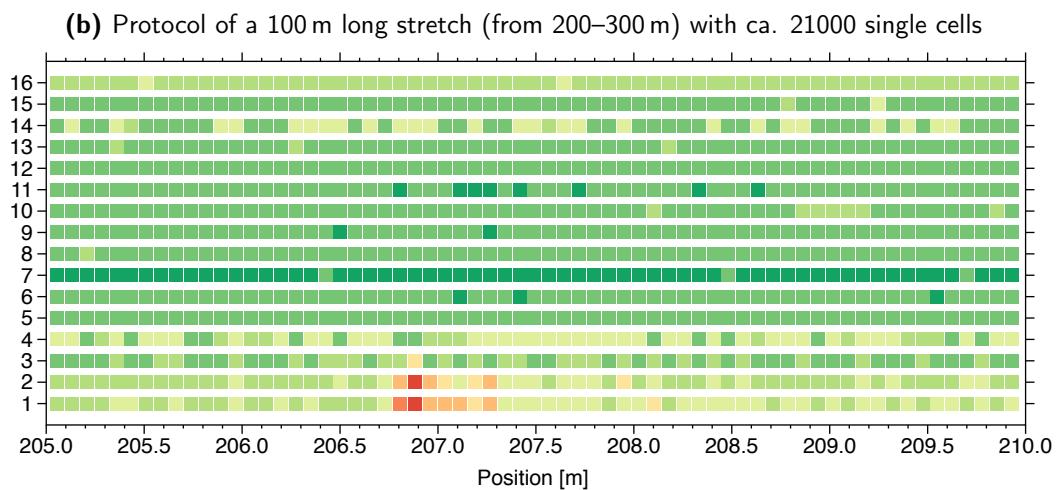
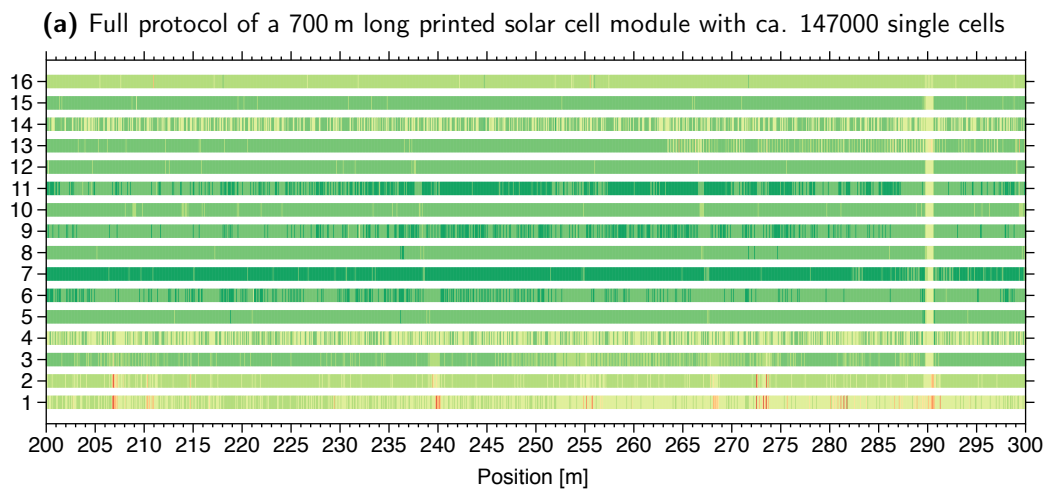
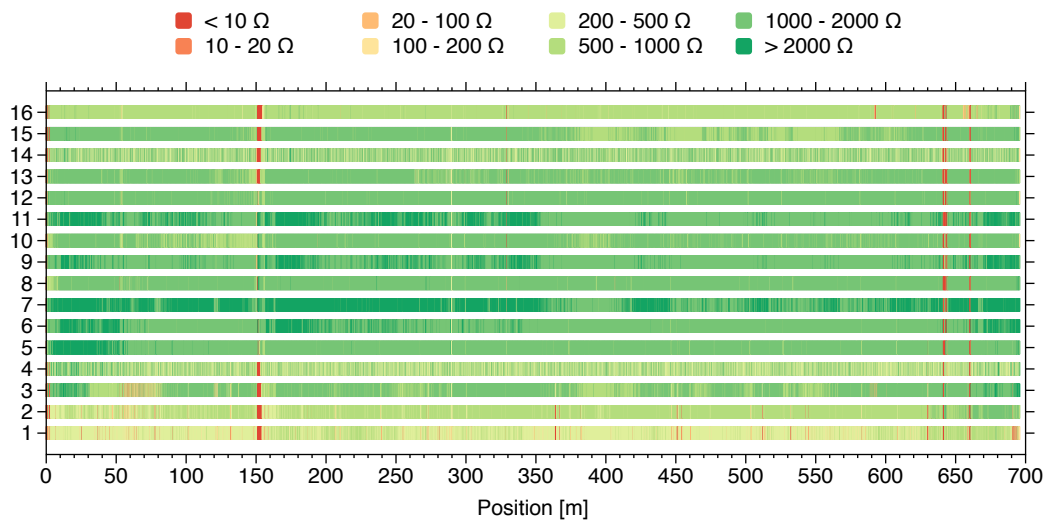


Figure 4.8.: Quality control data of a 700 m long Infinity print-run derived from the dark I-V curve to verify a functional solar cell ($R \gg 10 \Omega$).

Each of the 147000 cells from a 700 m long Infinity print run had to be switched following methods reported earlier.[41, 210] The quality control data protocol shown in Figure 4.8a revealed some problems (red color) after 150 m and around 650 m probably due to some registration problems. In these areas the cells most likely acted as short circuit and did not contribute to the module performance. It is clearly visible that the center stripes 5 to 11 had the best performance. The reason could be inhomogeneities of the active layer thickness across the web direction and pronounced impact of cross directional foil shrinkage on the outer stripes of the foil. Foil shrinkage and precise printing in registry is a general challenge and was handled by pre-shrinking the foil prior the first print. Zooming further into the data as illustrated in Figure 4.8b and 4.8c reveals the quality of each individual cell. The data output was used to select the best 100 m long stretches for the installation in the solar park, while areas of poor performing cells were avoided. Rolls of 100 m long modules were made out of the 700 m long mother roll during the encapsulation with UV-curable adhesive and barrier foil.

4.3. Back electrode printing

The highly conductive metal back electrode is a key component of organic solar cells and the majority of reports employ vacuum-based evaporation steps through shadow masks for the finalization of the layer stack. The purpose is an efficient current collection over large area, eventually as a back reflector, and for the serial connection of multiple cells to modules. Although it is not impossible to upscale patterned R2R metal evaporation for continuous large-scale fabrication of OVP devices it does present some bottlenecks in terms of processing speed, capital investment in equipment, technical yield and direct process energy. Solution-based printing processes seem to be more favorable as they can be very fast and versatile.

In small-scale devices the silver back electrode has been flexo printed,[199, 206] inkjet printed,[162, 163, 330, 338] spray coated,[246, 287, 288] or screen printed.[299, 302] Reports on R2R processed back electrodes using solution-based methods are very limited and are basically focused on silver formulations [38, 98, 194, 209] or carbon [210, 297] using semicontinuous flatbed or continuous rotary screen printing methods. Here, the question will be answered which of the available methods, namely flexography, inkjet (IJ), flatbed screen printing (FBSP), and rotary screen printing (RSP), is most suited for large-scale R2R processing of silver back electrodes with respect to technical yield, material use, and speed.

4.3.1. Experimental

The OPV layer stack is based on the IOne design introduced earlier comprising of Ag-grid|PEDOT:PSS|ZnO|P3HT:PCBM|PEDOT:PSS with varying back electrode silver grids. The front electrode was based on a hexagonal grid pattern, whereas the back electrode was based on a comb-like grid structure with finger widths of 150–200 μm and a spacing of 1 mm. The fundamental substrate was PET (Melinex ST506, DuPont Teijin Films). The Flextrode substrate (Ag-grid|PEDOT:PSS|ZnO) has been fabricated

using standard procedures as reported earlier.[41] The active layer was composed of P3HT (Sepiolid P200, BASF) and [60]PCBM (Merck) in a ratio of 1:1 (55 mg ml^{-1} in chlorobenzene) and slot-die coated at 3.5 m min^{-1} . The PEDOT:PSS back electrode (Orgacon EL-P 5010, Agfa) was rotary screen printed at 2 m min^{-1} . The printed modules were based on 16 serially connected cells but only single cells or small modules of 4 cells were used for the characterization. Barrier foil (Amcor) with a thickness of $72 \mu\text{m}$ and UV-curable adhesive (LP655, DELO) was used for the encapsulation and the lifetime study. The activation of the cells had been carried out through electrical switching as described elsewhere.[210]

A screen printer from ALRAUN Technik GmbH was used for intermittent R2R flatbed screen printing. The solvent-based silver paste (PV410, DuPont) was printed with a 120 mesh screen and dried at 140°C for 2 min in a 2 m long hot air oven. The overall speed was roughly 1 m min^{-1} .

Rotary screen printing was carried out on a RSI compact printing unit (Stork Print BV) with an electroformed nickel screen and a repeat length of 12". The screen parameters were 215 mesh, 25% open area, and a theoretical wet layer deposit of $20 \mu\text{m}$. The printing speed of the solvent-based silver paste (PV410, DuPont) was up to 10 m min^{-1} using a 2 m long hot air oven with 140°C and IR support.

Inkjet printing was carried out at 2 m min^{-1} using three piezo based DOD printheads (Kyocera) with a resolution of 600 dpi that were combined to enable a print width of 305 mm. Additionally, a corona station for surface treatment and a 2 m long hot air oven with 140°C was used. The corona station was set to a power of 300 W to enable sufficient wetting of the water-based nanoparticle silver ink (Suntronic U7089, Sun Chemical) on the PET substrate.

Flexo printing was carried using an anilox cylinder with a volume of 11 ml cm^{-3} and an elastomeric printing form with a hardness of 65 Shore. Water-based nanoparticle ink (PFI-722, PChem Associates) was printed with up to 10 m min^{-1} and dried using two 2 m long ovens at 140°C and IR support.

4.3.2. Results and discussion

The printing experiments were carried out using the most suitable ink type for each fabrication method based on its single-layer printability on plain substrate and the existing equipment. Although ink change is the nature of printing the inkjet setup was basically fixed to the employed water-based ink. The recirculation system and the adjusted printhead settings did not allow a quick ink swap.

The key layer for the subsequent deposition of silver is the thick back electrode PEDOT:PSS fabricated using rotary screen printing and the adjacent layers with different surface characteristics and wetting behaviors. These layers were not optimized regarding the silver ink and allow a direct comparison of the current ink and process interaction. The results lead to process recommendations and optimization that need to be addressed for future upscaling efforts.

The best printability has been achieved with both screen printing methods as can be seen in Figure 4.9 with the trade-off of high consumption. The silver paste with a high viscosity of 40–70 Pa·s and thixotropic behavior is forced through the screen and showed no dewetting or smearing of regardless the surface quality beneath. It stucked on the surface after the ink deposition and smoothed out the step sizes from the relatively thick PEDOT:PSS layers (2 μm) due to its own thickness d beyond 8 μm . The print quality and edge definition was slightly better for the flatbed screen printed silver due to the different mesh types but it was outperformed ten-fold in speed by rotary screen printing. The maximum final speed is generally limited just by the dryer length and could easily be increased in an optimized machine setup. The sheet resistances R_{sheet} were very low with less than $67 \text{ m}\Omega \square^{-1}$ as listed in Table 4.1. The ink consumption and a higher degree of ink waste was the bottleneck of screen printing but overall it gave best results in solar cell performance. Rotary screen printing has the capabilities of seamless prints and very high speeds that match with other process steps and allows inline fabrication of multiple layers.

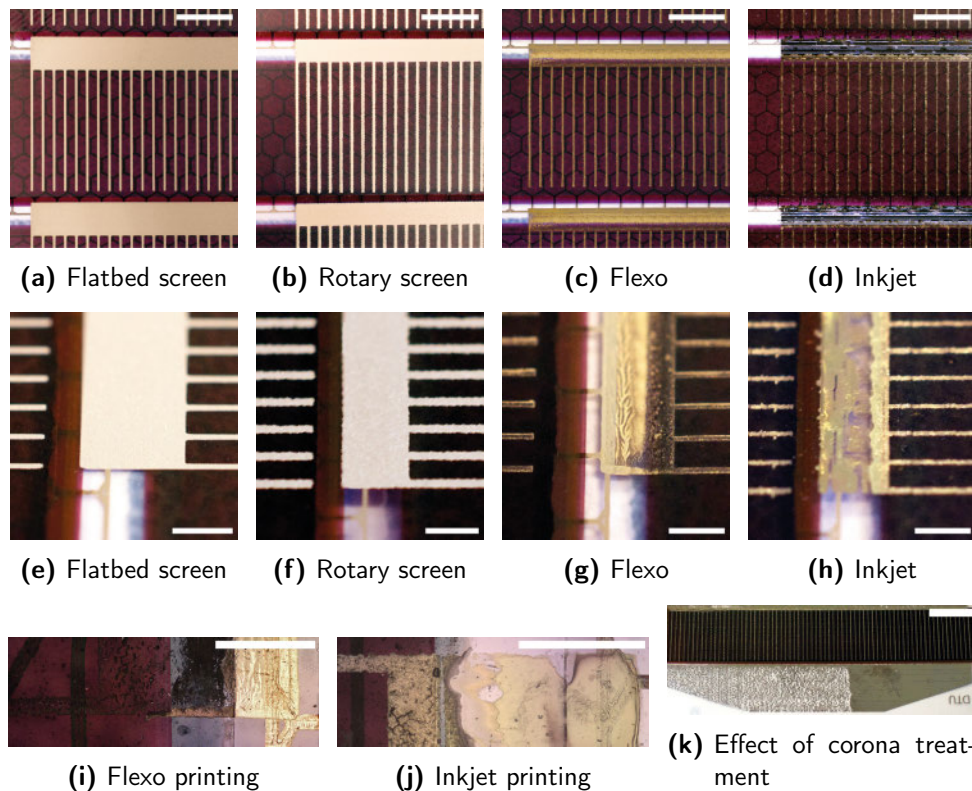


Figure 4.9.: (a-j) Silver back electrode print results of the four R2R printing methods. (k) Effect of corona treatment (right part) on the wetting of inkjet AgNP ink on PET. Scale bar is 5 mm (a-d), 2 mm (e-h), 1 mm (i,j), and 10 mm (k) Adapted from [164] © 2013 WILEY-VCH Verlag GmbH & Co. KGaA, Weinheim.

Table 4.1.: Process parameters and silver layer characteristics. Adapted from [164] © 2013 WILEY-VCH Verlag GmbH & Co. KGaA, Weinheim.

Method	v [m min ⁻¹]	R_{sheet}	d [μm]	Notes
FBSP (Ag)	1	67 m Ω □ ⁻¹	8	Hot air
RSP (Ag)	10	47 m Ω □ ⁻¹	10	Hot air, IR
IJ (AgNP)	2	38 Ω □ ⁻¹	0.5	Hot air, corona
Flexo (AgNP)	10	162 m Ω □ ⁻¹	1	Hot air, IR
RSP (PEDOT:PSS)	2	232 Ω □ ⁻¹	2	Hot air, IR

At first sight the print quality of the flexo printed silver layer was satisfying but revealed problems surfaces with different characteristics as can be seen in Figure 4.9. The ink transfer to the PET surface and silver from the front grid electrode was very good as expected and showed the typical viscous fingering effects (Figure 4.9g). Although the ink layer thickness was much lower than the screen printed ones it had a comparable sheet resistance of 162 m Ω □⁻¹ due to its optimized nanoparticle ink composition for low-temperature sintering. The problem during the processing was the almost non-existing ink transfer onto the PEDOT:PSS layer that had a roughness R_a of 400 nm. A change of the printing parameter such as nip pressure, speed, and anilox volume did not eliminate the problem and it was found that the surface parameters of the PEDOT:PSS layer and the ink characteristics must be insufficient to enable a high ink transfer ratio from the printing form to the pre-printed substrate. During the printing, PEDOT:PSS even got slightly dissolved by the water-based ink and residues were transferred back onto the printing form and accumulated under the doctor blade in a silver|PEDOT:PSS mixture. The silver layer was not connected on the PEDOT:PSS (see Figure 4.9i) and it did not contribute for an efficient current collection. Therefore, the electrical switching was very difficult to achieve. The ink consumption was very low compared to screen printing at much higher speed. Ink waste can be minimized with a controlled inking of the anilox cylinder to the end of print runs as experiments showed. It would be the ideal fabrication process if the surface interaction problems are solved.

The printability of the inkjet printed water-based AgNP ink was satisfying on PEDOT:PSS and PET despite some missing dots due to clogged nozzles. To achieve a homogeneous silver layer on PET the surface had to be corona treated to increase the surface energy (see Figure 4.9k), otherwise it showed dewetting and the formation of ink islands. This treatment was necessary but also caused some destructive impact on all previously printed layers. A solution might be a soft plasma treatment but was not available in the R2R setup. The optimum condition would be a complete process without additional surface treatments which could make other ink solvent systems necessary. The step height of PEDOT:PSS to PET is another critical challenge for the inkjet process that led to very little ink coverage next to PEDOT:PSS (see Figure 4.9j), which could brake the serial connection and limited the electrical switching. It might be explained with a down-flow of the low-viscous ink from the edge of the PEDOT:PSS layer. Furthermore, the electrical switching was limited due to the poor sheet resistance of the silver layer,

which was several orders of magnitude higher than in the other methods. The printing speed was just limited by the dryer length and can be much higher with up to 75 m min^{-1} for single head systems. Ink consumption was the lowest of all methods with virtually no waste due its principle of drops on demand. Some ink loss is produced during printhead flushing prior printing. The R2R system which was used here cannot not be used for ink compatibility testings due to the high ink volume internally. At least it is not practical and very expensive and tabletop systems would be the better choice.

After printing all the different back electrodes the solar cell performance was compared for single cells and small modules. Electrical switching was very easy and reliable for the screen printed cells due to thick silver grid lines and very good conductivity. The flexo and inkjet printed modules were difficult to switch so that copper stripes were taped between each cell to achieve a serial connection and good contact for the switching. The resulting J–V curves and solar cell parameters for each device and printing method are shown in Figure 4.10 and Table 4.2. It shows that screen printed back electrodes had the best performance as expected from the visual printing results and very good layer characteristics. They efficiencies varied from nearly 1.8% up to 2.1% and fill factors close to 50%. The flexo and inkjet printed cells had poor performances with a PCE <1% and low fill factors <31%. The very thin flexo printed silver and the low conductive inkjet silver on the PEDOT:PSS led to high series resistance. The current extraction over large area was basically carried out just through the back electrode PEDOT:PSS and resulted in a low current density. Poor switching performance led to a low shunt resistance and ultimately to the low fill factor. The back PEDOT:PSS layer was not completely switched (de-doped) and the hole conducting interface was not fully built up.[210]

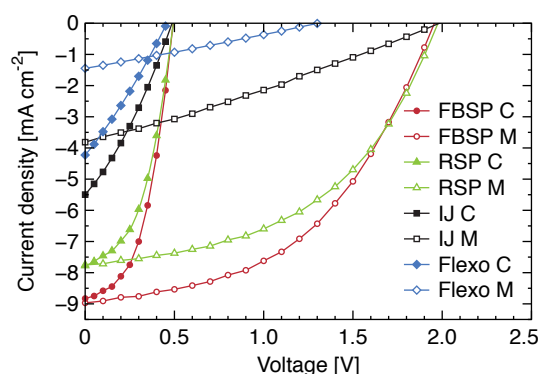


Figure 4.10.: J-V-curves of single cells and modules prepared with different back electrode printing methods. Adapted from [164] © 2013 WILEY-VCH Verlag GmbH & Co. KGaA, Weinheim

Table 4.2.: Solar cell and module parameters for each back electrode printing method. Adapted from [164] © 2013 WILEY-VCH Verlag GmbH & Co. KGaA, Weinheim

Method	Single cell					Module (4 cells)				
	A [cm ²]	V _{OC} [V]	J _{SC} [mA cm ⁻²]	FF [%]	PCE [%]	A [cm ²]	V _{OC} [V]	J _{SC} [mA cm ⁻²]	FF [%]	PCE [%]
FBSP	6	0.49	-8.82	48.4	2.10	24	1.96	-8.97	53.8	2.09
RSP	6	0.49	-7.77	46.8	1.79	24	1.98	-7.75	48.1	1.84
IJ	7	0.49	-5.49	31.0	0.83	28	1.98	-3.81	28.7	0.54
Flexo	6	0.46	-4.22	28.2	0.55	24	1.31	-1.44	26.3	0.12

4.3.3. Conclusion

Based on the results from the printing runs and the good solar cell performance it can be concluded that screen printing is the most robust method for the R2R fabrication of silver back electrodes. The interaction with the underlying surface characteristics is negligible due to lay-down of the thick and sticky ink paste. Rotary screen printing provides very high speeds using an appropriate drying system and has the advantage of gapless prints.

The interaction of flexo and inkjet printed silver ink, in this case water-based ink, with the pre-printed layers is very challenging due to their surface morphologies and ink attraction. Both methods potentially need a redevelopment of the PEDOT:PSS layer that is smoother and thinner to avoid the edge phenomena. Furthermore, the silver ink must be carefully evaluated to show a higher degree of compatibility. Both methods can achieve very high speeds once a compatible ink is found.

A recommended silver ink for flexo printing on the current thick PEDOT:PSS obviously needs higher viscosity, a higher degree of thixotropy, and high volume anilox rollers to decrease the surface interaction effects as can be observed during screen printing. The implementation of flexo printing for silver back electrodes is now carried out on the rollcoater, where full layer or grids are successfully printed by simply using solvent-based screen printing paste.[190, 199, 206] The proof of concept using screen printing paste (PV410, DuPont) for large-scale R2R flexo printing of back electrodes on thick PEDOT:PSS has been carried out for fully printed thermoelectric devices, where the silver layer was printed with 10 m min⁻¹. [408] An application for the fabrication of organic solar cells should be promoted.

4.4. Encapsulation

After the successful R2R fabrication of the complete OPV layer stack under ambient conditions it is the logical step to employ R2R encapsulation procedures for finishing the device fabrication, so that it withstands environmental impacts and shows long functional stability.

The stability and lifetime of organic solar cells still lacks a complete understanding of the involved processes such as photo-oxidation, photo-chemical processes, morphology

changes, and the interaction of interface layers, so that several reviews cover the whole spectra of this particular field of interest.[39, 409–412] Nevertheless, improvements in the OPV design and processing led to devices with lifetimes of several thousand hours.

The number of studies on the physical device encapsulation, especially on R2R large-scale processes, is rather small compared to the thousands of publications on OPV devices. It was shown that flexible barrier foils with medium water vapor transmission rates (WVTR) of $10^{-3} \text{ g m}^{-2} \text{ day}^{-1}$ or better are sufficient enough to enable lifetimes of several years, which is much less than the often proclaimed golden rule of $10^{-6} \text{ g m}^{-2} \text{ day}^{-1}$ for OLED devices.[413]

Flexible high performance barrier films are mostly organic–inorganic multilayer structures to increase the gas diffusion path length between occurring defects in the inorganic layer.[414–418] Rigid glass would be the ideal barrier, but cannot be handled in a R2R fashion, although highly flexible R2R-processible glasses (Corning Willow glass) entering the market and need to be tested for OPVs.[419] So far, glass is used for the encapsulation of small lab-scale devices but it has been shown for the manual encapsulation of large R2R produced polymer solar cells to enable building integrated photovoltaics (BIPV).[209]

The majority of small electro-optical demonstrators and test devices are encapsulated with stainless steel lids or glass sheets in conjunction with epoxy resins.[158, 420–424] Further encapsulation methods and procedures that have been studied are nanocomposite coatings,[425] polyurethane,[426] atomic layer deposition (ALD),[427–429] multilayer barriers with nitrogen spacers,[430] plasma-enhanced physical vapor deposition (PECVD),[431] parylene polymeric coatings,[432] stacked graphene,[433] and just solution-processed UV epoxy resins,[434] but they are all far from any practical application. Further reviews covering the broad range of encapsulation methods for OPV devices can be found elsewhere.[415, 435]

Here, large-scale R2R encapsulation procedures, namely UV-curable adhesive, hot-melt, and pressure sensitive adhesives (PSA), are evaluated that are not only practical relevant but also improve the stability against mechanical impacts, which is questionable for ultra thin film encapsulation such as graphene or ALD. Ultimately, the encapsulation speed should be in the same range or faster than all pre-processed layers to offer an efficient industrial upscaling potential. This section focuses on the experimental study of mechanical encapsulation methods using R2R lab equipment rather than on fundamental degradation processes.

4.4.1. Experimental

The solar cell modules used in this study were based on Flextrode substrate and the IOne concept as described earlier.[41, 43] Here, all layers were directly printed on barrier foil (Amcor Ceramis) with a thickness of $72 \mu\text{m}$, WVTR $0.04 \text{ g m}^{-2} \text{ day}^{-1}$, and OTR $0.01 \text{ cm}^3 \text{ day}^{-1} \text{ bar}^{-1}$. The solar cell layer stack comprised of Flextrode|P3HT:PCBM| $2 \times$ PEDOT:PSS|Ag, whereby all layers were fabricated with the known R2R procedures described earlier. Instead of honeycomb grids a slanted comb grid was used for front and back electrode to minimize the amount of direct overlaps.

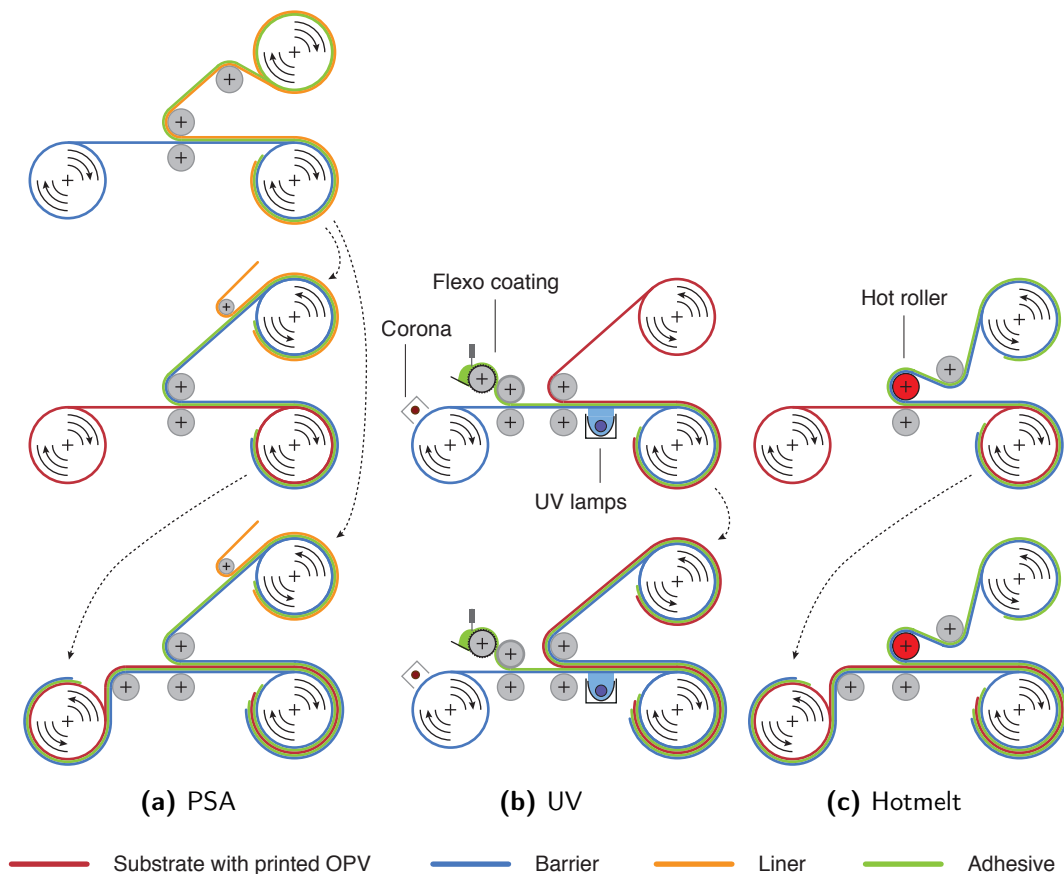


Figure 4.11.: Simplified schematics of three different R2R encapsulation strategies with its process flow from top to bottom. The dotted arrows symbolize the roll change during back- and frontside lamination.

The encapsulation was carried out using full R2R processes and three different adhesive strategies, namely PSA, UV-curable adhesive, and hotmelt. The barrier foil for encapsulation was the same as used for the solar cell substrate. Two sets of test modules were fabricated in which one had only a single backside lamination covering the printed layers and another set was double encapsulated with a backside and a second frontside lamination to enable edge-sealing with a 10 mm wide rim.[436] The UV-blocking layer on the Flextrode had been removed manually prior double-side encapsulation. The process workflow is illustrated in Figure 4.11 while photographs are shown in Figure 4.12.

The PSA encapsulation process required a pre-process where the barrier foil was laminated with the adhesive and a release liner. The adhesive was based on acrylate polymers (3M 467 MP, 60 μm) and laminated to the barrier at as speed of 20 m min^{-1} . The lamination onto the solar cell substrate was carried out at the same speed, whereas the final strength of the adhesive was achieved after some hours of resting time.

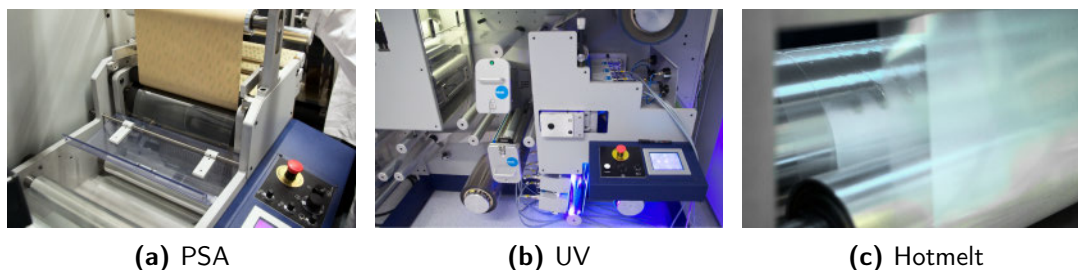


Figure 4.12.: Photographs of three different R2R encapsulation processes. (a) The PSA is laminated onto the barrier foil. (b) Photograph of the UV lamination machine. (c) Close-up of the melted hotmelt.

The high-viscous and solvent-free UV-curable epoxy resin (DELO LP655) was directly applied onto the corona-treated barrier foil prior entering the encapsulation nip using a flexo coating unit with an anilox volume of 30 ml m^{-2} . The R2R UV-curing was carried out at a speed of 2 m min^{-1} using a custom-built UV-LED lamp bank (DELO DELOLUX 20, 400 nm, 200 mW cm^{-2}) to achieve the recommended minimum exposure time of 16 s over the whole substrate width. The final thickness after curing was about $20 \mu\text{m}$, whereas the full strength was achieved within 24 h after exposure.

Hotmelt encapsulation was carried out at a speed of 1 m min^{-1} and a roller temperature of 140°C for a wrinkle-free lamination. The thick polyester-based hotmelt adhesive film (Glutex AU130, $145 \mu\text{m}$) had been applied onto the barrier foil prior encapsulation. A long melting zone was achieved by wrapping the foil around the hot roller ($\varnothing 95 \text{ mm}$) for an angular contact length of more than 200° . The adhesive film alone was highly flexible and stretchable but rather stiff in the final sandwich structure of the encapsulated solar cell. The smooth barrier film was not very sticky to the hotmelt and it showed tendencies of delamination upon bending the final device.

The encapsulated samples were tested under a solar simulator at 1000 W m^{-2} AM1.5G (ISOS-L-1 testing protocol,[437]) and an external cooling with a fan to a temperature of about 35°C . Each module consisted of 4 serially connected cells with a total active area of 28 cm^2 and an initial PCE of around 1.6%. The solar cell parameters were frequently measured with a Keithley 2400 Sourcemeter over a period of 900 h.

4.4.2. Results and discussion

Processing

Comparing the pure lamination speeds it was shown that the PSA method is superior to all other processes with 10–20× faster encapsulation and ease of handling, but taking the pre-lamination into account it is only 5–10× faster. The effective speed was cut down to 10 m min^{-1} . The sticky PSA does not allow coarse cross-directional alignment during the lamination run, which causes large wrinkles.

The UV-curable adhesive was directly applied during the lamination run and did not need any pre-processes. In theory, the barrier foil can be changed on-the-fly. The

current setup and choice of adhesive limited the speed to 2 m min^{-1} but can be increased by adding more LED lamps, increasing the temperature of the adhesive, and by choosing fast-curing adhesives with exposure time down to 1 s. Another UV-curable acrylic adhesive (DELO LP415) was tested as well and had much shorter curing times but showed destructive behavior on the active layer when not cured fast enough. It is the right choice for frontside laminations on the blank film. LP655 did not show any effects on the printed layers and could be left uncured for minutes without any negative interactions. The UV light exposes the adhesive through the barrier foil with applied UV-blocking filter (cut off at 380–390 nm). The adhesive used here cures within 320–440 nm, whereby a 365 nm irradiation would be the most efficient. The 400 nm light won't be cut off by the barrier and was therefore the only choice. The matching of the barrier filter, absorption of the photo-initiators, and the UV lamps is critical for an efficient upscaling to fast curing speeds. Once the adhesive is exposed with UV light it will cure further under visible light and will reach their final strength after 24 h in ambient atmosphere. The advantage of using UV light was the instant annealing during the lamination process. The solar cells showed very good J-shaped I–V-curves without inflection from the beginning, which was not the case for PSA and hotmelts.

The direct application of hotmelt on the substrate can only be carried out with special equipment such as heated slot-die heads or rollers, and would typically be outsourced to specialists and purchased as ready-to-use lamination foil. This process was emulated in-house by attaching a hotmelt foil to the barrier foil. Lamination above 1 m min^{-1} led to increased wrinkling and could only be minimized with highly increased web tension. The usage of thin hotmelts would most likely avoid these problems and allow higher speeds. The very thick hotmelts (probably too thick) were used to ensure bubble-free encapsulation on the textured printed layer, which has been observed with standard office lamination pouches during experimental tests. Industrial hotmelt processes run at high speeds with several tens of meters per minute and based on the results this process could see further application in the encapsulation of OPV.

A further advantage of UV-curable adhesives is the possibility to vary the coating thickness. The other methods are fixed to one thickness that has been applied onto the barrier. The $20 \mu\text{m}$ thick adhesive layer corresponded to a consumption of 28 g m^{-2} but could be easily adapted to other adhesive requirements by using other anilox cylinders. Other deposition methods such as slot-die coating or roll-coating would work as well. A second advantage of using the flexographic printing method is the possibility of a patterned adhesive deposition.

The encapsulation with PSA causes a lot of waste due to the protective liner made from polycoated kraft paper. It will be removed from the prepared barrier foil prior entering the lamination rollers and cannot be reused. Wastage of UV-curable adhesive is negligible for long runs because it is applied in a control way. The disadvantage is cleaning the machinery with solvents, whereby the PSA and hotmelt methods are dry processes.

Stability and lifetime

It has been shown in prior studies that double side edge-sealing is superior compared to single side lamination.[436] Another report showed that UV-curable adhesive is slightly better than PSA for edge-sealed devices.[198] Nevertheless, it was never shown if single backside lamination would be suitable enough, once the frontside is already based on a barrier foil. It could significantly cut down the energy payback time but also shorten the process time and lower the costs.[3]

The edge-sealing showed no bleaching of the active layer after >900 h of constant illumination. It was expected to observe the bleaching for single side encapsulation with all three adhesives but it only appeared on the PSA-based devices. Hotmelt devices had only very small areas of bleaching at the open edge, whereas modules with UV-curable adhesive showed no bleaching at all as can be seen in Figure 4.13. A possible reason is the dense structure of the epoxy resin or melted glue that has no impurities as the PSA. It has a much rougher surface once released from the liner, which will later on transform to tiny air inclusions during the lamination process as can be seen in Figure 4.13d. These homogeneously distributed inclusions had volumes <450 pl and might act as an additional starting point for an accelerated bleaching. The bleaching study already showed that single backside lamination could be already enough to reach a comparable lifetime to fully edge-sealed devices. Ultimately it should be the goal to produce a solar cell where the functional layers never reach the substrate edge. Then the single-side lamination itself acts as edge-sealing after cutting the modules.

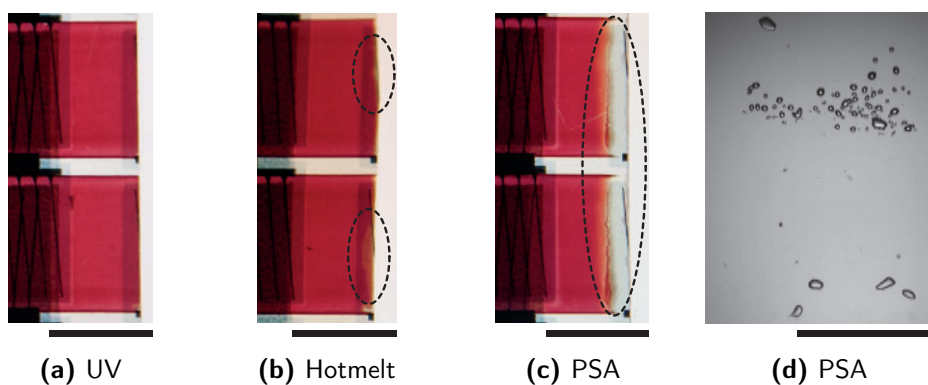


Figure 4.13.: (a-c) Edge bleaching behavior of single-side encapsulated modules. (d) Microscopic photograph of air inclusion in the PSA layer. Scale bar is 10 mm (a-b) and 1 mm (d). Adapted from [305] © 2013 WILEY-VCH Verlag GmbH & Co. KGaA, Weinheim.

The lifetime study has been carried out on various samples and the following datasets represent the average solar cell parameters of three samples per encapsulation method. All samples had been light-soaked for 24 h for stabilization of the parameters (burn-in) followed by the 900 h test period, which is shown Figure 4.14. The efficiency decreased linear for all samples from around 200 h onwards which is caused by the usage of the same barrier foil on all devices. The drop in degradation had its reason in the different encapsulation methods.

The degradation rate for UV-curable adhesive was the same for single side and double side encapsulation, and the best compared to all other methods with a T_{80} of >1000 h after burn-in. The edge-sealed PSA devices had a slightly faster degradation than the UV samples, which was already shown in a prior study.[198] The V_{OC} of these 3 device types was almost stable over the full test period. The hotmelt device with single side encapsulation had also good lifetime performance but showed a decreased voltage over time, which potentially came from the very thick adhesive and a higher oxygen uptake.

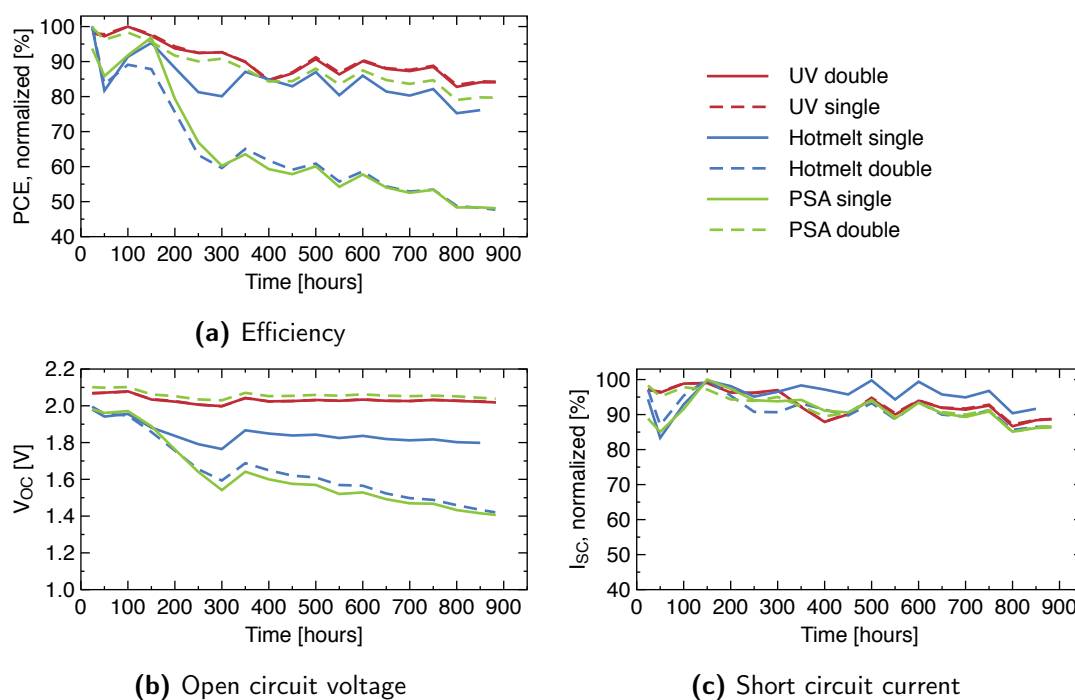


Figure 4.14.: Lifetime study of single and double-side encapsulated modules with three different adhesives. Adapted from [305] © 2013 WILEY-VCH Verlag GmbH & Co. KGaA, Weinheim.

The significantly faster degradation of the PSA single-side and the hotmelt double-side device was mainly due to the loss of voltage over time. The large bleaching of the active layer in the PSA device revealed poor barrier properties of the adhesives at the open edge, which causes oxygen ingress over time. The poor performance of the hotmelt device might come from the preparation process where it was heated twice and fed under high web tension leading to unpredictable interaction of the printed layers with the adhesive. The modules were tested furthermore on single cell level and it was shown that the voltage drop was caused by a voltage decrease over all cells and not just a single cell. Contact problems could therefore be excluded. The low decrease in current over the whole test period was very similar for all devices and encapsulation methods.

The drawback of the hotmelt was the whitish/opaque appearance that blocked some light through the frontside in the double-sealed devices. The adhesive color for just backside laminated devices is irrelevant. The flexibility was good except for the hotmelt devices this but should be improved by using much thinner adhesives.

4.4.3. Conclusion

The comparison of three adhesive types and two encapsulation schemes clearly showed that a single-side lamination with UV-curable adhesive is sufficient enough for organic solar cells that are directly fabricated on barrier foil. Extra layers of barrier foil can be avoided which lower the embodied energy, weight, and processing time significantly. Lamination with PSA outperformed all other methods in direct processing speed but it required pre-processing and double-side edge-sealing to reach similar lifetime performance. This produced not only more waste caused by the release liner but also decreased the effective speed significantly. The highest upscaling potential can be seen in fast-curing UV-curable adhesives or improved UV lamp setups with a higher dose. Hotmelt was good for single side lamination and could see more process improvements with thinner hotmelt layers and direct inline application of the glue during the lamination, which requires suitable equipment for coating hotmelts.

Single-side lamination has the advantage for very large modules where the ratio of open edges to module area is negligible. The solar cell modules based on the Infinity concept are 100 m long and the active layer has contact with the edge just on a length of <0.6 m.[43, 99] Although this save a lot of processing time and cost it was shown that a subsequent edge-sealing improves the handling and mechanical robustness.

Nevertheless, single-side encapsulation is very useful to produce cheap demonstrator modules as shown for the freeOPV modules.[107] Although the slot-die coated active layer has edge contact it was ensured that the distance to the active part of the module is large enough. In an ideal process everything would be printed in patterns so that no functional layer would ever have contact with the module edge. In this case single-side lamination could act as a true edge-seal.

5. Large-scale OPV installation scenarios and operation

So far, OPV cells and modules are basically fabricated with lab-scale methods and in small sizes. The maximum size of R2R produced modules was in the range of A3 sheets, just limited by the machinery and stripe-like layout based on patterned ITO-PET substrate. Although a lot of application scenarios such as BIPV are claimed to be the future throughout the OPV community, there is a lack of actual deployments beyond tiny dummy demonstrators.^a A fair exception should be made for the former company "Konarka Technologies" (filed for bankruptcy in 2012) that actually produced and sold OPV based solar modules. They even presented large installations for energy production with a solar powered bus stop shelter in San Francisco as the most prominent example.^b The theoretical maximum power was most likely in the range of $70 W_{\text{peak}}$ or less based on reverse engineering of available photographs and product datasheets (8 modules at $P_{\text{max}} = 8.6 W$).^c The projected energy production for 300 shelters was 43.000 kWh annually, but only one was ever built! Another example was a car park solar canopy with 30 flexible modules of most likely around $22.3 W_{\text{peak}}$ each, which adds up to $1338 W_{\text{peak}}$ under ideal conditions. One bottleneck of the modules produced by Konarka was the manual sheet-based finishing of the devices that required significant labour hours, which could be seen as a critical drawback in their upscaling plans.[407]

Large-scale produced flexible OPVs are still way behind the small record devices, not to mention 1st generation PV technology, and will probably never compete with them in efficiency. With full additive solution-based processing and the Infinity concept on hand, it will be shown here how to deploy OPV devices for actual large power output in the kW range. The whole infrastructure needs to be considered and put into account to justify OPV for energy production with low embodied energy and energy payback times (EPBT). Four concepts in form of a solar park, on- and offshore solar tubes, and a balloon will be described from the application and installation point of view. The full lifecycle assessment (LCA) and environmental impact assessment calculation will not be covered here in detail and are described just briefly with major numbers such as EPBT.[99, 438] Installation and performance evaluation covers the first half of this chapter while a failure mode analysis in the second half shows critical problems that appeared in the current

^aPress release Fraunhofer IAP: <http://www.iap.fraunhofer.de/en/Pressemitteilungen/2013/press-releases3.html> (12.12.2013)

^bThe website www.konarka.com is not accessible anymore due to the bankruptcy. The case-study can be downloaded using archive.org Internet Archive: https://web.archive.org/web/20120201092240/http://www.konarka.com/media/pdf/konarka_casestudy_sanfrancisco.pdf (07.12.2013)

^cPower Plastic 20 Series, datasheet: https://web.archive.org/web/20120516140525/http://konarka.com/media/pdf/konarka_20series.pdf (07.12.2013)

generation of devices with high power output. Nevertheless, destroyed modules can be easily repaired using methods described here. The whole chapter is based on four principal publications that describe the Infinity proof of concept, solar park, deployment scenarios, and failure modes.[43, 99, 438, 439]

5.1. Installation scenarios

First attempts in grid-connected OPVs were made in 2009 and showed the disadvantages of low performing large-scale organic solar cell modules during that time.[440] Individual ITO-based and R2R produced modules were cut from the roll, manually connected and encapsulated using the same glass panel manufacturing methods employed in the traditional silicon-based solar industry. It was shown that system costs and time consumption for the panel assembly cannot be justified for OPVs with low efficiency to fulfill cost-efficient energy production and scalability.

To overcome these bottlenecks the truly scalable Infinity concept was developed that employed only two points of contact independently from the module size. It avoids rigid glass encapsulation and allows very fast installation and maintenance so that low power conversion efficiency can be accepted. The main purpose was to enable energy production with minimized system EPBTs.

5.1.1. Solar park

The advantage of the Infinity concepts is the handling of rolls with discrete units of solar cells that can be directly rolled out. Tedious cutting of single cells or small submodules from the roll and manual wiring is avoided. The high voltage system with low current densities enables thin external wires to keep material usage and embodied energy low, while installation of high power producing OPV modules as a single unit ensures little labour during the setup.



Figure 5.1.: Panorama photograph of the first row of the solar park with six parallel installed solar cell modules of 100 m length each. Adapted from [99] © 2013 WILEY-VCH Verlag GmbH & Co. KGaA, Weinheim.

To demonstrate the potential for true energy production the solar cells were installed in a solar park with an overall mounting capacity of 1000 m². A panoramic view of the front-facing platform with 6 installed modules can be seen in Figure 5.1. The structure located on DTU Risø campus (N56.6962°–E12.1041°) is actually so big that it can be

clearly identified using satellite imagery.^d It comprises four wooden scaffold structures with wooden plates that face south with an inclination angle of 38°. Up to seven modules with a width of 305 mm can be mounted side-by-side on each of the four 100 m long platforms.

The installation of the modules directly from the roll enabled very fast mounting times exceeding 100 m min^{-1} , which is faster than the overall manufacturing speed of the solar cell module (1 m min^{-1}). To achieve this, the roll was mounted on a customized wagon that moved over the platform without touching the modules as can be seen in Figure 5.2. It was manually pushed along the platform but a motorized version with even higher installation speed would be the further development. Two tape dispensers enabled a simultaneous edge fixation of the module while rolling out. Installation was performed without any problems under different weather conditions including bright sunshine, light rain, and high wind loads. Special care was necessary considering the fact that handling with high voltage systems is very dangerous and only possible for trained people. Once the modules were illuminated, even under overcast conditions, high voltage developed that is invisible to the human eye. Safety precaution in form of protective gloves and full awareness of the risks was essential. The Infinity concept in this scale is therefore most likely reserved for professionals with appropriate background.

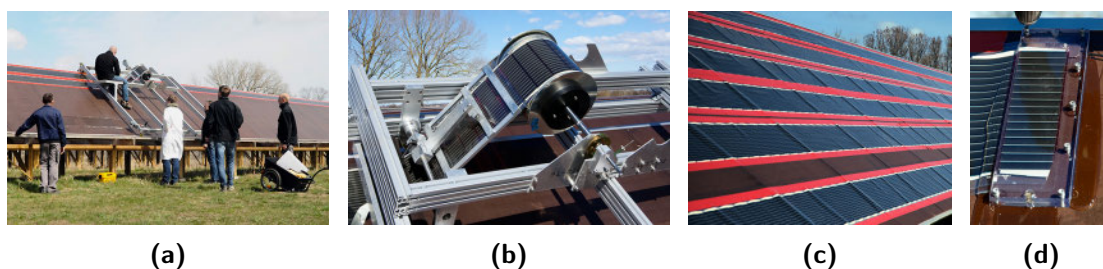


Figure 5.2.: (a) Roll mounting system with detailed photograph of the installation system (b) for rolling out and fixing the modules. (c) The solar cell modules are mounted on the wooden board and fixed with weather resistant duct tape (red). (d) Terminal connection at the end of a module. Adapted from [99, 438] © 2013 WILEY-VCH Verlag GmbH & Co. KGaA, Weinheim.

The electrical connection at the end of each module was carried out using PMMA panels and wired copper plates with soldered spikes that were punched through the barrier foil (Figure 5.2d). Polyurethane mixed on-site was used as sealant between the PMMA panels that were screwed onto the wooden panels. This method enabled a reliable, weather resistant and very fast connection. The installed modules were in connected to a resistive load for measurement purposes with results presented in Section 5.2.

A module with a length of 100 m delivered $>220 \text{ W}_{\text{peak}}$, which corresponded to an installation speed of $>200 \text{ W}_{\text{peak}} \text{ min}^{-1}$ just for the module. The installation time of under 1 min for a conventional silicon-based solar panel with the same power output would be hard to achieve. With the current installation concept it should be possible to install solar modules faster and less energy demanding than conventional panels, although a much larger land area is required due to the low efficiency.

^dSatellite view available on Google Maps, Bing Maps, and Apple Maps. Last time tested: 10.12.2013

Wooden base structures were used due to its origin as renewable source, corrosion resistance, durability, and $3\times$ lower emission rate than steel and concrete.[441] Life cycle assessment (LCA) calculations showed that the whole system of wooden scaffold, infrastructure, and OPV modules had an EPBT of only 6 month if placed in southern Europe.[99] The impact of the wood on the EPBT was found to be very little compared to the OPV modules considering the estimated structure lifetime of 15 years versus one year for the solar cells. It should be not noted that the risk of inflammation has to be taken into account and wood might not to be the best solution considering the fatal defects we observed in a later stage of the lifetime study and described in Section 5.3. PVC plates were additionally installed to prevent damages but were not as helpful as expected and increased the EPBT from 180 days to 320 days when located in a southern European location with $1700 \text{ kWh m}^{-2} \text{ yr}^{-1}$. [99, 439]

5.1.2. Alternative concepts

The installation of Infinity modules in the solar park configuration proved to be a successful concept for large-scale grid-power production with low environmental footprint but the pure size and investment of the structure could be seen as a barrier for the installation of such a setup. To provide energy in smaller scale and in search for lighter and fast deployable systems, three alternative concepts based on lightweight plastic-based structures had been developed and analyzed.[439] The concepts were offshore, onshore and airborne installations in form of air filled solar tubes and a flying balloon with mounted solar modules. The idea was not only to design sustainable solution but also to explore new territories for solar installation. A floating energy harvesting solution-based on OPV and very light structures can be a low cost alternative in terms of capital investment compared to rigid platform for heavy conventional modules. Additionally, open water provides installation area virtually for free while land mass is often rare or expensive. Furthermore, the onshore/offshore solar tubes and balloon concept could provide rapid response service and lightweight power supply for special applications as they can be easily transported anywhere without the risk of damage due to there flexibility.

The on- and offshore solar installation were based on self-supporting inflated tubes of low density polyethylene (LDPE) with a thickness of $200 \mu\text{m}$. To enable a leakage-free wiring a tube-in-tube method was developed, whereby the inner tube is fully seal after inflation. The Infinity module was cut into the desired length, placed between inner and outer tube, and kept in a fixed position once the inner tube was inflated and sealed. The outer tube was slightly longer to allow proper sealing and external fixation. The electrical wires were fed through the wrapped ends or directly through holes of the out tubes, which was later on taped.

All tube-module-tube units were prepared indoor and rolled up for further usage. The solar module length was between 3.4 and 10 m, which corresponds to a maximum V_{OC} of 1 kV. For the final installation outdoors the prepared units were rolled out and blown up in less than 5 s. The ends of the inner tube were closed using an automatic sealing machine. The inclination of the modules could be adjusted during the fixation of the units. The system's lifetime had been estimated with 2 years to calculate EPBT.

The offshore solar tubes were installed on the water at the pier of DTU Risø campus in the Roskilde Fjord and are shown in Figure 5.3b. The installation consisted of five parallel connected tubes with an active area of 5 m^2 that showed an efficiency of around 0.6% as summarized in Section 5.2.2. They were fixed with ropes to the pier to simulate the idea of a floating solar installation. Wind and waves were found to be the biggest problem that need to be solved in future installation concepts. Special care is necessary for the operation of electrical installations in wet environment as water and electricity is known to be very dangerous. Salt spray that might shade the solar cells was tested indoors and found to be less critical as it scatters the light and does not fully shadow the cells. The EPBT was calculated with 270 days.[439]



Figure 5.3.: Photographs of alternative solar cell installation concepts. Adapted from Ref. [439] with permission from The Royal Society of Chemistry.

A land-based onshore installation of the solar tubes was carried out in the area of the existing solar park. The prepared solar tubes unit were rolled out and blown up on-site. At first, six 3.4 m long module tubes (Figure 5.3a) were serially connected with six 6.8 m long ones to operate in the working range of the inverter (0.6–1 kV input voltage). Further extension with nine 10 m long modules gave a total active area of 25 m^2 and can be seen in Figure 5.5b. The long tubes were not inflated and kept flat on the ground due to difficulties in keeping the inclination stable. All tubes were parallel connected to enable a V_{OC} of around 1 kV and grid-connected with an inverter as described in Section 5.2.2. Wind and vegetation was found to be the challenging and could be handled through proper fixation and frequent gardening. The tubes were very resistant to rain water since it flows down immediately. The flat tubes as a subversion of the inflated tube concept should be kept tilted since water will be accumulated over time. Nevertheless, the short air-filled tubes were very stable even under heavy storm. The longer they are the more vulnerable they become to wind. The EPBT was calculated with 292 days.[439]

One could see the LDPE foil with an opaque/whitish appearance as a major drawback since it was covering the already low performing solar cells in the tubes but it was tested to be less critical. The transmittance was measured between 40 and 70% over the visible spectrum but the actual efficiency drop was considerably lower with just 8% as can be seen in Figure 5.4. The I_{SC} decreased by around 10% while the fill factor improved slightly. Although the foil showed a low transmittance it was believed that the efficiency could be kept high due to diffuse scattering of the transmitted light.

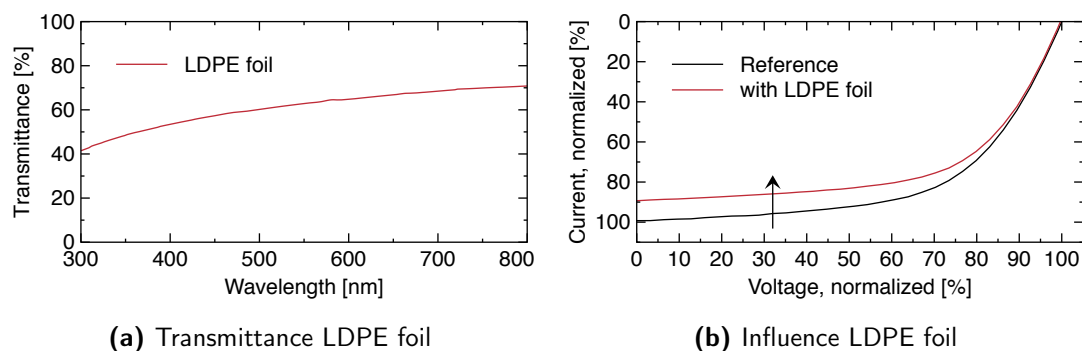


Figure 5.4.: (a) Transmittance of the LDPE foil was measured with 40–70%. (b) The actual effect on the solar cell performance is much lower than expected with just 10% loss in I_{SC} . Adapted from Ref. [439] with permission from The Royal Society of Chemistry.

The airborne installation scenario in form of a balloon with attached solar modules was kind of experimental but still successful. A possible application might be the powering of sensors and transmitters in weather balloons, or orbiting communication balloons,^e rather than grid-power generation. Foils of LDPE were sealed to a pillow-shaped balloon measuring 4 m×5 m along the edges while having a surface area of 40 m². The idealized volume was calculated to 17 m³ of Helium that would generate enough lift to raise the balloon itself plus 8 kg of additional load. Five Infinity modules with a combined active area of 2.5 m² were attached before filling the balloon. Cables of suitable length enabled a ground-based device characterization and power extraction. Finally, the balloon was filled with 16 m³ of Helium (Figure 5.5a) and raised to a height of roughly 10 m as can be seen in Figure 5.5b. The highly flexible and lightweight OPV modules were located on the top side of the balloon while be flattened due to the pressure of the balloon. The final inclination was adjusted during the fixation of the balloon using ropes on each corner. This experiment was carried out on a wind-free day since the ballon was very vulnerable to gusts of wind while tethered. The performance was shown to be good and presented in Section 5.2.2. The EPBT was calculated with 529 days but it should be noted that this kind of installation would never be made for long term power production.[439]

5.2. Performance

5.2.1. Solar park

Proof of concept

The first functional Infinity modules were produced before the solar park construction was finished. Some of the first long stretches were simply tested by rolling out on grass and characterized on voltage and current to get some rough numbers and the average amount of working cells.

^eIn 2013, Google started the Project Loon, a "balloon-powered internet for everyone"

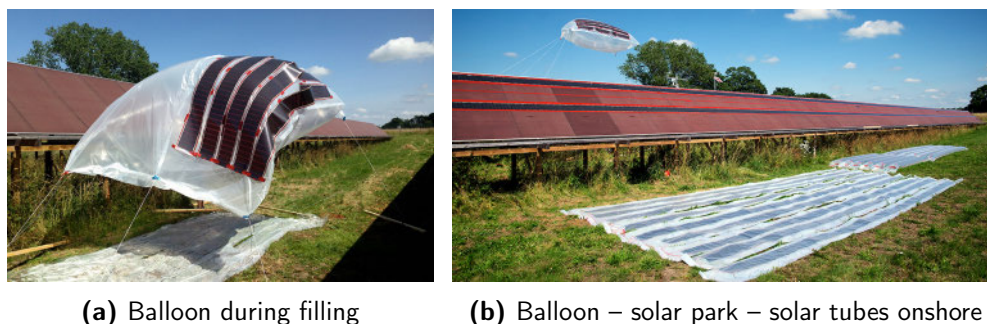


Figure 5.5.: Photographs of the alternative airborne solar installation in comparison to solar park and onshore solar tubes. Adapted from Ref. [439] with permission from The Royal Society of Chemistry.

After improving the fabrication yield the first test modules were manually taped on the wooden panels of the solar park construction. In the beginning the available equipment allowed only measurements with voltages up to 1000 V with the result of several destroyed multimeters due to underestimated performance of the modules. Later on, high voltage test probes with division factors of 1000× were used and allowed the use of standard multimeters for simple measurements.

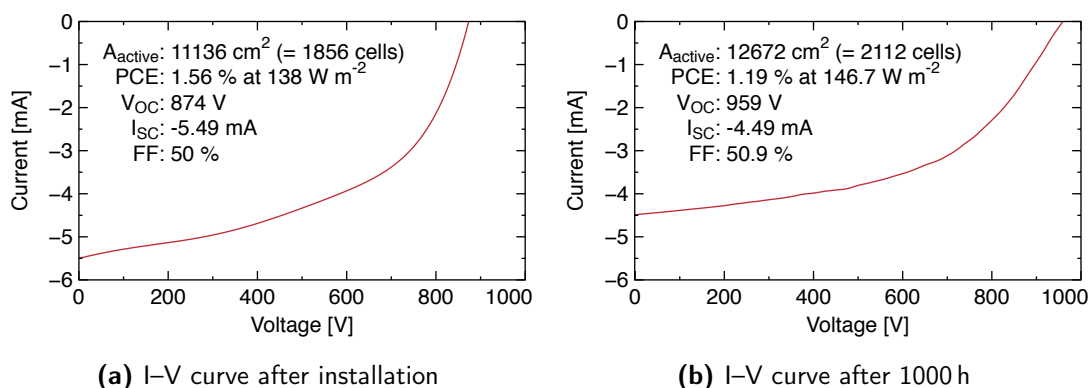


Figure 5.6.: Solar cell behavior of the first installed Infinity modules under overcast conditions. Adapted from [43] © 2013 WILEY-VCH Verlag GmbH & Co. KGaA, Weinheim.

The successful proof of concept was carried out on a 80 m long module with 16000 cells that had an $V_{OC} > 8100$ V. The module was based on the first generation grid design with honeycomb front electrodes and straight comb back electrodes. The maximum power point was measured through a resistive load and found to be at 125 W with a V_{OC} of 8.2 kV and a I_{SC} of -29 mA. A full I–V characterization as can be seen in Figure 5.6 was only possible on shorter modules with approximately 2000 cells and under overcast conditions to match the operating space of the source meter (Keithley 2410, 1000 V, 20 mA). The calculated efficiency was 1.56 % directly after installation and around 1.2 %

after 1000 h of outdoor operation. The fill factor was stable over the test period while the performance degradation was caused by a decreased current. The module was not optimized for operational stability and had just a backside lamination without a secondary edge-sealing. A smaller test module with just 80 cells was then fully edge-sealed using Amcor barrier foil and UV-curable adhesive to perform an accelerated indoor lifetime study under a solar simulator with 1000 W m^{-2} AM1.5G illumination and 85°C . The lifetime behavior over 1000 h can be seen in Figure 5.7. The T_{80} lifetime of 1350 h continuous illumination corresponds to more than one year of outdoor operation.

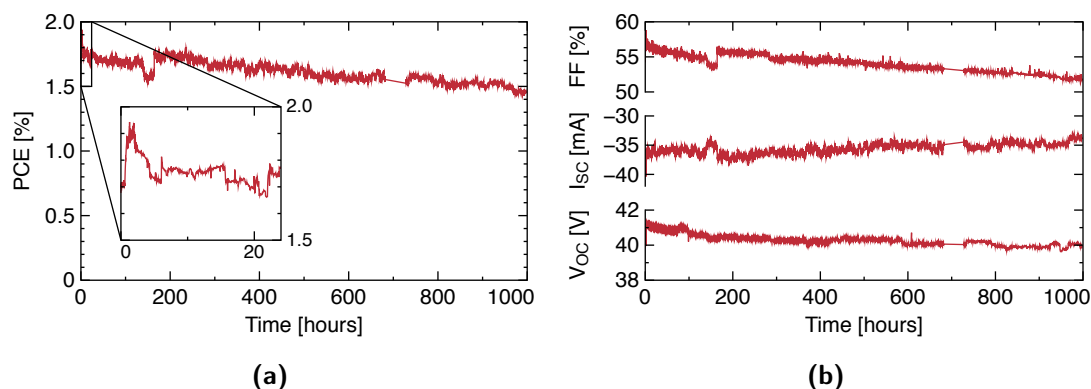


Figure 5.7.: Indoor lifetime study of a fully edge-sealed 80-cell Infinity module. (a) The T_{80} lifetime was calculated with around 1350 h (linear decay) after stabilization of the solar cell parameters in the first hours of operation (see insert). (b) The efficiency decay was mainly caused by a dropping fill factor and current. (a) Adapted from [43] © 2013 WILEY-VCH Verlag GmbH & Co. KGaA, Weinheim.

Large-scale installation

After successful testing smaller modules and one 80 m long module a set of six 100 m long modules were fabricated and installed as described before. The electrode design was based on the improved slanted grids for front and back electrode. The six modules with an overall cell count of around 126000 were connected in parallel and kept under resistive load for measurement purposes. At this time the transformation to $<1 \text{ kV}$ and grid-connection was not yet fully implemented for the 10 kV system.

The I–V characterization was performed by measuring voltage and current over a resistive load rather than doing an I–V sweep with a sourcemeter, which was not available in the parameter range. Sunny days without stable irradiance were chosen to avoid large fluctuation during the data collection. The I–V behavior of one module over its lifetime can be seen in Figure 5.8a. The PCE on the day of installation was measured with above 2% but dropped within the first days to a stabilized level of around 1.7%. The high fill factor of above 60% over the whole lifetime showed that it is possible to serially connect at least 21000 cells without significantly affecting the performance. Frequent measurements over 3000 h as can be seen in Figure 5.8b showed high stability with a calculated

T_{80} lifetime of around 3630 h (151 d) after stabilization and under the assumption of a linear decay. The cell temperature was measured with around $45\text{ }^{\circ}\text{C}$ under bright sun. Furthermore, the power output on sunny days with an irradiance around 1000 W m^{-2} never dropped below $200\text{ W}_{\text{peak}}$.

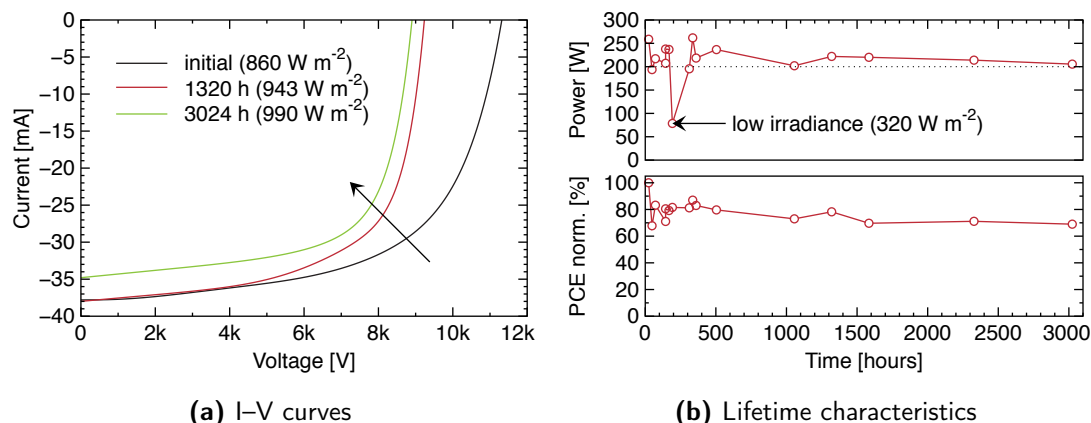


Figure 5.8.: (a) Solar cell characteristics of a single module with 14.7 m^2 active area. (b) PCE behavior and power output on a sunny day over 3000 h of outdoor operation. (b) Partially adapted from [99] © 2013 WILEY-VCH Verlag GmbH & Co. KGaA, Weinheim.

A characteristic I–V and power curve of a solar array with 6 parallel connected modules and an active area of 88.2 m^2 can be seen in Figure 5.9. The PCE and FF was calculated with 1.53% and 54%, respectively. The power output was in the range of $1330\text{ W}_{\text{peak}}$ for an irradiance of 990 W m^{-2} , which is an average of nearly $222\text{ W}_{\text{peak}}$ per module. The maximum output for a single module could be measured with around $260\text{ W}_{\text{peak}}$. The slightly lower performance of the module array was due to loss in fill factor and open circuit voltage caused most likely of a mismatch of the modules and the external electrical connection. The measurements show that it was possible to build a high power solar array with a minimum amount of terminal connections and wiring.

5.2.2. Alternative concepts

Beside the installation of the modules in the solar park some other experimental deployment concepts had been carried out. The offshore/onshore solar tubes and the balloon with solar panels were successfully deployed and characterized. The advantage of the Infinity concept is the variability in length so that it was possible to customize the panels for each application.

The five parallel connected solar tubes in the offshore configuration and the balloon were characterized by measuring voltage and current through a resistive load. The I–V curves and the solar parameters are shown Figure 5.10. Although the modules on the water were faced south to gain maximum irradiance the efficiency was rather low. The most likely reason was that some modules were partly shadowed and due to the handling

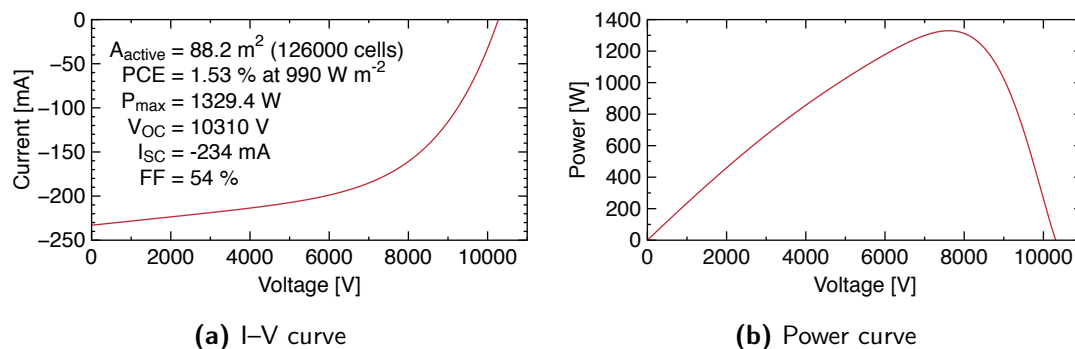


Figure 5.9.: Characteristics of 6 parallel connected modules at an irradiance of 990 W m^{-2} . The power output was in the range of $1330 \text{ W}_{\text{peak}}$. Adapted from [99] © 2013 WILEY-VCH Verlag GmbH & Co. KGaA, Weinheim.

while setting up the tubes on the water. Furthermore, the modules were already in use on the solar park on removed to build the tubes. The waves, although very small, caused some fluctuation in the current measurement and inclination. The V_{OC} of 657 V implied that all cells of a module contributed to the power generation. Measurement of the I_{SC} of each single solar tube showed almost the same current. The experiment revealed that waves and wind were the most critical factors of the design and that a stable platform might be beneficial to minimize mechanical impact.

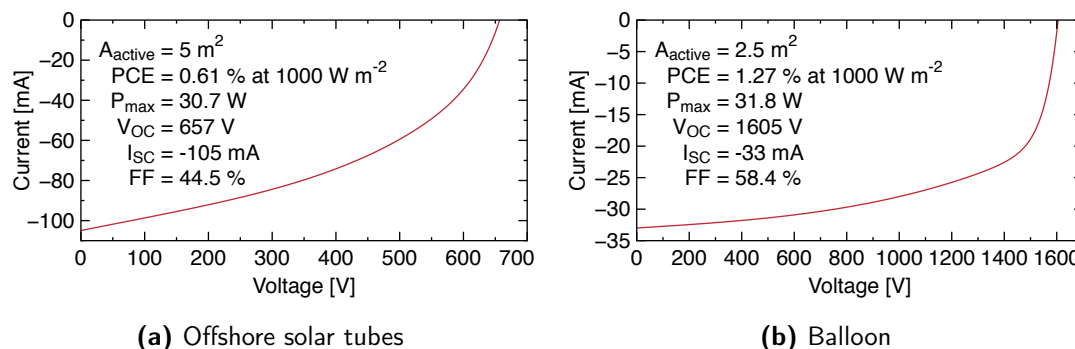


Figure 5.10.: Solar cell characteristics of alternative deployment strategies. Adapted from Ref. [439] with permission from The Royal Society of Chemistry.

The balloon with attached solar panels was a very experimental installation scenario but proved to be functional although it was far away from any practical application at this stage of the experiment. The high flexibility of the modules was very beneficial during the filling. Once the balloon was properly filled it was lifted and the side with the modules was faced towards the sun. The design did not allow proper inclination of all modules but the I-V measurement as shown in Figure 5.10b revealed acceptable results. The five modules were serially connected to a high voltage array with an V_{OC} of $>1600 \text{ V}$ and an output of nearly $32 \text{ W}_{\text{peak}}$. The PCE was calculated with 1.27 % for an active

area of 2.5 m^2 . The pronounced J-shape most likely came from the somehow wavy solar panels and inhomogeneous illumination. Wind and ballon movements made it difficult to measure the I–V characteristics under stable conditions.

The solar tubes mounted on ground next to the solar park were not characterized regarding the standard solar parameters. Here, the modules were directly grid-connected using a Danfoss TLX 6 kW inverter to actually generate electricity for the Danish power grid. Although the majority of the tubes were not inflated and the inclination was not perfect the modules with an overall active area of 25 m^2 could deliver around 200 W on average at a sunny day. The energy production and irradiance between July 7th and August 12th 2013 is shown in Figure 5.11. Irradiance data was recorded using a pyranometer on a solar tracker and not with the fixed pyranometer in the solar park. The record energy production per day was above 1 kWh with an accumulated output of 18 kWh over 5 weeks. Fast growing grass produced some shadow over time and had to be cut down. Heat and thermal expansion of the air filling caused some change in the inclination over time, which led to full shadowing of some modules. Manual adjustment had a noticeable impact on the output, which can be seen at point B in Figure 5.11. The rise in energy production was not necessarily related to the irradiance at this specific day. The energy production was not recorded further beyond the 5-week period.

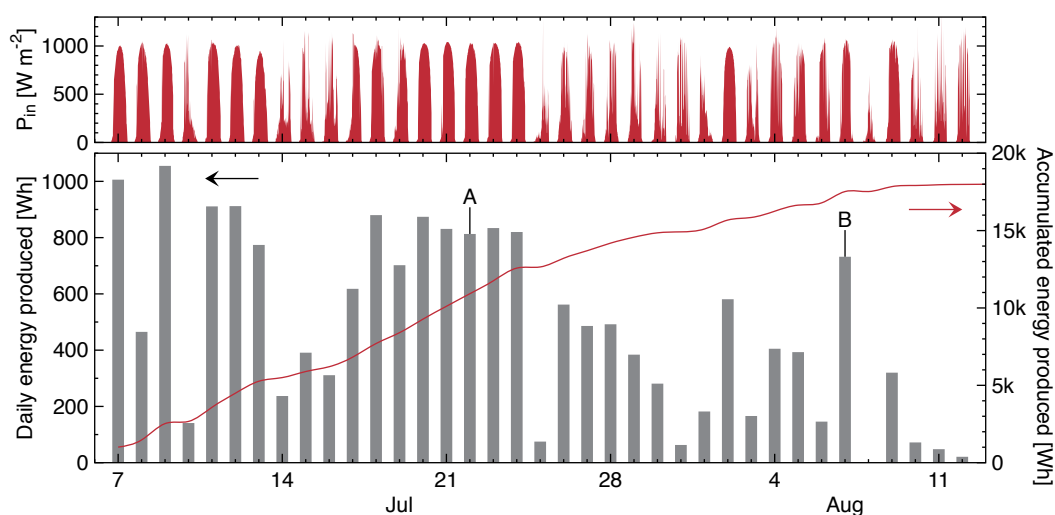


Figure 5.11.: Irradiance (top), daily energy production, and accumulated energy production of the onshore solar tubes over a duration of 5 weeks during summer 2013. At point A grass was cut and at point B the modules were adjusted additionally.

5.3. Failure modes and repair procedures

Until recently, actual large-scale power producing installations never really existed, with the consequence of limited to zero experience throughout the OPV community. The solar

bus shelter example based on 8 connected low-voltage high-current modules produced roughly 70 W, which is less than 1/3 of the output of just one large Infinity module presented here. The operation of such high power OPV devices was a completely new field and cannot be compared with any small lab-scale cells, which are typically operated under very low voltage and current. These lab operation modes will never lead to the fatal defects presented here but should be taken into account by anyone who is aiming to install OPV for energy production. Conventional PV systems are of high power and multiple defect scenarios have been observed due to the large installation base. Typical defects in silicon-based modules are shading, weak soldering, cracking, delamination, hot-spots, overheating, backsheet burn-throughs, and metal grid oxidation, which in worst case can lead to costly mass replacements of hundreds of modules in a solar park.[442–444]

It has been reported that R2R produced OPV modules with BIPV-like glass encapsulation can surpass strict IEC-61646 environmental chamber tests but they lacked of any practical high power output.[209] It will be shown here that similar defect scenarios known from silicon solar modules, namely delamination, punctures, hot-spots, water ingress, and burns can also appear on plastic foil based OPV installations that employ the high power producing Infinity module. All modules were tested under typical Danish weather conditions including heavy rain, thunderstorms, heat, and high irradiance.

5.3.1. Mechanical failures

The defects shown here are directly related to the high power production but also to the sheer amount of installed OPV modules that had a potential impact area of roughly 360 m². At this dimension the chance of scratches and punctures of the barrier is rather high. Animal behavior such as birds with claws and sharp beaks needs to be considered as well, although never directly observed. Bird drops were noticed in large amount and acted as partial shadows. A negative influence on the barrier properties might be the case over long term.

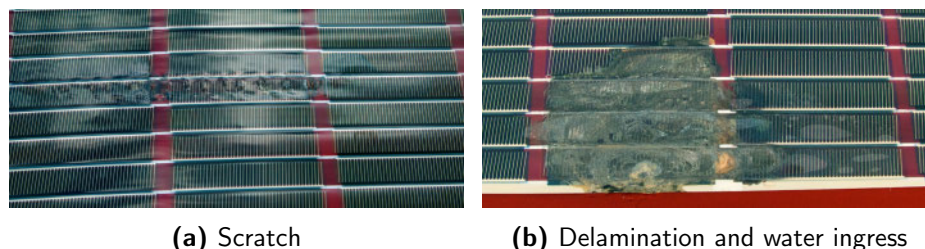


Figure 5.12.: Large-scale defects induced by (a) unintended scratching during installation and (b) delamination from the bottom side with subsequent water ingress. Adapted from [438] © 2013 WILEY-VCH Verlag GmbH & Co. KGaA, Weinheim.

Some delamination appeared after few thousand hours of operation considering the fact that the total edge length of the modules was 2400 m. Punctures, scratches and delamination were starting point for water and oxygen ingress that destroyed the layer interfaces, bleached active layers, dissolved PEDOT:PSS and oxidized the silver electrodes as shown in Figure 5.12. The defects tend to grow if not repaired.

5.3.2. Electrical failures, hot-spots, burns

Quality control of the OPV modules under operational conditions was carried out with IR thermal imaging methods (Fluke Ti125) to scan hundreds of square meters in short time. IR imaging is a common practice for conventional PV plants and can be performed using commercially available equipment.[442, 445] It was a reliable method to identify abnormal temperatures (hot-spots) caused by electrical failures that were not optically visual at first sight. Sample images of the inspection are shown in Figure 5.13. The hot-spots with an elevated temperature were clearly detectable at various locations inside the cells but also outside the active area in the printed silver electrodes.

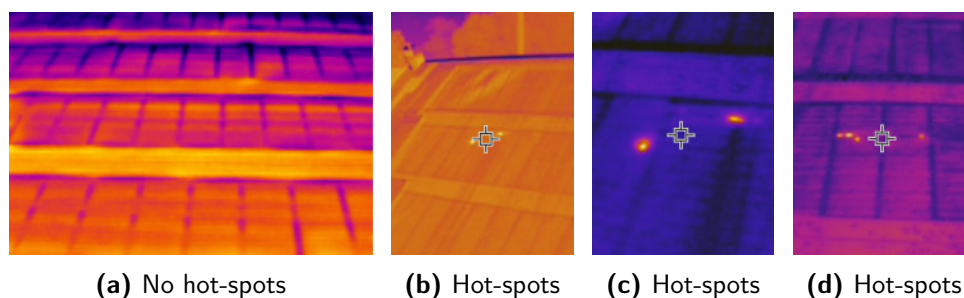


Figure 5.13.: IR imaging photographs of OPV modules under operational conditions. (b) Adapted from [438] © 2013 WILEY-VCH Verlag GmbH & Co. KGaA, Weinheim.

After the hot-spots had been located they could be studied in detail, whereby the spots inside the cells were caused by tiny burns in the area of direct overlap of the front and back electrode grid fingers as can be seen in Figure 5.14a - 5.14c. In the particular area the cell got shunted and the current started to accumulate at point of low resistance, followed by a localized heat increase. A reasonable failure source might be spikes from the printed silver grids, or pinholes in the intermediate layers that lower the distance between the front and back electrode grid. Unfortunately, it was impossible to further investigate the reasons *post mortem*. The temperature was above the melting point of the employed substrate and barrier foils, which was later on destroyed around the hot-spot. Such puncturing of laminates is a known problem in silicon-based PV system as well.[442] Another burn was observed outside the active area close to the edge (see Figure 5.14d) and it was investigated that the foil had been delaminated leading to water ingress. In this case electrical arcs between the high voltage electrode and the underlying mounting structure might have ignited the foil.

Another burning phenomena appeared outside on the flexo printed guidelines the cells, which was used for coating head registration and not cut off for some of the modules. These lines were not directly electrically connected but had been the source of propagating burns as can be seen in Figure 5.14e. The reason was found again in localized delamination and water ingress that led to standing arcs between the conductive line and the mounting structure. Arc lengths of 10 mm could be easily observed at the end of a freshly cut module. The guidelines had been removed for modules installed later.

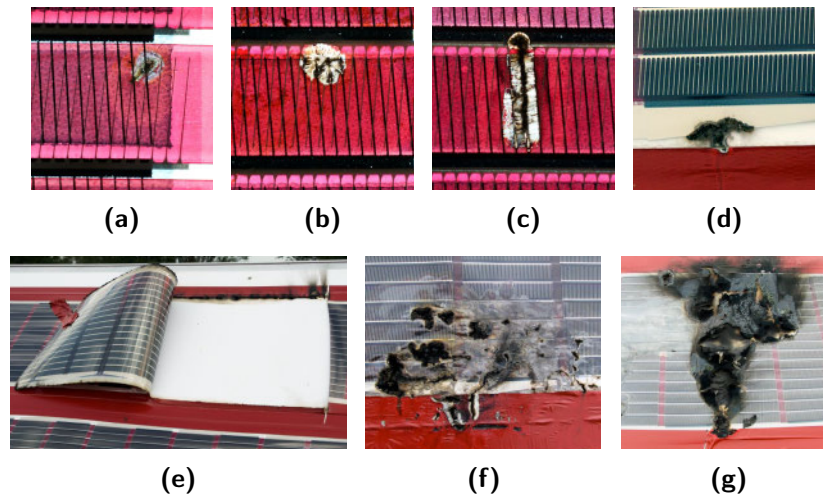


Figure 5.14.: Various burns observed for the modules under operational conditions most likely caused by shunts between front and back electrode (a-c), delamination and water ingress (d). Flipped module with a burned guideline on the topside (e). Large burns were spotted after thunderstorms and due to propagating small burns (f,g). Adapted from [438] © 2013 WILEY-VCH Verlag GmbH & Co. KGaA, Weinheim.

Quite surprisingly and not expect in such extent was that thunderstorms and heavy rain had the most fatal impact. An actual physical record of a lightning striking the solar cell array was never recorded but it was most likely that a lightning must have struck the construction or nearby and introduced a high electrical potential into the modules. In consequence, several fatal burns with multiple ignition points were distributed randomly over a large part of the array. The nature of solar cell is that they are "On" whenever light shines upon them, which can lead to rapid defect growth. The plastic foil starts to melt around an igniting hot-spot and will creep until extinguished by wind or rain. A glass encapsulation might reduce some of the problems but limits the upscaling capacities and increases embodied energy.

After observing the burns it was interesting to know how much they actually affect the solar cell parameters. Controlled indoor burning tests using a lighter on modules with 80 cells showed that small burn holes had only minor impact on the performance, whereby the fill factor was lowered by introducing a tiny kink close the maximum power point as can be seen in Figure 5.15a and Table 5.1. V_{OC} got slightly increased and I_{SC} was not lowered much as one would expect from the loss of active area. The I-V behavior of a module with a fully burned cell showed similarities to a module with a fully shadowed cell as can be seen in Figure 5.15b. The loss in I_{SC} was just around 10% and showed the strong contribution of the other cells in the module. The I-V curve had a strong inflection point with a sharp kink around V_{OC} .

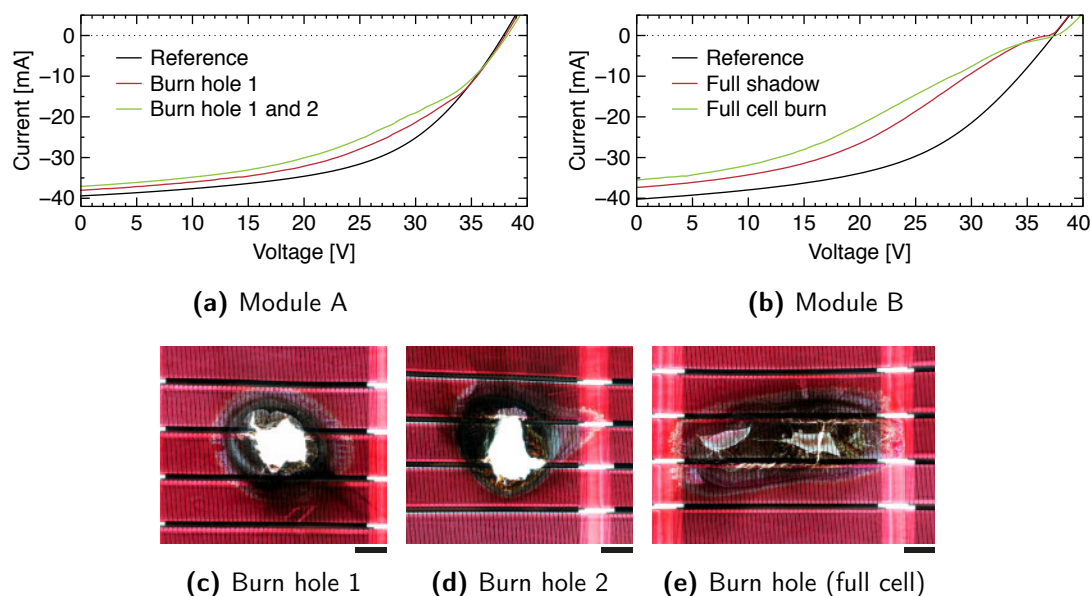


Figure 5.15.: Forced burning test on modules with 80 serially connected cells. The I–V curves of module A (a) show just small changes from burn hole 1 (c) and 2 (d), while module B (b) has a strong inflection point due to a full burned cell (e). Scale bar is 10 mm. Adapted from [438] © 2013 WILEY-VCH Verlag GmbH & Co. KGaA, Weinheim.

The forced burning tests on the relatively small module did not lead to any open circuit and the module was still functional with decreased performance. The burn holes in the high voltage outdoor module tended to grow further while the cell was still electrically connected. In some cases sparks could be seen that slowly melted the plastic foil but the following repair procedures prevented further damages.

5.3.3. Repair procedures

In case conventional wafer-based modules fail they need to be replaced completely, which can be very costly. The replacement of a single cell in the glass encapsulated module is not practical or not even possible. On the other hand, the flexible modules based on the Infinity concept allow fast repair procedure in case critical damages appear.

Scratches from the installation and identified punctures that are not critical could be covered with a second piece of barrier foil, pressure sensitive adhesive and some polyurethane to prevent water ingress. The damages were successfully closed without further evolution of the defects over time. Larger defects such as burn holes or delaminated areas that already affected the functionality of the module were removed by cutting the defective stretch out of the module. Short parts could be rewired using the same end connector plates, whereas larger stretches could be replaced with a fresh module as can be seen in Figure 5.16. The new module stretch was connected on each side with the known PMMA plates with copper inserts and spikes that punched through the foil and reconnected the printed silver electrodes. For each replacement using the cut & replace method only 16 cells per connection were lost, which is only 0.15% of a 100 m long module with 21000 cells.

Table 5.1.: Solar cell parameters of a forced burning test on modules with 80 serially connected cells. Adapted from [438] © 2013 WILEY-VCH Verlag GmbH & Co. KGaA, Weinheim.

	V_{OC} [V]	I_{SC} [mA]	FF [%]	PCE [%]
Module A	37.8	-39.4	53.6	1.33
+ Burn hole 1 (Fig. 5.15c)	38.0	-38.1	48.2	1.16
+ Burn hole 1 + 2 (Fig. 5.15c + 5.15d)	38.2	-37.1	45.0	1.06
Module B	37.4	-40.2	49.3	1.24
+ Shadowed cell	37.0	-37.3	38.4	0.88
+ Burned cell (Fig. 5.15e)	37.5	-35.5	33.3	0.74

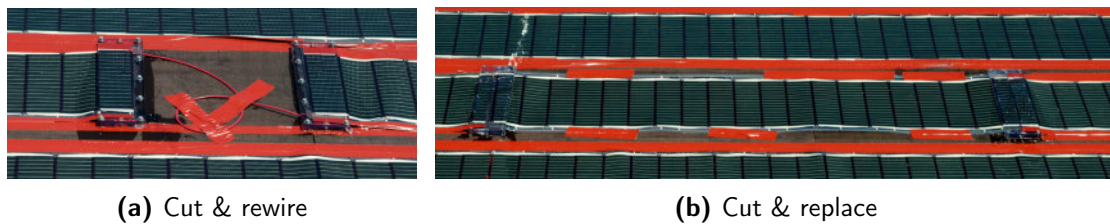


Figure 5.16.: Simple repair procedures of an Infinity module. Adapted from [438] © 2013 WILEY-VCH Verlag GmbH & Co. KGaA, Weinheim.

The operational stability of a 100 m long module was good and the power output on a cloud-free day never dropped below $205 W_{peak}$ during 3000 hours.[99] The first module withstood even heavy rainfall and thunderstorm without any impact. After 4000 h (166 days) the first burn holes appeared and needed to be fixed without replacing the whole module. The module was cut and rewired multiple times with an overall loss of around $0.5 m^2$ active area. The repaired module could still produce $>150 W_{peak}$ ($P_{in} = 920 W m^{-2}$) after half year of outdoor operation while having a decreased fill factor. The corresponding I–V and power curves are shown in Figure 5.17.

The repair procedures presented here clearly show the opportunities of large-scale OPV installations although they still have a lot of challenges to be solved. The defects itself have only minor impact on the performance if the size is smaller than a single cell. Large defects can be repaired using simple methods, whereby an expensive replacement of a complete module is not necessary.

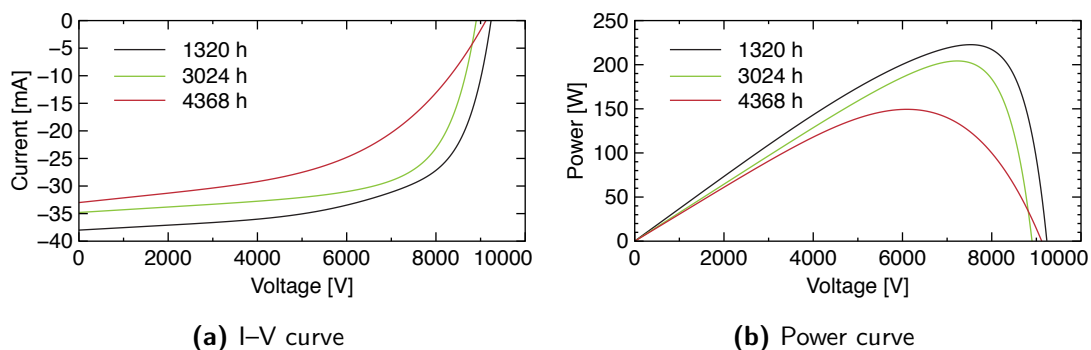


Figure 5.17.: Power and I–V curves of a module at a sunny day after 1320 h (5 d), 3024 h (126 d), and repaired after 4368 h (182 d) of outdoor operation. Adapted from [438] © 2013 WILEY-VCH Verlag GmbH & Co. KGaA, Weinheim.

6. Conclusion & outlook

This PhD thesis successfully describes the upscaling achievements of organic solar cells to device sizes that actually allow real power production beyond "gadget-size". One crucial step was the introduction of the ITO-free Flextrode electrode that can be printed and coated in very fast speeds. Currently available materials enable only low efficiencies of around 2% in a full ambient printing and coating process with the result that module sizes have to be huge for high power output, or small modules have to be manually wired. With the introduction of the Infinity concept it was possible for the first time to produce modules in virtually infinite large sizes. Special designed electrode layouts allowed a high voltage serial connection of thousands of single solar cells entirely through R2R printing and coating processes.

The best way to conclude the upscaling achievements is through a graphical illustration of the modules sizes fabricated throughout the time of this PhD thesis (see Figure 6.1). Several solar cell modules with lengths of 100 m (width 0.3 m) and 21000 serially connected cells could be produced and deployed in a solar park. Modules with an active area of 14.7 m² produced >220 W_{peak} with just two terminal connectors – no manual wiring or soldering was necessary. Up to 6 parallel-connected modules had an output of >1300 W_{peak}. Although the efficiency was <2% on the active area, it was proved to be viable concept that had energy payback times under half a year including the wooden solar park structure. Further deployment concepts such as solar tubes were tested and 18 kWh of energy could be fed back into the Danish power grid.

Working with high voltage and high power modules also revealed new challenges. First of all, handling with high voltage devices is dangerous and needs special awareness and training. Secondly, some new failure modes appeared in form of burning solar cells that nobody ever saw before or was not willingly to show. Although some fatal defects occurred it was possible to easily repair non-working parts of a module without replacing the whole module.

Important points that should be addressed in the future are better contacting schemes, improved encapsulation, higher efficiency and lifetime, and increased geometrical fill factors of the printed cells and modules on the substrate. Furthermore, the full implementation of the high voltage transformation to a voltage range that the inverter can handle has to be improved. The literature study about R2R compatible printing and coating methods also revealed some new interesting concepts that should be tested for a future large-scale OPV fabrication.

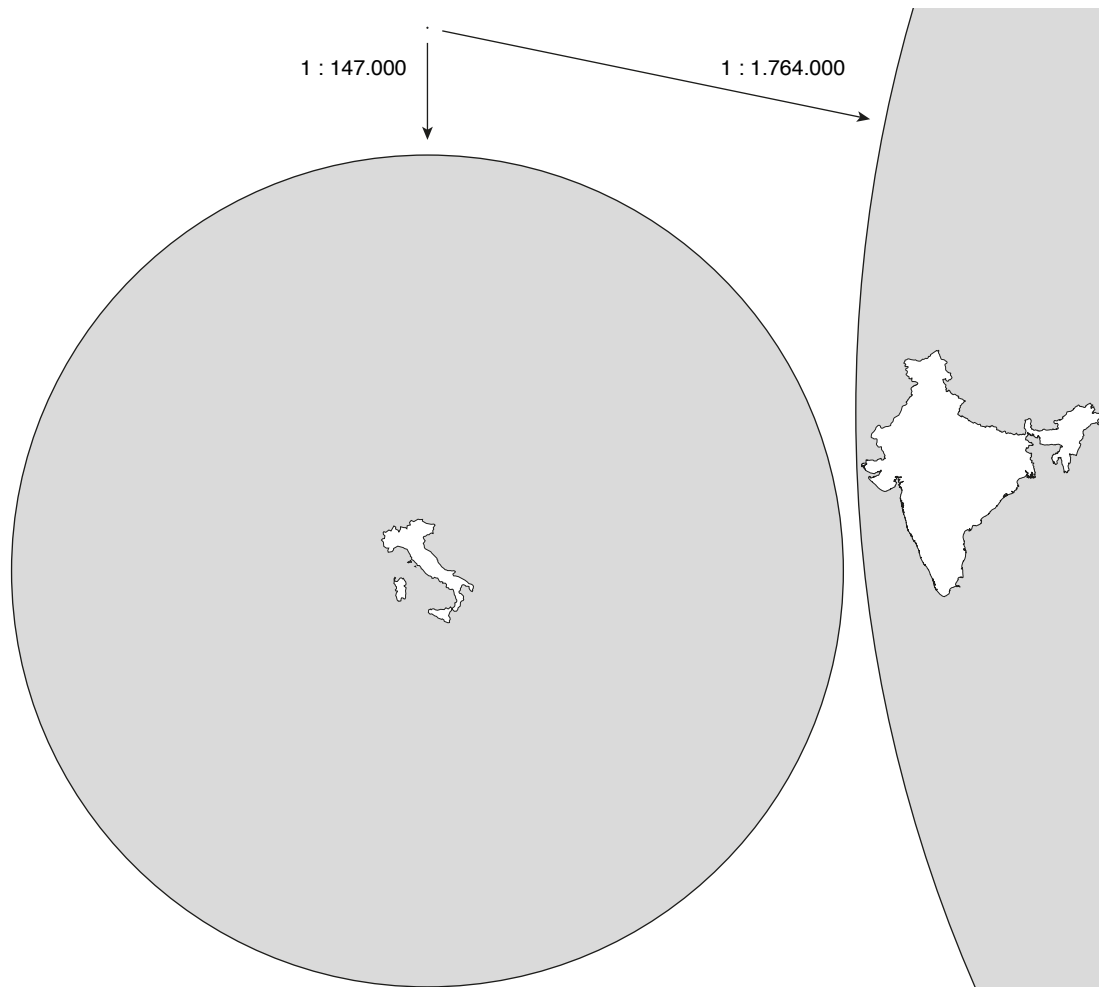


Figure 6.1.: Graphical illustration of the enormous upscaling achievements carried out with the Infinity solar cell module layout. It illustrates the upscaling of a 1 cm² solar cell (small dot) to a 100 m long solar cell module with 21000 serially connected cells and an active area of 147000 cm² (14.7 m²). Furthermore, it shows a secondary upscaling by a factor of 12 that illustrates twelve installed and tested Infinity modules during this PhD study (176 m²). Roughly the same scaling can be achieved when the area of Monaco is compared to Italy, and almost whole of India at full scale.

Bibliography

- [1] S. B. Darling and F. You, The case for organic photovoltaics, *RSC Adv.*, 2013, **3**, 17633–17648.
- [2] J. Nelson and C. J. M. Emmott, Can solar power deliver?, *Philosophical Transactions of the Royal Society A: Mathematical, Physical and Engineering Sciences*, 2013, **371**, 20120372.
- [3] N. Espinosa, M. Hösel, D. Angmo and F. C. Krebs, Solar cells with one-day energy payback for the factories of the future, *Energy Environ. Sci.*, 2012, **5**, 5117–5132.
- [4] M. A. Green, Silicon solar cells: state of the art, *Philosophical Transactions of the Royal Society A: Mathematical, Physical and Engineering Sciences*, 2013, **371**, 20110413.
- [5] K. L. Chopra, P. D. Paulson and V. Dutta, Thin-film solar cells: an overview, *Prog. Photovolt: Res. Appl.*, 2004, **12**, 69–92.
- [6] M. A. Green, K. Emery and Y. Hishikawa, Solar cell efficiency tables (version 42), *Prog. Photovolt: Res. Appl.*, 2013, **21**, 827–837.
- [7] C. Kost, T. Schlegl, J. Thomsen, S. Nold and J. Mayer, *Levelized Cost Of Electricity Renewable Energies*, Fraunhofer Institute for Solar Energy Systems ISE technical report, 2012.
- [8] J. Gong, J. Liang and K. Sumathy, Review on dye-sensitized solar cells (DSSCs) Fundamental concepts and novel materials, *Renewable and Sustainable Energy Reviews*, 2012, **16**, 5848–5860.
- [9] M. Riede, T. Mueller, W. Tress, R. Schueppel and K. Leo, Small-molecule solar cells - status and perspectives, *Nanotechnology*, 2008, **19**, 424001.
- [10] C. Deibel and V. Dyakonov, Polymer–fullerene bulk heterojunction solar cells, *Reports on Progress in Physics*, 2010, **73**, 096401.
- [11] J. Nelson, Polymer:fullerene bulk heterojunction solar cells, *Mater. Today*, 2011, **14**, 462–470.
- [12] A. J. Heeger, 25th Anniversary Article: Bulk Heterojunction Solar Cells: Understanding the Mechanism of Operation, *Adv. Mater.*, 2014, **26**, 10–28.
- [13] F. C. Krebs, Fabrication and processing of polymer solar cells: A review of printing and coating techniques, *Sol. Energy Mater. Sol. Cells*, 2009, **93**, 394–412.
- [14] C. Tang, Two-layer organic photovoltaic cell, *Appl. Phys. Lett.*, 1986, **48**, 183–185.
- [15] N. S. Sariciftci, D. Braun, C. Zhang, V. Srdanov, A. Heeger, G. Stucky and F. Wudl, Semiconducting polymer-buckminsterfullerene heterojunctions: Diodes, photodiodes, and photovoltaic cells, *Appl. Phys. Lett.*, 1993, **62**, 585–587.

- [16] H. Spanggaard and F. C. Krebs, A brief history of the development of organic and polymeric photovoltaics, *Sol. Energy Mater. Sol. Cells*, 2004, **83**, 125–146.
- [17] C. J. Brabec, V. Dyakonov and U. Scherf, *Organic Photovoltaics*, Wiley-VCH, 2008.
- [18] F. C. Krebs, *Polymer Photovoltaics: A Practical Approach*, SPIE Publications, 2008.
- [19] H. Hoppe and N. S. Sariciftci, Organic solar cells: An overview, *J. Mater. Res*, 2004, **19**, 1924–1945.
- [20] M. Helgesen, R. Søndergaard and F. C. Krebs, Advanced materials and processes for polymer solar cell devices, *J. Mater. Chem.*, 2010, **20**, 36–60.
- [21] J. D. Servaites, M. A. Ratner and T. J. Marks, Organic solar cells: A new look at traditional models, *Energy Environ. Sci.*, 2011, **4**, 4410–4422.
- [22] T. Ameri, G. Dennler, C. Lungenschmied and C. J. Brabec, Organic tandem solar cells: A review, *Energy Environ. Sci.*, 2009, **2**, 347–363.
- [23] T. Ameri, P. Khoram, J. Min and C. J. Brabec, Organic Ternary Solar Cells: A Review, *Adv. Mater.*, 2013, **25**, 4245–4266.
- [24] R. C. Chiechi, R. W. A. Havenith, J. C. Hummelen, L. J. A. Koster and M. A. Loi, Modern plastic solar cells: materials, mechanisms and modeling, *Mater. Today*, 2013, **16**, 281–289.
- [25] P. W. M. Blom, V. D. Mihailetschi, L. J. A. Koster and D. E. Markov, Device Physics of Polymer:Fullerene Bulk Heterojunction Solar Cells, *Adv. Mater.*, 2007, **19**, 1551–1566.
- [26] J. Halls, K. Pichler, R. Friend, S. Moratti and Holmes, AB, Exciton diffusion and dissociation in a poly(p-phenylenevinylene)/C60 heterojunction photovoltaic cell, *Appl. Phys. Lett.*, 1996, **68**, 3120–3122.
- [27] A. Haugeneder, M. Neges, C. Kallinger, W. Spirkl, U. Lemmer, J. Feldmann, U. Scherf, E. Harth, A. Gügel and K. Müllen, Exciton diffusion and dissociation in conjugated polymer/fullerene blends and heterostructures, *Phys. Rev. B*, 1999, **59**, 15346.
- [28] J. Piris, T. E. Dykstra, A. A. Bakulin, P. H. M. v. Loosdrecht, W. Knulst, M. T. Trinh, J. M. Schins and L. D. A. Siebbeles, Photogeneration and Ultrafast Dynamics of Excitons and Charges in P3HT/PCBM Blends, *J. Phys. Chem. C*, 2009, **113**, 14500–14506.
- [29] E. Bundgaard and F. C. Krebs, Low band gap polymers for organic photovoltaics, *Sol. Energy Mater. Sol. Cells*, 2007, **91**, 954–985.
- [30] M. C. Scharber, D. Mühlbacher, M. Koppe, P. Denk, C. Waldauf, A. Heeger and C. J. Brabec, Design Rules for Donors in Bulk-Heterojunction Solar Cells-Towards 10 % Energy-Conversion Efficiency, *Adv. Mater.*, 2006, **18**, 789–794.
- [31] L. Koster, V. Mihailetschi and P. W. M. Blom, Ultimate efficiency of polymer/fullerene bulk heterojunction solar cells, *Appl. Phys. Lett.*, 2006, **88**, 093511.
- [32] M. C. Scharber and N. S. Sariciftci, Efficiency of bulk-heterojunction organic solar cells, *Progress in Polymer Science*, 2013, **38**, 1929–1940.

- [33] C. Kästner, B. Muhsin, A. Wild, D. A. M. Egbe, S. Rathgeber and H. Hoppe, Improved phase separation in polymer solar cells by solvent blending, *J. Polym. Sci. B Polym. Phys.*, 2013, **51**, 868–874.
- [34] Y. Yao, J. Hou, Z. Xu, G. Li, Y. Yang and S. Inc, Effects of Solvent Mixtures on the Nanoscale Phase Separation in Polymer Solar Cells, *Adv. Funct. Mater.*, 2008, **18**, 1783–1789.
- [35] A. Gaur and P. Kumar, An improved circuit model for polymer solar cells, *Prog. Photovolt: Res. Appl.*, 2013.
- [36] B. Qi and J. Wang, Open-circuit voltage in organic solar cells, *J. Mater. Chem.*, 2012, **22**, 24315–24325.
- [37] J. Kim, K. Kim, S. H. Ko and W. Kim, Optimum design of ordered bulk heterojunction organic photovoltaics, *Sol. Energy Mater. Sol. Cells*, 2011, **95**, 3021–3024.
- [38] F. C. Krebs, S. A. Gevorgyan and J. Alstrup, A roll-to-roll process to flexible polymer solar cells: model studies, manufacture and operational stability studies, *J. Mater. Chem.*, 2009, **19**, 5442–5451.
- [39] M. Jørgensen, K. Norrman, S. A. Gevorgyan, T. Tromholt, B. Andreasen and F. C. Krebs, Stability of Polymer Solar Cells, *Adv. Mater.*, 2012, **24**, 580–612.
- [40] N. Espinosa, R. García-Valverde, A. Urbina and F. C. Krebs, A life cycle analysis of polymer solar cell modules prepared using roll-to-roll methods under ambient conditions, *Sol. Energy Mater. Sol. Cells*, 2011, **95**, 1293–1302.
- [41] M. Hösel, R. R. Søndergaard, M. Jørgensen and F. C. Krebs, Fast Inline Roll-to-Roll Printing for Indium-Tin-Oxide-Free Polymer Solar Cells Using Automatic Registration, *Energy Technology*, 2013, **1**, 102–107.
- [42] J.-S. Yu, I. Kim, J.-S. Kim, J. Jo, T. T. Larsen-Olsen, R. R. Søndergaard, M. Hösel, D. Angmo, M. Jørgensen and F. C. Krebs, Silver front electrode grids for ITO-free all printed polymer solar cells with embedded and raised topographies, prepared by thermal imprint, flexographic and inkjet roll-to-roll processes, *Nanoscale*, 2012, **4**, 6032–6040.
- [43] P. Sommer-Larsen, M. Jørgensen, R. R. Søndergaard, M. Hösel and F. C. Krebs, It is all in the pattern - high efficiency power extraction from polymer solar cells through high voltage serial connection, *Energy Technology*, 2013, **1**, 15–19.
- [44] R. Po, C. Carbonera, A. Bernardi and N. Camaioni, The role of buffer layers in polymer solar cells, *Energy Environ. Sci.*, 2011, **4**, 285–310.
- [45] K. Zilberberg, J. Meyer and T. Riedl, Solution processed metal-oxides for organic electronic devices, *J. Mater. Chem. C*, 2013, **1**, 4796–4815.
- [46] Y.-j. Lee, J. Yi, G. F. Gao, H. Koerner, K. Park, J. Wang, K. Luo, R. A. Vaia and J. W. P. Hsu, Low-Temperature Solution-Processed Molybdenum Oxide Nanoparticle Hole Transport Layers for Organic Photovoltaic Devices, *Adv. Energy Mater.*, 2012, **2**, 1193–1197.

- [47] N. Espinosa, H. F. Dam, D. M. Tanenbaum, J. W. Andreasen, M. Jørgensen and F. C. Krebs, Roll-to-Roll Processing of Inverted Polymer Solar Cells using Hydrated Vanadium(V)Oxide as a PEDOT:PSS Replacement, *Materials*, 2011, **4**, 169–182.
- [48] A. Ng, X. Liu, W. Y. Jim, A. B. Djurišić, K. C. Lo, S. Y. Li and W. K. Chan, P3HT : PCBM solar cells-The choice of source material, *J. Appl. Polym. Sci.*, 2014, **131**, –.
- [49] M. T. Dang, L. Hirsch and G. Wantz, P3HT:PCBM, Best Seller in Polymer Photovoltaic Research, *Adv. Mater.*, 2011, **23**, 3597–3602.
- [50] R. R. Søndergaard, M. Hösel and F. C. Krebs, Roll-to-Roll fabrication of large area functional organic materials, *J. Polym. Sci. B Polym. Phys.*, 2013, **51**, 16–34.
- [51] R. Søndergaard, M. Hösel, D. Angmo, T. T. Larsen-Olsen and F. C. Krebs, Roll-to-roll fabrication of polymer solar cells, *Mater. Today*, 2012, **15**, 36–49.
- [52] A. A. Tracton, *Coatings Technology*, CRC Press, Boca Raton, FL, 2007.
- [53] H. Kipphan, *Handbook of print media*, Springer Verlag, Berlin Heidelberg New York, 2001.
- [54] S. F. Kistler and P. M. Schweizer, *Liquid Film Coating*, Springer Science+Business Media, Dordrecht, 1997.
- [55] S. Magdassi, *The chemistry of inkjet inks*, World Scientific Publishing, Singapore, 2010.
- [56] O. A. Basaran, H. Gao and P. P. Bhat, Nonstandard Inkjets, *Annual Review of Fluid Mechanics*, 2013, **45**, 85–113.
- [57] S. F. Pond, *Inkjet technology and product development strategies*, Torrey Pines Research, Carlsbad, 2000.
- [58] L. Wengeler, M. Schmitt, K. Peters, P. Scharfer and W. Schabel, Comparison of large scale coating techniques for organic and hybrid films in polymer based solar cells, *Chemical Engineering and Processing: Process Intensification*, 2013, **68**, 38–44.
- [59] B. Derby, Inkjet Printing of Functional and Structural Materials: Fluid Property Requirements, Feature Stability, and Resolution, *Annual Review of Materials Research*, 2010, **40**, 395–414.
- [60] D. E. Riemer, The Theoretical Fundamentals of the Screen Printing Process, *Microelectronics International*, 1989, **6**, 8–17.
- [61] M. Hösel, D. Angmo and F. C. Krebs, in *Handbook of organic materials for optical and optoelectronic devices*, Woodhead Publishing Ltd, Sawsten, 2013, pp. 473–507.
- [62] G. H. Han, S. H. Lee, W.-G. Ahn, J. Nam and H. W. Jung, Effect of shim configuration on flow dynamics and operability windows in stripe slot coating process, *J Coat Technol Res*, 2014, **11**, 19–29.
- [63] C.-F. Lin, B.-K. Wang, S.-H. Lo, D. S.-H. Wong, T.-J. Liu and C. Tiu, Operating windows of stripe coating, *Asia-Pac. J. Chem. Eng.*, 2014, **9**, 134–145.
- [64] F. C. Krebs, Polymer solar cell modules prepared using roll-to-roll methods: Knife-over-edge coating, slot-die coating and screen printing, *Sol. Energy Mater. Sol. Cells*, 2009, **93**, 465–475.

- [65] M. Schmitt, P. Scharfer and W. Schabel, Slot die coating of lithium-ion battery electrodes: investigations on edge effect issues for stripe and pattern coatings, *J Coat Technol Res*, 2014, **11**, 57–63.
- [66] Y. C. Huang, T. Z. Wang, C. P. Tsai and T. J. Liu, Operating window of solution casting, part I: Newtonian fluids, *J. Appl. Polym. Sci.*, 2013, **129**, 507–516.
- [67] Y.-R. Chang, C.-F. Lin and T.-J. Liu, Start-up of slot die coating, *Polym. Eng. Sci.*, 2009, **49**, 1158–1167.
- [68] S. Didari, Z. Y. Ahmad, J. D. Veldhorst and T. Harrisa, The Mechanism of Air Entrainment in the Slot Die Coating Process, 2012.
- [69] K. Bhamidipati, S. Didari and T. A. L. Harris, Experimental Study on Air Entrainment in Slot Die Coating of High-Viscosity, Shear-Thinning Fluids, *Chemical Engineering Science*, 2012, **80**, 195–204.
- [70] J. Nam and M. S. Carvalho, Flow in tensioned-web-over-slot die coating Effect of die lip design, *Chemical Engineering Science*, 2010, **65**, 3957–3971.
- [71] J. Nam and M. S. Carvalho, Two-layer tensioned-web-over-slot die coating Effect of operating conditions on coating window, *Chemical Engineering Science*, 2010, **65**, 4065–4079.
- [72] C.-F. Lin, B.-K. Wang, C. Tiu and T.-J. Liu, On the pinning of downstream meniscus for slot die coating, *Adv. Polym. Technol.*, 2013, **32**, E249–E257.
- [73] C.-F. Lin, D. S. Hill Wong, T.-J. Liu and P.-Y. Wu, Operating windows of slot die coating: Comparison of theoretical predictions with experimental observations, *Adv. Polym. Technol.*, 2010, **29**, 31–44.
- [74] F. C. Krebs, All solution roll-to-roll processed polymer solar cells free from indium-tin-oxide and vacuum coating steps, *Org. Electron.*, 2009, **10**, 761–768.
- [75] D. Angmo, M. Hösel and F. C. Krebs, All solution processing of ITO-free organic solar cell modules directly on barrier foil, *Sol. Energy Mater. Sol. Cells*, 2012, **107**, 329–336.
- [76] L. Wengeler, K. Peters, M. Schmitt, T. Wenz, P. Scharfer and W. Schabel, Fluid-dynamic properties and wetting behavior of coating inks for roll-to-roll production of polymer-based solar cells, *J Coat Technol Res*, 2014, **11**, 65–73.
- [77] F. Jakubka, M. Heyder, F. Machui, J. Kaschta, D. Eggerath, W. Lövenich, F. C. Krebs and C. J. Brabec, Determining the coating speed limitations for organic photovoltaic inks, *Sol. Energy Mater. Sol. Cells*, 2013, **109**, 120–125.
- [78] L. Wengeler, R. Diehm, P. Scharfer and W. Schabel, Dependence of opto-electric properties of (semi-)conducting films in polymer based solar cells on viscous shear during the coating process, *Org. Electron.*, 2013, **14**, 1608–1613.
- [79] S. Shin, M. Yang, L. J. Guo and H. Youn, Roll-to-Roll Cohesive, Coated, Flexible, High-Efficiency Polymer Light-Emitting Diodes Utilizing ITO-Free Polymer Anodes, *Small*, 2013, **9**, 4036–4044.

- [80] A. Sandström, H. F. Dam, F. C. Krebs and L. Edman, Ambient fabrication of flexible and large-area organic light-emitting devices using slot-die coating, *Nat. Commun.*, 2012, **3**, 1–5.
- [81] J. Alstrup, M. Jørgensen, A. Medford and F. C. Krebs, Ultra Fast and Parsimonious Materials Screening for Polymer Solar Cells Using Differentially Pumped Slot-Die Coating, *ACS Appl. Mater. Interfaces*, 2010, **10**, 2819–2827.
- [82] B. Schmidt-Hansberg, M. Sanyal, M. F. G. Klein, M. Pfaff, N. Schnabel, S. Jaiser, A. Vorobiev, E. Müller, A. Colsmann, P. Scharfer, D. Gerthsen, U. Lemmer, E. Barrena and W. Schabel, Moving through the Phase Diagram: Morphology Formation in Solution Cast Polymer–Fullerene Blend Films for Organic Solar Cells, *ACS Nano*, 2011, **5**, 8579–8590.
- [83] B. Schmidt-Hansberg, M. Baunach, J. Krenn, S. Walheim, U. Lemmer, P. Scharfer and W. Schabel, Spatially resolved drying kinetics of multi-component solution cast films for organic electronics, *Chemical Engineering and Processing: Process Intensification*, 2011, **50**, 509–515.
- [84] M. Sanyal, B. Schmidt-Hansberg, M. F. G. Klein, A. Colsmann, C. Munuera, A. Vorobiev, U. Lemmer, W. Schabel, H. Dosch and E. Barrena, In Situ X-Ray Study of Drying-Temperature Influence on the Structural Evolution of Bulk-Heterojunction Polymer-Fullerene Solar Cells Processed by Doctor-Blading, *Adv. Energy Mater.*, 2011, **1**, 363–367.
- [85] M. Sanyal, B. Schmidt-Hansberg, M. F. G. Klein, C. Munuera, A. Vorobiev, A. Colsmann, P. Scharfer, U. Lemmer, W. Schabel, H. Dosch and E. Barrena, Effect of Photovoltaic Polymer/Fullerene Blend Composition Ratio on Microstructure Evolution during Film Solidification Investigated in Real Time by X-ray Diffraction, *Macromolecules*, 2011, **44**, 3795–3800.
- [86] B. Schmidt-Hansberg, M. F. G. Klein, K. Peters, F. Buss, J. Pfeifer, S. Walheim, A. Colsmann, U. Lemmer, P. Scharfer and W. Schabel, In situ monitoring the drying kinetics of knife coated polymer-fullerene films for organic solar cells, *J. Appl. Phys.*, 2009, **106**, 124501.
- [87] B.-K. Yu, D. Vak, J. Jo, S.-I. Na, S.-S. Kim, M.-K. Kim and D.-Y. Kim, Factors to be Considered in Bulk Heterojunction Polymer Solar Cells Fabricated by the Spray Process, *IEEE J. Sel. Topics Quantum Electron.*, 2010, **16**, 1838–1846.
- [88] G. S. Lonakar, M. S. Mahajan, S. S. Ghosh and J. V. Sali, Modeling thin film formation by Ultrasonic Spray method: A case of PEDOT:PSS thin films, *Org. Electron.*, 2012, **13**, 2575–2581.
- [89] K. Steirer, M. Reese, B. Rupert and N. Kopidakis, Ultrasonic spray deposition for production of organic solar cells, *Sol. Energy Mater. Sol. Cells*, 2009, **93**, 447–453.
- [90] X. Zhao, B. Lojewski, W. Yang, T. Zhu, B. Mi, Z. Gao, W. Huang and W. Deng, Electro-spray as a Fabrication Tool in Organic Photovoltaics, *Reviews in Nanoscience and Nanotechnology*, 2012, **1**, 172–186.
- [91] C. Giroto, B. Rand, J. Genoe and C. W. Lee, Exploring spray coating as a deposition technique for the fabrication of solution-processed solar cells, *Sol. Energy Mater. Sol. Cells*, 2009, **93**, 454–458.

- [92] C. Girotto, D. Moia, B. P. Rand and P. Heremans, High-Performance Organic Solar Cells with Spray-Coated Hole-Transport and Active Layers, *Adv. Funct. Mater.*, 2010, **21**, 64–72.
- [93] J.-W. Kang, Y.-J. Kang, S. Jung, M. Song, D.-G. Kim, C. Su Kim and S. H. Kim, Fully spray-coated inverted organic solar cells, *Sol. Energy Mater. Sol. Cells*, 2012, **103**, 76–79.
- [94] J.-W. Kang, Y.-J. Kang, S. Jung, D. S. You, M. Song, C. S. Kim, D.-G. Kim, J.-K. Kim and S. H. Kim, All-spray-coated semitransparent inverted organic solar cells: From electron selective to anode layers, *Org. Electron.*, 2012, **13**, 2940–2944.
- [95] J. E. Lewis, E. Lafalce, P. Toglia and X. Jiang, Over 30% transparency large area inverted organic solar array by spray, *Sol. Energy Mater. Sol. Cells*, 2011, **95**, 2816–2822.
- [96] S. Colella, M. Mazzeo, G. Melcarne, S. Carallo, G. Ciccarella and G. Gigli, Spray coating fabrication of organic solar cells bypassing the limit of orthogonal solvents, *Appl. Phys. Lett.*, 2013, **102**, 203307.
- [97] B. Zhang, H. Chae and S. Cho, Screen-Printed Polymer: Fullerene Bulk-Heterojunction Solar Cells, *Jpn. J. Appl. Phys.*, 2009, **48**, 020208.
- [98] F. C. Krebs, R. Søndergaard and M. Jørgensen, Printed metal back electrodes for R2R fabricated polymer solar cells studied using the LBIC technique, *Sol. Energy Mater. Sol. Cells*, 2011, **95**, 1348–1353.
- [99] F. C. Krebs, N. Espinosa, M. Hösel, R. R. Søndergaard and M. Jørgensen, 25th Anniversary Article: Rise to Power - OPV-Based Solar Parks, *Adv. Mater.*, 2014, **26**, 29–39.
- [100] A. Lindner, D. Bonn, E. Poire, M. Amar and J. Meunier, Viscous fingering in non-Newtonian fluids, *Journal of Fluid Mechanics*, 2002, **469**, 237–256.
- [101] A. C. Hübler, M. Bellmann, G. C. Schmidt, S. Zimmermann, A. Gerlach and C. Haentjes, Fully mass printed loudspeakers on paper, *Org. Electron.*, 2012, **13**, 2290–2295.
- [102] M. Hambsch, K. Reuter, H. Kempa and A. C. Hübler, Comparison of fully printed unipolar and complementary organic logic gates, *Org. Electron.*, 2012, **13**, 1989–1995.
- [103] J. Jo, J.-S. Yu, T.-M. Lee and D.-S. Kim, Fabrication of Printed Organic Thin-Film Transistors Using Roll Printing, *Jpn. J. Appl. Phys.*, 2009, **48**, 04C181.
- [104] A. C. Hübler, F. Doetz, H. Kempa, H. Katz, M. Bartzsch, N. Brandt, I. Hennig, U. Fuegmann, S. Vaidyanathan and J. Granstrom, Ring oscillator fabricated completely by means of mass-printing technologies, *Org. Electron.*, 2007, **8**, 480–486.
- [105] G. Schmidt, M. Bellmann, B. Meier, M. Hambsch, K. Reuter, H. Kempa and A. C. Hübler, Modified mass printing technique for the realization of source/drain electrodes with high resolution, *Org. Electron.*, 2010, **11**, 1683–1687.
- [106] C. F. Huebner, J. B. Carroll, D. D. Evanoff, Y. Ying, B. J. Stevenson, J. R. Lawrence, J. M. Houchins, A. L. Foguth, J. Sperry and S. H. Foulger, Electroluminescent colloidal inks for flexographic roll-to-roll printing, *J. Mater. Chem.*, 2008, **18**, 4942–4948.
- [107] F. C. Krebs, M. Hösel, M. Corazza, B. Roth, M. V. Madsen, S. A. Gevorgyan, R. R. Søndergaard, D. Karg and M. Jørgensen, Freely available OPV - The fast way to progress, *Energy Technology*, 2013, **1**, 378–381.

- [108] D. Deganello, J. Cherry, D. Gethin and T. C. Claypole, Patterning of micro-scale conductive networks using reel-to-reel Flexographic Printing, *Thin Solid Films*, 2010, **518**, 6113–6116.
- [109] L. B. Keng, W. L. Lai, C. W. A. Lu and B. Salam, 2011 IEEE 13th Electronics Packaging Technology Conference, 2011, pp. 517–520.
- [110] D. Deganello, J. A. Cherry, D. T. Gethin and T. C. Claypole, Impact of metered ink volume on reel-to-reel flexographic printed conductive networks for enhanced thin film conductivity, *Thin Solid Films*, 2012, **520**, 2233–2237.
- [111] N. Hoda and S. Kumar, Boundary integral simulations of liquid emptying from a model gravure cell, *Phys. Fluids*, 2008, **20**, 092106.
- [112] H. Kang, H. Sung, T. Lee, D. Kim and C. Kim, Liquid transfer between two separating plates for micro-gravure-offset printing, *Journal of Micromechanics and Microengineering*, 2009, **19**, 015025.
- [113] W.-X. Huang, S.-H. Lee, H. J. Sung, T.-M. Lee and D.-S. Kim, Simulation of liquid transfer between separating walls for modeling micro-gravure-offset printing, *INTERNATIONAL JOURNAL OF HEAT AND FLUID FLOW*, 2008, **29**, 1436–1446.
- [114] X. Yin and S. Kumar, Flow visualization of the liquid emptying process in scaled-up gravure grooves and cells, *Chemical Engineering Science*, 2006, **61**, 1146–1156.
- [115] S. Yu, S. Kang, K. Lee and S. Um, The analysis of film flow around rotating roller partially immersed ink, *Computational Science and Its Applications-ICCSA 2007*, 2007, **4706**, 951–960.
- [116] S. Ahn and Y. Na, On the ink transfer process in gravure printing, *Proceedings of the 2007 international conference on Computational science and Its applications-Volume Part II*, 2007, 907–918.
- [117] S. Elsayad, F. Morsy, S. El-Sherbiny and E. Abdou, Some factors affecting ink transfer in gravure printing, *Pigment and Resin Technology*, 2002, **31**, 234–240.
- [118] S. Lee and Y. Na, Effect of roll patterns on the Ink transfer in R2R printing process, *International Journal of Precision Engineering and Manufacturing*, 2009, **10**, 123–130.
- [119] R. Kitsomboonloha, S. J. S. Morris, X. Rong and V. Subramanian, Femtoliter-Scale Patterning by High-Speed, Highly Scaled Inverse Gravure Printing, *Langmuir*, 2012, **28**, 16711–16723.
- [120] J. A. Lee, J. P. Rothstein and M. Pasquali, Computational study of viscoelastic effects on liquid transfer during gravure printing, *Journal of Non-Newtonian Fluid Mechanics*, 2013, **199**, 1–11.
- [121] A. de la Fuente Vornbrock, D. Sung, H. Kang, R. Kitsomboonloha and V. Subramanian, Fully gravure and ink-jet printed high speed pBTTT organic thin film transistors, *Org. Electron.*, 2010, **11**, 2037–2044.
- [122] J. Noh, S. Kim, K. Jung, J. Kim, S. Cho and G. Cho, Fully Gravure Printed Half Adder on Plastic Foils, *IEEE Trans. Electron Devices*, 2011, **32**, 1555–1557.

- [123] H. Kempa, M. Hambsch, K. Reuter, M. Stanel, G. Schmidt, B. Meier and A. C. Hübler, Complementary Ring Oscillator Exclusively Prepared by Means of Gravure and Flexographic Printing, *IEEE Trans. Electron Devices*, 2011, **58**, 2765–2769.
- [124] H. Kang, R. Kitsomboonloha, J. Jang and V. Subramanian, High-Performance Printed Transistors Realized Using Femtoliter Gravure-Printed Sub-10 μm Metallic Nanoparticle Patterns and Highly Uniform Polymer Dielectric and Semiconductor Layers, *Adv. Mater.*, 2012, **24**, 3065–3069.
- [125] M. M. Voigt, A. Guite, D.-Y. Chung, R. U. A. Khan, A. J. Campbell, D. D. C. Bradley, F. Meng, J. H. G. Steinke, S. Tierney, I. McCulloch, H. Penxten, L. Lutsen, O. Douheret, J. Manca, U. Brokmann, K. Sönnichsen, D. Hülseberg, W. Bock, C. Barron, N. Blanckaert, S. Springer, J. Grupp and A. Mosley, Polymer Field-Effect Transistors Fabricated by the Sequential Gravure Printing of Polythiophene, Two Insulator Layers, and a Metal Ink Gate, *Adv. Funct. Mater.*, 2010, **20**, 239–246.
- [126] M. Hambsch, K. Reuter, M. Stanel, G. Schmidt, H. Kempa, U. Fügmann, U. Hahn and A. C. Hübler, Uniformity of fully gravure printed organic field-effect transistors, *Mater. Sci. Eng., B*, 2010, **170**, 93–98.
- [127] D. Sung, A. d. l. F. de La Fuente Vornbrock and V. Subramanian, Scaling and Optimization of Gravure-Printed Silver Nanoparticle Lines for Printed Electronics, *IEEE Transactions on Components and Packaging Technologies*, 2010, **33**, 105–114.
- [128] J. Noh, D. Yeom, C. Lim, H. Cha, J. Han, J. Kim, Y. Park, V. Subramanian and G. Cho, Scalability of Roll-to-Roll Gravure-Printed Electrodes on Plastic Foils, *Electronics Packaging Manufacturing, IEEE Transactions on*, 2010, **33**, 1–9.
- [129] A. de la Fuente Vornbrock, J. M. Ding, D. Sung, H.-Y. Tseng and V. Subramanian, Flexible Electronics & Displays Conference and Exhibition, 2005, pp. 1–7.
- [130] M. Pudas, N. Halonen, P. Granat and J. Vähäkangas, Gravure printing of conductive particulate polymer inks on flexible substrates, *Progress in organic coatings*, 2005, **4**, 310–316.
- [131] H. Park, H. Kang, Y. Lee, Y. Park, J. Noh and G. Cho, Fully roll-to-roll gravure printed rectenna on plastic foils for wireless power transmission at 13.56 MHz, *Nanotechnology*, 2012, **23**, 344006.
- [132] D.-Y. Shin, M. Jung and S. Chun, Resistivity transition mechanism of silver salts in the next generation conductive ink for a roll-to-roll printed film with a silver network, *J. Mater. Chem.*, 2012, **22**, 11755–11764.
- [133] C. Koidis, S. Logothetidis, C. Kapnopoulos, P. G. Karagiannidis, A. Laskarakis and N. A. Hastas, Substrate treatment and drying conditions effect on the properties of roll-to-roll gravure printed PEDOT:PSS thin films, *Mater. Sci. Eng., B*, 2011, **176**, 1556–1561.
- [134] P. Kopola, R. Sliz, S. Guillerez, M. Ylikunnari, D. Cheyns, M. Välimäki, M. Tuomikoski, J. Hast, G. Jabbour, R. Myllylä and A. Maaninen, Gravure printed flexible organic photovoltaic modules, *Sol. Energy Mater. Sol. Cells*, 2011, **95**, 1344–1347.
- [135] P. Kopola, S. Guillerez, H. Jin, M. Tuomikoski, A. Maaninen and J. Hast, High efficient plastic solar cells fabricated with a high-throughput gravure printing method, *Sol. Energy Mater. Sol. Cells*, 2010, **94**, 1673–1680.

- [136] C. Koidis, S. Logothetidis, S. Kassavetis, C. Kapnopoulos, P. G. Karagiannidis, D. Georgiou and A. Laskarakis, Effect of process parameters on the morphology and nanostructure of roll-to-roll printed P3HT:PCBM thin films for organic photovoltaics, *Sol. Energy Mater. Sol. Cells*, 2013, **112**, 36–46.
- [137] C. Koidis, S. Logothetidis, A. Ioakeimidis, A. Laskarakis and C. Kapnopoulos, Key factors to improve the efficiency of roll-to-roll printed organic photovoltaics, *Org. Electron.*, 2013, **14**, 1744–1748.
- [138] M. M. Voigt, R. C. I. Mackenzie, S. P. King, C. P. Yau, P. Atienzar, J. Dane, P. E. Keivanidis, I. Zadrazil, D. D. C. Bradley and J. Nelson, Gravure printing inverted organic solar cells: The influence of ink properties on film quality and device performance, *Sol. Energy Mater. Sol. Cells*, 2012, **105**, 77–85.
- [139] M. M. Voigt, R. C. I. Mackenzie, C. P. Yau, P. Atienzar, J. Dane, P. E. Keivanidis, D. D. C. Bradley and J. Nelson, Gravure printing for three subsequent solar cell layers of inverted structures on flexible substrates, *Sol. Energy Mater. Sol. Cells*, 2011, **95**, 731–734.
- [140] A. C. Hübler, B. Trnovec, T. Zillger, M. Ali, N. Wetzold, M. Mingeback, A. Wagenpfahl, C. Deibel and V. Dyakonov, Printed Paper Photovoltaic Cells, *Adv. Energy Mater.*, 2011, **1**, 1018–1022.
- [141] J. Ding, A. d. l. F. de La Fuente Vornbrock, C. Ting and V. Subramanian, Patternable polymer bulk heterojunction photovoltaic cells on plastic by rotogravure printing, *Sol. Energy Mater. Sol. Cells*, 2009, **93**, 459–464.
- [142] B. J. de Gans, P. C. Duineveld and U. S. Schubert, Inkjet Printing of Polymers: State of the Art and Future Developments, *Adv. Mater.*, 2004, **16**, 203–213.
- [143] A. Teichler, J. Perelaer and U. S. Schubert, Inkjet printing of organic electronics – Comparison of deposition techniques and state-of-the-art developments, *J. Mater. Chem. C*, 2013, **1**, 1910–1925.
- [144] H. Wijshoff, The dynamics of the piezo inkjet printhead operation, *Physics Reports*, 2010, **491**, 77–177.
- [145] G. D. Martin, S. D. Hoath and I. M. Hutchings, Inkjet printing - the physics of manipulating liquid jets and drops, *J. Phys.: Conf. Ser.*, 2008, **105**, 012001.
- [146] D. Soltman and V. Subramanian, Inkjet-Printed Line Morphologies and Temperature Control of the Coffee Ring Effect, *Langmuir*, 2008, **24**, 2224–2231.
- [147] B. J. Kang and J. H. Oh, Geometrical characterization of inkjet-printed conductive lines of nanosilver suspensions on a polymer substrate, *Thin Solid Films*, 2010, **518**, 2890–2896.
- [148] E. Fribourg-Blanc, D. M. T. Dang and C. M. Dang, Characterization of silver nanoparticle based inkjet printed lines, *Microsyst Technol*, 2013, **19**, 1961–1971.
- [149] R. D. Deegan, Pattern formation in drying drops, *Physical Review E*, 2000, **61**, 475–485.
- [150] R. D. Deegan, O. Bakajin, T. F. Dupont, G. Huber, S. R. Nagel and T. A. Witten, Capillary flow as the cause of ring stains from dried liquid drops, *Nature*, 1997, **389**, 827–829.

- [151] G. Cummins and M. P. Y. Desmulliez, Inkjet printing of conductive materials: a review, *Circuit World*, 2012, **38**, 193–213.
- [152] M. Singh, H. Haverinen, P. Dhagat and G. E. Jabbour, Inkjet Printing-Process and Its Applications, *Adv. Mater.*, 2009, **21**, 1–13.
- [153] S. H. Eom, H. Park, S. H. Mujawar, S. C. Yoon, S.-S. Kim, S.-I. Na, S.-J. Kang, D. Khim, D.-Y. Kim and S.-H. Lee, High efficiency polymer solar cells via sequential inkjet-printing of PEDOT:PSS and P3HT:PCBM inks with additives, *Org. Electron.*, 2010, **11**, 1516–1522.
- [154] A. Lange, W. Schindler, M. Wegener, K. Fostiropoulos and S. Janietz, Inkjet Printed Solar Cell Active Layers Based on a Novel, Amorphous Polymer, *J. Nanosci. Nanotechnol.*, 2013, **13**, 5209–5214.
- [155] A. Lange, W. Schindler, M. Wegener, K. Fostiropoulos and S. Janietz, Inkjet printed solar cell active layers prepared from chlorine-free solvent systems, *Sol. Energy Mater. Sol. Cells*, 2013, **109**, 104–110.
- [156] S. H. Eom, S. Senthilarasu, P. Uthirakumar, S. C. Yoon, J. Lim, C. Lee, H. S. Lim, J. Lee and S.-H. Lee, Polymer solar cells based on inkjet-printed PEDOT:PSS layer, *Org. Electron.*, 2009, **10**, 536–542.
- [157] A. Teichler, R. Eckardt, S. Hoepfener, C. Friebe, J. Perelaer, A. Senes, M. Morana, C. J. Brabec and U. S. Schubert, Combinatorial Screening of Polymer:Fullerene Blends for Organic Solar Cells by Inkjet Printing, *Adv. Energy Mater.*, 2010, **1**, 105–114.
- [158] Y. Galagan, E. W. C. Coenen, S. Sabik, H. H. Gortler, M. Barink, S. C. Veenstra, J. M. Kroon, R. Andriessen and P. W. M. Blom, Evaluation of ink-jet printed current collecting grids and busbars for ITO-free organic solar cells, *Sol. Energy Mater. Sol. Cells*, 2012, **104**, 32–38.
- [159] Y. Galagan, B. Zimmermann, E. Coenen, M. Jørgensen, F. C. Krebs, D. Tanenbaum, H. Gortler, S. Sabik, L. Slooff, S. C. Veenstra, J. Kroon and R. Andriessen, Current Collecting Grids for ITO-Free Solar Cells, *Adv. Energy Mater.*, 2012, **2**, 103–110.
- [160] Y.-C. Huang, F.-H. Hsu, H.-C. Cha, C.-M. Chuang, C.-S. Tsao and C.-Y. Chen, High-performance ITO-free spray-processed polymer solar cells with incorporating ink-jet printed grid, *Org. Electron.*, 2013, **14**, 2809–2817.
- [161] M. Neophytou, F. Hermerschmidt, A. Savva, E. Georgiou and S. A. Choulis, Highly efficient indium tin oxide-free organic photovoltaics using inkjet-printed silver nanoparticle current collecting grids, *Appl. Phys. Lett.*, 2012, **101**, 193302.
- [162] D. Angmo, J. Sweelssen, R. Andriessen, Y. Galagan and F. C. Krebs, Inkjet Printing of Back Electrodes for Inverted Polymer Solar Cells, *Adv. Energy Mater.*, 2013, **3**, 1239–1237.
- [163] J. J. van Franeker, W. P. Voorthuizen, H. Gortler, K. H. Hendriks, R. A. J. Janssen, A. Hadipour, R. Andriessen and Y. Galagan, All-solution-processed organic solar cells with conventional architecture, *Sol. Energy Mater. Sol. Cells*, 2013, **117**, 267–272.
- [164] M. Hösel, R. R. Søndergaard, D. Angmo and F. C. Krebs, Comparison of fast roll-to-roll flexographic, inkjet, flatbed and rotary screen printing of metal back electrodes for polymer solar cells, *Adv. Eng. Mater.*, 2013, **15**, 995–1001.

- [165] J. Liu, X. Gao, Y. Sun and Y. Han, A quasi-ordered bulk heterojunction of P3HT/PCBM solar cells fabricated by zone-casting, *Sol. Energy Mater. Sol. Cells*, 2013, **117**, 421–428.
- [166] J. Rysz, M. Josiek, M. M. Marzec and E. Moons, Pattern replication in blends of semi-conducting and insulating polymers casted by horizontal dipping, *J. Polym. Sci. B Polym. Phys.*, 2013, **51**, 1419–1426.
- [167] F. Nickel, C. Sprau, M. F. G. Klein, P. Kapetana, N. Christ, X. Liu, S. Klinkhammer, U. Lemmer and A. Colmann, Spatial mapping of photocurrents in organic solar cells comprising wedge-shaped absorber layers for an efficient material screening, *Sol. Energy Mater. Sol. Cells*, 2012, **104**, 18–22.
- [168] H. G. Jeon, C. Y. Cho, J. C. Shin and B. Park, Inverted polymer solar cells fabricated by pre-metered coating process, *J. Mater. Chem.*, 2012, **22**, 23022–23029.
- [169] B. Park and M. Han, Photovoltaic characteristics of polymer solar cells fabricated by pre-metered coating process, *Optics Express*, 2009, **17**, 13830–13840.
- [170] Z. Hu, J. Zhang, S. Xiong and Y. Zhao, Annealing-free, air-processed and high-efficiency polymer solar cells fabricated by a dip coating process, *Org. Electron.*, 2012, **13**, 142–146.
- [171] C. Sachse, L. Müller-Meskamp, L. Bormann, Y. H. Kim, F. Lehnert, A. Philipp, B. Beyer and K. Leo, Transparent, dip-coated silver nanowire electrodes for small molecule organic solar cells, *Org. Electron.*, 2013, **14**, 143–148.
- [172] T. Ghooos, O. Malinkiewicz, B. Conings, L. Lutsen, D. Vanderzande, H. J. Bolink and W. Maes, Solution-processed bi-layer polythiophene-fullerene organic solar cells, *RSC Adv.*, 2013, **3**, 25197–25203.
- [173] O. Malinkiewicz, M. Lenes, H. Brine and H. J. Bolink, Meniscus coated high open-circuit voltage bi-layer solar cells, *RSC Adv.*, 2012, **2**, 3335–3339.
- [174] J.-W. Lim, D.-Y. Cho, Jihoon-Kim, S.-I. Na and H.-K. Kim, Simple brush-painting of flexible and transparent Ag nanowire network electrodes as an alternative ITO anode for cost-efficient flexible organic solar cells, *Sol. Energy Mater. Sol. Cells*, 2012, **107**, 348–354.
- [175] D.-Y. Cho, K. Eun, S.-H. Choa and H.-K. Kim, Highly flexible and stretchable carbon nanotube network electrodes prepared by simple brush painting for cost-effective flexible organic solar cells, *Carbon*, 2014, **66**, 530–538.
- [176] S.-W. Heo, J.-Y. Lee, H.-J. Song, J.-R. Ku and D.-K. Moon, Patternable brush painting process for fabrication of flexible polymer solar cells, *Sol. Energy Mater. Sol. Cells*, 2011, **95**, 3041–3046.
- [177] S. Kim, S. Na, S. Kang and D. Kim, Annealing-free fabrication of P3HT: PCBM solar cells via simple brush painting, *Sol. Energy Mater. Sol. Cells*, 2010, **94**, 171–175.
- [178] J.-H. Lee, W.-S. Chung, N.-G. Park and K. Kim, Wiper coating method for PEDOT:PSS film on fabricating organic photovoltaic modules, *Curr. Appl Phys.*, 2010, **10**, e185–e188.
- [179] J. W. Jung and W. H. Jo, Annealing-Free High Efficiency and Large Area Polymer Solar Cells Fabricated by a Roller Painting Process, *Adv. Funct. Mater.*, 2009, **20**, 2355–2363.

- [180] A. Colsmann, F. Stenzel, G. Balthasar, H. Do and U. Lemmer, Plasma patterning of Poly(3,4-ethylenedioxythiophene):Poly(styrenesulfonate) anodes for efficient polymer solar cells, *Thin Solid Films*, 2009, **517**, 1750–1752.
- [181] I. Etxebarria, J. G. Tait, R. Gehlhaar, R. Pacios and D. Cheyuns, Surface treatment patterning of organic photovoltaic films for low-cost modules, *Org. Electron.*, 2013, **14**, 430–435.
- [182] M. Gebhardt, J. Hänel, F. Allenstein, C. Scholz and M. Clair, Laser Structuring of Flexible Organic Solar Cells, *Laser Technik Journal*, 2013, **10**, 25–28.
- [183] M. Gebhardt, J. Hänel, M. Clair and C. Scholz, Reel-to-reel machining with ultra short pulsed lasers, *Laser Technik Journal*, 2011, **8**, 29–32.
- [184] T. Petsch, J. Haenel, M. Clair, B. Keiper and C. Scholz, Laser processing of organic photovoltaic cells with a roll-to-roll manufacturing process, *Proc. of SPIE*, 2011, **7921**, 79210U–79210U–7.
- [185] P. Kubis, N. Li, T. Stubhan, F. Machui, G. J. Matt, M. M. Voigt and C. J. Brabec, Patterning of organic photovoltaic modules by ultrafast laser, *Prog. Photovolt: Res. Appl.*, 2013.
- [186] N. Li, P. Kubis, K. Forberich, T. Ameri, F. C. Krebs and C. J. Brabec, Towards large-scale production of solution-processed organic tandem modules based on ternary composites: Design of the intermediate layer, device optimization and laser based module processing, *Sol. Energy Mater. Sol. Cells*, 2014, **120**, 701–708.
- [187] S. Xiao, S. A. Fernandes and A. Ostendorf, Selective Patterning of ITO on flexible PET Substrate by 1064nm picosecond Laser, *Physics Procedia*, 2011, **12**, 125–132.
- [188] J. Haenel, B. Keiper, C. Scholz and M. Clair, Laser scribing of ITO and organic solar cells, *Proc. of SPIE*, 2010, **7771**, 77710G.
- [189] T. T. Larsen-Olsen, F. Machui, B. Lechene, S. Berny, D. Angmo, R. Søndergaard, N. Blouin, W. Mitchell, S. Tierney, T. Cull, P. Tiwana, F. Meyer, M. Carrasco-Orozco, A. Scheel, W. Lövenich, R. de Bettignies, C. J. Brabec and F. C. Krebs, Round-Robin Studies as a Method for Testing and Validating High-Efficiency ITO-Free Polymer Solar Cells Based on Roll-to-Roll-Coated Highly Conductive and Transparent Flexible Substrates, *Adv. Energy Mater.*, 2012, **2**, 1091–1094.
- [190] M. Helgesen, J. E. Carlé and F. C. Krebs, Slot-Die Coating of a High Performance Copolymer in a Readily Scalable Roll Process for Polymer Solar Cells, *Adv. Energy Mater.*, 2013, **3**, 1664–1669.
- [191] F. C. Krebs, V. Senkovskyy and A. Kiriyy, Preorganization of Nanostructured Inks for Roll-to-Roll-Coated Polymer Solar Cells, *Selected Topics in Quantum Electronics, IEEE Journal of*, 2010, **16**, 1821–1826.
- [192] W. Yue, T. T. Larsen-Olsen, X. Hu, M. Shi, H. Chen, M. Hinge, P. Fojan, F. C. Krebs and D. Yu, Synthesis and photovoltaic properties from inverted geometry cells and roll-to-roll coated large area cells from dithienopyrrole-based donor–acceptor polymers, *J. Mater. Chem. A*, 2013, **1**, 1785–1793.

- [193] F. C. Krebs, J. Fyenbo and M. Jørgensen, Product integration of compact roll-to-roll processed polymer solar cell modules: methods and manufacture using flexographic printing, slot-die coating and rotary screen printing, *J. Mater. Chem.*, 2010, **20**, 8994–9001.
- [194] F. C. Krebs, T. Tromholt and M. Jørgensen, Upscaling of polymer solar cell fabrication using full roll-to-roll processing, *Nanoscale*, 2010, **2**, 873–886.
- [195] F. C. Krebs and K. Norrman, Using Light-Induced Thermocleavage in a Roll-to-Roll Process for Polymer Solar Cells, *ACS Appl. Mater. Interfaces*, 2010, **2**, 877–887.
- [196] F. C. Krebs, T. D. Nielsen, J. Fyenbo, M. Wadstrøm and M. S. Pedersen, Manufacture, integration and demonstration of polymer solar cells in a lamp for the “Lighting Africa” initiative, *Energy Environ. Sci.*, 2010, **3**, 512–525.
- [197] M. Lilliedal, A. Medford, M. Madsen, K. Norrman and F. C. Krebs, The effect of post-processing treatments on inflection points in current-voltage curves of roll-to-roll processed polymer photovoltaics, *Sol. Energy Mater. Sol. Cells*, 2010, **94**, 2018–2031.
- [198] D. Angmo, S. A. Gevorgyan, T. T. Larsen-Olsen, R. R. Søndergaard, M. Hösel, M. Jørgensen, R. Gupta, G. U. Kulkarni and F. C. Krebs, Scalability and stability of very thin, roll-to-roll processed, large area, indium-tin-oxide free polymer solar cell modules, *Org. Electron.*, 2013, **14**, 984–994.
- [199] J. E. Carlé, T. R. Andersen, M. Helgesen, E. Bundgaard, M. Jørgensen and F. C. Krebs, A laboratory scale approach to polymer solar cells using one coating/printing machine, flexible substrates, no ITO, no vacuum and no spincoating, *Sol. Energy Mater. Sol. Cells*, 2013, **108**, 126–128.
- [200] R. Søndergaard, M. Manceau, M. Jørgensen and F. C. Krebs, New Low-Bandgap Materials with Good Stabilities and Efficiencies Comparable to P3HT in R2R-Coated Solar Cells, *Adv. Energy Mater.*, 2012, **2**, 415–418.
- [201] C. M. Amb, M. R. Craig, U. Koldemir, J. Subbiah, K. R. Choudhury, S. A. Gevorgyan, M. Jørgensen, F. C. Krebs, F. So and J. R. Reynolds, Aesthetically Pleasing Conjugated Polymer:Fullerene Blends for Blue-Green Solar Cells Via Roll-to-Roll Processing, *ACS Appl. Mater. Interfaces*, 2012, **4**, 1847–1853.
- [202] H. F. Dam and F. C. Krebs, Simple roll coater with variable coating and temperature control for printed polymer solar cells, *Sol. Energy Mater. Sol. Cells*, 2012, **97**, 191–196.
- [203] F. C. Krebs, J. Fyenbo, D. M. Tanenbaum, S. A. Gevorgyan, R. Andriessen, B. van Re-mortere, Y. Galagan and M. Jørgensen, The OE-A OPV demonstrator anno domini 2011, *Energy Environ. Sci.*, 2011, **4**, 4116–4123.
- [204] N. Espinosa, R. García-Valverde, A. Urbina, F. Lenzenmann, M. Manceau, D. Angmo and F. C. Krebs, Life cycle assessment of ITO-free flexible polymer solar cells prepared by roll-to-roll coating and printing, *Sol. Energy Mater. Sol. Cells*, 2012, **97**, 3–13.
- [205] J. E. Carlé, M. Helgesen, M. V. Madsen, E. Bundgaard and F. C. Krebs, Upscaling from single cells to modules – fabrication of vacuum- and ITO-free polymer solar cells on flexible substrates with long lifetime, *J. Mater. Chem. C*, 2014, **2**, 1290–1297.

- [206] T. R. Andersen, H. F. Dam, B. Andreasen, M. Hösel, M. V. Madsen, S. A. Gevorgyan, R. R. Søndergaard, M. Jørgensen and F. C. Krebs, A rational method for developing and testing stable flexible indium- and vacuum-free multilayer tandem polymer solar cells comprising up to twelve roll processed layers, *Sol. Energy Mater. Sol. Cells*, 2014, **120**, 735–743.
- [207] S. Schiefer, B. Zimmermann and U. Würfel, Layout optimization of organic wrap through solar cells by combined electrical and optical modeling, *Sol. Energy Mater. Sol. Cells*, 2013, **115**, 29–35.
- [208] S. Hong, J. Lee, H. Kang and K. Lee, Slot-die coating parameters of the low-viscosity bulk-heterojunction materials used for polymer solarcells, *Sol. Energy Mater. Sol. Cells*, 2013, **112**, 27–35.
- [209] F. Yan, J. Noble, J. Peltola, S. Wicks and S. Balasubramanian, Semitransparent OPV modules pass environmental chamber test requirements, *Sol. Energy Mater. Sol. Cells*, 2013, **114**, 214–218.
- [210] T. T. Larsen-Olsen, R. R. Søndergaard, K. Norrman, M. Jørgensen and F. C. Krebs, All printed transparent electrodes through an electrical switching mechanism: A convincing alternative to indium-tin-oxide, silver and vacuum, *Energy Environ. Sci.*, 2012, **5**, 9467–9471.
- [211] D. Angmo, T. T. Larsen-Olsen, M. Jørgensen, R. R. Søndergaard and F. C. Krebs, Roll-to-Roll Inkjet Printing and Photonic Sintering of Electrodes for ITO Free Polymer Solar Cell Modules and Facile Product Integration, *Adv. Energy Mater.*, 2012, **3**, 172–175.
- [212] M. Schrödner, S. Sensfuss, H. Schache, K. Schultheis, T. Welzel, K. Heinemann, R. Milker, J. Marten and L. Blankenburg, Reel-to-reel wet coating by variation of solvents and compounds of photoactive inks for polymer solar cell production, *Sol. Energy Mater. Sol. Cells*, 2012, **107**, 283–291.
- [213] T. T. Larsen-Olsen, T. R. Andersen, B. Andreasen, A. P. L. Böttiger, E. Bundgaard, K. Norrman, J. W. Andreasen, M. Jørgensen and F. C. Krebs, Roll-to-roll processed polymer tandem solar cells partially processed from water, *Sol. Energy Mater. Sol. Cells*, 2012, **97**, 43–49.
- [214] T. T. Larsen-Olsen, B. Andreasen, T. R. Andersen, A. P. L. Böttiger, E. Bundgaard, K. Norrman, J. W. Andreasen, M. Jørgensen and F. C. Krebs, Simultaneous multilayer formation of the polymer solar cell stack using roll-to-roll double slot-die coating from water, *Sol. Energy Mater. Sol. Cells*, 2012, **97**, 22–27.
- [215] B. Zimmermann, H. F. Schleiermacher, M. Niggemann and U. Würfel, ITO-free flexible inverted organic solar cell modules with high fill factor prepared by slot die coating, *Sol. Energy Mater. Sol. Cells*, 2011, **95**, 1587–1589.
- [216] T. R. Andersen, T. T. Larsen-Olsen, B. Andreasen, A. P. L. Böttiger, J. E. Carlé, M. Helgesen, E. Bundgaard, K. Norrman, J. W. Andreasen, M. Jørgensen and F. C. Krebs, Aqueous Processing of Low-Band-Gap Polymer Solar Cells Using Roll-to-Roll Methods, *ACS Nano*, 2011, **5**, 4188–4196.
- [217] M. Manceau, D. Angmo, M. Jørgensen and F. C. Krebs, ITO-free flexible polymer solar cells: From small model devices to roll-to-roll processed large modules, *Org. Electron.*, 2011, **12**, 566–574.

- [218] L. Wengeler, B. Schmidt-Hansberg, K. Peters, P. Scharfer and W. Schabel, Investigations on knife and slot die coating and processing of polymer nanoparticle films for hybrid polymer solar cells, *Chemical Engineering and Processing: Process Intensification*, 2011, **50**, 478–482.
- [219] Y. Galagan, I. G. de Vries, A. P. Langen, R. Andriessen, W. J. H. Verhees, S. C. Veenstra and J. M. Kroon, Technology development for roll-to-roll production of organic photovoltaics, *Chemical Engineering and Processing: Process Intensification*, 2011, **50**, 454–461.
- [220] L. Blankenburg, K. Schultheis, H. Schache, S. Sensfuss and M. Schrödner, Reel-to-reel wet coating as an efficient up-scaling technique for the production of bulk-heterojunction polymer solar cells, *Sol. Energy Mater. Sol. Cells*, 2009, **93**, 476–483.
- [221] F. C. Krebs, Roll-to-roll fabrication of monolithic large-area polymer solar cells free from indium-tin-oxide, *Sol. Energy Mater. Sol. Cells*, 2009, **93**, 1636–1641.
- [222] F. Padinger, C. J. Brabec, T. Fromherz, J. C. Hummelen and N. S. Sariciftci, Fabrication of large area photovoltaic devices containing various blends of polymer and fullerene derivatives by using the doctor blade technique, *Opto-Electronics Review*, 2000, **8**, 280–283.
- [223] Y. Lin, H. F. Dam, T. R. Andersen, E. Bundgaard, W. Fu, H. Chen, F. C. Krebs and X. Zhan, Ambient roll-to-roll fabrication of flexible solar cells based on small molecules, *J. Mater. Chem. C*, 2013, **1**, 8007–8010.
- [224] N. Shin, L. J. Richter, A. A. Herzing, R. J. Kline and D. M. DeLongchamp, Effect of Processing Additives on the Solidification of Blade-Coated Polymer/Fullerene Blend Films via In-Situ Structure Measurements, *Adv. Energy Mater.*, 2013, **3**, 938–948.
- [225] S.-L. Lim, E.-C. Chen, C.-Y. Chen, K.-H. Ong, Z.-K. Chen and H.-F. Meng, High performance organic photovoltaic cells with blade-coated active layers, *Sol. Energy Mater. Sol. Cells*, 2012, **107**, 292–297.
- [226] M. Neophytou, W. Cambarau, F. Hermerschmidt, C. Waldauf, C. Christodoulou, R. Pacios and S. A. Choulis, Inkjet-printed polymer-fullerene blends for organic electronic applications, *Microelectron. Eng.*, 2012, **95**, 102–106.
- [227] J. Ajuria, I. Ugarte, W. Cambarau, I. Etxebarria, R. Tena-Zaera and R. Pacios, Insights on the working principles of flexible and efficient ITO-free organic solar cells based on solution processed Ag nanowire electrodes, *Sol. Energy Mater. Sol. Cells*, 2012, **102**, 148–152.
- [228] J.-H. Chang, Y.-H. Chen, H.-W. Lin, Y.-T. Lin, H.-F. Meng and E.-C. Chen, Highly efficient inverted rapid-drying blade-coated organic solar cells, *Org. Electron.*, 2012, **13**, 705–709.
- [229] B. Schmidt-Hansberg, M. Sanyal, N. Grossiord, Y. Galagan, M. Baunach, M. F. G. Klein, A. Colmann, P. Scharfer, U. Lemmer, H. Dosch, J. Michels, E. Barrena and W. Schabel, Investigation of non-halogenated solvent mixtures for high throughput fabrication of polymer–fullerene solar cells, *Sol. Energy Mater. Sol. Cells*, 2012, **96**, 195–201.
- [230] W.-B. Byun, S. K. Lee, J.-C. Lee, S.-J. Moon and W. S. Shin, Bladed organic photovoltaic cells, *Curr. Appl Phys.*, 2011, **11**, S179–S184.

- [231] J. Ajuria, I. Etxebarria, W. Cambarau, U. Muñecas, R. Tena-Zaera, J. C. Jimeno and R. Pacios, Inverted ITO-free organic solar cells based on p and n semiconducting oxides. New designs for integration in tandem cells, top or bottom detecting devices, and photovoltaic windows, *Energy Environ. Sci.*, 2011, **4**, 453–458.
- [232] C.-Y. Chen, H.-W. Chang, Y.-F. Chang, B.-J. Chang, Y.-S. Lin, P.-S. Jian, H.-C. Yeh, H.-T. Chien, E.-C. Chen, Y.-C. Chao, H.-F. Meng, H.-W. Zan, H.-W. Lin, S.-F. Horng, Y.-J. Cheng, F.-W. Yen, I.-F. Lin, H.-Y. Yang, K.-J. Huang and M.-R. Tseng, Continuous blade coating for multi-layer large-area organic light-emitting diode and solar cell, *J. Appl. Phys.*, 2011, **110**, 094501.
- [233] B. Schmidt-Hansberg, H. Do, A. Colsmann, U. Lemmer and W. Schabel, Drying of thin film polymer solar cells, *The European Physical Journal-Special Topics*, 2009, **166**, 49–53.
- [234] Y. Chang, S. Tseng, C. Chen, H. Meng, E.-C. Chen, S.-F. Horng and C.-S. Hsu, Polymer solar cell by blade coating, *Org. Electron.*, 2009, **10**, 741–746.
- [235] C. N. Hoth, P. Schilinsky, S. A. Choulis and C. J. Brabec, Printing Highly Efficient Organic Solar Cells, *Nano Lett.*, 2008, **8**, 2806–2813.
- [236] C. Hoth, S. A. Choulis, P. Schilinsky and C. J. Brabec, On the effect of poly (3-hexylthiophene) regioregularity on inkjet printed organic solar cells, *J. Mater. Chem.*, 2009, **19**, 5398–5404.
- [237] W. Kylberg, F. A. de Castro, P. Chabreck, U. Sonderegger, B. T.-T. Chu, F. Nüesch and R. Hany, Woven Electrodes for Flexible Organic Photovoltaic Cells, *Adv. Mater.*, 2011, **23**, 1015–1019.
- [238] C. N. Hoth, R. Steim, P. Schilinsky, S. A. Choulis, S. Tedde, O. Hayden and C. J. Brabec, Topographical and morphological aspects of spray coated organic photovoltaics, *Org. Electron.*, 2009, **10**, 587–593.
- [239] J.-S. Yu, G. H. Jung, J. Jo, J.-S. Kim, J. W. Kim, S.-W. Kwak, J.-L. Lee, I. Kim and D. Kim, Transparent conductive film with printable embedded patterns for organic solar cells, *Sol. Energy Mater. Sol. Cells*, 2013, **109**, 142–147.
- [240] B. Park, Y. Chan Kim and S. H. Yun, All-solution-processed inverted polymer solar cells with low temperature, water-processable hybrid electron-collecting layers, *J. Mater. Chem. A*, 2013, **1**, 2030–2038.
- [241] J. Krantz, M. Richter, S. Spallek, E. Spiecker and C. J. Brabec, Solution-Processed Metallic Nanowire Electrodes as Indium Tin Oxide Replacement for Thin-Film Solar Cells, *Adv. Funct. Mater.*, 2011, **21**, 4784–4787.
- [242] N. Li, D. Baran, K. Forberich, M. Turbiez, T. Ameri, F. C. Krebs and C. J. Brabec, An Efficient Solution-Processed Intermediate Layer for Facilitating Fabrication of Organic Multi-Junction Solar Cells, *Adv. Energy Mater.*, 2013, **3**, 1597–1605.
- [243] F. Guo, X. Zhu, K. Forberich, J. Krantz, T. Stubhan, M. Salinas, M. Halik, S. Spallek, B. Butz, E. Spiecker, T. Ameri, N. Li, P. Kubis, D. M. Guldi, G. J. Matt and C. J. Brabec, ITO-Free and Fully Solution-Processed Semitransparent Organic Solar Cells with High Fill Factors, *Adv. Energy Mater.*, 2013, **3**, 1062–1067.

- [244] T. Stubhan, I. Litzov, N. Li, M. Salinas, M. Steidl, G. Sauer, K. Forberich, G. J. Matt, M. Halik and C. J. Brabec, Overcoming interface losses in organic solar cells by applying low temperature, solution processed aluminum-doped zinc oxide electron extraction layers, *J. Mater. Chem. A*, 2013, **1**, 6004–6009.
- [245] A. Savva, F. Petraki, P. Elefteriou, L. Sygellou, M. Voigt, M. Giannouli, S. Kennou, J. Nelson, D. D. C. Bradley, C. J. Brabec and S. A. Choulis, The Effect of Organic and Metal Oxide Interfacial layers on the Performance of Inverted Organic Photovoltaics, *Adv. Energy Mater.*, 2013, **3**, 391–398.
- [246] J. Krantz, T. Stubhan, M. Richter, S. Spallek, I. Litzov, G. J. Matt, E. Spiecker and C. J. Brabec, Spray-Coated Silver Nanowires as Top Electrode Layer in Semitransparent P3HT:PCBM-Based Organic Solar Cell Devices, *Adv. Funct. Mater.*, 2012, **23**, 1711–1717.
- [247] N. Li, T. Stubhan, D. Baran, J. Min, H. Wang, T. Ameri and C. J. Brabec, Design of the Solution-Processed Intermediate Layer by Engineering for Inverted Organic Multi junction Solar Cells, *Adv. Energy Mater.*, 2013, **3**, 301–307.
- [248] T. Ameri, J. Min, N. Li, F. Machui, D. Baran, M. Forster, K. J. Schottler, D. Dolfen, U. Scherf and C. J. Brabec, Performance Enhancement of the P3HT/PCBM Solar Cells through NIR Sensitization Using a Small-Bandgap Polymer, *Adv. Energy Mater.*, 2012, **2**, 1198–1202.
- [249] C. N. Hoth, P. Schilinsky, S. Choulis and C. J. Brabec, Photovoltaic Loss Analysis of Inkjet-Printed Polymer Solar Cells Using Pristine Solvent Formulations, *Macromol. Symp.*, 2010, **291-292**, 287–292.
- [250] T. Ameri, G. Denzler, C. Waldauf, P. Denk, K. Forberich, M. C. Scharber, C. J. Brabec and K. Hingerl, Realization, characterization, and optical modeling of inverted bulk-heterojunction organic solar cells, *J. Appl. Phys.*, 2008, **103**, 084506.
- [251] G. Denzler, K. Forberich, M. C. Scharber, C. J. Brabec, I. Tomiš, K. Hingerl and T. Fromherz, Angle dependence of external and internal quantum efficiencies in bulk-heterojunction organic solar cells, *J. Appl. Phys.*, 2007, **102**, 054516.
- [252] C. Waldauf, M. Morana, P. Denk, P. Schilinsky, K. Coakley, S. A. Choulis and C. J. Brabec, Highly efficient inverted organic photovoltaics using solution based titanium oxide as electron selective contact, *Appl. Phys. Lett.*, 2006, **89**, 233517.
- [253] P. Schilinsky, C. Waldauf and C. J. Brabec, Performance Analysis of Printed Bulk Heterojunction Solar Cells, *Adv. Funct. Mater.*, 2006, **16**, 1669–1672.
- [254] F. Padinger, C. J. Brabec, T. Fromherz, J. C. Hummelen and N. S. Sariciftci, Fabrication of large area photovoltaic devices containing various blends of polymer and fullerene derivatives by using the doctor blade technique, *Opto-Electronics Review*, 2000, **8**, 280–283.
- [255] Y.-R. Hong, P.-K. Chen, J.-C. Wang, M.-K. Lee, S.-F. Horng and H.-F. Meng, Simultaneous enhancement in both large-area coatability and photovoltaic performance of inverted organic solar cells with co-solvent, *Sol. Energy Mater. Sol. Cells*, 2014, **120**, 197–203.
- [256] M. Neophytou, E. Georgiou, M. M. Fyrillas and S. A. Choulis, Two step sintering process and metal grid design optimization for highly efficient ITO free organic photovoltaics, *Sol. Energy Mater. Sol. Cells*, 2014, **122**, 1–7.

- [257] Y.-C. Huang, H.-C. Chia, C.-M. Chuang, C.-S. Tsao, C.-Y. Chen and W.-F. Su, Facile hot solvent vapor annealing for high performance polymer solar cell using spray process, *Sol. Energy Mater. Sol. Cells*, 2013, **114**, 24–30.
- [258] J. G. Tait, B. P. Rand and P. Heremans, Concurrently pumped ultrasonic spray coating for donor:acceptor and thickness optimization of organic solar cells, *Org. Electron.*, 2013, **14**, 1002–1008.
- [259] T. Wang, N. W. Scarratt, H. Yi, A. D. F. Dunbar, A. J. Pearson, D. C. Watters, T. S. Glen, A. C. Brook, J. Kingsley, A. R. Buckley, M. W. A. Skoda, A. M. Donald, R. A. L. Jones, A. Iraqi and D. G. Lidzey, Fabricating High Performance, Donor-Acceptor Copolymer Solar Cells by Spray-Coating in Air, *Adv. Energy Mater.*, 2013, **3**, 505–512.
- [260] J.-H. Lee, T. Sagawa and S. Yoshikawa, Fast Screening of the Optimal Polymer Ratio for Organic Solar Cells Using a Spray-Coating Deposition Method for the Fullerene Mixture, *Energy Technology*, 2013, **1**, 85–93.
- [261] S. Kannappan, K. Palanisamy, J. Tatsugi, P.-K. Shin and S. Ochiai, Fabrication and characterizations of PCDTBT: PC71BM bulk heterojunction solar cell using air brush coating method, *J Mater Sci*, 2012, **48**, 2308–2317.
- [262] J.-H. Lee, T. Sagawa and S. Yoshikawa, Thickness dependence of photovoltaic performance of additional spray coated solar cells, *Thin Solid Films*, 2012, **529**, 464–469.
- [263] A. Abdellah, K. S. Viridi, R. Meier, M. Döblinger, P. Müller-Buschbaum, C. Scheu, P. Lugli and G. Scarpa, Successive Spray Deposition of P3HT/PCBM Organic Photoactive Layers: Material Composition and Device Characteristics, *Adv. Funct. Mater.*, 2012, **22**, 4078–4086.
- [264] M. Ali, M. Abbas, S. K. Shah, R. Tuerhong, A. Generosi, B. Paci, L. Hirsch and R. Gunnella, Realization of solution processed multi-layer bulk heterojunction organic solar cells by electro-spray deposition, *Org. Electron.*, 2012, **13**, 2130–2137.
- [265] S.-E. Park, S. Kim, K. Kim, H.-E. Joe, B. Jung, E. Kim, W. Kim, B.-K. Min and J. Hwang, Fabrication of ordered bulk heterojunction organic photovoltaic cells using nanopatterning and electrohydrodynamic spray deposition methods, *Nanoscale*, 2012, **4**, 7773–7779.
- [266] T. Fukuda, K. Takagi and Y. Liao, Insertion of fullerene layer for bulk heterojunction organic photovoltaic cell fabricated by electrospray deposition method, *Phys. Status Solidi RRL*, 2013, **7**, 1055–1058.
- [267] W. Nie, R. C. Coffin, J. Liu, Y. Li, E. D. Peterson, C. M. MacNeill, R. E. Nofle and D. L. Carroll, High efficiency organic solar cells with spray coated active layers comprised of a low band gap conjugated polymer, *Appl. Phys. Lett.*, 2012, **100**, 083301.
- [268] G. Susanna, L. Salamandra, T. M. Brown, A. Di Carlo, F. Brunetti and A. Reale, Airbrush spray-coating of polymer bulk-heterojunction solar cells, *Sol. Energy Mater. Sol. Cells*, 2011, **95**, 1775–1778.
- [269] W. Nie, R. Coffin, J. Liu, C. M. MacNeill, Y. Li, R. E. Nofle and D. L. Carroll, Exploring Spray-Coating Techniques for Organic Solar Cell Applications, *Sol. Energy Mater. Sol. Cells*, 2011, **2012**, 852–855.

- [270] J.-H. Lee, T. Sagawa and S. Yoshikawa, Morphological and topographical characterizations in spray coated organic solar cells using an additional solvent spray deposition, *Org. Electron.*, 2011, **12**, 2165–2173.
- [271] L.-M. Chen, Z. Hong, W. L. Kwan, C.-H. Lu, Y.-F. Lai, B. Lei, C.-P. Liu and Y. Yang, Multi-Source/Component Spray Coating for Polymer Solar Cells, *ACS Nano*, 2010, **4**, 4744–4752.
- [272] C. Yang, E. Zhou, S. Miyanishi, K. Hashimoto and K. Tajima, Preparation of Active Layers in Polymer Solar Cells by Aerosol Jet Printing, *ACS Appl. Mater. Interfaces*, 2011, **3**, 4053–4058.
- [273] X.-Y. Zhao, X. Wang, S. L. Lim, D. Qi, R. Wang, Z. Gao, B. Mi, Z.-K. Chen, W. Huang and W. Deng, Enhancement of the performance of organic solar cells by electrospray deposition with optimal solvent system, *Sol. Energy Mater. Sol. Cells*, 2014, **121**, 119–125.
- [274] Y.-J. Noh, S.-S. Kim, T.-W. Kim and S.-I. Na, Cost-effective ITO-free organic solar cells with silver nanowire–PEDOT:PSS composite electrodes via a one-step spray deposition method, *Sol. Energy Mater. Sol. Cells*, 2014, **120**, 226–230.
- [275] J. Weickert, H. Sun, C. Palumbiny, H. C. Hesse and L. Schmidt-Mende, Spray-deposited PEDOT:PSS for inverted organic solar cells, *Sol. Energy Mater. Sol. Cells*, 2010, **94**, 2371–2374.
- [276] K. Steirer, J. Berry, M. Reese and M. van Hest, Ultrasonically sprayed and inkjet printed thin film electrodes for organic solar cells, *Thin Solid Films*, 2009, **517**, 2781–2786.
- [277] Y. Kang, K. Lim, S. Jung, D. Kim, J. Kim, C. Kim, S. Kim and J. Kang, Spray-coated ZnO electron transport layer for air-stable inverted organic solar cells, *Sol. Energy Mater. Sol. Cells*, 2012, **96**, 137–140.
- [278] Y.-F. Lim, S. Lee, D. J. Herman, M. T. Lloyd, J. E. Anthony and G. G. Malliaras, Spray-deposited poly(3,4-ethylenedioxythiophene):poly(styrenesulfonate) top electrode for organic solar cells, *Appl. Phys. Lett.*, 2008, **93**, 193301.
- [279] D. Y. Choi, H. W. Kang, H. J. Sung and S. S. Kim, Annealing-free, flexible silver nanowire–polymer composite electrodes via a continuous two-step spray-coating method, *Nanoscale*, 2013, **5**, 977–983.
- [280] Y. Kim, J. Lee, H. Kang, G. Kim, N. Kim and K. Lee, Controlled electro-spray deposition of highly conductive PEDOT:PSS films, *Sol. Energy Mater. Sol. Cells*, 2012, **98**, 39–45.
- [281] A. Colsmann, M. Reinhard, T.-H. Kwon, C. Kayser, F. Nickel, J. Czolk, U. Lemmer, N. Clark, J. Jasieniak, A. B. Holmes and D. Jones, Inverted semi-transparent organic solar cells with spray coated, surfactant free polymer top-electrodes, *Sol. Energy Mater. Sol. Cells*, 2012, **98**, 118–123.
- [282] R. J. Peh, Y. Lu, F. Zhao, C.-L. K. Lee and W. L. Kwan, Vacuum-free processed transparent inverted organic solar cells with spray-coated PEDOT:PSS anode, *Sol. Energy Mater. Sol. Cells*, 2011, **95**, 3579–3584.
- [283] C. Sachse, N. Weiß, N. Gaponik, L. Müller-Meskamp, A. Eychmüller and K. Leo, ITO-Free, Small-Molecule Organic Solar Cells on Spray-Coated Copper-Nanowire-Based Transparent Electrodes, *Adv. Energy Mater.*, 2014, **4**, –.

- [284] S.-E. Park, S. Kim, D.-Y. Lee, E. Kim and J. Hwang, Fabrication of Silver Nanowire Transparent Electrodes using Electrohydrodynamic Spray Deposition for Flexible Organic Solar Cells, *J. Mater. Chem. A*, 2013, **1**, 14286–14293.
- [285] C.-C. Chen, L. Dou, R. Zhu, C.-H. Chung, T.-B. Song, Y. B. Zheng, S. Hawks, G. Li, P. S. Weiss and Y. Yang, Visibly Transparent Polymer Solar Cells Produced by Solution Processing, *ACS Nano*, 2012, **6**, 7185–7190.
- [286] L. Yang, T. Zhang, H. Zhou, S. C. Price, B. J. Wiley and W. You, Solution-Processed Flexible Polymer Solar Cells with Silver Nanowire Electrodes, *ACS Appl. Mater. Interfaces*, 2011, **3**, 4075–4084.
- [287] S. K. Hau, H.-L. Yip, K. Leong and A. K.-Y. Jen, Spraycoating of silver nanoparticle electrodes for inverted polymer solar cells, *Org. Electron.*, 2009, **10**, 719–723.
- [288] C. Girotto, B. Rand, S. Steudel, J. Genoe and C. W. Lee, Nanoparticle-based, spray-coated silver top contacts for efficient polymer solar cells, *Org. Electron.*, 2009, **10**, 735–740.
- [289] S. Kim, X. Wang, J. H. Yim, W. C. Tsoi, J.-S. Kim, S. Lee and J. C. deMello, Efficient organic solar cells based on spray-patterned single wall carbon nanotube electrodes, *J. Photon. Energy*, 2012, **2**, 021010.
- [290] L. La Notte, D. Mineo, G. Polino, G. Susanna, F. Brunetti, T. M. Brown, A. Di Carlo and A. Reale, Fabrication of Fully-Spray-Processed Organic Photovoltaic Modules by using an Automated Process in Air, *Energy Technology*, 2013, **1**, 757–762.
- [291] S.-I. Na, B.-K. Yu, S.-S. Kim, D. Vak, T.-S. Kim, J.-S. Yeo and D.-Y. Kim, Fully spray-coated ITO-free organic solar cells for low-cost power generation, *Sol. Energy Mater. Sol. Cells*, 2010, **94**, 1333–1337.
- [292] K.-J. Kim, Y.-S. Kim, W.-S. Kang, B.-H. Kang, S.-H. Yeom, D.-E. Kim, J.-H. Kim and S.-W. Kang, Inspection of substrate-heated modified PEDOT:PSS morphology for all spray deposited organic photovoltaics, *Sol. Energy Mater. Sol. Cells*, 2010, **94**, 1303–1306.
- [293] Y. Hames, S. E. San, T. Özdal, E. Aslan, H. Çabalak and H. Sar, Manufacturing of inorganic-organic hybrid solar cells by screen printing method, *Turkish J. Eng. Env. Sci.*, 2009, **34**, 261–264.
- [294] T. Aernouts, P. Vanlaeke, J. Poortmans and P. Heremans, Polymer solar cells: screen printing as a novel deposition technique, *Mater. Res. Soc. Symp. Proc.*, 2005, **836**, L3.9.1–L3.9.6.
- [295] F. C. Krebs, J. Alstrup, H. Spanggaard, K. Larsen and E. Kold, Production of large-area polymer solar cells by industrial silk screen printing, lifetime considerations and lamination with polyethyleneterephthalate, *Sol. Energy Mater. Sol. Cells*, 2004, **83**, 293–300.
- [296] S. Shaheen, R. Radspinner, N. Peyghambarian and G. Jabbour, Fabrication of bulk heterojunction plastic solar cells by screen printing, *Appl. Phys. Lett.*, 2001, **79**, 2996–2998.
- [297] N. Espinosa, F. O. Lenzmann, S. Ryley, D. Angmo, M. Hösel, R. R. Søndergaard, D. Huss, S. Däfinger, S. Gritsch, J. M. Kroon, M. Jørgensen and F. C. Krebs, OPV for mobile applications: an evaluation of roll-to-roll processed indium and silver free polymer solar cells through analysis of life cycle, cost and layer quality using inline optical and functional inspection tools, *J. Mater. Chem. A*, 2013, **1**, 7037–7049.

- [298] Y. Galagan, J.-E. J M Rubingh, R. Andriessen, C.-C. Fan, P. W. M. Blom, S. C Veenstra and J. M Kroon, ITO-free flexible organic solar cells with printed current collecting grids, *Sol. Energy Mater. Sol. Cells*, 2011, **95**, 1339–1343.
- [299] R. Søndergaard, M. Helgesen, M. Jørgensen and F. C. Krebs, Fabrication of Polymer Solar Cells Using Aqueous Processing for All Layers Including the Metal Back Electrode, *Adv. Energy Mater.*, 2010, **1**, 68–71.
- [300] H. J. van de Wiel, Y. Galagan, T. J. van Lammeren, J. F. J. de Riet, J. Gilot, M. G. M. Nagelkerke, R. H. C. A. T. Lelieveld, S. Shanmugam, A. Pagudala, D. Hui and W. A. Groen, Roll-to-roll embedded conductive structures integrated into organic photovoltaic devices, *Nanotechnology*, 2013, **24**, 484014.
- [301] T. Aernouts, P. Vanlaeke, W. Geens, J. Poortmans, P. Heremans, S. Borghs, R. Mertens, R. Andriessen and L. Leenders, Printable anodes for flexible organic solar cell modules, *Thin Solid Films*, 2004, **451-452**, 22–25.
- [302] F. C. Krebs, M. Jørgensen, K. Norrman, O. Hagemann, J. Alstrup, T. Nielsen, J. Fyenbo, K. Larsen and J. Kristensen, A complete process for production of flexible large area polymer solar cells entirely using screen printing—first public demonstration, *Sol. Energy Mater. Sol. Cells*, 2009, **93**, 422–441.
- [303] J. Goldstein, I. Yakupov and B. Breen, Development of large area photovoltaic dye cells at 3GSolar, *Sol. Energy Mater. Sol. Cells*, 2010, **94**, 638–641.
- [304] M. Hörteis and S. W. Glunz, Fine line printed silicon solar cells exceeding 20% efficiency, *Prog. Photovolt: Res. Appl.*, 2008, **16**, 555–560.
- [305] M. Hösel, R. R. Søndergaard, M. Jørgensen and F. C. Krebs, Comparison of UV-curing, hotmelt and pressure sensitive adhesive as roll-to-roll encapsulation methods for polymer solar cells, *Adv. Eng. Mater.*, 2013, **15**, 1068–1075.
- [306] M. Frey, F. Clement, S. Dilfer, D. Erath and D. Biro, Front-side Metalization By Means Of Flexographic Printing, *Energy Procedia*, 2011, **8**, 581–586.
- [307] S. Thibert, D. Chaussy, D. Beneventi, N. Reverdy-Bruas, J. Jourdan, B. Bechevet and S. Mialon, Silver ink experiments for silicon solar cell metallization by flexographic process, *Photovoltaic Specialists Conference (PVSC), 2012 38th IEEE*, 2012, 2266–2270.
- [308] J. Lee, A. Kim, S. M. Cho and H. Chae, Solvent effects on gravure-printed organic layers of nanoscale thickness for organic solar cells, *Korean J. Chem. Eng.*, 2012, **29**, 337–340.
- [309] C.-K. Cho, W.-J. Hwang, K. Eun, S.-H. Choa, S.-I. Na and H.-K. Kim, Mechanical flexibility of transparent PEDOT:PSS electrodes prepared by gravure printing for flexible organic solar cells, *Sol. Energy Mater. Sol. Cells*, 2011, **95**, 3269–3275.
- [310] S. Heusing, P. W. de Oliveira, E. Kraker, A. Haase, C. Palfinger and M. Veith, Wet chemical deposited ITO coatings on flexible substrates for organic photodiodes, *Thin Solid Films*, 2009, **518**, 1164–1169.
- [311] S. Logothetidis, D. Georgiou, A. Laskarakis, C. Koidis and N. Kalfagiannis, In-line spectroscopic ellipsometry for the monitoring of the optical properties and quality of roll-to-roll printed nanolayers for organic photovoltaics, *Sol. Energy Mater. Sol. Cells*, 2013, **112**, 144–156.

- [312] J. Yang, D. Vak, N. Clark, J. Subbiah, W. W. H. Wong, D. J. Jones, S. E. Watkins and G. Wilson, Organic photovoltaic modules fabricated by an industrial gravure printing proofer, *Sol. Energy Mater. Sol. Cells*, 2013, **109**, 47–55.
- [313] D.-Y. Chung, J. Huang, D. D. C. Bradley and A. J. Campbell, High performance, flexible polymer light-emitting diodes (PLEDs) with gravure contact printed hole injection and light emitting layers, *Org. Electron.*, 2010, **11**, 1088–1095.
- [314] M. Tuomikoski, P. Kopola, H. Jin, M. Ylikunnari, J. Hiitola-Keinanen, M. Välimäki, M. Aikio and J. Hast, Roll-to-roll manufacturing of organic photovoltaic modules, *Microelectronics and Packaging Conference, 2009. EMPC 2009.*, 2009, 1–4.
- [315] D. Tobjork, H. Aarnio, T. Mäkelä and R. Österbacka, Roll-to-Roll Fabrication of Bulk Heterojunction Plastic Solar Cells using the Reverse Gravure Coating Technique, *MRS Proceedings*, 2011, **1091**, 1091-AA05–45.
- [316] A. Kim, H. Lee, C. Ryu, S. Cho and H. Chae, Nanoscale Thickness and Roughness Control of Gravure Printed MEH-PPV Layer by Solvent Printing for Organic Light Emitting Diode, *J. Nanosci. Nanotechnol.*, 2010, **10**, 3326–3330.
- [317] H. Lee, A. Kim, S. M. Cho and H. Chae, Characterization of thermal annealing of gravure printed PVK/Ir(ppy)₃ organic light emitting layers, *Curr. Appl Phys.*, 2010, **10**, e143–e146.
- [318] M. Tuomikoski, R. Suhonen, M. Välimäki, T. Maaninen, A. Maaninen, M. Sauer, P. Rogin, M. Mennig, S. Heusing and J. Puetz, Manufacturing of polymer light-emitting device structures, *Proc. SPIE*, 2006, **6192**, 619204.
- [319] S. Tekoglu, G. Hernandez-Sosa, E. Kluge, U. Lemmer and N. Mechau, Organic Electronics, *Org. Electron.*, 2013, **14**, 3493–3499.
- [320] P. Kopola, M. Tuomikoski and R. Suhonen, Gravure printed organic light emitting diodes for lighting applications, *Thin Solid Films*, 2009, **517**, 5757–5762.
- [321] A. Kim, H. Lee, J. Lee, S. M. Cho and H. Chae, Bi-Layer Gravure Printed Nanoscale Thick Organic Layers for Organic Light Emitting Diode, *J. Nanosci. Nanotechnol.*, 2011, **11**, 546–549.
- [322] G. Hernandez-Sosa, N. Bornemann, I. Ringle, M. Agari, E. Dörsam, N. Mechau and U. Lemmer, Rheological and Drying Considerations for Uniformly Gravure-Printed Layers: Towards Large-Area Flexible Organic Light-Emitting Diodes, *Adv. Funct. Mater.*, 2013, **23**, 3164–3171.
- [323] A. Lange, A. Hollaender and M. Wegener, Modified processing conditions for optimized organic solar cells with inkjet printed P3HT:PC61BM active layers, *Mater. Sci. Eng., B*, 2013, **178**, 299–305.
- [324] A. Lange, M. Wegener, C. Boeffel, B. Fischer, A. Wedel and D. Neher, A new approach to the solvent system for inkjet-printed P3HT:PCBM solar cells and its use in devices with printed passive and active layers, *Sol. Energy Mater. Sol. Cells*, 2010, **94**, 1816–1821.
- [325] V. Fauzia, A. Umar, M. Salleh and M. Yahya, Optimizing of the inkjet printing technique parameters for fabrication of bulk heterojunction organic solar cells, *Semiconductor Electronics (ICSE), 2010 IEEE International Conference on*, 2010, 60–63.

- [326] T. Aernouts, T. Aleksandrov, C. Girotto, J. Genoe and J. Poortmans, Polymer based organic solar cells using ink-jet printed active layers, *Appl. Phys. Lett.*, 2008, **92**, 033306.
- [327] C. N. Hoth, S. A. Choulis, P. Schilinsky and C. J. Brabec, High Photovoltaic Performance of Inkjet Printed Polymer:Fullerene Blends, *Adv. Mater.*, 2007, **19**, 3973–3978.
- [328] G.-H. Lim, J.-M. Zhuo, L.-Y. Wong, S.-J. Chua, L.-L. Chua and P. K. H. Ho, A transition solvent strategy to print polymer:fullerene films using halogen-free solvents for solar cell applications, *Org. Electron.*, 2014, **15**, 449–460.
- [329] A. D. G. Del Mauro, R. Diana, I. A. Grimaldi, F. Loffredo, P. Morvillo, F. Villani and C. Minarini, Polymer solar cells with inkjet-printed doped-PEDOT:PSS anode, *Polym Compos*, 2013, **34**, 1493–1499.
- [330] S. Eom, S. Senthilarasu, P. Uthirakumar, C. Hong, Y. Lee, J. Lim, S. Yoon, C. Lee and S. Lee, Preparation and characterization of nano-scale ZnO as a buffer layer for inkjet printing of silver cathode in polymer solar cells, *Sol. Energy Mater. Sol. Cells*, 2008, **92**, 564–570.
- [331] P. Kopola, B. Zimmermann, A. Filipovic, H.-F. Schleiermacher, J. Greulich, S. Rousu, J. Hast, R. Myllylä and U. Würfel, Aerosol jet printed grid for ITO-free inverted organic solar cells, *Sol. Energy Mater. Sol. Cells*, 2012, **107**, 252–258.
- [332] Y. T. Gizachew, L. Escoubas, J. J. Simon, M. Pasquinelli, J. Loiret, P. Y. Leguen, J. C. Jimeno, J. Martin, A. Apraiz and J. P. Aguerre, Towards ink-jet printed fine line front side metallization of crystalline silicon solar cells, *Sol. Energy Mater. Sol. Cells*, 2011, **95**, S70–S82.
- [333] Y. Galagan, E. W. C. Coenen, R. Abbel, T. J. van Lammeren, S. Sabik, M. Barink, E. R. Meinders, R. Andriessen and P. W. M. Blom, Photonic sintering of inkjet printed current collecting grids for organic solar cell applications, *Org. Electron.*, 2013, **14**, 38–46.
- [334] J.-A. Jeong, J. Lee, H. Kim, H.-K. Kim and S.-I. Na, Ink-jet printed transparent electrode using nano-size indium tin oxide particles for organic photovoltaics, *Sol. Energy Mater. Sol. Cells*, 2010, **94**, 1840–1844.
- [335] J. Kim, S.-I. Na and H.-K. Kim, Inkjet printing of transparent InZnSnO conducting electrodes from nano-particle ink for printable organic photovoltaics, *Sol. Energy Mater. Sol. Cells*, 2012, **98**, 424–432.
- [336] H.-K. Kim, I.-K. You, J. B. Koo and S.-H. Kim, Organic solar cells fabricated on inkjet-printed indium tin oxide electrodes, *Surface & Coatings Technology*, 2012, **211**, 33–36.
- [337] G. Azzellino, A. Grimoldi, M. Binda, M. Caironi, D. Natali and M. Sampietro, Fully Inkjet Printed Organic Photodetectors with High Quantum Yield, *Adv. Mater.*, 2013, **25**, 6829–6833.
- [338] M. Senghor, M. Manceau, F. Ardiaca, R. de Bettignies, S. Berson, L. Dassas, S. Poughon, C. Dossou-Yovo and R. Noguera, High-speed inkjet printing for organic photovoltaic devices, *Proc. of SPIE*, 2012, **8477**, 84770M.

- [339] J. Perelaer, P. J. Smith, D. Mager, D. Soltman, S. K. Volkman, V. Subramanian, J. G. Korvink and U. S. Schubert, Printed electronics: the challenges involved in printing devices, interconnects, and contacts based on inorganic materials, *J. Mater. Chem.*, 2010, **20**, 8446–8453.
- [340] J. Perelaer and U. S. Schubert, Novel approaches for low temperature sintering of inkjet-printed inorganic nanoparticles for roll-to-roll (R2R) applications, *J. Mater. Res*, 2013, **28**, 564–573.
- [341] J. Greer and R. Street, Thermal cure effects on electrical performance of nanoparticle silver inks, *Acta Materialia*, 2007, **55**, 6345–6349.
- [342] J. K. Jung, S. H. Choi, I. Kim, H. C. Jung, J. Joung and Y. C. Joo, Characteristics of microstructure and electrical resistivity of inkjet-printed nanoparticle silver films annealed under ambient air, *Philosophical Magazine*, 2008, **88**, 339–359.
- [343] M. Hösel and F. C. Krebs, Large-scale roll-to-roll photonic sintering of flexo printed silver nanoparticle electrodes, *J. Mater. Chem.*, 2012, **22**, 15683–15688.
- [344] J. Jensen, M. Hösel, I. Kim, J.-S. Yu, J. Jo and F. C. Krebs, Fast switching ITO free electrochromic devices, *Adv. Funct. Mater.*, 2014.
- [345] M. Helgesen, J. E. Carlé, B. Andreasen, M. Hösel, K. Norrman, R. Søndergaard and F. C. Krebs, Rapid flash annealing of thermally reactive copolymers in a roll-to-roll process for polymer solar cells, *Polym. Chem.*, 2012, **3**, 2649–2655.
- [346] J. Wang, H. L. Duan, Z. P. Huang and B. L. Karihaloo, A scaling law for properties of nano-structured materials, *Proceedings of the Royal Society A: Mathematical, Physical and Engineering Sciences*, 2006, **462**, 1355–1363.
- [347] P. Buffat and J.-P. Borel, Size effect on the melting temperature of gold particles, *Phys. Rev. A*, 1976, **13**, 2287–2298.
- [348] W. Luo, W. Hu and S. Xiao, Size Effect on the Thermodynamic Properties of Silver Nanoparticles, *J. Phys. Chem. C*, 2008, **112**, 2359–2369.
- [349] J. Perelaer, A. W. M. de Laat, C. E. Hendriks and U. S. Schubert, Inkjet-printed silver tracks: low temperature curing and thermal stability investigation, *J. Mater. Chem.*, 2008, **18**, 3209–3215.
- [350] S.-J. L. Kang, *Sintering - Densification, Grain Growth, and Microstructure*, Elsevier Butterworth-Heinemann, Oxford, 1st edn., 2005.
- [351] A. Kamyshny, J. Steinke and S. Magdassi, Metal-based Inkjet Inks for Printed Electronics, *The Open Applied Physics Journal*, 2011, **4**, 19–36.
- [352] V. Gorshkov, V. Kuzmenko and V. Privman, Nonequilibrium Kinetic Study of Sintering of Dispersed Nanoparticles, *CrystEngComm*, 2013, **36**, 7177–7191.
- [353] A. T. Alastalo, H. Seppä, J. H. Leppäniemi, M. J. Aronniemi, M. L. Allen and T. Mattila, Modelling of nanoparticle sintering under electrical boundary conditions, *J. Phys. D: Appl. Phys.*, 2010, **43**, 485501.

- [354] Y. Min, M. Akbulut, K. Kristiansen, Y. Golan and J. Israelachvili, The role of interparticle and external forces in nanoparticle assembly, *Nature Materials*, 2008, **7**, 527–538.
- [355] M. Allen, A. Alastalo, M. Suhonen, T. Mattila, J. Leppaniemi and H. Seppa, Contactless Electrical Sintering of Silver Nanoparticles on Flexible Substrates, *IEEE Transactions on Microwave Theory and Techniques*, 2011, **59**, 1419–1429.
- [356] J. Perelaer, B. de Gans and U. Schubert, Ink-jet Printing and Microwave Sintering of Conductive Silver Tracks, *Adv. Mater.*, 2006, **18**, 2101–2104.
- [357] I. Reinhold, C. Hendriks, R. Eckardt, J. Kranenburg, J. Perelaer, R. Baumann and U. Schubert, Argon plasma sintering of inkjet printed silver tracks on polymer substrates, *J. Mater. Chem.*, 2009, **19**, 3384–3388.
- [358] M. Cherrington, T. C. Claypole, D. Deganello, I. Mabbett, T. Watson and D. Worsley, Ultrafast near-infrared sintering of a slot-die coated nano-silver conducting ink, *J. Mater. Chem.*, 2011, **21**, 7562–7564.
- [359] S. Magdassi, M. Grouchko, O. Berezin and A. Kamyshny, Triggering the Sintering of Silver Nanoparticles at Room Temperature, *ACS Nano*, 2010, **4**, 1943–1948.
- [360] J. Yeo, G. Kim, S. Hong, M. S. Kim, D. Kim, J. Lee, H. B. Lee, J. Kwon, Y. D. Suh, H. W. Kang, H. J. Sung, J.-H. Choi, W.-H. Hong, J. M. Ko, S.-H. Lee, S.-H. Choa and S. H. Ko, Flexible supercapacitor fabrication by room temperature rapid laser processing of roll-to-roll printed metal nanoparticle ink for wearable electronics application, *Journal of Power Sources*, 2014, **246**, 562–568.
- [361] J. West, J. W. Sears, S. Smith and M. Carter, in *Sintering of Advanced Materials - Fundamentals and Processes*, ed. Z. Z. Fang, Woodhead Publishing, 2010, pp. 275–288.
- [362] K. Schroder, S. McCool and W. Furlan, Broadcast Photonic Curing of Metallic Nanoparticle Films, *Presented at NSTI Nanotech May*, 2006.
- [363] T. Gebel, L. Rebohle, R. Fendler, W. Hentsch, W. Skorupa, M. Voelskow, W. Anwand and R. Yankov, Millisecond Annealing with Flashlamps: Tool and Process Challenges, *Advanced Thermal Processing of Semiconductors, 2006. RTP'06. 14th IEEE International Conference on*, 2006, 47–55.
- [364] M. J. Guillot, S. McCool and K. Schroder, Simulating The Thermal Response Of Thin Films During Photonic Curing, *Proceedings of the 12th International Conference on Nuclear Engineering*, 2012, 1–9.
- [365] J. West, M. Carter, S. Smith and J. Sears, in *Sintering - Methods and Products*, ed. V. Shatokha, InTech, 2012, pp. 173–188.
- [366] S. Farnsworth and K. Schroder, Photonic curing for millisecond-drying of thin films, *Specialist Printing Worldwide*, 2012, 34–36.
- [367] J. West, M. Carter, S. Smith, J. Sears and S. Rapid City, Photonic Curing of Silver Nanoparticle Based Inks, *Proceedings of NSTI-Nanotech 2010*, 2010, 210–213.
- [368] D. D. Liana, B. Raguse, L. Wiczorek, G. R. Baxter, K. Chuah, J. J. Gooding and E. Chow, Sintered gold nanoparticles as an electrode material for paper-based electrochemical sensors, *RSC Adv.*, 2013, **3**, 8683–8691.

- [369] H.-J. Hwang, W.-H. Chung and H.-S. Kim, In situ monitoring of flash-light sintering of copper nanoparticle ink for printed electronics, *Nanotechnology*, 2012, **23**, 485205.
- [370] J. Ryu, H. Kim and H. Hahn, Reactive sintering of copper nanoparticles using intense pulsed light for printed electronics, *Journal of Electronic Materials*, 2011, **40**, 42–50.
- [371] H.-S. Kim, S. R. Dhage, D.-E. Shim and H. T. Hahn, Intense pulsed light sintering of copper nanoink for printed electronics, *Appl. Phys. A*, 2009, **97**, 791–798.
- [372] N. Marjanovic, J. Hammerschmidt, J. Perelaer, S. Farnsworth, I. Rawson, M. Kus, E. Yenel, S. Tilki, U. S. Schubert and R. R. Baumann, Inkjet printing and low temperature sintering of CuO and CdS as functional electronic layers and Schottky diodes, *J. Mater. Chem.*, 2011, **21**, 13634–13639.
- [373] T. Araki, T. Sugahara, J. Jiu, S. Nagao, M. Nogi, H. Koga, H. Uchida, K. Shinozaki and K. Sugauma, Cu Salt Ink Formulation for Printed Electronics using Photonic Sintering, *Langmuir*, 2013, **29**, 11192–11197.
- [374] B.-Y. Wang, T.-H. Yoo, Y.-W. Song, D.-S. Lim and Y.-J. Oh, Cu Ion Ink for a Flexible Substrate and Highly Conductive Patterning by Intensive Pulsed Light Sintering, *ACS Appl. Mater. Interfaces*, 2013, **5**, 4113–4119.
- [375] W.-S. Han, J.-M. Hong, H.-S. Kim and Y.-W. Song, Multi-pulsed white light sintering of printed Cu nanoinks, *Nanotechnology*, 2011, **22**, 395705.
- [376] S. R. Dhage, H.-S. Kim and H. T. Hahn, Cu(In,Ga)Se₂ Thin Film Preparation from a Cu(In,Ga) Metallic Alloy and Se Nanoparticles by an Intense Pulsed Light Technique, *Journal of Electronic Materials*, 2010, **40**, 122–126.
- [377] S. H. Park and H. S. Kim, Flash light sintering of nickel nanoparticles for printed electronics, *Thin Solid Films*, 2014, **550**, 575–581.
- [378] S.-H. Park, S. Jang, D.-J. Lee, J. Oh and H.-S. Kim, Two-step flash light sintering process for crack-free inkjet-printed Ag films, *Journal of Micromechanics and Microengineering*, 2013, **23**, 015013.
- [379] W.-H. Chung, H.-J. Hwang, S.-H. Lee and H.-S. Kim, In situ monitoring of a flash light sintering process using silver nano-ink for producing flexible electronics, *Nanotechnology*, 2013, **24**, 035202.
- [380] J. Perelaer, R. Abbel, S. Wünscher, R. Jani, T. van Lammeren and U. S. Schubert, Roll-to-Roll Compatible Sintering of Inkjet Printed Features by Photonic and Microwave Exposure: From Non-Conductive Ink to 40 Conductivity in Less Than 15 Seconds, *Adv. Mater.*, 2012, **24**, 2620–2625.
- [381] T. Fałat, B. Płatek, J. Felba, A. Moscicki, A. Smolarek and K. Stojek, Photonic Sintering Process of Ink-Jet Printed Conductive Microstructures, *Electronic System-Integration Technology Conference (ESTC)*, 2012, 1–5.
- [382] R. Abbel, T. van Lammeren, R. Hendriks, J. Ploegmakers, E. J. Rubingh, E. R. Meinders and W. A. Groen, Photonic flash sintering of silver nanoparticle inks: a fast and convenient method for the preparation of highly conductive structures on foil, *MRS Communications*, 2012, **2**, 145–150.

- [383] I. Reinhold, M. Müller, M. Müller, W. Voit and W. Zapka, Spectrally Enhanced Photonic Sintering, *NIP 28 and Digital Fabrication 2012*, 2012, 424–430.
- [384] D.-J. Lee, S.-H. Park, S. Jang, H.-S. Kim, J. H. Oh and Y.-W. Song, Pulsed light sintering characteristics of inkjet-printed nanosilver films on a polymer substrate, *Journal of Micromechanics and Microengineering*, 2011, **21**, 125023.
- [385] S. Farnsworth, Processing Inkjet vs. Screen Printed Metal-Based Inks on Low-Temperature Substrates, *Coating International*, 2011, **44**, 16–18.
- [386] T. Falat, J. Felba, B. Platek, T. Piasecki, A. Moscicki and A. Smolarek, Low-temperature, photonic approach to sintering the ink-jet printed conductive microstructures containing nano sized silver particles, *Microelectronics and Packaging Conference (EMPC), 2011 18th European*, 2011, 1–4.
- [387] S. Ahmed, Sintering nanoparticle-based inks on challenging substrates, *Industrial + Specialty Printing*, 2011, 20–23.
- [388] J. Kang, J. Ryu, H. Kim and H. Hahn, Sintering of Inkjet-Printed Silver Nanoparticles at Room Temperature Using Intense Pulsed Light, *Journal of Electronic Materials*, 2011, **40**, 2268–2277.
- [389] K. C. Yung, X. Gu, C. P. Lee and H. S. Choy, Ink-jet printing and camera flash sintering of silver tracks on different substrates, *Journal of Materials Processing Tech.*, 2010, **210**, 2268–2272.
- [390] J. Jiu, H. Sugahara, M. Nogi, T. Araki, K. Suganuma, H. Uchida and K. Shinozaki, High-intensity pulse light sintering silver nanowire transparent films on polymer substrates: the effect the thermal properties of substrates on the performance of silver films, *Nanoscale*, 2013, **5**, 11820–11828.
- [391] J. Jiu, M. Nogi, T. Sugahara, T. Tokuno, T. Araki, N. Komoda, K. Suganuma, H. Uchida and K. Shinozaki, Strongly adhesive and flexible transparent silver nanowire conductive films fabricated with a high-intensity pulsed light technique, *J. Mater. Chem.*, 2012, **22**, 23561–23567.
- [392] R. Abbel, J. van den Boomen, T. van Lammeren, T. de Koning, J. J. P. Vaeton and E. R. Meinders, Current Collecting Grids for R2R Processed Organic Solar Cells, *MRS Proceedings*, 2011, **1323**, 87–92.
- [393] P. Saffman and G. Taylor, The penetration of a fluid into a porous medium or Hele-Shaw cell containing a more viscous liquid, *Proceedings of the Royal Society of London. Series A. Mathematical and Physical Sciences*, 1958, **245**, 312–329.
- [394] D.-J. Lee, J. H. Oh and H. S. Bae, Crack formation and substrate effects on electrical resistivity of inkjet-printed Ag lines, *Materials Letters*, 2010, **64**, 1069–1072.
- [395] M. Jørgensen, J. E. Carlé, R. R. Søndergaard, M. Lauritzen, N. A. Dagnæs-Hansen, S. L. Byskov, T. R. Andersen, T. T. Larsen-Olsen, A. P. L. Böttiger, B. Andreasen, L. Fu, L. Zuo, Y. Liu, E. Bundgaard, X. Zhan, H. Chen and F. C. Krebs, The state of organic solar cells—A meta analysis, *Sol. Energy Mater. Sol. Cells*, 2013, **119**, 84–93.

- [396] M. Panayotova and V. Panyotov, Indium - one of crucial metals for the sustainable society development, *Annual Of The University Of Mining And Geology St. Ivan Rilski*, 2013, **56**, 159–164.
- [397] H. Hoppe, M. Seeland and B. Muhsin, Optimal geometric design of monolithic thin-film solar modules: Architecture of polymer solar cells, *Sol. Energy Mater. Sol. Cells*, 2012, **97**, 119–126.
- [398] S. Na, S. Kim, J. Jo and D. Kim, Efficient and flexible ITO-free organic solar cells using highly conductive polymer anodes, *Adv. Mater.*, 2008, **20**, 4061–4406.
- [399] K. Leppänen, B. Augustine, J. Saarela, R. Myllylä and T. Fabritius, Solar Energy Materials & Solar Cells, *Sol. Energy Mater. Sol. Cells*, 2013, **117**, 512–518.
- [400] D. Angmo and F. C. Krebs, Flexible ITO-Free Polymer Solar Cells, *J. Appl. Polym. Sci.*, 2013, **129**, 1–14.
- [401] D. S. Hecht and R. B. Kaner, Solution-processed transparent electrodes, *MRS Bull.*, 2011, **36**, 749–755.
- [402] K. Tvingstedt and O. Inganäs, Electrode grids for ITO free organic photovoltaic devices, *Adv. Mater.*, 2007, **19**, 2893–2897.
- [403] S.-I. Na, D.-W. Park, S.-S. Kim, S.-Y. Yang, K. Lee and M.-H. Lee, ITO-free flexible polymer solar cells with ink-jet-printed Ag grids, *Semicond. Sci. Technol.*, 2012, **27**, 125002.
- [404] J. Zou, H.-L. Yip, S. K. Hau and A. K.-Y. Jen, Metal grid/conducting polymer hybrid transparent electrode for inverted polymer solar cells, *Appl. Phys. Lett.*, 2010, **96**, 203301.
- [405] Y. Galagan, E. W. C. Coenen, B. Zimmermann, L. H. Slooff, W. J. H. Verhees, S. C. Veenstra, J. M. Kroon, M. Jørgensen, F. C. Krebs and R. Andriessen, Scaling Up ITO-Free Solar Cells, *Adv. Energy Mater.*, 2014, **4**, –.
- [406] Y. Li, L. Mao, Y. Gao, P. Zhang, C. Li, C. Ma, Y. Tu, Z. Cui and L. Chen, ITO-free photovoltaic cell utilizing a high-resolution silver grid current collecting layer, *Sol. Energy Mater. Sol. Cells*, 2013, **113**, 85–89.
- [407] J. Chow, *Productivity and System Improvements in an Organic Photovoltaic Panel Manufacturing Facility*, Massachusetts Institute of Technology technical report, 2011.
- [408] R. R. Søndergaard, M. Hösel, N. Espinosa, M. Jørgensen and F. C. Krebs, Practical evaluation of organic polymer thermoelectrics by large-area R2R processing on flexible substrates, *Energy Science & Engineering*, 2013, **1**, 81–88.
- [409] M. Jørgensen, K. Norrman and F. C. Krebs, Stability/degradation of polymer solar cells, *Sol. Energy Mater. Sol. Cells*, 2008, **92**, 686–714.
- [410] N. Grossiord, J. M. Kroon, R. Andriessen and P. W. M. Blom, Degradation mechanisms in organic photovoltaic devices, *Org. Electron.*, 2012, **13**, 432–456.
- [411] E. Voroshazi, B. Verreet and P. Heremans, Long-term operational lifetime and degradation analysis of P3HT:PCBM photovoltaic cells, *Sol. Energy Mater. Sol. Cells*, 2011, **95**, 1303–1307.

- [412] J. U. Lee, J. W. Jung, J. W. Jo and W. H. Jo, Degradation and stability of polymer-based solar cells, *J. Mater. Chem.*, 2012, **22**, 24265–24283.
- [413] S. Cros, R. de Bettignies, S. Berson, S. Bailly, P. Maisse, N. Lemaitre and S. Guillerez, Definition of encapsulation barrier requirements: A method applied to organic solar cells, *Sol. Energy Mater. Sol. Cells*, 2011, **95**, S65–S69.
- [414] J. Fahlteich, M. Fahland, W. Schönberger and N. Schiller, Permeation barrier properties of thin oxide films on flexible polymer substrates, *Thin Solid Films*, 2009, **517**, 3075–3080.
- [415] J.-S. Park, H. Chae, H. K. Chung and S. I. Lee, Thin film encapsulation for flexible AM-OLED: a review, *Semicond. Sci. Technol.*, 2011, **26**, 034001.
- [416] S. Amberg-Schwab, U. Weber, A. Burger, S. Nique and R. Xalter, Development of Passive and Active Barrier Coatings on the Basis of Inorganic–Organic Polymers, *Monatshefte für Chemie/Chemical Monthly*, 2006, **137**, 657–666.
- [417] C. Charton, N. Schiller, M. Fahland, A. Holländer, A. Wedel and K. Noller, Development of high barrier films on flexible polymer substrates, *Thin Solid Films*, 2006, **502**, 99–103.
- [418] S.-W. Seo, E. Jung, H. Chae, S. J. Seo, H. K. Chung and S. M. Cho, Bending properties of organic–inorganic multilayer moisture barriers, *Thin Solid Films*, 2014, **550**, 742–746.
- [419] C.-S. Huang, H.-T. Lin, G.-S. Huang, J.-P. Hu, S.-T. Lu, C. T. Liu, S. Garner, J.-C. Lin, K.-T. Kuo, G. Merz, J. Tosch and C. Chang, Roll-to-roll Process on Ultra-thin Flexible Glass for Manufacturing the Multi-Touch Sensor Panel, *SID DIGEST*, 2013, 807–809.
- [420] D. M. Tanenbaum, M. Hermenau, E. Voroshazi, M. T. Lloyd, Y. Galagan, B. Zimmermann, M. Hösel, H. F. Dam, M. Jørgensen, S. A. Gevorgyan, S. Kudret, W. Maes, L. Lutsen, D. Vanderzande, U. Würfel, R. Andriessen, R. Rösch, H. Hoppe, G. Teran-Escobar, M. Lira-Cantu, A. Rivaton, G. Y. Uzunoglu, D. Germack, B. Andreasen, M. V. Madsen, K. Norrman and F. C. Krebs, The ISOS-3 inter-laboratory collaboration focused on the stability of a variety of organic photovoltaic devices, *RSC Adv.*, 2012, **2**, 882–893.
- [421] P. E. Burrows, V. Bulovic, S. R. Forrest, L. S. Sapochak, D. M. McCarty and M. E. Thompson, Reliability and degradation of organic light emitting devices, *Appl. Phys. Lett.*, 1994, **65**, 2922–2924.
- [422] M. Riede, C. L. Uhrich, J. Widmer, R. Timmreck, D. Wynands, G. Schwartz, W. Gnehr, D. Hildebrandt, A. Weiss, J. Hwang, S. Sundarraj, P. Erk, M. Pfeiffer and K. Leo, Efficient Organic Tandem Solar Cells based on Small Molecules, *Adv. Funct. Mater.*, 2011, **21**, 3019–3028.
- [423] R. Roesch, K.-R. Eberhardt, S. Engmann, G. Gobsch and H. Hoppe, Solar Energy Materials & Solar Cells, *Sol. Energy Mater. Sol. Cells*, 2013, **117**, 59–66.
- [424] S. B. Sapkota, M. Fischer, B. Zimmermann and U. Würfel, Solar Energy Materials & Solar Cells, *Sol. Energy Mater. Sol. Cells*, 2014, **121**, 43–48.
- [425] M. W. Möller, D. A. Kunz, T. Lunkenbein, S. Sommer, A. Nennemann and J. Breu, UV-Cured, Flexible, and Transparent Nanocomposite Coating with Remarkable Oxygen Barrier, *Adv. Mater.*, 2012, **24**, 2142–2147.

- [426] R. R. Søndergaard, T. Makris, P. Lianos, A. Manor, E. A. Katz, W. Gong, S. M. Tuladhar, J. Nelson, R. Tuomi, P. Sommeling, S. C. Veenstra, A. Rivaton, A. Dupuis, G. Teran-Escobar, M. Lira-Cantu, S. B. Sapkota, B. Zimmermann, U. Würfel, A. Matzarakis and F. C. Krebs, The use of polyurethane as encapsulating method for polymer solar cells—An inter laboratory study on outdoor stability in 8 countries, *Sol. Energy Mater. Sol. Cells*, 2012, **99**, 292–300.
- [427] S. Sarkar, J. H. Culp, J. T. Whyland, M. Garvan and V. Misra, Encapsulation of organic solar cells with ultrathin barrier layers deposited by ozone-based atomic layer deposition, *Org. Electron.*, 2010, **11**, 1896–1900.
- [428] C. Chang, C. Chou, Y. Lee, M. Chen and F. Tsai, Thin-film encapsulation of polymer-based bulk-heterojunction photovoltaic cells by atomic layer deposition, *Org. Electron.*, 2009, **10**, 1300–1306.
- [429] J. A. van Delft, D. Garcia-Alonso and W. M. M. Kessels, Atomic layer deposition for photovoltaics: applications and prospects for solar cell manufacturing, *Semicond. Sci. Technol.*, 2012, **27**, 074002.
- [430] J. Granstrom, M. Villet, T. Chatterjee, J. A. Gerbec, E. Jerkunica and A. Roy, Multilayer barrier films comprising nitrogen spacers between free-standing barrier layers, *Appl. Phys. Lett.*, 2009, **95**, 093306.
- [431] P. Mandlik, J. Gartside, L. Han, I.-C. Cheng, S. Wagner, J. A. Silvernail, R.-Q. Ma, M. Hack and J. J. Brown, A single-layer permeation barrier for organic light-emitting displays, *Appl. Phys. Lett.*, 2008, **92**, 103309.
- [432] M. R. Cavallari, C. M. Cuppoletti, G. Pucker, F. J. Fonseca, A. M. Andrade, S. Carturan, G. Maggioni, A. Quaranta, M. Buffa and M. Tonezzer, Degradation studies of rigid and flexible rr-P3HT:PCBM bulk heterojunction solar cells encapsulated with a parylene polymeric coating, *11th International Conference on Advanced Materials*, 2009.
- [433] Z. Liu, J. Li and F. Yan, Package-Free Flexible Organic Solar Cells with Graphene top Electrodes, *Adv. Mater.*, 2013, **25**, 4296–4301.
- [434] H. J. Lee, H. P. Kim, H.-M. Kim, J.-H. Youn, D.-H. Nam, Y.-G. Lee, J.-G. Lee, A. R. bin Mohd Yusoff and J. Jang, Solution processed encapsulation for organic photovoltaics, *Sol. Energy Mater. Sol. Cells*, 2013, **111**, 97–101.
- [435] J. Ahmad, K. Bazaka, L. J. Anderson, R. D. White and M. V. Jacob, Materials and methods for encapsulation of OPV: A review, *Renewable and Sustainable Energy Reviews*, 2013, **27**, 104–117.
- [436] D. M. Tanenbaum, H. F. Dam, R. Rösch, M. Jørgensen, H. Hoppe and F. C. Krebs, Edge sealing for low cost stability enhancement of roll-to-roll processed flexible polymer solar cell modules, *Sol. Energy Mater. Sol. Cells*, 2012, **97**, 157–163.
- [437] M. O. Reese, S. A. Gevorgyan, M. Jørgensen, E. Bundgaard, S. R. Kurtz, D. S. Ginley, D. C. Olson, M. T. Lloyd, P. Morvillo, E. A. Katz, A. Elschner, O. Haillant, T. R. Currier, V. Shrotriya, M. Hermenau, M. Riede, K. R. Kirov, G. Trimmel, T. Rath, O. Inganäs, F. Zhang, M. Andersson, K. Tvingstedt, M. Lira-Cantu, D. Laird, C. McGuinness, S. J. Gowrisanker, M. Pannone, M. Xiao, J. Hauch, R. Steim, D. M. DeLongchamp, R. Rösch,

- H. Hoppe, N. Espinosa, A. Urbina, G. Yaman-Uzunoglu, J.-B. Bonekamp, A. J. J. M. van Breemen, C. Girotto, E. Voroshazi and F. C. Krebs, Consensus stability testing protocols for organic photovoltaic materials and devices, *Sol. Energy Mater. Sol. Cells*, 2011, **95**, 1253–1267.
- [438] M. Hösel, R. R. Søndergaard, M. Jørgensen and F. C. Krebs, Failure Modes and Fast Repair Procedures in High Voltage Organic Solar Cell Installations, *Adv. Energy Mater.*, 2014.
- [439] N. Espinosa, M. Hösel, M. Jørgensen and F. C. Krebs, Large scale deployment of polymer solar cells on land, on sea and in the air, *Energy Environ. Sci.*, 2014, **3**, 855–866.
- [440] A. J. Medford, M. R. Lilliedal, M. Jørgensen, D. Aarø, H. Pakalski, J. Fyenbo and F. C. Krebs, Grid-connected polymer solar panels: initial considerations of cost, lifetime, and practicality, *Optics Express*, 2010, **18**, A272–A285.
- [441] Å. Jönsson, T. Björklund and A.-M. Tillman, LCA of concrete and steel building frames, *Int. J. LCA*, 1998, **3**, 216–224.
- [442] M. García, L. Marroyo, E. Lorenzo, J. Marcos and M. Pérez, Observed degradation in photovoltaic plants affected by hot-spots, *Prog. Photovolt: Res. Appl.*, 2013.
- [443] P. Sánchez-Friera, M. Piliouge, J. Peláez, J. Carretero and M. Sidrach de Cardona, Analysis of degradation mechanisms of crystalline silicon PV modules after 12 years of operation in Southern Europe, *Prog. Photovolt: Res. Appl.*, 2011, **19**, 658–666.
- [444] J. Muñoz, E. Lorenzo, F. Martínez-Moreno, L. Marroyo and M. García, An investigation into hot-spots in two large grid-connected PV plants, *Prog. Photovolt: Res. Appl.*, 2008, **16**, 693–701.
- [445] C. Buerhop, D. Schlegel, M. Niess, C. Vodermayr, R. Weißmann and C. J. Brabec, Reliability of IR-imaging of PV-plants under operating conditions, *Sol. Energy Mater. Sol. Cells*, 2012, **107**, 154–164.

A. Appendix

This thesis is based on the following publications:

- **M. Hösel**, R. R. Søndergaard, M. Jørgensen and F. C. Krebs, Fast inline roll-to-roll printing and coating of electrodes for indium-tin-oxide free polymer solar cells using automatic registration, *Energy Technology*, 2013, **1**, 102–107.
- **M. Hösel**, R. R. Søndergaard, D. Angmo and F. C. Krebs, Comparison of fast roll-to-roll flexographic, inkjet, flatbed and rotary screen printing of metal back electrodes for polymer solar cells, *Adv. Eng. Mater.*, 2013, **15**, 995–1001.
- **M. Hösel**, R. R. Søndergaard, M. Jørgensen and F. C. Krebs, Comparison of UV-curing, hotmelt and pressure sensitive adhesive as roll-to-roll encapsulation methods for polymer solar cells, *Adv. Eng. Mater.*, 2013, **15**, 1068–1075.
- **M. Hösel** and F. C. Krebs, Large-scale roll-to-roll photonic sintering of flexo printed silver nanoparticle electrodes, *J. Mater. Chem.*, 2012, **22**, 15683–15688.
- **M. Hösel**, R. R. Søndergaard, M. Jørgensen and F. C. Krebs, Failure modes and fast repair procedures in high voltage organic solar cell installations, *Adv. Energy Mater.*, 2014, in press.
- P. Sommer-Larsen, M. Jørgensen, R. R. Søndergaard, **M. Hösel** and F. C. Krebs, It is all in the pattern - high efficiency power extraction from polymer solar cells through high voltage serial connection, *Energy Technology*, 2013, **1**, 15–19.
- F. C. Krebs, N. Espinosa, **M. Hösel**, R. R. Søndergaard and M. Jørgensen, 25th Anniversary Article: Rise to Power - OPV-Based Solar Parks, *Adv. Mater.*, 2014, **26**, 29-39.
- N. Espinosa, **M. Hösel**, M. Jørgensen and F. C. Krebs, Large scale deployment of polymer solar cells on land, on sea and in the air, *Energy Environ. Sci.*, 2014, **7**, 855-866.
- R. Søndergaard, **M. Hösel**, D. Angmo, T. T. Larsen-Olsen and F. C. Krebs, Roll-to-roll fabrication of polymer solar cells, *Mater. Today*, 2012, **15**, 36–49.
- R. R. Søndergaard, **M. Hösel** and F. C. Krebs, Roll-to-Roll fabrication of large area functional organic materials, *J. Polym. Sci. B Polym. Phys.*, 2013, **51**, 16–34.

Fast Inline Roll-to-Roll Printing for Indium-Tin-Oxide-Free Polymer Solar Cells Using Automatic Registration

Markus Hösel, Roar R. Søndergaard, Mikkel Jørgensen, and Frederik C. Krebs*^[a]

Fast inline roll-to-roll printing and coating on polyethylene terephthalate (PET) and barrier foil was demonstrated under ambient conditions at web speeds of 10 m min^{-1} for the manufacture of indium-tin-oxide-free (ITO-free) polymer solar cells comprising a 6-layer stack: silver-grid/PEDOT:PSS/ZnO/P3HT:PCBM/PEDOT:PSS/silver-grid. The first and second layers were printed at the same time using inline processing at a web speed of 10 m min^{-1} where flexographic printing of a hexagonal silver grid comprises the first layer followed by rotary-screen printing of a PEDOT:PSS electrode as the second layer. The third and fourth layers were slot-die coated at the same time again using inline processing

at a web speed of 10 m min^{-1} of firstly zinc oxide as the electron transport layer followed by P3HT:PCBM as the active layer. The first three layers (silver-grid/PEDOT:PSS/ZnO) comprise a generally applicable ITO-free, semitransparent, electron-selective front electrode for inverted polymer solar cells. This electrode shows a low sheet resistance ($\sim 10 \Omega/\square$) and good optical transmission in the visible range ($\sim 60\%$). The solar cell stack was completed by rotary-screen printing of a hole-collecting PEDOT:PSS layer at 2 m min^{-1} and a comb-patterned silver-grid back electrode at the same speed. The solar cells were post processed by using fast roll-to-roll switching to a functional state.

Introduction

Indium tin oxide (ITO) has for decades been the only widely available transparent electrode for a number of technologies, that is, organic photovoltaics (OPVs) and organic/polymer light emitting diode (OLED/PLED) devices.^[1,2] Research in these areas has been driven by the potential for low-cost manufacture at high throughput using roll-to-roll (R2R) techniques, for which the use of indium is unfavorable because of its scarcity and high cost. It is, therefore, paramount that alternatives to ITO are found, but just as important is their actual implementation in the research communities to convince researchers to adopt the use of these new electrode types instead of ITO, which is unlikely to be sustainable for large-scale technologies. Numerous attempts to substitute ITO, particularly in OPVs, have been reported, including PEDOT:PSS [poly(3,4-ethylenedioxythiophene):poly(styrenesulfonate)],^[3,4] thin semitransparent metal layers,^[5-8] metal grid structures,^[9-13] metal nanowires,^[14-16] graphene,^[17-19] and carbon nanotubes^[20] with varying success. However, only the report in Ref. [11] has demonstrated the potential to be sufficiently scaleable for the final substrate to be produced at a speed and cost allowing for its consideration as a serious candidate for R2R printing.

Here we present a new flexible semitransparent substrate which, when used in the preparation of OPVs, provides similar performances to analogous modules prepared on ITO-covered substrates.^[1] This “flextrode” substrate is suitable for inverted-structure OPVs and is based on a high-conductivity PEDOT:PSS layer, which is coated with zinc oxide. For larger areas a flexo-printed silver grid reduces sheet resistance. We demonstrate how the ITO-free electrode material can be processed at high speed by printing several layers at

the same time using inline printing and coating. We show that a length of 1000 m is easily manufactured within a few hours having full 2-dimensional registration of the printed pattern. We see this as the first real candidate for a mass producible replacement for ITO, and to promote the use of such substrates in academic research, this substrate is made freely available.

Results and Discussion

The flextrode substrate suitable for large-area OPVs was prepared by flexographic printing of a honeycomb-patterned silver grid structure (2 mm pitch) by using a water-based silver-nanoparticle ink (PFI-722 from PChem Associates with 60 wt % Ag content). This was followed by rotary-screen printing PEDOT:PSS on top of and in registry with the silver grid exposing one side of the silver for subsequent direct contacting and serial interconnection of modules by printing. The highly conductive PEDOT:PSS (Heraeus Clevis PH1000) was diluted with isopropanol at a concentration of 10:3 by weight to ensure proper printing. The inline processing speed was 10 m min^{-1} and is in reality only limited by the drying speed (in $2 \times 2 \text{ m}^2$ ovens). Infrared dryers were used in conjunction with hot-air convection ovens at a tem-

[a] M. Hösel, R. R. Søndergaard, M. Jørgensen, F. C. Krebs
Department of Energy Conversion and Storage
Technical University of Denmark
Frederiksborgvej 399, 4000 Roskilde (Denmark)
E-mail: frkr@dtu.dk

Supporting Information for this article is available on the WWW under <http://dx.doi.org/10.1002/ente.201200029>.

perature of 140 °C. ZnO ink as a stabilized nanoparticle suspension in acetone (55 mg mL⁻¹) was finally coated on top by slot-die coating (10 m min⁻¹) to smooth the surface and leave a small part of the bottom electrode exposed for later contacting. Critical to the success is the formulation and the application of the ZnO ink because it is reactive towards the atmosphere. The nanoparticulate nature of the ZnO and the acetone solvent employed serve to dissolve the PEDOT:PSS surface slightly whereas the nanoparticles efficiently fill voids in the surface. The net result is a very smooth surface that is fully covered with ZnO. It should be emphasized that the ink formulation represents a 6-year effort of optimization and that the formulation of the ink and the details of the process depend quite closely on one another. The flextrode carrier substrate is either polyethylene terephthalate (PET, Dupont-Teijin, Melinex ST506) or barrier foil (Amcors, Ceramis). The three processing steps and a processing flowchart are shown in Figures 1 and 2.

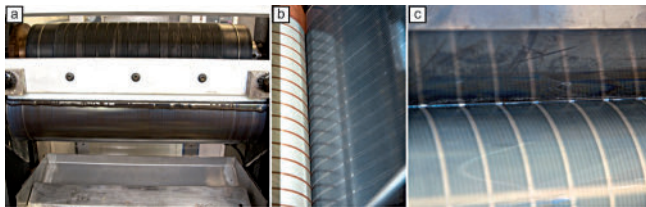


Figure 1. Processing of the flextrode substrate on PET: a) Flexo-printing of the silver grid; b) Rotary-screen printing of PEDOT:PSS; and c) slot-die coating of nanoparticle-based ZnO ink.

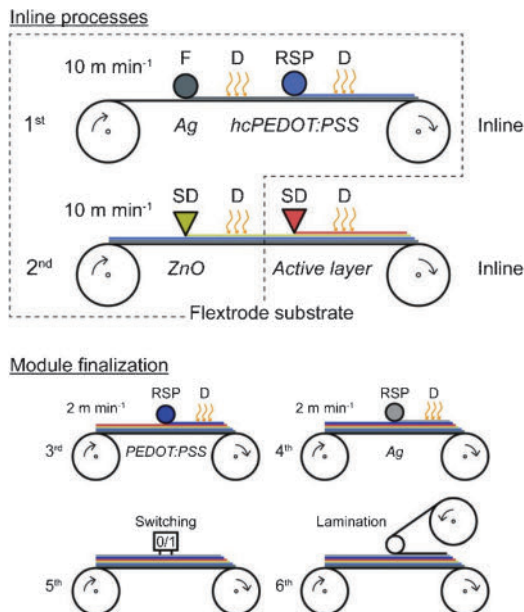


Figure 2. Flowchart visualizing the inline fabrication of the flextrode substrate and the solar cell module finalization. Currently, the silver grid together with highly conductive PEDOT:PSS layer, ZnO, and an active layer can be processed inline at 10 m min⁻¹. The illustrated processes are flexo-printing (F), rotary-screen printing (RSP), slot-die coating (SD), and drying (D).

When preparing small-area OPVs the silver grid is not necessary, and, therefore, the initial flexo-printing step of the silver grid was eliminated as demonstrated earlier.^[21] Using a silver grid lowers the sheet resistance of the front electrode but inherently blocks some of the surface from incoming light. Figure 3 a and b show the transmittance characteristics

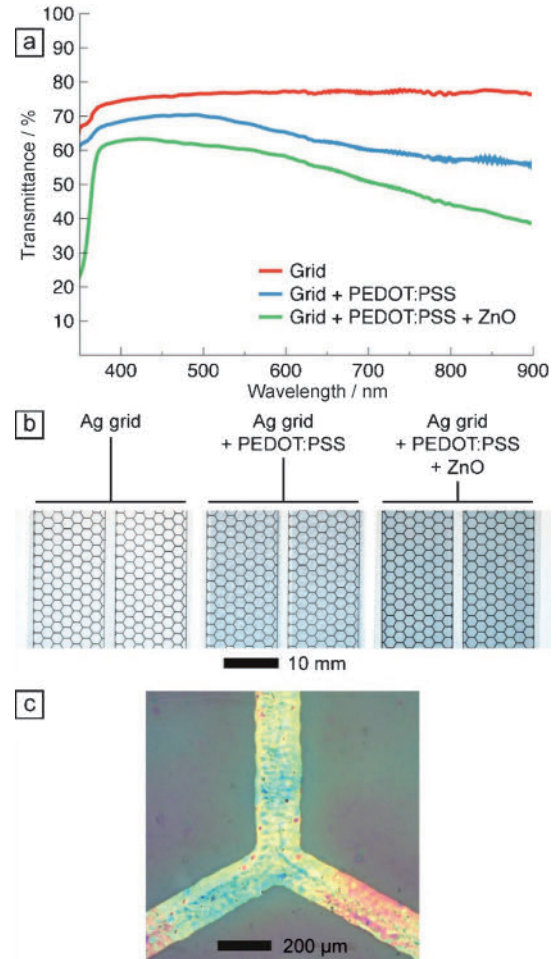


Figure 3. a) Illustration of the optical transmittance after each processing step. b) Photos of the substrate after each processing step. c) Optical microscopy image of the silver grid lines with a PEDOT:PSS layer on top.

for the substrate after each processing step, and the light blocking is clearly observed as the transmittance is reduced to around 80% after processing of the silver grid. The grid structure was built up on hexagonal elements with a dimension of 2 mm between two parallel sides, whereas the nominal line width of 100 μm from the flexo-printing form was increased to an average line width of approximately 160 μm during printing with a grid peak height of up to 750 nm. The efficient consumption of silver was ensured by using a low-volume anilox roller (1.5 mL m⁻², 480 L cm⁻¹) together with a sleeve-based elastomer printing form with a hardness of 65 Shore. An experimental run of ~1000 m flexo-printed grid on barrier foil led to a consumption of roughly 100 mL (200 g) of ink. The cost of the grid when employing inline

processing is essentially determined by costs of materials, drying, and cleaning as machine time is already accounted for in the processing of the PEDOT:PSS layer.

The rotary-screen printing of the PEDOT:PSS on top of the silver grid leads to an average sheet resistance of $10.4 \Omega/\square$ over the full layer area, which is much lower than the $60 \Omega/\square$ for a typical ITO electrode on PET used in R2R processing of organic solar cells.^[1,22] The sheet resistance of the grid and grid/PEDOT:PSS was measured over a defined number of squares as described in the Supporting Information. Rotary-screen printing of the PEDOT:PSS film was carried out using a 215 mesh screen with an open area of 25% that leads to a theoretical wet-ink deposit of 20 μm . The ink covers the silver grid lines and follows its metrology as shown in Figure 3c. Rainbow-colored optical interference patterns of the thin PEDOT:PSS film on the silver grid lines are clearly visible. When preparing the flextrode substrate comprising silver-grid/PEDOT:PSS/ZnO, the process is finished by slot-die coating of the electron-transporting (hole blocking) ZnO layer on top of the electrode stack (see process flow in Figure 2). Thus, the transparency is further reduced by a few percent to 60.3% at 550 nm and a maximum of 63.4% at 424 nm as summarized in Table 1. In addition to

width, excluding setup times) is approximately 60 s (10 mmin^{-1} , 3 individual runs). The complete process speed is in principle limited only by the dryer configuration and fully independent of the electrode design to this point. Exceptional process improvements can thus be achieved when the silver grid and the subsequent PEDOT:PSS layer are printed in an inline configuration. We are currently able to print both layers inline at 10 mmin^{-1} with minimal waste and improved register control because of decreased foil shrinkage. The calculated time for 1 m^2 of printed flextrode substrate is then reduced to 40 s with the advantage of less handling and rewinding processes.

Two continuous guidelines were simultaneously printed with the silver grid, which have been used for a camera-based real-time adjustment of the slot-die coating head for the final ZnO layer (and for the active layer in cases when the flextrode is prepared in situ). Printed marks were used to screen print the PEDOT:PSS layer in register on the underlying silver grid. Although these prints consume some silver ink and have no functionality for the electrode, they do help to decrease the human interaction for a fully automated process workflow. Finally, inkjet-printed barcodes printed during the first passage through the machine help to identify the

electrodes and solar cells during later processing. A strobe camera system was used to monitor the layer quality and overprint accuracy even at higher speeds than the described ones. The process optimization tools are shown in Figure 4 with its positioning in the machine setup (Figure 5).

The flextrode substrates as shown in Figure 6a and b can either be used for large-scale processing of ITO-free OPVs on full R2R systems or smaller roll-coater setups such as described in Refs. [23] and [24]. After cutting individual sample pieces (Figure 6c) the substrate is suitable for spin coating or other small-scale ink deposition processes such as rod coating or doctor blading.

OPV sample fabrication

Single ITO-free solar cells based on the flextrode/P3HT:PCBM/PEDOT:PSS/Ag structure [P3HT = poly(3-hexylthiophene), PCBM = [6,6]-phenyl- C_{61} -butyric acid methyl ester] have been successfully manufactured in a full R2R process and subsequently delivered an efficiency of up to 1.82% on an area of 6 cm^2 .^[11] The fill factor exceeded 51% with a current density of ca. 7 mA cm^{-2} .

Here, we verify the functional homogeneity of the flextrode substrate with a larger set of fully R2R-processed OPV modules with eleven serially connected cells. The modules (Figure 7b) with an active area of 66 cm^2 (module area $\approx 100 \text{ cm}^2$) were manufactured by using the structure: flextrode/P3HT:PCBM/2x-PEDOT:PSS/Ag, for which the P3HT:PCBM active layer was slot-die coated, and the PE-

Table 1. Key parameters of the flextrode layer stack.

	T [%] @ 550 nm	T_{max} [%]	R_{sheet} [Ω/\square]	R_{s} [nm]
Ag grid	77	77.8 (738 nm)	7.4 ± 0.8	–
Ag grid + PEDOT:PSS	68	70.4 (490 nm)	10.4 ± 2.6	80.5 ± 16.7 ^[a]
Ag grid + PEDOT:PSS + ZnO	60.3	63.4 (424 nm)	–	6.7 ± 4.1 ^[b]

[a] Measured on the PEDOT:PSS layer inside the grid cells. [b] Measured on the ZnO layer inside the grid cells.

making the flextrode substrate electron selective by enabling the hole-blocking characteristics, the ZnO layer also improves the surface roughness by an order of magnitude from approximately 80 nm down to below 7 nm on average. Similar to the PEDOT:PSS layer, the ZnO layer with a thickness of around 100 nm basically follows the metrology of the underlying layers but has a significantly better flattening effect. The ZnO layer was dried passing through two ovens (length = 2 m) at 70°C and 140°C , respectively, and coated at a web speed of 5 or 10 mmin^{-1} . Both layers were dried at 140°C in the case where the flextrode was prepared by coating both the ZnO and the active layer simultaneously using inline printing at 10 mmin^{-1} .

The electrodes were manufactured in a 16-stripe design with a width of 13 mm and a gap of 2 mm between the stripes, but other electrode layouts are also possible depending upon the requirement of the final solar cell and module design. Here, the flexo-printing and register-controlled rotary-screen printing enabled a 2-dimensional patterning leading to electrode stripes ($\approx 300 \text{ mm}$ length) along the web direction, whereas the ZnO layer was continuously slot-die coated in 16 stripes of 13 mm width. The manufacturing speed of the 1 m^2 flextrode substrate (based on 305 mm web

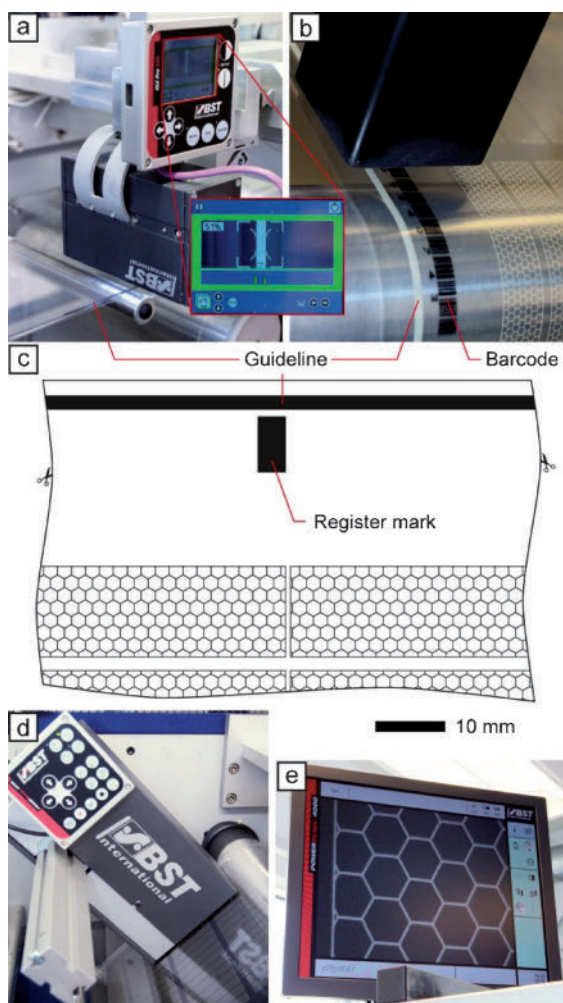


Figure 4. a) Camera-based guideline detection for the cross-directional real-time adjustment of the slot-die head. b) Inkjet printing of individual barcodes for substrate and device identification. c) Section of the silver-grid flexo-printing form including the guideline and register mark. d) Strobe camera for manipulating the printed layers at high speed. e) Camera output for monitoring the printed layers.

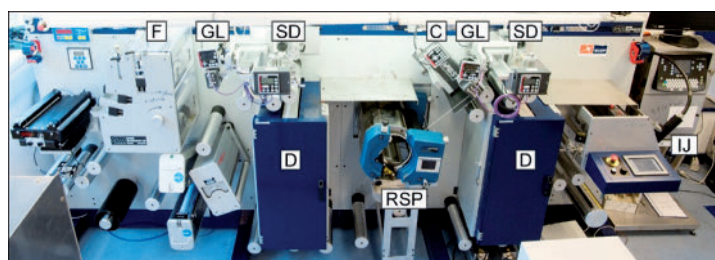


Figure 5. Process optimization tools, namely guideline detection (GL), strobe camera (C), and barcode inkjet printer (I) mounted on the R2R machine setup with flexo-printing (F), slot-die coating (SD), rotary-screen printing (RSP), and driers (D).

DOT:PSS (Agfa 5010) and the silver grid back electrode (Dupont 5025) were rotary-screen printed (see process flows 2, 3, and 4 in Figure 2). The modules were encapsulated from both sides by using a 72 μm -thick barrier foil (Amcor) using UV-curable glue (DELO LP655).

Light soaking for roughly 50 h at 1000 W m^{-2} (AM 1.5G) was performed to stabilize the cell parameters before I - V measurements. The I - V curves of ten randomly selected modules shown in Figure 7a have similar characteristics, with an average power conversion efficiency (PCE) of 1.50% (max. 1.60%), open-circuit voltage (V_{OC}) of 5.54 V (max. 5.63 V), short-circuit current (I_{SC}) of -32.09 mA (max. -33.01 mA) and fill factor (FF) of 55.64% (max. 57.34%). The average current density (J_{SC}) of approximately 5.3 mA cm^{-2} per cell seems to be limited by the lower transmittance of the semitransparent electrode compared to ITO-based cells with the same active-layer composition. Future optimizations of different grid designs and thinner grid lines with less shadow loss are promising for further improvement of the flextrode substrate and the solar cell characteristics.

R2R switching

A final electrical-switching treatment is necessary to transform the whole solar cell stack based on the structure flextrode/active layer/PEDOT:PSS/electrode to a fully functional photovoltaic device by dedoping the PEDOT:PSS layer at the active-layer/PEDOT:PSS interface.^[21] Compared to grid-free PEDOT:PSS/ZnO substrates for small area devices (stripe width < 3 mm), the additional silver grid reduces the sheet resistance, enables large device areas, and improves the serial connection with the printed back electrode. Furthermore, and most importantly, it allows the distribution of a short pulse with high current density and high electric field over several square centimeters. All R2R-manufactured flextrode-based large-area devices were switched using a customized R2R switching setup as shown Figure 8a. The switching head (Figure 8b and c) with its contact pin array is designed according to the specific module layout and connects to the bus bars of the silver comb back electrode. Proprietary software was used to control the whole switching procedure that includes: contact testing, applying the individual switching pulse per single cell, resistance measurement or dark I - V curve acquisition, and further switching cycles, if necessary in case of insufficient switching. All steps were performed in parallel for all cells and required approximately 15 s for a 16-cell module. Therefore, the switching of the 10 m flextrode substrate with 130 modules of roughly 6 cm width took about 32 min. The correct switching parameters for a roll of solar cell devices cannot be fully specified in advance and need some prior tests depending on the area, active layer thickness, and back electrode conductivity. Hereby, the software allows an individual adjustment of the electrical pulse length (typically 15 ms), current (up to 10 A, typically 0.2–0.5 A), voltage (up to 36 V, typically 29 V), threshold resistance (100–1000 Ω), and the number of switching cycles (optimum one cycle). After setting the individual parameters the machine runs automatically without further actions by the operator. Protocols of all switching parameters, especially the threshold resistance, allow for back-

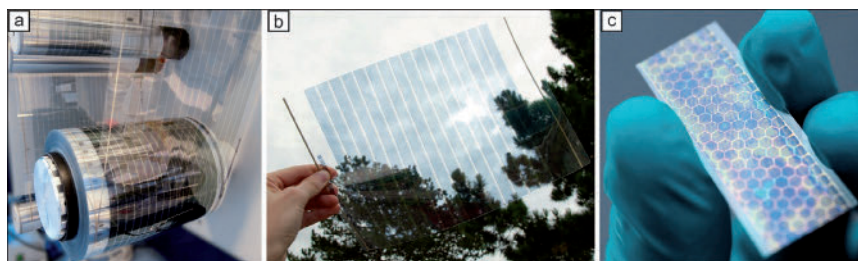


Figure 6. a) Hundreds of meters of flextrode substrate (PET) ready for further R2R processing. b) Flextrode substrate with 16 individual electrode stripes. c) Small flextrode cut-out suitable for OPV manufacturing using spin coating.

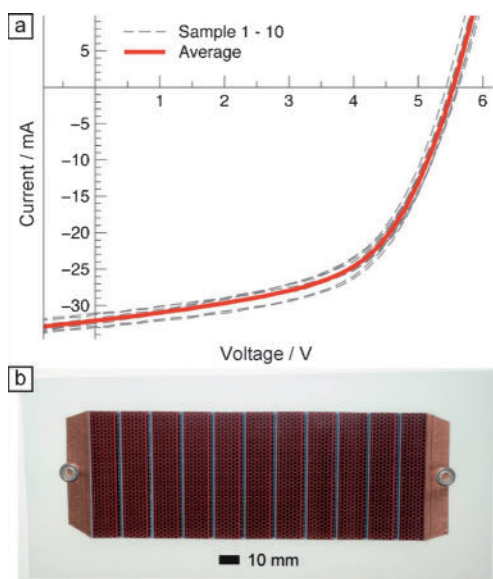


Figure 7. a) I - V curves (dashed lines) of ten randomly selected OPV modules containing eleven serial connected cells. The red line illustrates the average I - V curve. b) Fully encapsulated OPV module fabricated on the flextrode substrate.

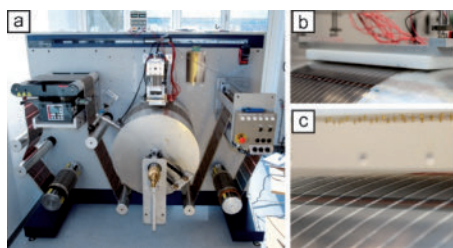


Figure 8. a) Photograph of the R2R switching setup with a mounted roll of fully R2R-processed solar cell modules. b) Switching of a solar cell module with the switching head in contact to the back-electrode bus bars. c) Lifted switching head showing the gold contact pin array.

tracking and identification of potentially unswitched cells using a log-file.

It should be pointed out that all switching procedures can be easily performed by hand using a current-voltage source and then shorting the wires connected to the device. A video demonstrating the simple procedure is available.^[25]

Conclusions

With our flextrode substrate we present an attractive ITO-free alternative for the fast manufacture of large-area OPVs with an inverted structure. The manufacturing is free of very scarce materials such as indium and allows fast, vacuum-free processing of individually designed electrodes. The sheet resistance of the combined silver grid and

PEDOT:PSS stack is almost six times lower than that of a typical flexible ITO-coated PET substrate. Fully R2R-processed solar cells and modules were successfully manufactured leading to PCEs of more than 1.8% on single cells and FFs of more than 60%. Modules could be manufactured with more than 1.6% PCE on the active area. A simple electrical-switching procedure is necessary to transform the solar cell to a functional device. This can be performed manually on small-scale devices or fully automated by using a customized R2R setup. To motivate the OPV scientific community performing research on ITO-free substrates, the flextrode comprising substrate/silver-grid/PEDOT:PSS/ZnO is available free of charge to all academics.

Acknowledgements

This work was supported by the Danish Ministry of Science, Innovation, and Higher Education through the EliteForsk initiative. We would like to thank Dr. Hanne Lauritzen for suggesting the name “flextrode”.

Keywords: inline printing • PEDOT/PSS • PET • slot-die coating • zinc oxide

- [1] F. C. Krebs, S. A. Gevorgyan, J. Alstrup, *J. Mater. Chem.* **2009**, *19*, 5442–5451.
- [2] A. Sandström, H. F. Dam, F. C. Krebs, L. Edman, *Nat. Commun.* **2012**, *3*, 1002.
- [3] Y. Zhou, H. Cheun, S. Choi, W. J. Potscavage, C. Fuentes-Hernandez, B. Kippelen, *Appl. Phys. Lett.* **2010**, *97*, 153304.
- [4] S. Choi, W. J. Potscavage, B. Kippelen, *Opt. Express* **2010**, *18*, A458–A466.
- [5] D. Angmo, M. Hösel, F. C. Krebs, *Sol. Energy Mater. Sol. Cells* **2012**, *107*, 329–336.
- [6] H. Schmidt, T. Winkler, I. Baumann, S. Schmale, H. Flügge, H. H. Johannes, S. Hamwi, T. Rabe, T. Riedl, W. Kowalsky, *Appl. Phys. Lett.* **2011**, *99*, 033304.
- [7] A. Haldar, S. D. Yambem, K.-S. Liao, N. J. Alley, E. P. Dillon, A. R. Barron, S. A. Curran, *Thin Solid Films* **2011**, *519*, 6169–6173.
- [8] D. S. Ghosh, R. Betancur, T. L. Chen, V. Pruneri, J. Martorell, *Sol. Energy Mater. Sol. Cells* **2011**, *95*, 1228–1231.
- [9] Y. Galagan, B. Zimmermann, E. Coenen, M. Jørgensen, F. C. Krebs, D. Tanenbaum, H. Gorter, S. Sabik, L. Slooff, S. C. Veenstra, J. Kroon, R. Andriessen, *Adv. Energy Mater.* **2012**, *2*, 103–110.
- [10] Y. Galagan, J.-E. J. M. Rubingh, R. Andriessen, C.-C. Fan, P. W. M. Blom, S. C. Veenstra, J. M. Kroon, *Sol. Energy Mater. Sol. Cells* **2011**, *95*, 1339–1343.

- [11] J.-S. Yu, I. Kim, J.-S. Kim, J. Jo, T. T. Larsen-Olsen, R. R. Søndergaard, M. Hösel, D. Angmo, M. Jørgensen, F. C. Krebs, *Nanoscale* **2012**, *4*, 6032–6040.
- [12] K. Tvingstedt, O. Inganäs, *Adv. Mater.* **2007**, *19*, 2893–2897.
- [13] P. He, C. Gu, Q. Cui, X. Guo, *Proc. SPIE* **2011**, *8312*, 83120A1.
- [14] T. Stubhan, J. Krantz, N. Li, F. Guo, I. Litzov, M. Steidl, M. Richter, G. J. Matt, C. J. Brabec, *Sol. Energy Mater. Sol. Cells* **2012**, *107*, 248–251.
- [15] D.-S. Leem, A. Edwards, M. Faist, J. Nelson, D. D. C. Bradley, J. C. de Mello, *Adv. Mater.* **2011**, *23*, 4371–4375.
- [16] J.-W. Lim, D.-Y. Cho, Jihoon-Kim, S.-I. Na, H.-K. Kim, *Sol. Energy Mater. Sol. Cells* **2012**, *107*, 348–354.
- [17] M. He, J. Jung, F. Qiu, Z. Lin, *J. Mater. Chem.* **2012**, DOI: 10.1039/c2m33784c.
- [18] Y.-Y. Choi, S. J. Kang, H.-K. Kim, W. M. Choi, S.-I. Na, *Sol. Energy Mater. Sol. Cells* **2012**, *96*, 281–285.
- [19] Y. Wang, X. Chen, Y. Zhong, F. Zhu, K. P. Loh, *Appl. Phys. Lett.* **2009**, *95*, 063302.
- [20] T. M. Barnes, J. D. Bergeson, R. C. Tenent, B. A. Larsen, G. Teeter, K. M. Jones, J. L. Blackburn, J. van de Lagemaat, *Appl. Phys. Lett.* **2010**, *96*, 243309.
- [21] T. T. Larsen-Olsen, R. R. Søndergaard, K. Norrman, M. Jørgensen, F. C. Krebs, *Energy Environ. Sci.* **2012**, *5*, 9467–9471.
- [22] Y. Galagan, I. G. de Vries, A. P. Langen, R. Andriessen, W. J. H. Verhees, S. C. Veenstra, J. M. Kroon, *Chem. Eng. Process.* **2011**, *50*, 454–461.
- [23] H. F. Dam, F. C. Krebs, *Sol. Energy Mater. Sol. Cells* **2012**, *97*, 191–196.
- [24] J. E. Carlé, T. R. Andersen, M. Helgesen, E. Bundgaard, M. Jørgensen, F. C. Krebs, *Sol. Energy Mater. Sol. Cells* **2013**, *108*, 126–128.
- [25] www.plasticphotovoltaics.com.

Received: October 18, 2012

Revised: November 3, 2012

Published online on January 6, 2013

DOI: 10.1002/adem.201300011

Comparison of Fast Roll-to-Roll Flexographic, Inkjet, Flatbed, and Rotary Screen Printing of Metal Back Electrodes for Polymer Solar Cells**

By Markus Hösel, Roar R. Søndergaard, Dechan Angmo and Frederik C. Krebs*

The majority of polymer solar cells reported today employs processing under high vacuum for one or more of the layers in the solar cell stack. Most notably the highly conducting metal back electrode is almost exclusively applied by evaporation of the pure metal. While it is not impossible to envisage mass production of polymer solar cells using vacuum processing it does present some drawbacks in terms of both processing speed, capital investment in processing equipment technical yield and direct process energy. From this point of view it is clear that vacuum processed electrodes should be avoided and electrodes should be printable using methods that provide a high degree of accuracy and high technical yield. When considering large area polymer solar cells (i.e., not laboratory devices) a few reports have employed printable back electrodes mostly by use of silver formulations^[1–4] but also carbon^[5] and copper has been discussed whereas copper is unlikely to yield the necessary cost reduction and resistance to oxidation. Most reports have employed flatbed or rotary screen printing whereas other methods are available and described later on. The important question to answer is which technique is most suited for manufacture of polymer solar cell modules in terms of technical yield, materials use and processing speed? Evidently the back electrode has to be of high conductivity, which implies the use of a thick electrode. Therefore thick film printing techniques such as the screen printing techniques have proven excellent while they do present disadvantages in speed due to significant drying requirements but also they do require significant amounts of material.^[2,6]

In this paper we employ four different roll-to-roll (R2R) printing methods for printing silver back electrodes for polymer solar cell modules based on the *IOne* process which is a fully printable, indium-tin-oxide (ITO), and vacuum free

technology that provide similar performance to ITO-based polymer solar cell modules when using poly(3-hexylthiophene) (P3HT) and [6,6]-phenyl-C61-butyric acid methyl ester ([60]PCBM) as the active layer. We analyze advantages and disadvantages for each method and also outline boundaries of their use and highlight a few areas where development could lead to disruptive progress for the polymer solar cell as a technology.

1. Results and Discussion

So far, the *ProcessOne* process introduced in 2009 was mainly used for the R2R fabrication of polymer solar cells and employed vacuum processed ITO on polyethylene terephthalate (PET) and subtractive etching processes for the transparent conductive electrode.^[1,2] The processing speeds of all layers were up to 2 m min^{-1} , which is far away from high volume outputs necessary for real-world applications, e.g. grid connected polymer solar cells. Furthermore, ITO accounts for more than 80% of the embodied energy in input materials.^[6] The challenge is to employ only additive fabrication processes (i.e. only add the material you need and where you need it) and much faster processing speeds for all layers without the use of vacuum steps. One crucial step is the economical fabrication of the silver back electrode responsible for current collecting and the serial connection of the solar cells to modules. Most of all small-scale record cells are fabricated with evaporated back electrodes, which are costly and challenging to transfer to a fast R2R process.

The recently introduced polymer solar cell process *IOne* is based on the *Flextrode* substrate and employs an ITO-free layer stack with the order PET/Ag-grid/PEDOT:PSS/ZnO/P3HT:PCBM/PEDOT:PSS/Ag as described in the experimental section and shown in Figure 1.^[7,8] All fabrication steps are additive and process optimized to compete with ITO-based cells fabricated under full R2R ambient conditions. The four fabrication methods of the final back electrode silver comb structure compared in this study utilize different silver inks that are most suitable for their specific technique based on its single-layer printability and our existing equipment. The key layer for the subsequent deposition of silver is the thick poly(3,4-ethylenedioxythiophene):poly(styrenesulfonate) (PEDOT:PSS) fabricated using rotary screen printing and the adjacent layers with different wetting behaviors.

[*] Prof. F. C. Krebs, M. Hösel, Dr. R. R. Søndergaard, D. Angmo
Department of Energy Conversion and Storage, Technical
University of Denmark, Frederiksborgvej 399, DK-4000
Roskilde, Denmark
E-mail: frkr@dtu.dk

[**] This work was supported by the the EU-Indian framework of the
“Largecells” project as part of the European Commission’s
Seventh Framework Programme (FP7/2007-2013, grant no.
261936).

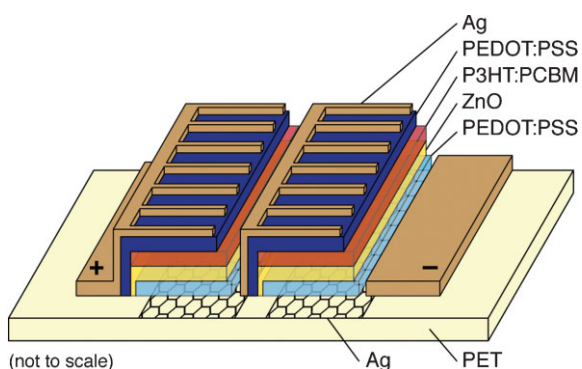


Fig. 1. Illustration of the fully R2R processed solar cell stack comprising the materials silver Ag, PEDOT:PSS, zinc oxide (ZnO), and P3HT:phenyl-C61-butiric acid methylester (P3HT:PCBM). The last Ag back electrode is printed using four different techniques.

Typically, screen printed silver back electrodes are used for inverted polymer solar cells as they show high conductivity and relatively low complexity during the fabrication, either small-scale or large-scale. The standard silver pastes are based on micron sized silver flakes dispersed in a variety of different solvents. The impact of different solvent types on the underlying layers and therefore on the performance of polymer solar cells can be studied using the light beam induced current (LBIC) technique and has been published elsewhere.^[3] Another deposition method of silver back electrodes that has been studied in inverted solar cells is spray coating. Silver nanowire and nanoparticle ink has been used for the back electrode with comparable solar cell parameters to ones with evaporated silver.^[9–11] The applicability in a structured R2R process is rather complicated although spray coated films can be patterned using a shadow mask. The use of a shadow mask also leads to a significant loss of precious ink if not recycled. Inkjet printing is a second contact-free deposition method of silver ink with its advantage of a full digital patterning and theoretically zero ink waste. Reports on inkjet printed silver back electrodes have until now been quite infrequent and only by use of specialized sheet-to-sheet inkjet printing setups with a limited amount of nozzles and slow production speed. Normal structured devices^[12] and inverted devices^[13] with full silver layers have successfully been manufactured but without mentioning critical drying times that are a limiting factor in a continuous process. Some more exotic methods are lamination and stamping procedures for the silver electrodes, but they are currently carried out only under lab-scale conditions.^[14–16] Flexography type printing of silver paste on inverted cells in an experimental small-scale roll-coater setup has been successfully carried out for a large amount of single solar cells with areas of 1 cm².^[17] Silver metallization of silicon solar cells using flexography has been studied as well and enabled printing of very fine line structures.^[18]

In this study we compare the most promising R2R printing technologies, namely flatbed screen printing, rotary screen printing, flexography, and inkjet printing, for their applicability in R2R large-scale production of serially connected

polymer solar cell modules. For each method we chose the most suitable silver ink, which already show good printability and functionality as a back electrode^[12] or as an electrode grid structure directly printed on the substrate.^[7,19,20] From the environmental point of view water-based silver inks were preferred, which is the case here for inkjet and flexography.

To fairly compare the results of printability and functionality of each silver deposition method we did not optimize the underlying PEDOT:PSS layer and chose the same type in all the experiments. This directly results in some process recommendations and structural optimizations that need to be addressed for future fast R2R production with alternative fabrication methods.

1.1. Printing Techniques and Printability

The working principles of each printing method has already been described in detail elsewhere.^[21,22] In brief, screen printing is based on a screen with closed and open areas defining the printing pattern. A squeegee moving over the screen forces the ink through the open areas onto the substrate. The amount of ink printed onto the substrate is defined by the screen thickness and relative open area. The ink paste has typically high viscosities above 20 Pa s with shear thinning characteristics (thixotropy). In flexo printing the ink is transferred from an anilox cylinder with a certain ink volume (in mL m⁻²) to the flexo printing form made from elastomeric material or photopolymer where the printing pattern presents a raised topography. Later on, the ink from the printing form is transferred to the substrate with slight pressure from the impression roller. The ink viscosity is typically below 1000 mPa s. Surface interactions define the final ink pick out and transfer to the substrate beside other printing parameters such as speed and nip pressure. A fully digital pattern and non-contact method is inkjet printing. The low viscous ink (<30 mPa s) is ejected out of tiny nozzles in droplets with volumes of above ten of picoliters. The droplets are typically generated with piezoelectric actuators inside the printhead. The printing quality and film formation on the substrate is highly dependent on surface interactions to achieve fine structures and full layers. Missing dots due to nozzle clogging are a major problem and can lead to gaps in the printed layers. All printing methods require drying steps that are often the speed-limiting factor caused by the dryer length.

We printed the same silver comb structure with all four technologies and achieved the best printability for both screen printing methods as shown in the comparison in Figure 2. The high viscous silver paste is forced through the screen and shows no dewetting regardless of the underlying surface. The applied layer thickness is several times thicker than the edge heights of PEDOT:PSS and all other layers beneath. Therefore it is a preferred method when it comes to print on different surfaces with micron sized steps and rough metrologies. Furthermore it allows relatively high speed with up to 10 m min⁻¹ just limited by the dryer length in our current R2R setup. The sheet resistance after drying is very low and is

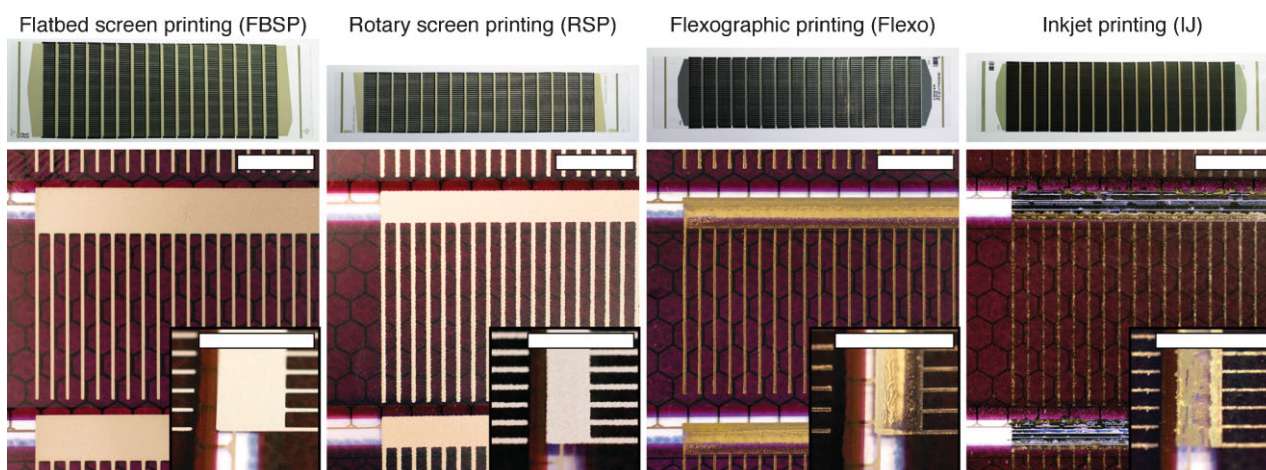


Fig. 2. Overview of the printed silver back electrodes with the fully R2R fabricated modules shown on the top. The macro-photographs show the layer and edge quality and the areas of serial connection. Scale bar is 5 mm.

summarized in Table 1, together with further printing parameters and layers thicknesses.

The macro-scale print quality of the flexo printed water-based silver ink is good (Figure 2) but reveals some challenging problems with respect to different surface materials and its impact on the ink transfer. The ink transfer onto the PET substrate and printing over the bottom silver grid for the serial connection is very satisfying and needs no further treatment although it is a water-based ink. The full layer sheet resistance achieved at a maximum speed of 10 m min^{-1} during this experiment is very good ($162 \text{ m}\Omega \square^{-1}$) and comparable to the screen printed silver electrode. The problem occurred here was the almost non-existing ink transfer to the rough PEDOT:PSS layer ($R_a \sim 400 \text{ nm}$) as shown in Figure 3. We tried different speeds, nip pressures and anilox volumes but it seems the ink transfer is just limited by the surface interaction of the used material combination which leads to different ink splitting ratios between printing form and pre-printed substrate. We also discovered a transfer of PEDOT:PSS back onto the printing roller and back into the inking cycle. This led to local agglomeration of a PEDOT:PSS/silver ink mixture under the doctor blade which scrapes off the excess ink from the anilox cylinder. Although the printed comb fingers are clearly observed they show no connected silver structures and do not increase the conductivity of the PEDOT:PSS for an efficient current collection. Furthermore, the electrical switching^[5] was

very difficult due to a limited distribution of the high current density during the short electrical pulse.

Inkjet printing with water-based silver ink enables satisfying quality on PEDOT:PSS and PET despite some missing dots. To achieve a homogeneous silver layer on PET the surface had to be corona treated to increase the surface

Table 1. Process parameters and silver layer parameters of the silver back electrode printed with four different methods. The parameters of the printed PEDOT:PSS are given as well.

Printing method	Speed [m min^{-1}]	R_s	Thickness [μm]	Comments
FBSP (Ag)	1	$67 \text{ m}\Omega \square^{-1}$	8	Hot air
RSP (Ag)	10	$47 \text{ m}\Omega \square^{-1}$	10	Hot air, IR
IJ (Ag)	2	$38 \Omega \square^{-1}$	0.5	Hot air, 300 W corona
Flexo (Ag)	10	$162 \text{ m}\Omega \square^{-1}$	1	Hot air, IR
RSP (PEDOT:PSS)	2	$232 \Omega \square^{-1}$	2	Hot air, IR

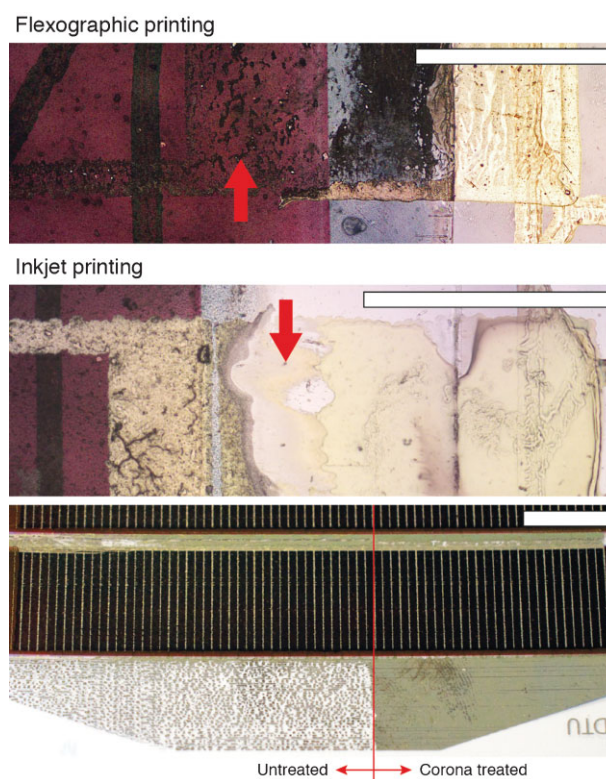


Fig. 3. (top) Microscopic image of flexo printed silver with limited ink transfer to the PEDOT:PSS surface (arrow) and good printing on PET. (center) Microscopic image of inkjet printed silver with good printability on the PEDOT:PSS surface and PET. Inkjet printing over the edge of PEDOT:PSS leads to smeared silver (arrow) and non-conductive areas. (bottom) Inkjet printing of silver with and without corona treatment. Scale bar is 1 mm (top, center) and 10 mm (bottom).

energy (Figure 3). This is a very critical process step because it has a destructive impact on all previously printed layers. A soft plasma treatment might reduce or prevent surface damage but was not available in the R2R setup. Generally speaking surface treatments should be avoided which could point to the need for the use of other solvent systems for the inkjet ink. The second problem that occurs here is the step height from PEDOT:PSS to PET. The microscopic image shown in Figure 3 shows areas of very little silver coverage, which leads to breaks in the serial connections. An explanation for this behavior can be a down-flow of the very low viscous ink from the PEDOT:PSS and an additional repulsion from poor wetting of low surface energy areas on the device structure. The full layer sheet resistance is several orders higher than the silver printed with the other methods and also limits the electrical switching process.

1.2. Speed and Material Consumption

Flexo printing enables a very high fabrication speed above 10 m min^{-1} and it can easily be increased as the silver ink is very fast drying with the help of infrared dryers. The material consumption can be controlled with the anilox volume and is less than 20% of the screen printed silver based on the dry layer thickness at comparable conductivity levels. Therefore, it would be the optimal silver back electrode fabrication method as it is faster with less ink consumption. Ink waste can almost be avoided by a controlled inking of the anilox cylinder.

Flatbed screen printing combined with an intermittent R2R setup achieves the best printing quality but is also the slowest. An increase in speed to more than 1 m min^{-1} is basically limited by the static printing process where the screen moves up and down with the squeegee moving back and forth. To avoid a contact of the screen with the wet layer the substrate has to move forward by the minimum size of the screen frame. A certain area of the substrates cannot be printed and it is therefore not possible to print continuous patterns. All other techniques allow for a seamless pattern design if necessary. The ink consumption is high based on the dry layer thickness and waste cannot be avoided as a lot of ink/paste has to be on the screen to enable proper ink flooding over the whole screen. Excess ink should not be used again in a production run if it has been exposed to air for too long time.

The ink consumption for rotary screen printing is slightly higher than flatbed but allows faster speeds and continuous pattern if necessary. The expected ink waste is similar for all screen printing processes and can be limited by a known consumption and controlled refilling over long runs. Processing speed should be easily increased to more than 10 m min^{-1} with longer dryers and less wet layer thickness. As rotary screen printing shows very good solar cell performances and speed of up to 10 m min^{-1} it matches to most of the other layer process speeds.

Inkjet printing of silver has the least ink consumption and theoretically no waste but also a much higher sheet resistance. It is a highly complex system with its ink circulation and needs frequent maintenance especially when not in use for long time.

Printhead cleaning und flushing of the nozzles produces some ink waste. A full ink exchange is time consuming and not practical for an R2R production system. Furthermore, ink compatibility-testing should be carried out on a lab-scale inkjet system. Finally, the speed of 2 m min^{-1} is only limited by the dryer length and can be much higher ($\leq 75 \text{ m min}^{-1}$ for single head systems and $\leq 300 \text{ m min}^{-1}$ for a four head system).

1.3. Device Performance

After printing a large amount of solar cell modules we compared their performance. Single cells were electrically switched manually to establish the compatibility with automated switching. This was very easy for the screen printed cells. The flexo- and inkjet printed modules however had to be taped with small copper stripes between each cell to achieve a serial connection and good contact during the switching procedure. The *JV*-curves in Figure 4 and their corresponding data in Table 2 reveal that the solar cells with screen printed back electrodes have the best performance as expected from the visual printing results and layer characteristics. They have efficiencies from nearly 1.8% up to 2.1% and fill factors close to 50%. The good performance is based on the highly conductive silver electrodes and the reliable switching of each cell.

The inkjet and flexo printed cell have poor performance with efficiencies below 1% and low fill factors with a maximum of 31%. The low conductive inkjet silver and the very thin flexo printed silver on the PEDOT:PSS leads to high series resistance. The current extraction over a large area is therefore limited by

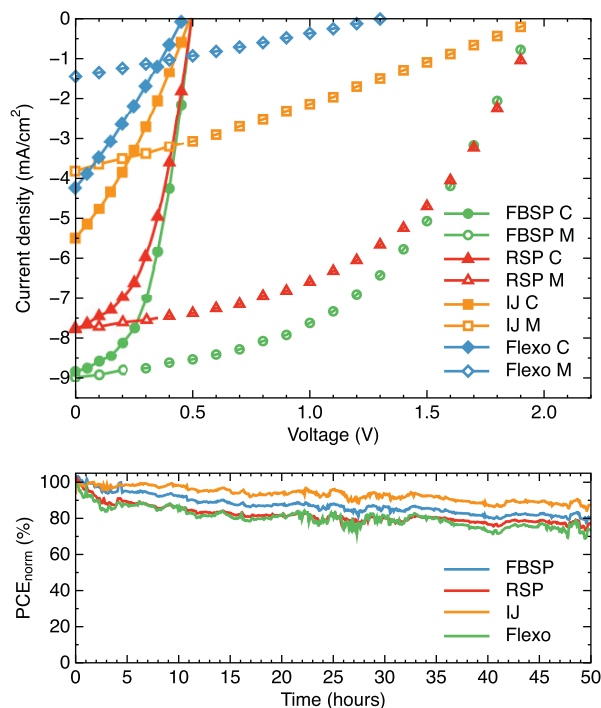


Fig. 4. (top) *JV*-curves of single cells (C) and 4-cell modules (M) for each printing method. (bottom) The normalized efficiency over 50 h of encapsulated devices under 1 sun conditions.

Table 2. Solar cell and module parameter for each printing method.

Single cell					
Printing method	A [cm ²]	V _{OC} [V]	J _{SC} [mA cm ⁻²]	FF [%]	PCE [%]
FBSP	6	0.493	-8.82	48.4	2.10
RSP	6	0.493	-7.77	46.8	1.79
IJ	7	0.487	-5.49	31.0	0.83
Flexo	6	0.458	-4.22	28.2	0.55
4-Cell module					
Printing method	A [cm ²]	V _{OC} [V]	J _{SC} [mA cm ⁻²] ^[a]	FF [%]	PCE [%]
FBSP	24	1.956	-8.97	53.8	2.09
RSP	24	1.976	-7.75	48.1	1.84
IJ	28	1.985	-3.81	28.7	0.54
Flexo	24	1.306	-1.44	26.3	0.12

^[a] J_{SC} is calculated based on the active area of a single cell.

the relatively low conductive PEDOT:PSS layer resulting in a low current density. The low fill factor is also caused by the low shunt resistance, which is caused by the limited electrical switching. The back PEDOT:PSS layer is not fully switched (doped) and acts like a simple Ohmic contact rather than a hole conducting interface.^[5] The low open circuit voltage of the flexo printed module is based on the difficult switching and some cells working poorly. The accelerated degradation behavior of fully edge sealed modules is in principle very similar for each printing method as shown in Figure 4.

1.4. Evaluation of the Different Techniques and Recommendations

The solar cell parameters show that a highly conductive and optimal printed silver grid structure over all different surfaces is necessary to fabricate single cells and in particular solar cell modules with serial connection. The limiting factor is not primarily the layer thickness, as thin layers from the flexo printing can achieve comparably low sheet resistances. The interaction of the ink/paste with the different surfaces and layer edges has the highest impact. The printing experiments show that screen printing is the most robust method, no matter which surface energy characteristics are present. Micron thick wet/dry layer thicknesses and silver flake pastes smooth out all edges and step heights from the underlying layers. Ink consumption can be reduced with slightly thinner layers, which also enables higher printing speeds.

In inkjet printing very thin layers of very low viscous inks can lead to problems at large layer step heights. Therefore the underlying layers should be very smooth over the whole device area. Flexography shows a high fabrication speed but also present challenges in printing on surfaces with minimized ink transfer capabilities from the flexo printing form. The silver ink and/or the PEDOT:PSS layer must be optimized for a complete ink transfer. The PEDOT:PSS layer should be thin and smooth to avoid edge problems as the flexo printed layer is thinner and low viscous. The silver ink should not dissolve the PEDOT:PSS to avoid transfer back onto the printing roller

during the printing process. The future applicability of flexo printing of silver back electrodes is very good if compatible silver inks can be transferred with the same quality as in screen printing. Therefore the ink will potentially need a higher viscosity and stronger thixotropic behavior so that it behaves like screen printing ink. It is also likely that water based inks are difficult to formulate efficiently for flexographic printing onto PEDOT:PSS unless the PEDOT:PSS is cured or cross linked to a higher degree than is customary today. Alternatively it might be necessary to formulate silver based inks in benign organic solvents for flexographic printing.

The running costs of inkjet printing are basically free as no physical printing form is required, whereas the investment costs in machinery for large scale R2R inkjet printing are very high compared to all other processes. A frequent printing is recommended to avoid nozzle clogging and precipitation of nanoparticle in the ink. The complexity of the setup is high and it is limited to a small range of inks. The master costs of flatbed screen printing and flexo are relatively low and last for a long time. Otherwise, flexo and rotary screen printing requires either costly but also very robust anilox cylinders or rotary printing forms. The rotary screen printing method has a high applicability with a large high-speed potential and a good solar cell performance. A summary of the four printing methods in terms of capacity and applicability can be found in Table 3.

2. Conclusions

It is clear from the experiments that all printing techniques can be employed and that flexo and inkjet would require that the solar cell stack and the back electrode inks were adapted better to each other. It has to be remembered that *ProcessOne* and *IOne* have evolved around the screen printing techniques and a shift to flexography or inkjet which are thin film printing techniques have some requirements. The most important one is topology, but also the surface energy becomes important for the lower viscosity of the inkjet and flexo inks. The solvent was

Table 3. Comparison of the different printing methods in terms of their theoretical capacity and its practical applicability for large-scale R2R production of silver back electrodes.

Printing method	Speed	Wet thickness [μm]	Resolution [μm]	Start/stop	Master cost	Complexity	Applicability
FBSP	Low	5–100	100	Yes	Low	Low	Limited
RSP	High	3–500	100	Yes ^[a]	High	Medium	Very good
IJ	Medium	1–5	<50	Yes	Free	High	Limited
Flexo	Very high	1–10	<50	Yes ^[a]	Low	Medium	Very good ^[b]

^[a] Stopping should be avoided. Risk of registration lost and drying of ink in anilox cylinder. Short run-in length;

^[b] with a compatible silver ink to enable ink transfer to PEDOT:PSS.

naturally shown to present challenges for a contact printing technique such as flexo when the substrate (water soluble PEDOT:PSS) interacts with the ink solvent (water). For inkjet this was less of a problem. In the end silver is silver and all devices were demonstrated to work. The differences observed are thus ascribed to the compatibility between the chosen solar cell stack, the ink and the method and we highlight the need to develop solar cell stacks that are compatible with flexo printing as this would represent the lowest cost, lowest materials consumption and fastest processing speed. The alternative of using benign organic solvents is still a possible solution whereas water-based inks does present the ultimate goal in ink formulation. Finally, the development of new printable hole extraction layers that are compatible with the use of water based silver inks is also a valiant subject for further development.

3. Experimental

3.1. Solar Cell Stack

The common solar cell layer stack for all experiments is Ag-grid/PEDOT:PSS/ZnO/P3HT:PCBM/PEDOT:PSS with varying back electrode silver grid fabricated on PET substrate (Melinex ST506, DuPont Teijin Films). In brief, the ITO-free front electrode (Ag-grid/PEDOT:PSS/ZnO) is also known as the Flextrode^[7] and is comprised of a flexo printed silver hexagonal grid (PFI-722, PChem Associates Inc.) with an additional rotary screen printed PEDOT:PSS layer (Clevios PH1000, Heraeus) on top of it. The processing speed used here was 15 and 10 m min⁻¹, respectively. Zinc oxide ZnO was slot-die coated from a nanoparticle dispersion in acetone (55 mg mL⁻¹) at a speed of 10 m min⁻¹. The active layer was composed of poly(3-hexylthiophene) P3HT (Sepiolid P200, BASF) and [60]PCBM (Merck) in a ratio of 1:1 (55 mg mL⁻¹ in chlorobenzene) and slot-die coated at 3.5 m min⁻¹. The PEDOT:PSS back electrode (Orgacon EL-P 5010, Agfa) was rotary screen printed at 2 m min⁻¹. Finally, the comb grid structure with a nominal finger width of 150–200 μm and a spacing of 1 mm was printed in register on the underlying layer stack using four different printing methods. All printing and coating steps are sufficiently dried using hot air (140 °C) and infrared dryers. We printed solar cell modules with 16 serial connected cells and used representative parts for the characterization of single cells and small modules of 4 cells. The R2R machine setups are described elsewhere.^[23,24] The devices for the lifetime study were encapsulated using 72 μm thick barrier foil (Amcor) and UV-curable adhesive (LP655, DELO). The solar cell had to be activated using the electrical switching method as described elsewhere.^[5]

3.2. Roll-to-Roll Flatbed Screen Printing

A screen printer from ALRAUN Technik GmbH was used for intermittent R2R screen printing. The solvent based silver paste (PV410, DuPont) was printed with a 120 mesh screen and dried at 140 °C for 2 min in a 2 m long hot air oven. The overall speed was 1 m min⁻¹.

3.3. Roll-to-Roll Rotary Screen Printing

Rotary screen printing was carried out on a RSI compact printing unit (Stork Print BV) with an electroformed nickel screen having a repeat length of 12". The screen had a 215 mesh size with 25% open area and a theoretical wet layer deposit of 20 μm . The solvent-based silver paste (PV410, DuPont) was printed with up to 10 m min⁻¹ and dried at 140 °C in a 2 m long oven. The drying was supported by infrared light.

3.4. Roll-to-Roll Inkjet Printing

Inkjet printing was carried out at 2 m min⁻¹ using drop-on-demand printheads (Kyocera) with a resolution of 600 dpi. Three combined heads enabled a print width of 305 mm. The R2R setup employed a corona station and a 2 m long hot air oven set to 140 °C. The corona treatment was set to a power of 300 W to achieve a sufficient wetting of the water-based nanoparticle silver ink (Suntronic U7089, Sun Chemical) on the PET substrate, although this process lead to a partial destruction of the underlying layers.

3.5. Roll-to-Roll Flexographic Printing

Flexographic printing was carried using an anilox cylinder with a volume of 11 mL cm⁻³ and an elastomeric printing form with hardness of 65 Shore. The water-based nanoparticle ink (PFI-722, PChem Associates Inc.) was printed with up to 10 m min⁻¹ and dried using two 2 m long oven set to 140 °C supported by infrared dryers.

3.6. Measurement Equipment

A Jandel RM3 4-point probe system was used to measure the sheet resistance of the printed silver layers. Layer thicknesses were measured using a Dektak profilometer. Finally, the solar cell parameters were measured under a solar simulator (metal halide lamp, 1000 W m⁻², AM1.5G) with a Keithley 2400 sourcemeter and proprietary control software.

Received: January 12, 2013

Final Version: April 24, 2013

Published online: June 20, 2013

- [1] F. C. Krebs, S. A. Gevorgyan, J. Alstrup, *J. Mater. Chem.* **2009**, *19*, 5442.
- [2] F. C. Krebs, T. Tromholt, M. Jørgensen, *Nanoscale* **2010**, *2*, 873.

- [3] F. C. Krebs, R. Søndergaard, M. Jørgensen, *Sol. Energy Mater. Sol. Cells* **2011**, *95*, 1348.
- [4] F. Yan, J. Noble, J. Peltola, S. Wicks, S. Balasubramanian, *Sol. Energy Mater. Sol. Cells* **2012**, *114*, 214.
- [5] T. T. Larsen-Olsen, R. R. Søndergaard, K. Norrman, M. Jørgensen, F. C. Krebs, *Energy Environ. Sci.* **2012**, *5*, 9467.
- [6] N. Espinosa, R. Garcia-Valverde, A. Urbina, F. C. Krebs, *Sol. Energy Mater. Sol. Cells* **2011**, *95*, 1293.
- [7] M. Hösel, R. R. Søndergaard, M. Jørgensen, F. C. Krebs, *Energy Technol.* **2013**, *1*, 102.
- [8] D. Angmo, S. A. Gevorgyan, T. T. Larsen-Olsen, R. Søndergaard, M. Hösel, M. Jørgensen, R. Gupta, G. U. Kulkarni, F. C. Krebs, *Org. Electron.* **2013**, *14*, 984.
- [9] J. Krantz, T. Stubhan, M. Richter, S. Spallek, I. Litzov, G. J. Matt, E. Spiecker, C. J. Brabec, *Adv. Funct. Mater.* **2012**, *23*, 1711.
- [10] C. Girotto, B. Rand, S. Steudel, J. Genoe, C. W. Lee, *Org. Electron.* **2009**, *10*, 735.
- [11] S. K. Hau, H.-L. Yip, K. Leong, A. K.-Y. Jen, *Org. Electron.* **2009**, *10*, 719.
- [12] S. Eom, S. Senthilarasu, P. Uthirakumar, C. Hong, Y. Lee, J. Lim, S. Yoon, C. Lee, S. Lee, *Sol. Energy Mater. Sol. Cells* **2008**, *92*, 564.
- [13] M. Senghor, M. Manceau, F. Ardiaca, R. de Bettignies, S. Berson, L. Dassas, S. Poughon, C. Dossou-Yovo, R. Noguera, *Proc. SPIE* **2012**, *8477*, 84770M.
- [14] W. Gaynor, J. Lee, P. Peumans, *ACS Nano* **2009**, *4*, 30.
- [15] M. Reinhard, R. Eckstein, A. Slobodskyy, U. Lemmer, A. Colmann, *Org. Electron.* **2013**, *14*, 273.
- [16] J.-Y. Lee, S. T. Connor, Y. Cui, P. Peumans, *Nano Lett.* **2010**, *10*, 1276.
- [17] J. E. Carlé, T. R. Andersen, M. Helgesen, E. Bundgaard, M. Jørgensen, F. C. Krebs, *Sol. Energy Mater. Sol. Cells* **2013**, *108*, 126.
- [18] S. Thibert, D. Chaussy, D. Beneventi, N. Reverdy-Bruas, J. Jourdan, B. Bechevet, S. Mialon, *Photovoltaic Specialists Conference (PVSC), 2012 38th IEEE*, Austin, TX **2012**, p. 2266.
- [19] D. Angmo, T. T. Larsen-Olsen, M. Jørgensen, R. R. Søndergaard, F. C. Krebs, *Adv. Energy Mater.* **2012**, *3*, 172–175.
- [20] R. R. Søndergaard, M. Hösel, M. Jørgensen, F. C. Krebs, *J. Polym. Sci. B: Polym. Phys.* **2013**, *51*, 132.
- [21] R. R. Søndergaard, M. Hösel, F. C. Krebs, *J. Polym. Sci. B: Polym. Phys.* **2013**, *51*, 16.
- [22] R. Søndergaard, M. Hösel, D. Angmo, T. T. Larsen-Olsen, F. C. Krebs, *Mater. Today* **2012**, *15*, 36.
- [23] F. C. Krebs, J. Fyenbo, M. Jørgensen, *J. Mater. Chem.* **2010**, *20*, 8994.
- [24] J.-S. Yu, I. Kim, J.-S. Kim, J. Jo, T. T. Larsen-Olsen, R. R. Søndergaard, M. Hösel, D. Angmo, M. Jørgensen, F. C. Krebs, *Nanoscale* **2012**, *4*, 6032.

Comparison of UV-Curing, Hotmelt, and Pressure Sensitive Adhesive as Roll-to-Roll Encapsulation Methods for Polymer Solar Cells**

By Markus Hösel, Roar R. Søndergaard, Mikkel Jørgensen and Frederik C. Krebs*

The most distinct advantage of the polymer solar cell is the possibility for roll-to-roll (R2R) fabrication compatibility based on printing and coating processes. The R2R encapsulation is the last crucial process step in the manufacturing workflow and is evaluated in this study. Polymer solar cell modules are directly printed on barrier foil and encapsulated with the same barrier foil either on the backside or on both sides of the device. The three lamination methods comprise of UV-curable epoxy resin, hotmelt, and pressure sensitive adhesive (PSA). It is shown that a single sided encapsulation with UV-curable adhesive is enough to achieve the same or better lifetime than double-sided encapsulation with all the adhesives utilized here. This is mainly due to the good edge sealing effect of the thin adhesive with no edge bleaching after 900 h of constant illumination. Although the fabrication of the PSA method is the fastest method (in this study) it generates a considerable amount of waste (paper liner) and two lamination steps are required to achieve a sufficient lifetime. We conclude that UV-curing presents the largest advantages of all methods with a good upscaling potential and low embodied energy due to the possibility for single sided encapsulation.

1. Introduction

In recent years, the field of polymer and organic photovoltaics (OPV) has seen a rapid growth in publications^[1] and in efficiencies up to 12% for small areas.^[2,3] Most of the record cells in the literature were produced under optimal conditions using spin-coating or evaporation, but with an undisclosed lifetime. Full solution processing using coating and printing techniques has also seen a lot of attraction to explore the most suitable methods such as slot-die coating, screen printing, inkjet, flexo, and gravure printing, either full roll-to-roll (R2R) or sheet-to-sheet.^[4–12] Most of the solar cells are fabricated on PET or glass substrates with indium tin oxide (ITO) as

transparent conductive electrode and show a high-embodied energy due to ITO.^[13] The transition to alternative materials such as silver grid or nanowire structures in conjunction with highly conductive polymers is the latest attempt to enable a vacuum free front electrode fabrication process and with possibilities for fast upscaling using only additive methods (i. e., material is deposited only where it is needed without extra patterning steps post-film formation).^[14–17]

Whereas materials and solar cell manufacturing research is demonstrating strong progress, the stability and lifetime of polymer solar cells still lacks a complete understanding. Several review publications cover the whole spectra of degradation phenomena with photo-oxidation, photo-chemical processes, morphology changes, and interface layers named as possible, and often competing reasons for the degradation of current polymer solar cells.^[18–22] Although the degradation issue is not solved the lifetime of OPV devices has reached several thousands of hours depending on the testing procedure. The fundamental degradation processes will not be covered by this report since we focus on the most suitable R2R encapsulation method.

The physical encapsulation for flexible devices and the practical procedures for applying the barrier itself to the solar cell is a field of limited resources so far. It has been shown that flexible barriers with water vapor transmission rates (WVTR)

[*] Prof. F. C. Krebs, M. Hösel, Dr. R. R. Søndergaard, Dr. M. Jørgensen
Department of Energy Conversion and Storage, Technical University of Denmark, Frederiksborgvej 399, DK-4000, Roskilde, Denmark
E-mail: frkr@dtu.dk

[**] This work was supported by Energinet.dk (project no. 10728) and the EU-Indian framework of the "Largecells" project as part of the European Commission's Seventh Framework Programme (FP7/2007-2013, grant no. 261936) and the Framework 7 ICT 2009 collaborative project ROTROT (grant no. 288565)

of $10^{-3} \text{ g m}^{-2} \text{ day}^{-1}$ or better are sufficient enough to achieve lifetimes of several years.^[23] The development in flexible high performance barrier films is mostly driven by organic–inorganic multi-layer structures to increase the gas diffusion path length between occurring defects (e.g., pinholes) in the inorganic layer.^[24–27] The best transparent barrier would of course be glass but this does only allow for sheet-to-sheet handling with limited output capacity. It is mainly used for the encapsulation of small-scale devices fabricated with spin-coating or evaporation but it has also been shown as a promising encapsulation method of R2R produced polymer solar cells for rigid building integrated photovoltaics.^[28] Stainless steel lids and glass sheets in conjunction with epoxy resins are still preferably used to seal functional photonic devices (OPV, OLED) under inert atmosphere and in lab-scale sizes.^[14,29–32]

Direct deposition of nanocomposite coatings,^[33] embedding in polyurethane,^[34] atomic layer deposition ALD,^[25,35–37] multilayer barriers with nitrogen spacers,^[38] plasma-enhanced physical vapor deposition PECVD,^[39] parylene polymeric coatings,^[40] stacked graphene,^[41] and just solution-processed UV epoxy resins^[42] are further processes that have been studied to extend the lifetime of organic electro-optical devices.

The lamination of barrier foil with UV-curable adhesive, hotmelt, or pressure sensitive adhesives (PSA) in a large-scale ambient R2R fabrication process seem to be the most suitable technologies for the upscaling and the manufacturing of flexible OPV modules, especially when it comes to really large-scale output for future energy production.^[43] Only simple converting machinery adopted from the printing industry would be required rather than complicated and delicate tools such as R2R ALD. The PSA method has been used for a long time to fabricate flexible OPV modules in a full R2R process,^[44,45] whereas UV-curable adhesives have been demonstrated to be superior in relation to the lifetime of flexible solar cells.^[5] Basic hotmelt lamination with an office laminator was demonstrated earlier.^[46] In this report we compare these three methods based on full R2R processes and its maximum achievable speed with our lab equipment. The final devices are made with the same batch of fully solution processed ITO-free solar cell modules and identical barrier foil. The only difference is the adhesive and the lamination procedure.

2. Experimental

2.1. Solar Cell Fabrication

The polymer solar cell modules were fully R2R produced based on the *IOne* process as described earlier.^[5,15,43] In brief, a silver electrode structure was flexo printed directly on thin barrier foil (Amcors Ceramis, $72 \mu\text{m}$ thick, WVTR $0.04 \text{ g m}^{-2} \text{ day}^{-1}$, OTR $0.01 \text{ cm}^3 \text{ d}^{-1} \text{ bar}^{-1}$, 305 mm wide) using water-based silver nanoparticle ink (PChem PFI-722). Contrary to all previous reports with a honeycomb grid design we used an optimized electrode layout with slanted comb electrodes in the direction of the current flow. On top of the silver electrode a

rotary screen printed poly(3,4-ethylenedioxythiophene):poly(styrenesulfonate) (PEDOT:PSS) layer (Heraeus Clevis PH1000) and a subsequently slot-die coated zinc oxide (ZnO) hole-blocking layer forms the ITO-free transparent electrode stack, which is known as *Flextrode*.^[47] The light absorbing active layer was slot-die coated on top of the electrode and contains poly(3-hexylthiophene):[6,6]-phenyl-C₆₁-butyric acid methyl ester (P3HT:PCBM, Plextronics, Merck) as donor:acceptor dissolved in chlorobenzene. Two layers of PEDOT:PSS (Agfa 5010) and the silver comb grid (Dupont 5025) were rotary screen printed as current collecting back-electrode. Here we also used an optimized design with slanted comb electrodes to achieve a maximum of two direct overlaps of front and back silver electrodes independently of the registration accuracy during the printing. The fabrication speed of all layers varied between 2 and 20 m min^{-1} and were dried using hot air convection ovens (max. $140 \text{ }^\circ\text{C}$) and IR-driers. After processing the complete layer stack of Ag-comb/PEDOT:PSS/ZnO/P3HT:PCBM/PEDOT:PSS/Ag-comb the devices were electrically switched to fully functional solar cells in an automatic setup as described earlier.^[47,48]

2.2. Encapsulation

The encapsulation of the solar cells was carried out with three different adhesive technologies, namely of PSA, UV-curable glue, and hotmelt. The barrier foil was the same type that the solar cells were printed on. Two sets of encapsulated modules were prepared in a full R2R process using the machine setups shown earlier.^[49] The first set of modules had only a single lamination on the backside covering the printed layers as illustrated in the processing workflow in Figure 1. A second set was laminated again with barrier foil on the front side to ensure a full edge sealing for small test modules.^[50] Hereby the modules have been cut out in advance to enable a 10 mm rim of barrier around the module. For the double-sided, lamination the UV-blocking layer from the solar cell barrier substrate was removed prior to lamination. The full R2R processing workflow for all methods and the simplified substrate paths through a R2R lamination machine is illustrated in Figure 1. In all cases, the substrate with the solar cells and the encapsulation foil was fed through two rollers under a certain pressure.

For the PSA encapsulation process the barrier foil with the laminated adhesive was prepared in a separate run prior to the lamination onto the solar cells. The adhesive based on acrylate polymers (3M 467 MP, $60 \mu\text{m}$) was laminated to the barrier together with a paper liner at 20 m min^{-1} and was put on stock for later use. The same speed was used for the lamination onto the solar cell substrate whereas the final adhesive strength was achieved after some hours of resting time.

Prior to the encapsulation with UV-curable adhesive a flexo coating/printing unit was used to apply the solvent-free epoxy resin (DELO-KATIOBOND LP655) onto the corona treated barrier substrate. The chemical components are 7-oxabicyclo[4.1.0]hept-3-ylmethyl 7-oxabicyclo[4.1.0]heptane-3-carboxylate with the reaction product bisphenol-A-(epichlorhydrin) and a small amount of [3-(2,3-epoxypropoxy)propyl]

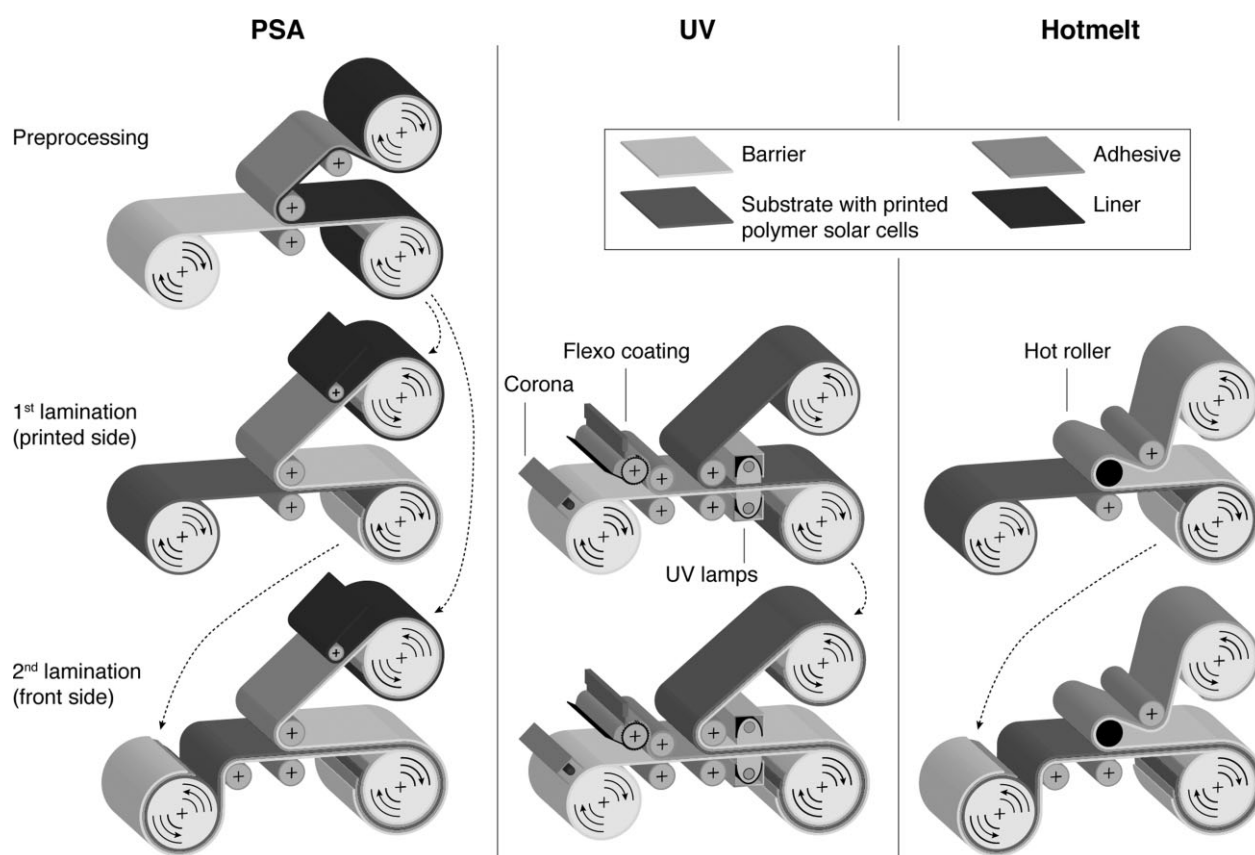


Fig. 1. Process workflow for the R2R encapsulation of flexible OPV modules.

trimethoxysilane. We also tested UV-curing acrylic adhesives (DELO LP415) that have monoalkyl or monoaryl or monoalkylaryl esters of acrylic acid; 1,3-butadiene, 2-methyl-, homopolymer, maleated, 2-[(2-methyl-1-oxo-2-propen-1-yl)oxy]ethyl esters 4-(1-oxo-2-propenyl)-morpholine; methacrylic acid; and phenyl bis(2,4,6-trimethylbenzoyl)-phosphine oxide cyclohexane as chemical components. This adhesive could also be made to work well but required fast curing to avoid destructive interaction with the active solar cell stack. In contrast the DELO LP655 could be left uncured on top of the active layer for prolonged periods of time with no adverse side effects and we therefore chose to work with LP655 in this study. For optimized fast mass production, we expect that LP415 works in a comparable manner. An anilox roller with a volume of 30 ml m^{-2} was used for the metering of the highly viscous adhesive. The final cured thickness of the adhesive is about $20 \mu\text{m}$. The R2R UV-curing was carried out at a speed of 2 m min^{-1} just limited by the length of the UV-LED lamp installation (DELO DELOLUX 20, 400 nm , 200 mW cm^{-2}) and the recommended minimum exposure time of 16 s. The final curing is achieved within 24 h after exposure.

The encapsulation with hotmelt adhesive was carried out at a speed of 1 m min^{-1} and a roller temperature of 140°C to achieve a wrinkle-free lamination. The polyester-based hotmelt adhesive film (Glutex AU130, $145 \mu\text{m}$) had been applied onto the barrier prior encapsulation. The barrier foil

with the hotmelt was wrapped around the hot roller for an angular contact length of more than 200° (roller diameter 95 mm) to enable a long melting zone before entering the nip and getting into contact with the solar cell substrate. The adhesive film itself is highly flexible and stretchable but shows rather stiff behavior in the final sandwich structure with tendencies of delamination from the smooth barrier film.

The solar cell modules with single and double lamination were tested under a solar simulator (Steuernagel KHS Solar Constant 1200, metal halide lamp) at AM1.5G illumination with an irradiance of 1000 W m^{-2} (ISOS-L-1 testing protocol). The solar cells have been externally cooled with a fan to a temperature of about 35°C . Each module consisted of four serially connected cells with a total active area of 28 cm^2 and an open circuit voltage V_{OC} of $\approx 2 \text{ V}$. The initial power conversion efficiency of the devices were in the range of 1.6%. The solar cell parameters were frequently measured with a Keithley 2400 Sourcemeter over a period of 900 h. The test samples under the solar simulator are shown in Figure 2.

3. Results and Discussion

3.1. Processing

The fabrication of the solar cell modules directly on the barrier film was straightforward based on our experience gained from previous reports where modules with thousands of serially connected cells were produced.^[43]

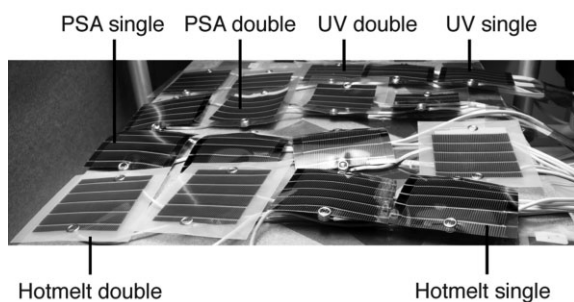


Fig. 2. Encapsulated solar cell modules under the solar simulator.

When the pure lamination speed from our experiments is compared, the PSA method is far superior in ease of handling being 10–20 times faster in processing compared to UV and hotmelt. But this is only true if a ready-to-use barrier foil with an applied PSA is available. In our case, the PSA had to be applied in advance which cuts to the effective speed from 20 to 10 m min^{-1} . The lamination of the substrate with the PSA and liner often requires some run-in to achieve alignment. The sticky PSA does not allow coarse cross-directional alignment during the substrate movement, as it results in large wrinkles.

The hotmelt also needs to be applied in advance by a supplier when no hotmelt applicator is available. The direct application of hot melt sealant can only be done with special heated slot-die heads and rollers. The UV curable adhesive is the only one where the application was carried out directly during the lamination run just before the barrier and the solar cell substrate are joined together with the pressurized rollers. The fast change of the barrier foil itself is a huge advantage. The speed of 2 m min^{-1} of the current UV process can be improved by longer illumination zones, increased temperature of the adhesive, and fast-curing adhesives where the minimum exposure time can be down to 1 s. The matching of the LED wavelength with the absorption spectra of the photo-initiators in the adhesive is very important as well. The exposure of the adhesive happens through the barrier foil that has an applied UV-blocking filter (cut-off at 380–390 nm). Therefore the adhesive must also react at longer wavelengths. In our case the curing takes place within 320–440 nm. After exposure to UV light the curing continues under visible light. The laminated modules will reach their final strength after 24 h in ambient atmosphere.

The speed of the hotmelt method was limited to 1 m min^{-1} due to increased wrinkling at higher speed. A lot of web tension had to be applied to minimize the effect. The speed can be easily increased when thinner hotmelts are used as the hot roller with a diameter of 95 mm and 140°C was sufficient enough to melt the $145 \mu\text{m}$ thick glue in short time. A thinner hotmelt would potentially also improve the lamination procedure regarding speed and wrinkling. We chose the very thick hotmelt to ensure a lamination without air entrapment between the relatively thick back electrode comb electrodes that has sometimes been shown to be the case during experiments with an office laminator and standard office

lamination pouches. It should be noted that an industrial hotmelt lamination process typically employs a direct application of the hotmelt (heated slot-die or roll-coater) shortly before the joining of the two substrates. High speeds with several tens of meters per minute can be achieved.

A further advantage of a direct application of the UV-curable adhesive in this experiment is the variety of coating thickness. We chose a high volume anilox cylinder with 30 ml m^{-2} that resulted in a $20 \mu\text{m}$ thick adhesive layer after curing. This corresponds to a consumption of 28 g m^{-2} (density 1.4 g cm^{-3}). In case other liquid adhesives are used or thinner layers are desired the anilox cylinder can be changed in very short time. Other deposition methods such as slot-die coating or roll-coating would work as well. A second advantage of using the flexographic printing method is the possibility of a patterned adhesive deposition.

Despite its preprocessing, the encapsulation with PSA also causes a lot of waste due to the protective liner (polycoated kraft paper) that has to be removed prior entering the lamination rollers. Hotmelt might also have this problem if it comes with a liner. Direct application of UV curable adhesive does not produce large amounts of waste as the adhesive ink can be applied in a controlled manner. For a longer run, less ink waste will be generated relative to the overall usage. The only disadvantage of the UV curable adhesive is that the equipment (rollers) needs to be cleaned with solvent after the run is completed. Neither PSA or hot melt requires this and they can both be viewed as clean or dry processes that allows the operator to touch the materials during handling which is a significant advantage at the practical operational level.

The lamination with UV-curable adhesives has the advantage that the solar cells can be directly used afterwards, which cannot be achieved with the other methods. The solar cells become instantly annealed due to the highly intense illumination with UV light during the lamination process. Measurements of encapsulated solar cells show very good J-shaped I-V-curves without inflection points compared to PSA and hotmelt encapsulated cells that exhibit an initial S-shape behavior. This will change to a J-shape after some time under the solar simulator or natural sunlight.

3.2. Backside (Single) Versus Frontside/Backside (Double) Lamination

A recent study had already shown that double lamination with PSA and an 10 mm rim around the solar cell module is superior compared to a single side lamination.^[50] The cells were printed on PET-ITO substrate without specific barrier functionality. Therefore, a double-sided lamination was necessary to achieve a particular barrier and UV-blocking effect on the illuminated front side. Further studies on printed ITO-free devices on barrier foil revealed that edge-sealed devices with UV-curable adhesive have slightly better lifetime than the ones with PSA.^[5] A single side lamination has not been carried out with the ITO-free devices.

In this report we compare the three R2R lamination methods described above with regard to the necessity of a second front

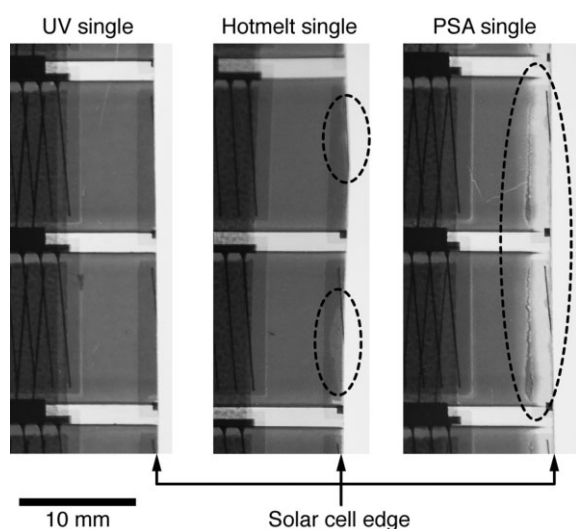


Fig. 3. Edge bleaching behavior of the active layer of single side encapsulated modules after 900 h of illumination. The use of UV curable epoxy resin shows no bleaching.

barrier, edge sealing, and lifetime behavior. The barrier itself accounts for a large part of the final device cost and implies also a lot of embodied energy that increases the energy payback time.^[51] If only one lamination layer on the backside is enough for a lifetime comparable to double edge sealing then this yields a shorter processing time and lower device cost.

As expected, a full edge sealing with all three adhesives shows no bleaching of the active layer after >900 h of illumination. On the other hand the more cost-efficient single side lamination has very surprising and promising results. We expected a similar bleaching of the P3HT:PCBM layer for all three adhesives but only PSA showed a remarkable edge effect with full bleaching. The modules with hotmelt adhesive have only very small areas of bleaching at the open edge whereas modules with UV-curable adhesive show no bleaching at all. Photographs for side-by-side comparison of all three single-side encapsulated modules can be seen in Figure 3. Although specific permeation properties of the adhesives are not specified the results show that the UV epoxy resin and the hotmelt are superior compared to PSA, which is in accordance to previously published results.^[5] One reason for this is obviously the dense structure formed out of the liquid epoxy resin or melted glue. The PSA has a rougher surface when released from the liner and pressed onto the printed solar cells. During the lamination process many inclusions (air bubbles) were built into the adhesive that form reservoirs of the current ambient conditions during the lamination. The inclusions (Figure 4) have volumes of up to 450 pL (calculation based on perfect spheres) and are homogeneously distributed over the whole laminate. Therefore the inclusions at the edge can be seen as an additional starting point for an accelerated bleaching. From these findings, it already shows that a single backside encapsulation with the UV-curable adhesive and barrier foil might be enough for a long lasting solar cell that is directly processed on barrier substrate.

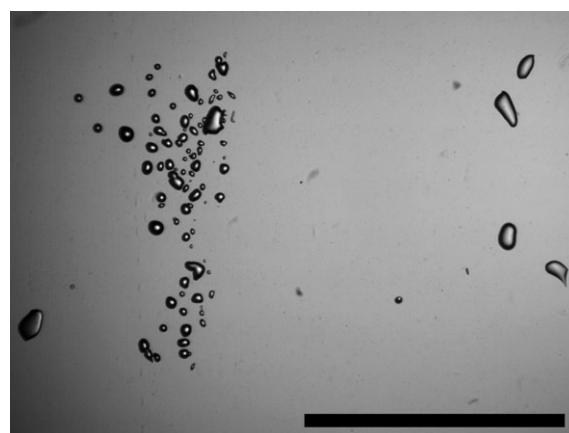


Fig. 4. Microscopic photograph of typical inclusions (air bubbles) after lamination with pressure sensitive adhesive (PSA). The calculated volume is in the range of 1.5–450 pL. Scalebar is 1 mm.

3.3. Lifetime

The encapsulated devices have been tested for 900 h under permanent illumination in ambient atmosphere using an external fan to cool the samples to $\approx 35^\circ\text{C}$. The solar simulator was calibrated to 1000 W m^{-2} and the samples were spread on a board as shown in Figure 2. Due to the size and number of the samples it was not possible to enable the same direct and total irradiation of all devices.^[52] Therefore the presented evolution of the solar cell parameters is an average from three samples per encapsulation method.

After encapsulation the samples have been light soaked for 24 h to stabilize the solar cell parameters. We observed a quite significant drop of efficiency during this “burn-in” period and started the lifetime study from 24 h onwards. The stabilization on a lower level within the first 24 h is a typical behavior for our R2R produced cells in conjunction specifically with the P3HT used. The main reason can be seen in the active layer composition and initial degradation processes, but the physical and chemical mechanisms remain unclear within the organic solar cell research community. It is observed for several different types of organic solar cells.^[29] The burn-in process depends very much on the type of materials used in the active layer and can show completely different results just by changing the supplier of the same polymer, although the remaining solar cell structure is unchanged. We observed different behaviors such as an initial improvement and drop afterwards or a drop of performance from the beginning as appeared here. The evolution of the solar cell parameters over the test period of 900 h is visualized in Figure 5. It can be seen that the normalized efficiency follows a linear degradation from 200 h onwards.

The parallelism of the linear fits is caused by the use of the same barrier foil and solar cells for all samples whereas the level of degradation has its reason in the different adhesives and encapsulation methods. It clearly shows that the UV-curable adhesive is superior to all other methods independently of single side encapsulation or edge sealing with front and back barrier foil. These modules end up with a T_{80} of

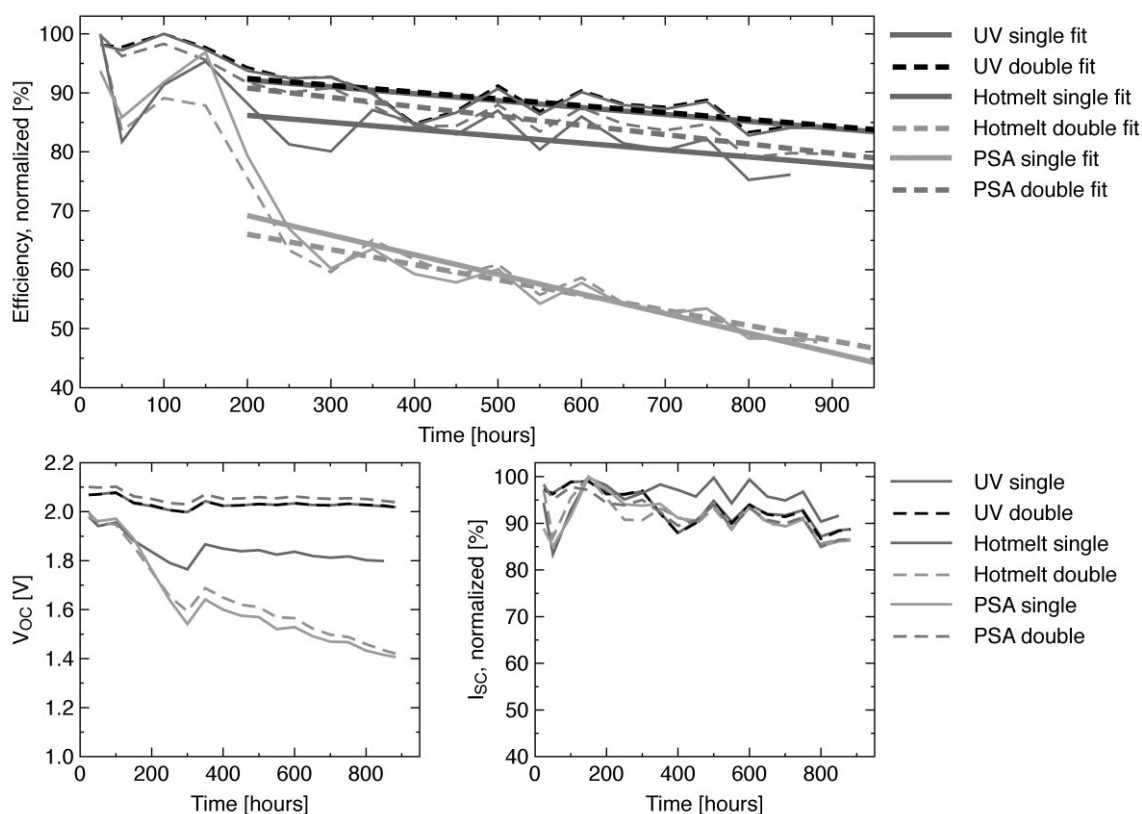


Fig. 5. Stability curves of normalized efficiency, open circuit voltage V_{OC} , and normalized short circuit current I_{SC} after 24 h of burn-in and ≈ 900 h continuous illumination. The curves represent the average of three samples per encapsulation method. The linear fit has been calculated from 200 h onwards.

>1000 h after burn-in. The results from the edge sealing analysis show virtually no differences for the UV epoxy resin. Exactly the same efficiency decay is evaluated during the test period for edge and non-edge sealed UV-encapsulated modules. The edge sealed PSA without any bleaching shows a faster degradation than the UV samples and is comparable to the results in a previous study even though the devices in the previous study were based on PET-ITO.^[5] The V_{OC} of the modules for these three samples is almost stable over the test period. The decreasing efficiency occurs due to the slightly decreasing current. The very good V_{OC} properties are caused by a very slow ingress of oxygen due to the good barrier properties of the adhesive for UV single side encapsulation or the edge sealing with PSA. The single side hotmelt also shows a good lifetime performance but exhibits a voltage drop over time. This may come from the very thick adhesive and a potentially higher oxygen uptake.

The single-sided PSA encapsulation and the double-sided hotmelt encapsulation show a significantly faster degradation mainly due to loss of voltage as seen in Figure 5. A large bleaching of the active layer was observed on the samples with single side PSA (Figure 3), which can be explained by the poor barrier properties of the adhesives at the open edge and the resulting oxygen ingress over time. The similar efficiency and voltage drop could be seen on the double hotmelt but was not expected from the bleaching results. The bad performance might come from our hotmelt process itself where the adhesive

is heated twice for short time in the nip zone resulting in an unpredictable interaction of the printed layers with the adhesive. Secondly, the modules are forced through the nip at high tension to avoid wrinkling which leads to an enhanced mechanical stress to the solar cell. The devices themselves are delicate to handle compared to all other test samples due to the stiff sandwich structure with the two adhesives as the thickest layers in the multilayer structure. A much thinner hotmelt layer in the range of the UV epoxy resin thickness would most likely improve handling and lifetime of the hotmelt devices.

The voltage drop of the specific devices is caused by a decreased voltage on all serially connected single cells and can be explained by a homogeneous degradation over the whole device and not by failure of a single cell, e.g., due to contact problems. For this, each module was placed on an upside-down solar simulator after the test period and every single cell has been contacted with probing needles through the barrier and adhesive to measure the open circuit voltage. The slight decrease in current over the 900 h is in principle similar for all encapsulation methods.

The flexibility of the UV and PSA devices is comparable, although the PSA device felt a bit softer than the one with the fully cured thin epoxy resin. The disadvantage of the hotmelt is its whitish/opaque appearance that blocks more light than the clear PSA and UV adhesives in the double sealed devices. The color of the adhesive has only a negligible impact on single backside laminated cells.

4. Conclusions

In this study we compared three R2R encapsulation methods on fully printed ITO-free polymer solar cells processed directly on barrier foil. The processing of solar cells directly on the barrier instead on ITO-PET substrate has the advantage of having a minimized embodied energy in the final device and that an extra encapsulation on the front side can be avoided. It has been shown earlier that an edge sealing is superior for PSA devices but here we conclude that a single-sided lamination with UV-curable epoxy resin just on the backside is enough to achieve the best performing encapsulation over a test period of 900 h. Although the lamination with PSA is currently much faster than all other methods it requires a preprocessing step and double-sided lamination to perform almost as good as single or double UV. The waste of the PSA process is considerably higher whereas the coating weight of the UV epoxy resin can be adjusted as required with minimized waste, especially for long runs. Upscaling is viewed as facile with fast curing adhesives or larger light curing setups for longer exposure times. The hotmelt process is also advantageous and has a comparable lifetime performance for single side lamination. The drawback is the low speed in the current setup. It can most likely be improved with thinner hotmelts or specialized coating equipment for a direct application of the hotmelt before the lamination.

The single backside lamination with UV-curable adhesives presents the largest advantages for large scale produced polymer solar cells on barrier where the ratio of open edges to module area is very small and only present at the beginning and end of the long modules.^[43] The lamination requires much less material input and lowers the cost of the device significantly which is necessary for a potential electrical grid connection of OPVs.

Received: May 8, 2013

Final Version: June 24, 2013

Published online: July 26, 2013

- [1] M. Jørgensen, J. E. Carlé, R. R. Søndergaard, M. Lauritzen, N. A. Dagnæs-Hansen, S. L. Byskov, T. R. Andersen, T. T. Larsen-Olsen, A. P. L. Böttiger, B. Andreasen, L. Fu, L. Zuo, Y. Liu, E. Bundgaard, X. Zhan, H. Chen, F. C. Krebs, *Sol. Energy Mater. Sol. Cells* **2013**. DOI: 10.1016/j.solmat.2013.05.034
- [2] M. A. Green, K. Emery, Y. Hishikawa, W. Warta, E. D. Dunlop, *Prog. Photovolt: Res. Appl.* **2013**, *21*, 1.
- [3] www.Heliatek.com
- [4] F. C. Krebs, S. A. Gevorgyan, J. Alstrup, *J. Mater. Chem.* **2009**, *19*, 5442.
- [5] D. Angmo, S. A. Gevorgyan, T. T. Larsen-Olsen, R. R. Søndergaard, M. Hösel, M. Jørgensen, R. Gupta, G. U. Kulkarni, F. C. Krebs, *Org. Electron.* **2013**, *14*, 984.
- [6] P. Kopola, J.-M. Kim, S. Guillerez, H. Jin, M. Tuomikoski, A. Maaninen, J. Hast, *Sol. Energy Mater. Sol. Cells* **2010**, *94*, 1673.
- [7] M. M. Voigt, R. C. I. Mackenzie, C. P. Yau, P. Atienzar, J. Dane, P. E. Keivanidis, D. D. C. Bradley, J. Nelson, *Sol. Energy Mater. Sol. Cells* **2011**, *95*, 731.
- [8] A. C. Hübler, B. Trnovec, T. Zillger, M. Ali, N. Wetzold, M. Mingeback, A. Wagenpfahl, C. Deibel, V. Dyakonov, *Adv. Energy Mater.* **2011**, *1*, 1018.
- [9] A. Lange, A. Hollaender, M. Wegener, *Mater. Sci. Eng. B* **2013**, *178*, 299.
- [10] C. N. Hoth, P. Schilinsky, S. A. Choulis, C. J. Brabec, *Nano Lett.* **2008**, *8*, 2806.
- [11] L. Wengeler, M. Schmitt, K. Peters, P. Scharfer, W. Schabel, *Chem. Eng. Process.: Process Intensification* **2013**, *68*, 38.
- [12] R. R. Søndergaard, M. Hösel, F. C. Krebs, *J. Polym. Sci. B Polym. Phys.* **2013**, *51*, 16.
- [13] N. Espinosa, R. Garcia-Valverde, A. Urbina, F. C. Krebs, *Sol. Energy Mater. Sol. Cells* **2011**, *95*, 1293.
- [14] Y. Galagan, E. W. C. Coenen, S. Sabik, H. H. Gorter, M. Barink, S. C. Veenstra, J. M. Kroon, R. Andriessen, P. W. M. Blom, *Sol. Energy Mater. Sol. Cells* **2012**, *104*, 32.
- [15] J.-S. Yu, I. Kim, J.-S. Kim, J. Jo, T. T. Larsen-Olsen, R. R. Søndergaard, M. Hösel, D. Angmo, M. Jørgensen, F. C. Krebs, *Nanoscale* **2012**, *4*, 6032.
- [16] J. Krantz, M. Richter, S. Spallek, E. Spiecker, C. J. Brabec, *Adv. Funct. Mater.* **2011**, *21*, 4784.
- [17] D. Y. Choi, H. W. Kang, H. J. Sung, S. S. Kim, *Nanoscale* **2013**, *5*, 977.
- [18] M. Jørgensen, K. Norrman, S. A. Gevorgyan, T. Tromholt, B. Andreasen, F. C. Krebs, *Adv. Mater.* **2012**, *24*, 580.
- [19] M. Jørgensen, K. Norrman, F. C. Krebs, *Sol. Energy Mater. Sol. Cells* **2008**, *92*, 686.
- [20] N. Grossiord, J. M. Kroon, R. Andriessen, P. W. M. Blom, *Org. Electron.* **2012**, *13*, 432.
- [21] J. U. Lee, J. W. Jung, J. W. Jo, W. H. Jo, *J. Mater. Chem.* **2012**, *22*, 24265.
- [22] E. Voroshazi, B. Verreet, J.-M. Kim, P. Heremans, *Sol. Energy Mater. Sol. Cells* **2011**, *95*, 1303.
- [23] S. Cros, R. de Bettignies, S. Berson, S. Bailly, P. Maise, N. Lemaitre, S. Guillerez, *Sol. Energy Mater. Sol. Cells* **2011**, *95*, S65.
- [24] J. Fahlteich, M. Fahland, W. Schönberger, N. Schiller, *Thin Solid Films* **2009**, *517*, 3075.
- [25] J.-S. Park, H. Chae, H. K. Chung, S. I. Lee, *Semicond. Sci. Technol.* **2011**, *26*, 034001.
- [26] S. Amberg-Schwab, U. Weber, A. Burger, S. Nique, R. Xalter, *Monatsh. Chem./Chem. Mon.* **2006**, *137*, 657.
- [27] C. Charton, N. Schiller, M. Fahland, A. Holländer, A. Wedel, K. Noller, *Thin Solid Films* **2006**, *502*, 99.
- [28] F. Yan, J. Noble, J. Peltola, S. Wicks, S. Balasubramanian, *Sol. Energy Mater. Sol. Cells* **2013**, *114*, 214.
- [29] D. M. Tanenbaum, M. hermenau, E. Voroshazi, M. T. Lloyd, Y. Galagan, B. Zimmermann, M. Hösel, H. F. Dam, M. Jørgensen, S. A. Gevorgyan, S. Kudret, W. Maes, L. Lutsen, D. Vanderzande, U. Würfel, R. Andriessen, R. Rösch, H. Hoppe, G. teran-Escobar, M. Lira-Cantu, A. Rivaton, G. Y. Uzunoglu, D. Germack, B. Andreasen, M.

- V. Madsen, K. Norrman, F. C. Krebs, *RSC Adv.* **2012**, *2*, 882.
- [30] P. E. Burrows, V. Bulovic, S. R. Forrest, L. S. Sapochak, D. M. McCarty, M. E. Thompson, *Appl. Phys. Lett.* **1994**, *65*, 2922.
- [31] M. Riede, C. L. Uhrich, J. Widmer, R. Timmreck, D. Wynands, G. Schwartz, W. M. Gnehr, D. Hildebrandt, A. Weiss, J. Hwang, S. Sundarraj, P. Erk, M. Pfeiffer, K. Leo, *Adv. Funct. Mater.* **2011**, *21*, 3019.
- [32] R. Roesch, K.-R. Eberhardt, S. Engmann, G. Gobsch, H. Hoppe, *Sol. Energy Mater. Sol. Cells* **2013**, *117*, 59.
- [33] M. W. Möller, D. A. Kunz, T. Lunkenbein, S. Sommer, A. Nennemann, J. Breu, *Adv. Mater.* **2012**, *24*, 2142.
- [34] R. R. Søndergaard, T. Makris, P. Lianos, A. Manor, E. A. Katz, W. Gong, S. M. Tuladhar, J. Nelson, R. Tuomi, P. Sommeling, S. C. Veenstra, A. Rivaton, A. Dupuis, G. teran-Escobar, M. Lira-Cantu, S. B. Sapkota, B. Zimmermann, U. Würfel, A. Matzarakis, F. C. Krebs, *Sol. Energy Mater. Sol. Cells* **2012**, *99*, 292.
- [35] S. Sarkar, J. H. Culp, J. T. Whyland, M. Garvan, V. Misra, *Org. Electron.* **2010**, *11*, 1896.
- [36] C. Chang, C. Chou, Y. Lee, M. Chen, F. Tsai, *Org. Electron.* **2009**, *10*, 1300.
- [37] J. A. van Delft, D. Garcia-Alonso, W. M. M. Kessels, *Semicond. Sci. Technol.* **2012**, *27*, 074002.
- [38] J. Granstrom, M. Villet, T. Chatterjee, J. A. Gerbec, E. Jerkunica, A. Roy, *Appl. Phys. Lett.* **2009**, *95*, 093306.
- [39] P. Mandlik, J. Gartside, L. Han, I.-C. Cheng, S. Wagner, J. A. Silvernail, R.-Q. Ma, M. Hack, J. J. Brown, *Appl. Phys. Lett.* **2008**, *92*, 103309.
- [40] M. R. Cavallari, C. M. Cuppoletti, G. Pucker, F. J. Fonseca, A. M. Andrade, S. Carturan, G. Maggioni, A. Quaranta, M. Buffa, M. Tonezzer, *11th International Conference on Advanced Materials* **2009**.
- [41] Z. Liu, J. Li, F. Yan, *Adv. Mater.* **2013**. DOI: 10.1002/adma.201205337
- [42] H. J. Lee, H. P. Kim, H.-M. Kim, J.-H. Youn, D.-H. Nam, Y.-G. Lee, J.-G. Lee, A. R. bin Mohd Yusoff, J. Jang, *Sol. Energy Mater. Sol. Cells* **2013**, *111*, 97.
- [43] P. Sommer-Larsen, M. Jørgensen, R. R. Søndergaard, M. Hösel, F. C. Krebs, *Energy Technol.* **2013**, *1*, 15.
- [44] F. C. Krebs, T. Tromholt, M. Jørgensen, *Nanoscale* **2010**, *2*, 873.
- [45] F. C. Krebs, J. Fyenbo, D. M. Tanenbaum, S. A. Gevorgyan, R. Andriessen, B. van Remoortere, Y. Galagan, M. Jørgensen, *Energy Environ. Sci.* **2011**, *4*, 4116.
- [46] F. C. Krebs, J. Alstrup, H. Spanggaard, K. Larsen, E. Kold, *Sol. Energy Mater. Sol. Cells* **2004**, *83*, 293.
- [47] M. Hösel, R. R. Søndergaard, M. Jørgensen, F. C. Krebs, *Energy Technol.* **2013**, *1*, 102.
- [48] T. T. Larsen-Olsen, R. R. Søndergaard, K. Norrman, M. Jørgensen, F. C. Krebs, *Energy Environ. Sci.* **2012**, *5*, 9467.
- [49] R. Søndergaard, M. Hösel, D. Angmo, T. T. Larsen-Olsen, F. C. Krebs, *Mater. Today* **2012**, *15*, 36.
- [50] D. M. Tanenbaum, H. F. Dam, R. Rösch, M. Jørgensen, H. Hoppe, F. C. Krebs, *Sol. Energy Mater. Sol. Cells* **2012**, *97*, 157.
- [51] N. Espinosa, M. Hösel, D. Angmo, F. C. Krebs, *Energy Environ. Sci.* **2012**, *5*, 5117.
- [52] S. A. Gevorgyan, J. E. Carlé, R. Søndergaard, T. T. Larsen-Olsen, M. Jørgensen, F. C. Krebs, *Sol. Energy Mater. Sol. Cells* **2013**, *110*, 24.

Large-scale roll-to-roll photonic sintering of flexo printed silver nanoparticle electrodes

Markus Hösel and Frederik C. Krebs*

Received 11th May 2012, Accepted 13th June 2012

DOI: 10.1039/c2jm32977h

In this report we employ static and roll-to-roll (R2R) photonic sintering processes on flexo printed silver nanoparticle-based electrode structures with a heat-sensitive 60 μm thin barrier foil as a substrate. We use large area electrode structures to visualize the increased optical footprint of single and quadruple flashes, and the R2R challenges in the form of overlapping exposures. It is shown that single flash exposure is enough to significantly increase the conductivity and adhesion without damaging the foil or build-up of cracks in the silver layer. Additional flash exposures or increased energies above the threshold level have only minor impact on the conductivity but lead to cracks and substrate deformation. A second silver nanoparticle ink was printed, which was already optimized for low-temperature drying. Here we show that photonic sintering has only a minor impact on the conductivity as the nanoparticles are already sintered. The advantage of single exposure is the ability to produce higher R2R processing speeds without overlapping, which is shown in the form of theoretical calculations.

Introduction

Current devices such as organic solar cells (OSCs) and organic light emitting diodes (OLEDs) employ transparent electrodes typically based on indium tin oxide (ITO), which is deposited by vacuum processes on the substrate. Enabling an energy efficient production and avoiding the use of scarce elements such as indium, a full solution based roll-to-roll (R2R) process using printing or coating of metal ink (*e.g.* silver nanoparticles) is beneficial. Depending on the device structure grids or full layer silver is applied as the first electrode by deposition directly on the substrate. This has been successfully demonstrated for OSCs^{1–3} and OLEDs.⁴ Printed touch screen grid electrodes⁵ and RFID antennas⁶ are devices currently fabricated by printing of silver based inks. R2R compatible printing methods such as screen-printing,³ gravure,^{7,8} flexography,⁹ and inkjet⁴ are typically used for the patterning of electrode structures on flexible polymer substrates.

Printing of nanoparticle silver often requires further processing steps such as sintering or prolonged thermal treatment to achieve the required conductivity.^{10,11} The most prominent and often time-consuming process is simple heating at high temperature (sometimes 200–300 °C) to allow evaporation of organic stabilizers, densification of the nanoparticles and the formation of a continuous percolation network.¹² Further technologies include electrical sintering,¹³ microwave assisted sintering,¹⁴ and plasma sintering.¹⁵ Flexible substrates such as heat-stabilized

polyethylene terephthalate (PET) only allow temperature regimes up to 140 °C for a short time span without damage or excessive shrinkage. One way to significantly improve the conductivity of printed silver nanoparticle ink on very thin and heat-sensitive PET substrates is the use of photonic sintering utilizing a R2R compatible xenon flash lamp system. Photonic sintering of silver and copper nanoparticle inks allows for room-temperature processing and was demonstrated by several groups.^{16–22} It should be noted that reported demonstrations have mostly been small test patterns and no large area structures close to real-world applications have been reported. The advantage of an intensive short-pulsed flashlight is the rapid heating of the metallic nanoparticle layer without damaging the substrate. The melting temperature of metallic nanoparticles varies inversely with the radius of the particle, which is below the bulk melting temperature.²³

In this study we use high-throughput R2R flexo printing of silver nanoparticle inks to form full layer electrodes directly on a 60 μm barrier foil close to the final application. The barrier film has already been used as an encapsulation material for organic solar cells.²⁴ Printing of electrodes directly on the barrier foil to avoid ITO on a thicker PET substrate with its vacuum-based production processes can significantly reduce the embodied energy and energy payback time of photovoltaic devices.²⁵ Sintering of the printed layers and the improvement in conductivity was performed with an additional R2R xenon flash lamp system. Silver layers optimized for flexographic printing that were conductive already after printing and drying showed only a small decrease in sheet resistance upon photonic sintering. A second type of silver nanoparticle ink most suited for inkjet printing was

Department of Energy Conversion and Storage, Technical University of Denmark, Frederiksborgvej 399, DK-4000 Roskilde, Denmark. E-mail: frkr@dtu.dk

not conductive after printing and drying and showed significant improvements in conductivity and adhesion after photonic sintering. Unlike other reports we were able to sinter silver nanoparticles with just a single flash exposure and less optical energy density.^{19,22} The process itself also revealed challenges in finding the right process settings to avoid too much impact on the surface morphology of the silver layer in the form of cracks and dimensional deformation of the substrate. As the flexo printed electrodes are designed for use in organic solar cells, printing of silver ink combined with photonic sintering can also see its application elsewhere, where superior surface quality after sintering is not required in the first instance. Examples of applications are printed RFID antennas or printed circuit boards (PCB). This report comprises experiments of photonic sintering of silver nanoparticle ink with results that can be adapted to any application, where heat-sensitive substrates are used and R2R processing is the desired fabrication method.

Experimental

Printing

The substrate used in this study was a 60 μm thin barrier foil from Amcor. Two different silver nanoparticle inks were printed on a roll-to-roll system as described elsewhere.²⁶ The commercial water-based flexo silver ink PFI-722 (PChem Associates) was printed at 15 m min^{-1} using an anilox volume of 1.5 ml m^{-2} (0.97 BCM) and an elastomeric printing form (65 Shore). The silver content of the ink was 60 wt%. Corona treatment was used for improved adhesion and print quality. The second silver ink (AgNP) was a dispersion of Ag nanoparticles (40–70 nm) in a 1 : 1 mixture of triethyleneglycolmonomethylether and *o*-xylene with a final concentration of 25 wt% as employed earlier¹ and filtered through a 2.7 μm filter prior to printing. Flexo printing was carried out at 10 m min^{-1} using an anilox volume of 11 ml m^{-2} (7.1 BCM) and an elastomeric printing form (40 Shore). Here, the barrier substrate was not corona treated to achieve better print quality. For each printing experiment the ink was

dried using hot-air ovens (140 $^{\circ}\text{C}$, 2 \times 2 m) and additional IR heating. The printed electrode pattern had a repeat size of 12 inches and consists of 16 stripes (13 mm wide, 2 mm gap) with a gap of 1 mm between the stripes along the print direction. Photographs of the printing processes are shown in Fig. 1a–d.

Photonic sintering

Photonic sintering was carried out using a commercial xenon flash lamp system (Sinteron 2000, Xenon Corp.) installed on a roll-to-roll system as shown in Fig. 1e and f. The system delivers electrical pulse energies from 150 to 2000 joules by changing the voltage setting between 1.6 and 3.8 kV. In this study the pulse duration was set to 0.5 ms with a maximum electrical pulse energy of 830 J and a flash frequency of 1.8 Hz. The air-cooled 16'' xenon linear flash lamp delivers a broadband spectrum from 190 nm to 1000 nm (lamp C). The distance d of the lamp housing from the unsupported substrate was set to 2'' (out of focus). The optical energy density values are based on datasets given in the system's manual and represent approximate numbers.

Characterization

The sheet resistance was measured with a 4-point probe resistance meter (Techno Science Instruments, India). Surface images were taken with an optical microscope from Lab Engineering Instruments, India. The size and morphology of the nanoparticle ink before and after sintering was examined with a field emission scanning electron microscope (FE-SEM, FEI Nova NanoSEM 600). Surface profilometry was carried out using a contactless 3D white light interferometer (Veeco Wyko NT9100) and a stylus profiler (Veeco Dektak 6m).

Results and discussion

Printing quality

In this study we flexo printed two types of silver nanoparticle inks, which showed good edge quality necessary for a

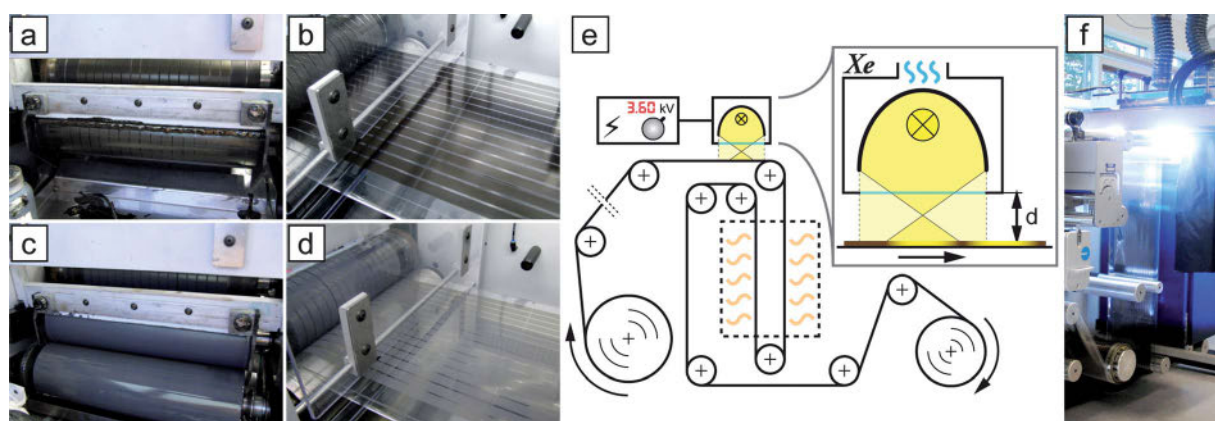


Fig. 1 R2R flexographic printing of silver nanoparticle ink directly on a thin barrier foil and R2R photonic sintering post-processing. (a) Anilox cylinder with doctor blade and scraped off excess PFI-722 ink. (b) Printed PFI-722 electrode stripes at 15 m min^{-1} shown as the wet layer. (c) Printing of the AgNP ink with the help of an ink bath and fountain roller due to lower ink viscosity (not necessary for PFI-722 ink). (d) Printed AgNP ink electrode stripes at 10 m min^{-1} shown as the wet layer. (e) A simplified schematic drawing of the roll-to-roll photonic sintering setup (not to scale), incl. a voltage pulse-forming controller and the xenon flash lamp system. The air-cooled lamp housing is mounted above the substrate at a variable distance d . An additional hot air dryer is situated below the flash lamp. (f) Photograph of the R2R photonic sintering machine with an open light shield at the moment of flashing.

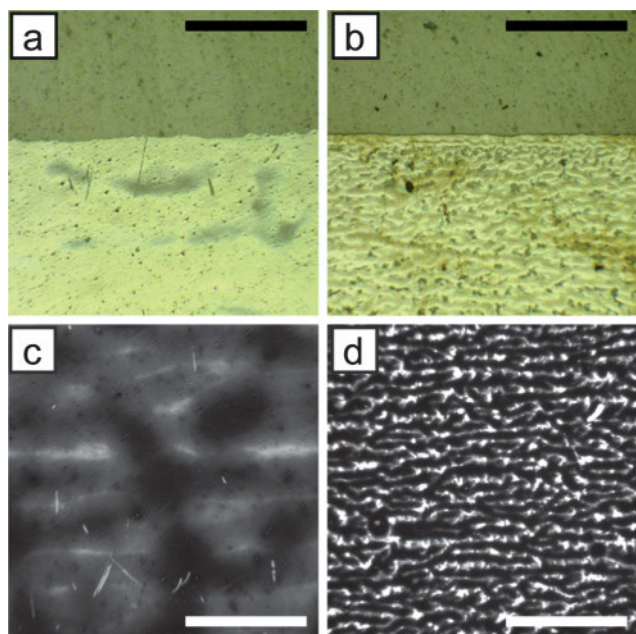


Fig. 2 Microscope images showing the edge quality of (a) AgNP ink and (b) PFI-722 ink. Microscope images (transmitted light) showing the viscous fingering effect of (c) AgNP ink and (d) PFI-722 ink. Dark areas correspond to thicker silver layers. The scale-bar is 500 μm .

well-defined electrode pattern. A typical property of printing technologies employing a nip such as flexography is ink splitting between the printing cylinder and substrate, resulting in viscous fingering (Saffman–Taylor instabilities^{27,28}) and therefore in an uneven layer thickness, as shown in Fig. 2. The optimized PFI-722 ink had much smaller finger patterns compared to the silver nanoparticle ink (AgNP), caused by the higher viscosity of the PFI-722 ink. The layer thickness was measured to be 150–200 nm for layers printed using the AgNP ink. The peak height of the viscous fingering of the PFI-722 ink was ≤ 250 nm, with a layer thickness of less than 400 nm measured at the edge of the electrode pattern. The uneven layer thickness over the large areas is the reason for using the sheet-resistance as a macroscopic performance parameter for the flash experiments. The calculation of resistivity values based on local thickness measurements would deliver incorrect results due to varying cross-sections in different areas. We chose the macroscopic sheet resistance as a measure of performance partly for this reason and partly because it is the most commonly employed parameter when evaluating electrodes used in final applications such as OSCs and OLEDs.

Conductivity development

The PFI-722 ink is already highly conductive directly after drying at 15 m min^{-1} in the printing machine and in principle needs no further treatment. The ink is optimized for fast and low temperature drying with hot air and IR. The sheet resistance was measured to be 1.55 $\Omega \square^{-1}$. In contrast, the AgNP ink showed no conductivity after printing and drying at 10 m min^{-1} . After an additional 4 min drying period at 140 $^{\circ}\text{C}$ conductivity was achieved, with a sheet resistance of 271 $\Omega \square^{-1}$. Interestingly, the same ink achieved high conductivity after 1 min at 130 $^{\circ}\text{C}$ when

using slot-die coating.¹ One reason for this can be seen in the thinner and less dense layer when printed with flexography. The effect of intensive pulsed flashlight sintering was tested on both printed silver layers to study the effect on sheet resistance and layer morphology.

The printed electrode patterns were sintered with single flash exposure (0.5 ms), quadruple exposure (4×0.5 ms) at 1.8 Hz, and R2R at different speeds up to 2.5 m min^{-1} . The voltage setting (pulse energy) was generally varied between minimum (1.6 kV) and maximum (3.8 kV) in 200 V steps. The optimum distance (in focus) of the flash housing from the substrate is 1'' with an optical footprint of 19 mm \times 305 mm. Here, we used a distance of 2'' to increase the footprint for potentially faster R2R processing.

The effect of different voltage settings on the sheet resistance of printed PFI-722 ink is visualized in Fig. 3 (top). The lowest sheet resistance of 1.15 $\Omega \square^{-1}$ can be achieved with a single flash and a voltage setting of 3.8 kV, corresponding to an optical energy density of approx. 1.75 J cm^{-2} . The sheet resistance decreases with increasing energy input. The good conductivity without flashing is caused by the already sintered silver nanoparticles after drying. The slight improvement obviously comes from further densification and grain growth of the silver nanoparticles.

The relative improvement is low compared to the AgNP ink, which shows no conductivity right after printing and good conductivity after flash exposure. The impact of single and quadruple exposures is illustrated in Fig. 3 (bottom). For single exposure, the sheet resistance linearly decreases down to

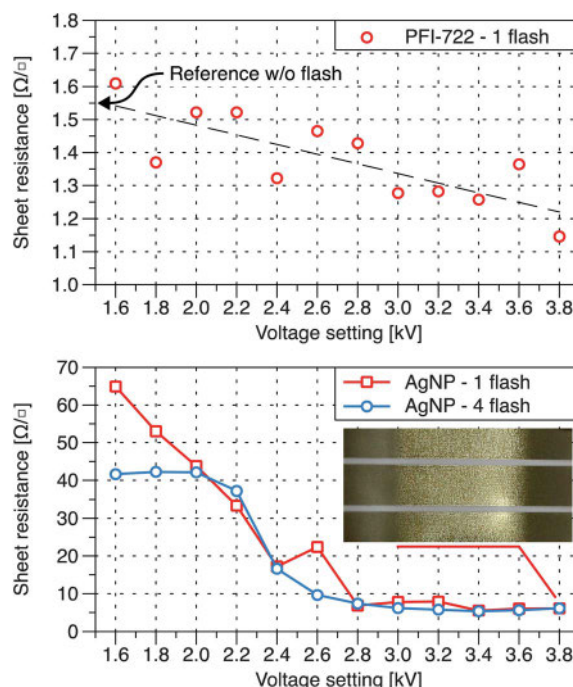


Fig. 3 (Top) Sheet resistance of the PFI-722 ink after single flash exposure. (Bottom) Sheet resistance of the AgNP ink after single and quadruple flash exposures. The sheet resistance change over 2.8 kV is negligible. The extraordinary value at 2.6 kV can be explained by contact problems due to the thin and sensitive silver layer. The inset shows the sintered area of the AgNP ink at 1 \times 3.8 kV.

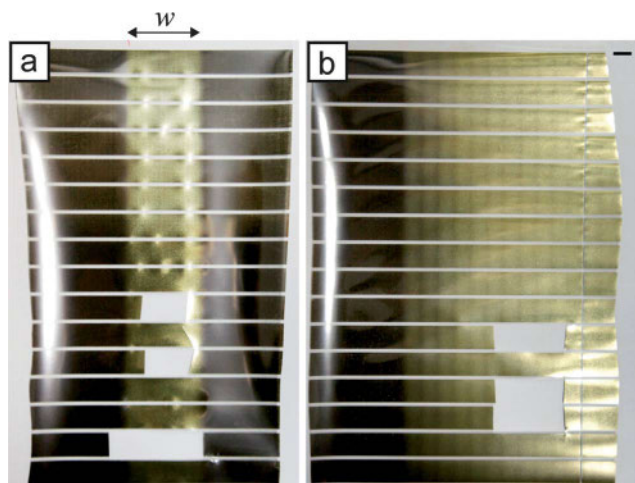


Fig. 4 (a) Barrier substrate with the flexo printed AgNP ink electrode pattern showing the exposure area of 4×3.2 kV flashes with the sintered width w . (b) R2R photonic sintered AgNP ink at 1 m min^{-1} , 2.8 kV and 140°C thermal treatment. The overlapped exposure areas are obvious. The substrates are shown from the backside with some cutouts for characterization purposes.

$6.83 \Omega \square^{-1}$ at a voltage setting of 2.8 kV (approx. 0.95 J cm^{-2}). No significant change occurs with further increasing energies whereas the minimum was found at $5.5 \Omega \square^{-1}$ at 3.4 kV. The impact of multiple flashes can only be measured in the low energy regime up to a voltage setting of 2.0 kV (approx. 0.48 J cm^{-2}). Further, the behavior is similar to single exposure with negligible differences in sheet resistance, compared to the initial value. In the case of R2R processing it means the substrate can run faster as no multiple flashes are required.

The effect of flash exposure on the AgNP ink was clearly visible from 2.8 kV onwards and the impact area was measured. A color change from black to golden occurred and the adhesion was significantly improved. Photographs of the color change are shown in Fig. 4. Before sintering the ink could be simply wiped off. Therefore, the high-energy input not only sintered the nanoparticles to result in higher conductivity, but also improved adhesion, which is a major advantage. The thin barrier foil substrate showed no deformation after single exposure at maximum energy. Small wrinkles appeared with 4 pulses at 1.8 Hz and voltage settings above 2.6 kV. The silver layer absorbed too much energy, which then dissipated into the substrate and heated it up causing permanent deformation.

The sintered width we achieved for a flash distance of $2''$ is larger than the optical footprint when being in focus at $1''$. The optical footprint is more than doubled with a sintered width of up to 42 mm after one flash (see Table 1). Multiple exposures on the same spot achieved up to 44 mm with blurred edges. Therefore, the R2R processing speed can be increased by a factor of two. The theoretical web speed v in m min^{-1} can be calculated with

$$v = \frac{f \times (w - w_0) \times 60}{1000} \quad (1)$$

where f is the flash frequency in Hz, w the sintered width in mm of a single flash, and w_0 the desired overlap in mm. An overlap of exposed areas is typically required, as the sintered area shows no

Table 1 Sintered width w of the AgNP ink for different voltage settings with single and quadruple exposures. Exposure widths below 2.8 kV were not optically visible. The achievable R2R web speed v is calculated based on the single flash exposure

kV	w [mm] 1 \times flash	v [m min^{-1}] no overlap	v [m min^{-1}] 5 mm overlap	w [mm] 4 \times flash
2.0	—	—	—	37
2.2	—	—	—	38
2.4	—	—	—	38
2.6	—	—	—	39
2.8	25	2.70	2.16	40
3.0	33	3.56	3.02	41
3.2	34	3.67	3.13	42
3.4	40	4.32	3.78	42
3.6	41	4.43	3.89	43
3.8	42	4.54	4.00	44

sharp edge caused by decreased optical energy density at the edge.

As the PFI-722 ink is already highly conductive without photonic treatment, R2R flash sintering was only conducted on flexo printed AgNP ink electrode patterns. Experiments were carried out at 1 m min^{-1} with different voltage settings and at 3 kV with increasing web speeds up to 2.5 m min^{-1} as shown in Fig. 5. The sheet resistance at 1 m min^{-1} is decreased compared to single flash, as the overlap at low speed leads to multiple exposures with increased evaporation of organic residues and further nanoparticle densification. The difference can be seen particularly for low voltage settings. As the silver nanoparticles are already sintered above 2.8 kV, multiple exposures have minor impact. Fig. 4b shows a R2R sintered sample from the substrate backside, exposed with 2.8 kV at 1 m min^{-1} and additional 140°C thermal treatment. It should be noted that the thermal treatment alone had no further impact on the sheet resistance.

R2R sintering with 3 kV at 2.5 m min^{-1} leads to higher sheet resistance. At 1 m min^{-1} the silver becomes continuously exposed with 6 pulses (23.7 mm overlap), and almost continuously with 2 pulses at 2 m min^{-1} (14.5 mm overlap). At 2.5 m min^{-1} the overlap is calculated with only 9.8 mm resulting in alternating single and double exposures. The R2R experiments clearly show the challenges in homogeneous sintering over a large area, with the interaction of web speed, exposure area and overlap. The exposure area itself depends on flash distance, optical energy density distribution and the material characteristics.

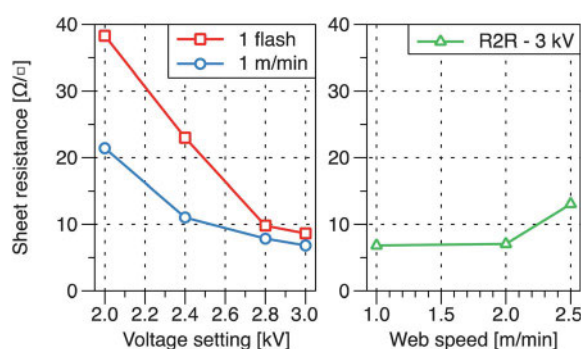


Fig. 5 (Left) sheet resistance for single exposure and R2R photonic sintering at 1 m min^{-1} with different voltage settings. (Right) sheet resistance at a fixed voltage setting of 3 kV with web speeds up to 2.5 m min^{-1} .

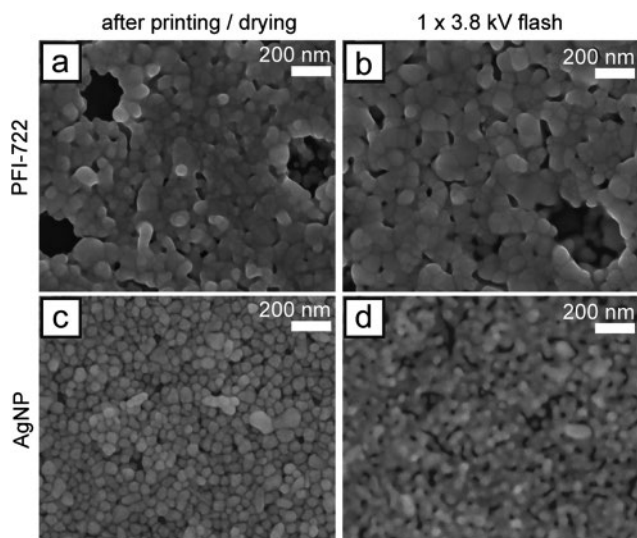


Fig. 6 FESEM images of PFI-722 ink before (a) and after photonic sintering at 3.8 kV (b). No major change in densification occurs, as the nanoparticles were already sintered. (c) AgNP ink before sintering shows nanoparticles with a size of 40–70 nm. (d) AgNP nanoparticles after single exposure are sintered and show a fused percolation network leading to increased conductivity.

The reason for the increase in conductivity of AgNP inks after photonic sintering is clearly visible in the scanning electron microscopy images, as shown in Fig. 6. The PFI-722 ink is already sintered after drying during the printing process. Photonic sintering has only a minor impact and leads only to minor densification. On the other hand, the AgNP ink is not conductive after drying with unsintered nanoparticles (40–70 nm) visible in Fig. 6c. Conductivity appears after a single flash, which evaporates organic compounds and fuses the nanoparticles together by forming a percolation network, as shown in Fig. 6d. Sintering of metallic nanoparticles at temperatures below the bulk melting temperature is possible because of a high surface-to-volume ratio and therefore a decreased melting temperature. After the solvent and organic residues that prevent direct contact of the nanoparticles are fully evaporated, the “softness” of the material leads to self-diffusion and an initial neck formation between the nanoparticles.¹¹ A bulk-like material is formed with increasing grain growth that results in the loss of nanoparticle material characteristics and an increased conductivity. With flashlight sintering the heat is generated through the enhanced photothermal effect.¹⁶ Once the particles are sintered they lose their nanoparticle behavior and only grain growth occurs. This explains the minor change in sheet resistance above voltage settings of 2.8 kV, as shown in Fig. 3.

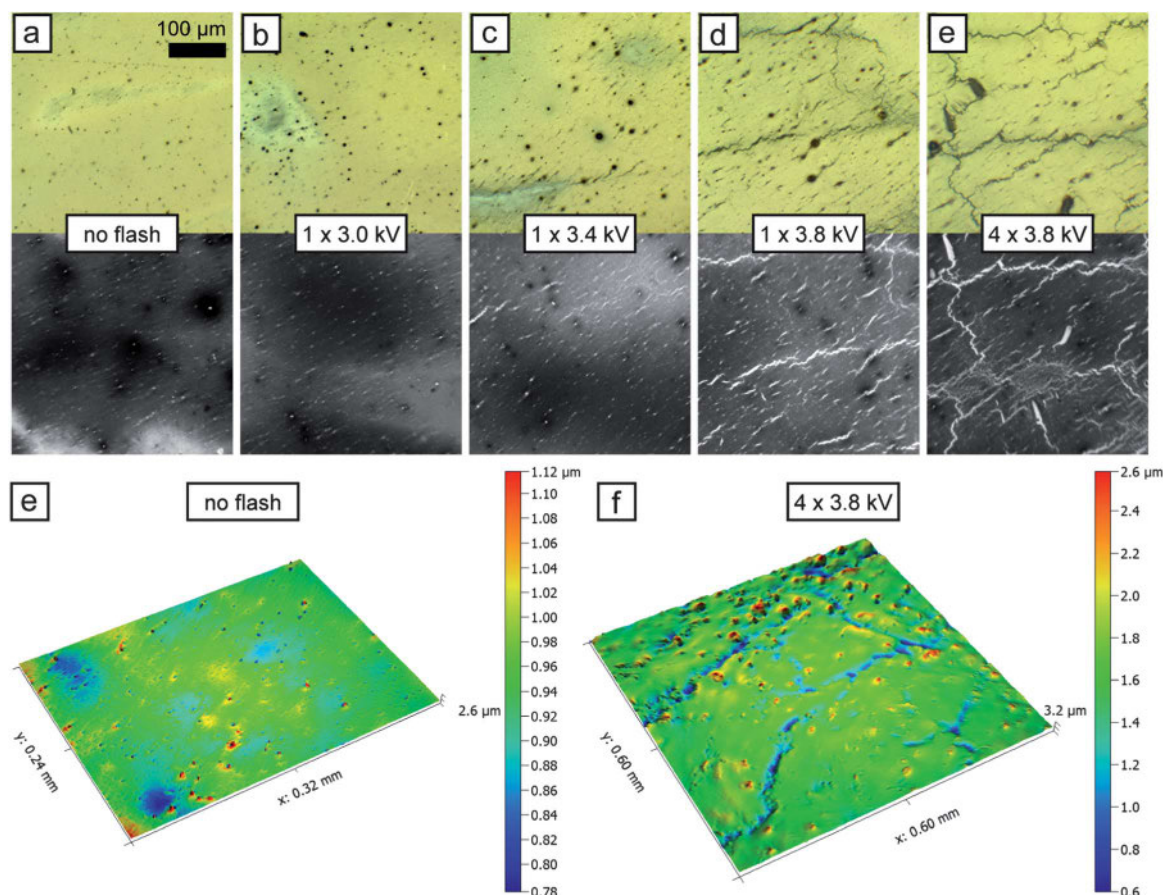


Fig. 7 Reflected light (top) and transmitted light (bottom) microscope images of AgNP layer surfaces with increasing energy input from (a) to (e). Crack formation starts at voltage settings of 3.4 kV (c). The corresponding white light interferometry images of the AgNP ink on the barrier foil before (e) and after quadruple exposure at 3.8 kV (f).

Surface morphology and crack formation

Surface damage and crack formation in the AgNP silver layer occurs at higher energy input. Finding the right level between conductivity and satisfying surface morphology is a challenging task and has to be considered for final process upscaling. Cracks appear with voltage settings above 3.4 kV for single exposure whereas multiple exposures at high voltage settings lead to significant surface damage (see Fig. 7). Silver layers printed using the PFI-722 ink showed no cracks. Fine line structures such as grids are very sensitive to cracks as they can completely interrupt the conductive lines. In our case, surface damage and cracks with hundreds of microns length have no influence on the sheet resistance because the percolation network is still intact over a large area. The reason for crack formation can be explained by volume shrinkage due to densification of the nanoparticles.²⁹ The impact of intense flashlight on varying layer thicknesses due to the fingering effect is visible in Fig. 7b and c in the form of the appearance of a different color. Thinner areas appear lighter and grey instead of yellowish golden for the homogeneous areas. The thin areas are almost crack-free but surrounded by small cracks, whereas the majority of cracks are observed in thicker areas due to inhomogeneous stress distribution³⁰ and the difference of the coefficient of thermal expansion (CTE)³¹ of silver and the barrier foil substrate, which is $19 \mu\text{m m}^{-1} \text{K}^{-1}$ and $\sim 59 \mu\text{m m}^{-1} \text{K}^{-1}$, respectively. Homogenous layers over large area and reduced energy input, in our case voltage settings below 3.4 kV, can result in crack-free and fully sintered silver electrodes.

Conclusion

Our main finding is that properly engineered low-temperature inks do not require additional processing steps such as flash sintering for significantly improving conductivity whereas nanoparticle metal based inks with higher sintering temperatures can benefit from processing steps such as flash sintering with respect to both conductivity and adhesion. For these nanoparticle-based inks we conclude that flash sintering is a mandatory requirement for achieving high conductivity. We showed that a single flash is already enough to achieve high conductivity without damaging the layer and thin barrier foil substrate. Photonic sintering is an ultra-fast technology and has potential for direct inline processing with fast printing technologies, when multiple flash systems are synchronized or the flash frequency of a single system gets increased. The necessity of multiple flashes has to be considered, which directly impacts the processing speed. The deposition of silver electrode structures directly on a thin barrier foil and post-treatment with photonic sintering processes can enable applications with reduced use of material and therefore minimized embodied energy. Possible applications can be seen in electrodes for organic solar cells, OLEDs or RFID antennas produced directly on the encapsulation and packaging foil.

Acknowledgements

This work was supported by the Danish Strategic Research Council (2104-07-0022), EUDP (j.no. 64009-0050 and 64011-0002), the EU-Indian framework of the “Largecells” project as

part of the European Commission’s Seventh Framework Programme (FP7/2007-2013, grant no. 261936). Thanks go to the Chemistry and Physics of Materials Unit group of Prof. G. U. Kulkarni from Jawaharlal Nehru Centre for Advanced Scientific Research (Bangalore, India) for using the surface characterization equipment.

References

- 1 F. C. Krebs, *Org. Electron.*, 2009, **10**, 761–768.
- 2 J. Zou, H.-L. Yip, S. K. Hau and A. K.-Y. Jen, *Appl. Phys. Lett.*, 2010, **96**, 203301.
- 3 Y. Galagan, J.-E. J. M. Rubingh, R. Andriessen, C.-C. Fan, P. W. M. Blom, S. C. Veenstra and J. M. Kroon, *Sol. Energy Mater. Cells*, 2011, **95**, 1339–1343.
- 4 S. Harkema, S. Mennema, M. Barink, H. Rooms, J. S. Wilson, T. van Mol and D. Bollen, *Proc. SPIE*, 2009, **7415**, 74150T.
- 5 J. Woerle and H. Rost, *MRS Bull.*, 2011, **36**, 789–793.
- 6 M. Jung, J. Kim, J. Noh, N. Lim, C. Lim, G. Lee, J. Kim, H. Kang, K. Jung and A. Leonard, *IEEE Trans. Electron. Devices*, 2010, **57**, 571–580.
- 7 J. Noh, D. Yeom, C. Lim, H. Cha, J. Han, J. Kim, Y. Park, V. Subramanian and G. Cho, *IEEE Trans. Electron. Packag. Manuf.*, 2010, **33**, 1–9.
- 8 M. Allen, C. Lee, B. Ahn, T. Kololuoma, K. Shin and S. Ko, *Microelectron. Eng.*, 2011, **88**, 3293–3299.
- 9 D. Deganello, J. Cherry, D. Gethin and T. C. Claypole, *Thin Solid Films*, 2010, **518**, 6113–6116.
- 10 J. Perelaer, P. J. Smith, D. Mager, D. Soltman, S. K. Volkman, V. Subramanian, J. G. Korvink and U. S. Schubert, *J. Mater. Chem.*, 2010, **20**, 8446–8453.
- 11 A. Kamyshny, J. Steinke and S. Magdassi, *Open Appl. Phys. J.*, 2011, **4**, 19–36.
- 12 J. Greer and R. Street, *Acta Mater.*, 2007, **55**, 6345–6349.
- 13 M. Allen, A. Alastalo, M. Suhonen, T. Mattila, J. Leppaniemi and H. Seppa, *IEEE Trans. Microwave Theory Tech.*, 2011, **59**, 1419–1429.
- 14 J. Perelaer, M. Klokkenburg, C. E. Hendriks and U. S. Schubert, *Adv. Mater.*, 2009, **21**, 4830–4834.
- 15 I. Reinhold, C. Hendriks, R. Eckardt, J. Kranenburg, J. Perelaer, R. Baumann and U. Schubert, *J. Mater. Chem.*, 2009, **19**, 3384–3388.
- 16 K. C. Yung, X. Gu, C. P. Lee and H. S. Choy, *J. Mater. Process. Technol.*, 2010, **210**, 2268–2272.
- 17 S. Farnsworth, *Coating Int.*, 2011, **44**, 16–18 (http://www.coating.ch/en_coa_Inhalt_7_11.ebs).
- 18 N. Marjanovic, J. Hammerschmidt, J. Perelaer, S. Farnsworth, I. Rawson, M. Kus, E. Yenel, S. Tilki, U. S. Schubert and R. R. Baumann, *J. Mater. Chem.*, 2011, **21**, 13634.
- 19 J. Kang, J. Ryu, H. Kim and H. Hahn, *J. Electron. Mater.*, 2011, **40**, 2268–2277.
- 20 K. Schroder, S. McCool and W. Furlan, *Presented at NSTI Nanotech May, 2006*.
- 21 R. Abbel, J. van den Boomen, T. van Lammeren, T. de Koning, J. J. P. Valetton and E. R. Meinders, *Mater. Res. Soc. Symp. Proc.*, 2011, **1323**, 87–92.
- 22 J. Perelaer, R. Abbel, S. Wünscher, R. Jani, T. van Lammeren and U. S. Schubert, *Adv. Mater.*, 2012, **24**, 2620–2625.
- 23 J. Wang, H. L. Duan, Z. P. Huang and B. L. Karihaloo, *Proc. R. Soc. London, Ser. A*, 2006, **462**, 1355–1363.
- 24 F. C. Krebs, T. Tromholt and M. Jørgensen, *Nanoscale*, 2010, **2**, 873–886.
- 25 N. Espinosa, M. Hösel, D. Angmo and F. C. Krebs, *Energy Environ. Sci.*, 2012, **5**, 5117–5132.
- 26 F. C. Krebs, J. Fyenbo and M. Jørgensen, *J. Mater. Chem.*, 2010, **20**, 8994–9001.
- 27 P. G. Saffman and G. Taylor, *Proc. R. Soc. London, Ser. A*, 1958, **245**, 312–329.
- 28 M. B. Amar and D. Bonn, *Phys. D*, 2005, **209**, 1–16.
- 29 J. West, M. Carter, S. Smith, J. Sears, and S. Rapid City, *Proc. of NSTI-Nanotech 2010*, 2010, pp. 210–213.
- 30 J. R. Greer and R. A. Street, *J. Appl. Phys.*, 2007, **101**, 103529.
- 31 D. J. Lee, J. H. Oh and H. S. Bae, *Mater. Lett.*, 2010, **64**, 1069–1072.

Failure Modes and Fast Repair Procedures in High Voltage Organic Solar Cell Installations

Markus Hösel, Roar R. Søndergaard, Mikkel Jørgensen, and Frederik C. Krebs*

Steadily increasing efficiencies of organic solar cells are frequently published but the practical demonstration of actual large-scale installations with high power output has been very limited. Here, the real-world challenges and opportunities of organic solar cells fabricated on thin plastic foil and mounted in solar cell arrays of more than 1 kW are shown. In this configuration defects in form of burns that have never been reported before are observed. The reason can be seen in the combination of high power production, water ingress, and the use of thin plastic foil as the substrate. Environmental impact such as lightning was also observed to cause randomly distributed burn holes that initiate self-sustained damaging under illumination. The large solar cell modules each with more than 220 W_{peak} are based only on serially connected cells and need no time-consuming manual wiring of single cells. Although burns that locally destroy the modules are observed the efficiency is not much affected. Simple repair procedures developed throughout the lifetime study enable the cut and replace of small pieces of the module. A complete replacement as it is carried out for malfunctioning conventional Si-based PV modules is not necessary. This enables cost-effective maintenance over the lifetime of the organic solar cells.

1. Introduction

Organic photovoltaics (OPV) and polymer solar cells have seen a steady rise in research effort around the world, with a resulting increase in power conversion efficiency breaking the 10% barrier.^[1–3] The record devices are preferably made on indium tin oxide (ITO) glass substrates under optimum laboratory conditions with a least one (often many) high vacuum evaporated layer(s). An extensive analysis of almost 9000 scientific publications revealed that the active area is typically well below 0.5 cm² and most often 0.04 cm².^[4] Such cells are ideal for studying material properties and the physics of the devices but they are of very little use in actual applications. Large-scale devices with active areas of at least tens of square centimeters, considering the low efficiency, are the key for a successful implementation of solar energy harvesting in low power electronic gadgets, building integrated photovoltaics (BIPV), or grid

connected solar parks. Monolithic and serial connected organic solar cells with active areas above 25 cm² have been successfully produced but are the minority in the field.^[5–12] Recently, we fabricated what is likely the world's largest serially connected organic solar cell module with an active area of more than 10 square meters each (max. 14.7 m² for a 100 m long module) for high-voltage power extraction of more than 220 W per module.^[13,14] The up-scaling factor from a typical <1 cm² lab-scale solar cell to this dimension is comparable to the area of Monaco vs. Italy. The operation of organic solar cells with such sizes and power outputs is a completely new field that has to be handled with special care considering the power levels we present here. Considering the current low efficiency of organic photovoltaics, any reasonable power extraction has to be realized by covering large areas, either on specifically designed solar parks or within building integrated photovoltaics

(BIPV) (e.g., laminated into glass).

Economical calculations for commercial-scale produced organic solar cell modules based on ITO-free substrates and evaporated back electrodes have been carried out and predict a feasible use of OPV devices as power sources.^[15] Ultimately, however, the organic solar cells should be fabricated using energy efficient roll-to-roll (R2R) full solution processes without the use of any vacuum steps to enable minimized energy pay-back times and low embodied energies.^[14,16–18]

Although several long term lifetime studies on a variety of different organic solar cell types have been carried out, demonstrating operational lifetimes of thousands of hours,^[19–22] there is a lack of experience with outdoor large-scale power producing installations based on organic photovoltaics and, as a consequence, large area processing is currently limited to very few groups in the OPV community. One report on large-scale OPVs aimed for BIPV realized passing of the strict IEC-61646 environmental chamber tests, but the achieved result only accounts for a single test sample without real world serial or parallel connection for high power extraction for potential grid-connection.^[22] The international standard IEC-61646 contains a list of requirements that need to be fulfilled by thin-film terrestrial photovoltaic modules. One test is the damp heat test (85 °C and 85% relative humidity for 1000 h) whereby the efficiency of the modules must not fall below 95% of the initial value. In

M. Hösel, Dr. R. R. Søndergaard, Dr. M. Jørgensen,
Prof. F. C. Krebs
Department of Energy Conversion and Storage
Technical University of Denmark
Frederiksborgvej 399, DK-4000, Roskilde, Denmark
E-mail: frkr@dtu.dk



DOI: 10.1002/aenm.201301625

the before mentioned 100 m long high-voltage solar cell modules outdoor lifetimes of at least 5000 h (data until now) has been successfully shown with power extraction of more than 220 W_{peak} per module.^[14]

As for silicon-based PV, the recording of solar cell parameters over the lifetime is only one side of reporting results. Especially for grid-connected large-scale installations multiple damage scenarios have been observed, which is something that has obviously never been witnessed in the field of OPVs because of the generally low voltage and current measurements performed in the laboratory. Such lab operation modes will not lead to the fatal defects we present here but anyone aiming to install OPV for energy production should be aware of such potentially catastrophic failure modes. Typical defects in silicon based systems are shading, weak soldering, cracking, delamination, hot-spots, overheating, backsheet burn-throughs, and metal grid oxidation.^[23–25] Some of these defects cannot be observed directly and technologies such as infrared thermal imaging must be used to identify defects in large solar PV plants for further inspection.^[26] Such defects often lead to a costly change of the whole module, which can add up to mass replacements of more than 1000 modules, as reported for a 1.8 MW_{peak} silicon-based PV plant.^[25]

Here, we present similar defect scenarios, namely delamination, punctures, hot-spots, water ingress, and burns that are particularly critical for thin plastic foil based solar cells, that appear in high-power-producing OPV installations fabricated on flexible plastic substrates fully exposed to the environment and without any BIPV-like glass encapsulations.^[14] In addition to this, we also show easy and fast repair procedures that do not require the replacement of the entire module.

2. Results and Discussion

2.1. High-Voltage Organic Solar Cell Installation

Current large-scale produced organic solar cells have to be connected in modules to enable any useful power generation that can ultimately be fed into the electric grid. So far, large organic solar cell modules often have a discrete size (e.g., a sheet size of A4 to A3, which corresponds to 0.62–0.125 m^2), limited by the manufacturing equipment. The electrical connection of these cells into modules in the final application is inevitable, as is well known from Si wafer-based solar modules. The manual wiring of printed sub-cells or sub-modules to reasonably large solar cell arrays is ineffective, time consuming, and costly. Each single terminal connection of the encapsulated sub-module is a weak point in the system and a potential area of oxygen and water ingress. The number of connectors in a power-generating module should ultimately be minimized to only two, i.e., the plus and minus terminals.

We solved this by developing a fully printable and “infinitely” long module with thousands of serially connected cells. Each module delivers more than 220 W_{peak} and has open circuit voltages of >10 kV. The “infinity” concept including the solar park setup and installation procedures has been reported in detail elsewhere.^[13,14] In brief, the flexible solar cell module has been fully R2R printed and coated on ordinary ITO-free plastic

substrates with a silver-grid/poly(3,4-ethylenedioxythiophene) poly(styrenesulfonate) (PEDOT:PSS)/ZnO layer structure as the semitransparent front electrode.^[17] The light absorbing layer P3HT:PCBM was slot-die coated. Rotary screen printing was used for the PEDOT:PSS back electrode and silver grid back electrode to serially connect every single cell along hundreds of meters of substrate. Encapsulation was carried out using UV-curable adhesive and PET multilayer-based barrier foil ($\approx 72 \mu\text{m}$ thick). The final module size was cut from the master rolls (1.3–2.2 km) to 100 m long modules with a width of 305 mm limited in length only by the mounting platform (100 m long). In the practical experiments up to 700 m of solar cell could be prepared without a single error. The active area of the 100 m module with $\approx 21\,000$ serially connected cells is 14.7 m^2 (total area $\approx 30 m^2$). Characteristic solar cell parameters of such a module after 1320 h (55 days) of outdoor operation and an irradiance of 943 $W m^{-2}$ are short circuit current $I_{\text{SC}} = -38 \text{ mA}$, open circuit voltage $V_{\text{OC}} = 9235 \text{ V}$, maximum power point current $I_{\text{MPP}} = -29.5 \text{ mA}$, maximum power point voltage $V_{\text{MPP}} = 7525 \text{ V}$, fill factor $\text{FF} = 63.2\%$, and power conversion efficiency $\text{PCE}_{\text{active}} = 1.61\%$.

The mounting of a 100 m long module took roughly 1 min (52 s) plus the additional electrical connection on each side of the module as shown in Figure 1.^[33] Pre-manufactured

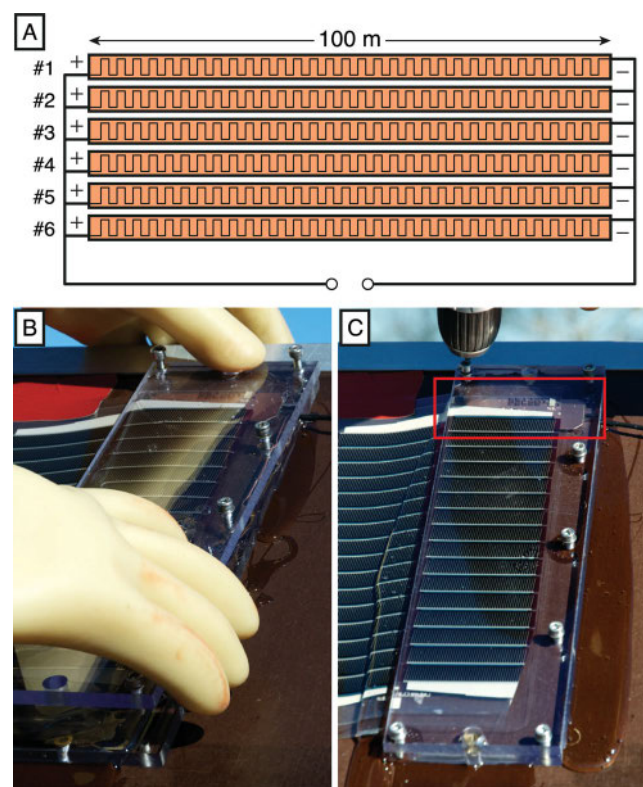


Figure 1. A) Schematics of the solar array layout consisting of 6 parallel-connected modules. Each module contains 21 000 serially connected cells. B) Photographs of the connection board at the end of one solar cell module: handling of high voltage equipment requires special protective gloves and C) electrical connection through the laminated module is carried out with multiple spikes that are punched through the laminate while mounting the top plate. The solar cells under the top plate are inactive.

poly(methyl methacrylate) (PMMA) plates were used as rigid connector base and were mounted on site. The cables were soldered to a printed circuit board (PCB) copper plate with soldered spikes that punch through the barrier foil and connect to the printed silver electrode. The small spikes prevent large damage in the barrier foil as manual delamination for an electrical connection is not required. Polyurethane was filled between the top and bottom PMMA plates to fully seal the open end of the module and prevented any water ingress. The layout of the module and the point of electrical connection allows that the solar cells under the top plate are not part of the serial network. The path length from the cut in the substrate to the first active cells is increased to roughly 8 cm. A long distance of the active cells to any edge of the module contributes to an improved lifetime.^[27]

So far, twelve modules (1200 m of printed solar cells) were installed in two arrays as described above. The schematic illustration in Figure 1A shows the principle connection plan of a 6-module array. The high voltage/low current design enables the use of thin printed conductors and thin external wires, which are later connected to a down converter and an inverter for grid connection. Complicated lamination of busbars for high current parallel connection are not required, which is a massive advantage. Our modules with $>220 W_{\text{peak}}$ require no further internal wiring or soldering as it would be required with all other smaller discretely processed OPV modules shown so far. The modules were installed and connected on a wooden structure and tested under Danish outdoor environmental conditions, which include thunderstorms, heavy rain, and solar irradiances of more than $1000 W m^{-2}$ during summertime. To the best of our knowledge, this is the first real-world large-scale installation of OPVs for power generation in the kilowatt range. The defect scenarios we demonstrate here are directly related to the high power production and could not be foreseen in any labs. The installed amount of OPV modules itself ($\approx 360 m^2$ surface area) is a huge area for all possible environmental impacts.

2.2. Mechanical Failures

Based on the area, the chance of having mechanical failures such as punctures in the barrier or scratches due to the installation is rather high. Even the influence of animal behavior should be considered at these dimensions. We noticed a large amount of small and big bird drops that act as cell shadows but may also influence the properties of the barrier substrate. Although never observed, the chance of birds with sharp beaks or claws damaging the foil is certainly present. Some delamination along the substrate edges ($\approx 2400 m$ total edge length) was also observed after a few thousand hours.

Punctures, edge delamination, and scratches can lead to water and oxygen ingress and can finally end up in further delamination in the certain area over time. The layer interfaces will be destroyed, the active layer will bleach, the PEDOT:PSS can dissolve, and the silver electrodes oxidize as shown in Figure 2. The affected area will have limited or no solar cell characteristics. These defects grow over time and can lead to further damage, as shown later. Various repair procedures are also described.



Figure 2. A) Photograph of large-scale defects induced by delamination from the bottom side. Water ingress leads to a propagating area of inactive solar cells. B) A long scratch caused during the installation affects three solar cells. Water and oxygen ingress changes the visual appearance of the cells.

2.3. Electrical Failures, Hot-Spots, and Burns

The R2R fabrication of the solar cells on substrate lengths beyond hundreds of meters produces 21 000 cells per 100 m based on our current design approach. In a serially connected cell array each cell needs to work, or at least has to have simple resistor characteristics. An open circuit must be avoided. Our experience shows that we can print close to 100% yield based on visual inspection during the fabrication, except during run-in for each layer. Before encapsulation each single cell is electrically tested in a custom built R2R setup and data are logged.^[17,28] Based on the logged dark $I-V$ curves and the shunt resistance we can decide between working and non-working cells (low resistance). The cells are not tested under illumination, neither before nor after encapsulation. Production runs in this dimension are based on pre-defined process parameters and well-studied layer stacks that allow a 100% yield of functional cells after the fabrication process. The solar cell modules are then installed outdoors and connected as described earlier.

For quality control and identification of any electrical failures that lead to abnormal temperatures (hot-spots) we used infrared (IR) imaging techniques (Fluke Ti125) for scanning hundreds of square meters in short time as shown in Figure 3. This is a reliable test method for conventional PV plants.^[25,26] Compared to other non-contact methods such as light-beam-induced current (LBIC),^[29] lock-in thermography,^[30,31] and luminescence imaging^[32] for defect analysis of cells at sub-millimeter scale in a lab environment the IR imaging is ideal for large-scale observation under operation conditions.

Fully functional cells and modules will have a homogeneous temperature distribution as shown in in Figure 3A. Any abnormalities such as hot-spots are normally not detectable with the naked eye, whereas IR imaging allows a fast localization for further investigation as shown in Figure 3B–D. We observed multiple hot-spots inside the cells and also outside along the printed conductive silver electrodes. Detailed studies of these

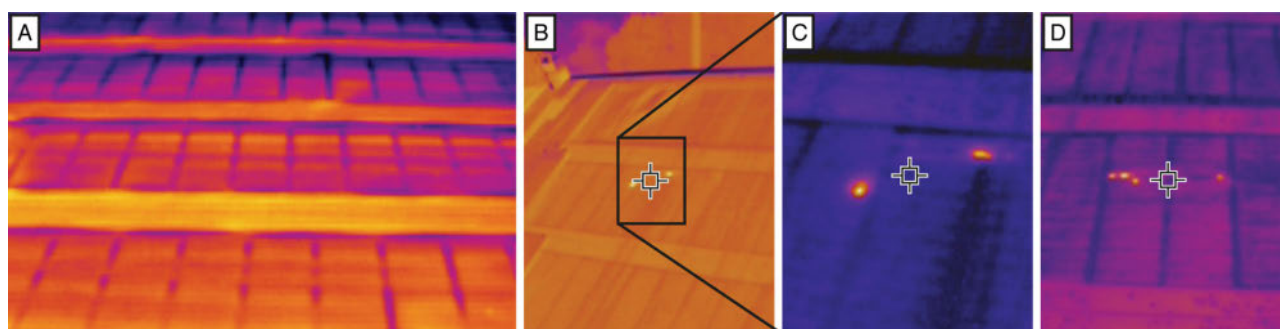


Figure 3. IR imaging photographs of OPV modules showing cells without failures (A), a hot-spot inside a cell and on the printed silver electrode outside the cells (B,C), and four hot-spots inside the cells (D).

spots revealed tiny burns with bleached active layer around the center as shown in **Figure 4A–C**. Based on the optical inspection we found the origin of the burn in the direct overlap of a front and back electrode grid finger. In the particular case that the individual cell is shunted and the current accumulated at the point of low resistance locally heats up the cell. Spikes in the printed silver grid or pinholes in the intermediate layers that decrease the distance between the electrodes might be a reasonable failure source while it is impossible to establish

this post mortem. The temperature of the hot-spot is above the melting point of the barrier foil, which is then destroyed locally. Similar overheating and puncturing of TEDLAR back-laminates has also been observed in Si-based modules.^[25]

Another localized burn is shown in **Figure 4D** that appeared outside of the cells on the printed silver electrode. Further investigation revealed a local delamination and water ingress from the edge of the foil. High voltage can form an electrical arc or sparks between the electrode and underlying structure leading to ignition of the foil locally.

Some of the modules we installed still had a conductive guideline present on the outer edges of the substrate. The lines are printed together with the front silver electrode and act as cross directional registration guides for the slot-die coating processes.^[17] These lines were not connected to the high-voltage network but were the source of propagating burns along the printed guideline as shown in **Figure 4E**. The solar cells were not necessarily affected by the burning. The reason for the burning guideline was established as being due to localized delamination and water ingress thus forming an electrical connection with standing sparks between the mounting structure and the conductive line. We could observe continuous sparks up to a centimeter from the conductive silver electrode to ground on the open end of a freshly cut module. Careful handling with high-voltage protective gloves was necessary in all handling involving open-ended foil. The challenge of burns induced by the printed guideline was avoided later on by removing the guidelines before encapsulation.

Another highly destructive source was thunderstorms and light bolts. Anyone who installs large area electrical constructions (e.g., PV plants) should be aware of it and consider countermeasures such as distributed lightning conductors. We observed multiple large burns such as those shown in **Figure 4F,G** directly after thunderstorms combined with heavy rain. While we did not physically record an event of lightning striking the solar cell array we believe that a lightning must have struck the construction and introduced a high electrical potential into the modules that consequently led to the observed ignition and burns distributed randomly over a large part of the array.

The drawback of plastic foil in combination with solar cells is that solar cells are “ON” whenever light shines upon them. It is not possible to easily switch them off, which can lead to

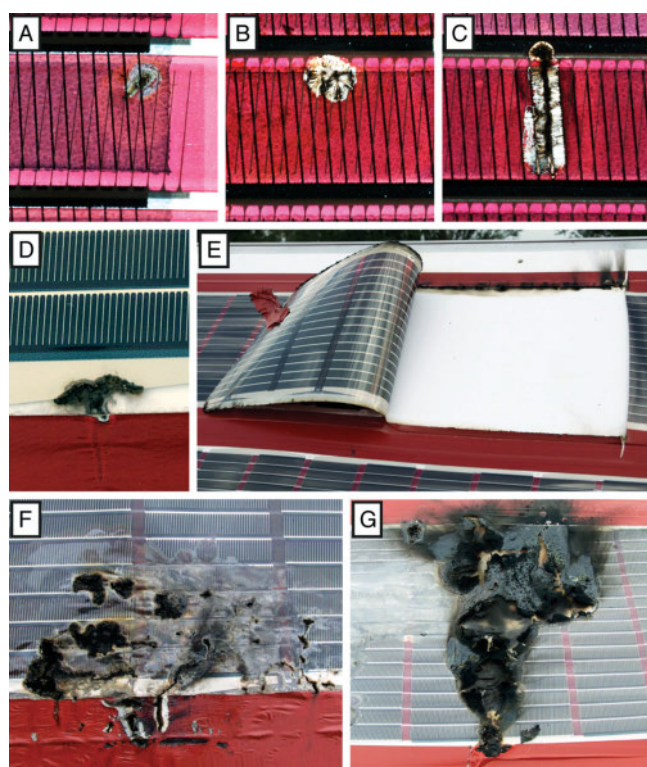


Figure 4. Different burns observed for the modules under operational conditions. A–C) In-cell burns caused by shunts between front and back electrode. D) Burning at the outer silver electrode caused by delamination and water ingress that lead to sparks. E) A flipped module with a burned guideline on the topside. F,G) Large burns after thunderstorms and from propagating small burns.

growth of defects. Once a shunt starts melting and igniting the foil it will propagate until it is extinguished, e.g., by wind or rain. As long the defective area is electrically connected sparks can appear and further destroy the solar cells so even if any fire is extinguished, the defect will still propagate. The burn holes can grow drastically and cause a full disconnection of a module. We believe this applies to all large-scale plastic-based solar cell installations and is not limited to our design. A cost-intensive full glass encapsulation (such as proclaimed for BIPV) might reduce these problems but this limits the upscaling and introduces several further processes (e.g., sealing and wiring) after the R2R manufacturing. Consequently the energy payback time and embodied energy in a large-scale glass enclosed plastic solar cell will increase as well. In the work presented here we simply roll out the foil and connect.

2.4. Repair Procedures

We previously showed that we can install the flexible OPV modules very fast and produce more than 1.3 kW with six parallel connected modules.^[14] As we describe here, we also observed multiple problems in form of burns that can limit the performance once they start. Such findings were never published before or at least nobody has been willing to present such data. Nevertheless, we are presenting the worst-case scenarios that can appear in plastic-based high-power-producing OPV installations and, more positively, how they can be fixed. The infinity design and the large-scale deployment of the flexible solar cells without further BIPV-like glass integration enable multiple rapid repair procedures. The costly replacement of the entire module in case of defects as carried out for conventional PV systems is not required.

The main repair techniques are based on the same connector plates as introduced for the principle electrical connection of a module on each side. Small scratches and detected pinholes that do not need to be cut out in the first instance can be covered with additional barrier foil, pressure-sensitive adhesive, and polyurethane as shown in **Figure 5A**. We successfully closed scratches caused during the deployment and saw no further evolution of the defects.

In case of burns that cause further damages the defective part needs to be removed. Small sections can be bypassed with a wire that is mounted in the same way as the terminal connectors (**Figure 5B**). The pre-manufactured PMMA plates combined with polyurethane allow a rigid and fully sealed connection. Large sections with defects should be cut, removed and replaced to avoid a large power drop on the module and a mismatch with other parallel-connected modules in the system. After cutting the module, preferably with a non-conductive ceramic knife or scissors, a fresh part of the same length will be inserted (**Figure 5C**). The PMMA plate with copper inserts and spikes punch through each end of the foil and reconnects the printed silver electrodes. If the cut is made in the middle of the individual solar cells then only one sub-module (16 cells) in the serial network is lost per reconnection. For two connectors required for cut and replace, the area loss on the whole module with 21 000 cells is $\approx 0.15\%$ and therefore negligible. The length of the replaced part is close to unimportant.

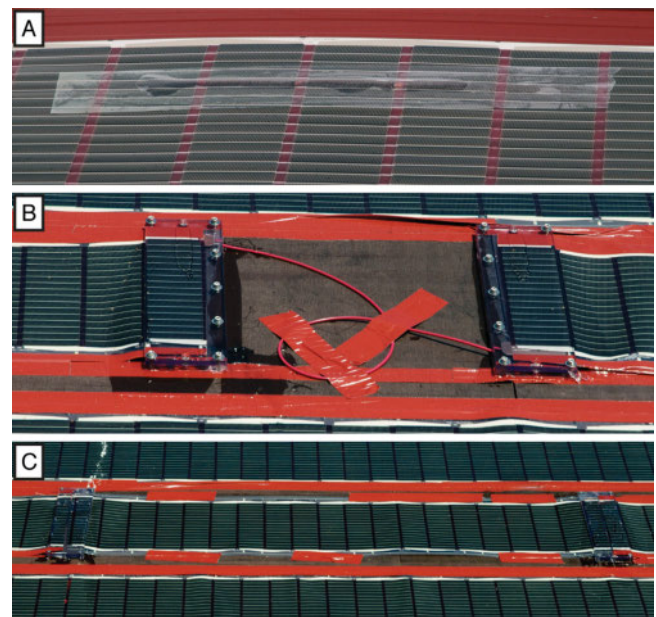


Figure 5. Photographs of different repair procedures with A) simple covering of scratches with additional barrier foil and polyurethane, B) cut out of defect areas and rewiring, and C) cut out of defect area and replacement with new cells.

2.5. Impact on Solar Cell Performance

We observed different defects during the test period with small or large burns, but that did not directly lead to a full loss of functionality. Experimental indoor tests on 80-cell modules have been carried out and showed that partially burned cells have only a minor impact on the module performance. The cells were burned on purpose with a flame. Photographs and the corresponding I - V curves are shown in **Figure 6**. Small burn holes lower the fill factor and introduce a tiny kink close to the maximum power point. There is only a minor impact on the V_{OC} and I_{SC} . The loss in I_{SC} is much smaller than one would expect from the area loss of one cell. All other working cells still contribute to the high current and average it out, although it is a serial connection. A second burn hole lowers the fill factor slightly more but the module still shows moderate performance. In the case where a single cell is fully burned then the I_{SC} is still fairly high with a loss of only around 10%. The I - V curve tends to show a strong inflection point with a sharp kink around V_{OC} , as shown in **Figure 6**. The behavior is similar to the full shadowing of the same cell prior to burning. The solar cell parameters of the tested modules can be found in **Table 1**.

None of the forced burning scenarios that we carried out for the indoor IV tests led to loss of the serial connection and the module was still operational, albeit at a decreased performance level. The problem with burning plastic is its propagating behavior. In the high-voltage outdoor experiment we observed sparks at the edges of extinguished burn holes due to a still existing electrical connection. As a result, the holes tend to grow and melt further. Cutting out the destroyed part followed

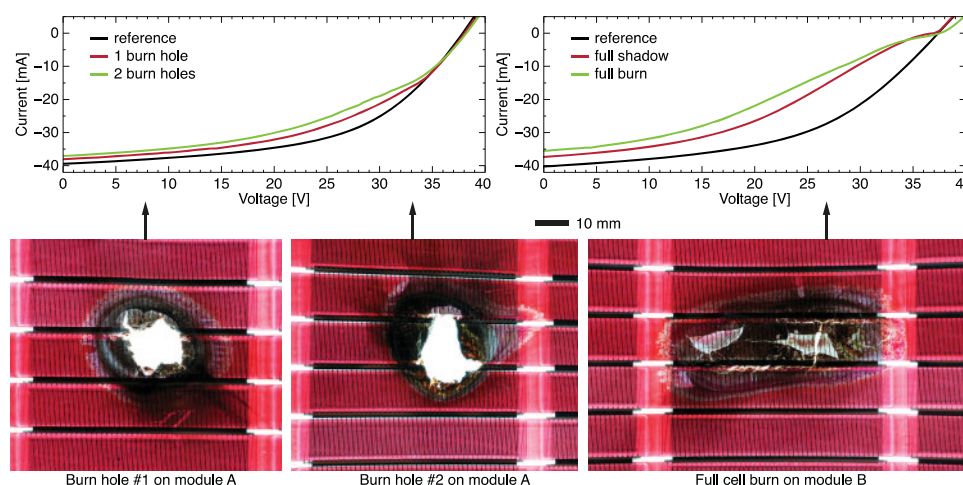


Figure 6. I - V curves of a module with 80 serially connected cells under AM1.5G illumination (1000 W m^{-2}). Top: The I - V curves show the behavior with one or two partially burn holes in a single cell of the module. Center: The I - V curves show the behavior with a fully shadowed cell and the same cell fully burned afterwards. The effect is similar. The corresponding photographs of the burned cells are shown in the bottom row.

by reconnection of the module with our repair procedures was found to fully prevent further damages in that area.

The 100 m long modules exhibited good operational stability after an initial burn-in (stabilization of solar cell parameters) in the first days. The power output on a clear day with an irradiance of $\approx 1000 \text{ W m}^{-2}$ never dropped below $205 \text{ W}_{\text{peak}}$ during the first 3000 h.^[14] The first module we installed withstood multiple thunderstorms and heavy rainfall without any impact. After around 4000 h of outdoor study some burns appeared and the module was fixed following our repair procedures. All in all around 3 m of substrate ($\approx 0.5 \text{ m}^2$ active area) had to be cut out and rewired at multiple points. The affected parts were not replaced with fresh cells. The module still produced more than $150 \text{ W}_{\text{peak}}$ at <1 sun ($\approx 920 \text{ W m}^{-2}$) after half-year of outdoor operation (4368 h). The corresponding I - V and power curves are shown in **Figure 7**. An expensive replacement of the whole module was not necessary.

3. Conclusion

In this study we clearly show the challenges and the opportunities of large-scale high-power-producing organic solar cell

installations based on thin plastic foil. The observed failure modes in form of burns and propagating catastrophic defects caused by internal and external impacts had only small effects on the I - V behavior of modules if the failure size was smaller than a single cell. Larger burns may destroy the module locally and could lead to an open circuit. For these cases we developed multiple repair procedures that enable a fast and reliable fix of the affected module without replacing it completely. A module with several repairs still showed good performance after a half-year outdoors. An expensive replacement of the whole module was not necessary, as would have been the case for conventional PV modules.

Table 1. Solar cell parameters of 80-cell modules with burned cells.

	V_{oc} [V]	I_{sc} [mA]	FF [%]	Efficiency [%]
Module A	37.8	-39.4	53.6	1.33
Module A + burn hole #1	38.0	-38.1	48.2	1.16
Module A + burn hole #1 and #2	38.2	-37.1	45.0	1.06
Module B	37.4	-40.2	49.3	1.24
Module B + shadowed cell	37.0	-37.3	38.4	0.88
Module B + burned cell	37.5	-35.5	33.3	0.74

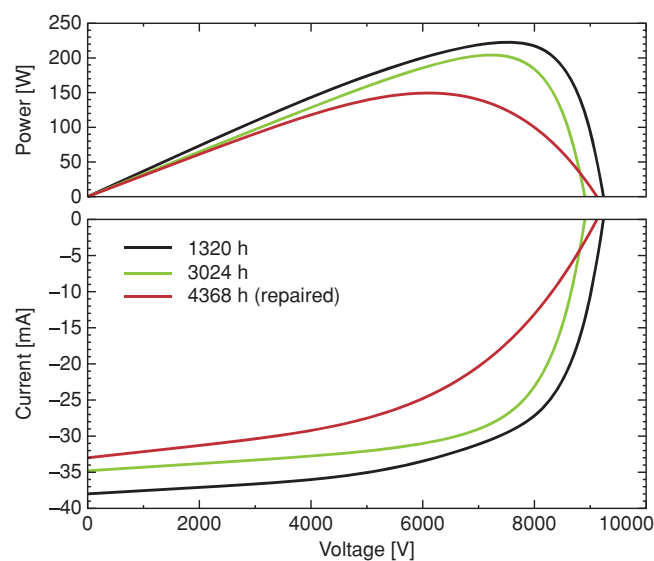


Figure 7. Power and I - V curves of a module after 1320 h (55 days), 3024 h (126 days), and 4368 h (182 days) of outdoor operation. Burns appeared after 4000 h and had to be repaired by cutting out the destroyed parts. The repaired module still produced more than $150 \text{ W}_{\text{peak}}$.

Acknowledgements

This work has been supported by Energinet.dk (project no. 10728), the Danish Ministry of Science, Innovation and Higher Education under a Sapere Aude Top Scientist grant (no. DFF – 1335–00037A) and an Elite Scientist grant (no. 11–116028).

Received: October 25, 2013

Revised: November 27, 2013

Published online:

- [1] M. A. Green, K. Emery, Y. Hishikawa, *Prog. Photovolt: Res. Appl.* **2013**, *21*, 827.
- [2] J. E. Carlé, F. C. Krebs, *Sol. Energy Mater. Sol. Cells* **2013**, *119*, 309.
- [3] J. You, L. Dou, K. Yoshimura, T. Kato, K. Ohya, T. Moriarty, K. Emery, C.-C. Chen, J. Gao, G. Li, Y. Yang, *Nat. Commun.* **2013**, *4*, 1446.
- [4] M. Jørgensen, J. E. Carlé, R. R. Søndergaard, M. Lauritzen, N. A. Dagnæs-Hansen, S. L. Byskov, T. R. Andersen, T. T. Larsen-Olsen, A. P. L. Böttiger, B. Andreasen, L. Fu, L. Zuo, Y. Liu, E. Bundgaard, X. Zhan, H. Chen, F. C. Krebs, *Sol. Energy Mater. Sol. Cells* **2013**, *119*, 84.
- [5] H. Jin, C. Tao, M. Velusamy, M. Aljada, Y. Zhang, M. Hamsch, P. L. Burn, P. Meredith, *Adv. Mater.* **2012**, *24*, 2572.
- [6] C. L. Uhrich, R. Meerheim, T. Mueller, F. Lindner, K. Walzer, B. Maennig, A. Weiss, M. Pfeiffer, *Proc. SPIE* **2012**, 847705.
- [7] F. C. Krebs, T. Tromholt, M. Jørgensen, *Nanoscale* **2010**, *2*, 873.
- [8] M. Manceau, D. Angmo, M. Jørgensen, F. C. Krebs, *Org. Electron.* **2011**, *12*, 566.
- [9] Y. Galagan, D. J. D. Moet, D. C. Hermes, P. W. M. Blom, R. Andriessen, *Org. Electron.* **2012**, *13*, 3310.
- [10] R. Tipnis, J. Bernkopf, S. Jia, J. Krieg, S. Li, M. Storch, D. Laird, *Sol. Energy Mater. Sol. Cells* **2009**, *93*, 442.
- [11] L. Blankenburg, K. Schultheis, H. Schache, S. Sensfuss, M. Schrödner, *Sol. Energy Mater. Sol. Cells* **2009**, *93*, 476.
- [12] N. Su Kang, B.-K. Ju, T. Wan Lee, D. H. Choi, J.-M. Hong, J.-W. Yu, *Sol. Energy Mater. Sol. Cells* **2011**, *95*, 2831.
- [13] P. Sommer-Larsen, M. Jørgensen, R. R. Søndergaard, M. Hösel, F. C. Krebs, *Energy Technology* **2013**, *1*, 15.
- [14] F. C. Krebs, N. Espinosa, M. Hösel, R. R. Søndergaard, M. Jørgensen, *Adv. Mater.* **2014**, *26*, 29.
- [15] C. J. Mulligan, M. Wilson, G. Bryant, Ben Vaughan, X. Zhou, W. J. Belcher, P. C. Dastoor, *Sol. Energy Mater. Sol. Cells* **2013**, *120(A)*, 9.
- [16] R. Søndergaard, M. Hösel, D. Angmo, T. T. Larsen-Olsen, F. C. Krebs, *Mater. Today* **2012**, *15*, 36.
- [17] M. Hösel, R. R. Søndergaard, M. Jørgensen, F. C. Krebs, *Energy Technol.* **2013**, *1*, 102.
- [18] N. Espinosa, M. Hösel, D. Angmo, F. C. Krebs, *Energy Environ. Sci.* **2012**, *5*, 5117.
- [19] D. M. Tanenbaum, M. Hermenau, E. Voroshazi, M. T. Lloyd, Y. Galagan, B. Zimmermann, M. Hösel, H. F. Dam, M. Jørgensen, S. A. Gevorgyan, S. Kudret, W. Maes, L. Lutsen, D. Vanderzande, U. Würfel, R. Andriessen, R. Rösch, H. Hoppe, G. Teran-Escobar, M. Lira-Cantu, A. Rivaton, G. Y. Uzunoglu, D. Germack, B. Andreasen, M. V. Madsen, K. Norrman, F. C. Krebs, *RSC Adv.* **2012**, *2*, 882.
- [20] S. A. Gevorgyan, M. V. Madsen, H. F. Dam, M. Jørgensen, C. J. Fell, K. F. Anderson, B. C. Duck, A. Mescheloff, E. A. Katz, A. Elschner, R. Roesch, H. Hoppe, M. Hermenau, M. Riede, F. C. Krebs, *Sol. Energy Mater. Sol. Cells* **2013**, *116*, 187.
- [21] M. Jørgensen, K. Norrman, S. A. Gevorgyan, T. Tromholt, B. Andreasen, F. C. Krebs, *Adv. Mater.* **2012**, *24*, 580.
- [22] F. Yan, J. Noble, J. Peltola, S. Wicks, S. Balasubramanian, *Sol. Energy Mater. Sol. Cells* **2013**, *114*, 214.
- [23] P. Sánchez-Friera, M. Piliouguine, J. Peláez, J. Carretero, M. Sidrach de Cardona, *Prog. Photovolt: Res. Appl.* **2011**, *19*, 658.
- [24] J. Muñoz, E. Lorenzo, F. Martínez-Moreno, L. Marroyo, M. García, *Prog. Photovolt: Res. Appl.* **2008**, *16*, 693.
- [25] M. García, L. Marroyo, E. Lorenzo, J. Marcos, M. Pérez, *Prog. Photovolt: Res. Appl.* **2013**.
- [26] C. Buerhop, D. Schlegel, M. Niess, C. Vodermyer, R. Weißmann, C. J. Brabec, *Sol. Energy Mater. Sol. Cells* **2012**, *107*, 154.
- [27] D. M. Tanenbaum, H. F. Dam, R. Rösch, M. Jørgensen, H. Hoppe, F. C. Krebs, *Sol. Energy Mater. Sol. Cells* **2012**, *97*, 157.
- [28] T. T. Larsen-Olsen, R. R. Søndergaard, K. Norrman, M. Jørgensen, F. C. Krebs, *Energy Environ. Sci.* **2012**, *5*, 9467.
- [29] F. C. Krebs, R. Søndergaard, M. Jørgensen, *Sol. Energy Mater. Sol. Cells* **2011**, *95*, 1348.
- [30] J. Bachmann, C. Buerhop-Lutz, R. Steim, P. Schilinsky, J. Hauch, E. Zeira, C. J. Brabec, *Sol. Energy Mater. Sol. Cells* **2012**, *101*, 176.
- [31] H. Hoppe, J. Bachmann, B. Muhsin, K.-H. Drüe, I. Riedel, G. Gobsch, C. Buerhop-Lutz, C. J. Brabec, V. Dyakonov, *J. Appl. Phys.* **2010**, *107*, 014505.
- [32] M. Seeland, R. Rösch, H. Hoppe, *J. Appl. Phys.* **2011**, *109*, 064513.
- [33] A video showing the roll-out of a solar cell module is available on www.plasticphotovoltaics.org (accessed January, 2014).

DOI: 10.1002/ente.201200055

It is all in the Pattern—High-Efficiency Power Extraction from Polymer Solar Cells through High-Voltage Serial Connection

Peter Sommer-Larsen, Mikkel Jørgensen, Roar R. Søndergaard, Markus Hösel, and Frederik C. Krebs*^[a]

Among all known energy technologies, polymer solar cells offer the shortest unit manufacturing time, using a relatively small amount of earth-abundant materials. The efficiencies of state-of-the-art polymer solar cells are approaching those of inorganic solar cells for very small millimeter-sized active areas^[1] but are still outperformed by the established technologies when it comes to module performance and operational stability. The challenge currently addressed is to improve the module efficiency while simultaneously finding truly scalable methods both for the fast manufacturing and implementation into a larger system.

Polymer solar cell modules were first connected to the electrical grid in April 2009, for which the system was manufactured using similar methods to those employed for crystal-line-Si solar panels.^[2] In that work, the roll-processed flexible polymer solar cells were cut into small modules and handled as discrete units, encapsulated using hot-melt sealants on glass plates, and tediously connected using metal strips before frame mounting on a tracking system. Unsurprisingly, the analysis showed the many shortcomings of organic photovoltaics (OPV) compared to silicon PV. It was, however, the first instance of a direct comparison as laboratory reports often compare the efficiency of a mm²-sized single-junction polymer solar cell with the performance of large industrially produced silicon solar cell panels. One particular lesson learned was that, to take advantage of OPV, it should certainly not be integrated in a fashion similar to that of silicon PV. This also becomes evident when one performs a life-cycle analysis to provide a measure of the value of a given energy-producing technology through the energy pay-back time (EPBT). Also the energy return factor (ERF) is used to establish how many times an energy producing unit pays back the energy invested in it during manufacture. Here polymer solar cells are particularly attractive because they enable significantly shorter EPBTs and larger ERFs than any other PV technology (or any other renewable energy technology for that matter) provided that they are applied in a thin-film structure. Currently an EPBT of significantly less than one year is possible with an efficiency of 1–2% for large-area flexible modules. Polymer solar cells could potentially reach EPBTs on the order of 1 day provided that higher efficiencies are reached and renewable energy is employed in the manufacture.^[3] This is realistic and does not

affect the manufacturing speed when the energy input during manufacture is very low because polymer solar cells do not require any high-temperature steps (processing temperature < 140 °C).

The question is, of course, how one can utilize the polymer solar cell in its thin-film form while maintaining the advantages of a short EPBT by avoiding adding extra materials or time consuming process steps that would effectively lengthen the EPBT. The natural answer is to employ the uncut roll of manufactured polymer solar cells directly, by handling the long stretch of continuous polymer solar cell foil as one discrete unit. However, to employ this method, the individual solar cells cannot be reconfigured after the fast roll-to-roll processing employed during manufacture, which presents a few challenges. First, the polymer solar cells are manufactured by using continuous roll-to-roll coating and printing of thin films and, thus, will be unable to transport a large electrical current. The well-known solution to this challenge is to employ a serial connection. The serial connection is employed today for nearly all solar cell technologies, but typically only to approximately 1000 V at the system level by stringing wafers together using metal strips. To make use of the distinctive features of polymer solar cells, much higher voltages would be required, significantly higher than the few hundred volts employed in traditional modules. One distinct difficulty with serially connected silicon solar cell modules is that the entire system performance can be compromised if one cell performs more poorly than the others in the series. In such a configuration, one faulty cell can effectively ruin the overall performance of the array. A typical cause for inhomogeneous performance could be uneven solar illumination of a large array through shadowing from trees or buildings or it could be caused by the accumulation of dust or dirt on the surface. The latter can of course be handled through cleaning but for silicon PV, shadowing can lead to an abnormally large current density and charge build-up which can destroy the shadowed cell. For silicon PV this can be effectively resolved through use of a bypass diode, but this solution cannot be employed in the case of polymer solar cells if the low EPBT and fast manufacturing are to be maintained.

In this study, we analyzed the typical *I*–*V* characteristics of a polymer solar cell architecture that is fully printable and free from indium tin oxide (ITO) and then explored the serial connection of many polymer solar cells of this kind. We surprisingly found that, in contrast to traditional PV, a large, effectively infinite series of polymer solar cells of this type are relatively insensitive to partial shadowing. The explanation for this result can be found in the generally lower fill factor and current density observed for polymer solar cells as compared to silicon PV and the counter-diode-

[a] Dr. P. Sommer-Larsen, Dr. M. Jørgensen, Dr. R. R. Søndergaard, M. Hösel, Prof. F. C. Krebs
Department of Energy Conversion and Storage
Technical University of Denmark
Frederiksborgvej 399
4000 Roskilde (Denmark)
E-mail: frkr@dtu.dk

characteristics that many polymer solar cell architectures exhibit, which in essence acts as a built-in bypass diode. For the roll-to-roll-processed polymer solar cells studied here, a fill factor in the range of 50–60% was observed whereas it is up to 80% for silicon PV. The lower fill factor implies lower performance at the single solar cell level but in this case also produces more robust performance for very large serially connected arrays. In Figure 1 we illustrate the effect by comparing a small array of 80 serially connected silicon solar cells with the equivalent of 80 serially connected polymer solar cells. Initial experiments using polymer solar cells were based on the processing method/architecture called “ProcessOne”,^[4] which is the ITO-based analogue to the ITO- and vacuum-free roll-to-roll process employed in this work called “IOne”. The ProcessOne solar cells have fill factors in the range of 40–50%, and the complete blocking of one cell was observed to have negligible effect on the performance of the array. The nonideal diode behavior and relatively low internal resistance effectively prevented charge build-up and the internal electric fields never developed to a level where they would become destructive because the current densities were low.

An analysis of a standard equivalent circuit model for solar cells was employed, for which N solar cells are interconnected that each generate a photocurrent (I_L), and represent diodes that can be described by the Shockley diode equation. Each cell is additionally modeled with a shunt resistance in parallel and an electrical interconnect that is modeled as a series resistance. For a set of serially connected solar cells (Figure 1A), each cell experiences a voltage drop. For a given current running through each cell, the total voltage (v) of the series is the sum of the voltage drops over each cell, which is given by Equation 1 and Equation 2:

$$v = \sum_n v^{(n)} \quad (1)$$

and

$$v^{(n)} = V^{(n)}(i) \quad (2)$$

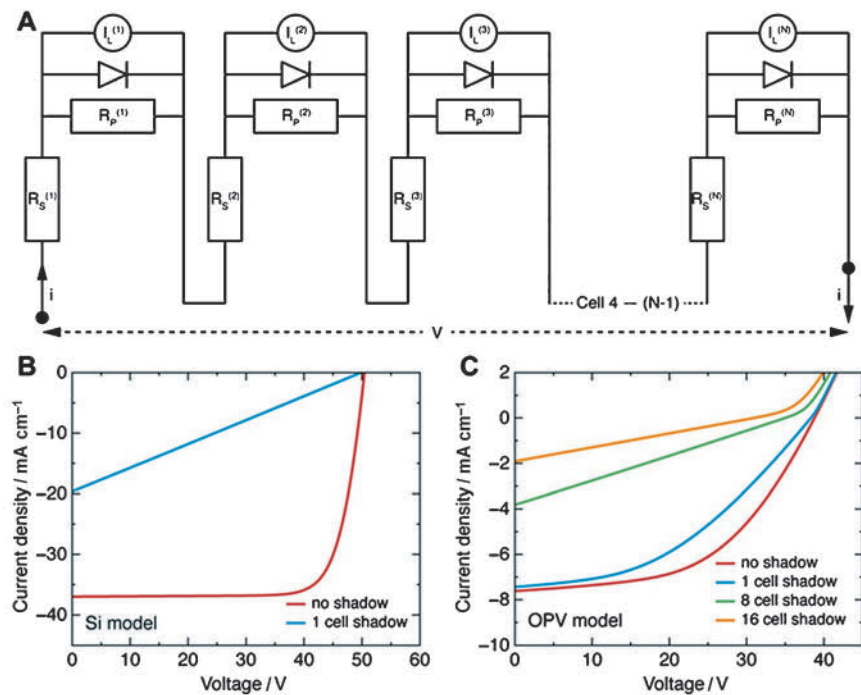


Figure 1. Simulation of the I – V behavior for serially connected solar cells. A) An illustration of the equivalent-circuit model for a large array of serially connected solar cells. B) Simulated I – V curve (current as function of voltage) for 80 serially connected cells with parameters in the equivalent-circuit model corresponding to silicon solar cells. The red curve corresponds to all cells generating approximately the same photocurrent and the blue curve corresponds to the situation when one cell is shadowed, so that it does not produce photocurrent as shown in the inset. C) I – V curves for 80 serially connected cells with parameters in the equivalent-circuit model corresponding to polymer solar cells. The red curve corresponds to all cells generating approximately the same photocurrent and the blue curve corresponds to the situation when one cell is shadowed so that it does not produce photocurrent. We further show how the I – V behavior evolves as 8 or 16 cells are shadowed as shown in the green and yellow curves.

Here $V^{(n)}(i)$ is the functional form for the potential generated over each cell when a current (i) passes through that cell (based on the equivalent-circuit description of the cells). The model set consists of 80 equivalent serially connected cells for which each has parameters typical for crystalline-Si solar cells. The I – V curves are shown in Figure 1 for the fully illuminated case and the case where one cell is shadowed. In the latter case the array produces a significantly reduced short-circuit current and fill factor (as shown in Figure 1B). In the case of OPV, a similar set of serially connected solar cells with typical OPV parameters was tested (also shown for the IOne technology employed in the latter part of this work, which exhibits higher fill factors). We introduced up to 10% variation in the parameters for each individual cell to demonstrate the robustness of the array. In spite of the higher fill factor (as compared to ProcessOne devices) it is clear that the output of the polymer solar cell array is much less sensitive to shadowing (Figure 1C) than the silicon solar cell array.

We have thus designed a process for the realization of large arrays of serially connected polymer solar cells by using roll-to-roll printing. We have extensive experience with automatic roll-to-roll printing, coating, and testing of thousands of polymer solar cell modules on web lengths of up to 1 km, but the practical realization of an effectively infinite

connected array along the roll presents some unique challenges. From the outset it is clear that the most catastrophic failure one can have is if a single cell in the array presents an open circuit, and this would prevent any power extraction from the array. A short-circuited solar cell is less critical but would of course generate a series resistance within the array causing poorer performance. Based on this analysis it is clear that the technical yield of the manufacturing process needs to be very high, that is, in excess of 99.999% for foil lengths on the order of 100 m. At first, this seemed unreasonable until we investigated the possible topologies for such a large array that would be compatible with the printing and coating methods required for the process. The ITO- and vacuum-free process employed here is known as the IOne process and is a significantly refined version of the original ITO-based roll-to-roll process for polymer solar cells called ProcessOne. The IOne process comprises a combination of the fast flexographic printing of a highly conducting silver grid, the necessary registration marks, and pilot lines.^[5,6] This is followed by rotary-screen printing and slot-die coating steps. All steps have been executed with a web speed in excess of 10 mmin^{-1}

and in this example the web width was 305 mm. Importantly, slot-die coating only allows for 1-dimensional patterning of the layers applied, whereas both flexographic- and rotary-screen printing methods allow full 2-dimensional control of the pattern with a resolution better than $100 \mu\text{m}$. The polymer solar cell pattern thus has to accommodate the combination of 1- and 2-dimensional film-forming methods. The IOne process comprises six printing and coating steps, and each is associated with drying and curing as illustrated in Figure 2. Each step generates some shrinkage in the cross-web direction and elongation in the web direction. In ordinary processing of discrete modules this is easily handled, but for a long, effectively infinitely connected array the entire polymer solar cell roll represents one single (but large) module, and this brings new challenges. We experimented with several designs and found a meandering pattern to present a very efficient solution for the combination of 1- and 2-dimensional patterns. The registration for slot-die coating was achieved through a combination of registration marks and linear pilot lines. The pattern is shown in Figure 2 and illustrates the effectively infinite connection of solar cells ach-

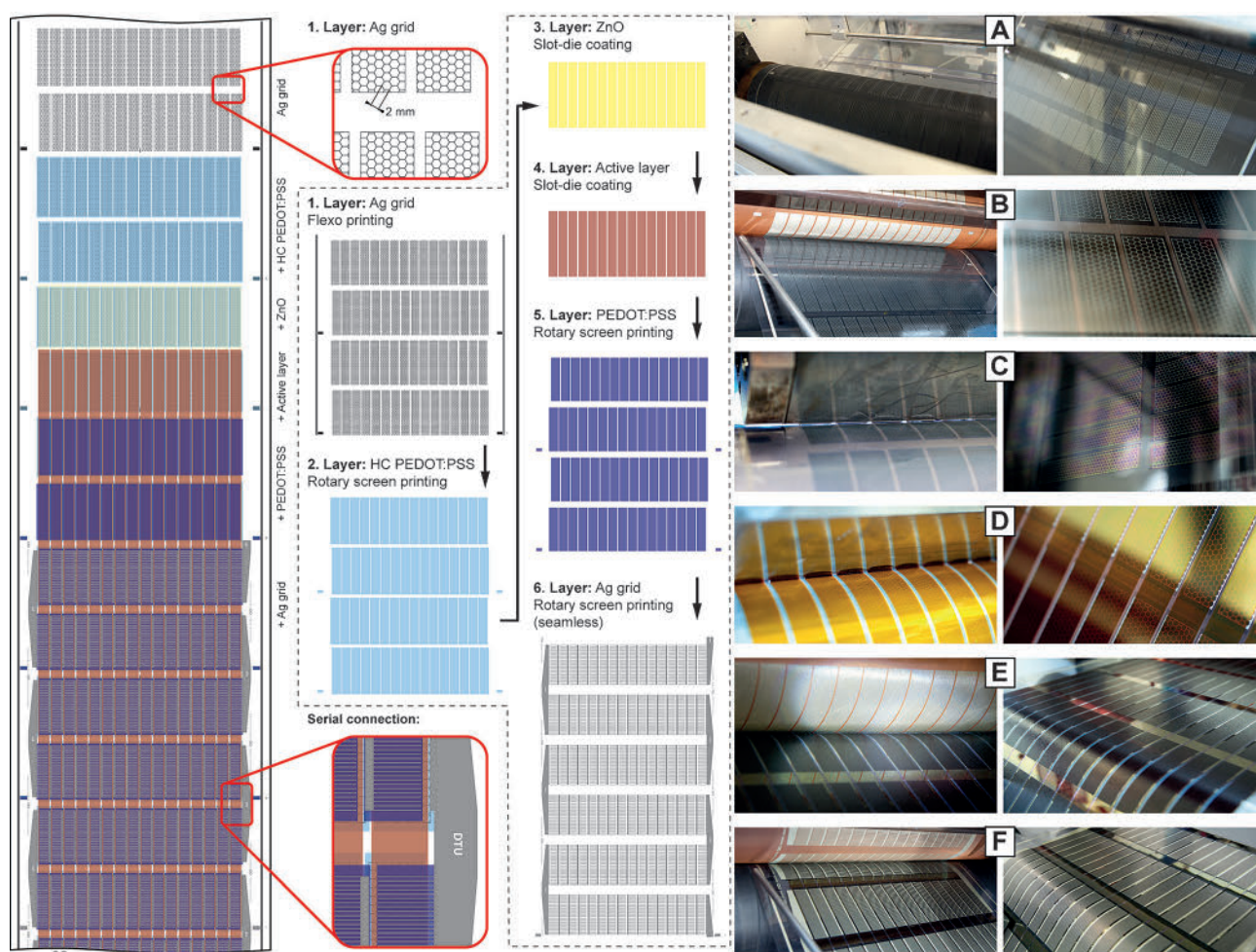


Figure 2. A process illustration for the modules employed in solar cell fabrication (the web direction is shown vertically, left), for which a diagram is shown for the process step of each layer (1–6). On the right-hand side, the processing of each layer is shown as a series of photographs of the printing form for the wet film (left photos) and the dried layer (right photos) for each of the processed layers (A–F).

ieved through printing. It should be noted that the serial connection is achieved in the final printing step as this was found to be the most materials-efficient method when encountering the loss of material during start/end of a printing run. The foil shrinkage in the cross-web direction was handled through tooling of the printing forms, and elongation in the direction along the web was handled through registration and slippage in the open areas of the pattern.

We printed and tested a series of 16000 serially connected solar cells (a length of 80 meters) and found that all of the cells remained operational (Figure 3). The array was tested outside in sunlight with overcast weather conditions. The high voltages achieved did not allow for full I - V characterization of the large array (as no source meter is available in the 10000 kV range), but shorter lengths of approximately 2000 serially connected cells (which presented open-circuit voltages of around 1000 V) allowed us to perform the full I - V measurements. We intentionally tested the cells under overcast weather conditions to fit the operating range of the source meter (Keithley 2410, 1000 V, 20 mA). Here we observed an approximate power conversion efficiency of 1.6% and a fill factor of approximately 50% for the shorter array when initially deployed and the efficiency remained at approximately 1.2% after 1000 h. The voltage and fill factor are relatively stable with operation time and the primary

cause of performance degradation is a drop in the current. It should be stressed that these modules were not packaged, with the exception of a back lamination protecting the printed layers against the mechanical handling of the array. We encapsulated a small piece of the foil (comprising 80 serially connected cells) to fit under a solar simulator for accelerated testing and demonstrated accelerated lifetimes corresponding to outdoor operation well in excess of 1 year. The full 80 m array was tested with respect to open-circuit voltage, short-circuit current, and maximum power point through a resistive load. Here we found the same performance: 8.2 kV, 29 mA, and a maximum power of 125 W.

The results of this study show that the polymer solar cell, with its currently inferior performance, can be installed rapidly in a form that takes full advantage of its low carbon footprint and low materials usage. Furthermore, the polymer solar cell array does present several operational differences when compared to the traditional silicon-based solar cells by allowing for the efficient serial connection of a very large array without loss and exhibiting robustness towards partial shadowing. The approach that we demonstrate here realizes the goal of renewable energy production using polymer solar cells, by deliberately making use of its advantages of fast production and robust high voltage serial connection through printing. This demonstration could be used as a platform for

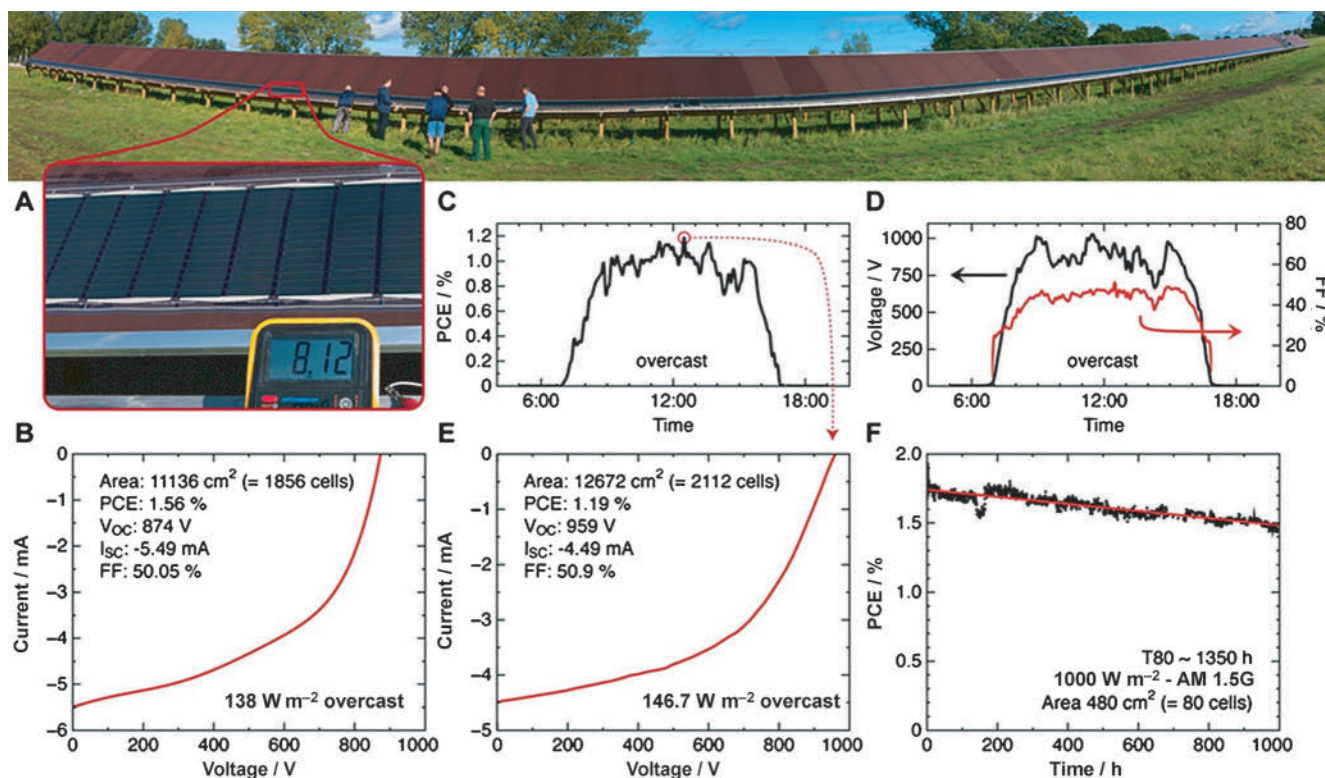


Figure 3. A) A panoramic view of the 80 m foil comprising 16000 serially connected cells (top). A voltmeter shows the total voltage of 8.12 kV for the 80 m array illuminated at full sun. B) An I - V curve for 1856 serially connected cells at the beginning of the experiment. C) The daily performance on an overcast day after ageing for 1000 h showing the power conversion efficiency (PCE). D) Plots of the open-circuit voltage (V_{oc}) and fill factor (FF) after 1000 h. E) A representative I - V curve is also shown for 2112 serially connected cells. F) Accelerated indoor testing of a small array comprising 80 serially connected cells under a metal halide based solar simulator (AM1.5G, 1000 W m^{-2} irradiance, $T = 85^\circ \text{C}$). The T_{80} (the time necessary to reach 80% of the initial performance) of 1350 h corresponds to an outdoor lifetime of more than one year.

development to direct the ongoing research on new and more efficient materials for OPVs such that they fit the device structure and printing/coating methods we have demonstrated in this work. This procedure would allow for the direct application of progress within materials development as the large areas employed and use of the sun as light source would ensure a higher level of consistency to make the comparison of performance and testing between different laboratories more straightforward.

Acknowledgements

This work was supported by the Danish Ministry of Science, Innovation, and Higher Education through the EliteForsk initiative and the 2011 Grundfos Award.

Keywords: PEDOT/PSS • photovoltaics • polymers • roll-to-roll processing • rotary-screen printing

- [1] M. A. Green, K. Emery, Y. Hishikawa, W. Warta, E. D. Dunlop, *Prog. Photovoltaics* **2012**, *20*, 606–614.
- [2] A. J. Medford, M. R. Lilliedal, M. Jørgensen, D. Aarø, H. Pakalski, J. Fyenbo, F. C. Krebs, *Optics Express* **2010**, *18*, A272–A285.
- [3] N. Espinosa, M. Hösel, D. Angmo, F. C. Krebs, *Energy Environ. Sci.* **2012**, *5*, 5117–5132.
- [4] F. C. Krebs, S. A. Gevorgyan, J. Alstrup, *J. Mater. Chem.* **2009**, *19*, 5442–5451.
- [5] T. T. Larsen-Olsen, R. R. Søndergaard, K. Norrman, M. Jørgensen, F. C. Krebs, *Energy Environ. Sci.* **2012**, *5*, 9467–9471.
- [6] M. Hösel, R. R. Søndergaard, M. Jørgensen, F. C. Krebs, *Energy Technol.* **2013**, DOI: 10.1002/ente.201200029.

Received: December 4, 2012

25th Anniversary Article: Rise to Power – OPV-Based Solar Parks

Frederik C. Krebs,* Nieves Espinosa, Markus Hösel, Roar R. Søndergaard, and Mikkel Jørgensen

Dedicated to Markus C. Scharber

A solar park based on polymer solar cells is described and analyzed with respect to performance, practicality, installation speed, and energy payback time. It is found that a high voltage installation where solar cells are all printed in series enables an installation rate in Watts installed per minute that far exceed any other PV technology in existence. The energy payback time for the practical installation of polymer solar cell foil on a wooden 250 square meter platform in its present form is 277 days when operated in Denmark and 180 days when operated in southern Spain. The installation and de-installation rate is above 100 m min^{-1} , which, with the present performance and web width, implies installation of $>200 \text{ W min}^{-1}$. In comparison, this also exceeds the overall manufacturing speed of the polymer solar cell foil with a width of 305 mm which is currently 1 m min^{-1} for complete encapsulated and tested foil. It is also significant that simultaneous installation and de-installation which enables efficient schemes for decommissioning and recycling is possible. It is highlighted where research efforts should most rationally be invested in order to make grid electricity from OPV a reality (and it is within reach).

solar cells but certainly also to *Advanced Materials*. Mirroring the conventional PV technologies,^[2] the majority of research focus in OPV has since been devoted to improving the power conversion efficiency^[2] and the justification for the polymer solar cell and polymer solar cell research most often reads that it is a low cost solar cell that will prove immensely useful to society (in the future) provided that a certain efficiency goal is reached. In an effort to reach the somewhat arbitrarily chosen high efficiency goal, the focus on when the polymer solar cell is good enough or how it should be made has been lost. The most focused attempt to direct research and highlight status have been the compilation of road-maps for the OPV technology by several independent organs (OE-A, IDTechEx, PlasticsElectronics, EU etc.) and while the frequent (often yearly) update of these road-maps are in general

1. Introduction

The polymer solar cell is about the same age as *Advanced Materials* and, during these 25 years, the journal has contributed significantly to the success of the polymer solar cell by bringing forward some of the most important contributions to the field, the most cited one being a paper by Markus C. Scharber et al. that described design rules on how to reach 10% power conversion efficiency for polymer solar cells.^[1] The article was published at a time when power conversion efficiencies above 1% was only reached by a select group of people leading the field with efficiencies in the 2–3% range. The importance of the article was enormous as it showed that 10% was in principle possible by careful selection of materials parameters that were readily measurable by the chemist developing materials and today the maximum performance for OPV has been reported to exceed the 10% claimed possible much earlier. The work of Scharber was thus true to the art and vision of polymer

agreement there has been a tendency for the required levels (in efficiency, stability and process) to increase thus always pushing the societal interest of the technology 5–10 years into the future, while stipulating the most important current research goals and the currently achieved parameters.^[3,4]

In this report we attempt to turn things upside down and instead refocus at the polymer solar cell in the form we would ideally like to apply it and also how we would ideally prepare it. We then examine how a certain performance in stability, efficiency and process affect the general view of what the polymer solar cell is and certainly also of how it should be. Most importantly this alludes to where research efforts should be placed if the goal of electrical energy available from OPV is to be reached.

We finally describe our practical experience with the installation of polymer solar cells in a solar park with a platform capacity of 1000 square meters comprised in four tilted rows of 250 square meters (100 meters long by 2.5 meters high). The present solar park is viewed as a small prototype for a much larger scale solar park and includes the infrastructure needed for efficient use of the same installation–de-installation system on all rows through a train-based system that can be automated. The intended size of the system is 1 000 000 square meters or more and we highlight that energy production based on such a system is possible with the presently available materials and that materials selected correctly according to the Scharber

Prof. F. C. Krebs, Dr. N. Espinosa, M. Hösel,
Dr. R. R. Søndergaard, Dr. M. Jørgensen
Department of Energy Conversion and Storage
Technical University of Denmark
Frederiksborgvej 399, DK-4000, Roskilde, Denmark
E-mail: frkr@dtu.dk



DOI: 10.1002/adma.201302031

rule would make energy production a profitable business (for professionals).

2. The Distinction of the Polymer Solar Cell

Of all known renewable energy technologies the polymer solar cell is the only one that inherently enables fast manufacture of a given energy producing unit with a very thin outline using only abundant elements. The original vision of the polymer solar was that it could be printed endlessly, but, as the science developed, the archetypal solar cell was prepared in tiny format under inert and clean conditions on glass plates using techniques that are not scalable (i.e., indium-tin-oxide (ITO) electrodes, vacuum processing, reactive metals, and spin-coating). The approach successfully demonstrated the desired high efficiency which is a scientific hallmark in its own right, but while showing that it is a technological possibility it has also become far removed from being a technological reality.

2.1. The Fast Processing

Unlike any other solar cell technology all layers in the polymer solar cell can be processed from a liquid ink and since the required layer thickness for each layer in the solar cell stack is generally very thin it is possible to form the layers using fast printing and coating processes. There are of course limitations to the achievable web speeds but the range of 60–300 m min⁻¹, typically encountered in the printing industry, is readily accessible and even 60 m min⁻¹ is sufficient to enable an overall manufacturing speed of around 10 m min⁻¹ which is estimated to be sufficient for production of 1 GW_{peak} every day without too large a capital investment in machinery. The low temperatures employed during drying and curing also add to the possibility for high-speed processing. In terms of film formation the current approach is a suitable mixture of different printing and coating techniques.^[5] The advantage of the printing methods is that the ink usage can be minimized in contrast to coating where a typical loss of 10–25% is encountered and also that fine 2-dimensional patterns can be realized. The printing techniques currently employed are however inferior to coating when it comes to formation of thin and smooth layers. Ideally only printing will be used for the entire process but this will require a massive investment in development of both ink systems and printing methodologies which is unlikely to be justified until the need is there. The currently available methods largely suffice to develop OPV as an energy producing technology.

2.2. The Embodied Energy

One of the central parameters used to view and compare an energy technology is how efficient it is at converting the source energy into the form of energy that we would like to use (i.e., the conversion of sunlight, wind or wave energy into electrical energy). The appeal of this is of course that the power conversion efficiency is a scalar property that can be



Frederik C. Krebs is currently professor at the technical university of Denmark (DTU) with research focus on foil-based energy systems (thermoelectrics, PEMFCs, photocatalysts, light emitting devices, solar cells). In the context of OPV interests range from synthesis of new materials and stability, advanced device structures (tandem polymer solar cells), roll-to-roll processing, large scale manufacture, product integration, lifecycle analysis, recycling, installation, and operation, to energy production from solar parks based on polymer solar cells.

directly compared. More importantly is however the expense at which this efficiency is reached, the speed at which it can be realized and the materials and energy consumed in the process. Such an analysis known as a life cycle analysis (LCA) is a complex method that gains accuracy only by having complete detail of the entire process.^[6] LCA does however enable one to compare the efficacy of a given technology in terms of how quickly it conquers back the energy invested in its making and here polymer solar cells outperform all other PV technologies even on a laboratory scale described here. This measure, known as the energy pay-back time (EPBT), is very useful to compare different renewable technologies. Currently an EPBT of ca. 90 days is possible for polymer solar cells with an efficiency of around 2% which is currently reached on flexible ITO-free modules. Polymer solar cells potentially enable an EPBT of 1 day^[7] provided that higher practical large-scale efficiencies are reached and renewable energy is employed in the manufacture. This is realistic because the energy input (process heat) during manufacture is very low since the technology does not require any high-temperature steps (<<140 °C) as mentioned above. Once operational the energy balance of the inputs during the lifespan of an energy system must be evaluated. In other words, the embodied energy must weigh less -or have a lower value- than the energy delivered by the system during its operational phase (i.e., the solar cells, the installation, the decommissioning etc.). Energy is needed to create energy systems in the extraction and processing of raw materials, in the manufacture of finished products and components, in the construction phase, and in the transport of materials/products to site. We can draw boundaries around the considered lifecycle stages, and assess the inputs and outputs that cross the boundary; this is at the heart of LCA. As a methodology it is transparent, repeatable and clearly defined in the ISO14040 series.^[6] It helps to generate a framework for future decision-making and it is highly appropriate for evaluating the energy investment made in an energy system and in determining the EPBT and also the energy return factor (ERF) which is the number of times the system pays back the energy invested in it.

Table 1. Lifecycle energy in MJ per kW h_{el}, energy payback time (EPBT) in years and global warming potential (GWP) in kg CO₂ per kW h_{el} for several alternative energy technologies.

Energy source/Technology	Location	EPBT [years]	Embedded energy [MJ per kW h _{el}]	GWP [kg CO ₂ per kW h _{el}]	Ref.
Wind	Global average	0.39	0.066	0.027	[8]
PV technologies					
Mono and poly Si	US-Global average	1.65–4.14	11.9	0.032–0.36	[9,10]
Amorphous Si	US-Global average	1.13	2.55	0.011–0.226	[11,12]
CdTe	European average	0.73–1.61	9.22	0.025	[13,14]
OPV ^{a)}	Denmark/Europe	0.2–4	44.50	0.01–0.06	[7,15,16]
Hydropower	Germany-Canada	0.5	0.14	0.013–0.04	[17]
Geothermal	Germany	0.54	0.54	0.041	[17]
Biomass	China	5–10	–	0.045	[18]
Natural gas	Australia	–	12.91	0.751	[19]

^{a)}Note that these LCA values are given for the production of the modules and not for the whole installation, which is the object of this study.

2.3. Comparison with Other Renewable Technologies

It is clear that low efficiency does imply a large area or volume for harvesting energy. Shown in Table 1 is the energy intensity or energy embedded in several energy technologies per kW h_{el} produced during their operational lifetimes.^[7–19] The efficiency and lifetime of OPV is much lower than other competitors, so key to achieving low values of EPBT reside in a low embodied energy; both the energy attributable to the materials and to the manufacturing of a functional unit which is usually measured in processed area (i.e., per square meter). A low embodied energy enables a fast EPBT and also underlines that any gain in efficiency and lifetime is quickly paid back at several levels (see Table 1). Since OPV is currently at the level and even surpassing some technologies it also implies that it has the potential to significantly outperform all renewable energy technologies in existence pending even slight improvements in efficiency and lifetime over the currently achievable levels.

The geographical location has a significant impact on the EPBT and the few LCA studies devoted to OPV reach the same conclusions and are in general agreement. The minor variation in the findings can be attributed to the specific design of the technology, the LCA methodology adopted and especially the scope, assumptions and availability of inventory data, the inclusion/exclusion of Balance of System (BoS) in the inventory data (the collection of all inputs and outputs), and the use of theoretical (or estimated) data vs. case study data. In this work we employ case study data that are fully rooted in fact and observation with no assumptions made on processing parameters, materials consumption or speed.

2.4. Realizing the Low-Carbon-Footprint Potential of OPV

There is a need to provide the energy production markets with effective payback opportunities, and the energy consumed and carbon emitted over the lifecycle of these alternatives must be weighed up against the energy and carbon they are intended to save; that is to say, the output from the lifecycle analysis should

negatively influence emission. The assessment of the emissions is linked to the life-cycle analysis of the energy, relying on prevailing energy structures to convert mega joules of energy to kilograms of CO₂. Analogously to the embodied energy, we can define the embodied carbon of any product or service in relation to the carbon emissions associated with the product or service over its lifetime and it can be seen as the primary factor in determining the carbon mitigation potential of a technology.^[20] In general, we can cover carbon emitted by energy systems in two distinct areas: emissions associated with manufacturing and construction – fixed emissions – and emissions occurring during operation. In the case of PV systems, the latter are zero, or very small if we count the replacement of some electronic equipment or BoS components. Table 1 includes a list of the life-cycle global warming potential (GWP) for the main non-nuclear electricity technologies, in kilograms of equivalent CO₂. If we compare present-day PV technology (at a southern European location) with other energy options we see that PV has considerably lower greenhouse gas (GHG) emissions than fossil options such as natural gas. But in comparison with wind energy present-day PV still presents comparable GHG emission levels, and slightly higher levels if we install PV systems in lower-irradiation regions (i.e., Denmark). The OPV analyzed in this work on the other hand shows very good promise for further reduction of the GHG emissions, down to the current values of 7 g per kW h_{el} and even lower.

3. Solar Parks Based on Polymer Solar Cells

Whereas state-of-the-art polymer solar cells are approaching the polycrystalline and thin-film inorganic solar cells in terms of efficiency on very small square millimeter sized active areas,^[2] they dwarf the established technologies when it comes to module performance and operational stability. The challenge here is to find truly scalable methods both for the manufacture and the implementation into a larger system that accommodates both advantages and disadvantages. This was made obvious with the first electricity grid connected polymer solar

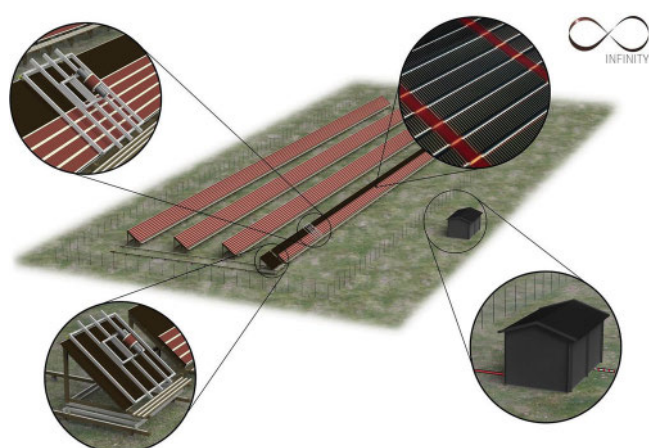


Figure 1. Solar park according to the Infinity concept showing how rows of tilted platforms serve as the mounting surface for foil-based OPV. New foil can be mounted while simultaneously demounting the old foil using a wagon that rolls along the row. At the end of the rows, a train system allows one to move the wagon from row to row. It is a high voltage installation and does require a fence around it. The rows that are 100 m long result in a voltage build-up along the row of >10 kV, achieved through serial connection of the 21 000 individual junctions along each lane of solar cell foil. Down-conversion to <1 kV takes place inside the fence and is transferred in subterranean cables to a building where inversion and grid connection takes place.

cell plant that was demonstrated in April 2009.^[21] The system was comprised of glass panels manufactured using the same methods currently employed for silicon solar panels. This implied that the flexible polymer solar cells were cut into individual small modules from the roll, tediously connected using metal strips and encapsulated using hotmelt sealant on glass plates with final frame mounting on a tracking system. An analysis showed not surprisingly that this method would never enable OPV. A financial analysis showed the majority of the cost of the system was in the mounting structure (glass, frame, sealants) and the time associated with assembly. The report was useful in the sense that it was the first time that an OPV panel could be truly compared to a silicon panel with equal size. The OPV system in question is still in service even if the performance has dropped significantly over the four years it has been in operation. Based on this knowledge a new truly scalable concept (the infinity concept) was developed where discrete handling of solar cells is avoided and only two points of contact is involved in order to make installation and maintenance significantly faster than, for example, silicon-based solar cells, such that the lower efficiency was acceptable.

The infinity concept^[22] is illustrated in **Figure 1** and shows how one handles the long roll of solar cells as one discrete unit with application directly from the roll and thus avoids the tedious cutting and handling of individual cells and modules as described earlier. By printing all the individual solar cell junctions in series it is possible to extract the energy at opposite ends of the rows using just two points of contact which is a scalable approach that allows for long lengths of solar cell foil. The high voltage elegantly solves the issue of high current densities and enables a thin and light-weight system using only thin wires, a system which is true to the art of keeping

materials usage and embodied energy as low as possible, while also ensuring as little labour as possible in the installation itself.

3.1. The Roll-to-Roll Manufacture

The philosophy that the roll of material can be handled manually whereas the individual cells or modules cannot, is truly enabling and compatible with roll-to-roll manufacture of an in principle infinite series connected array of solar cells. This was demonstrated in 2012^[22] when it was proven possible and also proven that high voltages could be stably generated and energy meaningfully extracted with very little loss. The challenges in the roll-to-roll processing of serially connected solar cells that exceed many thousand are significant and printing and coating registration becomes paramount to keep the technical yield high. Currently the infinity modules are prepared on roll lengths of 1.5–2.2 km which comprise 315 000–462 000 serially connected single solar cells. In order to make this possible the technical yield has to be exceptionally high and currently we have at best achieved 700 m of foil with 100% technical yield (147 000 solar cells). For the current installation the strict requirement is that stretches of 100 m (21 000 solar cells in series) has to be without error and this is easily achievable as illustrated in the following. In our first demonstration we employed a flexo printed hexagonal metal grid structure in the front electrode and a rotary screen printed comb shaped grid structure in the back electrode.^[22] This was robust enough to make 80 m of foil consistently and without error (16 000 solar cells in series). The challenge with printed (ITO-free) electrodes is shorts from silver-silver contacts between the grid structures and this is generally observed whenever grid lines cross. For a 2D grid such as a honeycomb grid combined with a comb grid the number of potential shorting points are large and uncontrolled since the registration in the web direction does vary on a scale comparable to or slightly smaller than the grid spacing employed in the comb (1 mm spacing). We redeveloped the grid structure by making many experiments and found that the desirable double comb metal electrode structure with comb lines being exactly out of phase is impossible in the current module design due to unpredictable shrinkage of the web during processing, which also takes place at approximately the same length scale as the comb repetition length. We instead developed a $+5^\circ/-5^\circ$ slanted comb structure where the Moiré effect is deliberately exploited to ensure that typically one cross of comb grid lines is observed per unit cell and maximally two as illustrated in **Figure 2**.

The Infinity philosophy^[22] was still followed using the same combination of printing and coating techniques with this new grid structure having a comb line spacing of 1.5 mm. We also chose to print the back silver electrode in two much faster printing steps making registration in both web and cross web direction less critical. The overall manufacturing speed of the foil in a form ready for installation was 1 m min^{-1} and even if this is fast for lab scale, manufacture for large scale energy production clearly will need much higher speed. The manufacturing speed of each complete, tested and encapsulated single

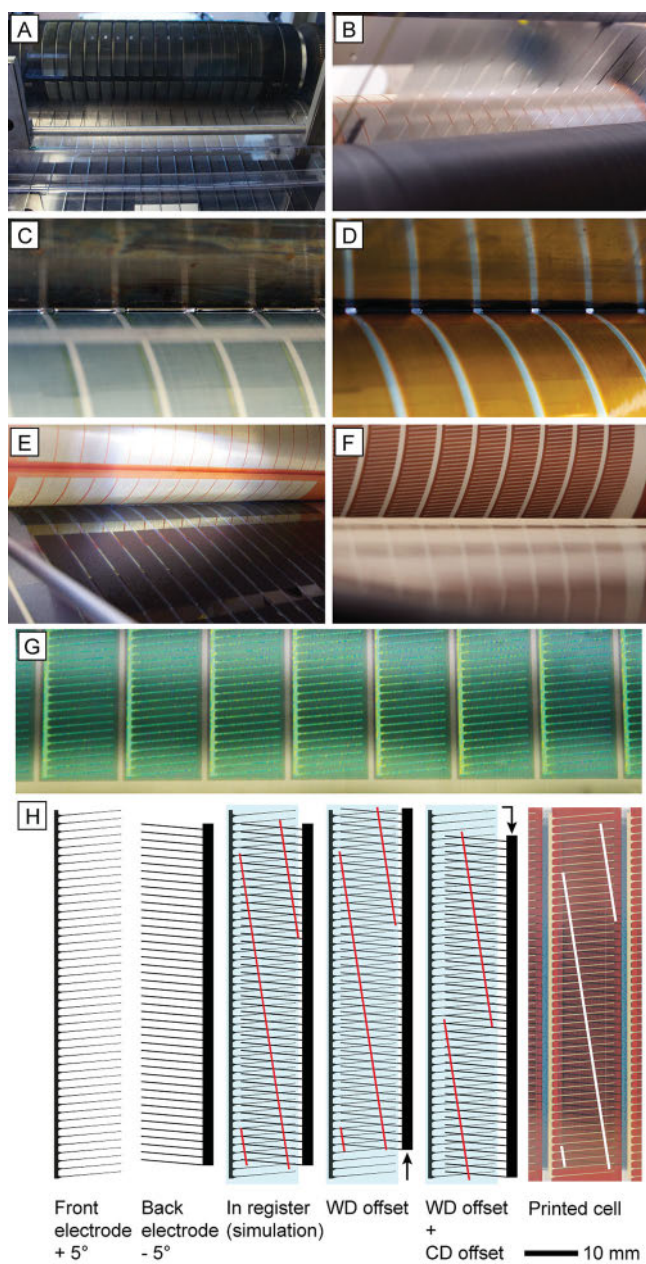


Figure 2. R2R processing of the solar cells employed in this work. Flexographic printing of the front silver grid (A) rotary screen printing of front PEDOT:PSS electrodes (B) slot-die coating of ZnO (C) slot-die coating of P3HT:PCBM active layer (D) rotary screen printing of back PEDOT:PSS (E) Rotary screen printing the back silver electrode (F). A photograph of the front slanted silver grid with PEDOT:PSS (G) Illustrations of the $+5^\circ/-5^\circ$ slanted comb grid electrode pair with graphical illustrations of front and back grid electrodes illustrating the comb electrodes separately (left part) overlaid with the red lines showing the crossing points depending on the registry or an offset in the web-direction (WD) or with an additional offset in the cross-web direction (CD) (middle part) and for the final solar cell with white lines showing the crosses (right part) (H).

junction with a ca. 7 cm^2 active area is <0.3 seconds which in its own right is a significant speed. The potential of the technology is junction manufacturing speeds in the range of milliseconds.

3.2. The Roll-Platform-Roll Methodology to Installation–Operation–De-installation

Having an efficient roll-to-roll process leading to hundreds of meters of deployable solar cell foil calls for use of roll processing also in the installation ideally such that the foil can be cut to the desired length (in this case 100 m) only at the stage at which it has been laid out. The process is illustrated in Figure 3 and proved to be straight forward. We have experience with installation under a high wind loading of up to 12 m s^{-1} wind speed with 18 m s^{-1} gusts and also installation in light rain and wind speed of 10 m s^{-1} . We have installed in full sunlight (mid-day) and under overcast conditions and observe no differences in the quality of performance of the installation or foil. One important aspect with the experiment was to establish the speed and ease of the installation. We found that the foil could be installed at a rate exceeding 100 m min^{-1} using relatively manual handling (see video on website in ref.^[30]) and estimate that further development of automated systems should enable an installation rate of $2\text{--}300 \text{ m min}^{-1}$. This demonstrates that OPV can be installed at a rate that exceeds the intended manufacturing rate and from this point of view the technology is proven ready. Another important parameter enabling comparison with silicon is how fast a watt is installed. With the current performance of the foil 100 meters of foil give $>220 \text{ W}_{\text{peak}}$. This corresponds to an installation rate of $>200 \text{ W}_{\text{peak}} \text{ min}^{-1}$. It should be underlined that wider web widths and higher power conversion efficiency would yield installation rates of several $\text{kW}_{\text{peak}} \text{ min}^{-1}$ which is largely sufficient for global installation of $>1 \text{ GW}_{\text{peak}} \text{ day}^{-1}$. A typical silicon solar cell panel also yields on the order of $200 \text{ W}_{\text{peak}}$ but cannot foreseeably be installed at the same rate. We thus firmly believe to have established that OPV can already be installed in a faster and less energy demanding fashion than traditional PV even with the currently achievable performance (which is low). It should be added that the energy that can be extracted per area using OPV is significantly lower than for state of the art silicon solar cells by a factor of $5\text{--}10$ ^[2] and this implies that a correspondingly larger land mass or area must be available for any given power rating. It is clear that this is a significant drawback and will require that the land areas used for OPV are of a very low cost in comparison (by a factor of $5\text{--}10$). It is likely that OPV will have to be explored in areas that are currently not in use, for example desert regions^[23] or off-shore regions. Another aspect is that the flexible foil is likely to be replaced and the system illustrated here also enables simultaneous de-installation and installation (not shown). This is estimated to be necessary in the case of scaled use of silver electrodes where recycling will be necessary. In the case where a fully carbon-based OPV foil is employed then recovery and combustion might be profitable as it would release around ca. 5 MJ of heat per square meter of the currently employed foil which could be used in large scale systems as process heat for drying.

3.3. Operation and Stability (and also Safety)

The system could be operated stably while a high voltage installation needless to say does require some safety precautions and

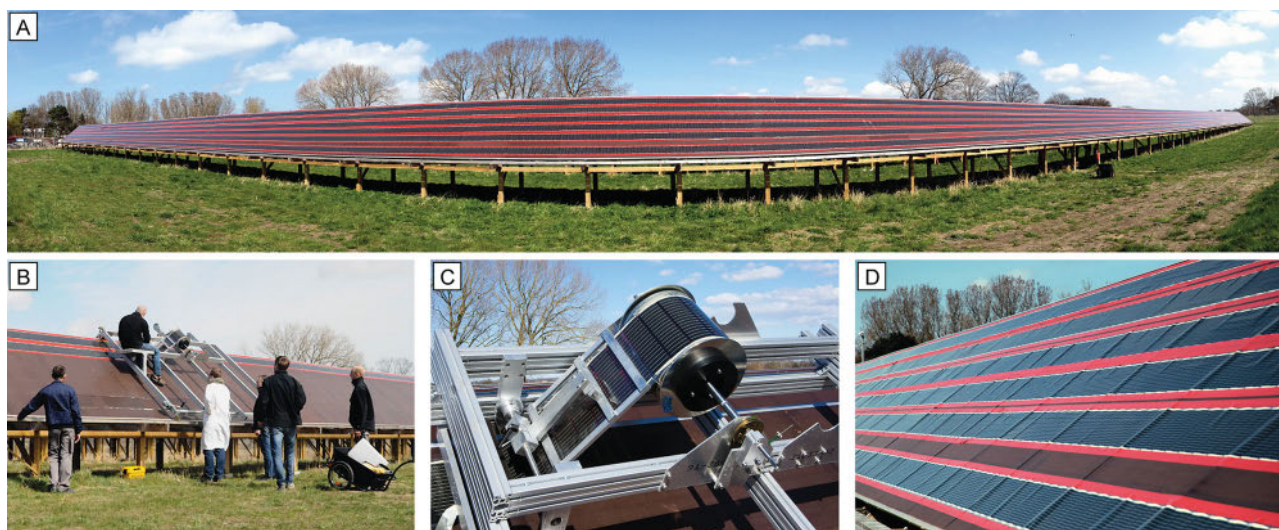


Figure 3. The front row of the solar park with 6 lanes of 100 m stretches of solar cell foil in a web width of 305 mm (A). The roll mounting of the foil is shown (B) along with a close-up photograph of the application with a guide (C). A view along the row showing dilation around connections in the platform (D).

specialized handling. We therefore do not see this solution as generally applicable to the public but find that it is most likely reserved for professionals wishing to produce and sell electricity to the grid. We should add that we never encountered any problems with high voltages during processing and handling rolls of foil while on the roll. Once the foil is rolled out (even under low light pressures) high voltages does develop and it is important that this is performed by people who are fully aware of the object at hand and it is perhaps the right moment to reiterate that the most dangerous aspect of electricity is that it is invisible to the human eye and a complication for solar cells is that they cannot be switched off.

In terms of performance the solar cells with the improved grid structure showed an initial power conversion efficiency of >2% over the active area of 14.7 m² on a 100 m stretch and after an initial drop they stabilized at a relatively constant power conversion efficiency of 1.6–1.8%. The fill factor was above 60% showing that it is possible to connect ca. 21 000 solar cells in series and achieve a high fill factor. When connecting 6 such lanes of 100 m in parallel a performance as shown in **Figure 4** was obtained with a slightly lower performance of 1.53% mainly due to loss in fill factor and open circuit voltage (over an active area of 88.2 m²). The Infinity foil has been shown to inherently inhibit a large resistance to effects from partial shading and the observed deterioration initially could be due to initial shading by bird droppings (there is a bird colony close to the solar park). In spite of this we did not observe any adversities as a result of this nor did we make attempts to wash or clean the solar cells even if this would be possible by suitable modification of the installation wagon.

3.4. Energy Payback Times and Energy Return Factors

By carrying out an LCA using the manufacturing and installation data as input we found a short EPBT of 6 months for the

present installation in its entirety (0.49 years) in a southern European setting. The energy payback time of the solar park is the sum of the EPBT of the components. **Figure 5** shows that the OPV modules have the highest influence on the EPBT as compared to the rest of the solar park installation. Especially the use of a wooden scaffold was found to influence the EBPT to a very little degree due to the longer lifetime of the structure. We estimate 15 years for the installation (platform, fence etc.), which is much longer than the PV modules where we estimate a lifetime of 1 year. The 1 year lifetime is likely to be underestimated and the present technology can possibly endure several years with a performance above T_{80} (the time to reach 80% of the initial performance). If this is the case as we gain experience with long term operation this would imply an EPBT as low as 0.32 years. The expected operational lifespan of electronic components such as cabling and the inverter has been considered to be 10 years.

The emissions related to the installation of the solar park include the manufacturing of all the components and it totals at 12 922 kg CO_{2eq} considering that the electricity mix of Denmark releases 420 g CO₂ per kW h. With the solar park in the current location, the carbon footprint is 0.112 kg CO_{2 eq} per kW h. If the installation were located in southern Spain, the carbon footprint would be 0.072 kg CO_{2 eq} per kW h of electricity produced.

3.5. Critical View on Wood as Scaffold Material

Wood-based materials have several advantages, due to their origin as a renewable resource, the emissions released in comparison with concrete or metallic structures are 3 times lower, and further wood has advantages such as being corrosion resistant, durable when installed in a fashion that allows it to dry, etc. There are, however, two critical challenges with respect to its use that must be mentioned. The source and origin of the wood is important and may negatively impact biological

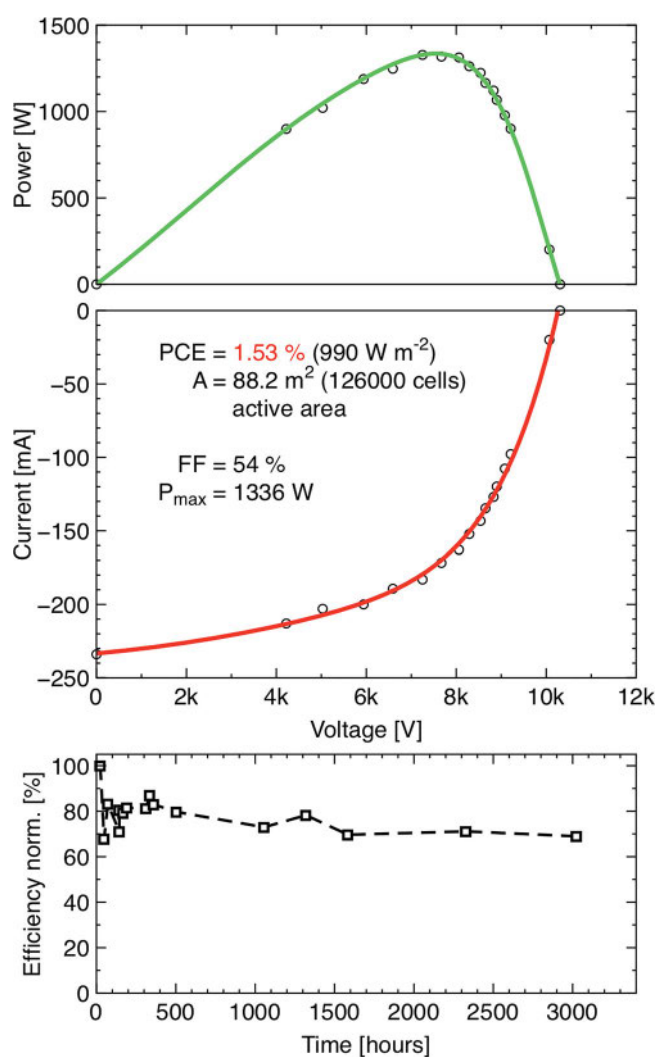


Figure 4. The power extracted from 6 stretches of 100 m solar cell foil at full sun (top). The IV-curve from the 126 000 solar cells shows a high fill factor of 54% (middle). After an initial drop in efficiency it stabilized at 1.5% mainly due to a drop in fill factor (below).

diversity that by many is viewed as a future threat on the same importance scale as climate change currently is. The risk of inflammation is also there especially in our case where high

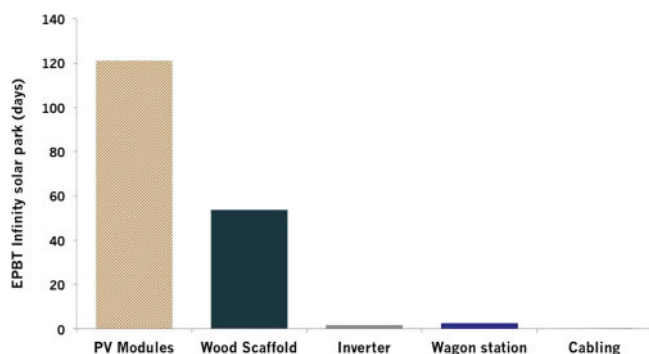


Figure 5. Energy payback time (EPBT) in days for the different components of the solar park presented here.

voltages are an integral part of the installation even if we have not observed this yet. The biological issue is subject to variation in different parts of the world. Deforestation is a critical issue in tropical forests, but not in boreal forests in the Nordic countries and while we have employed wood that was sustainably produced we also assume that the wood used in large scale solar parks would be obtained sustainably. Unsustainable forest management causes 20% of the climate change, and 25% of the forest trade is estimated to be illegal according to the World Wildlife Fund (WWF). Sustainability of forestry is not limited to ecology but also influence human rights for workers, indigenous people, outdoor people, long term economy for local societies etc. Since forestry is much more complicated to assess, compared to for example metals, it is necessary to stick to relevant certification systems.^[24]

4. Materials and Devices for Solar Parks: A New Research Direction

Until now the approach to making polymer solar cells a success has been to develop materials that yield the highest efficiency in an often unrealistic laboratory setting involving materials with low abundance or toxic chemicals and processes that are not scalable. Most often the important issue of operational stability has also been neglected and it is only recently that this has gained appreciation as being important. When viewed from above this approach has been extremely successful when it comes to demonstrating that polymer solar cells has the capacity to yield a high power conversion efficiency that is comparable to many inorganic solar cell technologies. The approach has however failed at progressing beyond academic reports due to the complex fundamental challenges associated with creating efficient materials that are also stable, scalable and that fit in a large scale process. We have attempted the roll-to-roll processing of nearly every reported high efficiency material shortly after its publication and have only a small selection of materials that yield good large scale performance when roll-to-roll processed in large area and P3HT:PCBM still remains the best overall performer. It should also be noted that the power conversion efficiencies do not reach anywhere near the high efficiencies reported for very small areas in scientific publications. The finding of my group and the conclusion after many years of attempting is that things have to be turned upside down to be successful and it is unrealistic that one can take a material that is optimized for achieving high efficiency in a specific laboratory setting and assume or expect that it can perform similarly when subjected to a large scale process that has several limitations or requirements when comparing to the laboratory experiment. We have attacked this problem intensively since the first high efficiency materials were reported 5 years ago without success and now have firm evidence that another approach is needed. One could say that instead of making the process fit the material, the material has to fit the process. By taking the end product (i.e., a solar park based on the Infinity concept) and the known processing space into account when making materials selection and adaptation the natural selection of materials is forced to meaningfully comply with where we would like to end up. Once a material has been identified we

are granted immediate success as the newly developed material can be put straight to work by installation in our energy producing system. It should finally be emphasized that the newly developed materials must have a simple and low cost synthesis. It is unlikely that a multistep synthetic route to a high performance material can be justified on the basis of high efficiency. Multistep- synthetic materials are known to be justified within medical products but it is highly unlikely to be the case for bulk materials for large scale energy production. Activities along the lines outlined above are hopefully stimulated by this report and several solar parks in different geographical locations would be highly warranted.

4.1. Materials for Processes

In addition to the active material which by many is viewed as the work horse of the organic solar cells, there are several other layers in the polymer solar cells stack that play an equally important role in achieving high performance. Adhesives, printable conductors, printable interlayers and substrates are an integral part of the polymer solar cell and they need to fit the process flow that has been selected for manufacture of the polymer solar cell based on other parameters than stability and efficiency. Most often operator safety, printability, coatibility, curing method, curing time, materials usage, embodied energy, technical yield and cost are elements that enter the selection. The optimal choice of the process parameters and the materials for it present near infinite variation and having fixed the application, installation method, manufacturing method and module design it is important to fix as many additional parameters as possible and here the adhesive is especially important since it is a quite costly material that enter the process in significant volume and it plays a decisive role when it comes to the operational stability of the final roll of solar cells. The semi-transparent conductor which today most rationally comprise PEDOT:PSS is another highly important material that embodies a lot of energy (both in the material and the process) and development in this area is also key to future success. This reduces to the fact that the scientific community needs a common platform for testing and optimizing new materials very much in the same manner as the spincoater, vacuum evaporator, cleanroom, glovebox, ITO-glass substrates etc. have played a decisive role in the development of highly efficient miniature laboratory OPV. My group has worked for many years to build the foundation that enables such a change. A common solar test platform^[25] and a mini roll coater^[26,27] that enable facile scaling to R2R machinery using very small quantities of active material (commercially available from an external company). More importantly the flexible ITO-free substrate^[28] that is employed in the Infinity-concept is made available for free to academics thus in principle enabling the change from ITO to something that is more sustainable and being offered for free it is the largest encouragement we can offer. Finally a common module platform in which new materials can be tested and compared has been developed recently. It comprises an ITO-free structure similar to the Infinity concept and complete and functional modules are available also for free.^[28] New materials across all levels (active materials, conductors, adhesives, transport layers

etc.) can be tested on this platform and directly compared and if they constitute progress they can be applied in i.e. an Infinity solar park. The most important aspect is the philosophy dictating that it should be free for academics and serving the common aim of propagating OPV as a future energy producing technology. Studying materials for the desired processes thus represent a new research direction that should be encouraged.

4.2. Silver Freedom and Recycling

The current approach employs only printing and coating methods on flexible substrates and does not use ITO. Since approximately the same performance is achieved with this new method as compared to the ITO approach it does constitute significant progress. Before heralding this as enabling it should be underlined that the Infinity process employ printed silver grids instead of ITO and silver has about the same natural abundance as indium so the advantage from this point of view is reduced to having enabled printed electrodes and avoidance of vacuum processing that while significant does not stand as tall as one could have hoped for. It has been shown that carbon can be used instead of silver for active areas with a small outline and resulting limits on the size of the active area.^[29] An all carbon method is clearly desirable but also implies more use of carbon in electrodes since it is a poorer electrical conductor. Central to the question of carbon vs. silver is the recycling of the solar cells after de-installation and indeed whether de-installation is necessary. In the case of a carbon-based solar cell the solar cell foil has a thickness of ca. 100 μm in its installed form and can release 5 MJ in heat if combusted properly after its service life. It could however be more efficient simply to install new solar cell foil on top of the old foil and handle the waste once the installation is deconstructed (i.e., after 15 years of operation as assumed here). In the case of solar foil based on silver electrodes the silver does constitute a materials resource and since silver is potentially very easy to recover the use of silver in the electrodes might be justified since the de-installation scheme demonstrated here allows for facile recovery of the solar foil in a compact form post-usage (in the form of a roll). Combustion, recovery and re-use of the silver is thus very likely to be an advantage and may justify use of silver over a pure carbon technology. This is currently a research topic that is highly advisable to pursue.

4.3. Moisture and Oxygen Barrier Foil

The barrier foil together with the adhesive constitute the majority of the Infinity solar foil by weight and volume and it thus plays a crucial role in the energy balance, cost and environmental impact of the OPV technology. Barrier foil and adhesive also account for the entry paths of water and oxygen into the solar cell stack and since these paths must be minimized (or ideally eliminated) there is a large research effort devoted to finding the optimum balance between operational service life for a given solar cell architecture and the use and cost of the barrier and adhesive. The barrier foil should ideally be available at very low cost and free from toxic materials and processing

steps in its manufacture. The current version comprises thin polymer layers with thin impervious coatings that are laminated together and comprise a UV-filter/hardcoating for the improvement of outside weather stability. It is unlikely that the plastic used in the barrier material can be recycled for re-use in OPV since this requires high purity and quality for drawing thin plastic foil with few defects. While it is likely that combustion comprise the most rational decommissioning method the possibility for developing barriers or barrier components that could be partially recycled constitute a valiant research goal.

4.4. Large Scale Installation and Operation

It is clear that the installation of large sized solar parks following this concept that efficiently explores all the advantages of the polymer solar cell while avoiding or accommodating the disadvantages should be considered as reserved for professionals wishing to produce and supply electricity by renewable means. Installing, operating and maintaining safety in a high voltage installation is unlikely to be realistically deployed in a public setting and private households. This however is no different from how for instance nuclear power plants are operated today and we do not view this as an impediment to the implementation of high-voltage solar parks based on OPV. It is however clear that the supply chain, the people operating the solar parks and the decommissioning is not available today and this large infrastructure will have to be scaled to meet these needs. To underline the scale of it we can take as an example the production and installation of 1 GW_{peak} of polymer solar cells with the presently achieved performance (Figure 3 and Figure 4). This would require 137 square kilometers of solar cell foil underlining the need for not only better materials but also better module design that has a higher geometric fill factor. It is clear that an improvement is possible but probably not more than by a factor of around ten. It should however be clear that the scale is manageable with the ideas demonstrated in this work.

5. Conclusions

We have demonstrated the manufacture and installation of a solar park based on polymer solar cells following a concept that takes advantage of the uniquely defining quantities for OPV while elegantly manoeuvring around the challenges for OPV when viewed in the context of traditional inorganic solar cells that are panel-based. We find that it is possible to install OPV at a rate much faster than any other PV technology and extract energy efficiently with thin cables using a high voltage installation. We demonstrate and describe the use of such an installation that also inherently enables recovery for recycling or decommissioning (while installing new material). We further discuss the new research directions that would further strengthen and support this effort and highlight that new and advanced materials must be developed for the context of the application (the solar park), the manufacturing method (fast roll-to-roll processing) using only abundant materials and flexible substrates (low cost barriers and adhesives). We have

emphasized that such a change requires new platforms and we have described how this has been made freely available to the academic community (ITO-free substrates and a new polymer solar cell module process as a vector for research). We have shown that the research is deeply rooted in, and directed by life cycle analysis and illustrate how a short energy pay-back time for the solar park demonstrated here is possible by choice of a wooden structure, roll-based installation and high voltage connections. The current solar park has an energy payback time of 180 days everything included when operated in a southern European setting which implies that OPV can be used for energy production already today. We also conclude that realistic improvements to the OPV technology will revolutionize use of solar energy.

Acknowledgements

This article is part of an ongoing series celebrating the 25th anniversary of *Advanced Materials*. We are indebted to technical assistance from Kristian Larsen and Torben Kjær during erection and maintenance of the solar park and for legislative and projecting assistance from Esben Højrup, Christian Henriksen, and Allan A. Murphy in the initial and planning phases. This work was supported by the Danish Ministry of Science, Innovation and Higher Education through the EliteForsk initiative, through the 2011 Grundfos Award and Energinet.dk (project no. 10728).

Received: May 6, 2013

Revised: July 12, 2013

Published online: October 8, 2013

- [1] M. C. Scharber, D. Mühlbacher, M. Koppe, P. Denk, C. Waldauf, A. J. Heeger, C. J. Brabec, *Adv. Mater.* **2006**, *18*, 789.
- [2] A. McEvoy, L. Castañer, T. Markvart, *Solar Cells, 2nd ed.*, Elsevier, **2013**.
- [3] *Roadmap for Organic and Printed Electronics, 4th ed.*, OE-A, Organic Electronic Association, 2011.
- [4] *Renewable Energy Technologies: Cost Analysis Series, Solar Photovoltaics*, International Renewable Energy Agency (IRENA), June 2012.
- [5] a) R. Søndergaard, M. Hösel, D. Angmo, T. T. Larsen-Olsen, F. C. Krebs, *Mater. Today* **2012**, *15*, 36; b) R. R. Søndergaard, M. Hösel, F. C. Krebs, *J. Polym. Sci., Part B: Polym. Phys.* **2013**, *51*, 16.
- [6] *ISO 14040*, International Organisation for Standardisation (ISO), Geneva, Switzerland, **1997**.
- [7] N. Espinosa, M. Hösel, D. Angmo, F. C. Krebs, *Energy Environ. Sci.* **2012**, *5*, 5117.
- [8] L. Schleisner, *Renewable Energy* **2000**, *20*, 279.
- [9] E. A. Alsema, M. J. de Wild-Scholten, presented at the European Photovoltaic Solar Energy Conf. and Exhibition, **2005**, Barcelona, Spain.
- [10] K. Knapp, T. Jester, *Sol. Energy* **2001**, *71*, 165.
- [11] R. H. Crawford, G. J. Treloar, R. J. Fuller, M. Bazilian, *Renewable Sustainable Energy Rev.* **2006**, *10*, 559.
- [12] G. A. Keoleian, G. M. Lewis, *Renewable Energy* **2003**, *28*, 271.
- [13] M. Raugei, S. Bargigli, S. Ulgiati, *Energy* **2007**, *32*, 1310.
- [14] K. Kato, T. Hibino, K. Komoto, S. Ihara, S. Yamamoto, H. Fujihara, *Sol. Energy Mater. Sol. Cells* **2001**, *67*, 279.
- [15] A. L. Roes, E. A. Alsema, K. Blok, M. K. Patel, *Prog. Photovoltaics: Res. App.* **2009**, *17*, 372.
- [16] R. García-Valverde, J. A. Cherni, A. Urbina, *Prog. Photovoltaics: Res. App.* **2010**, *18*, 535.

- [17] M. Pehnt, *Renewable Energy* **2006**, 31, 55.
- [18] D. Y. C. Leung, X. L. Yin, C. Z. Wu, *Renewable Sustainable Energy Rev.* **2004**, 8, 565.
- [19] *Life-Cycle Energy Balance and Greenhouse Gas Emissions of Nuclear Energy in Australia*, Consultancy Report ISA, The University of Sydney, Australia **2006**.
- [20] H. Hondo, *Energy* **2005**, 30, 2042.
- [21] A. J. Medford, M. R. Lilliedal, M. Jørgensen, D. Aarø, H. Pakalski, J. Fyenbo, F. C. Krebs, *Opt. Express* **2010**, 18, A272.
- [22] P. Sommer-Larsen, M. Jørgensen, R. R. Søndergaard, M. Hösel, F. C. Krebs, *Energy Technol.* **2013**, 1, 15.
- [23] *Clean Power from Deserts the DeserteC Concept for Energy, Water and Climate Security WhiteBook, 4th ed.*, Protext Verlag, Bonn, February 2009, http://www.desertec.org/fileadmin/downloads/DESERTEC-WhiteBook_en_small.pdf.
- [24] L. H. Gulbrandsen, *J. Environ. Dev.* **2005**, 14, 338.
- [25] F. C. Krebs, K. O. Sylvester-Hvid, M. Jørgensen, *Prog. Photovoltaics: Res. App.* **2011**, 19, 97.
- [26] H. F. Dam, F. C. Krebs, *Sol. Energy Mater. Sol. Cells* **2012**, 97, 191.
- [27] J. E. Carlé, T. R. Andersen, M. Helgesen, E. Bundgaard, M. Jørgensen, F. C. Krebs, *Sol. Energy Mater. Sol. Cells* **2013**, 108, 126.
- [28] a) M. Hösel, R. R. Søndergaard, M. Jørgensen, F. C. Krebs, *Energy Technol.* **2013**, 1, 102; b) F. C. Krebs, M. Hösel, M. Corazza, B. Roth, M. V. Madsen, S. A. Gevorgyan, R. R. Søndergaard, K. Dieter, M. Jørgensen, *Energy Technol.* **2013**, 1, 378.
- [29] T. T. Larsen-Olsen, R. R. Søndergaard, K. Norrman, M. Jørgensen, F. C. Krebs, *Energy Environ. Sci.* **2012**, 5, 9467.
- [30] Website with news from R&D in organic photovoltaics by DTU Energy Conversion at the Technical University of Denmark, <http://www.plasticphotovoltaics.org>, accessed: September 2013.

Large scale deployment of polymer solar cells on land, on sea and in the air†

Cite this: *Energy Environ. Sci.*, 2014, 7, 855

Nieves Espinosa, Markus Hösel, Mikkel Jørgensen and Frederik C. Krebs*

With the development of patterns that connect all cells in series, organic photovoltaics have leapt a step forward being ahead of other solar and even other energy technologies in terms of manufacturing speed and energy density. The important questions of how they are meant to be installed for producing power and what the requirements are yet to be explored. We present here the installation of organic solar cell modules in different settings (terrestrial, marine and airborne). For the evaluation of these installations deployed at DTU, we have used the life cycle assessment tools, and calculated key parameters in order to assess their environmental impact. The novel technology when installed in a solar park system can generate more than 1300 kW h kW_p⁻¹ of electricity a year, which means that the whole system can pay the energy invested back before the first year of operation, in 320 days. If this electricity is fed back to the same electricity supply system that was used for manufacturing the potential saving of more than 13 GJ of primary energy per kW_p per year can be reached. With the real data logged, a dynamic energy payback time has been furthermore calculated for the case of the solar tube installation, giving a value of 1.1 years.

Received 25th September 2013
Accepted 17th December 2013

DOI: 10.1039/c3ee43212b

www.rsc.org/ees

Broader context

Fast modes of manufacture warrant fast modes of installation and low impact energy technology requires low impact installation methods. The polymer solar cell when printed in quasi-infinite rolls is best installed directly from the roll and new methods of installation are enabled. We demonstrate very low impact installation methods of polymer solar cells on land, on sea and in air, all possible due to the unique properties of OPV. We find that short system energy pay-back times are possible even with these laboratory/pilot scale printed polymer solar cells and highlight that closing the observed gap in performance between laboratory hero cells and large scale devices as presented here will be the birth of the best performing renewable energy technology ever conceived.

1. Introduction

Greenhouse gas accounting and ecological foot printing as a result of electricity generation are concerns that every energy technology with the ambition to enter the energy supply chain must consider to counteract global warming. We employ the term of an ecological footprint for the technology and imply this as the complete measure on human demand on Earth's ecosystems. It does include not only the carbon emission footprint (CO_{2eq} per kW per h_{el} generated) but also other categories that account for human welfare and biocapacity use in general. It is clear that renewable energies and PV in particular present the smallest carbon factor emissions.^{1,2} Photovoltaics have a steep learning curve and one of the PV technologies, the organic photovoltaic (OPV) family, has been shown to have the smallest ecological footprint and the shortest energy payback time possible.³⁻⁶ The prospect of organic photovoltaics as being a

competitive energy technology however requires that new forms of installation are employed such that their advantages can be fully explored in comparison to other forms of energy.

A good tool to properly compare energy options is Life-Cycle Assessment (LCA). As a tool it was developed to compare clearly defined end-product alternatives but it has been rapidly incorporated at all levels and today LCA is employed at even the very high strategic levels including decision- and policy-making. Life-cycle assessment is currently used for assessing a wide range of products and activities, from eco-labelling to product design as well as food production, transportation alternatives and to assess the sustainability of energy systems.⁷

In this work, we present an evaluation of the sustainability of different grid-connected installations for organic solar modules deployed at DTU through use of the LCA tool. The photovoltaic modules used in these installations have been manufactured according to the Infinity-concept, which is a refined version of the IOne process.⁸⁻¹⁰ This route has been proven to be one of the most successful to OPV manufacturing using the bulk hetero-junction concept and its main feature is the low requirement of energy, both in the materials and in the process: no indium-tin-oxide is used, no vacuum steps are involved, only printing

DTU, Energy Conversion and Storage, Frederiksborgvej, 399, Roskilde, Denmark.
E-mail: frkr@dtu.dk

† Electronic supplementary information (ESI) available. See DOI: 10.1039/c3ee43212b

and coating steps are used and furthermore the processing takes place directly on the barrier foil at low temperature and high speed. This ultra-small cumulative energy demand (CED) results in a low energy payback time (EPBT), that is the time it takes for them to generate the same amount of energy that is embodied in the materials and spent during their manufacture. A further aspect is that a high voltage (a consequence of a quasi-infinite serial connection) is employed which is one of the best ways to transport electrical energy at little loss through thin printed conductors.

The first electricity grid-connected organic photovoltaic installation was demonstrated in 2009,¹¹ and recently a solar park based on the Infinity concept^{2,10} has been inaugurated at DTU. The main motivation of this solar park is the proof-of-concept for OPV in the context of large-scale electrical grid power production with a low environmental footprint. This mind-set is also reflected in the design; from the modules manufacturing, throughout the careful selection of the components based only on sustainability criteria and all the way to the materials in the support structure. For example, a wood-based structure has been used for the solar park since it presents several advantages but mostly due to its truly renewable origin: the emissions released when making a wooden structure as compared to concrete or metallic structures are 3 times lower¹² and further wood has advantages such as being corrosion resistant and durable when installed in a fashion that allows it to dry. The fast manner in which the modules are meant to be installed and uninstalled on the structure, the mounting surface, and the number of replacements possible are also reflections of the mind-set.

Lighter forms and rapidly deployable systems, apart from being useful in energy production on a large scale, could potentially provide benefits on a smaller scale as well; such as for example emergency communications in the wake of a disaster – when existing networks have been damaged – or in the case of remote applications integrating sensors that have to send/receive data.¹³ Therefore, alternative forms of installations based on light plastic structures were designed with the idea of designing a sustainable solution to that challenge. These new concepts are offshore, onshore and airborne light installations that were realized at DTU and they have been proven and analysed in this work. Our concept for offshore installations is foreseen to be lighter and having a lower impact than other offshore systems that comprise conventional inorganic technologies, such as the deployment termed Solar Islands.[‡] While these islands are floating and comprise robust rotating platforms for silicon modules, our offshore design can be a really low cost alternative in terms of capital investment since they do not require heavy construction works and steel platforms to support heavy modules. Offshore OPV could complement other offshore energy technologies such as offshore wind farm that produces 160 MW in an area of 20 km².§ If organic solar modules are placed in between the wind mills occupying 50% of

this area, with our present 0.8% total area power conversion efficiency (PCE) solar cells, 80 MW of additional power could be produced. With our first successful prototypes the technological gap between traditional and latest technologies could be filled and be part of portable land or offshore deployment units, by supplying a rapid response service. In addition they are light and can be transported anywhere without being subject to damage due to their flexibility.

2. Life cycle assessment methodology

Until now, large-scale energy producing installations that integrate OPV modules, as the ones presented in this work, have not been built up or even assessed. Evaluating different choices for the deployment of a solar installation requires a methodology that permits us to establish analogies between them. Life cycle assessment (LCA) has proven to be a very powerful tool and very useful so far in the context of OPV spanning the fabrication of modules^{3-5,14} and applications that include them.^{15,16} The main reason is that LCA studies provide an image of how this product will eventually impact the environment along its lifespan; but furthermore this tool keeps track of energy forms used in the final product or service, so that we are left with a real picture of what has been taken from nature to give shape to the product or installation. The cumulative energy demand – CED – in primary energy units (MJ_{EPE}) accounts for these total energy needs and it has in this work been calculated with our own processing data and the Ecoinvent database. It has served to obtain the energy payback time (EPBT), calculated as the CED divided by the energy that the modules generate in their lifetime (E_{GEN}) following International Energy Agency guidelines.¹⁷ Going further we also explore how many times the system returns the energy embedded in its fabrication if any, and this figure is termed energy return of investment (EROI). E_{GEN} and both indicators have been calculated using the following equations, where G is the irradiation in kW h per m² per year units, PR is the performance ratio, ¶ η is the module efficiency on the total area and P_p is the power peak installed – all the values considered for the assessment are gathered in Section 4.2.

$$E_{\text{GEN}} = \frac{G * PR * \eta}{P_p}$$

$$\text{EPBT} = \frac{\text{CED}}{E_{\text{GEN}}}$$

$$\text{EROI} = \frac{L E_{\text{GEN}}}{\text{CED}} = \frac{L}{\text{EPBT}}$$

‡ Solar island prototype in Switzerland. <http://www.solar-islands.com>.

§ Based on data from Horns Rev 1 Offshore Wind Farm in Blåvandshuk (Denmark).

¶ Performance ratio is the internationally introduced measure for an entire PV system. It accounts for the overall effect of losses due to array temperature, incomplete utilization of the irradiation and failures of the system components.

Cumulative energy demand is correlated with the energy payback time, so the lower is the former the faster the system pays back the energy invested, and that is a way to lower the EPBT. However, there is a reciprocal relationship between EPBT and PCE – since the energy generated by the system, E_{GEN} , depends on the radiation level and on the power conversion efficiency (PCE) of the PV system. While the conversion efficiency is often used as the metric to evaluate the performance and potential usefulness of a technology or system, usually more complex processes or materials are required. It has been discussed elsewhere¹⁸ that it may happen that for a particular OPV technology an increase in efficiency is also accompanied by such an increase in CED that balances out and in the end does not result in a shorter EPBT. The most powerful use of LCA, when used to evaluate energy options, is to direct research and development towards a sustainable product rather than being directed by some artificial goal of high power conversion efficiency. The latter is a valiant cause but not at any cost.

Since energy payback time does not take into account the whole scale of the problem at hand or the potential unavailability of elements or components, life cycle impact assessment (LCIA) of the installations has been performed through use of the commonly available LCA software: SimaPro. Two methods representing different approaches that are included in this software have been considered. First, CML 2000 was selected as a midpoint method and ReCiPe 2008 for the endpoint approach. Both approaches differ in the way in which the environmental relevance of category indicators is taken into account.¹⁹ In the former approach²⁰ relevance is given to the potential for causing damage (problem-oriented), while the latter focuses on the damage in itself (damage-oriented). The CML baseline version includes nine impact categories, from which we have extracted eight. The other method ReCiPe⁷ is a hybrid method that connects the midpoint and the endpoint-oriented methods, allowing the user to choose. In this work we chose the endpoint methodology and included indicators such as climate change, human toxicity or fossil depletion. The characterisation factors of impacts are expressed in different units (see Table 1) and we have chosen to present them normalized and weighted for a better comparison between the different deployments explored in this work. Therefore, the metric is given in the dimensionless unit Pt, obtained by weighting all the impact loads.

The level of uncertainty in the two approaches differs; the endpoint approach has a higher level of uncertainty when compared to midpoint level. Two basic kinds of uncertainties have to be distinguished: the first one is due to the calculation and modelling (used to describe a physical phenomenon), the other one is introduced as far as the inventory dataset may be reliable and accurate. The soundness of every impact indicator is scored ('+++ = high reliability to '+' = very low reliability) in Table 1. The scores for the reliability of the calculation methods are representative of today's state of the art for impact assessment within the LCA framework; additional work is in progress to improve the indicators related to human and ecosystem

Table 1 Impact category indicators considered in this life cycle analysis, their units and the expected reliability on the calculation methods

Impact category	Unit	Reliability in calculation methods
Cumulative energy demand	MJ EPE	+++
Abiotic depletion	kg eq. Sb	+
Global warming potential	g eq. CO ₂	+++
Acidification potential	g eq. SO ₂	++
Eutrophication potential	g eq. PO ₄	+
Photochemical oxidation	g eq. ethylene	+
Climate change human health	DALY	+
Particulate matter formation	DALY	+
Ionising radiation	DALY	+
Metal depletion	\$	+++
Fossil depletion	\$	+++
Agricultural land occupation	Species, year	+
Climate change ecosystems	Species, year	+
Urban land occupation	Species, year	+
Terrestrial ecotoxicity	kg 1,4 DB	+
Ozone layer depletion	kg eq. CFC-11	+
Human toxicity	kg 1,4 DB	+

health. The confidence in the inventory dataset in this study is very high, since it builds on real data recorded from pilot-scale production equipment and processes.

A third LCIA methodology was employed to calculate the carbon footprint of the produced modules and their installation in different forms. The Greenhouse Gas Protocol, the most used tool to quantify and manage greenhouse gas emissions, displays four types of carbon emissions: fossil based carbon originating from fossil fuels; biogenic carbon originating from plants and trees; carbon from land transformation; and carbon uptake (*i.e.* the CO₂ that has been stored in plants and trees as they grow).

3. The four installation scenarios

3.1 Solar park installation

The concept of the solar park has been reported in detail in recent publications^{2,10} and it is constructed using wooden scaffolds and plates that are facing south at an inclination angle of 38 degrees (Fig. 1). Each of the four rows of 100 m long platforms that comprise the solar park has a theoretical mounting area of 250 m² for solar cells, and the whole solar park setup has a size that is visible using satellite imagery highlighting that OPV has increased enormously in scale.²¹ Up to 7 stripes of solar cell modules currently manufactured in a width of 305 mm can be mounted side-by-side using a special wagon that holds one roll and moves from one end of the scaffold to the other while rolling out the OPV. Currently the stripes are fixed using weather-proof tape that is attached while rolling out the module. The power output from 6 parallel-connected modules on the platform with a cumulated active area of 88.2 m² is more than 1330 W at roughly 1 sun illumination that corresponds to an efficiency of more than 1.5% on the active area after burn-in. The average output per

|| SimaPro Software 7.3.3, PRE Consultants, 2011.

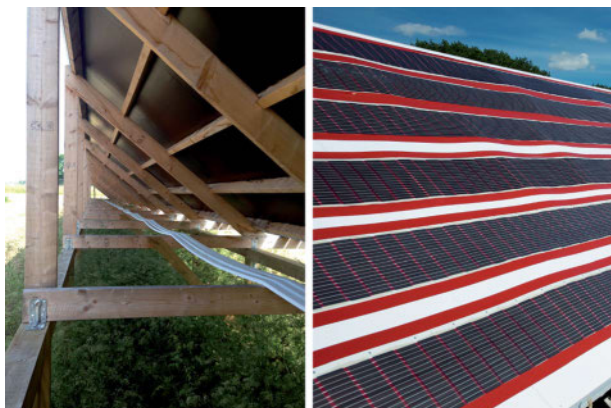


Fig. 1 Photograph of the wooden scaffold structure of the solar park installation (left) with six solar cell module strips mounted on top of PVC plates (right).

stripe was more than 220 W or 2.2 W per meter of Infinity module. For grid-connection, a down conversion of the high voltage system is necessary (the open circuit voltage of each 100 m stretch is above 10.000 V).

3.2 Tube-in-tube concept

The alternative on- and offshore installation designs are based on a self-supporting inflated tube of low density polyethylene (LDPE) with a thickness of 200 μm that have been first built in small dummy setups to learn how to fabricate them in an efficient way. To avoid any air leakage from cable feed-through we developed a tube-in-tube concept where the inner tube is fully sealed. The workflow of setting up the tubes is illustrated in Fig. 2.

We prepared tubes with solar cell module lengths of 3.4 m ($A_{\text{active}} \text{ ca. } 0.5 \text{ m}^2$), 6.8 m ($A_{\text{active}} \text{ ca. } 1 \text{ m}^2$), and 10 m ($A_{\text{active}} \text{ ca.}$

1.5 m^2). The inner tubes were slightly longer than the modules, and correspondingly the outer tubes to enable sealing and fixation with ropes (offshore) or hooks (onshore). An automatic sealing machine was used for closing the tubes, leaving one end open for a couple of centimetres to enable the final inflation, which was completed in just 5 seconds. During the preparation, the inner tube and an Infinity solar cell module were fed together into the outer tube. The manual preparation of the sets was feasible up to a module length of 10 meters corresponding to 1 kV open circuit voltage. The solar cells were electrically connected using cables soldered to push buttons that allow a fast mounting with the counterpart of the push button on the module. When the inner tube was inflated the solar cell stripe was fixed by the pressure of the inner tube against the outer one, however the final inclination of solar cells was adjusted by turning the cells and tubes towards the sun.

3.3 Offshore solar tube installation (on water)

The offshore version of the tubes was set up at the pier of DTU Risø campus in the Fjord of Roskilde and had a total of 5 parallel-connected tubes with a total active area of 5 m^2 . Each tube was connected with ropes to the pier to demonstrate the basic idea of the floating solar installation (we also made pilot experiments with a single tube during the winter of 2013). A photograph of the installation with the cells facing south and an I - V -curve is shown in Fig. 3. The maximum power output was $>30 \text{ W}$ with an efficiency of 0.6%, which was lower than expected. We ascribe this to some challenges in the installation where the modules experienced some rough handling as a result of the land-to-water method of installation and it is likely that the deployment from a float should be explored in the future. Although the modules are not perfectly inclined we measured almost the same current output from each module. The distance between each tube allows a shadow-free illumination over most of the day. Waves and wind can be seen as the most

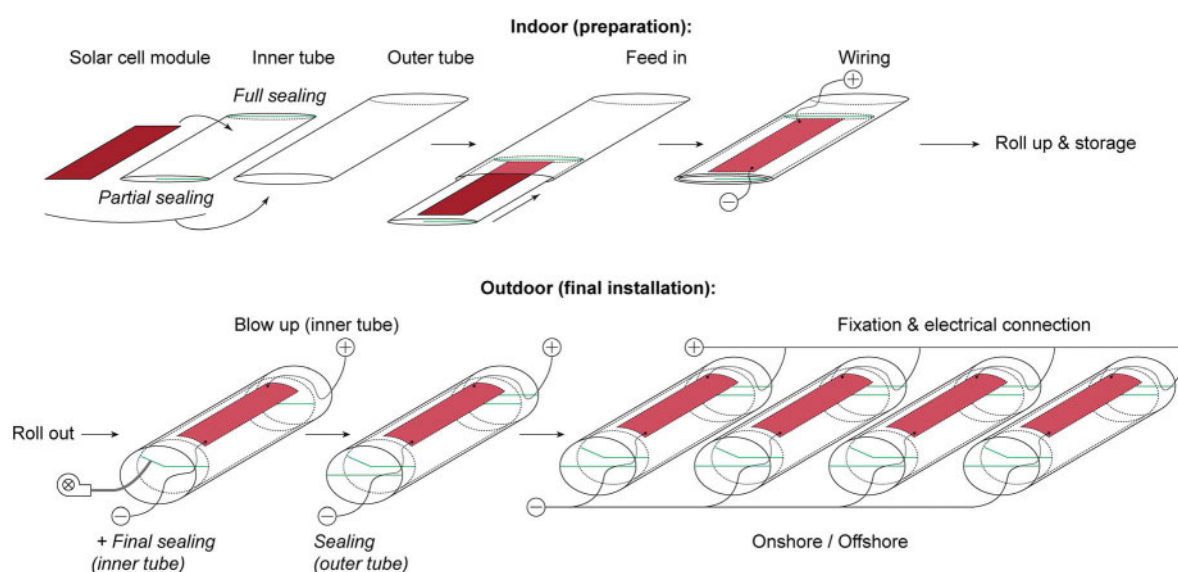


Fig. 2 Preparation and installation workflow of the tube-in-tube mounting concept.

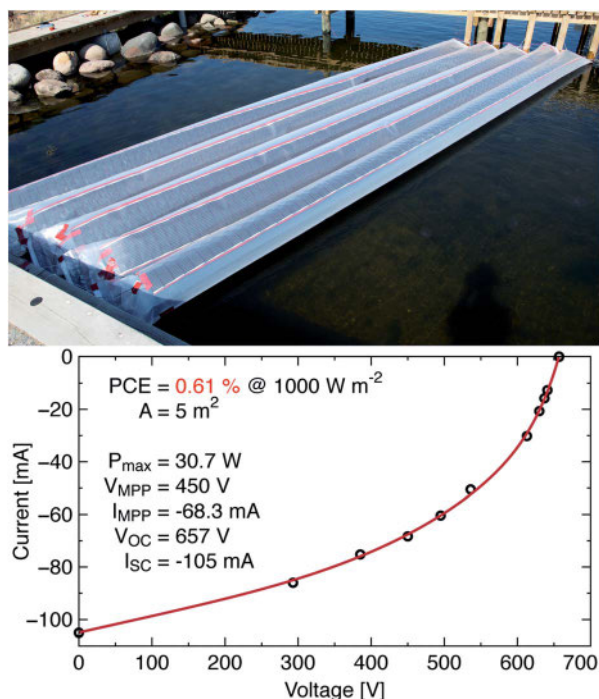


Fig. 3 Photograph of the offshore solar cell installation with five tubes of an overall length of ca. 7.5 m (top) and a corresponding I - V -curve (bottom).

critical factor that has to be considered for future offshore platforms based on this design. Bending and crumpling on long stretches must be avoided.

3.4 Onshore solar tube installation (on land)

An onshore or ground-based version of the tubes has been installed in the front row of the solar park at DTU. Here a first set of six tubes with 3.4 m long modules (Fig. 4) was extended with six modules of 6.8 m to generate enough power to be handled through the inverter (0.6–1 kV input voltage). Finally, nine 10 m long modules were added to give a total module area of ca. 50 m². The long tubes were not inflated because of difficulties in keeping the inclination of solar cells stable. Therefore, the flat version of solar cells in LDPE tubes can be seen as a further installation scenario. A photograph of the full setup side by side with the other land-based



Fig. 4 Ground-based onshore solar cell installation with the rolled-up tubes prior to blow-up (left) and the final setup of six 3.4 m solar cell modules (right).

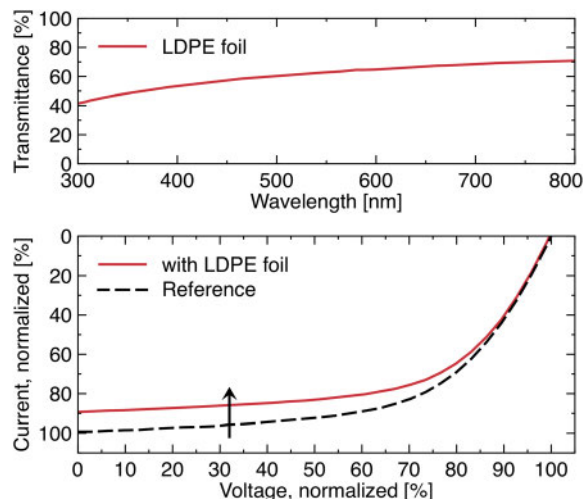


Fig. 5 Transmittance spectrum of the opaque LDPE foil that covers the solar cells (top). I - V -curve behaviour of a solar cell with and without LDPE foil on top (bottom). The efficiency drops by 8%.

installations is also shown in Fig. 6. All the tubes were connected to the inverter, delivering around 200 W on average to the grid. Since the tubes were grid-connected on the 5th July 2013, they have performed stably.

Compared to the properly fixed and inclined solar cells from the wooden solar park structure we saw a drop in efficiency for the solar cell inside the tubes. The main reasons are the different inclinations for each individual tube and in some cases partial shadowing. Furthermore, the opaque LDPE foil blocks some light due to a direct transmittance of 50–70% over the whole visual spectrum. Interestingly, this only results in an 8% drop of efficiency with improved fill factor as can be seen from the normalized I - V -curves in Fig. 5. We ascribe this to part of the transmission loss being due to diffuse scattering, which is collected by the solar cell.

3.5 Balloon solar installation (balloon)

The last and by far the most experimental installation scenario is the tethered balloon with mounted solar cells. Foils of LDPE with a surface area of 40 m² were sealed to form a pillow-shaped balloon with the size of 4 m × 5 m along the edges. Five solar cell modules with a combined active area of 2.5 m² were attached on one half of the top side of the balloon and connected in series to increase the voltage. Long cables enabled a ground-based power extraction. The volume of the idealized pillow shaped helium balloon was calculated so that 17 m³ would generate enough lift and up to 8 kg of additional load. Finally, we filled the balloon with 16 m³ of helium and floated it to a height of roughly 10 m. The balloon was aligned and held with ropes so that the solar cells had a good inclination for the I - V measurements. Photographs and a corresponding I - V -curve are shown in Fig. 6.

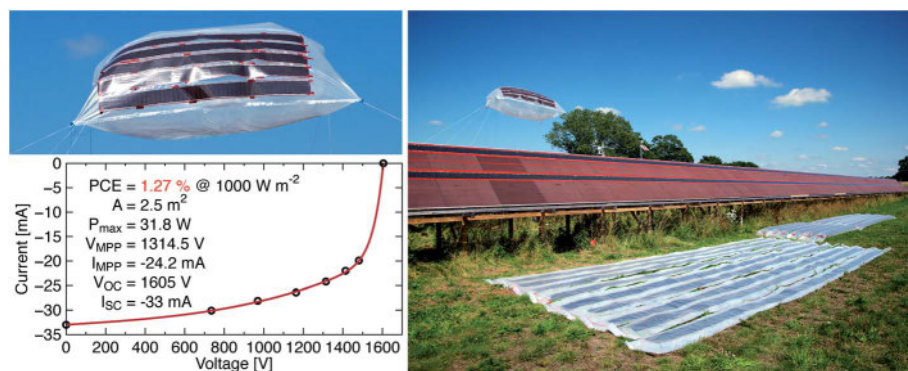


Fig. 6 Photograph of the helium-filled balloon with attached solar cells and an I - V -curve (left). The photograph on the right shows three installation scenarios combined – balloon, wooden solar park structure (with just 2 stripes of solar cells), and tubes (flat, and blown-up in the background).

4. The assessment of the OPV installations

The OPV modules are integrated in different structures or installations and they constitute a building block or a structural element; therefore we present a separate and detailed LCA analysis for them in the first section. Following that we have analysed the different balance of systems (BOS) of the different installations in which the modules produced by the same manufacturing route were integrated.

4.1 The assessment of the organic modules

Energy analyses of several manufacturing routes for producing organic solar modules in a semi industrial environment have already been performed using the LCA methodology. It was firstly applied for an ITO-based route named ProcessOne³ which highlighted that ITO accounted for an excessive amount of the embodied energy and the direct process energy. This led to development of ITO-free modules following different routes that were analysed using the LCA methodology. Several approaches were studied including an aluminium-chromium electrode,^{22,23} silver and also carbon based electrodes.^{5,24} Recently, a preliminary evaluation of the organic solar cell modules was done. They were prepared by the route known as

IOne⁸⁻¹⁰ and were mounted in a solar park and analysed.² Since our analysis work is always based on a real manufacturing set up and OPV is at an early development stage, slight improvements have been made in the speed, in the power for curing the adhesives, optimisations in printing forms, *etc.* All these changes can affect from moderately to strongly the needs of energy and materials. We therefore present here a refined analysis of the already published work, with the recent improvements included.

The modules are printed on a flexible ITO-free substrate called Flextrode²⁵ that is employed in the Infinity-concept, and which is now free available to academics.²¹ Thanks to the pattern employed in the Infinity-concept, it is possible to manufacture an infinite serial connection of both cells and modules in the direction of the web thus stepping up voltage along the web or roll. The modules are printed on a plastic barrier substrate from Amcor with a front electrode, PEDOT:PSS and ZnO – taken together this is called the Flextrode. The finalisation of the module is made with the active material, in this case P3HT:PCBM, a second layer of PEDOT:PSS and the silver back electrode. The top encapsulation is made with a UV curable adhesive. This results in an initial 2.2% efficiency on the active area. The module lifetime is 1 year and the functional unit considered for the LCA is one square meter of processed foil, in which the active area is 50% of total area ratio.

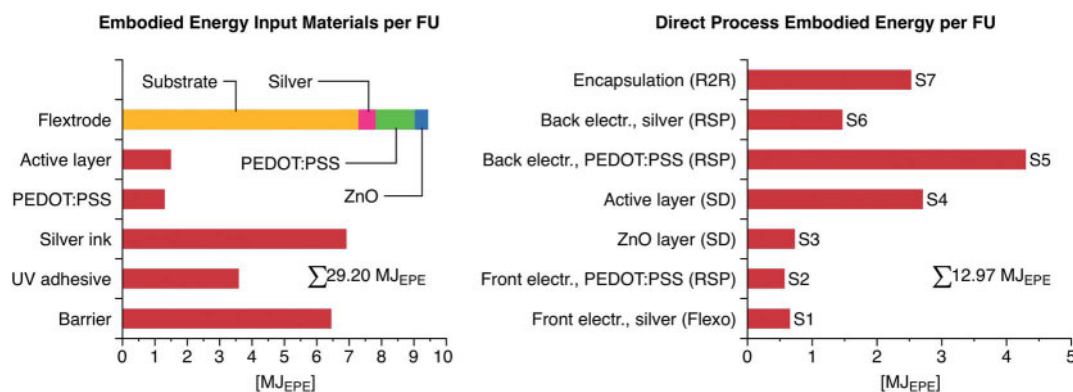


Fig. 7 Energy embodied in the materials and spent in the process of manufacturing 1 m² of organic modules produced with the Infinity pattern.

We show the results for the calculations on cumulative energy demand for 1 m² of modules in Fig. 7, where it can be observed that (in agreement with previous studies) the share of the energy that has to be used in the materials still remains two thirds of the total energy and one third being employed in the manufacturing phase of the modules. However, there has been a tremendous optimization of the IOne process with regard to the former routes which is reflected in the achieved reduction of energy required; from the several hundreds of MJ_{EPE} that were required for the manufacture of ProcessOne to IOne where only 42.17 MJ_{EPE} are needed. In Fig. 7 it is clear that the substrate containing four different materials (the Flextrode) requires a considerable part of the total materials energy. On the other hand the most expensive material in terms of energy to be deposited is by far PEDOT:PSS, due to the slow processing at 2 m min⁻¹ and to the use of infrared lamps for drying it (see ESI for more details on the data†).

4.2 The balance of systems assessment

The OPV modules, all of them manufactured in similar batches of 700 m length, were hosted in four different installations: solar park, onshore, offshore and a balloon – all shown in Fig. 3, 4 and 6. Their components and the structures are detailed in Table 2 (see also the ESI†). Each installation was conceived for a different purpose, and therefore had a different size. The solar park was originally devised for the sustainable production of electrical energy from OPV on a large scale, while the tubes and the balloon were envisaged for shorter operational lifetimes, being useful as a portable energy source or in communication systems. Their lifetimes and components employed in the systems are different. The lifetime of the structure defines the lifetime of the system. The wood based solar park is considered to last for 15 years, and since the lifetime of the modules is here assumed to be 1 year it is assumed that 15 replacements of modules will have to take place. In the case of the tubes either if they are onshore or offshore it has been estimated that they last for 2 years. The balloon is only considered to last for one month.

4.2.1. Inventory. The construction of the deployed OPV systems is detailed in the previous section, but to assess them we first present the list of all components and the energy associated with them, which includes not only their manufacture from raw materials but also their assembly into systems.

In the search for sustainable materials for the solar park scaffold, as the platform that serve for the installation/

deinstallation of the modules wood was chosen as shown in Fig. 1. The energy embedded in the scaffold has been taken as the average from a relevant study²¹ and from the Ecoinvent database,²⁶ resulting roughly in 270 GJ_{EPE}. We have explored using wood as the mounting surface but have also explored other mounting surfaces to ensure a more even surface in the joints between mounting plates and also to observe differences in electrical insulation. PVC foam plus wood was thus chosen in this study on the scale of 250 m² each. While other materials are possible the purpose here was not to exhaustively test all conceivable materials but rather to take two at opposite ends of the scale in terms of sustainability (wood is best, PVC is worst) and see how they impact the overall picture. So the combination PVC foam plus wood resulted in a CED of 615.7 GJ_{EPE} with data taken from Ecoinvent database.

For the other deployments, a much lighter structure made of low-density polyethylene (LDPE) tubes served as a support for onshore and offshore tubes, already explained in the previous section. Plastic film, LDPE, with a thickness of 200 μm was used, resulting in 3.5 and 1 GJ_{EPE}, respectively for onshore and offshore installations.

The cabling in the solar park is guided back from the end of each row (where the positive and negative terminals of the series are) to the middle of the rows and from thereon they are led through a subterranean tube to a hut with the inverter. The copper, cables and associated materials for their conduction to the endpoint were included in this study, but the hut was not. For the onshore tube installation, the cabling was guided in the same manner through the same system. For the other deployments cabling was 2.5 mm² section insulated copper cable, with an energy that was extracted from the Energy Inventory from Bath University.²⁷

The cabling reaches the inverter inside the hut. This inverter detailed in Table 2 has been used for all installations, which may be evidently oversized for the onshore and offshore tubes, and for the balloon system. For the LCA calculations of each system the energy needed for an ideal inverter with right power has been scaled and taken into account.

Results are shown in Fig. 8. In the energy invested in the structure for the solar park, the introduction of PVC as the mounting surface has a strong impact; it almost doubles the embodied energy thus underlining the need to use sustainable low energy materials as mounting surfaces. Wood alone is here found to be the best choice. In all the installations the energy embodied in the structure accounts from 47% to

Table 2 Main features and characteristics of components and materials required for the four OPV installations

Components	Park	Onshore	Offshore	Balloon
OPV module area	960 m ²	50 m ²	10 m ²	2.5 m ²
Structure	17 m ³ wood, 960 m ² supportive PVC, 1 cm	45 kg LDPE, 200 μm	10 kg LDPE, 200 μm	5.40 kg LDPE, 200 μm
Inverter	Inverter 6 kW Danfoss, TLX series	Inverter 50 W ^a	Inverter 250 W	Inverter 37 W
Cabling (copper wire)	500 m, 10 mm ²	82 m, 2.5 mm ²	40 m, 2.5 mm ²	30 m, 2.5 mm ²
Wagon station	35 m aluminium profiles	—	—	—
Power installed (<i>W_p</i>)	7860	403.2	80	20
Lifetime of the system	15 years	2 years	2 years	1 month

^a An estimated inverter has been considered for the accountancy, although 6 kW was used in these experiments.

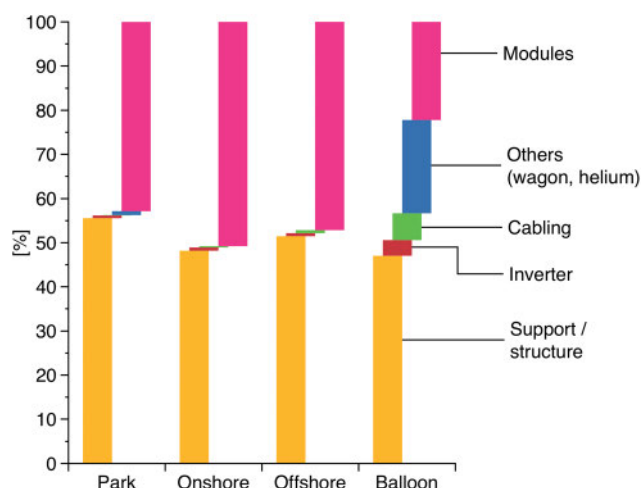


Fig. 8 Breakdown of cumulative energy demand required for every component in the balance of system of each installation (shown in percentages).

55% with respect to the total energy for the installation, while the modules represent from 22% to 50%. Inverters and cabling energy represent a little amount, being in all cases below 1%. For the balloon, a big share is embedded in helium that accounts for 21% of the total energy – see ESI† for details on the data.

After all the accountancy, the solar park including PVC embeds a total of 670 GJ_{EPE}, the onshore tubes account for 5.25 GJ_{EPE}, the offshore for 1.61 GJ_{EPE} and the balloon for 0.95 GJ_{EPE}. However, since they were all built in different sizes, in order to make fair comparisons, for each installation all the requirements of energy have been scaled to 1 m² of installed OPV modules per year of lifetime. So we have therefore scaled the energy requirements for the structure, cabling, inverter and other elements that were necessary for 1 m² of OPV modules and have then made the comparison. Once scaled, the solar park is still the deployment with the highest energy associated, even though they all fall close ranging from 83 to 180 MJ_{EPE} per m² per year. Table 3 illustrates this comparison of the installations and also shows the kind of energy that is required.

4.2.2. Assessment. For the evaluation of the impact of PV systems, the energy payback time – EPBT – was calculated for the different installations (see in Table 3). In order to have a comparison with other technologies and provide meaningful numbers, we have calculated an EPBT under standard conditions; assuming that the modules are installed in a location under 1700 kW h per m² per year irradiation (typical of Southern-Europe), that they have PCE of 1.6% in active area – or 0.8% in the total area – and that they work with a performance ratio of 0.8. The value for the performance ratio for the deployments on air or on water might be considered high for such systems since there are factors that influence negatively; e.g. the longer length required would incur in larger power losses. However, because the modules last for relatively short time which means that other components would not barely degrade, and because of the beneficial effect of the lower temperature that the cells would be working at, they would balance out the negative influences on the PR. The conversion factors used from primary to electrical or thermal energy are 0.35 and 0.85 respectively. In the case of the solar park, 1328.85 kW h per kW_p per year of electricity can be thus generated so that if this electricity is fed back to the same electricity supply system that was used for manufacturing, then we can save 13.66 GJ of primary energy per kW_p per year. Energy payback times and energy return factors of the installations – shown in Table 3 – are comparable with the latest and best published results for silicon based technologies in the range of 0.9–0.7 years for EPBTs and from 13–16 value for EROIs.²⁸ It is clear that the balloon does not pay back the energy used in its manufacture, however it was not conceived as an installation that had to do that, but for its use in emergency systems.

The first stripes of modules were installed in the solar park already in August 2012 though they could not be connected to the grid unattended due to a high voltage regulation. However, the tubes were grid-connected on the 5th July 2013 and the electricity output was logged: 1 kW h per sunny day has been summed up from the start date. In order to see whether the assumed conditions – for a southern location – were over-estimated, a dynamic EPBT for the onshore tube installation was estimated based on the real data. This real EPBT, plotted in Fig. 9, is based on the actual energy produced during

Table 3 The primary energy consumption of the BOS components sized to 1 m² of OPV modules –1.6% PCE – for the four types of installations, and the energy payback times and EROI of the systems functioning in a location with 1700 kW h per m² per year and a PR of 0.8. L stands for lifetime

	Park	Onshore	Offshore	Balloon
BOS component				
Support/structure (MJ _{EPE} m ⁻²)	54.71	40.01	46.03	96.89
Inverter (MJ _{EPE} m ⁻²)	0.61	0.61	0.61	0.61
Cabling (MJ _{EPE} m ⁻²)	0.08	0.25	0.62	1.86
Others (MJ _{EPE} m ⁻²) (Wagon station/helium)	0.88	—	—	38.66
Modules (MJ _{EPE} m ⁻²)	42.17	42.17	42.17	42.17
Total	98.45	83.05	89.43	180.20
E _{GEN} (MJ _{EPE} per m ² per year)	111.90	111.90	111.90	111.90
EPBT (years)	0.88	0.74	0.80	1.61
EROI (L/EPBT)	17.04	2.50	2.69	0.05

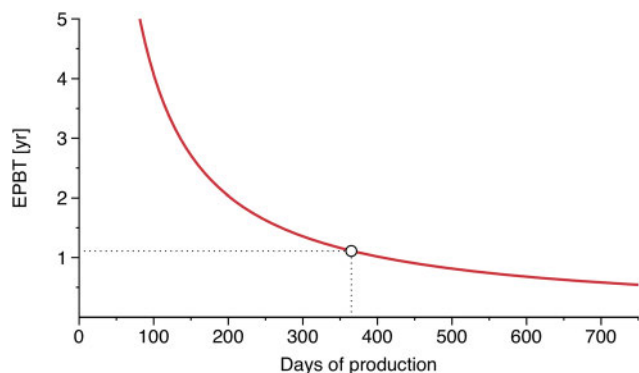


Fig. 9 Energy payback time in years for the onshore tube installation, based on real energy produced and fed into the Danish electricity grid. The dot marks one year of energy production where the energy embedded would be almost paid back (EPBT = 1.11 years).

summertime in Denmark and fed into the Danish electricity grid. We found the real EPBT was 30% larger than the theoretical in Table 3. The plot in Fig. 9 shows how the EPBT started

being 400 years and rapidly decreased to reach a 1.1 years level at the end of the first year of operation.

4.2.3. Environmental impact assessment. The sustainability of the installations has been evaluated by means of the SimaPro software. Three methods have been selected that allow for assessing accurately the environmental impact of the installations. In Fig. 10 and 11 we present respectively the impact score on the most relevant categories of a functional unit of OPV modules; *i.e.* 1 m² being installed in each of the four installations, following both CML and ReCiPe methods. The metric for ReCiPe scores is given in the dimensionless unit Pt, obtained by weighting all the impact loads. In the case of CML methodology data are normalized from the software. Normalisation data are described elsewhere²⁹ and more details about weighting and normalization of impact factors can be found in the ESI.†

For the modules produced by the Infinity route, silver accounts for 45% of the total impact by ReCiPe and 68% of the categories of CML methodology; thus underlining that efficient recycling schemes for silver needs to be developed or that silver must be entirely avoided in the finally refined OPV technology. The fossil fuel depletion category is highly impacted with

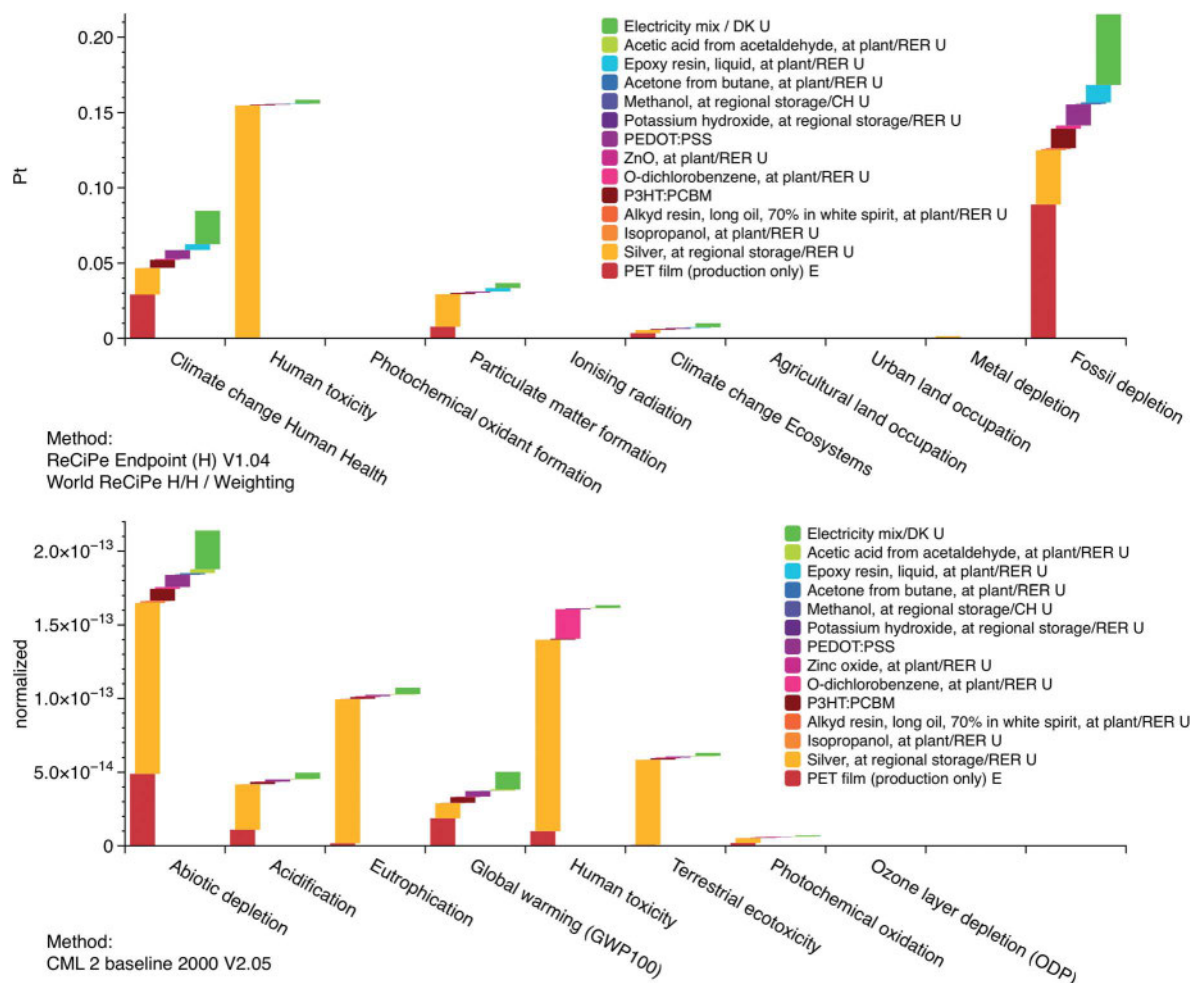


Fig. 10 Weighted environmental impacts of OPV modules analyzed by ReCiPe (top graph) and normalized impacts by CML (bottom graph). Both are LCA methodologies available in SimaPro. RER stands for average Europe and U for unit process in SimaPro.

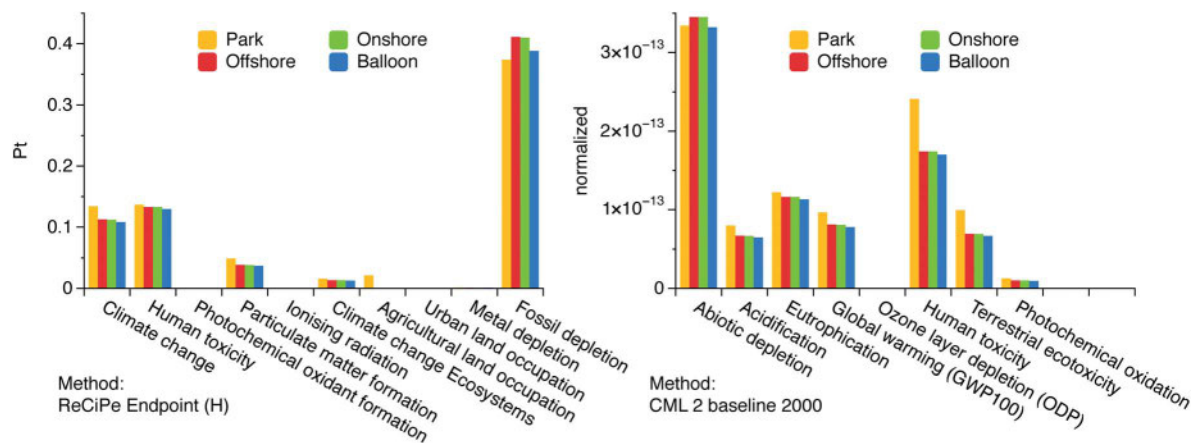


Fig. 11 Environmental impact of the four installations by two different assessment methods in SimaPro: CML and ReCiPe.

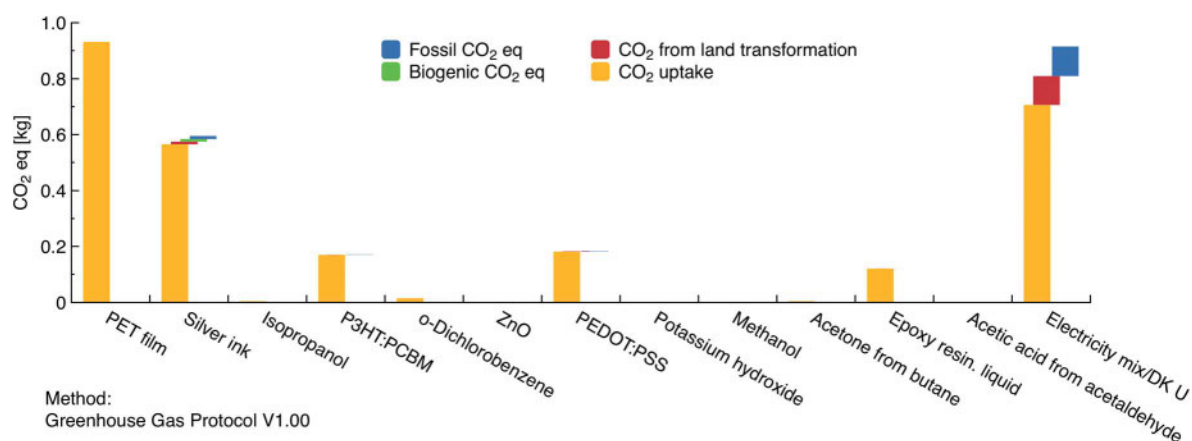


Fig. 12 Greenhouse gas emissions corresponding to one square meter of organic solar cells prepared by the IOne manufacturing route.

respect to the others and the main cause is the use of PET and electricity.

The most impacted category from the CML method is in every case abiotic depletion with *ca.* 40%, and then human toxicity. For the offshore, onshore and the balloon system the OPV modules are responsible for this impact with a 50% share, followed by the LDPE plastic foil. In the solar park however the use of PVC causes 60% of the impact in all categories, yet again highlighting the need for carefully choosing the material used as a mounting surface.

Using the ReCiPe methodology, we found similar results. Fossil fuel depletion is the most impacted category for all the installations up to 67% in the case of the balloon, and even for the modules. For the onshore and offshore installations, and the balloon the source of the fossil depletion is the LDPE plastic foil, while in the solar park it is due to the PVC (when used).

We have also applied the Greenhouse Gas Protocol embedded in SimaPro to calculate the equivalent CO₂ in kilograms per functional unit of module produced. And we found that the corresponding emissions were a total of 2.94 kg CO₂eq., that if rated per kW h of energy produced (known as the emission factor) amounts to 57.55 g of equivalent CO₂ (detailed in

Fig. 12). The latest publications in the PV field state emission factors for thin-film technologies ranging between 57 and 17 g of equivalent CO₂.¹ Therefore it is clear that OPV is well placed in comparison with well-established PV technologies when tackling environmental issues.

5. Discussion

The polymer and organic solar cell has been the subject of intense study with the aim of realising the vision of a low cost widely distributed green energy producing technology. As a photovoltaic technology the organic solar cell is distinct from the other photovoltaic technologies but it is also an extremely diverse solar cell. The record efficiency is claimed to be very high and approaching other thin film photovoltaics³⁰ whereas a sober view of the current status is best found by looking at all the organic solar cell data published and comparing this to other PV technologies. In a recent database study this enormous task was undertaken and it does show that the organic solar cell as a general rule falls below all other technologies.³¹ This of course does not rule out the fact that the technology can be developed to reach the record efficiencies claimed in a few

laboratories but it does show that the majority of competent researchers fall short of reaching the claimed potential. A question one could ask is whether the currently reachable performance is sufficient on its own such that efforts in scaling and development of methods can be pursued. It is likely that such developments can be carried out in parallel with performance enhancing efforts and if they can co-develop such that the future high performing OPV is directly compatible with the scaling and deployment methods then time is saved. Scaling and deployment efforts can also establish if OPV is already good enough as it is, or alternatively give an accurate view of exactly how good the performance will have to be before it is viable. It is clear that OPV has advantages that no other PV technology has. It is also clear that OPV has disadvantages that are mostly associated with low performance and relatively short stability. In terms of stability, OPV is still inferior to *i.e.* crystalline silicon. OPV however does seem to exhibit outside stability of several years as this has been demonstrated in several independent studies.^{32,33} One advantage is that the OPV can be fully printed and this enables the manufacture of endless solar cell foil that following the Infinity concept can be cut to any length and most interestingly that the performance is independent of the length of foil (at least up to 700 metres). It has been demonstrated for 100 metre stretches of foil that there is no difference in performance between a single cell and more than twenty thousand solar cells connected in series. This fact is unique and it enables the printing of interconnections such that no extra wires or strings need to be applied in post-production steps to make a module, one could say that the roll of solar cell is the module regardless of size. This simple fact has enormous implications when it comes to scaling since the question of scalability is reduced to clever ways of deployment rather than having to deal also with manual issues of contacting and connecting single devices into modules and systems post-production. We already demonstrated that the polymer solar cell can have an energy payback below one year even when manufactured under laboratory conditions.² The objective of the present work was to progress beyond what is possible with conventional solar cells and identify novel methods of fast and low impact deployment that has not been possible hitherto.

The solar park that we already had explored has served as a starting point and we have analysed this with respect to the impact that small changes in the scaffold would have on its energy balance. In the calculation the building time of the scaffold has been neglected. The result has been found to be sensitive while not extraordinarily sensitive (we showed it here for PVC mounting plates). We then progressed beyond this to establish if a low cost technology that can be readily deployed could be subject to simple installation means, and if possible it would enable us to explore territories that are not easily accessible with traditional solar cells. Most traditional solar cells are heavy and rigid thus making them difficult to deploy in a different context than on-land. The polymer solar cells are light and flexible thus potentially enabling one to explore both airborne and waterborne installation methods. We chose polyethylene as the carrier material simply because of its availability and flexibility. We developed the concept of having the solar cell

laminated between two tubes where the inner tube could be air filled (Fig. 2). The inner tube could be air-filled and its deployment worked equally well on land or on the surface of sea water (Fig. 3, 4 and 6). When installing on land one could also simply avoid air filling the inner tube. Nevertheless, the air filling is likely to be the most robust method with respect to precipitation in the form of rain or snow. The airborne experiment was mostly included to demonstrate that the lightness enables it but it is unlikely to be practical in the long run simply because tethering is a challenge over time when subject to weathering. This is also true for both land based and water based installations but the requirements are less strict and most straightforward for the land based version. One surprising outcome is that the energy payback time for the entire on-shore installation is just over 1 year based on the actual data which is very significant since the calculation included everything. We can conclude that both the on-shore and the water surface installations are viable methods of deployment of OPV modules. In response to one of the reviewer comments we also explored the effect of salt spray and dried salt on the solar cells surface which can be expected for the off-shore installation (even if we did not observe it). This demonstrated a relatively small drop in efficiency similar to the LDPE foil employed in the tubes which we ascribe to the optically transparent nature of sea salt which scatters light (see ESI†).

6. Outlook

There is a large gap between the average performance that can be reached for polymer cells and the best reported data. As this gap hopefully closes the polymer solar cell will move from being an already viable technology to a highly competitive energy technology. We have shown that currently available OPV technology can be manufactured and deployed in a setting where the energy is delivered back during the lifetime of the solar cell. When the performance gap is closed the polymer solar cell will outperform many if not all known energy technologies in terms of manufacturing speed, scalability, speed of deployment and removal, environmental foot print and energy payback time. If significant research efforts were focussed on closing the gap in the relevant polymer solar cell technology, *i.e.* the Infinity concept, then the ambitious goal of a fossil free future will move remarkably close.

Acknowledgements

This work has been supported by Energinet.dk (project no. 10728) and by the Danish Ministry of Science, Innovation and Higher Education under a Sapere Aude Top Scientist grant (no. DFF - 1335-00037A).

References

- 1 H. C. Kim, V. Fthenakis, J.-K. Choi and D. E. Turney, *J. Ind. Ecol.*, 2012, **16**, S110–S121.
- 2 F. C. Krebs, N. Espinosa, M. Hösel, R. R. Søndergaard and M. Jørgensen, *Adv. Mater.*, 2014, **26**, 26–39.

- 3 N. Espinosa, R. García-Valverde, A. Urbina and F. C. Krebs, *Sol. Energy Mater. Sol. Cells*, 2011, **95**, 1293–1302.
- 4 A. L. Roes, E. A. Alsema, K. Blok and M. K. Patel, *Progress in Photovoltaics: Research and Applications*, 2009, **17**, 372–393.
- 5 N. Espinosa, M. Hösel, D. Angmo and F. C. Krebs, *Energy Environ. Sci.*, 2012, **5**, 5117–5132.
- 6 J. Peng, L. Lu and H. Yang, *Renewable Sustainable Energy Rev.*, 2013, **19**, 255–274.
- 7 M. Goedkoop, R. Heijungs, M. Huijbregts, A. De Schryver, J. Struijs and R. Van Zelm, A life cycle impact assessment method which comprises harmonised category indicators at the midpoint and the endpoint level, ReCiPe 2008, 2009.
- 8 D. Angmo, S. A. Gevorgyan, T. T. Larsen-Olsen, R. R. Søndergaard, M. Hösel, M. Jørgensen, R. Gupta, G. U. Kulkarni and F. C. Krebs, *Org. Electron.*, 2013, **14**, 984–994.
- 9 J.-S. Yu, I. Kim, J.-S. Kim, J. Jo, T. T. Larsen-Olsen, R. R. Søndergaard, M. Hösel, D. Angmo, M. Jørgensen and F. C. Krebs, *Nanoscale*, 2012, **4**, 6032–6040.
- 10 P. Sommer-Larsen, M. Jørgensen, R. R. Søndergaard, M. Hösel and F. C. Krebs, *Energy Technol.*, 2013, **1**, 15–19.
- 11 A. J. Medford, M. R. Lilledal, M. Jørgensen, D. Aarø, H. Pakalski, J. Fyenbo and F. C. Krebs, *Opt. Express*, 2010, **18**, A272.
- 12 Å. Jönsson, T. Björklund and A.-M. Tillman, *Int. J. Life Cycle Assess.*, 1998, **3**, 216–224.
- 13 A. Valcarce, T. Rasheed, K. Gomez, S. Kandeepan, L. Reynaud, R. Hermenier, A. Munari, M. Mohorcic, M. Smolnikar and I. Bucaille, in *Personal Satellite Services*, ed. R. Dhaou, A.-L. Beylot, M.-J. Montpetit, D. Lucani and L. Mucchi, Springer International Publishing, Cham, 2013, pp. 13–25.
- 14 R. García-Valverde, J. A. Cherni and A. Urbina, *Progress in Photovoltaics: Research and Applications*, 2010, **18**, 535–558.
- 15 N. Espinosa, R. García-Valverde and F. C. Krebs, *Energy Environ. Sci.*, 2011, **4**, 1547–1557.
- 16 N. Espinosa, F. O. Lenzmann, S. Ryley, D. Angmo, M. Hösel, R. R. Søndergaard, D. Huss, S. Dafinger, S. Gritsch, J. M. Kroon, M. Jørgensen and F. C. Krebs, *J. Mater. Chem. A*, 2013, **1**, 7037–7040.
- 17 V. Fthenakis, R. Frischknecht, M. Raugei, H. C. Kim, E. A. Alsema, M. Held and M. J. de Wild-Scholten, *Methodology Guidelines on Life Cycle Assessment of Photovoltaic Electricity*, International Energy Agency, 2011.
- 18 N. Espinosa and F. C. Krebs, *Sol. Energy Mater. Sol. Cells*, 2014, **120**, 692–700.
- 19 J. C. Bare, P. Hofstetter, D. W. Pennington and H. A. U. Haes, *Int. J. Life Cycle Assess.*, 2000, **5**, 319–326.
- 20 J. B. Guinee, *Handbook on Life Cycle Assessment: Operational Guide to the ISO Standards*, Kluwer Academic Publishers, Dordrecht, 2002.
- 21 <http://Plasticphotovoltaics.org>.
- 22 M. Manceau, D. Angmo, M. Jørgensen and F. C. Krebs, *Org. Electron.*, 2011, **12**, 566–574.
- 23 N. Espinosa, R. García-Valverde, A. Urbina, F. Lenzmann, M. Manceau, D. Angmo and F. C. Krebs, *Sol. Energy Mater. Sol. Cells*, 2012, **97**, 3–13.
- 24 D. Angmo, M. Hösel and F. C. Krebs, *Sol. Energy Mater. Sol. Cells*, 2012, **107**, 329–336.
- 25 M. Hösel, R. R. Søndergaard, M. Jørgensen and F. C. Krebs, *Energy Technol.*, 2013, **1**, 102–107.
- 26 <http://Ecoinvent.ch>.
- 27 C. Jones, *Inventory Carbon Energy V2*, Bath University, HammondJones, 2011.
- 28 S. A. Mann, M. J. de Wild-Scholten, V. M. Fthenakis, W. G. J. H. M. van Sark and W. C. Sinke, *Progress in Photovoltaics: Research and Applications*, 2013, DOI: 10.1002/pip.2363.
- 29 M. A. J. Huijbregts, L. Breedveld, G. Huppes, A. de Koning, L. van Oers and S. Suh, *J. Cleaner Prod.*, 2003, **11**, 737–748.
- 30 M. A. Green, K. Emery, Y. Hishikawa, W. Warta and E. D. Dunlop, *Progress in Photovoltaics: Research and Applications*, 2013, **21**, 827–837.
- 31 M. Jørgensen, J. E. Carlé, R. R. Søndergaard, M. Lauritzen, N. A. Dagnæs-Hansen, S. L. Byskov, T. R. Andersen, T. T. Larsen-Olsen, A. P. L. Böttiger, B. Andreasen, L. Fu, L. Zuo, Y. Liu, E. Bundgaard, X. Zhan, H. Chen and F. C. Krebs, *Sol. Energy Mater. Sol. Cells*, 2013, **119**, 84–93.
- 32 M. Jørgensen, K. Norrman and F. C. Krebs, *Sol. Energy Mater. Sol. Cells*, 2008, **92**, 686–714.
- 33 J. A. Hauch, P. Schilinsky, S. A. Choulis, R. Childers, M. Biele and C. J. Brabec, *Sol. Energy Mater. Sol. Cells*, 2008, **92**, 727–731.



Roll-to-roll fabrication of polymer solar cells

As the performance in terms of power conversion efficiency and operational stability for polymer and organic solar cells is rapidly approaching the key 10-10 targets (10 % efficiency and 10 years of stability) the quest for efficient, scalable, and rational processing methods has begun. The 10-10 targets are being approached through consistent laboratory research efforts, which coupled with early commercial efforts have resulted in a fast moving research field and the dawning of a new industry. We review the roll-to-roll processing techniques required to bring the magnificent 10-10 targets into reality, using quick methods with low environmental impact and low cost. We also highlight some new targets related to processing speed, materials, and environmental impact.

Roar Søndergaard, Markus Hösel, Dechan Angmo, Thue T. Larsen-Olsen, and Frederik C. Krebs*

Department of Energy Conversion and Storage, Technical University of Denmark, Frederiksborgvej 399, DK-4000 Roskilde, Denmark

*E-mail: frkr@dtu.dk

In order to reach its full potential, the imminent realization of the 10 %-10 yr target within the laboratory must transcend into a realistic industrial process. While this may seem trivial to many and even obvious to some, there are challenges that have perhaps been taken too lightly in laboratory reports. Often tiny spin coated devices prepared on rigid glass through toxic solvent processing and metal evaporation is said to be roll-to-roll and industry compatible. The view held here is that claiming to be roll-to-roll and industrially compatible without such instruments is similar to claiming that one can learn how to swim on a floor.

Solution processing, low cost, low energy budget, flexible solar cells, are keywords associated with organic solar cells, and through several decades the driving force for research within the field of polymer solar

cells has been the huge potential of the technology to enable high throughput production of cheap solar cells. The evolution started with small area cells that used simple and relatively inexpensive techniques such as spin coating and thermal evaporation for the fabrication¹. The unstable nature of conjugated polymers when illuminated in the presence of oxygen, and the reactive nature of low work function metals such as calcium towards water quickly led to the preparation of organic photovoltaic (OPV) devices in the protective atmosphere of a glove box. The main reason was the desire to raise power conversion efficiencies towards levels that are meaningful in the context of global energy supply. Claims of meeting these goals have now been made for small area solar cells (a few mm² to around 1 cm²) with efficiencies reaching 8 – 9 %^{2,3}, (and reports above 10 % from Mitsubishi) but the field of organic solar

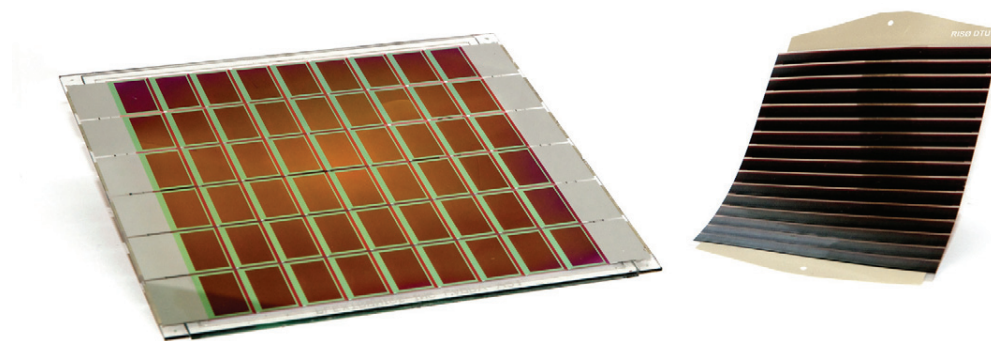


Fig. 1 An illustration of possibly the most refined example of an OPV module prepared using the laboratory route, comprising rigid glass substrate, spin coating, metal evaporation, getter materials, and a glass seal with a thick outline of several millimeters (left) and a flexible fully solution processed polymer solar cell module with a thickness of around one hundred microns (right).

cells is now facing the huge challenge of returning focus towards the original goal of large area production using a high throughput process. Such a shift in methodology does not automatically appear.

The general fabrication methods of spin coating and high vacuum thermal evaporation are not compatible with high throughput production which should preferably be performed in a continuous process such as roll-to-roll (R2R) processing. As a consequence of both the economical aspect of acquiring and running the necessary machinery and the focus on high efficiencies, the number of participants working with large area solar cells in true roll-to-roll coating processes has previously been limited. It should also be highlighted that the power conversion efficiency is considerably lower for larger area devices (currently < 3.5 %) ². In order for the organic solar cell to succeed as a technology, more effort must be directed towards large area fabrication combined with high throughput processing such as roll-to-roll methods. In this report we review some of the different printing and coating techniques that are fully compatible with R2R processing, and which could potentially be used in future mass production.

Film and device formation

An enormous palette of film forming techniques has been developed and many of them might be suitable for processing one or more of the layers in a polymer solar cell. In terms of development, an interesting distinction of the polymer and organic solar cell (when compared to most of the existing inorganic solar cell technologies) is that the development of processing methods for inorganic solar cells have been driven and defined by the solar cell technology. For polymer and organic solar cells, the possibility of solution processing has overturned this picture, and the wide selection of printing and coating techniques available may end up being what defines polymer solar cell technology.

When looking at OPVs as a technology it is important to consider our current position, which is in the doorway between the controlled and safe laboratory environment (behind us) and the outside world and field of application (in front of us). As our premise, we have the spin coating technique and the solution processed laboratory device. Our desire is to

find the right combination of techniques that will yield the same result albeit on a larger scale, by a factor of > 1 000 000 in terms of both processed area and processing time (and several other parameters). In Fig. 1 we illustrate this by presenting a very refined version of a rigid solar cell module prepared using the laboratory method with good performance in terms of stability and efficiency ⁴. In comparison we also illustrate a similarly sized flexible module prepared without a vacuum, produced entirely through roll-to-roll methods, using mainly water as the processing solvent. Both modules were prepared on laboratory scale equipment but while the total processing time for the rigid module is measured in days, the total processing time for the flexible roll-to-roll processed module is measured in seconds. The potential for increasing the throughput speed is present in both cases but the upper limit is inherently slower for the rigid module than for the roll-to-roll processed module.

In the most refined laboratory polymer cell, high performance is achieved through a delicate and highly empirical relationship between the processing method, the solvents, the additives, the drying, the materials, the substrate, and perhaps even the operator. When having to change virtually all these parameters in the effort to upscale, one may ask whether the laboratory performance should automatically be taken for granted in the large area roll-to-roll processed device? The answer is of course that it should not. A good argument in support of this view is that several high performing materials were reported years ago, but there have been no reported examples of high performing large area devices prepared by roll-to-roll methods using these materials (and it is not because it has not been attempted). The reason is that we have to re-invent or re-discover the processing conditions for the new setting which is not at all obvious, especially when considering that there are boundary conditions involved in fast roll-to-roll processing (speed, temperature, drying, multilayer processing, solvents, materials). In addition to this we do not know which printing or coating method will be the best choice for each layer in the polymer solar cell, which is typically comprised of five or more layers. There may thus be different film forming methods that are optimal for each layer in the stack. To approach the challenge constructively it is necessary to be confronted

with these facts and use them as a guide. One should take the view that for a given materials selection there is a rational choice of both film forming methods and operating parameters.

In the following we will describe many of the available film forming methods with a view towards how they are particularly suited for processing polymer solar cells using roll-to-roll methods. We also stress that there are several important choices that should be made early on to avoid redoubling development efforts. As an example, an intimate part of a printing or coating technique is the solvent employed. We already know that the processing of OPVs on the gigawatt scale does not leave room for the use of any solvents other than water and perhaps some alcohols. Any effort spent using environmentally harmful chlorinated and/or aromatic organic solvents is thus likely to prove to be a wasted effort. A final point is that the OPV technology allows for very low processing temperatures and very thin outlines with low embodied energy. Life cycle analysis (LCA)⁵⁻⁸ and financial analysis of roll-to-roll processed OPVs⁹⁻¹² are also tools that are used to direct research, and which have demonstrated that roll-to-roll processing of OPVs could yield very short energy pay-back times (EPBT) using simple approaches. By avoiding scarce elements such as indium, avoiding the use of vacuum processing, and using only solar heat and solar electricity, an energy payback time of

the order of 1 day has been demonstrated to be possible¹³. This shows that researchers should be encouraged to go where it is difficult and try and address the difficult properties, rather than go where it is easy and then try and address the difficult properties. We should thus start out directly with roll-to-roll processing in the ambient atmosphere without a vacuum, using only environmentally benign solvents and processing methods. From here we should develop stable, low cost, and efficient solar cells. Any efforts reaching those latter properties in a manner that is not scalable at the 1-gigawatt-a-day level are likely to be in vain.

Printing techniques (wet films through contact)

Since the development of the printing press by Johannes Gutenberg (1440) 'the art of printing' has evolved to include a multitude of techniques; some of which are represented in Fig. 2. These techniques each have their own advantages and disadvantages, but they all rely on the same principle of transferring ink from a solid printing form to a substrate. Printing implies the transferring of a motif to a substrate through physical contact between the object carrying the motif and the substrate, and further implies that the pattern is two-dimensional. One exception to this rule is ink-jet printing where there is no direct contact.

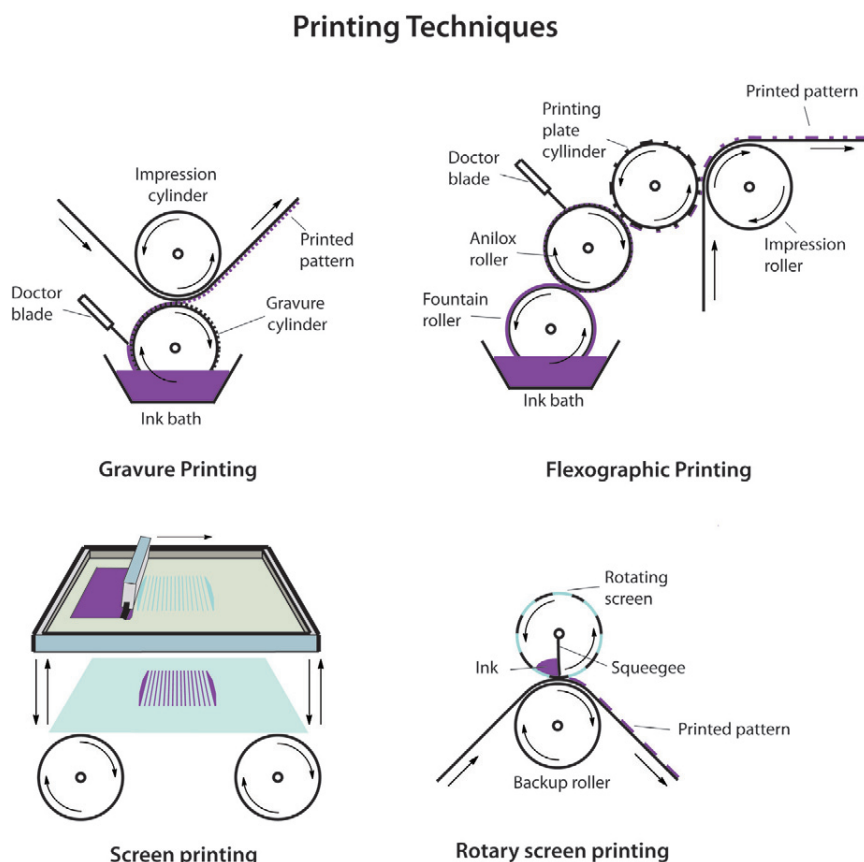


Fig. 2 Illustrations of the principles behind the four printing techniques; gravure printing, flexographic printing, screen printing, and rotary screen printing.

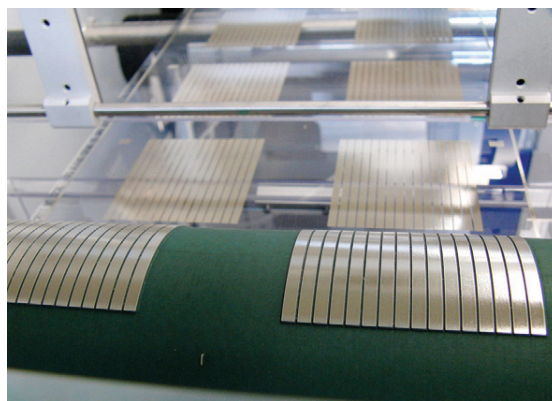
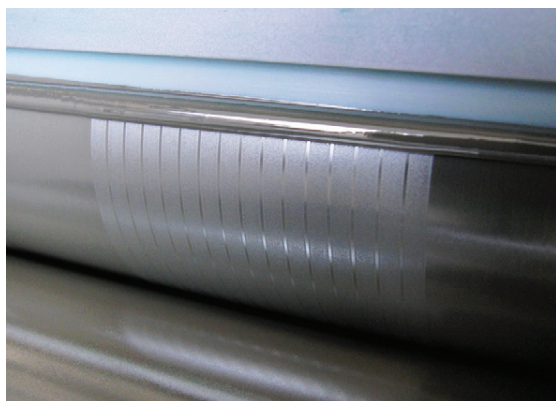


Fig. 3 The fountain roller disengaged from the anilox showing the negative print of the motif after ink pickout from the printing cylinder (left). The printing cylinder with the relief carrying the ink (in this case a silver paste) during printing. The final printed pattern on the web can be observed in the background (right).

Gravure printing

A commonly encountered printing technique in our everyday life is gravure printing which is widely used in the printing of magazines and high volume print runs like catalogues. As illustrated in Fig. 2, the technique relies on the transfer of ink, from tiny engraved cavities forming the pattern on the gravure cylinder, to the web by surface tension as the web is brought into contact with the gravure cylinder by pressure from the softer impression cylinder. The shape and thickness of the final imprint is defined by the pattern and depth of the cavities in the gravure cylinder. The engraved cells on the gravure cylinder are continuously filled from the ink bath and a doctor blade ensures removal of excess ink, ensuring that the ink is only present in the cavities. Gravure printing is suitable for the printing of low viscous inks at very high speeds, of up to 15 m/s, but careful optimization of the ink's surface tension is important, as the quality of the print is highly dependent on ink rheology, web speed, and the pressure of the impression cylinder. The use of gravure printing for the preparation of solar cells has only been reported in very few cases¹⁴⁻¹⁷.

Flexographic printing

Flexographic printing is a R2R technology that differs from gravure printing mainly in the fact that the transfer of the ink is performed from a relief opposed to cavities (see Fig. 2). The final pattern stands out from the printing plate which is typically made from rubber or a photopolymer. The flexo system consists of fountain rollers that continuously transfer ink to the ceramic anilox roller which has engraved cells/micro cavities embedded into the exterior. This allows the collection of ink which is then transferred to the relief on the printing cylinder that performs the final transfer to the web. The ink pick out from the anilox corresponding to the negative pattern of the motif can be observed directly as shown in Fig. 3. Roll-to-roll flexographic printing is a relatively new technology for organic solar cells and has so far not been used for direct processing of the active layer, but examples of its use include the processing of modified PEDOT:PSS¹⁸, processing of a wetting agent on the surface of the active layer¹⁹, and the patterning of conductive grids (roll-to-

roll) with a line width below 50 μm , which could potentially be used as electrode structures for ITO-free organic solar cells²⁰.

Screen printing

Screen printing is, in contrast to flexographic and gravure printing, a method that inherently allows for the formation of a very thick wet layer and thereby also very thick dry films, which can be useful for printed electrodes where high conductivity is needed. The typical wet layer thicknesses are in the range of 10 – 500 micron. There are two types of screen printing: flat-bed screen printing and rotary screen printing. The principle of the two methods is the same and outlined in Fig. 2. Photographs of the techniques in operation are shown in Fig. 4. The squeegee moves relative to the screen and forces the ink paste through the opening of the mesh, which define the desired motif. There are significant differences in the operation of the two techniques. The advantages of flat-bed screen printing (Fig. 4) are that the mask is low cost and it is possible to make one print at a time and make adjustments between each print if needed. For development and laboratory work this is a clear asset. In terms of production it is also possible to print on very large areas (on the scale of 10 square meters). Rotary screen printing differs in that the ink is contained inside the rotating cylinder with a fixed internal squeegee and the ink is less exposed to the surroundings. The mask is a lot more expensive than the flat-bed printing mask, but in terms of speed, edge definition/resolution, and achievable wet thickness, rotary screen printing is by far superior to flat-bed screen printing by at least an order of magnitude as it is a true roll-to-roll printing technique. It is the two-dimensional printing technique that allows for the largest wet thickness achievable (> 300 micron). Because of the cost of the mask, the more delicate operation, the more difficult adjustment, and the relatively time consuming cleaning procedures, rotary screen printing is not as well suited for laboratory work as the flat-bed technique. The printing techniques have proven particularly useful for the printing of the front and back electrodes for polymer solar cells²¹⁻²³ but also screen printing of active layers^{24,25} have been reported.

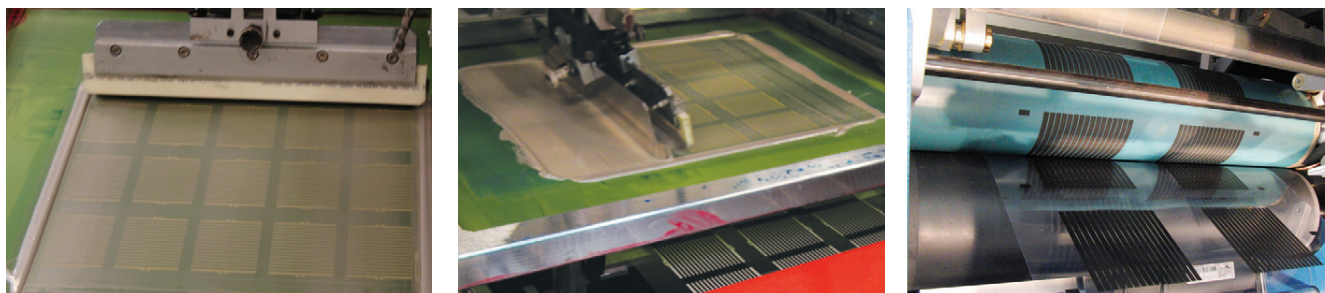


Fig. 4 Flat-bed screen printing of silver paste showing the squeegee after passage over the motif (left) and the squeegee during a printing cycle showing how the ink is forced through. The printed motif can be seen in the lower part of image (middle). A photograph of rotary screen printing of conducting graphite ink onto a clear polyester foil (right).

The coating techniques (wet films through a meniscus)

Whereas all of the printing techniques inherently allow for two-dimensional printing in the lateral plane through physical contact, the coating techniques lead to a continuous wet layer along the length of the web without contact between the coating head and the web. The coating itself is a result of continuous feeding of ink to a meniscus that is standing between the "coating head" and the web. Most of the coating techniques are thus zero-dimensional in the sense that no pattern is created as it is simply an even coat over the substrate. Most often, however, the control of the wet thickness is far superior to any of the printing techniques and very even layers can be prepared.

The two coating techniques that have found most use this far for roll-to-roll processing of polymer solar cells are slot-die coating and knife coating^{26,27}. These two techniques have been illustrated schematically in Fig. 5. Knife coating is very similar to doctor blading and laboratory results from laboratory doctor blading can be transferred quite readily to roll-to-roll knife coating. The knife coating process has an ink reservoir before the knife that serves to supply the meniscus with new ink as it is gradually deposited behind the knife as the web passes by. In the case of slot-die coating, it is possible to coat stripes of a well-defined width along the web direction and it is the only film forming technique which inherently allows for one-dimensional patterning. This aspect has enabled the very convincing demonstration of slot-die coating for the manufacture of polymer solar cells. In slot-die coating, the ink is supplied to the meniscus via a slot and a pump and it thus becomes possible to adjust the wet thickness by controlling either the speed of the web or the ink supply (or both). The natural limits to the achievable wet thicknesses depend on the coating window which is defined mostly by the ink properties and the web surface properties, but also by the coating geometry. Some examples of both slot die coating and knife coating are shown in Fig. 6 where the strength of slot die coating is evident. Many tightly spaced stripes can be coated at the same time at web speeds of a few meters per minute. This has been explored in several large demonstrations of polymer solar cell technology^{22,28-31}, of which the most elaborate example in terms of both miniaturization of the module,

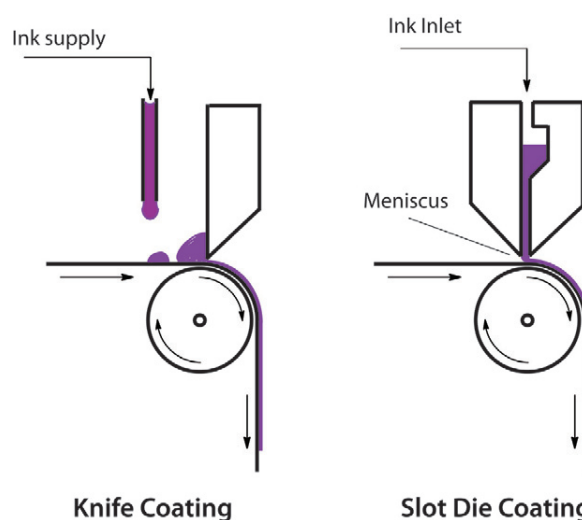


Fig. 5 A schematic illustration of knife coating where excess ink is kept ahead of the knife that is in close proximity to the web (left). Slot-die coating relies on the meniscus standing between a coating head with a slot from which ink is supplied to the standing meniscus thus forming a continuous (or striped) wet film (right).

complexity of the product integration, and the number of units produced is that of the OE-A demonstrator in 2011³².

Wet film formation without contact

Organization of the different film forming techniques according to the distinct categories of coating and printing is not straight forward and a few of the techniques that have been used for OPV have been named without taking the definitions above into account. In ink-jet printing, a two-dimensional pattern can be printed by specifically addressing each pixel in an area with (or without) an ink droplet. The third dimension (thickness) can in principle be achieved by printing multiple layers or by adding more ink to one spot. The method is entirely without contact between the printing head and the substrate as the ink droplet is ejected into the free space that exists between the nozzle and the substrate.

There are two types of droplet formation employed in inkjet printing as shown in Fig. 7. One where droplets are generated continuously and



Fig. 6 (a) Photograph of the standing meniscus during slot-die coating of the active layer of the OPV comprising many very tightly spaced stripes. (b) A total of 48 stripes (3 mm wide spaced by 1 mm) are coated simultaneously. (c) Knife coating with the open ink reservoir and the manual feed hose.

deflected onto the desired spot (pixel) on the substrate and one where droplets are only ejected on demand from a nozzle immediately in front of the pixel at the given time. In the former case speed can be very fast but since only one nozzle is used there are limits to the area that can be covered. On the other hand the drop on demand (DOD) system requires many nozzles. In early systems, the DOD systems were limited by the achievable web speeds and resolution, but today high resolution systems are commercially available that are capable of fast web speeds. From an industrial point of view, ink jet printing is a relatively new processing method with some speed limitations and restrictions on ink

formulations. The latter point in particular has put restraints on the use of the technology for organic solar cells. Inkjet printing of organic solar cells has so far been limited to small scale devices (0.03 – 1 cm², up to 3.7 % PCE) to process either the PEDOT:PSS³³ layer, the P3HT:PCBM³⁴⁻³⁶ layer, or both^{37,38}, and has in one case³⁹ been used for screening blend ratios, concentrations, solvent ratios, and film thicknesses. None of the reports on ink-jet printing in the context of OPV have been performed using R2R-processing and in all cases glass was used as the substrate. Although still largely untested in R2R processing, the possibility for complex pattern formation in high resolution from a digital master

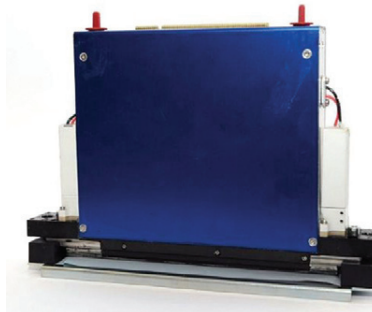
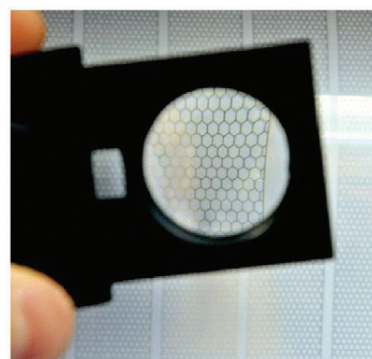
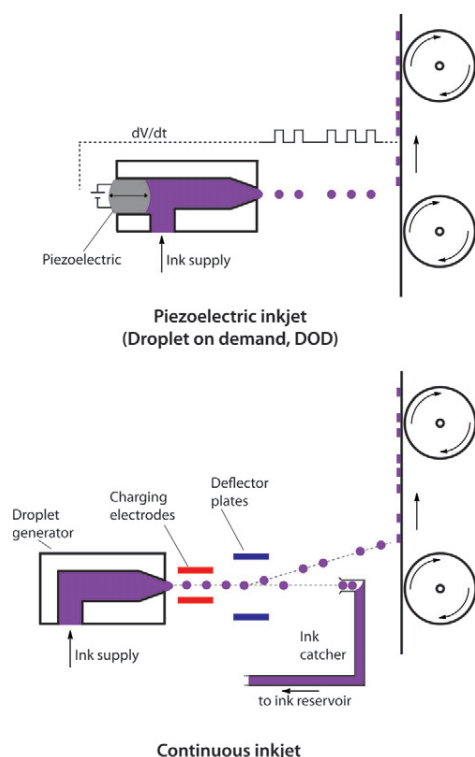


Fig. 7 (Left) Graphical illustrations of the principles behind drop-on-demand (DOD, here piezoelectric) inkjet printing and continuous inkjet printing. Photographs of (top right) a full roll-to-roll ink-jet printed pattern using a DOD system in a full width of 305 mm capable of printing with a resolution of 600 DPI and (bottom right) the 600 DPI printing head.

makes the ink-jet technique an extremely interesting future candidate for OPV processing.

Another film forming technique is spray coating, that like ink-jet printing achieves film formation through droplets and without physical contact between the coating head and the web. Similar to ink jet printing, the name is slightly misleading (no continuous wet film). Similar to ink-jet printing the ink is applied through droplets but where ink-jet printing achieves high graphical resolution through control of the droplets, spray coating does not allow for control of the pattern and is thus inherently a zero-dimensional coating technique. It is possible to pattern through a shadow mask but it is likely to prove impractical outside of the laboratory. Spray coating has been employed in several literature reports for the preparation of many of the layers in the OPV stack including the active area⁴⁰⁻⁴³, silver back electrode^{44,45}, a combination of both hole transport layer and active layer^{46,47}, and in one case three layers (electron transport layer, active layer, and hole transport layer)⁴⁸. Small laboratory sized roll-coaters has been developed where spray coating has been explored but so far there are no examples of roll-to-roll coated OPV prepared via spray coating⁴⁹. A final technique that deserves mention is brush painting of the layers in the polymer solar cell stack. The use of a brush for film formation is possibly the oldest and most difficult one to model as it comprises a mixture of multiple parameters. It relies on ink that is withheld between the fibers of a brush through the surface tension of the ink. When brought into contact with the substrate, a meniscus forms between the fibers

and the ink that is pulled out of the brush as it is moved across the surface of the substrate. The technique allows for some patterning depending on the brush size and it is thus a mixture of contact, meniscus, and two-dimensional patterning. It has not been employed in a roll-to-roll context until now but has been reported in the context of OPV in several instances and thus deserves mention⁵⁰⁻⁵². It is conceivable that a roll-to-roll brush method could be developed for film formation in OPV.

Exotic coatings

In this section we will briefly review some of the techniques that certainly have the potential to become impactful when it comes to the formation of the polymer solar cell stack but that have been termed exotic since they are beyond what is presently possible or at the limit of it. This far we have viewed the film forming techniques according to the way the ink is dispensed and the way the different techniques can lead to a zero, one or three-dimensional pattern in the horizontal plane and we have viewed the formation of one wet layer comprised of one ink. Now imagine that we could apply several wet layers simultaneously on top of each other or process the layers dry without solvent. The former presenting a lot of challenges in terms of ink formulation and application and the latter elegantly avoiding problems with toxic solvents and while yielding control similar to vacuum processing achieves this without it through use of electrostatic forces or simply through dry nanoparticles that are merged in a separate process or through adhesive forces (Fig. 8).

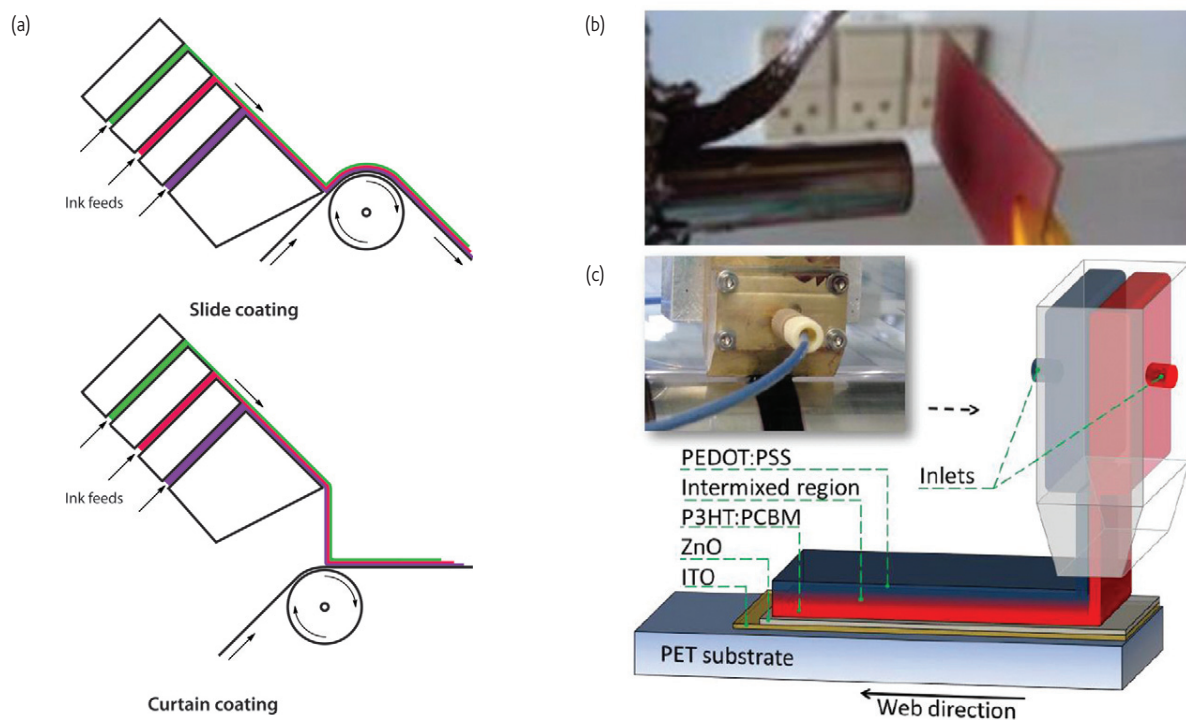


Fig. 8 (a) Graphical illustrations of slide and curtain coating, (b) dry coating of insoluble native polythiophene directly from the gas phase through nanoparticles, and (c) graphical illustration of double slot-die coating with a photograph showing double slot-die coating of a bilayer comprising P3HT:PCBM and PEDOT:PSS.

Curtain and slide coating techniques allow for the simultaneous formation of many layers (> 10), and ideally these techniques allow for the formation of the entire solar cell stack in one or two single coating steps. This would imply faster overall solar cell processing, less web handling, and less energy requirements (for machinery and drying) without having to increase the web speed. As our current understanding and capacity for ink formulation for the individual layers of the polymer solar cell stack is elaborate, it is currently inconceivable that we will be able to realize simultaneous formation of all the layers in the near future. A critical requirement of those two techniques is the web speed which has to be very high in order for the methods to work (typically $5 - 20 \text{ m s}^{-1}$).

There are some other film forming methods that qualify as exotic but have been used to form some of the layers in polymer solar cell stacks. One such method is double slot-die coating which is possible at much lower web speeds and on a much smaller scale than curtain and slide coating, and also allows for a much simpler control of the ink flow. The potential for double slot-die coating is large and it is the only multilayer

coating technique that has been employed for organic solar cells in a full R2R process (and in general). Larsen-Olsen *et al.* proved that it was possible to simultaneously coat an aqueous nanoparticle dispersion of P3HT:PCBM and an aqueous dispersion of PEDOT:PSS on top of doped zinc oxide, preprocessed using single slot-die coating from water (See Fig. 8)⁵³. The resulting cells showed relatively poor device performance, which was attributed to the far from perfect layer separation, due to the complex nature of the bilayer formation process. It did however demonstrate that it was possible to simultaneously form two layers of the solar cell stack.

The dry processing of the active layer has been described as worthy of investigation¹. The use of dry ink systems is quite well known to most people from photocopiers and laser printers that rely on an electrostatic patterning of the dry ink in the form of micron sized particles. For OPVs there is a requirement for sub-micron film thickness which implies that the ink particles would have to be nanometer sized. It is a challenge to form dry nanometer sized particles that do not aggregate. In order to

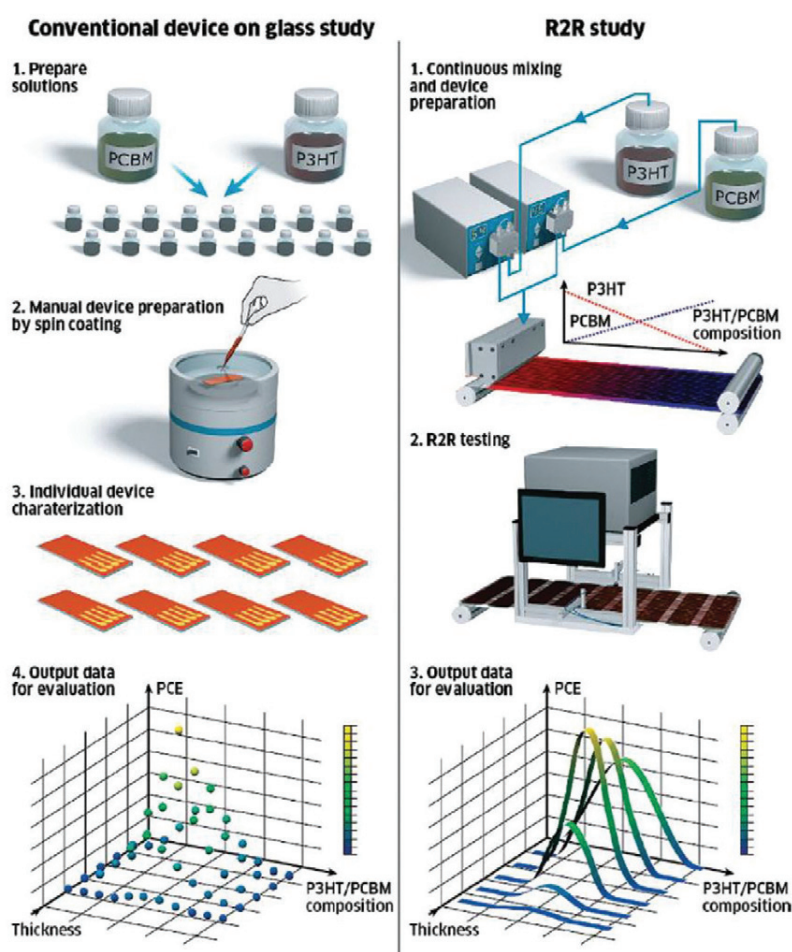


Fig. 9 Comparison between conventional spin-coating and differentially pumped roll-to-roll coating visualizing how a gradient of P3HT versus PCBM can be explored with great ease using slot-die coating. Reproduced with permission from⁵⁵ © 2010, American Chemical Society.

achieve dry coating of conjugated polymer systems, early experiments employed the gas phase formation of insoluble nanoparticles of native polythiophene mixed with PCBM⁵⁴. The dry nanoparticles are formed in a gas stream and deposited directly from the gas phase onto the substrate (Fig. 8).

Advanced processing during coating and printing

One is often met with the argument that roll-to-roll processing is technical and not at the forefront of science. We would hold the opposite argument and claim that it both enable and provides considerably more control over and insight into complex phenomena. To give just two examples; think of the double slot-die coating technique described above, which gives access to complex segregated wet films with a complex topology both laterally and horizontally. A second example is the differentially pumped slot-die coating technique developed by Alstrup *et al.*⁵⁵, where two or more ink solutions are mixed and supplied to a modified slot-die coating head as illustrated in Fig. 9. With two ink solutions it is thus possible to set up a gradient mixing and coating two inks along a roll. This enables a whole new method to explore the very large parameter space of compositions and layer thicknesses for organic solar cells. In contrast to conventional spin-coating techniques it is for instance straightforward to analyze the composition diagram between the donor and acceptor with several hundred solar cells having different compositions in a single run using very little ink material in a matter of minutes. In a similar way the thickness of, e.g., the active layer can be explored using a gradient of the optimized donor/acceptor versus solvent to create a concentration gradient while keeping the wet thickness constant during the slot-die coating process⁵⁶.

Drying and advanced processing post film formation

The most common processing technique employed post film formation is drying of the wet film. Traditionally this has been achieved by heating the wet film, thus removing the solvents and leaving a dry film of the desired

material. In recent years UV-curing has been developed for many adhesive systems as an approach to solvent free ink even though it is not a dry ink (at least not until it is fully cured). Drying and curing are complex processes that warrant a review of their own, but to give an example the very common process of hot air drying and UV curing have also been applied for screen printed silver back electrodes in inverted type OPVs²². Several different silver inks were compared with respect to power conversion efficiency and it was found that the only UV curable ink tested resulted in the highest PCE. A later study using light beam induced current (LBIC) measurements concluded that the solvent based silver inks degraded the current production in the adjoining active layer while this was not the case for the UV curable ink and nor was it for a specially developed water based thermally curing ink⁵⁷. The use of an intense source of light to thermocleave polymer side chains in a R2R coating process of OPV is another example⁵⁸.

Using an oven set at 140 °C to thermocleave a polymer required four hours, making this an impractically slow process, while using a custom build lamp with narrow wavelength high intensity (Fig. 10) enabled much faster web speeds of 0.2 – 0.4 m/min.

With the introduction of lasers capable of delivering ultra short pulses (pico- to femtosecond), new possibilities of performing selective laser patterning have emerged with a potential use in R2R processed organic solar cells. Because of the short pulse duration very little heat is generated and it is thus possible to selectively remove a thin layer without destroying what is beneath. Initial reports related to solar cells have primarily been focused on the patterning of ITO on glass and PET⁵⁹⁻⁶¹. So far the technology has yet to prove that functioning laser patterned solar cells can be produced, and cost wise the concept of removing applied material is generally not a preferred pathway in production if it can be avoided, but it has the potential to be a useful tool for niche productions.

One distinct advantage is that it can be used for scribing and this may prove useful in future OPV modules when very large geometric fill factors become important. Currently it is possible to reach geometric fill factors of 45 – 67 % using slot die coating and screen printing. With great accuracy this can possibly be increased to around 85 % but it is

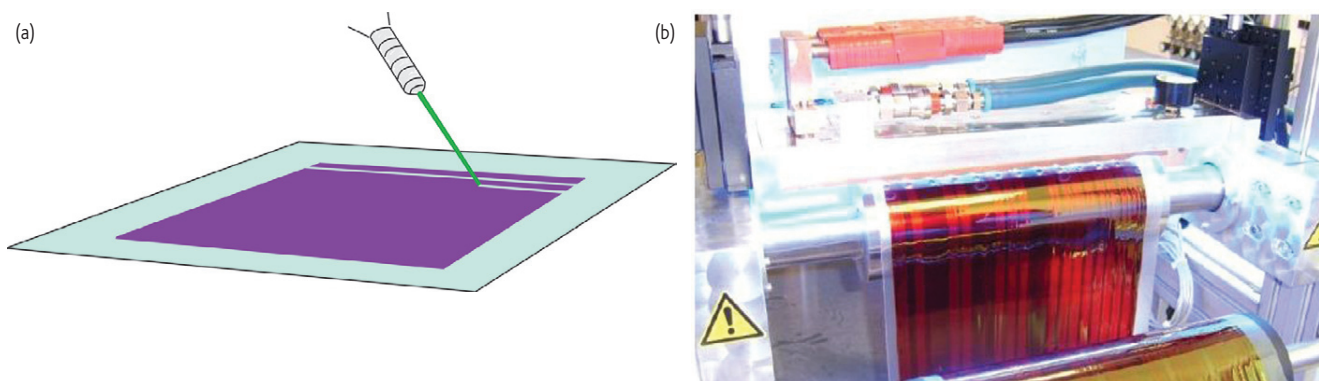


Fig. 10 (a) A Schematic drawing of patterning of the layers post processing and (b) the use of intense light with a specific wavelength or pulse length to selectively address, for instance, the active layer.

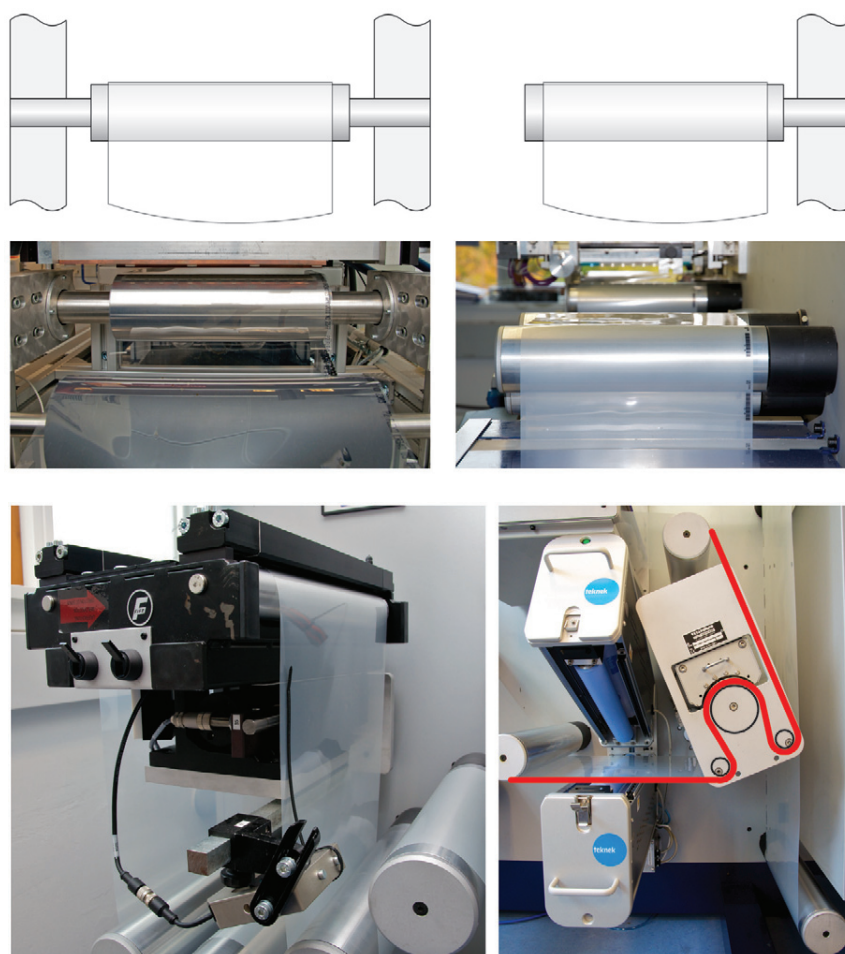


Fig. 11 Double sided roller mounting in schematic form with a photograph below (left) and cantilevered roller mounting with a schematic and a photograph (right). Below some web control and web processing tools are shown. A web guide used to correct the foil direction such that the edge of the foil is within ± 150 microns (lower left). A web cleaning and corona treating for higher surface energy is also shown. The red line shows how the web is guided through the corona treater (middle). A photograph of a nip which is used to separate different web tension zones between unwinder and rewinder on the machine (right).

unlikely to be taken further. Here laser scribing is likely to enable geometric fill factors in the 90 – 100 % range.

Machinery and web control

There are two basic ways that a roller carrying foil through a roll-to-roll machine can be constituted: double sided mounting and cantilevered, as illustrated in Fig. 11. Each system has its own advantages and disadvantages. The double sided roller mounting is particularly suited for large roller and web widths and heavy duty work yielding a stable machine, whereas a distinct disadvantage is the feeding of the machine with foil that has to be threaded like a sewing machine. The cantilevered machine on the other hand is well suited for narrow webs and does not allow for a web width much greater than 50 cm. For laboratory work and small production the cantilevered system is very well suited and allows for fast threading of the machine as everything can be accessed from one side.

Lamination

After the entire solar cell stack has been printed it needs to be encapsulated on the printed side for several reasons. The most important reason is operational stability. Another almost equally important factor during processing and handling is mechanical protection of the delicate printed layer stack. The process of lamination is in principle very simple and can be carried out in a number of ways using simple equipment, and the same basic principle of joining two lines of web by applying pressure as they are fed between two rollers. The use of cold lamination typically employs a pressure sensitive adhesive that is lined and applied to the laminate by a lamination process followed by removal of the liner and lamination onto the solar cell stack²². This is very simple and easy to control at the laboratory level at high speeds ($> 20 \text{ m min}^{-1}$ is easily accessible). Hot melt lamination uses the same principle, but here the laminate already has an adhesive material on it, which becomes adhesive

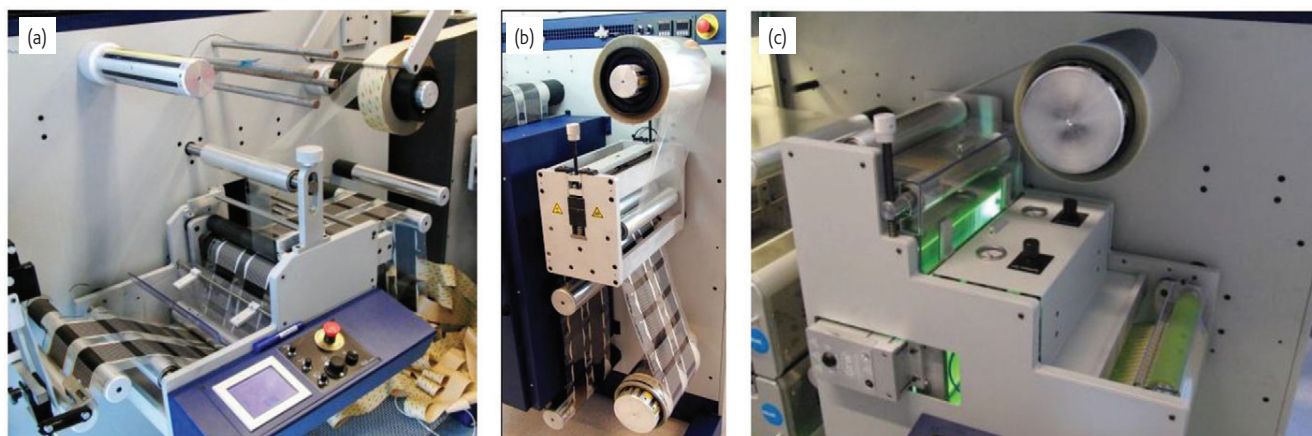


Fig. 12 Photographs of cold, hot-melt, and UV-lamination. (a) Cold lamination using lined pressure sensitive adhesives is shown for the lamination of solar cells. (b) A hot melt station is shown along with (c) a UV-lamination station.

when heated. The laminate and the substrate carrying the solar cells are then forced together between the heated rollers where the adhesive melts and forms a tight seal. UV lamination requires that an uncured adhesive or glue is applied by printing or coating immediately prior to bringing the two foils together. In the laminator the glue is cured by application of UV-light. In terms of operation, hot-melt is by far the easiest with cold lamination being slightly more complicated because one has to handle sticky adhesive and this implies that only one side of the foil can be handled (the non-sticky one). UV-lamination is by far the most complicated since it also involves a printing or coating step. Flexographic printing of the UV-curing adhesive is typically employed.

In terms of the adhesive thickness there are some limitations to the cold lamination where typically 50 microns of adhesive can be handled with ease. It is possible to employ pressure sensitive adhesives as thin as 20 microns, but it does present some challenges and the major drawback of cold lamination is the relatively thick adhesive layers that

must be employed. Hot lamination on the other hand enables very thin adhesives to be employed and this may be an advantage in some cases but can present problems if the surface topography of the solar cells is rough (i.e., for a screen printed grid with a thickness of 5 – 20 microns). UV-lamination gives the widest accessible range of adhesive thickness and is in principle only limited by the printing method chosen and the curability of the adhesive (1 – 100 microns is achievable). Photographs of the different roll-to-roll lamination techniques in Fig. 12 show the relative similarity.

Inks and materials

As previously mentioned, one of the extremely important issues in high throughput production is finding suitable inks based on nontoxic/nonpolluting solvents, with water being both the cheapest and most environmentally friendly. The majority of materials used in solar cells today do not fulfill this demand, PEDOT:PSS being the only component

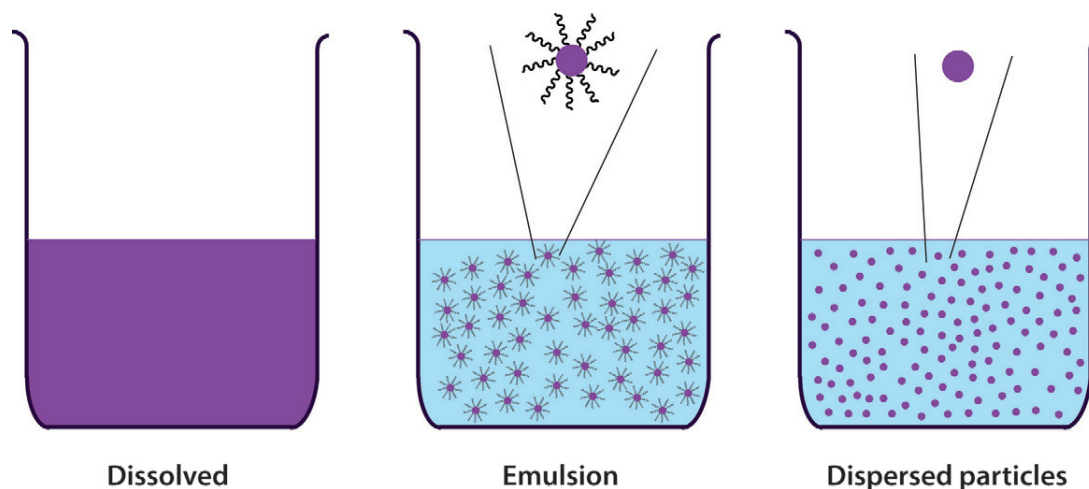


Fig. 13 Illustration of the basic types of ink formulations, which are fully dissolved, emulsions and dispersed particles.

that is generally processed from aqueous solution, so new approaches to processing (particularly the active layer) need to be developed. If we wish to process everything from water, careful consideration towards the potential of damaging layers that have already been processed need to be taken. Generally, ink formulations can be divided into three categories as indicated in Fig. 13: dissolved material (each separate molecule is fully solvated), emulsions (the material is kept in solution by additives which allows for micelle formation), and particulate solutions or pastes (solid particles are suspended in solution). The careful exploitation of different ink formulations might be the answer to how to replace the present use of orthogonal solvents (polar and non-polar) for every new layer, as each formulation type allows for the processing of different types of material.

With respect to non-transparent electrodes, silver is at present the only real candidate, and has been limited in R2R processing to the use of screen printing of highly viscous inks (paste) with relatively large silver particles, which ensures good conductivity. As previously mentioned, several types of silver paste are commercially available which can either be cured thermally or with UV light. None of these are water based, but screen printable water based silver pastes can be prepared quite easily using an aqueous binder, silver flakes, and water⁶². Low viscosity aqueous silver inks containing nanoscale particles are further commercially available, and could have potential use in solar cells processed by methods like gravure, flexographic, and inkjet printing. When using small particles sintering of the silver layer is required by either thermal or other treatment in order to achieve good connectivity^{63,64}.

As for the transparent electrodes ITO is still the leading material although extensive efforts are made towards replacing it because of the high cost of the material.

Regarding the processing of charge selective layers, the most widely used hole transport layer is PEDOT:PSS, which is commercially available in a large variety of inks that have been tailored with respect to conductivity, viscosity, and surface tension for different application purposes. As already shown in this review, a large variety of R2R techniques can be employed in the application of PEDOT:PSS. For electron selective layers, only the use of zinc oxide from acetone⁶⁵, methanol⁵⁵, or water solution⁶⁶ have been reported in R2R processes.

With respect to the processing of the active layers, chlorinated solvents have been used in the majority of R2R reports, but water based processing methods based on emulsified solutions have shown promising initial results as it is possible to process hydrophobic active components^{53,62,66,67}. Because the micelle stage only exists in solution (the micelle collapses upon removal of the solvent) the active layer is insoluble in aqueous solutions after drying of the solvent and further processing from water can be carried out without damaging the layer. Using emulsified low-band-gap polymers in inverted structured R2R processed solar cells (4 cm²) Andersen *et al.* thus achieved a PCE of 0.55 %⁶⁶, and Larsen-Olsen *et al.* used an emulsified aqueous solution to process one of the active layers in the first ever report of R2R processed organic tandem solar cells⁶⁷.

Testing the roll

At the end of processing polymer solar cells using roll-to-roll methods, one ends up with a roll of material. While some testing can be carried out during the processing of the individual layers, the functionality of the solar cell itself, i.e., the production of electrical energy upon being subject to illumination, has to be carried out at the very end, on the very roll that is the end product. One can thus view inline monitoring techniques as useful for guiding the process, but they can not guarantee the final performance. Therefore we also need roll-to-roll instrumentation to test functionality. The techniques that have proven useful for process control are the camera techniques, providing two-dimensional information using transmission, reflection, and dark field imaging of the printed or coated films, revealing detail on film thickness variations, registration, and particle detection. These techniques are non-contact techniques and apply to individual layers during manufacture. Once the solar cell modules have been prepared, the camera techniques still apply and new two-dimensional imaging techniques become possible that can complement the camera techniques. Methods such as light beam induced current (LBIC) mapping⁵⁷, dark lock-in thermographic imaging⁶⁸, electroluminescence imaging, and photoluminescence imaging^{69,70}. Most of those techniques require electrical contact with the device module to enable extraction of information regarding solar cell function. Some techniques that also require electrical contact are zero-dimensional in the sense that they will tell you about the malfunction of the device but not the location of the problem. IV and IPCE measurements are of this type. A roll-to-roll characterizer is shown in Fig. 14. It enables the recording of IV-curves, LBIC images, IPCE data and the photographic imaging of modules. The speed of the instrument is on the order of 1 m min⁻¹.

Device integration and application

The final aspect of the manufacture of OPVs using roll-to-roll methods is of course what happens after production and testing. There have not been many well documented examples of OPV integration, application, and demonstration and clearly this represents an entire topic on its own that will develop in time once the OPV technology becomes widely available.

What will be required before one can take full advantage of the polymer solar cell technology is that the device or product integration is also achieved using a roll-to-roll technique, or at least a technique that allows for the OPV to enter the process on a roll. Otherwise the major strength that roll-to-roll technology has to offer is lost. The earliest demonstration example in a significant volume is possibly that of the solar hat, where a small solar cell module was used to charge a battery for a radio. A part of the process was roll-to-roll based, but during the manufacture of the solar cells the roll was broken up into sheets and the solar cells were finally processed in sheets. This early example was thus far from what has been specified above, but was an important part of the learning process²⁴. A second example is that of a small lamp for the "lighting Africa" project, and here the solar cell was

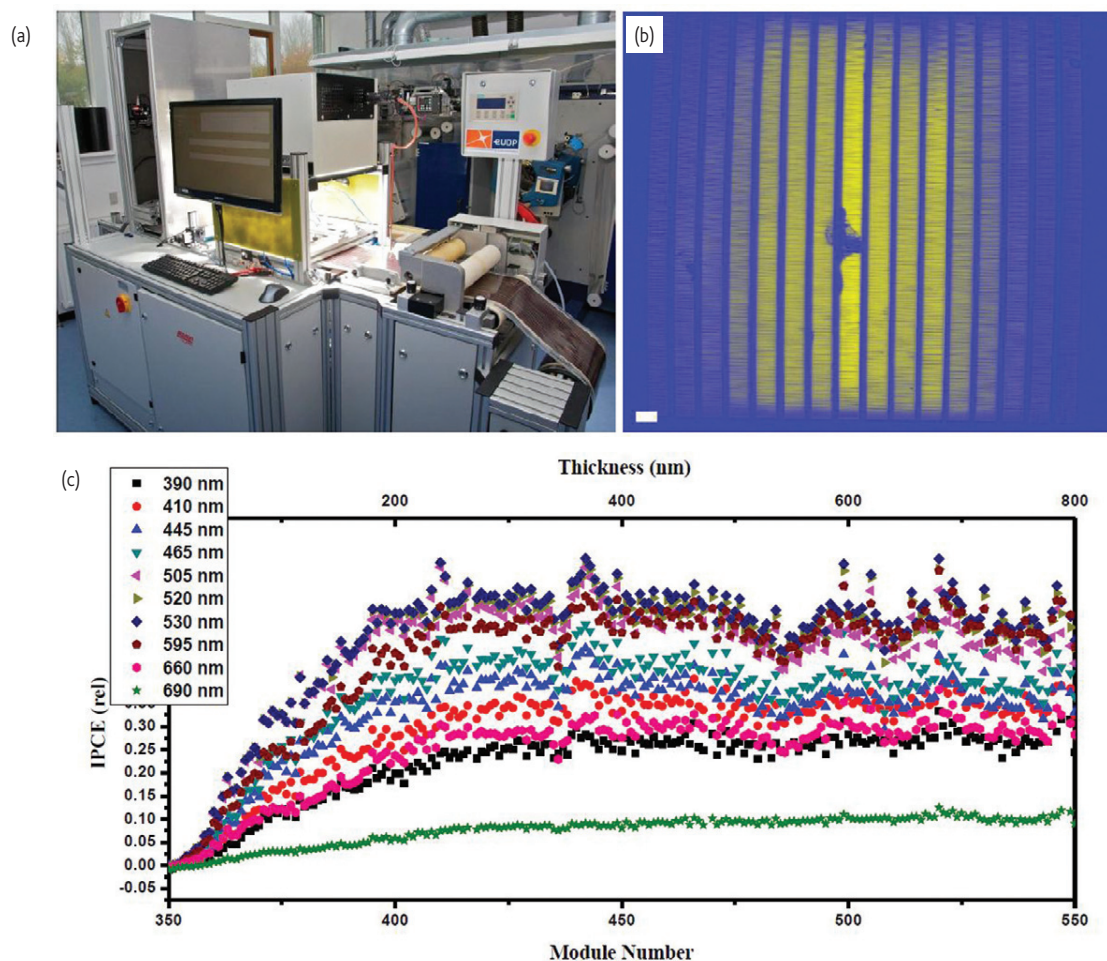


Fig. 14 (a) A photograph of a roll-to-roll testing machine allowing for solar simulation and two-dimensional imaging of devices (LBIC, photographic imaging, and IPCE). (b) An example of an LBIC image acquired roll-to-roll showing a defect (the resolution is 100 micron, the size of the imaged module is 305 x 250 mm, and data the acquisition time is around 1 second). (c) IPCE data for polymer solar cells along a roll recorded at different wavelengths using a powerful diode array.

entirely roll-to-roll processed, but the final confectioning of the lamp was made by handling the discrete unit. This example was a step forward in terms of processing and made use of the advantages that roll-to-roll processing has to offer⁷¹. The third example was the first instance of product integration in a fully automatic manner, even though the final confectioning was made by sheet processing where several units were handled simultaneously¹⁹. This final example was taken further in an experiment of miniaturization and product integration, where 10 000 units comprising > 30 discrete steps were produced through roll-to-roll processing and sheet based handling of 15 units at a time³².


Summary and outlook

It is clear that roll-to-roll processing is at the heart of OPVs in the future and that the successful realization of low cost OPVs will be closely linked to this. There are however also other requirements and roll-to-roll processing and roll-to-roll methodologies are only one part of a large equation. In addition to efficient processing, efficient process control



Fig. 15 Illustration of the OE-A demonstrator for 2011 and an example of the laser cutting the processed sheets into the final product.

during manufacture is required, and new materials and processes are urgently needed. Some of the most important materials and processes are those that will enable the printing of semitransparent electrodes and complete processes that are built around enabling complete fabrication of efficient solar cells. The materials and processes should of course give access to OPVs that provide operational stability of > 10 years and they should be efficient (> 10 %). A particular requirement to the OPV is that it has as thin an outline as possible with low materials consumption, to achieve a low embodied energy. The processing should not be environmentally harmful and should, through use of the lowest possible temperatures, require a very low input energy for manufacture. This, taken together, will enable short energy payback times, and < 10 days should be possible. Manufacture of the entire solar cell stack at an overall speed of > 10 m min⁻¹ will enable the manufacture of a daily energy

production capacity of more than 1 GW_{peak} and thus, in principle, fully address man-kinds future energy needs. 

Acknowledgements

This work has been supported by the Danish Strategic Research Council (2104-07-0022) and EUDP (j.no. 64009-0050). Partial financial support was also received from the European Commission as part of the Framework 7 ICT 2009 collaborative project HIFLEX (grant no. 248678), partial financial support from the EU-Indian framework of the “Largecells” project that received funding from the European Commission’s Seventh Framework Programme (FP7/2007–2013, grant no. 261936), partial financial support was also received from the European Commission as part of the Framework 7 ICT 2009 collaborative project ROTROT (grant no. 288565) and from PVERA-NET (project acronym POLYSTAR).

REFERENCES

- Krebs, F. C., *Sol Energy Mater Sol Cells* (2009) **93**, 394.
- Green, M. A., et al., *Prog Photovolt* (2011) **19**, 565.
- Service, R. F., *Science* (2011) **332**, 293.
- Tipnis, R., et al., *Sol Energy Mater Sol Cells* (2009) **93**, 442.
- Espinosa, N., et al., *Sol Energy Mater Sol Cells* (2011) **95**, 1293.
- Espinosa, N., et al., *Energy & Env Sci* (2011) **4**, 1547.
- Espinosa, N., et al., *Sol Energy Mater Sol Cells* (2012) **97**, 3.
- García-Valverde, R., et al., *Prog Photovolt: Res Appl* (2010) **18**, 535.
- Nielsen, T. D., et al., *Sol Energy Mater Sol Cells* (2010) **94**, 1553.
- Azzopardi, B., et al., *Energy & Env Sci* (2011) **4**, 3741.
- Kalowekamo, J., and Baker, E., *Sol Energy* (2009) **83**, 1224.
- Powell, C., et al., *Sol Energy* (2009) **83**, 1977.
- Espinosa, N., et al., *Energy & Env Sci* (2012) **5**, 5117.
- Ding, J. M., et al., *Sol Energy Mater Sol Cells* (2009) **93**, 459.
- Kopola, P., et al., *Sol Energy Mater Sol Cells* (2010) **94**, 1673.
- Kopola, P., et al., *Sol Energy Mater Sol Cells* (2011) **95**, 1344.
- Voigt, M. M., et al., *Sol Energy Mater Sol Cells* (2011) **95**, 731.
- Hübner, A., et al., *Adv Energy Mater* (2011) doi: 10.1002/aenm.201100394.
- Krebs, F. C., et al., *J Mater Chem* (2010) **20**, 8994.
- Deganello, D., et al., *Thin Solid Films* (2010) **518**, 6113.
- Galagan, Y., et al., *Sol Energy Mater Sol Cells* (2011) **95**, 1339.
- Krebs, F. C., et al., *Nanoscale* (2010) **2**, 873.
- Manceau, M., et al., *Org Electron* (2011) **12**, 566.
- Krebs, F. C., et al., *Sol Energy Mater Sol Cells* (2009) **93**, 422.
- Zhang, B., et al., *Jpn J Appl Phys* (2009) **48**, 020208.
- Krebs, F. C. *Sol Energy Mater Sol Cells* (2009) **93**, 465.
- Wengeler, L., et al., *Chem Eng Process* (2011) **50**, 478.
- Blankenburg, L., et al., *Sol Energy Mater Sol Cells* (2009) **93**, 476.
- Galagan, Y., et al., *Chem Eng Process* (2011) **50**, 454.
- Krebs, F. C., et al., *J Mater Chem* (2009) **19**, 5442.
- Zimmermann, B., et al., *Sol Energy Mater Sol Cells* (2011) **95**, 1587.
- Krebs, F. C., et al., *Energy & Env Sci* (2011) **4**, 4116.
- Eom, S. H., et al., *Org Electron* (2009) **10**, 536.
- Aernouts, T., et al., *Appl Phys Lett* (2008) **92**, 033306.
- Hoth, C. N., et al., *Adv Mater* (2007) **19**, 3973.
- Hoth, C. N., et al., *Nano Lett* (2008) **8**, 2806.
- Eom, S. H., et al., *Org Electron* (2010) **11**, 1516.
- Lange, A., et al., *Sol Energy Mater Sol Cells* (2010) **94**, 1816.
- Teichler, A., et al., *Adv Energy Mater* (2011) **1**, 105.
- Chen, L. M., et al., *ACS Nano* (2010) **4**, 4744.
- Giroto, C., et al., *Sol Energy Mater Sol Cells* (2009) **93**, 454.
- Park, S. Y., et al., *Sol Energy Mater Sol Cells* (2011) **95**, 852.
- Susanna, G., et al., *Sol Energy Mater Sol Cells* (2011) **95**, 1775.
- Giroto, C., et al., *Org Electron* (2009) **10**, 735.
- Hau, S. K., et al., *Org Electron* (2009) **10**, 719.
- Giroto, C., et al., *Adv Func Mater* (2011) **21**, 64.
- Na, S. I., et al., *Sol Energy Mater Sol Cells* (2010) **94**, 1333.
- Lewis, J. E., et al., *Sol Energy Mater Sol Cells* (2011) **95**, 2816.
- Dam, H. F., and Krebs, F. C., *Sol Energy Mater Sol Cells* (2012) **97**, 191.
- Heo, S. W., et al., *Sol Energy Mater Sol Cells* (2011) **95**, 3041.
- Kim, S. S., et al., *Sol Energy Mater Sol Cells* (2010) **94**, 171.
- Kim, S. S., et al., *Adv Mater* (2007) **19**, 4410.
- Larsen-Olsen, T. T., et al., *Sol Energy Mater Sol Cells* (2012) **97**, 22.
- Nan, Y.-X., et al., *Nanotechnology* (2011) **22**, 475301.
- Alstrup, J., et al., *ACS Appl Mater Interfaces* (2010) **2**, 2819.
- Bundgaard, E., et al., *Macromolecules* (2010) **43**, 8115.
- Krebs, F. C., et al., *Sol Energy Mater Sol Cells* (2011) **95**, 1348.
- Krebs, F. C., and Normann, K., *ACS Appl Mater Interfaces* (2010) **2**, 877.
- Haenel, J., *Proc SPIE* (2010) **7771**, 77710G.
- Schoonderbeek, A., et al., *J Laser Micro/Nanoeng* (2010) **5**, 248.
- Xiao, S., *Proc SPIE* (2011) **7921**, 79210I.
- Søndergaard, R., et al., *Adv Energy Mater* (2011) **1**, 68.
- Grouchko, M., et al., *ACS Nano* (2011) **5**, 3354.
- Perelaer, J., et al., *J Mater Chem* (2010) **20**, 8446.
- Espinosa, N., et al., *Materials* (2011) **4**, 169.
- Andersen, T. R., et al., *ACS Nano* (2011) **5**, 4188.
- Larsen-Olsen, T. T., et al., *Sol Energy Mater Sol Cells* (2012) **97**, 43.
- Bachmann, J., et al., *Sol Energy Mater Sol Cells* (2010) **94**, 642.
- Rösch, R., et al., *Sol Energy Mater Sol Cells* (2012) **97**, 176.
- Seeland, M., et al., *J Appl Phys* (2011) **109**, 064513.
- Krebs, F. C., et al., *Energy & Env Sci* (2010) **3**, 512.

Roll-to-Roll Fabrication of Large Area Functional Organic Materials

Roar R. Søndergaard, Markus Hösel, Frederik C. Krebs

Department of Energy Conversion and Storage, Technical University of Denmark, Frederiksborgvej 399, DK-4000 Roskilde, Denmark

Correspondence to: F. C. Krebs (E-mail: frkr@dtu.dk)

Received 16 August 2012; accepted 17 September 2012; published online 19 October 2012

DOI: 10.1002/polb.23192

ABSTRACT: With the prospect of extremely fast manufacture of very low cost devices, organic electronics prepared by thin film processing techniques that are compatible with roll-to-roll (R2R) methods are presently receiving an increasing interest. Several technologies using organic thin films are at the point, where transfer from the laboratory to a more production-oriented environment is within reach. In this review, we aim at giving an overview of some of the R2R-compatible techniques that can be used in such a transfer, as well the

current status of R2R application within some of the existing research fields such as organic photovoltaics, organic thin film transistors, light-emitting diodes, polymer electrolyte membrane fuel cells, and electrochromic devices. © 2012 Wiley Periodicals, Inc. *J Polym Sci Part B: Polym Phys* 51: 16–34, 2013

KEYWORDS: coating; organic thin films; polymer solar cells; printing; processing; R2R; roll-to-roll; techniques

INTRODUCTION In recent years, the need for cheap and fast processing of larger areas of thin organic films has become an increasingly important goal within a number of research fields that have emerged from the idea that solution processing of organic electronics has the potential for just that. In this context, roll-to-roll (R2R) vacuum free processing on flexible substrates has always been the final goal. Most of these technologies are now at the “verge of delivery” where science must be taken out of the protected environment of the laboratory, where it has proven successful for small-scale devices, in order to show that a transfer to large-scale production is actually possible. This might sound tedious, but the fact is that such a transfer is extremely challenging. First, all the preferred processing procedures in the laboratory and those suitable for R2R processing are generally not the same. Spin coating is, for example, among the most popular methods when it comes to small-scale processing of thin polymeric films in the laboratory, because it is easy to use and it is fairly cheap to acquire the necessary equipment, but the process does not comply well with larger areas and too much material is wasted for it to be compatible with high throughput production. Another example is vacuum deposition of electrodes, which because of the need for high vacuum is very time-consuming and a cost driver, which is why alternative techniques are necessary for larger production scale.

Second, there is a huge difference between preparing and aligning a small multilayer structure typically on a solid substrate like glass, and the precise coating and/or printing of large areas with the same accuracy on flexible substrates

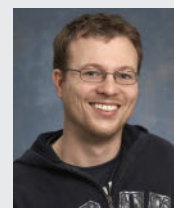
that moves with speeds on the order of 1–20 m/min (or preferably in the range of 60–300 m/min). This requires a high degree of technical skill, and the combination of scientific knowhow on how to tune the chemical and physical properties of the ink that is to be processed, with the technical knowhow of different processing procedures and the conditions they apply to. This simple challenge may very well become a bottleneck in the further development as such combined skills are not necessarily present in a research group.

This review is aimed at giving an overview of a series of R2R coating and printing techniques that can be used in the processing of organic thin films. We also review the devices that can be prepared using these techniques and give a broad overview of the recent progress within its applications in different research fields. Technical details on machine configurations and setups will not be covered as it is already well described elsewhere in literature.^{1–3}

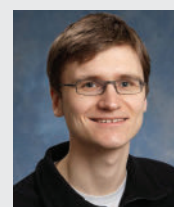
FILM PREPARATION METHODS

A large palette of different printing and coating techniques can be used for R2R processing on flexible substrates such as PET (polyethylene terephthalate), but depending on the ink and processing surface one particular choice is often critical for success or at least significantly better than the others. An essential difference between the coating and the printing techniques is that printings (with the exception of inkjet printing) are contact processes and enable a patterned deposition of the functional ink. Coating methods can either

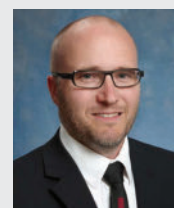
Roar R. Søndergaard received his PhD from Risø DTU—National Laboratory for Sustainable Energy and has a background in organic synthesis. Through synthesis and device preparation he has previously worked within areas of molecular wires, water processed organic solar cells, and improved stability of polymers for roll-to-roll (R2R)-processed organic solar cells. He is currently working as a researcher at DTU Energy Conversion where he is focusing on large-scale manufacture and optimization of R2R-processed organic solar cells through different processing methods.



Markus Hösel received his Diploma degree (Dipl.-Ing.) in Microtechnology/Mechatronics from the Chemnitz University of Technology (CUT) in 2007. After working as a construction engineer at a printing machine manufacturer and as a research associate at CUT, he is currently pursuing his PhD at DTU Energy Conversion under the mentorship of Prof. Frederik C. Krebs. His research interest is focused on roll-to-roll large-scale fabrication methods for organic photovoltaics.



Frederik C. Krebs received his PhD from the Technical University of Denmark (2000) and has since then worked in the field of functional organic materials for application as solar cells, fuel cells, electrochromics, light-emitting devices, and photocatalysis. A focus area has been polymer solar cells manufactured by roll-to-roll methods for solar energy conversion. He is currently a professor at DTU Energy Conversion within areas of research that include new materials with low bandgap and novel processing capability, large area processing and manufacture of polymer solar cells, all aspects of roll-to-roll printing-coating-processing and testing, life cycle analysis, stability and lifetime testing, degradation mechanism studies, outside testing and demonstration.



be contact-based or contact-free and are in general used for large-scale full-layer deposition of thin films. Patterning in coating is somehow limited, and is in reality restricted, to stripes. In the following section, we describe only the most prominent solution-based deposition technologies in the field of thin film electronics. A detailed description of the plethora of existing coating methods is beyond the scope of this review. Technical details to each film preparation method (coating/printing) can be found elsewhere in literature.³⁻⁸

Slot-Die Coating and Knife Coating

R2R coating is a one-dimensional continuous appliance of ink in a stripe with a defined width. In knife coating (often also referred to as blade coating), the ink is supplied in front of the knife which is placed very close to the substrate (see Fig. 1). As the substrate moves the fixed knife pushes the ink in front of it allowing only what corresponds to the gap to pass underneath the edge. The wet layer thickness can thus be regulated by adjusting the distance between the knife and the substrate and to some extent by the processing speed. The coating thickness can be estimated as being roughly half of the gap height. The technique is suitable for processing of wide areas without any pattern.

In slot-die coating, the ink is pumped through a coating head placed very close to the substrate, but without touching it. The constant supply of ink forms a standing meniscus between the moving substrate and the coating head. This

creates a continuous coat of quite even thickness over a large area. In case the slot-die head is fitted with a meniscus guide it is possible to coat stripes in variable width depending on the shape of the meniscus guide (see Fig. 2). Because of the use of a pump it is possible to regulate the wet layer thickness with very high precision as it is defined by the pumping speed, the width of the meniscus, and the web

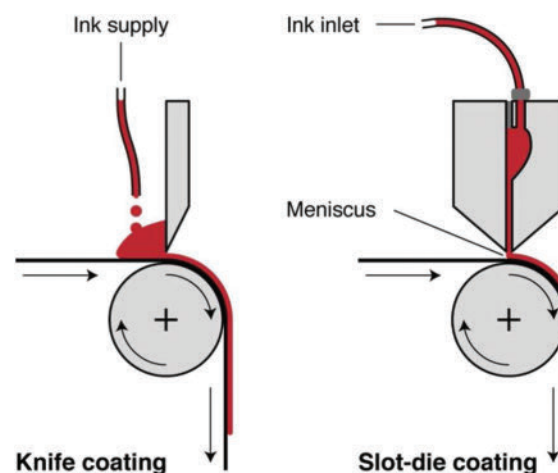


FIGURE 1 Schematic illustration of knife coating and slot-die coating process.

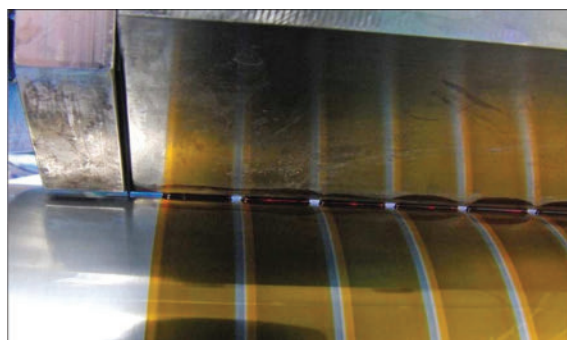


FIGURE 2 Picture of slot-die coating using a meniscus guide.

speed. It is therefore classified as a premeasured coating method.

Both knife and slot-die coating can be used for inks with large varieties in viscosity and solvents, and compared to many other coating and printing techniques they are also relatively forgiving with respect to wetting of the substrate as the ink is “poured” into the substrate compared to printing techniques where surface tension and surface energy play a more significant role in the transfer of the ink. Dewetting of the formed film will occur if the surface tension of the ink is larger than the surface energy of the substrate. The wetting of inks with a high surface tension (i.e., water-based inks and dispersions) can be achieved by pretreatment of the substrate with processes such as corona or plasma treatment that raises the surface energy of the substrate (this is in general valid for all coating and printing methods).

Processing speeds for both knife and slot-die coating can be performed at speeds ranging from 0.1 to 200 m/min. Currently, manufacture of functional thin films (e.g., for organic solar cells) has been reported at speeds lower than 5 m/min. This is possibly linked to the need for a thermal treatment of the active layer post film formation. In laboratory-scale or pilot-scale equipment, the oven length is often limited and therefore processing speed is drying length dependent rather than ink coatability/printability dependent.

Screen Printing

Opposed to the one-dimensional R2R coating, all the R2R printing techniques are two dimensional (2D) and thus allow for/require a defined pattern. In screen printing, the desired pattern is defined by the open area of an otherwise filled mesh. A squeegee, which moves relative to the mesh, then forces the ink through the open area and onto the substrate. The wet layer thickness is defined by the thickness as well as the open area of the mesh and generally relative thick wet layers can be achieved (10–500 μm). The technique is generally only useful for rather high-viscosity inks with thixotropic (shear-thinning) behavior, as inks with lower viscosities will simply run through the mesh.

There are two types of screen printing—flat bed and rotary screen printing—as illustrated in Figure 3. Flat bed screen printing is a stepwise process, where the screen is lowered on top of the substrate, the squeegee is then swiped over

the screen resulting in the transfer of the ink, and finally the screen is lifted and the substrate is manually changed or moved forward after which the process can be repeated. Stepwise processes are generally not desirable in R2R processing as they are more time-consuming, but flat bed screen printing has been successfully adapted to R2R processing. The screens used are easily patterned in a variety of sizes and are fairly low in cost. This makes flat bed screen printing a powerful tool for small laboratory systems, either in a tabletop configuration or in a small- to medium-scale R2R configuration.

Fully continuous processing is best achieved through rotary screen printing, which uses the same principle as flat bed printing but in this case the web of the screen is folded into a tube and the squeegee and the ink are placed inside the tube. As the screen rotates with the same speed as the substrate the ink is continuously pushed through the open area of the screen by the stationary squeegee, making a full print upon every rotation. Much higher processing speeds can be achieved by use of rotary screen printing (>100 m/min) compared to flat bed (0–35 m/min), but the screens are quite expensive and they are much more difficult to clean because of the restricted access to the inside of the screen. The process furthermore requires a longer adjustment run-in (adjusting the print with previously processed layers) compared to flat bed. This gives a higher initial waste, but once the process is running the procedure is very reliable.

Gravure Printing

Gravure printing is a widely used printing technique commonly used in the printing of high-volume catalogs and magazines. The technique relies on surface tension transfer of ink from small engraved cavities in the gravure cylinder to the substrate. Good contact between the substrate and the gravure cylinder is ensured by use of a softer impression cylinder, and the final imprint is defined by the patterning of the cavities in the gravure cylinder. The cavities are continuously refilled by passing an ink bath and excess ink is removed by use of a doctor blade. A more advanced ink filling method is achieved by using a chambered doctor blade system, which can be advantageous for inks containing highly volatile solvents. The gravure cell volume and the pick-out ratio mainly define the transferred wet layer thickness on the substrate. Gravure printing applies well for printing of low-viscosity inks and is well suited for very high processing speeds (up to 15 m/s). Gravure offset printing, gravure coating, and reverse gravure coating are further methods based on an engraved gravure cylinder, whereas it is only patterned for the printing process.

Flexographic Printing

In flexographic printing, the transfer of ink happens through direct contact of a soft printing plate cylinder, typically made of rubber or a photopolymer, onto which the desired motif stands out as a relief (like on a traditional stamp). The inking of the printing plate cylinder is provided via a ceramic anilox roller with engraved microcavities embedded into the exterior surface. The anilox cylinder is continuously supplied

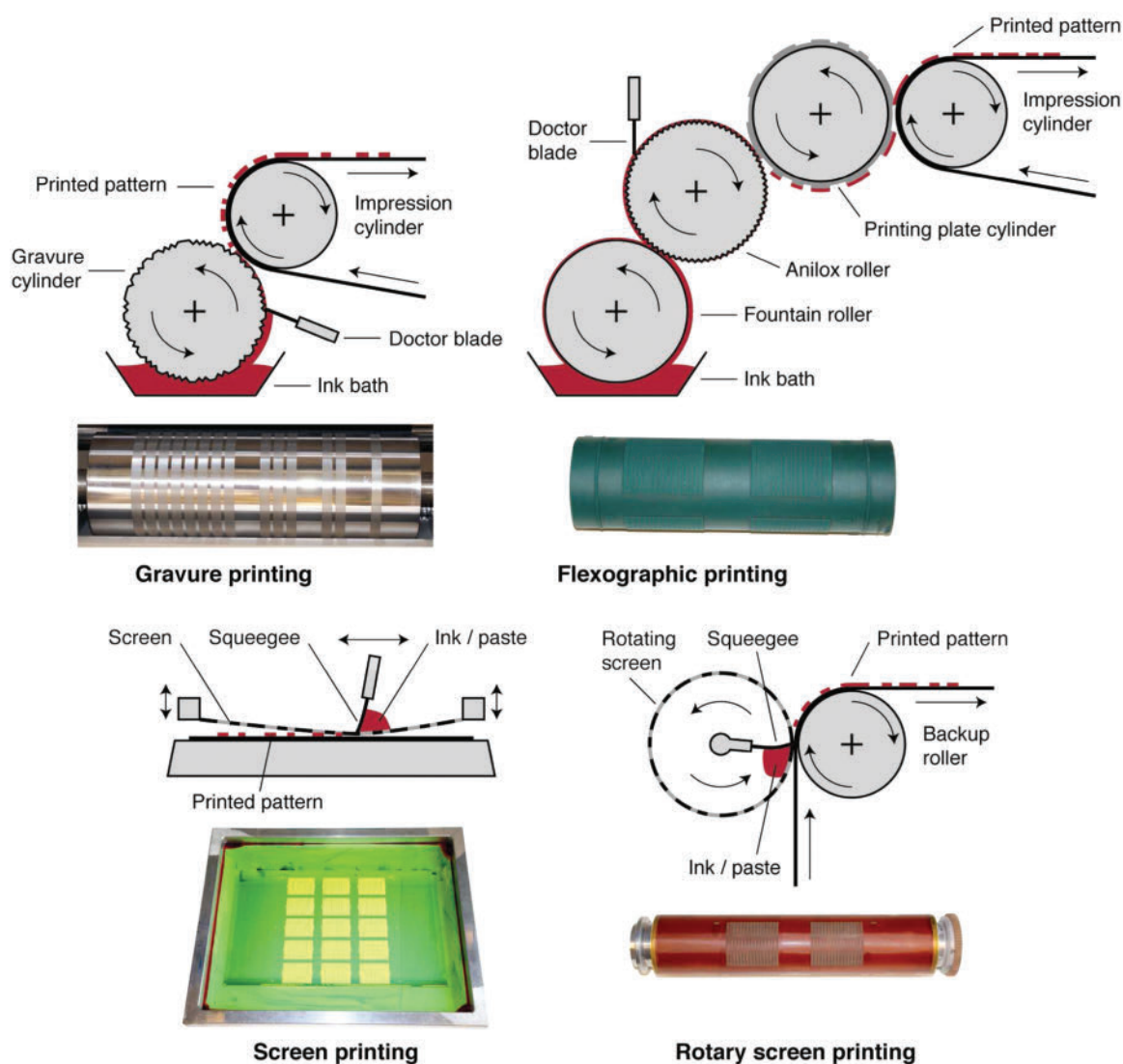


FIGURE 3 Schematic illustration of printing techniques with permanent printing forms, namely gravure printing, flexographic printing, and screen printing in flatbed or rotary design. Underneath each illustration is a picture of a corresponding printing form.

with ink by contact with a fountain roller that is partly immersed in an ink bath. Similar to gravure printing excess ink on the anilox is removed by a doctor blade ensuring good control of the wet layer thickness, which is defined by the volume of the cavities in the anilox cylinder (anilox volume) and the transfer rates from the printing plate cylinder to the substrate. The inking principle based on a chambered doctor blade system is also suitable in this case (similar to the gravure process).

Inkjet Printing

In contrast to the traditional printing techniques where the ink is transferred from or through a permanent printing form to the substrate, inkjet printing is classified as a full digital nonimpact printing method with images generated on demand. Two-dimensional patterning is obtained by a pixelated pattern with a defined resolution. Each pixel will either

receive a droplet of ink or not, as shown in Figure 4. The most abundantly used method, referred to as drop-on-demand (DOD), uses a piezoelectric material to shoot droplets from a nozzle which is situated ~ 1 mm from the substrate. The DOD system requires many nozzles which in the early days caused limitation in web speeds and resolution, but today both high web speeds and high resolution can be achieved with the available commercial systems. The pattern shown in Figure 4 was printed on a R2R inkjet printer capable of a resolution of 600 DPI with web speeds ≤ 75 m/min. The major advantage of the inkjet printing technique compared to other 2D techniques is the possibility to change/adjust the printed pattern easily on a computer without the need to manufacture a physical printing form (i.e., it uses a digital master). Inkjet printing is a relatively new technology on an industrial scale and presents some limitation with respect to processing speeds and ink formulation. Especially

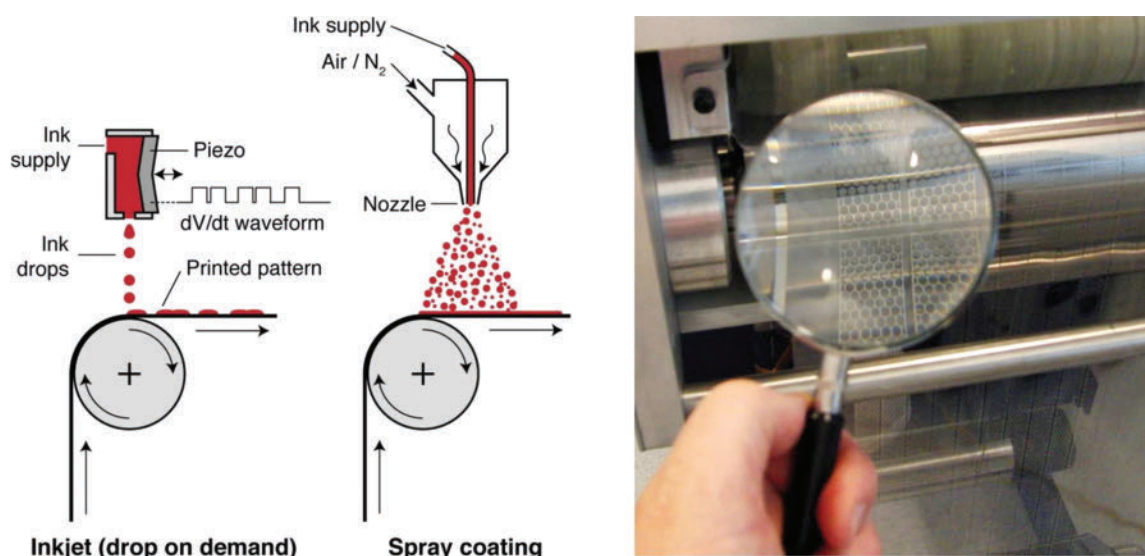


FIGURE 4 Left: Schematic illustration of piezo-based drop on demand inkjet printing and spray coating. Right: Example of a R2R inkjet printed silver pattern.

the latter point has put constraints on the use of the technology for organic film formation.

Spray Coating

Although spray coating cannot be counted as a printing method, it shows similarities to inkjet printing. In spray coating, a continuous spray of ink is generated in a nozzle instead of being digitally timed drops as in the case of DOD inkjet. In pneumatic-based systems, the ink gets atomized at the spray nozzle where pressurized air or gas (e.g., nitrogen) breaks up the liquid bulk into droplets.⁹ The liquid properties (surface tension, density, and viscosity), the gas flow properties, and the nozzle design influence the entire atomization process. The kinetic energy of the droplets helps them to spread upon impact on the substrate. Furthermore, the quality of the coated layer is based on several process parameters such as the distance of the spray nozzle to substrate, coating speed, and the number of sprayed layers. Other forms of spray generation are ultrasonication with a directed carrier gas¹⁰ or electrospraying.¹¹ Pattern formation with spray coating is only possible with the help of shadow masks. The spray method has a high R2R compatibility, but the disadvantage of ink mist has to be considered, as it can cause contamination of the processing equipment. The ink loss when using a shadow mask and the low edge resolution is also a fundamental disadvantage. As a coating method for fully covering layers, it can be used in conjunction with laser ablation or other patterning methods postfilm formation.

CURRENT STATUS WITHIN DIFFERENT RESEARCH FIELDS

R2R coating and printing is an emerging processing method within the field of organic/polymer thin film device fabrication. "True" R2R equipment is very costly to acquire, and as a consequence reports of "true" R2R processing are limited to very few groups. To give a broader picture of how the above described processing methods have been used so far,

we have chosen to include R2R-"compatible" processing techniques (sheet-to-sheet processing and the use of nonflexible substrates) in our overview of the current status of the field. It is important to stress though that there are huge differences between a process being claimed as R2R-compatible and true R2R processing, and the results obtained using the compatible processing will not be directly transferable to R2R! Table 1 gives a summary over various processing of layers in polymer-based devices including electrodes, blocking layers, and active layers and other layers in organic photovoltaic (OPV), organic thin film transistor (OTFT), polymer light-emitting diode (PLED), and electrochromic (EC) devices. The table also illustrates the fact that different coating or printing methods might be suited for processing of a specific layer, while proving less useful for the processing of others. Fixing the eye on a single technique for the processing of a whole device thus might prove less efficient than using several different techniques optimized for each specific layer. Figure 5 shows typical device architectures of OPVs, OTFTs, PLEDs, and EC devices.

Large Area Organic Solar Cells

Organic solar cells are as indicated in Figure 5 multilayer structures of typically a transparent electrode, a hole or electron blocking layer, the active layer (comprising a bulk heterojunction of a polymeric absorber, which acts as a donor material and an acceptor material typically a fullerene), a hole or electron blocking layer (the opposite of the one placed on top of the transparent electrode), and finally a back electrode.

A large palette of R2R techniques have been used in the preparation of organic solar cells, with slot-die coating at present being the most abundantly used for processing of hole/electron blocking layers and the active layer. On the other hand, screen printing is by far the most widely used

TABLE 1 Overview of Reported Polymer Thin Film Devices Using R2R or R2R-Compatible Techniques

Device Type	Processed Polymer, Electrode or Intermediate Layer	Processing Method	R2R (y/n)	Comments and Device Parameters	Ref.
OPV	- PEDOT:PSS - ZnO - P3HT:PCBM - PEDOT:PSS - Carbon back electrode	- rotary screen printing - slot-die - slot-die - screen printing	y	- ITO and silver free - on PET (PCE: 1.6%, 16 stripe modules, 15.5 cm ²)	12
OPV	- semitransparent silver front electrode - PEDOT:PSS - ZnO - P3HT:PCBM - PEDOT:PSS - silver back electrode	- thermally R2R imprinted grid which is subsequently filled, flexo, and inkjet. - rotary screen printing - slot-die - slot-die - screen printing	y	- ITO-free - study of embedded versus raised silver front grids prepared by different R2R methods - on PET (embedded, PCE: 1.92%, 6 cm ²) - on PET (flexo, PCE: 1.82%, 6 cm ²) - on PET (inkjet, PCE: 0.79%, 6 cm ²)	13
OPV	- PEDOT:PSS	- slot-die	y	- ITO-free on PET (2.3–3.11%, 0.25 cm ²)	14
OPV	- Al-Cr - P3HT:PCBM - PEDOT:PSS - silver back electrode	- R2R evaporated - slot-die - slot-die - screen printing	y	- ITO-free - on Kapton (PCE: 0.5%, 16 stripe modules, 235 cm ²)	15
OPV	- silver front electrode (semitransparent) - ZnO - P3HT:PCBM - PEDOT:PSS - silver back electrode	- slot-die - slot-die - slot-die - screen printing	y	- on PET (barrier foil), ITO-free - PCE: 0.44% (best), 16 stripe module, 35.5 cm ²	16
OPV	- glue/ZnO - P3HT:PCBM - PEDOT:PSS	- gravure - gravure - flexo	y	- ITO-free - on paper (PCE: 1.31%, 0.09 cm ² , at 600 W/m ²)	17
OPV	- ZnO - P3HT:PCBM - PEDOT:PSS - silver back electrode	- slot-die - slot-die - slot-die - screen printing	y	- "ProcessOne" - on PET (PCE: 1.78%, 8 stripe modules, 120 cm ²)	18
OPV	- ZnO - P3HT:PCBM - PEDOT:PSS - silver back electrode	- slot-die - slot-die - slot-die - screen printing	y	- on PET (PCE: average ≈ 2% (13,500 modules, 16 stripes, 15.4 cm ²) - Manufacture of more than 10,000 units of a module integrated flashlight demonstrator	19
OPV	- ZnO - P3HT:PCBM - PEDOT:PSS - silver back electrode (using a variety of silver inks)	- slot-die - slot-die - slot-die - screen printing	y	- on PET (PCE: 1.18% (±0.13), 150 modules, 16 stripe, 360 cm ²) - on PET (PCE: 1.22% (±0.11), 300 modules, 16 stripe, 160 cm ²) - on PET (PCE: 1.79% (±0.09), 600 modules, 16 stripe, 96 cm ²)	20

TABLE 1 (Continued)

Device Type	Processed Polymer, Electrode or Intermediate Layer	Processing Method	R2R (y/n)	Comments and Device Parameters	Ref.
OPV	- ZnO - P1/PCBM or P2/PCBM - PEDOT:PSS - silver back electrode	- slot-die - slot-die - slot-die - screen printing	y	- on PET (P1, avg. PCE for 100 cells: $1.24\% \pm 0.13\%$, 4.2 cm^2) - on PET (P2, avg. PCE for 100 cells: $0.29\% \pm 0.06\%$, 4.2 cm^2)	21
OPV	- ZnO - PDTTDABT/PCBM - PEDOT:PSS - silver back electrode	- slot-die - slot-die - slot-die - screen printing	y	- on PET (PCE: 0.60% , 16 stripe module, 96 cm^2)	22
OPV	- ZnO - P3HT:PCBM - <i>n</i> -octanol as wetting agent - PEDOT:PSS - silver back electrode	- slot-die - slot-die - flexo - slot-die - rotary screen printing	y	on PET (PCE: $1.96\% \pm 0.34\%$, 1,960 modules, 16 stripes, 15.5 cm^2)	23
OPV	- ZnO - side chain cleavable copolymer:PCBM - PEDOT:PSS - silver back electrode	- slot-die - slot-die + flash light annealing - slot-die - screen printing	y	- on PET R2R coated (PCE: 0.5% , 16 stripe module, 35.5 cm^2) - on PET roll coated (PCE: 0.63% , 1 cm^2)	24
OPV	- ZnO - PG3:PCBM - PEDOT:PSS - silver back electrode	- slot-die - slot-die - slot-die - screen printing	y	- on PET (PCE $> 0.7\%$, 4.2 cm^2) - on PET (PCE: 0.3% , 12 stripe module, 450 cm^2)	25
OPV	- P3HT:PCBM - PEDOT:PSS - silver back electrode	- slot-die - slot-die - screen printing	y	- single roll coater with a 300-mm diameter roll - on PET (PCE: 1.57% , 1 cm^2)	26
Hybrid OPV	- ZnO - P3MHOCT/ZnO np - PEDOT:PSS - silver back electrode	- knife or slot-die - slot-die - slot-die or screen printing - screen printing	y	on PET (PCE: 0.84% , 8 stripe module, 120 cm^2)	27
Hybrid OPV	- ZnO - P3HT:PCBM/ZnO np or P3MHOCT/ZnO np - PEDOT:PSS - silver back electrode	- screen printing - screen printing - screen printing - screen printing	y	on PET (2,124 modules, 133 cm^2)	28
OPV	- PEDOT:PSS - P3HT:PCBM	- slot-die - slot-die	y	on PET (3 stripe module)	29
OPV	- PEDOT:PSS - P3HT:PCBM	- slot-die - slot-die	y	on PET (PCE: 1.7% , 0.25 cm^2)	30
OPV	- PEDOT:PSS - P3HT:ICBA	- slot-die	y	- solvent study - on PET (PCE: 3.2% , 0.25 cm^2)	31
OPV	- silver front electrode grid	- screen printing	n	- ITO-free - on PEN (PCE: 1.93% , 4 cm^2)	32
OPV	- PEDOT:PSS - P3HT:PCBM	- slot-die - slot-die	n	- ITO-free - on PET (PCE: 2.2% , 11 stripe module, 13.2 cm^2) - on glass (PCE: 2.5% , 11 stripe module, 13.2 cm^2)	33

TABLE 1 (Continued)

Device Type	Processed Polymer, Electrode or Intermediate Layer	Processing Method	R2R (y/n)	Comments and Device Parameters	Ref.
OPV	- PEDOT:PSS - P3HT:PCBM	- gravure - gravure	n	- on polycarbonate (PCE: 1.68%, 0.03 cm ²)	34
OPV	- PEDOT:PSS - P3HT:PCBM	- gravure - gravure	n	- on PET (PCE: 1.68%, 8 stripe module, 15.45 cm ²)	35
OPV	- PEDOT:PSS - P3HT:PCBM	- gravure - gravure	n	- on PET (PCE: 2.8%, 0.019 cm ²)	36
OPV	- TiO _x - P3HT:PCBM - PEDOT:PSS	- gravure - gravure - gravure	n	- on PET (PCE: 0.6%, 0.045 cm ²)	37
OPV	- PEDOT:PSS	- inkjet	n	- on glass (PCE: 3.16%, 0.09 cm ²)	38
OPV	- P3HT:PCBM	- inkjet	n	- on glass (PCE: 1.4%, ~0.03 cm ²)	39
OPV	- P3HT:PCBM	- inkjet	n	- on glass (PCE: 2.9%, 0.2 cm ²)	40
OPV	- P3HT:PCBM	- inkjet or knife	n	- on glass (PCE: 3.47% (0.2 cm ²) - on glass (PCE: 4.05 (0.2 cm ²)	41
OPV	- PEDOT:PSS - P3HT:PCBM	- inkjet - inkjet	n	- on glass (PCE: 3.71% (0.09 cm ²)	42
OPV	- PEDOT:PSS - P3HT:PCBM	- inkjet - inkjet	n	- on glass (PCE: 2.40% (0.16 cm ²)	43
OPV	- P3HT:PCBM	- spray	n	- on glass (PCE: 2.91% (unknown area)	44
OPV	- PEDOT:PSS - P3HT:PCBM	- knife or spray - spray	n	- on glass (PCE: 2.7–3.1%, ~0.02 cm ²)	45
OPV	- P3HT:PCBM	- spray	n	- on glass (PCE: 3.2%, 0.11 cm ²)	10
OPV	- P3/PCBM	- spray	n	- on glass (PCE: 5.84%, 0.12–0.15 cm ²)	46
OPV	- P3HT:PCBM	- spray	n	- on glass (PCE: 2.17%, 0.01 cm ²)	47
OPV	- P3HT:PCBM	- spray	n	- successive deposition of donor and acceptor material - on glass (0.9 or 0.25 cm ² cells)	48
OPV	- PEDOT:PSS back electrode	- spray	n	- vacuum free - on glass (PCE: 0.5%, ~0.07 cm ²)	49
OPV	- P3HT:PCBM	- spray	n	- on glass (PCE: 2.84%, 0.03 cm ²)	50
OPV	- P3HT:PCBM	- spray	n	- on glass (PCE: 0.48%, 0.64 cm ²)	51
OPV	- P3HT:PCBM	- spray	n	- on glass (PCE: 4.1%, 0.25 cm ²)	52
OPV	- Cs ₂ CO ₃ - P3HT:PCBM - PEDOT:PSS	- spray	n	- on glass (PCE: 1.2%, 0.04 cm ²)	53
OPV	- PEDOT:PSS - P3HT:PCBM	- spray	n	- on glass (PCE: 3.52%, 0.03 cm ²)	54
OPV	- PEDOT:PSS - P3HT:PCBM	- spray	n	- on glass (PCE: 2.17%, 0.0466 cm ²)	55
OPV	- silver back electrode	- spray	n	- on glass (40–100 μΩ cm) - on glass (PCE: 2.5%, 0.03 cm ²)	56
OPV	- silver back electrode	- spray	n	- on flexible substrate (PCE: 1.4%, area not given) - on glass (PCE: 3%, area not given)	57
OPV	- P3HT:PCBM	- screen printing	n	- on glass (PCE: 2.38%, 3 cm × 1 cm in series)	58

TABLE 1 (Continued)

Device Type	Processed Polymer, Electrode or Intermediate Layer	Processing Method	R2R (y/n)	Comments and Device Parameters	Ref.
Hybrid OPV	- PEDOT:PSS - P3HT/unknown nanoparticles	- knife or slot-die - knife or slot-die	n	- on glass (PCE: 1.18%, 0.0785 cm ²)	59
OTFT	- PEDOT:PSS electrodes - PTPA2 semiconductor - butylene copolymer dielectric - PMMA dielectric	- gravure - gravure - gravure	y	- 50,000 transistors (75% yield) - on PET substrate - on/off ratio < 100	60
OTFT	- silver source/drain electrodes - P3HT semiconductor - PVP dielectric - PEDOT:PSS gate electrodes	- inkjet - reverse gravure coating - reverse gravure coating - inkjet	y/n	- on PEN substrate - on/off ratio 10 ² - threshold voltage 0.5 V	61
OTFT	- PEDOT:PSS source/drain - F8T2 semiconductor - butadiene-styrene copolymer dielectric - BaTiO ₃ dielectric - silver gate electrode	- offset printing - gravure - gravure - flexo - flexo	y/n	- on PET substrate - channel length 100 μm - on/off ratio 320 - mobility 1.3 × 10 ⁻³ cm ² /V s - seven-stage ring oscillator frequency 4 Hz	62
OTFT	- silver electrodes - PVP dielectric - TIPS-pentacene active layer	- all inkjet	n	- on polyarylate substrate - mobility 0.02 cm ² /V s - on/off ratio 10 ⁴ - threshold voltage -1.2 V	63
OTFT	- P3HT - PVP, PVA, PMMA, PHEMA dielectrics - silver gate electrodes	- all gravure	n	- on polyethersulfone (PES) substrate - on/off ratio > 10 ⁴ - mobility 0.04 cm ² /V s	64
OTFT	- silver source/drain and gate electrodes - PVP dielectric - pBTTT semiconductor	- gravure/inkjet - gravure - gravure	n	- on PEN substrate - channel length < 20 μm - on/off ratio 10 ⁶ - mobility 0.06 cm ² /V s	65
OTFT	- triarylamine copolymer semiconductor - perfluoropolymer dielectric (Cytop) - silver gate electrodes	- screen printing/gravure - inkjet - inkjet	n	- on PEN substrate - on/off ratio > 10 ⁴ - mobility > 0.026 cm ² /V s	66
PLED (LEC)	- ZnO - blend of polymer "Super Yellow" and KCF ₃ SO ₃ in poly(ethylene oxide) - PEDOT:PSS	- slot-die - slot-die - slot-die	(y)	- on PET, up to 3 cm ² - brightness 150 cd/m ² (10 V) - current eff. 0.6 cd/A at 50 cd/m ²	67
PLED	- phenyl-substituted poly(<i>para</i> -phenylene vinylene) (Super Yellow) - poly(ethylene oxide) - ZnO - PEDOT:PSS	- knife - knife - knife - knife	n	- on glass - 5.26 cd/A - 14,120 cd/m ² (7.8 V) on 0.06 cm ²	68
PLED	- PEDOT:PSS - blue-emitting polymer in <i>o</i> -xylene	- gravure - gravure	n	- on glass, 30 cm ² - luminance 1,000 cd/m ² (5.4 V)	69

TABLE 1 (Continued)

Device Type	Processed Polymer, Electrode or Intermediate Layer	Processing Method	R2R (y/n)	Comments and Device Parameters	Ref.
PLED	- MEH-PPV	- inkjet	n	- on glass, - luminance 1,850 cd/m ² (9 V) - efficiency 0.17 cd/A	70
PLED	-MEH-PPV/rubrene	- gravure	n	- on glass - > 400 cd/m ² (9 V)	71
OLED	- PEDOT:PSS - small molecules in PVK host solution	- knife - knife	n	- on glass, 6 cm ² - 25 cd/A (10 V) - max. 20,000 cd/m ²	72
OLED	-Small molecules in PVK host solution	- screen printing	n	- on glass - 63.2 cd/A and 650 cd/m ² (17.1 V) - max. 21,000 cd/m ² (35 V)	73
EC	- ECP-magenta - MCCP	- slot-die and spray - slot-die	(y)	- magenta → transparent - single roll coater - on PET [$\Delta T \sim 45.4\text{--}39.1\%$ (10–2.3 s), >10 cm ²]	74
EC	- ProDOT–phenylene polymer	- spray	n	- yellow → “transparent” - on glass [$\Delta T \sim 73\text{--}30\%$ (10–0.25 s)]	75
EC	- ECP-orange - ECP-red	- spray - spray	n	- red or orange → “transparent” - on glass ($\Delta T \sim 47\text{--}52\%$, t_{95} : 3.9–7.1 s) - on glass ($\Delta T \sim 38\text{--}60\%$, t_{95} : 1.1–4.9 s)	76
EC	- four disubstituted ProDOT polymers	- spray	n	- red or light purple → “transparent” → purple - on glass (ΔT : 51–80%, t_{95} : 0.37–2.2 s, $\sim 2\text{--}6$ cm ²)	77
EC	- disubstituted ProDOT polymers	- spray	n	- film thickness and morphology study	78
EC	- ProDOT-benzothiadiazole copolymer	- spray	n	- blue → transparent (light green) - on glass [$\Delta T \sim 42\text{--}39\%$ (10–1 s)]	79
EC	- two green polymers	- spray	n	- green → light green - on glass ($\Delta T \sim 39\text{--}36\%$, 10–1 s) - on glass ($\Delta T \sim 44\text{--}40\%$, 10–1 s)	80
EC	- polyaniline-silica colloidal composite - PEDOT-silica colloidal composite	- inkjet - inkjet	n	- on PET - electrochromic patterns	81
EC	- water-dispersible polyaniline composite materials with carbon nanotube	- inkjet		- yellow → green → blue - on PET, glossy photopaper, glass and PVDF	82
EC	- coating of electrolyte	- “screen printing” (screen is a precut barrier foil)	n	- on polyester substrate	83

TABLE 1 (Continued)

Device Type	Processed Polymer, Electrode or Intermediate Layer	Processing Method	R2R (y/n)	Comments and Device Parameters	Ref.
EC	- PEDOT:PSS - V_2O_5	- screen printing - screen printing	n	- on Mylar substrate	84
LS	- PEDOT:PSS - P(VDF-TrFE)	- flexo - screen printing	N	- on paper (sound pressure level 63.8 dB at 5,000 Hz, max. 80 dB, driving voltage ~50 V, and area 16 and 128 cm ²)	85

Only layers that have been processed by R2R or R2R-compatible techniques have been mentioned and they do not represent the complete device stack. A distinction has been made between "true" R2R processing and R2R-compatible processing.

OPV, organic photovoltaic; OTFT, organic thin film transistor; PLED, polymer light-emitting diode; EC, electrochromic; LS, loudspeaker; P3HT, poly(3-hexylthiophene); PCBM, phenyl-C61-butyric acid methyl ester; PEN, poly(ethylene 2,6-naphthalate); PEDOT:PSS, poly(3,4-ethylenedioxythiophene) poly(styrenesulfonate); P3MHOCT, polythiophene carrying tertiary ester groups; np, nanoparticle; ICBA, indene-C₆₀-bisadduct; P1 and P2, polymers are based on an alkoxy-substituted benzothia-

diazole acceptor unit and unsubstituted benzodithiophene donor units; P3, poly[4,8-bis(1-pentylhexyloxy)benzo[1,2-b:4,5-b']dithiophene-2,6-diyl-*alt*-2,1,3-benzoxadiazole-4,7-diyl]; PG3, polymer based on benzothiadiazole, dialkoxythiophene, and thiophene; ProDOT, 3,4-propylenedioxythiophene; ECP-orange, polymer of bis(ethylhexyloxy)-thiophene; ECP-red, copolymer of bis(ethylhexyloxy)-thiophene and dimethoxythiophene; PVDF, poly(vinylidene fluoride); ΔT , difference in transmittance between the oxidized state and the reduced state in EC devices; t_{95} , time to reach 95% of full optical contrast between neutralized and fully oxidized states in EC devices; P(VDF-TrFE), poly(vinylidene fluoride-trifluoroethylene).

for processing of the back electrode, and is a good example of how different processing procedures can be more suitable than others for the processing of a specific layer.

Krebs et al. introduced a new fabrication method for all R2R-processed OPVs on indium tin oxide (ITO)-coated PET substrates in 2009,¹⁸ with an architecture of PET|ITO|ZnO|active layer|PEDOT:PSS|silver, which has since been referred to as "ProcessOne." The first three layers (ZnO, active layer, and PEDOT:PSS) were processed using slot-die coating, and finally a silver back electrode was slot-die coated or flat bed screen printed to finalize the stack before it was laminated. Since then, numerous productions of solar cells and modules based on this method have been published,^{20–26} and solar modules produced according to this have been used in interlaboratory studies,^{86,87} round robins,^{88,89} and in demonstrators of various kinds that have mostly involved sound, light, or in one case a laser (see Fig. 6).^{19,23,28,90} The ProcessOne solar modules based on P3HT:PCBM are presently at a stage with a lifetime of 1 year (T_{80}) when exposed to outdoor weather conditions.

Various examples of the use of R2R-processed low-bandgap (LBG) polymers have been reported^{21,22,24,25} with efficiencies approaching what can be achieved with P3HT:PCBM. These are, however, still generally inferior in performance, which can be ascribed to the fact that it takes a large effort (and a lot of material) to fully explore a new polymer. This goes to show that direct transfer of small-scale technology cannot always be expected, as the use of several different LBG polymers in small-scale devices has proven to be more efficient than P3HT:PCBM, when prepared in a glove box and with evaporation of electrodes. In a more special case, Helgesen et al. used a R2R photonic flash lamp to remove the side chains of the used polymer by selective heating of the active layer to high temperatures without heat damaging the flexible plastic substrate. The reason for removing solubilizing side chains in this extra step was to improve device stability

as the solubilizing side chains are known to induce instability to the polymer.²⁴

Another of the more exotic examples of R2R-processed solar cells was presented by Hübler et al. who have prepared fully R2R-processed solar cells on paper using a combination of gravure and flexo printing.¹⁷ The processing starts with gravure printing of a glue onto a paper substrate. The glue patterned paper is then brought into contact with a zinc-coated transfer foil, transferring the zinc only onto the patterned glue, and the surface of the zinc is then oxidized creating a thin hole blocking layer. The active layer (P3HT:PCBM) is now coated on top of the ZnO by use of gravure printing, and the device is finalized by flexo printing a thin layer of PEDOT:PSS as a transparent back electrode. Small devices (0.09 cm²) showed maximum efficiencies of 1.31% at 600 W/m². Figure 7 shows a picture of the final device.

One of the interesting things about the report from Hübler et al., besides the fact that they use paper as substrate, is that the architecture is ITO-free. ITO has for decades been the preferred transparent electrode material in many types of electronic devices, because of its high transparency combined with a low sheet resistance, but the scarcity of indium makes ITO quite expensive and the cost of indium accounts for the majority of the device cost. Much effort has been put into finding alternatives, and Galagan et al. showed that a silver collecting grid, screen printed on a PEN substrate and subsequently spin-coating of a high-conducting PEDOT:PSS solution on top, is a way of substituting ITO.³² Good efficiencies (1.93%, 4 cm²) were obtained using P3HT:PCBM for the active layer (spin-coated in glove box) and evaporative deposition of LiF/Al as the electrode, but the use of spin-coating, inert atmosphere, and low-pressure deposition makes the procedure difficult to transfer to a R2R setting.

Other examples where full R2R processing is actually achieved have recently been presented though.^{12–14} Larsen-

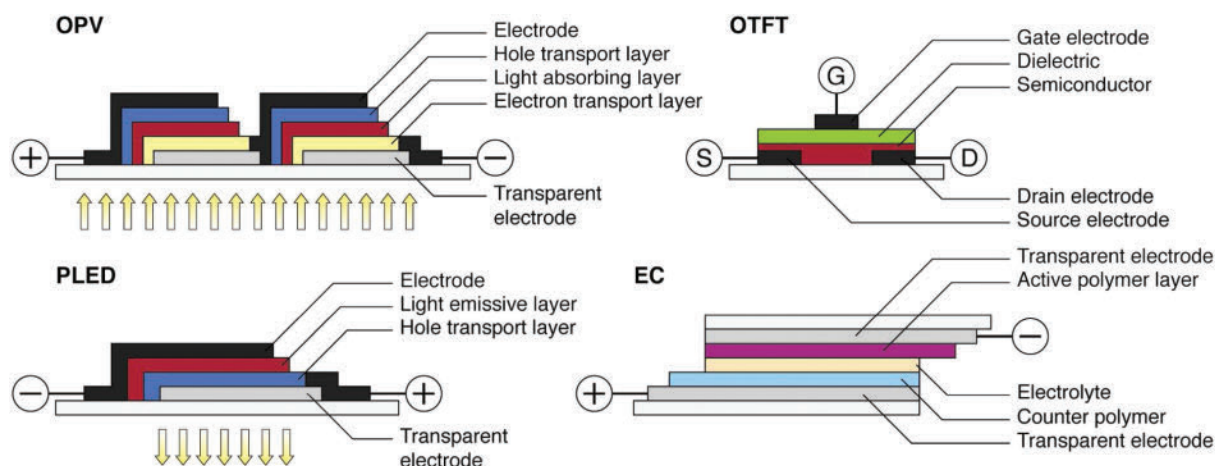


FIGURE 5 Device architecture of typical devices of OPVs (here shown as a full R2R-processable module with inverted structure), OTFT (top-gate bottom-contact structure), PLED (conventional structure), and EC devices (absorptive/transmissive multilayer structure).

Olsen et al. showed that the use of high-conductive PEDOT:PSS with or without a preprocessed silver collecting grid can be used as a substitute for ITO in inverted structure devices and modules with good results.^{12,14} By appliance of a short pulse at high negative bias to the solar cell, it is possible to electrochemically “switch” (reduce) a thin layer of the top PEDOT causing a permanent conductivity change rendering it a rectifying junction. Further studies on the use of different types of front grids in the same process were carried out by Yu et al. showing that thermally embedded silver grids and flexo printed silver grids result in solar cells with similar efficiencies (slightly better for the embedded grid), whereas solar modules with inkjet printed silver front grid performed poorer, which was ascribed to the lower conductivity of the grid.¹³

Besides the previously mentioned example of use of paper as substrate by Hübler et al., the use of gravure printing for the preparation of solar cells has only been reported in very few cases.^{34–37} Kopola et al. reported the use of a desktop

gravure printability tester (on PET, not R2R process) to process the hole transport layer (PEDOT:PSS) as well as the active layer (P3HT:PCBM) of single cells³⁶ and of small modules.³⁵ In both reported cases, the back electrode consisted of evaporated calcium and silver resulting in efficiencies of 2.8% for single cells (19 mm²) and 1.9% for small modules (five cells in series, 9.6 cm²) after optimization of the PEDOT:PSS ink with surfactants, wetting agents, and solvent mixtures.

Figure 8 shows an example of the necessity to optimize ink and processing conditions to obtain a smooth and homogeneous active layer and an example of a final flexible device. Voigt et al. recently reported the use of sheet-to-sheet gravure printing of inverted structured cells on PET after performing a systematic study of the wetting behavior of each

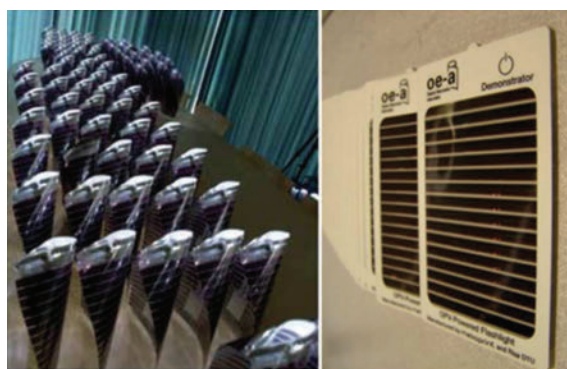


FIGURE 6 Examples of ProessOne fabricated demonstrators. Left: picture of a very simple integrated lamp for the “Lighting Africa” project. Right: picture of a module powered flashlight. Reprinted from Ref. 90 and Ref. 19, with permission from The Royal Society of Chemistry 2010 and The Royal Society of Chemistry 2011, respectively.

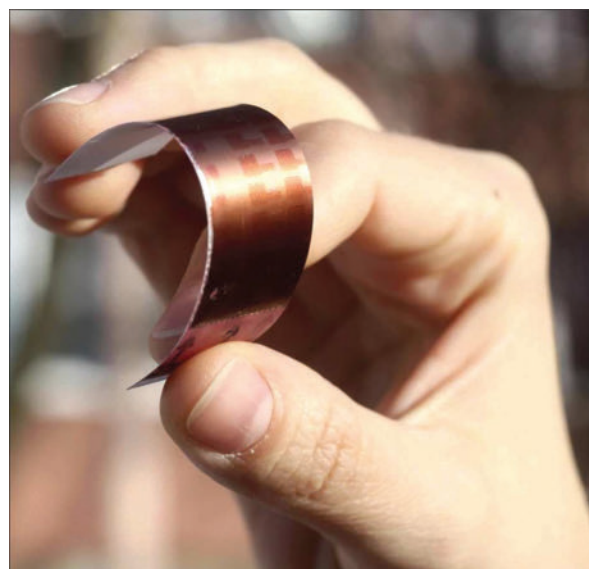


FIGURE 7 Picture of OPV printed on paper. Reprinted from Ref. 17, with permission from 2011 WILEY-VCH Verlag GmbH & Co. KGaA.

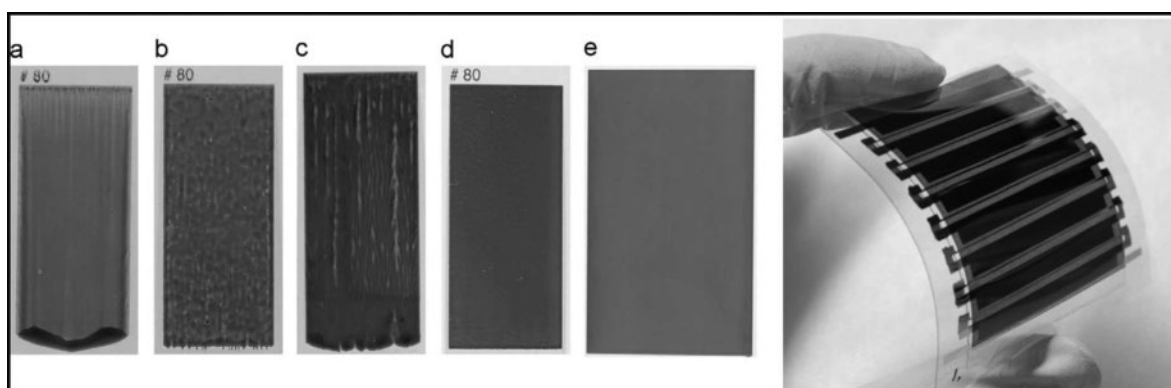


FIGURE 8 Left: Pictures of the optimization of ink and processing conditions for gravure processed P3HT:PCBM. Right: Picture of a gravure printed flexible organic solar cell module. Reprinted from Refs. 35 and 36, with permission from 2010 Elsevier B.V.

layer.³⁷ In this case, three of the layers (TiO_x, P3HT:PCBM, and PEDOT:PSS) were processed by gravure, and the cells were finalized by evaporation of a back gold electrode (4.5 mm², 0.6% PCE).

Also, flexo printing has only had limited application in solar cells and has so far not yet been used for processing of the active layer. The potential of flexographic printing as an extremely fast processing method has so far proven best for the preparation of front grid silver electrodes that were prepared at high speeds (25 m/min).¹³

Among the more specialized coating procedures used for R2R OPV fabrications can be mentioned double-slot-die coating, introduced in organic solar cells by Larsen-Olsen et al. in order to approach a further increase in the production throughput by simultaneous deposition of several layers of the solar cell stack.⁹¹ The double slot-die method illustrated in Figure 9 was used to coat an aqueous suspension of P3HT:PCBM nanoparticles and aqueous PEDOT:PSS at the same time with a processing speed of 1 m/min. Although the solar cells showed a poor performance (PCE of 0.03%) because of the complex bilayer formation process, it demonstrates the potential as a future processing method to lower the energy payback time of organic solar cells.

Another specialized processing method especially for research and development purposes is the differentially pumped slot-die coating.⁹² Hereby two components of the functional ink are mixed together with the ability to generate changing material ratios over the length of the running web. The fast screening method was used to determine the optimum donor-acceptor ratio and film thickness for organic solar cells. The specially designed slot-die head with very low dead volume requires very little amount of material, which makes it an ideal tool to screen new materials in a wide parameter space compared to spin coating. Furthermore, it directly shows the R2R processability. The process has later been used on several occasions to optimize donor/acceptor blends.^{21,22,25}

Electrochromes

Electrochromic devices are based on materials exhibiting electrochromic behavior (materials that present two discrete op-

tical appearances when in a reduced or oxidized electrochemical state). Testing of the electrochromic properties is usually performed by coating the polymer on a substrate with a transparent electrode (typically ITO), followed by immersing into an electrolyte solution together with an expendable counter electrode. The electrochromic properties, such as color change, change in transmittance (ΔT), and switching times, can then be examined through electrochemical oxidation and reduction of the polymer. When wanting to build a thin device the use of a simple counter electrode is generally not preferable because of the slow deterioration of this, but as a substitute one can make use of a complementary redox compound (a material that is reduced when the electrochrome is oxidized and vice versa) deposited on a second substrate also with a transparent electrode. The final device then consists of the two coated substrates with the electrolyte sandwiched in between as shown in Figure 5.

The processing of polymeric ECs has been reported by use of spray coating,^{74,76–80} inkjet printing,^{81,82} screen printing,^{83,84}

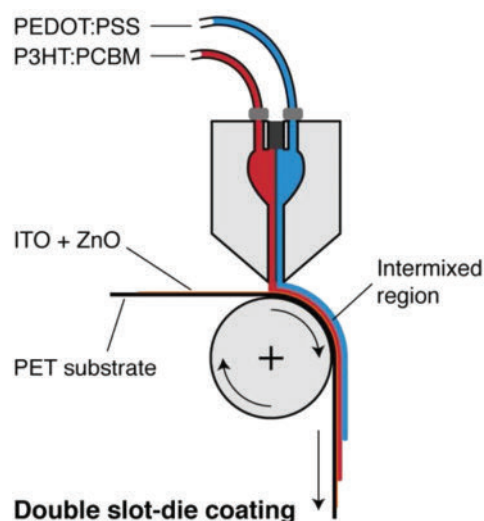


FIGURE 9 Schematic illustration of the double slot-die setup for the simultaneous coating of the P3HT:PCBM active layer and PEDOT:PSS.



FIGURE 10 Left: Picture of slot-die coating and spray coating of polymer electrochromes on a single roll system. Middle: Pictures of an integrated polymer electrochromic/polymer solar cell demonstrator. Right: Examples of inkjet printed electrochromic devices. Reprinted from Ref. 74 and Ref. 81, with permission from 2012 Wiley Periodicals, Inc and The Royal Society of Chemistry 2008, respectively.

and slot-die coating.⁷⁴ Jensen et al. recently presented results showing that slot-die coating (or spray coating) of the electrochromic layers on flexible substrates can be achieved using a single roll coater with a roll having a diameter of 300 mm.⁷⁴ By use of the EC commonly known as ECP-Magenta and a minimally color changing polymer (MCCP) as complementary redox compound, which were both slot-die coated on separate PET/ITO substrates, it was possible to make electrochromic devices $>10 \text{ cm}^2$, which could switch between magenta and a colorless state. Pictures of the coatings are shown in Figure 10. By connecting an electrochromic device ($40 \text{ mm} \times 40 \text{ mm}$) directly with polymer solar cell modules or with batteries charged by polymer solar cells, they furthermore fabricated a demonstrator showing how different polymer thin film technologies can be combined to a final product. The small-scale approach was later upscaled to full R2R processing of ITO-free $18 \text{ cm} \times 18 \text{ cm}$ electrochromic windows printed directly on barrier foil using flexographic printing of metal grids and slot-die coating of the electrochromic polymers (ECP-magenta and MCCP).⁷⁴

With respect to spray coating especially the group of Reynolds has contributed to finding a series of polymers of different colors and optimizing the conditions for the use of this technique.^{76–80} As can be seen from Table 1, a multitude of different colored polymer are available, and recently Dyer et al. could announce that the color palette for spray-processable polymer electrochromics is complete.⁹³

The use of inkjet printing of polymer electrochromes is highly useful when wanting to create patterned EC devices. This is well illustrated in a report by Shim et al., who showed that printing composite dispersions of polyaniline- or PEDOT-covered silica nanoparticles onto PET/ITO enabled preparation of electrochromic devices with good resolution (see Fig. 10).⁸¹

Screen printed flexible electrochromic devices were reported as early as in 1999 by Brotherston et al., who used a combination of PEDOT and V_2O_5 screen printed, respectively, onto separate ITO-coated Mylar substrates and finalized with an electrolyte sandwiched between the two substrates.⁸⁴ The

technique has not become widely used, as the only other example of the use of “screen printing” for electrochromic device preparation is the use of a precut barrier film and a screen printing squeegee for the processing of the electrolyte.⁸³ As no actual screen was used in this latter example, the term screen printing should be taken with modification.

Thin Film Transistors

Although organic solar cells have so far been the most prominent technology to use R2R processing of functional polymer materials, printing is also one of the experimental techniques in a variety of fabrication methods for organic thin film transistors.⁹⁴ In recent years, efforts have been made to R2R manufacture devices including organic thin film transistors to enable integrated circuitry such as inverters⁹⁵ and ring oscillators.⁹⁶ Still, most of the devices containing polymer materials are fabricated by sheet-to-sheet methods using R2R-compatible processes such as inkjet,^{63,97} gravure,^{64,65} screen printing,⁶⁶ and spray coating.⁹⁸ Kang et al., for example, utilize an optimized microgravure process to print silver patterns and poly(4-vinyl phenol) (PVP) dielectric layers.⁹⁹ A transistor with record transition frequencies of $>300 \text{ kHz}$ was achieved with a spin-coated organic semiconductor poly(2,5-bis(3-alkylthiophen-2-yl)thieno[3,2-b] thiophene) (pBTTT).

The transition from batch to R2R processing has partly been carried by Tobjörk et al. by using R2R reverse gravure coating for the deposition of a polymer semiconductor (P3HT) layer and a polymer dielectric PVP for the fabrication of low-voltage organic transistors with an on/off ratio of 100 and threshold voltage of 0.5 V.⁶¹ Silver source/drain electrodes and PEDOT:PSS polymer gate electrodes were sheet-to-sheet inkjet printed. Figure 11 (top) illustrates the processing methods used as well as the final device. The first integrated circuit fabricated completely by means of mass-printing technologies was reported by Huebler et al.⁶² The seven-stage ring oscillator contains organic field effect transistors in a top gate architecture with PEDOT:PSS source/electrodes prepared by offset lithographic printing. Gravure printing was used for the poly(9,9-dioctyl-fluorene-co-bithiophene) (F8T2) semiconductor

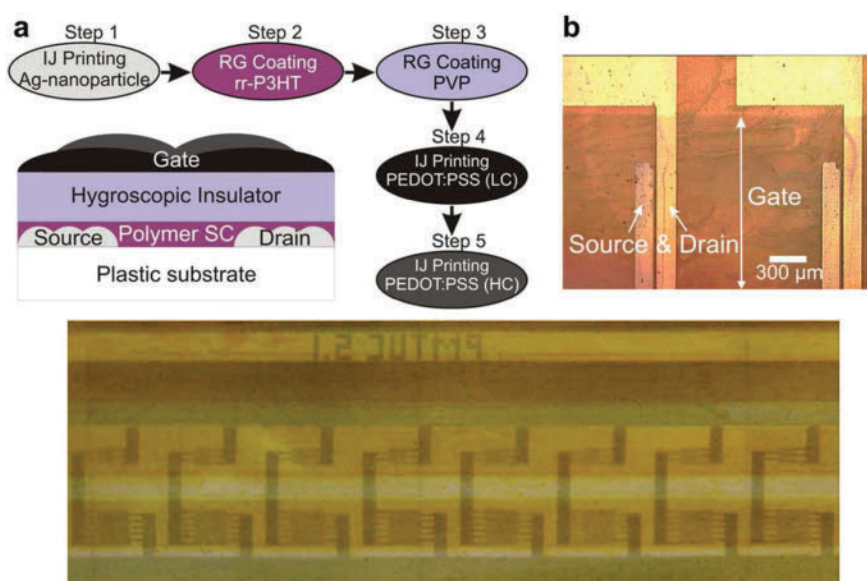


FIGURE 11 Top: Process flow, cross section and optical microscope picture of an all-printed OTFT including inkjet printing R2R reverse gravure coating. Bottom: Photographic image of a fully printed seven-stage ring oscillator. Reprinted from Ref. 61 and Ref. 62, with permission from 2008 Elsevier B.V. and 2007 Elsevier B.V., respectively.

layer and the first butadiene-styrene-copolymer low- k dielectric layer. The device was finalized with flexographic printing of a high- k BaTiO₃ dielectric layer and silver gate electrodes. Although the frequency reached was only 3.9 Hz, it demonstrates the processability with mass-printing technologies with speeds in the order of 1 m/s. A picture of the seven-stage ring oscillator is shown in Figure 11 (bottom).

A combined R2R flexo and gravure process was used to realize PEDOT:PSS source/drain electrodes with channel length down to 10 μm .¹⁰⁰ A negative image of the electrodes was flexo printed from an amorphous perfluorinated poly(alkenyl vinyl ether). A secondary full layer gravure print of PEDOT:PSS leads to a self-formation of the electrodes. Full devices such as OFETs, inverters, and ring oscillators were fabricated with gravure printing of F8T2 semiconductor and dielectric material (butylene copolymer and PMMA). Flexo printing was utilized for the copper electrodes.

Full R2R gravure processing was used for the manufacturing of all-polymer field effect transistors with a yield of $\sim 75\%$ out of a random selection of 50,000 produced transistors.⁶⁰ The report highlights a special electrode layout to avoid longitudinal registration problems. The polymer materials used were PEDOT:PSS (source/drain, gate), PMMA and butylene copolymer (dielectric), and an amorphous poly(triphenylamine) (PTPA2) as semiconductor.

Polymer Light-Emitting Diodes

PLED is a class of organic light-emitting diodes (OLED) where the light-emitting layer is based on polymers opposed to small molecules, which are typically deposited by evaporation processes.^{101–104} OLEDs in general are widely explored and are already in use for display and lighting applications. The layer structure of PLEDs is almost identical to organic solar cells with a light-emitting layer instead of a light-absorbing

layer as seen in Figure 5. Common conjugated polymer materials used as emitting layer are polyphenylene vinylenes such as poly[2-methoxy-5-(2'-ethylhexyloxy)-1,4-phenylenevinylene] (MEH-PPV).¹⁰¹ Another approach is the dispersion of small-molecule emitters in a nonconjugated polymer matrix, such as poly(methyl methacrylate) (PMMA) or polyvinylcarbazole (PVK).¹⁰² One advantage of using polymers is their solubility that enables the solution-based manufacturing similar to organic solar cells with a variety of potential printing and coating processes. Although the processing advantage is present, reports on R2R manufacturing are rare.

Various studies with R2R-compatible methods have been made and show the applicability of slot-die coating,⁶⁷ screen printing,^{73,105,106} blade coating,^{68,72,107} gravure printing,^{69,71,108,109} and inkjet printing,^{70,110,111} which has its advantages for pixel-based display applications. The following reports are highlighted for their closest potential in R2R up scaling. A sample device is shown in Figure 12.

Youn et al. fabricated a PLED based on the yellow-emitting phenyl-substituted poly(*para*-phenylene vinylene) (Super Yellow).⁶⁸ All layers including PEDOT:PSS, ZnO, and an ionic solution containing tetra-*n*-butylammonium tetrafluoroborate were blade-slit coated with a high layer uniformity on ITO-coated glass substrates. The luminous efficiency of the in-air processed samples reached 5.26 cd/A.

On another occasion standard multilayer blade coating has been used to coat several small-molecule materials and PVK host solutions to build multicolored light-emitting devices.⁷² The conducting polymer PEDOT:PSS was blade coated as well. The applied layer thicknesses were below 100 nm with uniformities within 10%. The report covers challenges in uniform layer formation, drying and interaction of solvents in the multilayer approach to prevent dissolution. Large-area

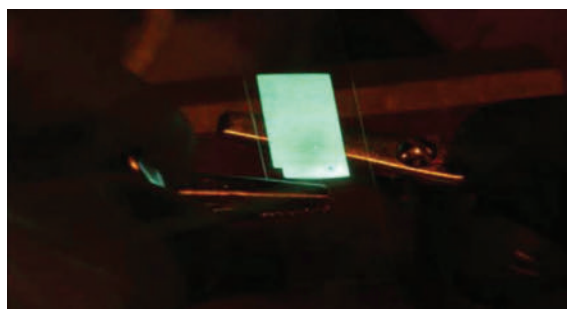


FIGURE 12 Photograph of a flexible PLED device (30 mm × 15 mm) with a slot-die-coated PEDOT:PSS layer and a gravure printed light-emitting polymer layer. Reprinted from Ref. 108, with permission from 2009 Elsevier B.V.

devices with 6 cm² active area and efficiencies up to 25 cd/A for green phosphorescent OLED materials were fabricated.

Gravure printing was used by Kopola et al. to prove the feasibility of large-scale fabrication of PLEDs for lighting applications.⁶⁹ PEDOT:PSS and a blue-emitting polymer dissolved in *o*-xylene was gravure printed on ITO-coated glass with an active area of up to 30 cm². Brightness levels of up to 1000 cd/m² at 5.4 V were achieved. Ink modification and printing form optimization played an important role to achieve homogenous layers for a uniform light generation.

Finally, a fully slot-die-coated light-emitting device based on the light-emitting electrochemical cell (LEC) technology has been demonstrated by Sandström et al.⁶⁷ For the first time, devices were fabricated fully under ambient conditions using roll coating on PET foil. This included air processing of the back electrode. The authors used the emissive conjugated polymer "Super Yellow" and an electrolyte consisting of potassium triflate (CF₃SO₃K) in poly(ethylene oxide) (PEO). Active areas of around 3 cm² have been achieved with brightness levels of up to 150 cd/m² at 10 V. The highest current efficiency was recorded with 0.6 cd/A at 50 cd/m². The processing of the devices was shown to be very reliable because of a thick active layer and air-stable materials. Figure 13 shows pictures of the slot-die coating and the final device.

The achieved results for gravure, blade, and slot-die coating will enable an upcoming transition to full R2R processing of cost-friendly and vacuum-free manufacturing of large area light sources on flexible substrates. Inkjet printing methods will most likely be seen in display manufacturing.

Fuel Cells

Steenberg et al. have lately reported the preparation of 40-mm-thick poly[2,2'(*m*-phenylene)-5,5'-bibenzimidazole] (PBI) films for fuel cells using both knife coating and slot-die coating.¹¹² The membranes proved to have identical properties compared to traditionally cast membranes resulting in an increase in manufacturing speed by a factor of 100.

Loudspeakers

A last example that shows a quite exotic application of thin film processed organic polymers can be found in a recent

publication by Hübler et al. on all-printed polymer loudspeakers.⁸⁵ By utilizing flexographic and screen printing methods, they successfully applied PEDOT:PSS electrodes and the piezo electric polymer poly(vinylidene fluoride-trifluoroethylene) (P(VDF-TrFE)) on standard coated paper substrate. The loudspeakers with effective areas of 16 and 128 cm² lead to sound pressure levels of 63.8 db at 5000 Hz.

SUMMARY AND OUTLOOK

Processing of organic thin films using R2R techniques clearly holds a promising future and for several technologies the realization of fast and low-cost manufacture lies within reach. There are issues though that still need to be overcome. Replacement of ITO as transparent electrode has commenced, but full integration of these new initiatives needs to be performed as they are still in their infant stage. Another key optimization parameter that needs improvement is the registration during R2R processing, which is used to align the different layers. Ultra-precise multilayer processing plays an important role for many types of devices such as organic TFTs, and better control of registration will be needed—especially for processing at very high speeds.

On the long term, a key feature for high throughput production will be that it does not harm the environment. A true large-scale production can only be realized by processing from water, and more research is needed on how this can be achieved. The use of different types of ink formulations (such as dissolved solutions, emulsions, and dispersed nanoparticles) as replacements to the typical use of orthogonal solvents for the processing of multilayer devices could be one suggestion on how to do this, but other solutions could prove more fruitful. One thing is clear though—if processing of large areas of organic thin films is to be realized through large-scale production, the typical toxic and chlorinated solvents that are generally used for processing of conjugated polymers must be replaced with something less harmful. In addition to solvent substitutions, processing procedures need to be more effective and new materials that can sustain processing in the ambient need to be developed. In-line processing (where several layers are processed right after each other during the same run) and even lower drying temperatures are ways of improving effectiveness. For the materials it is more difficult

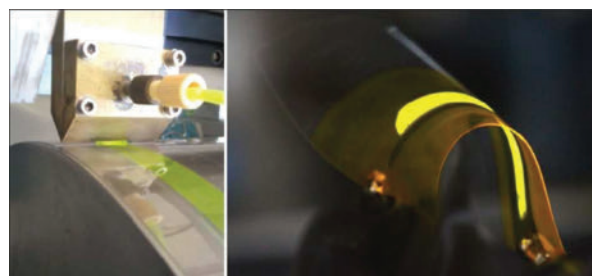


FIGURE 13 Left: Close-up photograph of the slot-die coating process of the light-emitting polymer layer "Super Yellow". Right: Photograph of the final LEC device showing a bidirectional light emission and device conformability. Reprinted from Ref. 67, with permission from 2012 Macmillan Publishers Limited.

to define a specific strategy, but ideally these should be developed in tandem with the solvent substitutions, thus approaching the two issues simultaneously.

ACKNOWLEDGMENTS

This work has been supported partially by the EU Indian framework of the "Largecells" project that received funding from the European Commission's Seventh Framework Programme (FP7/2007–2013; grant no. 261936); partial financial support was also received from the European Commission as part of the Framework 7 ICT 2009 collaborative project ROTROT (grant no. 288565).

REFERENCES AND NOTES

- Kim, C. H.; Jo, J.; Lee, S. H. *Rev. Sci. Instrum.* **2012**, *83*, 065001–065008.
- Søndergaard, R. R.; Hösel, M.; Angmo, D.; Larsen-Olsen, T. T.; Krebs, F. C. *Mater. Today* **2012**, *15*, 36–49.
- Krebs, F. C. *Sol. Energy Mater. Sol. Cells* **2009**, *93*, 394–412.
- Kipphan, H. *Handbook of Print Media*; Springer Verlag: Berlin, **2001**.
- Magdassi, S. *The Chemistry of Inkjet Inks*; World Scientific Publishing: Singapore, **2010**.
- Pond, S. F. *Inkjet Technology and Product Development Strategies*; Torrey Pines Research: Carlsbad, **2000**.
- Tracton, A. A. *Coatings Technology*; CRC Press: Boca Raton, FL, **2007**.
- Wengeler, L.; Schmitt, M.; Peters, K.; Scharfer, P.; Schabel, W. *Chem. Eng. Process.* **2012**; DOI: 10.1016/j.cep.2012.03.004.
- Yu, B. K.; Vak, D.; Jo, J.; Na, S. I.; Kim, S. S.; Kim, M. K.; Kim, D. Y. *IEEE J. Sel. Top. Quantum Electron.* **2010**, *16*, 1838–1846.
- Steirer, K. X.; Reese, M. O.; Rupert, B. L.; Kopidakis, N.; Olson, D. C.; Collins, R. T.; Ginley, D. S. *Sol. Energy Mater. Sol. Cells* **2009**, *93*, 447–453.
- Kim, Y.; Lee, J.; Kang, H.; Kim, G.; Kim, N.; Lee, K. *Sol. Energy Mater. Sol. Cells* **2012**, *98*, 39–45.
- Larsen-Olsen, T. T.; Søndergaard, R. R.; Norrman, K.; Jørgensen, M.; Krebs, F. C. *Energy Environ. Sci.* **2012**; DOI: 10.1039/c2ee23244h.
- Yu, J.-S.; Kim, I.; Kim, J.-S.; Jo, J.; Larsen-Olsen, T. T.; Søndergaard, R. R.; Hösel, M.; Angmo, D.; Jørgensen, M.; Krebs, F. C. *Nanoscale* **2012**, *4*, 6032–6040.
- Larsen-Olsen, T. T.; Machui, F.; Lechene, B.; Berny, S.; Angmo, D.; Søndergaard, R.; Blouin, N.; Mitchell, W.; Tierney, S.; Cull, T.; Tiwana, P.; Meyer, F.; Carrasco-Orozco, M.; Scheel, A.; Lövenich, W.; de Bettignies, R.; Brabec, C. J.; Krebs, F. C. *Adv. Energy Mater.* **2012**, *14*, 1091–1094.
- Manceau, M.; Angmo, D.; Jørgensen, M.; Krebs, F. C. *Org. Electron.* **2011**, *12*, 566–574.
- Angmo, D.; Hösel, M.; Krebs, F. C. *Sol. Energy Mater. Sol. Cells* **2012**; DOI: 10.1016/j.solmat.2012.07.004.
- Hübner, A.; Trnovec, B.; Zillger, T.; Ali, M.; Wetzold, N.; Mingebach, M.; Wagenfahl, A.; Deibel, C.; Dyakonov, V. *Adv. Energy Mater.* **2011**, *1*, 1018–1022.
- Krebs, F. C.; Gevorgyan, S. A.; Alstrup, J. *J. Mater. Chem.* **2009**, *19*, 5442–5451.
- (a) Krebs, F. C.; Fyenbo, J.; Tanenbaum, D. M.; Gevorgyan, S. A.; Andriessen, R.; van Remoortere, B.; Galagan, Y.; Jørgensen, M. *Energy Environ. Sci.* **2011**, *4*, 4116–4123; (b) Angmo, D.; Larsen-Olsen, T. T.; Jørgensen, M.; Søndergaard, R. R.; Krebs, F. C. *Adv. Energy Mater.* **2012**; DOI: 10.1002/aenm.201200520.
- Krebs, F. C.; Tromholt, T.; Jørgensen, M. *Nanoscale* **2010**, *2*, 873–886.
- Søndergaard, R.; Manceau, M.; Jørgensen, M.; Krebs, F. C. *Adv. Energy Mater.* **2012**, *2*, 415–418.
- Bundgaard, E.; Hagemann, O.; Manceau, M.; Jørgensen, M.; Krebs, F. C. *Macromolecules* **2010**, *43*, 8115–8120.
- Krebs, F. C.; Fyenbo, J.; Jørgensen, M. *J. Mater. Chem.* **2010**, *20*, 8994–9001.
- Helgesen, M.; Carlé, J. E.; Andreasen, B.; Hösel, M.; Norrman, K.; Søndergaard, R.; Krebs, F. C. *Polym. Chem.* **2012**, *3*, 2649–2655.
- Amb, C. M.; Craig, M. R.; Koldemir, U.; Subbiah, J.; Choudhury, K. R.; Gevorgyan, S. A.; Jørgensen, M.; Krebs, F. C.; So, F.; Reynolds, J. R. *ACS Appl. Mater. Interfaces* **2012**, *4*, 1847–1853.
- Dam, H. F.; Krebs, F. C. *Sol. Energy Mater. Sol. Cells* **2012**, *97*, 191–196.
- Krebs, F. C. *Sol. Energy Mater. Sol. Cells* **2009**, *93*, 465–475.
- Krebs, F. C.; Jørgensen, M.; Norrman, K.; Hagemann, O.; Alstrup, J.; Nielsen, T. D.; Fyenbo, J.; Larsen, K.; Kristensen, J. *Sol. Energy Mater. Sol. Cells* **2009**, *93*, 422–441.
- Galagan, Y.; de Vries, I. G.; Langen, A. P.; Andriessen, R.; Verhees, W. J.; Veenstra, S. C.; Kroon, J. M. *Chem. Eng. Process.* **2011**, *50*, 454–461.
- Blankenburg, L.; Schultheis, K.; Schache, H.; Sensfuss, S.; Schrödner, M. *Sol. Energy Mater. Sol. Cells* **2009**, *93*, 476–483.
- Schrödner, M.; Sensfuss, S.; Schache, H.; Schultheis, K.; Welzel, T.; Heinemann, K.; Milker, R.; Marten, J.; Blankenburg, L. *Sol. Energy Mater. Sol. Cells* **2012**; DOI: 10.1016/j.solmat.2012.06.048.
- Galagan, Y.; Rubingh, J. M.; Andriessen, R.; Fan, C. C.; Blom, W. M.; Veenstra, C.; Kroon, M. *Sol. Energy Mater. Sol. Cells* **2011**, *95*, 1339–1343.
- Zimmermann, B.; Schleiermacher, H.; Niggemann, M.; Wuerfel, U. *Sol. Energy Mater. Sol. Cells* **2011**, *95*, 1587–1589.
- Ding, J. M.; Vornbrock, A. D.; Ting, C.; Subramanian, V. *Sol. Energy Mater. Sol. Cells* **2009**, *93*, 459–464.
- Kopola, P.; Aernouts, T.; Sliz, R.; Guillerez, S.; Ylikunnari, M.; Cheynds, D.; Valimäki, M.; Tuomikoski, M.; Hast, J.; Jabbour, G.; Mäylä, R.; Maaninen, A. *Sol. Energy Mater. Sol. Cells* **2011**, *95*, 1344–1347.
- Kopola, P.; Aernouts, T.; Guillerez, S.; Jin, H.; Tuomikoski, M.; Maaninen, A.; Hast, J. *Sol. Energy Mater. Sol. Cells* **2010**, *94*, 1673–1680.
- Voigt, M. M.; Mackenzie, R. C. I.; Yau, C. P.; Atienzar, P.; Dane, J.; Keivanidis, P. E.; Bradley, D. D. C.; Nelson, J. *Sol. Energy Mater. Sol. Cells* **2011**, *95*, 731–734.
- Eom, S. H.; Senthilarasu, S.; Uthirakumar, P.; Yoon, S. C.; Lim, J.; Lee, C.; Lim, H. S.; Lee, J.; Lee, S. H. *Org. Electron.* **2009**, *10*, 536–542.
- Aernouts, T.; Aleksandrov, T.; Girotto, C.; Genoe, J.; Poortmans, J. *Appl. Phys. Lett.* **2008**, *92*, 033306.
- Hoth, C. N.; Choulis, S. A.; Schilinsky, P.; Brabec, C. J. *Adv. Mater.* **2007**, *19*, 3973–3978.
- Hoth, C. N.; Schilinsky, P.; Choulis, S. A.; Brabec, C. J. *Nano Lett.* **2008**, *8*, 2806–2813.
- Eom, S. H.; Park, H.; Mujawar, S. H.; Yoon, S. C.; Kim, S. S.; Na, S. I.; Kang, S. J.; Khim, D.; Kim, D. Y.; Lee, S. H. *Org. Electron.* **2010**, *11*, 1516–1522.

- 43** Lange, A.; Wegener, M.; Boeffel, C.; Fischer, B.; Wedel, A.; Neher, D. *Sol. Energy Mater. Sol. Cells* **2010**, *94*, 1816–1821.
- 44** Chen, L. M.; Hong, Z.; Kwan, W. L.; Lu, C. H.; Lai, Y. F.; Lei, B.; Liu, C. P.; Yang, Y. *ACS Nano* **2010**, *4*, 4744–4752.
- 45** Hoth, C. N.; Steim, R.; Schilinsky, P.; Choulis, S. A.; Tedde, S. F.; Hayden, O.; Brabec, C. J. *Org. Electron.* **2009**, *10*, 587–593.
- 46** Nie, W. Y.; Coffin, R. C.; Liu, J. W.; Li, Y.; Peterson, E. D.; MacNeill, C. M.; Nofhle, R. E.; Carroll, D. L. *Appl. Phys. Lett.* **2012**, *100*, 083301.
- 47** Ali, M.; Abbas, M.; Shah, S. K.; Tuerhong, R.; Generosi, A.; Paci, B.; Hirsch, L.; Gunnella, R. *Org. Electron.* **2012**, *13*, 2130–2137.
- 48** Abdellah, A.; Virdi, K. S.; Meier, R.; Döblinger, M.; Müller-Buschbaum, P.; Scheu, C.; Lugli, P.; Scarpa, G. *Adv. Funct. Mater.* **2012**, *22*, 4078–4086.
- 49** Peh, R. J.; Lu, Y. R.; Zhao, F. L.; Lee, C. L. K.; Kwan, W. L. *Sol. Energy Mater. Sol. Cells* **2011**, *95*, 3579–3584.
- 50** Giroto, C.; Rand, B. P.; Genoe, J.; Heremans, P. *Sol. Energy Mater. Sol. Cells* **2009**, *93*, 454–458.
- 51** Park, S. Y.; Kang, Y. J.; Lee, S.; Kim, D. G.; Kim, J. K.; Kim, J. H.; Kang, J. W. *Sol. Energy Mater. Sol. Cells* **2011**, *95*, 852–855.
- 52** Susanna, G.; Salamandra, L.; Brown, T. M.; Di Carlo, A.; Brunetti, F.; Reale, A. *Sol. Energy Mater. Sol. Cells* **2011**, *95*, 1775–1778.
- 53** Lewis, J. E.; Lafalce, E.; Toglia, P.; Jiang, X. *Sol. Energy Mater. Sol. Cells* **2011**, *95*, 2816–2822.
- 54** Giroto, C.; Moia, D.; Rand, B. P.; Heremans, P. *Adv. Funct. Mater.* **2011**, *21*, 64–72.
- 55** Na, S. I.; Yu, B. K.; Kim, S. S.; Vak, D.; Kim, T. S.; Yeo, J. S.; Kim, D. Y. *Sol. Energy Mater. Sol. Cells* **2010**, *94*, 1333–1337.
- 56** Giroto, C.; Rand, B. P.; Steudel, S.; Genoe, J.; Heremans, P. *Org. Electron.* **2009**, *10*, 735–740.
- 57** Hau, S. K.; Yip, H. L.; Leong, K.; Jen, A. K. *Org. Electron.* **2009**, *10*, 719–723.
- 58** Zhang, B.; Chae, H.; Cho, S. M. *Jpn. J. Appl. Phys.* **2009**, *48*, 020208.
- 59** Wengeler, L.; Schmidt-Hansberg, B.; Peters, K.; Scharfer, P.; Schabel, W. *Chem. Eng. Process.* **2011**, *50*, 478–482.
- 60** Hamsch, M.; Reuter, K.; Stanel, M.; Schmidt, G.; Kempa, H.; Fügmann, U.; Hahn, U.; Hübler, A. C. *Mater. Sci. Eng. B* **2010**, *170*, 93–98.
- 61** Tobjörk, D.; Kaihovirta, N. J.; Mäkelä, T.; Pettersson, F. S.; Österbacka, R. *Org. Electron.* **2008**, *9*, 931–935.
- 62** Huebler, A. C.; Doetz, F.; Kempa, H.; Katz, H. E.; Bartzsch, M.; Brandt, N.; Hennig, I.; Fuegmann, U.; Vaidyanathan, S.; Granstrom, J.; Liu, S.; Sydorenko, A.; Zillger, T.; Schmidt, G.; Preissler, K.; Reichmanis, E.; Eckerle, P.; Richter, F.; Fischer, T.; Hahn, U. *Org. Electron.* **2007**, *8*, 480–486.
- 63** Chung, S.; Kim, S. O.; Kwon, S. K.; Lee, C.; Hong, Y. *IEEE Electron Device Lett.* **2011**, *32*, 1134–1136.
- 64** Voigt, M. M.; Guite, A.; Chung, D. Y.; Khan, R. U. A.; Campbell, A. J.; Bradley, D. D. C.; Meng, F. S.; Steinke, J. H. G.; Tierney, S.; McCulloch, I.; Penxten, H.; Lutsen, L.; Douheret, O.; Manca, J.; Brokmann, U.; Sönnichsen, K.; Hülsenberg, D.; Bock, W.; Barron, C.; Blanckaert, N.; Springer, S.; Grupp, J.; Mosley, A. *Adv. Funct. Mater.* **2010**, *20*, 239–246.
- 65** Vornbrock, A. D.; Sung, D. V.; Kang, H. K.; Kitsomboonloha, R.; Subramanian, V. *Org. Electron.* **2010**, *11*, 2037–2044.
- 66** Verilhac, J. M.; Benwadih, M.; Seiler, A. L.; Jacob, S.; Bory, C.; Bablet, J.; Heitzman, M.; Tallal, J.; Barbut, L.; Frère, P.; Sicard, G.; Gwoziecki, R.; Chartier, I.; Coppard, R.; Serbutoviez, C. *Org. Electron.* **2010**, *11*, 456–462.
- 67** Sandström, A.; Dam, H. F.; Krebs, F. C.; Edman, L. *Nat. Commun.* **2012**, *3*, 1002.
- 68** Youn, H.; Jeon, K.; Shin, S.; Yang, M. *Org. Electron.* **2012**, *13*, 1470–1478.
- 69** Kopola, P.; Tuomikoski, M.; Suhonen, R.; Maaninen, A. *Thin Solid Films* **2009**, *517*, 5757–5762.
- 70** Kwon, J. T.; Eom, S. H.; Moon, B. S.; Shin, J. K.; Kim, K. S.; Lee, S. H.; Lee, Y. S. *Bull. Korean Chem. Soc.* **2012**, *33*, 464–468.
- 71** Kim, A.; Lee, H.; Lee, J.; Cho, S. M.; Chae, H. *J. Nanosci. Nanotechnol.* **2011**, *11*, 546–549.
- 72** Chen, C. Y.; Chang, H. W.; Chang, Y. F.; Chang, B. J.; Lin, Y. S.; Jian, P. S.; Yeh, H. C.; Chien, H. T.; Chen, E. C.; Chao, Y. C.; Meng, H. F.; Zan, H. W.; Lin, H. W.; Horng, S. F.; Cheng, Y. J.; Yen, F. W.; Lin, I. F.; Yang, H. Y.; Huang, K. J.; Tseng, M. R. *J. Appl. Phys.* **2011**, *110*, 094501.
- 73** Lee, D. H.; Choi, J. S.; Chae, H.; Chung, C. H.; Cho, S. M. *Displays* **2008**, *29*, 436–439.
- 74** (a) Jensen, J.; Dam, H. F.; Reynolds, J. R.; Dyer, A. L.; Krebs, F. C. *J. Polym. Sci. Part B: Polym. Phys.* **2012**, *50*, 536–545; (b) Søndergaard, R. R.; Hösel, M.; Jørgensen, M.; Krebs, F. C. *J. Polym. Sci. Part B: Polym. Phys.* **2013**; DOI: 10.1002/polb.23189.
- 75** Amb, C. M.; Kerszulis, J. A.; Thompson, E. J.; Dyer, A. L.; Reynolds, J. R. *Polym. Chem.* **2011**, *2*, 812–814.
- 76** Dyer, A. L.; Craig, M. R.; Babiarz, J. E.; Kiyak, K.; Reynolds, J. R. *Macromolecules* **2010**, *43*, 4460–4467.
- 77** Reeves, B. D.; Grenier, C. R. G.; Argun, A. A.; Cirpan, A.; McCarley, T. D.; Reynolds, J. R. *Macromolecules* **2004**, *37*, 7559–7569.
- 78** Mortimer, R. J.; Graham, K. R.; Grenier, C. R.; Reynolds, J. R. *ACS Appl. Mater. Interfaces* **2009**, *1*, 2269–2276.
- 79** Amb, C. M.; Beaujuge, P. M.; Reynolds, J. R. *Adv. Mater.* **2010**, *22*, 724–728.
- 80** Beaujuge, P. M.; Ellinger, S.; Reynolds, J. R. *Adv. Mater.* **2008**, *20*, 2772–2776.
- 81** Shim, G. H.; Han, M. G.; Sharp-Norton, J. C.; Creager, S. E.; Foulger, S. H. *J. Mater. Chem.* **2008**, *18*, 594–601.
- 82** Small, W. R.; Masdarolomoor, F.; Wallace, G. G.; in het Panhuis, M. J. *J. Mater. Chem.* **2007**, *17*, 4359–4361.
- 83** Andersson, P.; Forchheimer, R.; Tehrani, P.; Berggren, M. *Adv. Funct. Mater.* **2007**, *17*, 3074–3082.
- 84** Brotherston, I. D.; Mudigonda, D. S. K.; Osborn, J. M.; Belk, J.; Chen, J.; Loveday, D. C.; Boehme, J. L.; Ferraris, J. P.; Meeker, D. L. *Electrochim. Acta* **1999**, *44*, 2993–3004.
- 85** Hübler, A. C.; Bellmann, M.; Schmidt, G. C.; Zimmermann, S.; Gerlach, A.; Haentjes, C. *Org. Electron.* **2012**, *13*, 2290–2295.
- 86** Gevorgyan, S. A.; Medford, A. J.; Bundgaard, E.; Sapkota, S. B.; Schleiermacher, H. F.; Zimmermann, B.; Würfel, U.; Chafiq, A.; Lira-Cantu, M.; Swonke, T.; Wagner, M.; Brabec, C. J.; Haillat, O. O.; Voroshazi, E.; Aernouts, T.; Steim, R.; Hauch, J. A.; Elschner, A.; Pannone, M.; Xiao, M.; Langzettel, A.; Laird, D.; Lloyd, M. T.; Rath, T.; Maier, E.; Trimmel, G.; Hermenau, M.; Menke, T.; Leo, K.; Rösch, R.; Seeland, M.; Hoppe, H.; Nagle, T. J.; Burke, K. B.; Fell, C. J.; Vak, D.; Singh, T. B.; Watkins, S. E.; Galagan, Y.; Manor, A.; Katz, E. A.; Kim, T.; Kim, K.; Sommeling, P. M.; Verhees, W. J. H.; Veenstra, S. C.; Riede, M.; Christoforo, M. G.; Currier, T.; Shrotriya, V.; Schwartz, G.; Krebs, F. C. *Sol. Energy Mater. Sol. Cells* **2011**, *95*, 1398–1416.
- 87** Søndergaard, R.; Makris, T.; Lianos, P.; Manor, A.; Katz, E. A.; Gong, W.; Tuladhar, S. M.; Nelson, J.; Sommerling, P.;

- Veenstra, S. C.; Rivaton, A.; Dupuis, A.; Teran-Escobar, G.; Lira-Cantu, M.; Sabkota, S. B.; Zimmermann, B.; Würfel, U.; Krebs, F. C. *Sol. Energy Mater. Sol. Cells* **2012**, *99*, 292–300.
- 88** Krebs, F. C.; Gevorgyan, S. A.; Gholamkhash, B.; Holdcroft, S.; Schlenker, C.; Thompson, M. E.; Thompson, B. C.; Olson, D.; Ginley, D. S.; Shaheen, S. E.; Alshareef, H. N.; Murphy, J. W.; Youngblood, W. J.; Heston, N. C.; Reynolds, J. R.; Jia, S. J.; Laird, D.; Tuladhar, S. M.; Dane, J. G. A.; Atienzar, P.; Nelson, J.; Kroon, J. M.; Wienk, M. M.; Janssen, R. A. J.; Tvingstedt, K.; Zhang, F. L.; Andersson, M.; Inganäs, O.; Lira-Cantu, M.; de Bettignies, R.; Guillerez, S.; Aernouts, T.; Cheyng, D.; Lutsen, L.; Zimmermann, B.; Würfel, U.; Niggemann, M.; Schleiermacher, H. F.; Liska, P.; Grätzel, M.; Lianos, P.; Katz, E. A.; Lohwasser, W.; Jannson, B. *Sol. Energy Mater. Sol. Cells* **2009**, *93*, 1968–1977.
- 89** Tanenbaum, D. M.; Hermenau, M.; Voroshazi, E.; Lloyd, M. T.; Galagan, Y.; Zimmermann, B.; Hösel, M.; Dam, H. F.; Jørgensen, M.; Gevorgyan, S. A.; Kudret, S.; Maes, W.; Lutsen, L.; Vanderzande, D.; Würfel, U.; Andriessen, R.; Rösch, R.; Hoppe, H.; Teran-Escobar, G.; Lira-Cantu, M.; Rivaton, A.; Uzunoglu, G. Y.; Germack, D.; Andreasen, B.; Madsen, M. V.; Norrman, K.; Krebs, F. C. *RSC Adv.* **2012**, *2*, 882–893.
- 90** Krebs, F. C.; Nielsen, T. D.; Fyenbo, J.; Wadstrøm, M.; Pedersen, M. S. *Energy Environ. Sci.* **2010**, *3*, 512–525.
- 91** Larsen-Olsen, T. T.; Andreasen, B.; Andersen, T. R.; Böttiger, A. P. L.; Bundgaard, E.; Norrman, K.; Andreasen, J. W.; Jørgensen, M.; Krebs, F. C. *Sol. Energy Mater. Sol. Cells* **2012**, *97*, 22–27.
- 92** Alstrup, J.; Jørgensen, M.; Medford, A. J.; Krebs, F. C. *ACS Appl. Mater. Interfaces* **2010**, *2*, 2819–2827.
- 93** Dyer, A. L.; Thompson, E. J.; Reynolds, J. R. *ACS Appl. Mater. Interfaces* **2011**, *3*, 1787–1795.
- 94** Wen, Y. G.; Liu, Y. Q.; Guo, Y. L.; Yu, G.; Hu, W. P. *Chem. Rev.* **2011**, *111*, 3358–3406.
- 95** Hamsch, M.; Reuter, K.; Kempa, H.; Hübner, A. C. *Org. Electron.* **2012**, *13*, 1989–1995.
- 96** Kempa, H.; Hamsch, M.; Reuter, K.; Stanel, M.; Schmidt, G. C.; Meier, B.; Hübner, A. C. *IEEE Trans. Electron Devices* **2011**, *58*, 2765–2769.
- 97** Sirringhaus, H.; Kawase, T.; Friend, R. H.; Shimoda, T.; Inbasekaran, M.; Wu, W.; Woo, E. P. *Science* **2000**, *290*, 2123–2126.
- 98** Chan, C. K.; Richter, L. J.; Dinardo, B.; Jaye, C.; Conrad, B. R.; Ro, H. W.; Germack, D. S.; Fischer, D. A.; DeLongchamp, D. M.; Gundlach, D. J. *Appl. Phys. Lett.* **2010**, *96*, 133304.
- 99** Kang, H.; Kitsomboonloha, R.; Jang, J.; Subramanian, V. *Adv. Mater.* **2012**, *24*, 3065–3069.
- 100** Schmidt, G. C.; Bellmann, M.; Meier, B.; Hamsch, M.; Reuter, K.; Kempa, H.; Hübner, A. C. *Org. Electron.* **2010**, *11*, 1683–1687.
- 101** Bernius, M. T.; Inbasekaran, M.; O'Brien, J.; Wu, W. S. *Adv. Mater.* **2000**, *12*, 1737–1750.
- 102** So, F.; Krummacker, B.; Mathai, M. K.; Poplavskyy, D.; Choulis, S. A.; Choong, V. E. *J. Appl. Phys.* **2007**, *102*, 091101.
- 103** AlSalhi, M. S.; Alam, J.; Dass, L. A.; Raja, M. *Int. J. Mol. Sci.* **2011**, *12*, 2036–2054.
- 104** Wu, H. B.; Ying, L.; Yang, W.; Cao, Y. *Chem. Soc. Rev.* **2009**, *38*, 3391–3400.
- 105** Pardo, D. A.; Jabbour, G. E.; Peyghambarian, N. *Adv. Mater.* **2000**, *12*, 1249–1252.
- 106** Birnstock, J.; Blässing, J.; Hunze, A.; Scheffel, M.; Stössel, M.; Heuser, K.; Wörle, J.; Wittmann, G.; Winnacker, A. *Proc. SPIE* **2002**, *4464*, 68–75.
- 107** Tseng, S. R.; Meng, H. F.; Lee, K. C.; Horng, S. F. *Appl. Phys. Lett.* **2008**, *93*, 153308.
- 108** Michels, J. J.; de Winter, S. H. P. M.; Symonds, L. H. G. *Org. Electron.* **2009**, *10*, 1495–1504.
- 109** Tuomikoski, M.; Suhonen, R.; Valimäki, M.; Maaninen, T.; Maaninen, A.; Sauer, M.; Rogin, P.; Mennig, M.; Heusing, S.; Puetz, J.; Aegerter, M. A. *Proc. SPIE* **2006**, *6192*, 619204.
- 110** Lee, S.-H.; Hwang, J. Y.; Kang, K.; Kang, H. In *International Symposium on Optomechatronic Technologies (ISOT)*, **2009**; pp 71–76.
- 111** Tekin, E.; Holder, E.; Kozodaev, D.; Schubert, U. S. *Adv. Funct. Mater.* **2007**, *17*, 277–284.
- 112** Steenberg, T.; Hjuler, H. A.; Terkelsen, C.; Sanchez, M. T. R.; Cleemann, L. N.; Krebs, F. C. *Energy Environ. Sci.* **2012**, *5*, 6076–6080.

Thermoelectrical Generators / Superconducting Components
High Temperature Polymer Electrolyte Membrane Fuel Cells

Energy Conversion

Magnetism
Electrochemistry
Defect Chemistry

Colloidal Chemistry / Electrochemistry

Polymer Solar Cells

Solid State Physics

Electron Microscopy

Ceramic Membranes

Solid Oxide Fuel Cells

Shaping Processes / Electron Microscopy / Solid State Physics / Computational Materials Design

Modelling / Heterostructures

Solid Oxide Electrolysis Cells

Computational Materials Design

X-Ray and Neutron Scattering

High Temperature Polymer Electrolyte Membrane Electrolysis Cells

Fuel Cells and Hydrogen Test Center

Shaping Processes / Defect Chemistry

Electrochemical Flue Gas Purification

Batteries / Hydrogen Storage

Synthesis / Colloidal Chemistry / Heterostructures / X-Ray and Neutron Scattering

Magnetic Refrigeration

Energy Storage

Sintering

Fuel Cells

Synthetic Fuels

Sintering

Magnetism

Synthesis

Modelling

Department of Energy Conversion and Storage
Technical University of Denmark
Risø Campus
Frederiksborgvej 399
4000 Roskilde
Denmark
www.ecs.dtu.dk

ISBN 978-87-92986-15-3